Lecture Notes in Applied and Computational Mechanics 63

Ulrich Langer
Martin Schanz
Olaf Steinbach
Wolfgang L. Wendland
Editors

Fast Boundary Element Methods in Engineering and Industrial Applications

Springer

Lecture Notes in Applied and Computational Mechanics

Volume 63

Lecture Notes in Applied and Computational Mechanics

Edited by F. Pfeiffer and P. Wriggers

Further volumes of this series found on our homepage: springer.com

Vol. 63 Langer, U., Schanz, M., Steinbach, O., Wendland, W. L. (Eds.)
Fast Boundary Element Methods in Engineering and Industrial Applications
272 p. 2012 [978-3-642-25669-1]

Vol. 61 Frémond, M., Maceri, F. (Ed.)
Mechanics, Models and Methods in Civil Engineering
498 p. 2012 [978-3-642-24637-1]

Vol. 59 Markert, B., (Ed.)
Advances in Extended and Multifield Theories for Continua
219 p. 2011 [978-3-642-22737-0]

Vol. 58 Zavarise, G., Wriggers, P. (Eds.)
Trends in Computational Contact Mechanics
354 p. 2011 [978-3-642-22166-8]

Vol. 57 Stephan, E., Wriggers, P.
Modelling, Simulation and Software Concepts for Scientific-Technological Problems
251 p. 2011 [978-3-642-20489-0]

Vol. 54: Sanchez-Palencia, E., Millet, O., Béchet, F.
Singular Problems in Shell Theory
265 p. 2010 [978-3-642-13814-0]

Vol. 53: Litewka, P.
Finite Element Analysis of Beam-to-Beam Contact
159 p. 2010 [978-3-642-12939-1]

Vol. 52: Pilipchuk, V.N.
Nonlinear Dynamics: Between Linear and Impact Limits
364 p. 2010 [978-3-642-12798-4]

Vol. 51: Besdo, D., Heimann, B., Klüppel, M., Kröger, M., Wriggers, P., Nackenhorst, U.
Elastomere Friction
249 p. 2010 [978-3-642-10656-9]

Vol. 50: Ganghoffer, J.-F., Pastrone, F. (Eds.)
Mechanics of Microstructured Solids 2
102 p. 2010 [978-3-642-05170-8]

Vol. 49: Hazra, S.B.
Large-Scale PDE-Constrained Optimization in Applications
224 p. 2010 [978-3-642-01501-4]

Vol. 48: Su, Z.; Ye, L.
Identification of Damage Using Lamb Waves
346 p. 2009 [978-1-84882-783-7]

Vol. 47: Studer, C.
Numerics of Unilateral Contacts and Friction
191 p. 2009 [978-3-642-01099-6]

Vol. 46: Ganghoffer, J.-F., Pastrone, F. (Eds.)
Mechanics of Microstructured Solids
136 p. 2009 [978-3-642-00910-5]

Vol. 45: Shevchuk, I.V.
Convective Heat and Mass Transfer in Rotating Disk Systems
300 p. 2009 [978-3-642-00717-0]

Vol. 44: Ibrahim R.A., Babitsky, V.I., Okuma, M. (Eds.)
Vibro-Impact Dynamics of Ocean Systems and Related Problems
280 p. 2009 [978-3-642-00628-9]

Vol.43: Ibrahim, R.A.
Vibro-Impact Dynamics
312 p. 2009 [978-3-642-00274-8]

Vol. 42: Hashiguchi, K.
Elastoplasticity Theory
432 p. 2009 [978-3-642-00272-4]

Vol. 41: Browand, F., Ross, J., McCallen, R. (Eds.)
Aerodynamics of Heavy Vehicles II: Trucks, Buses, and Trains
486 p. 2009 [978-3-540-85069-4]

Vol. 40: Pfeiffer, F.
Mechanical System Dynamics
578 p. 2008 [978-3-540-79435-6]

Vol. 39: Lucchesi, M., Padovani, C., Pasquinelli, G., Zani, N.
Masonry Constructions: Mechanical Models and Numerical Applications
176 p. 2008 [978-3-540-79110-2]

Vol. 38: Marynowski, K.
Dynamics of the Axially Moving Orthotropic Web
140 p. 2008 [978-3-540-78988-8]

Vol. 37: Chaudhary, H., Saha, S.K.
Dynamics and Balancing of Multibody Systems
200 p. 2008 [978-3-540-78178-3]

Fast Boundary Element Methods in Engineering and Industrial Applications

Ulrich Langer, Martin Schanz,
Olaf Steinbach, and Wolfgang L. Wendland (Eds.)

Springer

Editors
Prof. Dr. Ulrich Langer
Institut für Numerische Mathematik
Johannes Kepler Universität Linz
4040 Linz, Austria

Prof. Dr. Olaf Steinbach
Institut für Numerische Mathematik
Technische Universität Graz
8010 Graz, Austria

Prof. Dr. -Ing. Martin Schanz
Institut für Baumechanik
Technische Universität Graz
8010 Graz, Austria

Prof. Dr. -Ing. Dr. h. c. Wolfgang L. Wendland
Institut für Angewandte Analysis und
Numerische Simulation
Universität Stuttgart
70569 Stuttgart, Germany

ISSN: 1613-7736
ISBN: 978-3-642-25669-1
DOI 10.1007/ 978-3-642-25670-7
Springer Heidelberg New York Dordrecht London

e-ISSN: 1860-0816
e-ISBN: 978-3-642-25670-7

Library of Congress Control Number: 2011944752

Printed on acid-free paper

Springer is part of Springer Science+Business Media (www.springer.com)

Preface

This volume on mathematical aspects and applications of fast boundary element methods in engineering and industry contains eight contributions on the state of the art in this field. This book is strongly related to the annual Söllerhaus workshops on *Fast Boundary Element Methods in Industrial Applications*[1] where recent trends and new methodologies are discussed to solve todays challenging problems in almost all areas of applications. The stimulating atmosphere of the Söllerhaus workshops contributed a lot to new developments and new interdisciplinary cooperations which are also documented within this book. This spirit of strong cooperations between mathematicians and engineers, with direct applications in industry, follows an already long–ongoing history. To underline this, we just mention the volumes *Boundary Element Topics* (Springer 1997), *Boundary Element Analysis. Mathematical Aspects and Applications* (Springer 2007), and the special issue of *Computing and Visualization in Science* (Volume 8, 2005), which indicate the development of the mathematical foundations of boundary integral equation methods and the applications of fast boundary element methods.

Nowadays, fast boundary element methods are a powerful tool for the simulation of physical phenomena in different fields of applications. In particular, boundary integral equation techniques are well suited for the solution of partial differential equations in unbounded exterior domains, or for problems which are considered in complicated geometries, but with simple physical model assumptions. The latter also involves applications with nonlinear interface or transmission conditions, as they appear in multiphysics simulations. Several of these aspects are covered within this book. An efficient and accurate numerical simulation of time–dependent problems both in time and frequency domain belongs still to the most challenging problems. This book includes contributions on the mathematical analysis of boundary integral formulations, the numerical analysis of boundary element methods and the construction of robust and efficient preconditioning strategies, and the design and implementation of fast boundary element methods to solve challenging problems of interest.

[1] see http://www.numerik.math.tu-graz.ac.at/tagungen

The aim of this book is to present some of the current developments of fast boundary element methods and their applications. We are aware that such a book can not cover all aspects in the analysis and applications of fast boundary element methods. There are no contributions, e.g., for adaptive fast boundary element methods. Other missing topics include the use of fast boundary element methods for the simulation of complex multiphysics problems including the coupling with finite element methods, as well as related inverse and shape optimization problems. In fact, this book may serve to present some of the basic tools to handle the above mentioned problems. The ongoing work on the solution of these problems will be reported on future workshops and conferences, and the results will be documented in future publications as well.

We would like to thank all authors for their contributions to this volume. Moreover, we also thank all anonymmous referees for their work, their criticism, and their suggestions. These hints were very helpful to improve the contributions. Finally, we would like to thank Dr. T. Ditzinger of Springer Heidelberg for the continuing support and patience while preparing this volume.

Graz, Linz, Stuttgart
September 2011

Ulrich Langer
Martin Schanz
Olaf Steinbach
Wolfgang L. Wendland

Contents

Differential Forms and Boundary Integral Equations for Maxwell-Type Problems

Stefan Kurz and Bernhard Auchmann

Abstract. We present boundary-integral equations for Maxwell-type problems in a differential-form setting. Maxwell-type problems are governed by the differential equation $(\delta \mathrm{d} - k^2)\omega = 0$, where $k \in \mathbb{C}$ holds, subject to some restrictions. This problem class generalizes **curl curl**- and div **grad**-types of problems in three dimensions. The goal of the paper is threefold: 1) Establish the Sobolev-space framework in the full generality of differential-form calculus on a smooth manifold of arbitrary dimension and with Lipschitz boundary. 2) Introduce integral transformations and fundamental solutions, and derive a representation formula for Maxwell-type problems. 3) Leverage the power of differential-form calculus to gain insight into properties and inherent symmetries of boundary-integral equations of Maxwell-type.

1 Introduction

It is the goal of this paper to express the theory of boundary-integral equations for Maxwell-type problems in the language of differential-form calculus. Maxwell-type problems are governed by the differential equation

$$(\delta \mathrm{d} - k^2)\omega = 0,$$

where $k \in \mathbb{C}$ fulfills either $k = 0$ or $0 \leq \arg k < \pi, k \neq 0$ [27, eq. (9.13)]. The exterior derivative d and coderivative δ will be defined in Sect. 2.1. This problem class generalizes **curl curl**- and div **grad**-types of problems in three dimensions.

Stefan Kurz
Tampere University of Technology, Department of Electronics, 33101 Tampere, Finland
e-mail: stefan.kurz@tut.fi

Bernhard Auchmann
CERN/TE, Geneva 1211, Switzerland
e-mail: bernhard.auchmann@cern.ch

U. Langer et al. (Eds.): Fast Boundary Element Methods, LNACM 63, pp. 1–62.
springerlink.com

It encompasses electro- and magnetostatics (potential problems), eddy-current and diffusion-type problems, as well as scattering problems.

In the authors' view, differential-form calculus features a range of advantages over classical vector analysis, that are particularly interesting in the field of boundary-integral equations. We give four examples: (i) Being independent of dimension, operators of the same class act upon fields on the domain and on the boundary. (ii) For a comprehensive treatment of the subject, only two families of functional spaces are required on the domain and on the boundary, respectively. The two families are related via Hodge duality. (iii) Involved computations with cross-products of normal vectors and tangent vectors are replaced by more elegant tools. (iv) A discretization of the functional spaces in terms of discrete differential forms is readily available and, in fact, an integral part of the differential-form setting. In this context HIPTMAIR writes in [17, p. 239ff.]: "Suitable finite elements for electromagnetic fields should be introduced and understood as discrete differential forms. ... Finite elements that lack an interpretation as discrete differential forms have to be used with great care.". For establishing spaces of discrete differential forms on two-dimensional surfaces we also point to [7, Sect. 4.1.].

The reader will find that, in many ways, the theory and proofs outlined in this paper are reminiscent of vector-analysis literature. This is not surprising, since a major part of our work consisted in translating classical proofs to the more general differential-form setting. In other places, presumably well-known subjects may look strangely unfamiliar. Study of the theory from the viewpoint of differential-form calculus reveals structural layers that are often hidden or obscured by the nature of vector analysis. For examples we point to the definition of generalized integral transforms, the image spaces of Sobolev spaces under the Hodge operator, or the symmetry of Calderón projectors under dual transformations. We hope that, with this work, we can help to spark the curiosity for differential-form calculus in the community, and do our share to lay the groundwork for future progress in the field. After all, ROTA wrote [31, p. 46], "Exterior algebra is not meant to prove old facts, it is meant to disclose a new world."

From a historical perspective, the idea to generalize Maxwell's equations, using p-forms in n-dimensional Euclidean space, was first put forward in a seminal paper by WEYL in 1952 [38]. Comparable work for the static case, that is, for potential problems, was accomplished by KRESS in 1972 [23]. Related work about higher dimensional electromagnetic scattering on Lipschitz domains in $\mathbb{R}^n$ was published by JAWERTH and MITREA in 1995 [21]. Recently, PAULY has published a series of papers, where the low frequency asymptotics for generalized Maxwell equations have been examined under rather general assumptions [29].

In Sect. 2 we give a concise summary of relevant topics of differential-form calculus. This summary is intended mainly for reference purposes. Readers who are not familiar with the formalism might want to consult [20], [16, Chap. A] or [2, Sect. 2]. Sect. 2 also includes contributions on topics such as integral transformations, and fundamental solutions of Helmholtz-type equations. So-called

translation isomorphisms are introduced, that carry the differential-form setting in three-dimensional Euclidean space over to the classical vector-analysis setting. Sect. 3 presents a differential-form based Sobolev-space framework that sets the scene for the discussion of Maxwell-type problems, their solutions, and boundary data. The section builds upon a 2004 work by WECK [36]. Translation isomorphisms are used to establish the link with Sobolev spaces in classical calculus. Sect. 4 is devoted entirely to the representation formula for Maxwell-type problems. The results generalize the Kirchhoff and Stratton-Chu formulae. In Sect. 5 we introduce boundary-integral operators and establish some of the properties that are required to prove the well-posedness of boundary-value problems. Finally, Sect. 6 studies properties of the Calderón projector and reveals a powerful symmetry with respect to dual transformations.

In our notation, we seek to strike a balance between readability on the one hand, and the addition of information that helps to interpret the compact differential-form notation on the other hand. If in doubt, we tend to favor the former over the latter, assuming that the generality and elegance of differential-form calculus best serve the readers' interest. For example, operators in Sect. 2 are defined for forms of arbitrary degrees, and on (Riemannian) manifolds of arbitrary dimension. We therefore do not generally distinguish in our notation between, for example, the Hodge operators acting on forms of various degrees on a domain Ω, and the Hodge operators acting upon the traces of said forms on the boundary Γ. The metric tensor which applies in the definition of each operator is clear from the context. A generalization that we did not adopt is to introduce graded Sobolev spaces on the entire exterior algebra of differential forms. We have opted for spaces of homogeneous degree and highlight the degree in the notation. All along the text, the relationship to results of classical vector analysis is established in framed paragraphs, to keep the paradigms separate in the main body of the paper.

2 Differential Forms – Preliminaries

In this section, we intend to summarize important results of differential-form calculus. Throughout the paper, n denotes the dimension of the problem domain; the degree of forms is frequently denoted by p and q, which are always related by $q = n - p$.

Powers of minus one followed by operators, as in $(-1)^{pq}\mathrm{op}_1\,\mathrm{op}_2\,\phi$, are to be read as follows: The degree p refers to the differential form that the sequence of operators acts upon from the left. In this example, p is the degree of the form ϕ. n is always the dimension of the problem domain, even if operators and forms on the domain boundary are considered; and $q = n - p$ following the above rule.

2.1 Basic Definitions

We introduce differential forms on a smooth, orientable Riemannian manifold (M, g) of finite dimension n, where g denotes the metric tensor. We have $\mathbb{R}^3$, or

a subset thereof, with Euclidean metric in mind. Throughout this section V denotes a vector space over a field $\mathbb{F}$, where $\mathbb{F}$ may be either $\mathbb{R}$ or $\mathbb{C}$.

A *simple p-vector* may be thought of as an ordered p-tuple of vectors that belong to a vector space V. The p-tuple is interpreted as a p-parallelepiped with oriented volume. An elementary permutation in the tuple changes the orientation. A change of orientation is indicated by a change of sign of the simple p-vector. More precisely, a simple p-vector is an equivalence class of ordered p-tuples of vectors that (i) span the same subspace of V; (ii) span p-parallelepipeds of identical oriented volume. *p-vectors* are linear combinations of simple p-vectors. They form a vector space $\Lambda^p V$ of dimension $\binom{n}{p}$, $0 \le p \le n$. Up to dimension $n = 3$ all p-vectors are simple p-vectors. We find $\Lambda^1 V = V$, $\Lambda^p V = \emptyset$ for $p > n$ and for $p < 0$, and we set $\Lambda^0 V = \mathbb{F}$.

Alternatively, p-vectors are defined in [15] via an isomorphism that identifies $\Lambda^p V$ with the vector space of skew-symmetric tensors of rank p over V.

Let $(\mathbf{e}_i \,|\, 1 \le i \le n)$ denote an ordered basis of V. We pick an *ordered basis of* $\Lambda^p V$

$$(\mathbf{e}_J \,|\, J \in \mathscr{J}_p^n),$$

where $J = j_1 j_2 \dots j_p$ is a multiindex,

$$\mathscr{J}_p^n = \{J = j_1 j_2 \dots j_p \,|\, 1 \le j_1 < j_2 < \dots < j_p \le n\},$$

and $\mathbf{e}_J$ is the equivalence class that contains the p-tupel $(\mathbf{e}_{j_1}, \mathbf{e}_{j_2}, \dots, \mathbf{e}_{j_p})$.

The *exterior product*, or wedge product, is a bilinear mapping

$$\wedge : \Lambda^k V \times \Lambda^\ell V \to \Lambda^{k+\ell} V : (\mathbf{v}, \mathbf{w}) \mapsto \mathbf{v} \wedge \mathbf{w},$$

defined by the following properties:

(i) $\wedge$ is associative, $(\mathbf{u} \wedge \mathbf{v}) \wedge \mathbf{w} = \mathbf{u} \wedge (\mathbf{v} \wedge \mathbf{w})$, $\mathbf{u} \in \Lambda^j V$;
(ii) $\wedge$ is graded anticommutative, $\mathbf{v} \wedge \mathbf{w} = (-1)^{k\ell} \mathbf{w} \wedge \mathbf{v}$ for $\mathbf{v} \in \Lambda^k V$ and $\mathbf{w} \in \Lambda^\ell V$;
(iii) $1 \wedge \mathbf{v} = \mathbf{v}$ for all $\mathbf{v} \in \Lambda^k V$.

To compute the exterior product we first relate the basis vectors of V to those of $\Lambda^p V$. Let $K = k_1 k_2 \dots k_p$ be an arbitrary p-index, and $\sigma(K)$ a permutation of K. Then we define

$$\mathbf{e}_{k_1} \wedge \dots \wedge \mathbf{e}_{k_p} = \begin{cases} +\mathbf{e}_{\sigma(K)} & \sigma(K) \in \mathscr{J}_p^n, \quad \sigma \text{ even}, \\ -\mathbf{e}_{\sigma(K)} & \sigma(K) \in \mathscr{J}_p^n, \quad \sigma \text{ odd}, \\ 0 & \text{otherwise}. \end{cases} \tag{1}$$

Next we define for basis vectors $\mathbf{e}_I \in \Lambda^k V$, $\mathbf{e}_J \in \Lambda^\ell V$

$$\begin{aligned} \mathbf{e}_I \wedge \mathbf{e}_J &= (\mathbf{e}_{i_1} \wedge \dots \wedge \mathbf{e}_{i_k}) \wedge (\mathbf{e}_{j_1} \wedge \dots \wedge \mathbf{e}_{j_\ell}) \\ &= \mathbf{e}_{i_1} \wedge \dots \wedge \mathbf{e}_{i_k} \wedge \mathbf{e}_{j_1} \wedge \dots \wedge \mathbf{e}_{j_\ell}, \end{aligned}$$

where $I \in \mathscr{J}_k^n$, $J \in \mathscr{J}_\ell^n$. The right hand side is defined by (1), or zero for $k+\ell > n$, respectively. Finally, the exterior product extends by linearity to the entire spaces. We say that $\Lambda^p V$ is the p-th exterior power of V. The direct sum $\Lambda V = \Lambda^0 V \oplus \Lambda^1 V \oplus \cdots \oplus \Lambda^{n-1} V \oplus \Lambda^n V$ is again a vector space. The pair $(\Lambda V, \wedge)$ has the structure of a graded algebra. It is called the *exterior algebra* over V.

Recall that a *tangent vector* on a manifold can be defined as a directional-derivative operator. Coordinates $(x^1, ..., x^n)$ on a patch $U \subset M$ induce a canonical coordinate basis $(\partial_{x^1}, ..., \partial_{x^n})$ of the tangent space $T_X M$. Here TM is the tangent bundle over M, and $T_X M$ is a fibre in a point $X \in U$. *Cotangent vectors*, on the other hand, are elements of the dual space $T_X^* M$, the cotangent space. In particular, the differential of a scalar function λ on M taken at a point X is a cotangent vector. The action of a cotangent vector $(\mathrm{d}\lambda)_X \in T_X^* M$ on a vector $\mathbf{v} \in T_X M$ equals the directional derivative of λ in direction of $\mathbf{v}$, $(\mathrm{d}\lambda)_X(\mathbf{v}) = \mathbf{v}(\lambda)$. The canonical coordinate basis of the cotangent space in a point $X \in U$ reads $(\mathrm{d}x^1, ..., \mathrm{d}x^n)$, and we see that $\mathrm{d}x^i(\partial_{x^j}) = \partial_{x^j}(x^i) = \delta_j^i$, with δ_j^i the Kronecker delta.

A vector field $\mathbf{v}$ is a section of TM. The space of smooth vector fields (component functions are C^∞) is denoted $\mathscr{X}_1(M)$. The space of smooth differential 1-forms is denoted $\mathscr{F}^1(M)$; its elements are smooth sections of the cotangent bundle. Note that the definitions of $\mathscr{X}_1(M)$ and $\mathscr{F}^1(M)$ require smoothness of the manifold M.

A p-vector field is a section of the p-th exterior power of the tangent bundle $\Lambda^p TM$, whose fibres are the spaces $\Lambda^p T_X M$. The space of *smooth p-vector fields* is denoted $\mathscr{X}_p(M)$, and the space of *smooth differential p-forms* $\mathscr{F}^p(M)$.

Coordinate bases of $\mathscr{X}_p(M)$ and $\mathscr{F}^p(M)$ are given in $U \subset M$ by $(\partial_{x^J} \,|\, J \in \mathscr{J}_p^n)$ and $(\mathrm{d}x^J \,|\, J \in \mathscr{J}_p^n)$, respectively. Hence the *basis representation*

$$\omega = \sum_{J \in \mathscr{J}_p^n} \omega_J \, \mathrm{d}x^J \in \mathscr{F}^p(M),$$

where $\omega_J \in C^\infty(M)$ are the component functions.

In the sequel, we will encounter function spaces of differential forms. A generic function space of p-forms defined on M will be denoted $\mathscr{H}\Lambda^p(M)$. For instance, $\mathscr{F}^p(M) = C^\infty \Lambda^p(M)$.

We denote by

$$\langle \cdot \,|\, \cdot \rangle_X : \Lambda^p T_X^* M \times \Lambda^p T_X M \to \mathbb{F}$$

the algebraic *duality product* at a point $X \in M$.

The exterior product above extends naturally to p-forms and p-vector fields. An alternative notation is given by

$$\mathrm{j} : \mathscr{F}^\ell(M) \times \mathscr{F}^k(M) \to \mathscr{F}^{\ell+k}(M) : (\omega, \eta) \mapsto \mathrm{j}_\eta \omega = \eta \wedge \omega,$$

and, analogously,

$$\mathrm{j} : \mathscr{X}_\ell(M) \times \mathscr{X}_k(M) \to \mathscr{X}_{\ell+k}(M) : (\mathbf{v}, \mathbf{w}) \mapsto \mathrm{j}_{\mathbf{w}} \mathbf{v} = \mathbf{w} \wedge \mathbf{v}.$$

The *interior products or contractions*

$$\mathrm{i} : \mathscr{X}_k(M) \times \mathscr{F}^\ell(M) \to \mathscr{F}^{\ell-k}(M) : (\mathbf{v}, \omega) \mapsto \begin{cases} \mathrm{i}_\mathbf{v}\omega, & \text{for} \quad \ell \geq k, \\ 0, & \text{for} \quad \ell < k, \end{cases}$$

and

$$\mathrm{i} : \mathscr{F}^\ell(M) \times \mathscr{X}_k(M) \to \mathscr{X}_{k-\ell}(M) : (\omega, \mathbf{v}) \mapsto \begin{cases} \mathrm{i}_\omega\mathbf{v}, & \text{for} \quad \ell \leq k, \\ 0, & \text{for} \quad \ell > k \end{cases}$$

are defined by dualities

$$\langle \mathrm{i}_\mathbf{v}\omega | \mathbf{w} \rangle_X = \langle \omega | \mathrm{j}_\mathbf{v}\mathbf{w} \rangle_X, \quad \langle \phi | \mathrm{i}_\omega\mathbf{v} \rangle_X = \langle \mathrm{j}_\omega\phi | \mathbf{v} \rangle_X,$$

for all $\mathbf{w} \in \mathscr{X}_{\ell-k}(M)$, $\phi \in \mathscr{F}^{k-\ell}(M)$, and $X \in M$. The use of the notation $\mathrm{i}_\mathbf{v}$, $\mathrm{j}_\mathbf{v}$ as a shorthand for $\mathrm{i}(\mathbf{v}, \cdot)$, $\mathrm{j}(\mathbf{v}, \cdot)$ is a mere matter of convenience.

General properties of interior and exterior products are

(i) $\mathrm{i}_\mathbf{v}\mathrm{i}_\mathbf{w} = (-1)^{ij}\mathrm{i}_\mathbf{w}\mathrm{i}_\mathbf{v}, \quad \mathrm{j}_\mathbf{v}\mathrm{j}_\mathbf{w} = (-1)^{ij}\mathrm{j}_\mathbf{w}\mathrm{j}_\mathbf{v},$
(ii) $\mathrm{i}_\mathbf{u}\mathrm{i}_\mathbf{u} = 0, \quad \mathrm{j}_\mathbf{u}\mathrm{j}_\mathbf{u} = 0,$
(iii) $\mathrm{i}_\mathbf{u}(\omega \wedge \eta) = \mathrm{i}_\mathbf{u}\omega \wedge \eta + (-1)^k \omega \wedge \mathrm{i}_\mathbf{u}\eta,$

where $\mathbf{v} \in \mathscr{X}_i(M)$, $\mathbf{w} \in \mathscr{X}_j(M)$, $\omega \in \mathscr{F}^k(M)$, $\eta \in \mathscr{F}^\ell(M)$, and $\mathbf{u} \in \mathscr{X}_1(M)$. Equivalent dual properties to (i) and (ii) hold for differential forms.

Consider the differential

$$\mathrm{D}\varphi : T_X M \to T_{\varphi(X)} N : \mathbf{w} \mapsto \mathrm{D}\varphi(\mathbf{w})$$

of a smooth map $\varphi : M \to N$ from a manifold M to a manifold N. It naturally extends to p-vectors $\mathbf{v}, \mathbf{w} \in \Lambda^p T_X M$ by the exterior compound

$$\mathrm{D}\varphi(\mathbf{v} \wedge \mathbf{w}) = \mathrm{D}\varphi(\mathbf{v}) \wedge \mathrm{D}\varphi(\mathbf{w}).$$

In case φ is a diffeomorphism, $\mathrm{D}\varphi$ induces a *pushforward operator*

$$\varphi_* : \mathscr{X}_p(M) \to \mathscr{X}_p(N) : \mathbf{v} \mapsto \varphi_*\mathbf{v},$$

by defining $\varphi_*\mathbf{v}_X = \mathrm{D}\varphi(\mathbf{v}_X)$ in all points $X \in M$. The *pullback operator*

$$\varphi^* : \mathscr{F}^p(N) \to \mathscr{F}^p(M) : \omega \mapsto \varphi^*\omega$$

is defined by duality at every point $X \in M$,

$$\langle \varphi^*\omega | \mathbf{v} \rangle_X = \langle \omega | \mathrm{D}\varphi(\mathbf{v}_X) \rangle_{\varphi X},$$

where $\omega \in \mathscr{F}^p(N)$, $\mathbf{v} \in \mathscr{X}_p(M)$. Note that φ is not required to be a diffeomorphism in this case.

The *exterior derivative* is a linear map

$$\mathrm{d} : \mathscr{F}^p(M) \to \mathscr{F}^{p+1}(M) : \omega \mapsto \mathrm{d}\omega$$

defined by the following properties:

(i) For $\gamma \in C^\infty(M)$, $\mathrm{d}\gamma$ is the differential of γ;
(ii) $\mathrm{dd} = 0$, (first Poincaré lemma);
(iii) $\mathrm{d}(\omega \wedge \eta) = \mathrm{d}\omega \wedge \eta + (-1)^p \omega \wedge \mathrm{d}\eta$, for $\omega \in \mathscr{F}^p(M)$.

The exterior derivative commutes with the pullback, i.e., $\mathrm{d}\varphi^* = \varphi^* \mathrm{d}$ holds. Its action on $\mathbf{v} = \mathbf{v}_1 \wedge \ldots \wedge \mathbf{v}_{p+1} \in \Lambda^{p+1} T_X M$ is given by

$$\langle \mathrm{d}\omega | \mathbf{v} \rangle_X = \sum_{i=1}^{p+1} (-1)^{i-1} \langle \nabla_{\mathbf{v}_i} \omega | \mathbf{v}_1 \wedge \ldots \wedge \hat{\mathbf{v}}_i \wedge \ldots \wedge \mathbf{v}_{p+1} \rangle_X ,$$

where $\nabla_{\mathbf{v}_i} \omega$ denotes the directional derivative of ω at X in direction $\mathbf{v}_i$, and $\hat{\mathbf{v}}_i$ is omitted.

Forms in the kernel of d are called *closed forms*, forms in the image of d are called *exact forms*.

The integration of differential p-forms can be reduced to multivariate integration of scalar functions in coordinates. *Stokes' theorem* on an embedded p-dimensional compact submanifold S, $\varphi : S \to M$, reads for $\omega \in \mathscr{F}^{p-1}(M)$

$$\int_{\varphi(S)} \mathrm{d}\omega = \int_{\partial\varphi(S)} \omega,$$

where ∂ is the boundary operator. It shows that the following operator equations are equivalent:

$$\mathrm{dd} = 0 \quad \text{and} \quad \partial\partial = 0.$$

Moreover, with the above properties of the exterior derivative, we find the integration-by-parts rule

$$\int_{\varphi(S)} \mathrm{d}\omega \wedge \eta + (-1)^k \int_{\varphi(S)} \omega \wedge \mathrm{d}\eta = \int_{\partial\varphi(S)} \omega \wedge \eta,$$

for $\omega \in \mathscr{F}^k(M)$, and $\eta \in \mathscr{F}^{p-k-1}(M)$.

An *orientation* of M is given by a consistent orientation of all tangent spaces of M. An orientation of $T_X M$ is given by a fixed ordering of the vectors of a basis. Hence, a non-vanishing n-vector field, called *volume vector-field* $\mathbf{m} \in \mathscr{X}_n(M)$ defines an orientation on M, and $-\mathbf{m}$ represents the opposite orientation. Likewise, a *volume form* $\mu \in \mathscr{F}^n(M)$ with $\langle \mu | \mathbf{m} \rangle_X > 0$ everywhere represents the same orientation of M. Henceforth we require without loss of generality that $\langle \mu | \mathbf{m} \rangle_X = 1$ holds everywhere.

The *Poincaré isomorphism* [15, p. 151] is defined using the above volume form and volume vector-field (remember $q = n - p$)

$$\mathrm{p} : \mathscr{F}^q(M) \to \mathscr{X}_p(M) : \eta \mapsto \mathrm{i}_\eta \mathbf{m}.$$

The inverse is given by

$$\mathrm{p}^{-1} : \mathscr{X}_p(M) \to \mathscr{F}^q(M) : \mathbf{v} \mapsto (-1)^{pq} \mathrm{i}_\mathbf{v} \mu.$$

An important property of the Poincaré isomorphism is

$$\langle \omega | \mathrm{p}\eta \rangle \ \mu = (-1)^{pq} \omega \wedge \eta, \tag{2}$$

where $\omega \in \mathscr{F}^p(M)$, $\eta \in \mathscr{F}^q(M)$, and the point-wise duality product defines a smooth scalar function on M.

We prefer defining the Riemannian metric tensor as a *Riesz isomorphism* between smooth vector fields and 1-forms, $\mathrm{g} : \mathscr{X}_1(M) \to \mathscr{F}^1(M)$. The definition is extended to p-vector fields and p-forms

$$\mathrm{g} : \mathscr{X}_p(M) \to \mathscr{F}^p(M)$$

by the exterior compound, $\mathrm{g}(\mathbf{v} \wedge \mathbf{w}) = \mathrm{g}\mathbf{v} \wedge \mathrm{g}\mathbf{w}$. The Riesz isomorphism defines a point-wise *inner product*

$$\Lambda^p T_X M \times \Lambda^p T_X M \to \mathbb{F} : (\mathbf{v}, \mathbf{w}) \mapsto \langle \mathbf{v}, \mathbf{w} \rangle_X = \langle \mathrm{g}\mathbf{v} | \overline{\mathbf{w}} \rangle_X$$

in a point $X \in M$, and, analogously,

$$\Lambda^p T_X^* M \times \Lambda^p T_X^* M \to \mathbb{F} : (\omega, \eta) \mapsto \langle \omega, \eta \rangle_X = \langle \omega | \mathrm{g}^{-1} \overline{\eta} \rangle_X,$$

where the bar denotes complex conjugation of the component functions in the case $\mathbb{F} = \mathbb{C}$. The metric tensor is required to be smooth in the sense that on all coordinate patches U the functions $g_{ij} : U \to \mathbb{F}$, defined by $X \mapsto \langle \partial_{x^i}, \partial_{x^j} \rangle_X$, are smooth.

The inner products induce the corresponding point-wise *norms* on $\Lambda^p T_X M$ and $\Lambda^p T_X^* M$

$$|\mathbf{v}|_X = \sqrt{\langle \mathbf{v}, \mathbf{v} \rangle_X} \quad \text{and} \quad |\omega|_X = \sqrt{\langle \omega, \omega \rangle_X}.$$

In what follows, duality product $\langle \cdot | \cdot \rangle$, inner product $\langle \cdot, \cdot \rangle$, and norm $|\cdot|$, acting on smooth p-forms and p-vector fields, denote point-wise evaluations that define smooth scalar functions on M.

We select a unit volume form, i.e., $|\mu| = 1$ everywhere. This connects volume form and metric, which would otherwise be unrelated. The *Hodge operator* can then be defined by

$$* : \mathscr{F}^p(M) \to \mathscr{F}^q(M) : \phi \mapsto (-1)^{pq} \mathrm{p}^{-1} \mathrm{g}^{-1} \phi,$$

and we see that $*\phi = \mathrm{i}(\mathrm{g}^{-1}\phi, \mu)$. The Hodge operator is an isomorphism. It fulfills $** = (-1)^{pq}$, and its inverse is given by $*^{-1} = (-1)^{pq} * = (-1)^{pq} \mathrm{g}\,\mathrm{p}$. The standard textbook definition

$$\langle \omega, \overline{\phi} \rangle \ \mu = \omega \wedge *\phi, \tag{3}$$

where $\phi \in \mathscr{F}^p(M)$, can be linked to the explicit definition by setting $\eta = *\phi$ in (2).

Let $\mathscr{D}\Lambda^p(M) \subset \mathscr{F}^p(M)$ denote the space of *test forms*, that are smooth, compactly supported p-forms on $M \setminus \partial M$ [20]. For $\omega, \eta \in \mathscr{D}\Lambda^p(M)$ we define the inner product

$$\langle \omega, \eta \rangle_{L^2(M)} = \int_M \langle \omega, \eta \rangle \, \mu = \int_M \omega \wedge * \overline{\eta},$$

and the norm $|\omega|^2_{L^2(M)} = \langle \omega, \omega \rangle_{L^2(M)}$. Completion of $\mathscr{D}\Lambda^p(M)$ with respect to this norm yields the Hilbert space $L^2\Lambda^p(M)$ of *square integrable p-forms*.

At this point we introduce the *coderivative*[1]

$$\delta : \mathscr{F}^p(M) \to \mathscr{F}^{p-1}(M) : \omega \mapsto \delta\omega = (-1)^p * ^{-1} \mathrm{d} * \omega, \tag{4}$$

and note the property

$$\delta\delta = 0.$$

The coderivative is defined to be the adjoint operator of the exterior derivative in the L^2 inner product,

$$\langle \mathrm{d}\omega, \eta \rangle_{L^2(M)} = \langle \omega, \delta\eta \rangle_{L^2(M)},$$

where the intersection of the support of $\omega \in \mathscr{F}^p(M)$ and $\eta \in \mathscr{F}^{p+1}(M)$ must be compact in $M \setminus \partial M$.

Forms in the kernel of δ are called *coclosed forms*, forms in the image of δ are called *coexact forms*.

Eventually, we define the *Laplace-Beltrami operator*

$$\Delta : \mathscr{F}^p(M) \to \mathscr{F}^p(M) : \omega \mapsto \Delta\omega = (\mathrm{d}\delta + \delta\mathrm{d})\omega. \tag{5}$$

Forms in the kernel of Δ are called *harmonic forms*.

We can now link up with the notation of classical vector analysis. The scalar and vector fields of 3D Euclidean vector analysis are recovered by the translation isomorphisms,

$$\Upsilon^0 : \quad \mathrm{Id}_{\mathscr{F}^0(M)}, \tag{6a}$$

$$\Upsilon^1 : \quad \mathscr{F}^1(M) \to \mathscr{X}_1(M) : \quad \omega \mapsto \mathrm{g}^{-1}\omega, \tag{6b}$$

$$\Upsilon^2 : \quad \mathscr{F}^2(M) \to \mathscr{X}_1(M) : \quad \omega \mapsto \mathrm{p}\omega, \tag{6c}$$

$$\Upsilon^3 : \quad \mathscr{F}^3(M) \to \mathscr{F}^0(M) : \quad \omega \mapsto *\omega. \tag{6d}$$

Note that the usual definition $\Upsilon^2 : \omega \mapsto \mathrm{g}^{-1} * \omega$ coincides with the above definition since for $n = 3$ we find $*^{-1} = * = \mathrm{gp}$ and therefore $\mathrm{g}^{-1} * = \mathrm{p}$.

[1] When comparing with [36] please note that the coderivative is defined there with an additional minus sign.

The differential operators of vector analysis are derived from the exterior derivative by

$$\begin{aligned}\mathbf{grad} &= \Upsilon^1\,\mathrm{d}\,(\Upsilon^0)^{-1},\\ \mathbf{curl} &= \Upsilon^2\,\mathrm{d}\,(\Upsilon^1)^{-1},\\ \mathrm{div} &= \Upsilon^3\,\mathrm{d}\,(\Upsilon^2)^{-1}.\end{aligned}$$

The identities $\mathbf{curl}\,\mathbf{grad} = \mathbf{0}$ and $\mathrm{div}\,\mathbf{curl} = 0$ follow directly from the first Poincaré lemma $\mathrm{dd} = 0$.

Integration of a 1-form $\alpha \in \mathscr{F}^1(M)$ along an oriented curve C that is embedded in M by $\varphi : C \to M$ is related to the integration of the tangential component of a vector:

$$\int\limits_{\varphi(C)} \alpha = \int\limits_{\varphi(C)} \mathbf{a}\cdot\mathbf{t}\,\mathrm{d}s,$$

where $\mathbf{a} = \Upsilon^1\alpha$, $\mathrm{d}s$ is the metric arc-length differential, and $\mathbf{t}$ is the unit tangent vector field to C. We have used the dot-product notation for the inner product.

Similarly,

$$\int\limits_{\varphi(A)} \beta = \int\limits_{\varphi(A)} \mathbf{b}\cdot\mathbf{n}\,\mathrm{d}a,$$

where A is an inner-oriented surface, embedded in M, $\mathbf{b} = \Upsilon^2\beta$, $\mathrm{d}a$ is the metric area differential, and $\mathbf{n}$ is the unit normal vector field to A. If $(\mathbf{v}_1,\mathbf{v}_2)$ defines an orientation of T_XA in $X \in A$, $\mathbf{v}_1,\mathbf{v}_2 \in T_XA$, then $\mathbf{n}_X$ is chosen such that $(D\varphi(\mathbf{v}_1), D\varphi(\mathbf{v}_2), \mathbf{n}_X)$ is consistent with the orientation of T_XM.

Eventually we find

$$\int\limits_{\varphi(V)} \omega = \int\limits_{\varphi(V)} w\,\mathrm{d}v,$$

where $w = \Upsilon^3\omega$, $\mathrm{d}v$ is the metric volume differential, and V is an inner-oriented domain that is embedded in M, $\varphi(V) \subset M$. We note that $\mathrm{d}v = \mu$ in (3).

Stokes' theorem with $\omega \in \mathscr{F}^{p-1}(M)$, and the embedded p-dimensional submanifold S, $\varphi : S \to M$,

$$\int\limits_{\varphi(S)} \mathrm{d}\omega = \int\limits_{\partial\varphi(S)} \omega$$

encompasses the classical theorems for $n = 3$, $p = 1,2,3$,

$$\int\limits_{\varphi(C)} \mathbf{grad}\, f\cdot\mathbf{t}\,\mathrm{d}s = f|_{\partial\varphi(C)}, \qquad \text{fundamental theorem of calculus,}$$

$$\int\limits_{\varphi(A)} \mathbf{curl}\,\mathbf{v}\cdot\mathbf{n}\,\mathrm{d}a = \int\limits_{\partial\varphi(A)} \mathbf{v}\cdot\mathbf{t}\,\mathrm{d}s, \qquad \text{Stokes' theorem,}$$

$$\int_{\varphi(V)} \operatorname{div} \mathbf{w}\, \mathrm{d}v = \int_{\partial\varphi(V)} \mathbf{w}\cdot\mathbf{n}\, \mathrm{d}a, \quad \text{Gauss' theorem.}$$

The coderivative corresponds to classical operators:

$$\begin{aligned}
\Upsilon^2\, \delta\, (\Upsilon^3)^{-1} &= -\mathbf{grad},\\
\Upsilon^1\, \delta\, (\Upsilon^2)^{-1} &= \mathbf{curl},\\
\Upsilon^0\, \delta\, (\Upsilon^1)^{-1} &= -\operatorname{div}.
\end{aligned}$$

Eventually, we recover the scalar and vector Laplace operators from

$$\begin{aligned}
\Upsilon^0\, \Delta\, (\Upsilon^0)^{-1} &= -\operatorname{div}\mathbf{grad} &&= -\Delta_{\mathrm{s}},\\
\Upsilon^1\, \Delta\, (\Upsilon^1)^{-1} &= -\mathbf{grad}\operatorname{div} + \mathbf{curl}\,\mathbf{curl} &&= -\Delta_{\mathrm{v}},\\
\Upsilon^2\, \Delta\, (\Upsilon^2)^{-1} &= \mathbf{curl}\,\mathbf{curl} - \mathbf{grad}\operatorname{div} &&= -\Delta_{\mathrm{v}},\\
\Upsilon^3\, \Delta\, (\Upsilon^3)^{-1} &= -\operatorname{div}\mathbf{grad} &&= -\Delta_{\mathrm{s}},
\end{aligned}$$

where Δ_{s} and Δ_{v} denote the classical scalar and vector Laplace operators, respectively.

2.2 Integral Transformations

Motivated by the notion of electromagnetic fields and sources, we distinguish between the source manifold M and the observation manifold N of an integral transformation. Forms in the domain of the transformation are defined on the source manifold; the image under the transformation is defined on the observation manifold. The transformation kernels are expressed in terms of double forms. In this section, source- and observation manifolds are both modeled by the Euclidean space $M = N = \mathbb{R}^n$, though. The source manifold will be chosen differently in Sect. 2.4, as the boundary of a domain $\Omega \subset M$. At this point we will take full advantage of the differential-form based framework.

The parallel transport of a vector $\mathbf{v} \in T_X M$ from X to X' is denoted by $\Gamma_X^{X'}\mathbf{v} = \mathbf{v}' \in T_{X'}M$. Note that in Euclidean space parallel transport is path independent. Therefore, a vector $\mathbf{v}$ anchored at X can be uniquely extended throughout the entire manifold M. The resulting vector field is called covariantly constant, and the space of covariantly constant vector fields is denoted by $\mathscr{X}_1^{\mathrm{const}}(M)$. The parallel transport $\Gamma_X^{X'}$ carries over naturally to p-vectors and p-covectors, hence $\mathscr{X}_p^{\mathrm{const}}(M)$ and $\mathscr{F}^{\mathrm{const},p}(M)$. These spaces are closed with respect to the Euclidean metric and the Hodge operator in the sense that $\mathscr{F}^{\mathrm{const},p}(M) = \mathrm{g}\big(\mathscr{X}_p^{\mathrm{const}}(M)\big)$ and $\mathscr{F}^{\mathrm{const},q}(M) = *\big(\mathscr{F}^{\mathrm{const},p}(M)\big)$, respectively. Eventually, Cartesian coordinates refer to orthonormal covariantly constant basis fields.

Let $f : M \times M \to \mathbb{F} : (X,X') \mapsto f(X,X')$ denote a scalar kernel function. With the help of this kernel, we define the integral transformation $\mathscr{T}$ for scalar functions σ by

$$\begin{aligned}(\mathscr{T}\sigma)(X') &= \int_M f(X,X')\sigma(X)\,\mu = \int_M f(X,X') * \sigma(X) \\ &= \langle \sigma(X), \overline{f}(X,X') \rangle_{L^2(M)},\end{aligned}$$

provided the integral exists. μ denotes the unit volume form on M. The generalization to p-forms $\omega \in \mathscr{F}^p(M)$ is obtained by requiring that

$$\langle \mathscr{T}\omega | \mathbf{v} \rangle_{X'} = \int_M f(X,X') \langle \omega | \mathbf{v} \rangle_X \,\mu = \int_M f(X,X')\,\omega(X) \wedge *\mathbf{g}\mathbf{v}, \tag{7}$$

for $\mathbf{v} \in \mathscr{X}_p^{\text{const}}(M)$, which amounts to integration by Cartesian components. For the second equality we used (3). Equation (7) provides a preliminary definition for the integral transformation of p-forms. For the definition of layer potentials and boundary integral operators we wish to have an equivalent explicit definition, which is provided next.

At this point it is useful to introduce *double forms*, a concept that goes back to DE RHAM [30, pp. 30-33]. Applications in the context of electromagnetic Green kernels have been reported in [34, 35].

A double form of bi-degree (p,r) over the product manifold $M \times N$ may be regarded for each point in M as a p-covector valued r-form on N, or for each point in N as a r-covector valued p-form on M [34, Sect. 3]. Given a pair of points $(X,X') \in M \times N$ on the source and observation manifold, respectively, a double form evaluates to a tensor product of covectors. The covector in the observation point X' is marked by a prime. In the presence of double forms, we need to distinguish between operators acting on the source and on the observation side of the tensor product. Unary and binary operators acting on the observation side are either evaluated in X' or marked with a prime.

We call double forms of bi-degree (p,p) double p-forms. In electrical engineering literature, the vector proxies of double p-forms are often called dyadics [33].

The *identity double p-form* is defined for $(X,X') \in M \times M$ by

$$\boxed{\langle I_p(X,X') | \Gamma_X^{X'} \mathbf{v} \rangle_{X'} = (\mathbf{g}\,\mathbf{v})_X,} \tag{8}$$

where $\mathbf{v} \in \Lambda^p T_X(M)$. It naturally extends to $\mathbf{v} \in \mathscr{X}_p(M)$.

The *integral transformation of p-forms* $\omega \in \mathscr{F}^p(M)$ is defined by

$$\boxed{(\mathscr{T}\omega)(X') = \langle \omega(X), \overline{f}(X,X') I_p(X,X') \rangle_{L^2(M)}.} \tag{9}$$

The conjugation of f compensates for the conjugation which is inherent to the L^2 inner product. The double p-form $\overline{f}(X,X')I_p(X,X')$ is the extension of the scalar kernel $\overline{f}(X,X')$ to p-forms.

To show that (7) and (9) are equivalent we rewrite (7) with (8),

$$\langle \mathscr{T}\omega|\mathbf{v}\rangle_{X'} = \int_M f(X,X')\omega(X)\wedge *\langle I_p(X,X')|\mathbf{v}\rangle_{X'},$$

where we took into account $\mathbf{v}\in\mathscr{X}_p^{\text{const}}(M)$. By linearity, we obtain (9), and vice versa.

A basis representation of the identity double p-form on a coordinate patch $U\subset M$ is given by

$$I_p(X,X') = \det(g_{JK})\left(\Gamma_X^{X'}\mathrm{d}x^J\right)\otimes \mathrm{d}x^K, \tag{10}$$

where we adopt the summation convention for the multi-indices $J,K\in\mathscr{J}_p^n$. (g_{JK}) denotes the $p\times p$ submatrix of (g_{jk}). Equation (10) can be seen by picking a basis vector $\mathbf{v}=\partial_{x^I}\in\Lambda^p T_X M$, $p>0$, $X\in U\subset M$ in (8). With $I_p(X,X')$ according to (10) we obtain from (8)

$$\langle I_p(X,X')|\Gamma_X^{X'}\partial_{x^I}\rangle_{X'} = \det(g_{JK})\delta_I^J\mathrm{d}x^K = \det(g_{IK})\mathrm{d}x^K = (\mathrm{g}\,\partial_{x^I})_X.$$

By convention, we set $I_0(X,X')=1$, and use I_p and f as shorthands for $I_p(X,X')$ and $f(X,X')$.

In Cartesian coordinates, $n=3$, we obtain the simple expressions

$$\begin{aligned}
I_0 &= 1,\\
I_1 &= \mathrm{d}x'\otimes\mathrm{d}x+\mathrm{d}y'\otimes\mathrm{d}y+\mathrm{d}z'\otimes\mathrm{d}z,\\
I_2 &= \mathrm{d}x'\wedge\mathrm{d}y'\otimes\mathrm{d}x\wedge\mathrm{d}y+\mathrm{d}y'\wedge\mathrm{d}z'\otimes\mathrm{d}y\wedge\mathrm{d}z+\mathrm{d}z'\wedge\mathrm{d}x'\otimes\mathrm{d}z\wedge\mathrm{d}x,\\
I_3 &= \mathrm{d}x'\wedge\mathrm{d}y'\wedge\mathrm{d}z'\otimes\mathrm{d}x\wedge\mathrm{d}y\wedge\mathrm{d}z.
\end{aligned}$$

Lemma 1. *The identity double p-form fulfills the following properties:*

$$*I_p = (*^{-1})'I_q, \tag{11a}$$
$$\mathrm{d}I_p = \mathrm{d}'I_p = 0. \tag{11b}$$

For convolution-type scalar kernels $f(X,X')$, i.e., for scalar kernels $f:M\times M\to\mathbb{F}$ that depend only on the Euclidean distance $d(X,X')$ between X and X' it also holds that

$$\mathrm{d}(fI_p) = \delta'(fI_{p+1}), \tag{11c}$$
$$\delta(fI_p) = \mathrm{d}'(fI_{p-1}), \tag{11d}$$
$$\Delta(fI_p) = \Delta'(fI_p). \tag{11e}$$

We give an example for (i) in Cartesian coordinates, for $n=3$, $p=1$:

$$\begin{aligned}*I_1 &= *(\mathrm{d}x'\otimes\mathrm{d}x+\mathrm{d}y'\otimes\mathrm{d}y+\mathrm{d}z'\otimes\mathrm{d}z)\\ &= \mathrm{d}x'\otimes\mathrm{d}y\wedge\mathrm{d}z+\mathrm{d}y'\otimes\mathrm{d}z\wedge\mathrm{d}x+\mathrm{d}z'\otimes\mathrm{d}x\wedge\mathrm{d}y\\ &= (*^{-1})'(\mathrm{d}y'\wedge\mathrm{d}z'\otimes\mathrm{d}y\wedge\mathrm{d}z+\mathrm{d}z'\wedge\mathrm{d}x'\otimes\mathrm{d}z\wedge\mathrm{d}x+\mathrm{d}x'\wedge\mathrm{d}y'\otimes\mathrm{d}x\wedge\mathrm{d}y)\\ &= (*^{-1})'I_2.\end{aligned}$$

Proof. (i) is shown by observing that for $\mathbf{v}\in\Lambda^pT_XM$

$$\begin{aligned}\langle *I_p|\Gamma_X^{X'}\mathbf{v}\rangle_{X'} &= (*\mathrm{g}\mathbf{v})_X = (-1)^{pq}(\mathrm{g}*\mathbf{v})_X\\ &= (-1)^{pq}\langle I_q|*'\Gamma_X^{X'}\mathbf{v}\rangle_{X'} = (-1)^{pq}\langle *'I_q|\Gamma_X^{X'}\mathbf{v}\rangle_{X'},\end{aligned}$$

where we used (8). The Hodge operator on p-forms is dual to the Hodge operator on p-vectors. More precisely, for a p-vector $\mathbf{v}$ and a q-vector $\mathbf{w}$ we find

$$\langle *\mathrm{g}\mathbf{v}|\mathbf{w}\rangle = \langle \mathrm{g}\mathbf{v}|*\mathbf{w}\rangle = \langle \mathrm{g}*\mathbf{v}|**\mathbf{w}\rangle = (-1)^{pq}\langle \mathrm{g}*\mathbf{v}|\mathbf{w}\rangle,$$

since the Hodge map is an isometry. (ii) holds, because I_p is covariantly constant. This can be seen from the fact that its Cartesian component functions are constant. To show (iii-v), let f denote a convolution-type kernel, so that for fixed (X,X') we find

$$(\mathrm{d}'f)_{X'} = -\Gamma_X^{X'}(\mathrm{d}f)_X. \tag{12}$$

Let $\mathbf{v}\in\Lambda^pT_XM$ and consider

$$\begin{aligned}\langle \mathrm{d}(fI_p)|\Gamma_X^{X'}\mathbf{v}\rangle_{X'} &= (\mathrm{d}f\wedge\mathrm{g}\mathbf{v})_X = \langle I_{p+1}|\Gamma_X^{X'}(\mathrm{g}^{-1}\mathrm{d}f\wedge\mathbf{v})\rangle_{X'}\\ &= -\langle I_{p+1}|(\mathrm{g}^{-1}\mathrm{d})'f\wedge\Gamma_X^{X'}\mathbf{v}\rangle_{X'} = -\langle \mathrm{i}'\big((\mathrm{g}^{-1}\mathrm{d})'f,I_{p+1}\big)|\Gamma_X^{X'}\mathbf{v}\rangle_{X'},\end{aligned}$$

where we used (8), (11b), and (12). Therefore,

$$\begin{aligned}\mathrm{d}(fI_p) &= -\mathrm{i}'\big((\mathrm{g}^{-1}\mathrm{d})'f,I_{p+1}\big) = (-1)^{p+1}(*^{-1})'(\mathrm{d}'f\wedge *'I_{p+1})\\ &= (-1)^{p+1}(*^{-1}\mathrm{d}*)'(fI_{p+1}) = \delta'(fI_{p+1}),\end{aligned}$$

where we took into account (4), (11b), and that for a 1-form $\phi=\mathrm{g}\mathbf{u}$ and p-form ω we have $\mathrm{i}(\mathbf{u},\omega)=(-1)^{p-1}*^{-1}(\phi\wedge*\omega)$. (iv) results from (iii), by exchanging unprimed with primed points, because f and I_p are symmetric in X and X'. Eventually, (v) is a consequence of (iii) and (iv). □

2.3 Fundamental Solution of the Helmholtz Equation

In this section, M is defined in the same way as in Sect. 2.2. That is, source- and observation manifolds are both modeled by the Euclidean space $M=\mathbb{R}^n$.

Let $\delta(X,X')$ denote the n-dimensional Dirac delta distribution of source and observation point. Using this kernel, the transformation (9) reduces to the identity map from source- to observation-manifold, $\mathscr{T}\omega=\mathrm{Id}\,\omega=\omega$, as can be seen from (7).

Moreover, let $g_n(X,X')$ denote the standard *fundamental solution* of convolution type of the scalar Helmholtz equation,

$$(\Delta - k^2) g_n(X,X') = \delta(X,X'). \tag{13}$$

With boundary integral equations in mind, we restrict ourselves to dimension $n \geq 2$. We find, e.g., in [25, Ch. 2.2, 2.3][2], [27, Ch. 8, 9]

$$g_n(X,X') = \begin{cases} \frac{i}{4}\left(\frac{k}{2\pi r}\right)^{(n/2)-1} H^{(1)}_{(n/2)-1}(kr), & 0 \leq \arg k < \pi, k \neq 0, \\ \frac{1}{2\pi} \ln \frac{r_0}{r}, \quad r_0 > 0, & k = 0, n = 2, \\ \frac{1}{(n-2)S_n(1)} r^{2-n}, & k = 0, n \geq 3, \end{cases} \tag{14}$$

where $r = d(X,X')$ is the Euclidean distance between X and X', $H^{(1)}$ denotes the Hankel function of the first kind, and $S_n(1)$ is the Euclidean measure of the unit sphere in n dimensions. For $n = 3$

$$g_3(X,X') = \frac{\exp(ikr)}{4\pi r}, \quad 0 \leq \arg k < \pi.$$

The *Green operator* $\mathscr{G}$ related to the Helmholtz operator $\Delta - k^2$ for p-forms is the integral transformation (9) with the scalar kernel $\overline{f} = \overline{g}_n$. The extension of this kernel to p-forms, the *Green kernel*, is denoted by

$$\boxed{G_p = \overline{g}_n I_p.} \tag{15}$$

Lemma 2. *The following properties of the Green operator and the Green kernel hold:*

(i) The Green operator provides a right inverse of the Helmholtz operator,

$$(\Delta - k^2)\mathscr{G} = \mathrm{Id}. \tag{16}$$

(ii) Locally, the expression takes the form

$$(\Delta - \overline{k}^2) G_p = \delta(X,X') I_p, \tag{17}$$

i.e. G_p is a fundamental solution of the adjoint Helmholtz operator on p-forms.

Proof. We use the notation Δ_p for the Laplace-Beltrami operator in order to emphasize that the operator is acting on p-forms. For flat Euclidean space and Cartesian coordinates we find for multi-indices $J \in \mathscr{J}^n_p$ and by using the summation convention,

$$\Delta_p \omega = (\Delta_0 \omega_J) dx^J.$$

[2] Be aware that in [25] the factor r is missing in the denominator of the first case, and that $\nabla^2 = \Delta_s = -\Delta$, where Δ is the Laplace-Beltrami operator according to (5).

That is, the Laplace-Beltrami operator acting on a p-form can be computed in Cartesian coordinates by applying scalar Laplace-Beltrami operators to its component functions. This is a particular case of the so-called Weitzenböck identities [22]. From this result we can infer that in Euclidean space, for $\mathbf{v} \in \mathscr{X}_p^{\text{const}}(M)$,

$$\Delta_0 \langle \omega | \mathbf{v} \rangle = \langle \Delta_p \omega | \mathbf{v} \rangle. \tag{18}$$

From (7), (13), and (18) we derive

$$\begin{aligned} \langle (\Delta_p - k^2) \mathscr{G} \omega | \mathbf{v} \rangle &= (\Delta_0 - k^2) \langle \mathscr{G} \omega | \mathbf{v} \rangle \\ &= \int_M (\Delta_0 - k^2)' g_n(X, X') \langle \omega | \mathbf{v} \rangle \, \mu \\ &= \int_M \delta(X, X') \langle \omega | \mathbf{v} \rangle \, \mu = \langle \mathrm{Id}\, \omega | \mathbf{v} \rangle, \end{aligned}$$

which proves (i). By using (9), (11e), and (16) we prove (ii):

$$\begin{aligned} \int_M \omega \wedge * \big((\Delta - \overline{k}^2) G_p \big) &= \int_M \omega \wedge * \big((\Delta - \overline{k}^2)' G_p \big) \\ &= (\Delta - \overline{k}^2)' \int_M \omega \wedge * G_p \\ &= (\Delta - \overline{k}^2) \overline{\mathscr{G}} \omega = \mathrm{Id}\, \omega = \int_M \omega \wedge * \delta(X, X') I_p. \end{aligned}$$

□

2.4 Single-Layer and Double-Layer Potentials

In this section Ω denotes a bounded open subset of Euclidean space M with smooth boundary $\partial\Omega$. We shall regard the boundary Γ as a smooth manifold embedded into $\overline{\Omega}$ by $\imath : \Gamma \to \overline{\Omega} : \imath\Gamma = \partial\Omega$. We introduce integral transformations from the boundary Γ to the domain Ω, where Ω plays the role of the observation manifold, and Γ that of the source manifold. The theory is extended to the case of Lipschitz boundaries in subsequent sections.

The *tangential trace* for smooth forms is defined by pullback,

$$\boxed{\mathrm{t} : \mathscr{F}^p(\Omega) \to \mathscr{F}^p(\Gamma) : \omega \mapsto \imath^* \omega,} \tag{19}$$

and the *normal trace* is given by

$$\boxed{\mathrm{n} : \mathscr{F}^p(\Omega) \to \mathscr{F}^{p-1}(\Gamma) : \omega \mapsto *^{-1} \mathrm{t} * \omega.} \tag{20}$$

In contrast to the tangential trace, the normal trace is a metric-dependent concept.

We define the *single- and double-layer potentials* to be the integral transformations from Γ to Ω

$$\boxed{\begin{aligned}\Psi_{\mathrm{SL}} &: \mathscr{F}^p(\Gamma) \to \mathscr{F}^p(\Omega): \quad \omega \mapsto \langle \omega, \mathrm{t} G_p \rangle_{L^2(\Gamma)}, && \text{(21a)}\\ \Psi_{\mathrm{DL}} &: \mathscr{F}^p(\Gamma) \to \mathscr{F}^p(\Omega): \quad \omega \mapsto -*\,\mathrm{d}\,\Psi_{\mathrm{SL}}(*^{-1}\omega). && \text{(21b)}\end{aligned}}$$

Recall that the L^2 inner product in (21a) is p-form valued, because it contains a double p-form as second factor.

Remark 1. An alternative definition of the double-layer potential reads

$$\Psi_{\mathrm{DL}} : \mathscr{F}^p(\Gamma) \to \mathscr{F}^p(\Omega) : \omega \mapsto \delta' \langle \omega, \mathrm{n} G_{p+1} \rangle_{L^2(\Gamma)}.$$

The equivalence can be seen from

$$\begin{aligned}\delta' \langle \omega, \mathrm{n} G_{p+1} \rangle_{L^2(\Gamma)} &= (-1)^{p(q-1)} \delta' \langle \omega, * * \mathrm{n} G_{p+1} \rangle_{L^2(\Gamma)} \\ &= (-1)^{q-1} (\delta *)' \langle *^{-1}\omega, \mathrm{t} G_{q-1} \rangle_{L^2(\Gamma)} \\ &= -(*\mathrm{d})' \langle *^{-1}\omega, \mathrm{t} G_{q-1} \rangle_{L^2(\Gamma)}, \end{aligned} \tag{22}$$

where we used $*\mathrm{n} = \mathrm{t}*$ and (11a), as well as that for p-forms there holds $\delta * = (-1)^{p+1} * \mathrm{d}$.

Lemma 3. *The single- and double-layer potentials exhibit the following properties in Ω:*

$$\begin{aligned}&(i) && \delta \Psi_{\mathrm{SL}} - \Psi_{\mathrm{SL}} \delta = 0, && \text{(23a)}\\ &(ii) && (\Delta - k^2) \Psi_{\mathrm{SL}} = 0, && \text{(23b)}\\ &(iii) && * \Psi_{\mathrm{DL}} = (-1)^{p+1} \mathrm{d}\, \Psi_{\mathrm{SL}} *, && \text{(23c)}\\ &(iv) && \delta \Psi_{\mathrm{DL}} = 0, && \text{(23d)}\\ &(v) && \mathrm{d}\, \Psi_{\mathrm{DL}} - \Psi_{\mathrm{DL}} \mathrm{d} = k^2 *^{-1} \Psi_{\mathrm{SL}} *, && \text{(23e)}\\ &(vi) && * \mathrm{d}\, \Psi_{\mathrm{DL}} = (-1)^p \mathrm{d}\, \Psi_{\mathrm{SL}} * \mathrm{d} + k^2 \Psi_{\mathrm{SL}} *, && \text{(23f)}\\ &(vii) && (\delta \mathrm{d} - k^2) \Psi_{\mathrm{DL}} = 0. && \text{(23g)}\end{aligned}$$

Remark 2.

1. Property (v) shows that the double-layer potential respects the de Rham sequence for $k = 0$.
2. Properties (iii) and (vi) will be used in the proof of the jump relations in Sect. 4.4.

Proof. (i) is shown by

$$\begin{aligned}\delta \Psi_{\mathrm{SL}} \omega &= \delta' \langle \omega, \mathrm{t} G_p \rangle_{L^2(\Gamma)} = \langle \omega, \mathrm{t}\, \mathrm{d} G_{p-1} \rangle_{L^2(\Gamma)} \\ &= \langle \omega, \mathrm{d}\, \mathrm{t} G_{p-1} \rangle_{L^2(\Gamma)} = \langle \delta \omega, \mathrm{t} G_{p-1} \rangle_{L^2(\Gamma)} \\ &= \Psi_{\mathrm{SL}} \delta \omega,\end{aligned}$$

and (ii) is seen from

$$\begin{aligned}(\Delta - k^2)\Psi_{\mathrm{SL}}\omega &= (\Delta - k^2)'\langle \omega, \mathrm{t}G_p\rangle_{L^2(\Gamma)}\\ &= \langle \omega, \mathrm{t}(\Delta - \overline{k}^2)G_p\rangle_{L^2(\Gamma)}\\ &= \langle \omega, \delta(X,X')\,\mathrm{t}I_p\rangle_{L^2(\Gamma)} = 0,\end{aligned}$$

where we used (11c) and (11e). (iii) and (iv) are direct consequences of the definitions (21). (vi) is obtained from combining (iii) and (v). (v) is shown by

$$\begin{aligned}\mathrm{d}\Psi_{\mathrm{DL}} &= -\mathrm{d}*\mathrm{d}\,\Psi_{\mathrm{SL}}*^{-1} = (-1)^{q-1}*\delta\mathrm{d}\,\Psi_{\mathrm{SL}}*^{-1}\\ &= (-1)^{q-1}*\big((\Delta - k^2) - \mathrm{d}\delta + k^2\big)\Psi_{\mathrm{SL}}*^{-1}\\ &= (-1)^{q}*\mathrm{d}\,\Psi_{\mathrm{SL}}\delta*^{-1} + (-1)^{q-1}k^2*\Psi_{\mathrm{SL}}*^{-1}\\ &= -*\mathrm{d}\,\Psi_{\mathrm{SL}}*^{-1}\mathrm{d} + (-1)^{(p+1)(q-1)}k^2*\Psi_{\mathrm{SL}}*\\ &= \Psi_{\mathrm{DL}}\mathrm{d} + k^2*^{-1}\Psi_{\mathrm{SL}}*,\end{aligned}$$

and (vii) is seen from

$$\begin{aligned}\delta\mathrm{d}\,\Psi_{\mathrm{DL}} &= \delta k^2*^{-1}\Psi_{\mathrm{SL}}*\\ &= (-1)^{p+1}k^2*^{-1}\mathrm{d}\,\Psi_{\mathrm{SL}}*\\ &= -k^2*\mathrm{d}\,\Psi_{\mathrm{SL}}*^{-1} = k^2\Psi_{\mathrm{DL}}.\end{aligned}$$

□

3 Sobolev Spaces of Differential Forms

Throughout this section we adopt the following notation. Ω denotes a bounded open subset of a smooth orientable Riemannian manifold M with Lipschitz boundary $\partial\Omega$. We require that Ω is homeomorphic to an open ball. The theory can be extended to the topologically non-trivial case, compare [19], but we do not delve into this. We shall regard the boundary Γ as a Lipschitz manifold embedded into $\overline{\Omega}$ by $\iota : \Gamma \to \overline{\Omega} : \iota\Gamma = \partial\Omega$.

3.1 Sobolev Spaces on the Domain

Let $\mathscr{D}\Lambda^p(\overline{\Omega})$ be the restriction of $\mathscr{D}\Lambda^p(M)$ to Ω, and

$$\mathscr{D}\Lambda^p(\Omega) = \{\phi \in \mathscr{D}\Lambda^p(M) | \operatorname{supp}\phi \subset \Omega\},$$

respectively. The inner product of p-forms on Ω is defined by

$$\langle \omega, \eta\rangle_{L^2(\Omega)} = \int_\Omega \omega \wedge *\overline{\eta},$$

and $|\cdot|_{L^2(\Omega)}$ denotes the corresponding norm. $L^2\Lambda^p(\Omega)$ is the completion of $\mathscr{D}\Lambda^p(\overline{\Omega})$ with respect to this norm. We call $\eta \in L^2\Lambda^{p+1}(\Omega)$ the *weak derivative* of $\omega \in L^2\Lambda^p(\Omega)$ iff

$$\langle \eta, \phi \rangle_{L^2(\Omega)} = \langle \omega, \delta\phi \rangle_{L^2(\Omega)},$$

for all $\phi \in \mathscr{D}\Lambda^{p+1}(\Omega)$. $\pi \in L^2\Lambda^{p-1}(\Omega)$ is called the *weak coderivative* of $\omega \in L^2\Lambda^p(\Omega)$ iff

$$\langle \pi, \psi \rangle_{L^2(\Omega)} = \langle \omega, \mathrm{d}\psi \rangle_{L^2(\Omega)},$$

for all $\psi \in \mathscr{D}\Lambda^{p-1}(\Omega)$. We can now define *Sobolev spaces of differential p-forms on* Ω. Let

$$H\Lambda^p(\Omega) = L^2\Lambda^p(\Omega).$$

Define

$$\boxed{H\Lambda^p(\mathrm{d},\Omega) = \{\omega \in H\Lambda^p(\Omega) \,|\, \mathrm{d}\omega \in H\Lambda^{p+1}(\Omega)\},}$$

where d has to be understood in the weak sense.

We denote by

$$|\omega|_{H\Lambda^p(\mathrm{d},\Omega)} = |\omega|_{L^2(\Omega)} + |\mathrm{d}\omega|_{L^2(\Omega)}$$

the graph norm associated with $H\Lambda^p(\mathrm{d},\Omega)$. The following sequence is exact [2, (2.6)][3]

$$\cdots \xrightarrow{\mathrm{d}} H\Lambda^p(\mathrm{d},\Omega) \xrightarrow{\mathrm{d}} H\Lambda^{p+1}(\mathrm{d},\Omega) \xrightarrow{\mathrm{d}} \cdots \quad . \tag{24}$$

The notations are to be read as follows: The Sobolev space $H^k\Lambda^p(\Omega)$ contains p-forms over Ω that have component functions in $H^k(\Omega)$, $k \geq 0$. For $H^k\Lambda^p(\mathrm{D},\Omega)$, the forms, as well as the derivation D of the forms in the weak sense, are in the respective $H^k\Lambda^p(\Omega)$ space. For $k = 0$, the index is omitted.

The Hodge star operator naturally extends to $L^2\Lambda^p(\Omega)$ and we define the image spaces

$$H\Lambda^p(\delta,\Omega) = *H\Lambda^q(\mathrm{d},\Omega),$$

with the norm

$$|\omega|_{H\Lambda^p(\delta,\Omega)} = |*\omega|_{H\Lambda^q(\mathrm{d},\Omega)}.$$

It is easy to see that these spaces are characterized by

$$\boxed{H\Lambda^p(\delta,\Omega) = \{\omega \in H\Lambda^p(\Omega) \,|\, \delta\omega \in H\Lambda^{p-1}(\Omega)\},}$$

where δ has to be understood in the weak sense. The sequence of these Sobolev spaces is, again, exact,

$$\cdots \xrightarrow{\delta} H\Lambda^p(\delta,\Omega) \xrightarrow{\delta} H\Lambda^{p-1}(\delta,\Omega) \xrightarrow{\delta} \cdots \quad .$$

Note that the maps

$$\boxed{\begin{aligned} *&: H\Lambda^p(\mathrm{d},\Omega) \to H\Lambda^q(\delta,\Omega),\\ *&: H\Lambda^p(\delta,\Omega) \to H\Lambda^q(\mathrm{d},\Omega) \end{aligned}}$$

are isometric isomorphisms.

Eventually, for use in Sect. 4, we introduce the space

$$H\Lambda^p(\delta\mathrm{d},\Omega) = \{\omega \in H\Lambda^p(\mathrm{d},\Omega) \,|\, \delta\mathrm{d}\omega \in H\Lambda^p(\Omega)\},$$

equipped with the graph norm, as well as the subspaces of closed and coclosed p-forms,

$$\begin{aligned} H\Lambda^p(\mathrm{d}0,\Omega) &= \{\omega \in H\Lambda^p(\mathrm{d},\Omega) | \mathrm{d}\omega = 0\} \subset H\Lambda^p(\mathrm{d},\Omega),\\ H\Lambda^p(\delta 0,\Omega) &= \{\omega \in H\Lambda^p(\delta,\Omega) | \delta\omega = 0\} \subset H\Lambda^p(\delta,\Omega),\\ H\Lambda^p(\delta\mathrm{d}0,\Omega) &= \{\omega \in H\Lambda^p(\delta\mathrm{d},\Omega) | \delta\mathrm{d}\omega = 0\} \subset H\Lambda^p(\delta\mathrm{d},\Omega). \end{aligned}$$

For $n = 3$, $p = 0,\ldots,n$, $H\Lambda^p(\mathrm{d},\Omega)$ encompasses a number of well-known spaces,

$$\begin{aligned} H^1(\Omega) &= \Upsilon^0 H\Lambda^0(\mathrm{d},\Omega),\\ \mathbf{H}(\mathbf{curl},\Omega) &= \Upsilon^1 H\Lambda^1(\mathrm{d},\Omega),\\ \mathbf{H}(\mathrm{div},\Omega) &= \Upsilon^2 H\Lambda^2(\mathrm{d},\Omega),\\ L^2(\Omega) &= \Upsilon^3 H\Lambda^3(\mathrm{d},\Omega). \end{aligned}$$

Note that the translation isomorphisms (6) naturally extend to the Sobolev space setting. We can therefore redefine the differential operators of classical vector analysis

$$\begin{aligned} \mathbf{grad} &= \Upsilon^1\, \mathrm{d}\, (\Upsilon^0)^{-1} : H^1(\Omega) \to \mathbf{H}(\mathbf{curl},\Omega),\\ \mathbf{curl} &= \Upsilon^2\, \mathrm{d}\, (\Upsilon^1)^{-1} : \mathbf{H}(\mathbf{curl},\Omega) \to \mathbf{H}(\mathrm{div},\Omega),\\ \mathrm{div} &= \Upsilon^3\, \mathrm{d}\, (\Upsilon^2)^{-1} : \mathbf{H}(\mathrm{div},\Omega) \to L^2(\Omega). \end{aligned}$$

The sequence (24) translates to

$$H^1(\Omega) \xrightarrow{\mathbf{grad}} \mathbf{H}(\mathbf{curl},\Omega) \xrightarrow{\mathbf{curl}} \mathbf{H}(\mathrm{div},\Omega) \xrightarrow{\mathrm{div}} L^2(\Omega)\cdot$$

In the next section we will proceed to introduce traces of the above Sobolev spaces. In the argument we will need $H^1\Lambda^p(\Omega)$, the space of p-forms ω with component functions ω_I in $H^1(\Omega)$,

$$H^1\Lambda^p(\Omega) = \{\omega \in L^2\Lambda^p(\Omega) \,|\, \omega_I \in H^1(\Omega), I \in \mathscr{J}_p^n\}.$$

Different coordinates on Ω are related by smooth transition maps, so that this definition is independent from their choice, and the norms

$$|\omega|^2_{H^1\Lambda^p(\Omega)} = \sum_{I\in\mathscr{J}_p^n} |\omega_I|^2_{H^1(\Omega)}$$

are equivalent. Note that $H\Lambda^0(\mathrm{d},\Omega) = H^1\Lambda^0(\Omega)$. Moreover, we will encounter

$$H^1\Lambda^p(\mathrm{d},\Omega) = \{\omega \in H^1\Lambda^p(\Omega)\,|\,\mathrm{d}\omega \in H^1\Lambda^{p+1}(\Omega)\},$$

and

$$H^1\Lambda^p(\delta,\Omega) = \{\omega \in H^1\Lambda^p(\Omega)\,|\,\delta\omega \in H^1\Lambda^{p-1}(\Omega)\},$$

equipped with their respective graph norms.

3.2 Sobolev Spaces on the Boundary

The Lipschitz manifold Γ has well-defined tangent spaces almost everywhere. Their orientation is chosen to be consistent with the orientation of Ω. The induced Riemannian metric allows for the definition of a Hodge operator, which maps p-forms to $(q-1)$-forms. It is shown in [36, Remark 1] that the $L^2\Lambda^p(\Gamma)$ spaces are well defined, with the inner product

$$\langle\omega,\eta\rangle_{L^2(\Gamma)} = \int_\Gamma \omega\wedge *\overline{\eta}$$

for $\omega,\eta \in L^2\Lambda^p(\Gamma)$. Let $\hat{\omega} = \mathrm{t}\,\omega$ denote the tangential trace according to (19). It is shown in [36, Sect. 2] that the tangential trace can be extended to $H^1\Lambda^p(\Omega)$. This extension may be defined even in the case of a Lipschitz boundary. We then define

$$\boxed{H_\parallel^{1/2}\Lambda^p(\Gamma) = \mathrm{t}\,H^1\Lambda^p(\Omega)}$$

equipped with the norm

$$|\hat{\omega}|_{H_\parallel^{1/2}\Lambda^p(\Gamma)} = \inf_{\hat{\omega}=\mathrm{t}\,\omega}\{|\omega|_{H^1\Lambda^p(\Omega)}\}.$$

The infimum is taken over all $\omega \in H^1\Lambda^p(\Omega)$ satisfying $\hat{\omega} = \mathrm{t}\,\omega$. Denote $H_\parallel^{-1/2}\Lambda^p(\Gamma)$ the topological dual of $H_\parallel^{1/2}\Lambda^p(\Gamma)$, with $L^2\Lambda^p(\Gamma)$ as pivot space.

It is shown in [36, Lemma 5] that the Hodge operator $*$ may be restricted to $H_\parallel^{1/2}\Lambda^p(\Gamma)$ and extended by continuity to $H_\parallel^{-1/2}\Lambda^p(\Gamma)$. This allows us to define the image spaces

$$\boxed{H_\perp^{\pm1/2}\Lambda^p(\Gamma) = *H_\parallel^{\pm1/2}\Lambda^{q-1}(\Gamma),}$$

with the norm

$$|\hat{\omega}|_{H_{\perp}^{1/2}\Lambda^p(\Gamma)} = |*\,\hat{\omega}|_{H_{\parallel}^{1/2}\Lambda^{q-1}(\Gamma)}.$$

Note that the maps

$$\boxed{\begin{aligned} &*: H_{\parallel}^{\pm 1/2}\Lambda^p(\Gamma) \to H_{\perp}^{\pm 1/2}\Lambda^{q-1}(\Gamma), \\ &*: H_{\perp}^{\pm 1/2}\Lambda^p(\Gamma) \to H_{\parallel}^{\pm 1/2}\Lambda^{q-1}(\Gamma) \end{aligned}}$$

are isometric isomorphisms, and the following inclusions hold [36, Thm. 2],

$$\begin{aligned} H_{\parallel}^{1/2}\Lambda^p(\Gamma) \subset L^2\Lambda^p(\Gamma) \subset H_{\parallel}^{-1/2}\Lambda^p(\Gamma), \\ H_{\perp}^{1/2}\Lambda^p(\Gamma) \subset L^2\Lambda^p(\Gamma) \subset H_{\perp}^{-1/2}\Lambda^p(\Gamma). \end{aligned}$$

Remark 3.

1. For smooth boundaries, the spaces $H_{\parallel}^{1/2}\Lambda^p(\Gamma)$ and $H_{\perp}^{1/2}\Lambda^p(\Gamma)$ are identical.
2. A fully intrinsic characterization of the spaces $H_{\parallel}^{1/2}\Lambda^p(\Gamma)$ and $H_{\perp}^{1/2}\Lambda^p(\Gamma)$ is available in the case of polyhedral domains for $n = 3$, $p = 1$. This has been shown in [8, 9]. In this case, the boundary consists of a finite number of smooth faces, and on each face the space $H_{\parallel}^{1/2}\Lambda^1(\Gamma)$ coincides with

$$H^{1/2}\Lambda^1(\Gamma) = \{\hat{\omega} \in L^2\Lambda^1(\Gamma) \,|\, \hat{\omega}_I \in H^{1/2}(\Gamma), I \in \mathscr{J}_1^{n-1}\}.$$

   The faces meet in edges, where forms in $H_{\parallel}^{1/2}\Lambda^1(\Gamma)$ exhibit a weak tangential and forms in $H_{\perp}^{1/2}\Lambda^1(\Gamma)$ a weak normal continuity (related to boundedness of the functionals $\mathscr{N}_{ij}^{\parallel}$ and $\mathscr{N}_{ij}^{\perp}$ defined in [8, Prop. 4.3.]).

Since $H^1\Lambda^p(\mathrm{d},\Omega)$ is a subspace of $H^1\Lambda^p(\Omega)$, the space $Y = *\,\mathrm{t}H^1\Lambda^{q-2}(\mathrm{d},\Omega)$ is a well defined subspace of $H_{\perp}^{1/2}\Lambda^{p+1}(\Gamma)$, and we equip it with the norm

$$|\hat{\omega}|_Y = \inf_{\hat{\omega}=*\,\mathrm{t}\,\omega} \{|\omega|_{H^1\Lambda^{q-2}(\mathrm{d},\Omega)}\}.$$

The infimum is taken over all $\omega \in H^1\Lambda^{q-2}(\mathrm{d},\Omega)$ satisfying $\hat{\omega} = *\,\mathrm{t}\,\omega$. We are now in the position to define the exterior derivative on the boundary in the weak sense

$$\mathrm{d}: H_{\perp}^{-1/2}\Lambda^p(\Gamma) \to Y' : \hat{\omega} \mapsto \mathrm{d}\,\hat{\omega}$$

by [36, Lemma 3]

$$\begin{aligned} \langle \mathrm{d}\,\hat{\omega} | \hat{\eta} \rangle_Y &= (-1)^p \langle \hat{\omega}, *^{-1}\,\mathrm{t}\,\mathrm{d}\,\eta \rangle_{H_{\perp}^{1/2}\Lambda^p(\Gamma)}, \\ \eta \in H^1\Lambda^{q-2}(\mathrm{d},\Omega), &\quad \hat{\eta} = *\,\mathrm{t}\,\eta \in Y. \end{aligned} \tag{25}$$

The duality pairing between Y' and Y is denoted by $\langle\cdot|\cdot\rangle_Y$, and between $H_\perp^{\mp 1/2}\Lambda^p(\Gamma)$ by $\langle\cdot|\cdot\rangle_{H_\perp^{1/2}\Lambda^p(\Gamma)}$, respectively. Note that $H_\perp^{-1/2}\Lambda^{p+1}(\Gamma)$ is a subspace of Y'. This motivates the definition

$$\boxed{H_\perp^{-1/2}\Lambda^p(\mathrm{d},\Gamma) = \{\hat{\omega} \in H_\perp^{-1/2}\Lambda^p(\Gamma) \,|\, \mathrm{d}\,\hat{\omega} \in H_\perp^{-1/2}\Lambda^{p+1}(\Gamma)\},}$$

equipped with the graph norm.

We may now restrict the definition of the exterior derivative to

$$\mathrm{d} : H_\perp^{-1/2}\Lambda^p(\mathrm{d},\Gamma) \to H_\perp^{-1/2}\Lambda^{p+1}(\Gamma) : \hat{\omega} \mapsto \mathrm{d}\,\hat{\omega}.$$

From (25) we infer that $\mathrm{d}\,\mathrm{d} = 0$, so that the image of d lies even in the smaller space $H_\perp^{-1/2}\Lambda^{p+1}(\mathrm{d},\Gamma)$, and we can refine the definition to read

$$\boxed{\mathrm{d} : H_\perp^{-1/2}\Lambda^p(\mathrm{d},\Gamma) \to H_\perp^{-1/2}\Lambda^{p+1}(\mathrm{d},\Gamma) : \hat{\omega} \mapsto \mathrm{d}\,\hat{\omega}.}$$

This final definition lends itself to the definition of the de Rham complex on Γ.

It is shown in [36, Thm. 3] that the extension of the tangential trace t from $H^1\Lambda^p(\Omega)$ to

$$\boxed{\mathrm{t} : H\Lambda^p(\mathrm{d},\Omega) \to H_\perp^{-1/2}\Lambda^p(\mathrm{d},\Gamma)}$$

is well defined, linear and continuous. Moreover [36, Thm. 4], it is surjective and hence admits a continuous right inverse t^{-1}. The latter may be chosen such that its image lies in $H^1\Lambda^p(\mathrm{d},\Omega)$. The definitions and properties of d and t that we gave so far are summarized by the following exact sequence diagram: [3]

$$\begin{array}{ccccccc}
\cdots & \xrightarrow{\mathrm{d}} & H\Lambda^p(\mathrm{d},\Omega) & \xrightarrow{\mathrm{d}} & H\Lambda^{p+1}(\mathrm{d},\Omega) & \xrightarrow{\mathrm{d}} & \cdots \\
 & & \downarrow{\scriptstyle \mathrm{t}} & & \downarrow{\scriptstyle \mathrm{t}} & & \\
\cdots & \xrightarrow{\mathrm{d}} & H_\perp^{-1/2}\Lambda^p(\mathrm{d},\Gamma) & \xrightarrow{\mathrm{d}} & H_\perp^{-1/2}\Lambda^{p+1}(\mathrm{d},\Gamma) & \xrightarrow{\mathrm{d}} & \cdots
\end{array} \tag{26}$$

Remark 4.

1. The diagram (26) commutes, which can be proven by density arguments [36, Remark 2],
$$\mathrm{td} = \mathrm{dt}. \tag{27}$$
2. From the standard trace theorem for scalar functions in $H^1(\Omega)$ we conclude that $H_\perp^{-1/2}\Lambda^0(\mathrm{d},\Gamma) = H^{1/2}(\Gamma) = H_\parallel^{1/2}\Lambda^0(\Gamma)$.

[3] Since Ω was required to be homeomorphic to an open ball, the sequences are exact, up to one-dimensional cohomology groups $\mathscr{H}^0(\Omega)$, $\mathscr{H}^0(\Gamma)$, and $\mathscr{H}^{n-1}(\Gamma)$.

There is an L^2-adjoint version of the diagram (26). To obtain it, define the spaces

$$H_{\|}^{-1/2}\Lambda^p(\delta,\Gamma) = *H_{\perp}^{-1/2}\Lambda^{q-1}(\mathrm{d},\Gamma),$$

that are characterized by

$$\boxed{H_{\|}^{-1/2}\Lambda^p(\delta,\Gamma) = \{\hat{\omega} \in H_{\|}^{-1/2}\Lambda^p(\Gamma) \,|\, \delta\,\hat{\omega} \in H_{\|}^{-1/2}\Lambda^{p-1}(\Gamma)\},}$$

where $\delta = (-1)^p *^{-1} \mathrm{d} *$ is the coderivative on p-forms. The norm is given by

$$|\hat{\omega}|_{H_{\|}^{-1/2}\Lambda^p(\delta,\Gamma)} = |*\,\hat{\omega}|_{H_{\perp}^{-1/2}\Lambda^{q-1}(\mathrm{d},\Gamma)}.$$

Finally, we extend the definition of the normal trace for smooth forms in (20) by

$$\boxed{\mathrm{n} : H\Lambda^p(\delta,\Omega) \to H_{\|}^{-1/2}\Lambda^{p-1}(\delta,\Gamma) : \omega \mapsto \hat{\omega} = *^{-1}\mathrm{t} * \omega,} \tag{28}$$

which inherits its properties from the tangential trace map [36, Thm. 7]. It is well defined, linear, surjective, and admits a right inverse n^{-1} the image of which lies in $H^1\Lambda^p(\delta,\Omega)$.

With these definitions we obtain the L^2-adjoint version of the diagram (26), that is again an exact sequence:

$$\begin{array}{ccccccc}
\cdots & \xrightarrow{\delta} & H\Lambda^p(\delta,\Omega) & \xrightarrow{\delta} & H\Lambda^{p-1}(\delta,\Omega) & \xrightarrow{\delta} & \cdots \\
 & & \mathrm{n}\downarrow & & -\mathrm{n}\downarrow & & \\
\cdots & \xrightarrow{\delta} & H_{\|}^{-1/2}\Lambda^{p-1}(\delta,\Gamma) & \xrightarrow{\delta} & H_{\|}^{-1/2}\Lambda^{p-2}(\delta,\Gamma) & \xrightarrow{\delta} & \cdots
\end{array} \tag{29}$$

Remark 5.

1. The diagram (29) commutes, since from (4), (27) and (28)
$$\mathrm{n}\delta = -\delta\mathrm{n}. \tag{30}$$
2. From the definitions it follows that $H_{\|}^{-1/2}\Lambda^0(\delta,\Gamma) = H_{\|}^{-1/2}\Lambda^0(\Gamma) = H^{-1/2}(\Gamma)$.
3. Up to sign, the diagram (29) can be thought of as the image of the diagram (26) under Hodge star operators.
4. There exists a Hodge decomposition [36, Thm. 11] of the spaces $H_{\perp}^{-1/2}\Lambda^p(\mathrm{d},\Gamma)$ and $H_{\|}^{-1/2}\Lambda^p(\delta,\Gamma)$, respectively, which generalizes the results obtained in [4, 9].

It has been shown in [36, Thm. 8] that the L^2 inner product on the boundary Γ can be extended to a *sesquilinear form*

$$b(\cdot,\cdot) : H_{\|}^{-1/2}\Lambda^p(\delta,\Gamma) \times H_{\perp}^{-1/2}\Lambda^p(\mathrm{d},\Gamma) \to \mathbb{F}.$$

For $(\omega,\eta)\in H\Lambda^{p+1}(\delta,\Omega)\times H\Lambda^{p}(\mathrm{d},\Omega)$ the integration by parts formula

$$b(\mathrm{n}\omega,\mathrm{t}\eta)=\langle\omega,\mathrm{d}\eta\rangle_{L^2(\Omega)}-\langle\delta\omega,\eta\rangle_{L^2(\Omega)} \tag{31}$$

holds. In fact, in the light of the surjectivity of the traces and the existence of suitable right inverses, (31) provides the definition of $b(\cdot,\cdot)$. A comparison with (52) confirms that $b(\mathrm{n}\omega,\mathrm{t}\eta)$ reduces to $\langle\mathrm{n}\omega,\mathrm{t}\eta\rangle_{L^2(\Gamma)}$ in the smooth case.

Let us now relate the results (26) and (29) to the language of classical vector analysis in $n=3$ dimensions. We denote the outer normal to Ω by $\mathbf{n}$, defined almost everywhere on $\partial\Omega$. Note that classical calculus defines the traces on $\partial\Omega=\imath\Gamma$, whereas with differential-forms we defined them on Γ by pullback. According to the definitions in [5, 11], we have to consider the following trace spaces and operators,

$$\begin{aligned}
\gamma:&\quad H^1(\Omega) &&\to H^{1/2}(\partial\Omega): && u\mapsto u\big|_{\partial\Omega},\\
\gamma_n:&\quad \mathbf{H}(\mathrm{div},\Omega) &&\to H^{-1/2}(\partial\Omega): && \mathbf{u}\mapsto \mathbf{u}\cdot\mathbf{n}\big|_{\partial\Omega},\\
\gamma_\tau:&\quad \mathbf{H}(\mathbf{curl},\Omega) &&\to \mathbf{H}^{-1/2}(\mathrm{div}_\Gamma,\partial\Omega): && \mathbf{u}\mapsto \mathbf{u}\times\mathbf{n}\big|_{\partial\Omega},\\
\pi_\tau:&\quad \mathbf{H}(\mathbf{curl},\Omega) &&\to \mathbf{H}^{-1/2}(\mathrm{curl}_\Gamma,\partial\Omega): && \mathbf{u}\mapsto \mathbf{u}-\gamma_n(\mathbf{u})\mathbf{n}\big|_{\partial\Omega}.
\end{aligned}$$

All trace operators are defined for smooth test functions in the first place and then extended to the respective function spaces. They are all well defined, linear, continuous, surjective, and admit continuous right inverses. Be aware that in [5, Def. 1] we find $\gamma_\tau:\mathbf{u}\mapsto\mathbf{n}\times\mathbf{u}\big|_{\partial\Omega}$, while in [11, Def. 2.1], [18, Def. $\gamma_{\mathbf{t}}^{\times}$], [19, Def. $\gamma_\times$] we have $\gamma_\tau:\mathbf{u}\mapsto\mathbf{u}\times\mathbf{n}\big|_{\partial\Omega}$. We follow the latter definition.
We define translation isomorphisms on the boundary,

$$\hat{\Upsilon}^0:\quad H_\perp^{-1/2}\Lambda^0(\mathrm{d},\Gamma)\to H^{1/2}(\partial\Omega): \qquad \omega\mapsto\quad \gamma\mathrm{t}^{-1}\,\omega, \tag{32a}$$

$$\hat{\Upsilon}^1:\quad H_\perp^{-1/2}\Lambda^1(\mathrm{d},\Gamma)\to \mathbf{H}^{-1/2}(\mathrm{curl}_\Gamma,\partial\Omega): \qquad \omega\mapsto\quad \pi_\tau\Upsilon^1\mathrm{t}^{-1}\,\omega, \tag{32b}$$

$$\hat{\Upsilon}^{\tilde{1}}:\quad H_\perp^{-1/2}\Lambda^1(\mathrm{d},\Gamma)\to \mathbf{H}^{-1/2}(\mathrm{div}_\Gamma,\partial\Omega): \qquad \omega\mapsto -\gamma_\tau\Upsilon^1\mathrm{t}^{-1}\,\omega, \tag{32c}$$

$$\hat{\Upsilon}^2:\quad H_\perp^{-1/2}\Lambda^2(\mathrm{d},\Gamma)\to H^{-1/2}(\partial\Omega): \qquad \omega\mapsto\quad \gamma_n\Upsilon^2\mathrm{t}^{-1}\,\omega. \tag{32d}$$

Remark 6. The translation isomorphisms are extensions of the following maps, which are valid for smooth forms and smooth boundaries: $\hat{\Upsilon}^0:\omega\mapsto\imath_*\omega$, $\hat{\Upsilon}^1:\omega\mapsto\imath_*\mathrm{g}^{-1}\omega$, $\hat{\Upsilon}^{\tilde{1}}=\hat{\Upsilon}^1*:\omega\mapsto\imath_*\mathrm{p}\,\omega$, $\hat{\Upsilon}^2:\omega\mapsto\imath_**\omega$. These translation isomorphisms coincide with the definitions in [3] and [17, p. 246].

We are now in the position to define the surface differential operators of vector analysis on Γ, in terms of the exterior derivative d,

$$\begin{aligned}
\mathbf{grad}_\Gamma=&\quad \hat{\Upsilon}^1\,\mathrm{d}\,(\hat{\Upsilon}^0)^{-1}:H^{1/2}(\partial\Omega) &&\to\mathbf{H}^{-1/2}(\mathrm{curl}_\Gamma,\partial\Omega),\\
\mathrm{curl}_\Gamma=&\quad \hat{\Upsilon}^2\,\mathrm{d}\,(\hat{\Upsilon}^1)^{-1}:\mathbf{H}^{-1/2}(\mathrm{curl}_\Gamma,\partial\Omega)&&\to H^{-1/2}(\partial\Omega),
\end{aligned}$$

$$\begin{aligned}\mathbf{curl}_\Gamma &= -\hat{\Upsilon}^{\tilde{1}}\,\mathrm{d}\,(\hat{\Upsilon}^0)^{-1} : H^{1/2}(\partial\Omega) &&\to \mathbf{H}^{-1/2}(\mathrm{div}_\Gamma,\partial\Omega),\\ \mathrm{div}_\Gamma &= -\hat{\Upsilon}^2\,\mathrm{d}\,(\hat{\Upsilon}^{\tilde{1}})^{-1} : \mathbf{H}^{-1/2}(\mathrm{div}_\Gamma,\partial\Omega) &&\to H^{-1/2}(\partial\Omega).\end{aligned}$$

From the general theory we know that the following sequences are exact, provided the boundary Γ is homeomorphic to a sphere:

$$\begin{array}{ccccc} H^{1/2}(\partial\Omega) & \xrightarrow{\mathbf{grad}_\Gamma} & \mathbf{H}^{-1/2}(\mathrm{curl}_\Gamma,\partial\Omega) & \xrightarrow{\mathrm{curl}_\Gamma} & H_*^{-1/2}(\partial\Omega) \\ \| & & \downarrow -\mathsf{R} & & \| \\ H^{1/2}(\partial\Omega) & \xrightarrow{\mathbf{curl}_\Gamma} & \mathbf{H}^{-1/2}(\mathrm{div}_\Gamma,\partial\Omega) & \xrightarrow{\mathrm{div}_\Gamma} & H_*^{-1/2}(\partial\Omega) \end{array}$$

We used $H_*^{-1/2}(\partial\Omega) = \{u \in H^{-1/2}(\partial\Omega)\,|\,\langle u|1\rangle_{H^{1/2}(\partial\Omega)} = 0\}$ to eliminate the cohomology group $\mathscr{H}^2(\partial\Omega)$. $\langle\cdot|\cdot\rangle_{H^{1/2}(\partial\Omega)}$ denotes the duality pairing between the $H^{\mp 1/2}(\partial\Omega)$ spaces. The rotation operator

$$\mathsf{R} : \mathbf{H}^{-1/2}(\mathrm{curl}_\Gamma,\partial\Omega) \to \mathbf{H}^{-1/2}(\mathrm{div}_\Gamma,\partial\Omega) : \gamma_\tau = -\mathsf{R}\,\pi_\tau \tag{33}$$

renders the diagram commutative. Note that $\mathsf{R}\,\hat{\Upsilon}^1 = \hat{\Upsilon}^{\tilde{1}}$. The rotation operator extends the vectorial operator $\mathbf{n}\times\cdot$, compare [11, Def. *r*], [18, Def. *R*]. In [19], however, we find $\mathsf{R} = -\mathbf{n}\times\cdot$.

4 Representation Formula

The goal of this section is to collect, unify, and generalize existing knowledge about scalar and vectorial representation formulae in electromagnetics. We refer to the definition of Ω in Sect. 3, where we now consider the Euclidean space $M = \mathbb{R}^n$ with $n \geq 2$. We denote by Ω^{c} the complement of $\overline{\Omega}$ in M, such that $\partial\Omega = -\partial\Omega^{\mathrm{c}}$, and $\Omega \cup \partial\Omega \cup \Omega^{\mathrm{c}} = M$. On Ω^{c} we denote $L^2_{\mathrm{loc}}\Lambda^p(\Omega^{\mathrm{c}})$ the space of p-forms that are square-integrable on each compact subdomain of Ω^{c}, and define the derived Sobolev spaces accordingly.

In Sect. 4.1 we introduce Maxwell-type problems and the space of solutions thereof. Sect. 4.2 proceeds to define radiation and decay conditions. In Sect. 4.3 we prove the status of a representation formula that represents elements of the solution space in terms of integral transformations of their boundary data. Sect. 4.4 proves the so-called jump relations of the respective terms of the representation formula. The properties and proofs carry over to classical calculus by means of the translation isomorphisms (6) and (32).

4.1 Maxwell-Type Problems, Solution Spaces, and Trace Operators

We call *Maxwell-type equation* the second-order equation

$$\boxed{(\delta \mathrm{d} - k^2)\omega = 0 \quad \text{in} \quad \Omega \cup \Omega^{\mathrm{c}},} \tag{34}$$

compare Fig. 1, for a p-form ω, $0 \le p < n$. We require that the constant $k \in \mathbb{C}$ fulfills either $k = 0$ or $0 \le \arg k < \pi, k \neq 0$.

We could have chosen the Helmholtz-type equation $(\delta \mathrm{d} + \mathrm{d}\delta - k^2)\omega = 0$ as starting point as well. Since we will work with the gauge condition

$$\delta\omega = 0 \quad \text{in} \quad \Omega \cup \Omega^{\mathrm{c}} \tag{35}$$

both equations are equivalent. For a more general account see [21].

Domains Ω, Ω^{c}, Ω^R and manifolds Γ, Γ^R are defined in Fig. 1. The terms "interior" and "exterior" refer to the domains Ω and Ω^{c}, respectively.

Every form that is eligible to be a solution of a boundary-value problem of Maxwell type must be an element of the space

$$\begin{aligned} Y^p(\Omega \cup \Omega^{\mathrm{c}}) = \{\omega \in H_{\mathrm{loc}}\Lambda^p(\delta\mathrm{d}, \Omega \cup \Omega^{\mathrm{c}}) \cap H_{\mathrm{loc}}\Lambda^p(\delta 0, \Omega \cup \Omega^{\mathrm{c}}) \\ | \, (\delta\mathrm{d} - k^2)\omega = 0\}. \end{aligned} \tag{36}$$

The definition implies (34) as well as (35). We call *Maxwell solutions* those elements of $Y^p(\Omega \cup \Omega^{\mathrm{c}})$ that fulfill a radiation or decay condition in Ω^{c}, see Sect. 4.2. The space of Maxwell solutions is denoted by $X^p(\Omega \cup \Omega^{\mathrm{c}}) \subset Y^p(\Omega \cup \Omega^{\mathrm{c}})$, and the restriction of this space to the domain of the interior problem reads $X^p(\Omega) = Y^p(\Omega)$.

Remark 7.

1. For $\omega \in H_{\mathrm{loc}}\Lambda^p(\delta\mathrm{d}, \Omega \cup \Omega^{\mathrm{c}}) \cap H_{\mathrm{loc}}\Lambda^p(\delta, \Omega \cup \Omega^{\mathrm{c}})$, the operators in (34) and (35) are well defined. This motivates the above definition of a solution space for Maxwell-type problems.
2. The gauge condition (35) for $p > 0$ is a consequence of (34) for $k \neq 0$, while for $k = 0$ it is an additional requirement that we impose. On topologically non-trivial domains, the periods of $\mathrm{t} * \omega$ have to vanish.

The interior *Dirichlet, Neumann, and normal traces* of Maxwell solutions are defined by

$$\begin{aligned} &\gamma_{\mathrm{D}} : H\Lambda^p(\mathrm{d}, \Omega) \to H_{\perp}^{-1/2}\Lambda^p(\mathrm{d}, \Gamma) &&: \omega \mapsto \mathrm{t}\,\omega, && \text{Dirichlet trace,} && (37a) \\ &\gamma_{\mathrm{N}} : H\Lambda^p(\delta\mathrm{d}, \Omega) \to H_{\parallel}^{-1/2}\Lambda^p(\delta, \Gamma) &&: \omega \mapsto \mathrm{n}\,\mathrm{d}\,\omega, && \text{Neumann trace,} && (37b) \\ &\mathrm{n} : \ H\Lambda^p(\delta, \Omega) \to H_{\parallel}^{-1/2}\Lambda^{p-1}(\delta, \Gamma) &&: \omega \mapsto \mathrm{n}\,\omega, && \text{normal trace,} && (37c) \end{aligned}$$

where the definition of the normal trace is given in (28).

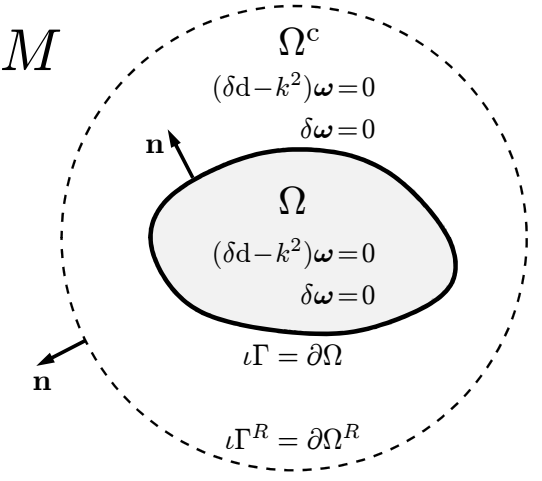

Fig. 1 Setting of the problem. Ω denotes a bounded subset of the Euclidean space M, homeomorphic to an open ball. Its Lipschitz boundary $\partial\Omega$ is represented by an embedded Lipschitz manifold Γ. Ω^{c} is the complement of $\overline{\Omega}$ in M. $\Omega^R \subset M$, homeomorphic to an open ball, is chosen such that $\Omega^R \ni \Omega$. Its smooth boundary $\partial\Omega^R$ ("far boundary") is represented by an embedded smooth manifold Γ^R. The normal-vector field $\mathbf{n}$ defines outer normals to both boundaries.

Remark 8.

1. The interior trace operators γ_{D} and γ_{N} are well defined, linear, continuous, and surjective, as a consequence of the properties of t and n laid out in Sect. 3.2.
2. The exterior Dirichlet, Neumann, and normal traces $\gamma_{\mathrm{D}}^{\mathrm{c}}$, $\gamma_{\mathrm{N}}^{\mathrm{c}}$, and n^{c}, as well as the trace operators on Γ^R, γ_{D}^R, γ_{N}^R, and n^R, are defined in the same way, and the same mapping properties apply.

4.2 Asymptotic Conditions

Any Maxwell solution of (34) is required to fulfill an asymptotic condition at infinity. For $k \neq 0$ the condition is called a radiation condition, for $k = 0$ it is called a decay condition. Let $\mathbf{n}$ denote an outward directed unit normal-vector field to a large sphere Γ^R with radius R, compare Fig. 1. X denotes an arbitrary point on Γ^R.

1. *Case $k \neq 0$.* The *radiation condition* reads

$$\left.\begin{aligned} |(\gamma_{\mathrm{N}}^R - ik\gamma_{\mathrm{D}}^R)\omega|_{L^2(\Gamma^R)} &= o(1), \\ |\mathrm{n}^R\omega|_{L^2(\Gamma^R)} &= o(1). \end{aligned}\right\} \tag{38}$$

We present the radiation condition in an L^2 sense because it directly relates to the energy arguments that are used to establish uniqueness of solutions [14, Thm. 2.4]. Lemma 4 provides strong versions of the radiation condition.

Lemma 4. *The following radiation conditions are equivalent to* (38)*, under the assumption of uniformity for* $R \to \infty$*:*

$$\left.\begin{aligned} |(\gamma_{\mathrm{N}}^R - ik\gamma_{\mathrm{D}}^R)\omega|_X &= o(R^{-(n-1)/2}), \\ |\mathrm{n}^R\omega|_X &= o(R^{-(n-1)/2}), \end{aligned}\right\} \tag{39}$$

$$|\mathrm{i}_{\mathbf{n}}\mathrm{d}\omega - ik\omega|_{\iota X} = o(R^{-(n-1)/2}). \tag{40}$$

For the latter condition see also [21, eq. (1)].

Proof. The Euclidean measure $S_n(R)$ of a sphere of radius R in n dimensions is $\mathscr{O}(R^{n-1})$ for $R \to \infty$. This proves the validity of (39).

For a smooth p-form ω it holds on a smooth submanifold that

$$\begin{aligned} \mathrm{t}\mathrm{i}_{\mathbf{n}}\omega &= (-1)^{pq}\mathrm{t}\mathrm{i}_{\mathbf{n}} * * \omega = (-1)^{pq}(-1)^q * \mathrm{t} * \omega \\ &= (-1)^{pq}(-1)^q(-1)^{(p-1)q} *^{-1} \mathrm{t} * \omega \\ &= \mathrm{n}\omega. \end{aligned} \tag{41}$$

For the second equality see [24, eq. (32)]. With the decomposition techniques from [24] it can easily be shown that the Pythagoras' theorem

$$|\omega|_{\iota X}^2 = |\mathrm{t}\omega|_X^2 + |\mathrm{n}\omega|_X^2$$

holds pointwise, where the moduli on the right hand side refer to the induced metric, and therefore $|\mathrm{t}\omega|_X, |\mathrm{n}\omega|_X \leq |\omega|_{\iota X}$. Condition (40) can be inferred from (39) with the help of (41), and vice versa. □

Condition (40) encompasses the Sommerfeld radiation condition for $p = 0$,

$$\frac{\partial u}{\partial r} - iku = o(R^{-(n-1)/2}),$$

and the Silver-Müller radiation condition for $p = 1, n = 3$,

$$|\mathbf{curl}\,\mathbf{u} \times \mathbf{n} - ik\mathbf{u}| = o(R^{-1}).$$

The following corollary will be useful in Section 5.1.

Corollary 1. *Let* $\omega \in X^p(\Omega^{\mathrm{c}} \cap \Omega^R)$*. Then for* $k \neq 0$ *the Dirichlet and Neumann traces fulfill*

$$|\gamma_{\mathrm{D}}^R\omega|_{L^2(\Gamma^R)} = \mathscr{O}(1), \quad |\gamma_{\mathrm{N}}^R\omega|_{L^2(\Gamma^R)} = \mathscr{O}(1), \tag{42}$$

i.e. the Dirichlet and Neumann traces on the far boundary are bounded as $R \to \infty$*.*

Proof. Substituting ω by $\mathrm{d}\omega$, $\omega \in H\Lambda^p(\delta\mathrm{d}, \Omega^{\mathrm{c}} \cap \Omega^R)$ in (31) on $\Omega^{\mathrm{c}} \cap \Omega^R$ and using the fact that ω is a Maxwell solution yields

$$-b(\gamma_{\mathrm{N}}^{\mathrm{c}}\omega,\gamma_{\mathrm{D}}^{\mathrm{c}}\eta)+\langle\gamma_{\mathrm{N}}^{R}\omega,\gamma_{\mathrm{D}}^{R}\eta\rangle_{L^2(\Gamma^R)}=\langle\mathrm{d}\omega,\mathrm{d}\eta\rangle_{L^2(\Omega^{\mathrm{c}}\cap\Omega^R)}-k^2\langle\omega,\eta\rangle_{L^2(\Omega^{\mathrm{c}}\cap\Omega^R)}.$$

Note that on the far boundary Γ^R we encounter sufficient regularity so to work with the L^2 inner product rather than the sesquilinear form $b(\cdot,\cdot)$. We set $\eta=\omega$, multiply by $\overline{k}$ and take the imaginary part,

$$\begin{aligned}&-\Im\mathrm{m}\big(\overline{k}b(\gamma_{\mathrm{N}}^{\mathrm{c}}\omega,\gamma_{\mathrm{D}}^{\mathrm{c}}\omega)\big)+\Im\mathrm{m}\big(\overline{k}\langle\gamma_{\mathrm{N}}^{R}\omega,\gamma_{\mathrm{D}}^{R}\omega\rangle_{L^2(\Gamma^R)}\big)\\&\quad=-(\Im\mathrm{m}\,k)\big(\langle\mathrm{d}\omega,\mathrm{d}\omega\rangle_{L^2(\Omega^{\mathrm{c}}\cap\Omega^R)}+|k|^2\langle\omega,\omega\rangle_{L^2(\Omega^{\mathrm{c}}\cap\Omega^R)}\big).\end{aligned}$$

From the radiation condition we obtain

$$\begin{aligned}o(1)&=|\gamma_{\mathrm{N}}^{R}\omega-ik\gamma_{\mathrm{D}}^{R}\omega|^2_{L^2(\Gamma^R)}\\&=|\gamma_{\mathrm{N}}^{R}\omega|^2_{L^2(\Gamma^R)}+|k|^2|\gamma_{\mathrm{D}}^{R}\omega|^2_{L^2(\Gamma^R)}-2\Im\mathrm{m}\,\big(\overline{k}\langle\gamma_{\mathrm{N}}^{R}\omega,\gamma_{\mathrm{D}}^{R}\omega\rangle_{L^2(\Gamma^R)}\big).\end{aligned}$$

Combining both equations yields

$$\begin{aligned}\Im\mathrm{m}\big(\overline{k}b(\gamma_{\mathrm{N}}^{\mathrm{c}}\omega,\gamma_{\mathrm{D}}^{\mathrm{c}}\omega)\big)&=(\Im\mathrm{m}\,k)\big(|\mathrm{d}\omega|^2_{L^2(\Omega^{\mathrm{c}}\cap\Omega^R)}+|k|^2|\omega|^2_{L^2(\Omega^{\mathrm{c}}\cap\Omega^R)}\big)\\&\quad+\tfrac{1}{2}\big(|\gamma_{\mathrm{N}}^{R}\omega|^2_{L^2(\Gamma^R)}+|k|^2|\gamma_{\mathrm{D}}^{R}\omega|^2_{L^2(\Gamma^R)}\big)+o(1).\end{aligned}\tag{43}$$

The left hand side is bounded, due to the continuity of the trace operators and of $b(\cdot,\cdot)$. Since we required $\Im\mathrm{m}\,k\geq 0$, we know that the right hand side consists of four non-negative terms, each of which must be bounded for $R\to\infty$. This proves the claim (42). □

Remark 9. This result generalizes the case $p=0$ that is discussed in [27, eq. (9.17)-(9.19)].

2. *Case $k=0$.* The *decay condition* reads

$$\boxed{|\omega|_{\imath X}\begin{cases}=\mathscr{O}(R^{2-n}), & n\geq 3,\\ \leq\left|b\ln\frac{R}{r_0}\right|+\mathscr{O}(R^{-1}), & n=2,\end{cases}}\tag{44}$$

uniformly for $R\to\infty$, where $b\in\mathbb{C}$ and $r_0>0$ are constants. For a motivation, see [27, Thm. 8.9]. Condition (44) implies the same asymptotic behaviour for the Dirichlet and normal traces $\gamma_{\mathrm{D}}^{R}\omega$ and $\mathrm{n}^R\omega$, respectively.

It can be shown that $\omega\in X(\Omega^{\mathrm{c}}\cap\Omega^R)$ subject to (44) also fulfills

$$|\mathrm{d}\omega|_{\imath X}\begin{cases}=\mathscr{O}(R^{1-n}), & n\geq 3,\\ \leq|b|R^{-1}+\mathscr{O}(R^{-2}), & n=2,\end{cases}\tag{45}$$

uniformly for $R\to\infty$. The proof of this assertion is based on the theory of generalized spherical harmonics. For $p=0$ it can be found in [27], as part of the

proof of Thm. 8.9. We skip the general case, while pointing out that the required background can be found in [37]. Condition (45) implies the same asymptotic behaviour for the Neumann trace $\gamma_{\mathrm{N}}^{R}\omega$.

For $p=0$, the above conditions (44) and (45) are sharp. For $p>0$ it can even be shown that by condition $\delta\omega=0$ we gain one order of decay, i.e. $|\omega|_{\imath X}=\mathscr{O}(R^{1-n})$ and $|\mathrm{d}\omega|_{\imath X}=\mathscr{O}(R^{-n})$, $n\geq 2$.[4] This implies $b=0$ for $p=1$.

Remark 10. The asymptotic conditions guarantee that a representation formula for Maxwell solutions exists without extra terms due to the far boundary. It must be noted that the conditions do not generally ensure that the forms decay rapidly enough for $X^p(\Omega^{\mathrm{c}})\subset L^2\Lambda^p(\Omega^{\mathrm{c}})$ to hold. For the scope of this paper, we circumvent the problem by using the spaces $L^2_{\mathrm{loc}}\Lambda^p(\Omega^{\mathrm{c}})$. However, if one is aiming at variational formulations in the domain Ω^{c}, the issue generally has to be remedied by replacing $L^2\Lambda^p(\Omega^{\mathrm{c}})$ with Beppo-Levi-type weighted spaces $L^2_s\Lambda^p(\Omega^{\mathrm{c}})$ [29], and building the theory in terms of weighted Sobolev spaces.[5]

4.3 Representation Formula for Maxwell Solutions

We define the jump of some trace γ_{X} of a form ω as

$$[\![\gamma_{\mathrm{X}}]\!]\omega=\gamma_{\mathrm{X}}^{\mathrm{c}}\omega-\gamma_{\mathrm{X}}\omega,$$

and refer to the definitions of the single- and double-layer potentials in Sect. 2.4.

The *boundary data* (β,γ,φ) of forms $\omega\in X^p(\Omega\cup\Omega^{\mathrm{c}})$ are defined as

$$\boxed{\begin{aligned}\beta&=[\![\gamma_{\mathrm{D}}]\!]\,\omega\in H_{\perp}^{-1/2}\Lambda^p(\mathrm{d},\Gamma),&\text{(46a)}\\ \gamma&=[\![\gamma_{\mathrm{N}}]\!]\,\omega\in H_{\parallel}^{-1/2}\Lambda^p(\delta,\Gamma),&\text{(46b)}\\ \varphi&=[\![\mathrm{n}]\!]\,\omega\ \ \in H_{\parallel}^{-1/2}\Lambda^{p-1}(\delta 0,\Gamma).&\text{(46c)}\end{aligned}}$$

Theorem 1. *A Maxwell solution $\omega\in X^p(\Omega\cup\Omega^{\mathrm{c}})$ can be represented in terms of integral transformations of its boundary data by*

$$\boxed{\omega=-\Psi_{\mathrm{SL}}\,\gamma+\Psi_{\mathrm{DL}}\,\beta-\mathrm{d}\,\Psi_{\mathrm{SL}}\,\varphi.}\tag{47}$$

Eq. (47) is called the *representation formula*.

Remark 11. We note that the Neumann data obey the additional restriction

$$\delta\gamma=-k^2\varphi,\quad \delta\varphi=0.\tag{48}$$

[4] For $n=3, p=1$ see [1], proof of Proposition 3.1.

[5] For the vectorial case $n=3$, $p=1$, $s=-1$ see [18, 19].

Consider the surface current density $\mathbf{k} \in \mathbf{H}^{-1/2}(\mathrm{div}_\Gamma, \partial\Omega)$ and the surface charge density $\sigma \in H^{-1/2}(\partial\Omega)$. For $p = 1$, $(\mathbf{k}, \sigma)$ can be defined as vector and scalar proxies of the differential forms (γ, φ), respectively. The first equation in (48) then translates into

$$\mathrm{div}_\Gamma \mathbf{k} + i\omega\sigma = 0,$$

the continuity equation, where ω is the angular frequency. Therefore, (48) is called generalized continuity equation.

For the proof we proceed in three steps: First, we derive in Lemma 5 representation formulae for smooth forms on Ω, $\Omega^c \cap \Omega^R$, and $(\Omega \cup \Omega^c) \cap \Omega^R$, respectively. Second, we show in Lemma 6 that the terms related to the far boundary vanish for $R \to \infty$, provided that the smooth forms fulfill the asymptotic condition. Third, Lemma 7 demonstrates that the layer potentials are well-defined for boundary data in the relevant Sobolev spaces.

Lemma 5. *Forms $\omega \in Y^p(\Omega) \cap \mathscr{F}^p(\Omega)$ can be represented by*

$$\omega = \Psi_{\mathrm{SL}}(\gamma_{\mathrm{N}}\omega) - \Psi_{\mathrm{DL}}(\gamma_{\mathrm{D}}\omega) + \mathrm{d}\,\Psi_{\mathrm{SL}}(\mathrm{n}\omega). \tag{49}$$

Forms $\omega \in Y^p(\Omega^c \cap \Omega^R) \cap \mathscr{F}^p(\Omega^c \cap \Omega^R)$ can be represented by

$$\omega = -\Psi_{\mathrm{SL}}(\gamma_{\mathrm{N}}^c\omega) + \Psi_{\mathrm{DL}}(\gamma_{\mathrm{D}}^c\omega) - \mathrm{d}\,\Psi_{\mathrm{SL}}(\mathrm{n}^c\omega) + M\omega, \tag{50}$$

where the term $M\omega$ contains integral transformations of Dirichlet and Neumann data on the far boundary Γ^R. Eventually, forms $\omega \in Y^p((\Omega \cup \Omega^c) \cap \Omega^R) \cap \mathscr{F}^p((\Omega \cup \Omega^c) \cap \Omega^R)$ can be represented by

$$\omega = -\Psi_{\mathrm{SL}}\,\gamma + \Psi_{\mathrm{DL}}\,\beta - \mathrm{d}\Psi_{\mathrm{SL}}\,\varphi + M\omega. \tag{51}$$

Proof. Representation Formula on Ω

For smooth forms $\psi \in \mathscr{F}^{p+1}(\Omega), \eta \in \mathscr{F}^p(\Omega)$, we start from the integration by parts formula

$$\langle \delta\psi, \eta\rangle_{L^2(\Omega)} - \langle \psi, \mathrm{d}\eta\rangle_{L^2(\Omega)} = -\langle \mathrm{n}\psi, \mathrm{t}\eta\rangle_{L^2(\Gamma)}. \tag{52}$$

Substituting ψ by $\mathrm{d}\omega$, $\omega \in \mathscr{F}^p(\Omega)$, yields *Green's first identity*

$$\langle \delta\mathrm{d}\omega, \eta\rangle_{L^2(\Omega)} - \langle \mathrm{d}\omega, \mathrm{d}\eta\rangle_{L^2(\Omega)} = -\langle \mathrm{nd}\omega, \mathrm{t}\eta\rangle_{L^2(\Gamma)}.$$

We insert the k^2 term, rewrite the equality with arguments swapped, and then subtract both equations. We thus find *Green's second identity of the **curl curl** type*

$$\begin{aligned}&\langle(\delta\mathrm{d}-k^2)\omega,\eta\rangle_{L^2(\Omega)}-\langle\omega,(\delta\mathrm{d}-\overline{k}^2)\eta\rangle_{L^2(\Omega)}\\&\quad=\langle\gamma_{\mathrm{D}}\omega,\gamma_{\mathrm{N}}\eta\rangle_{L^2(\Gamma)}-\langle\gamma_{\mathrm{N}}\omega,\gamma_{\mathrm{D}}\eta\rangle_{L^2(\Gamma)}.\end{aligned}\tag{53}$$

For completeness and further reference we also give *Green's second identity of the* ***grad*** div *type*,

$$\langle\mathrm{d}\delta\omega,\eta\rangle_{L^2(\Omega)}-\langle\omega,\mathrm{d}\delta\eta\rangle_{L^2(\Omega)}=\langle\mathrm{t}\delta\omega,\mathrm{n}\eta\rangle_{L^2(\Gamma)}-\langle\mathrm{n}\omega,\mathrm{t}\delta\eta\rangle_{L^2(\Gamma)}.\tag{54}$$

Now, replacing η by the fundamental solution (15), equation (53) becomes an integral transformation between p-forms. Moreover, we require that ω is a solution of (34) and obtain

$$\omega-\langle\omega,\mathrm{d}\delta G_p\rangle_{L^2(\Omega)}=\langle\gamma_{\mathrm{N}}\omega,\gamma_{\mathrm{D}}G_p\rangle_{L^2(\Gamma)}-\langle\gamma_{\mathrm{D}}\omega,\gamma_{\mathrm{N}}G_p\rangle_{L^2(\Gamma)}.\tag{55}$$

The second term can be decomposed via integration by parts (52),

$$\langle\omega,\mathrm{d}\delta G_p\rangle_{L^2(\Omega)}=\langle\delta\omega,\delta G_p\rangle_{L^2(\Omega)}+\langle\mathrm{n}\omega,\mathrm{t}\delta G_p\rangle_{L^2(\Gamma)}.\tag{56}$$

The domain integral on the right-hand side vanishes due to the gauge condition (35).

With (55) and (56) we can write down a first version of the representation formula for $\omega\in Y^p(\Omega)\cap\mathscr{F}^p(\Omega)$,

$$\omega=\langle\gamma_{\mathrm{N}}\omega,\gamma_{\mathrm{D}}G_p\rangle_{L^2(\Gamma)}-\langle\gamma_{\mathrm{D}}\omega,\gamma_{\mathrm{N}}G_p\rangle_{L^2(\Gamma)}+\langle\mathrm{n}\omega,\mathrm{t}\delta G_p\rangle_{L^2(\Gamma)}.$$

The p-form ω is not defined for observation points X' on the boundary $\partial\Omega$.

With the help of (11c, d) we obtain a second version of the representation formula,

$$\omega=\langle\gamma_{\mathrm{N}}\omega,\mathrm{t}G_p\rangle_{L^2(\Gamma)}-\delta\langle\gamma_{\mathrm{D}}\omega,\mathrm{n}G_{p+1}\rangle_{L^2(\Gamma)}+\mathrm{d}\,\langle\mathrm{n}\omega,\mathrm{t}G_{p-1}\rangle_{L^2(\Gamma)},\tag{57}$$

which effectively constitutes a Hodge decomposition of ω for $k=0$, i.e., ω is represented by (57) as sum of a harmonic, a coexact and an exact form.

Finally, with the definitions (21), and with (22), the representation formula (57) can be cast into the compact form (49),

$$\omega=\Psi_{\mathrm{SL}}(\gamma_{\mathrm{N}}\omega)-\Psi_{\mathrm{DL}}(\gamma_{\mathrm{D}}\omega)+\mathrm{d}\,\Psi_{\mathrm{SL}}(\mathrm{n}\omega).$$

The definition of the layer potentials can be extended to $\Omega\cup\Omega^{\mathrm{c}}$, admitting observation points $X'\in\Omega^{\mathrm{c}}$ as well. By construction, $\omega=0$ for $X'\in\Omega^{\mathrm{c}}$.

Representation Formula on $\Omega^{\mathrm{c}}\cap\Omega^R$

The same line of reasoning can be applied to the bounded exterior domain $\Omega^{\mathrm{c}}\cap\Omega^R$, which yields (50) for $X'\in\Omega^{\mathrm{c}}\cap\Omega^R$

$$\omega=-\Psi_{\mathrm{SL}}(\gamma_{\mathrm{N}}^{\mathrm{c}}\omega)+\Psi_{\mathrm{DL}}(\gamma_{\mathrm{D}}^{\mathrm{c}}\omega)-\mathrm{d}\,\Psi_{\mathrm{SL}}(\mathrm{n}^{\mathrm{c}}\omega)+M\omega.$$

The extra term $M\omega$ collects the boundary integrals on the far boundary Γ^R,

$$M\omega = \langle \gamma_{\mathrm{N}}^R \omega, \gamma_{\mathrm{D}}^R G_p \rangle_{L^2(\Gamma^R)} - \langle \gamma_{\mathrm{D}}^R \omega, \gamma_{\mathrm{N}}^R G_p \rangle_{L^2(\Gamma^R)} + \langle \mathrm{n}^R \omega, \mathrm{t}^R \delta G_p \rangle_{L^2(\Gamma^R)}. \tag{58}$$

By construction, $\omega = 0$ for $X' \in \Omega$.

Representation Formula on $(\Omega \cup \Omega^{\mathrm{c}}) \cap \Omega^R$

Adding up (49) and (50), we obtain the representation formula (51) which is valid for $X' \in (\Omega \cup \Omega^{\mathrm{c}}) \cap \Omega^R$,

$$\omega = -\Psi_{\mathrm{SL}}\, \gamma + \Psi_{\mathrm{DL}}\, \beta - \mathrm{d}\, \Psi_{\mathrm{SL}}\, \varphi + M\omega. \qquad \square$$

Remark 12. If $\omega \in Y^p(\Omega \cup \Omega^{\mathrm{c}}) \cap \mathscr{F}^p(\Omega \cup \Omega^{\mathrm{c}})$, then $M\omega$ is independent of the exact location and shape of Γ^R. This can be seen by introducing another $\Omega^{\tilde{R}} \ni \Omega^R$, and applying Green's identities on the annulus $\Omega^{\tilde{R}} \setminus \overline{\Omega}^R$.

Lemma 6. *If* $\omega \in X^p(\Omega \cup \Omega^{\mathrm{c}}) \cap \mathscr{F}^p(\Omega \cup \Omega^{\mathrm{c}})$*, i.e.,* ω *satisifies the radiation condition* (40) *for* $k \neq 0$ *or the decay condition* (44) *for* $k = 0$*, then* $|M\omega|_{X'} = o(1)$ *for all* $X' \in \Omega^{\mathrm{c}} \cap \Omega^R$ *as* $R \to \infty$*. Consequently, the far-boundary terms in* (50) *and* (51) *vanish.*

To prove Lemma 6 we need the following corollary about norms of the Green kernel. Consider some trace of the form $\gamma_{\mathrm{X}}^R G_p$. For a fixed observation point X' this expression gives a covector-valued form on Γ^R. To define a norm, we first take the point-wise norm of the covector anchored in X'. This leaves us with an ordinary form on Γ^R, whose L^2 norm we will then consider. We therefore define

$$\left|\gamma_{\mathrm{X}}^R G_p\right|_{L^2(\Gamma^R)}^{X'} = \left|\left|\gamma_{\mathrm{X}}^R G_p|_{X'}\right|\right|_{L^2(\Gamma^R)}.$$

Equivalently,

$$\left|\gamma_{\mathrm{X}}^R G_p\right|_{L^2(\Gamma^R)}^{X'} = \sup \left|\gamma_{\mathrm{X}}^R \langle G_p, \eta \rangle_{X'}\right|_{L^2(\Gamma^R)} = \sup \left|\gamma_{\mathrm{X}}^R (\overline{g}_n \eta)\right|_{L^2(\Gamma^R)},$$

where the supremum is taken here and subsequently over all covariantly constant p-forms $\eta \in \mathscr{F}^{\mathrm{const},p}(\Omega \cup \Omega^{\mathrm{c}})$ subject to $|\eta|_{X'} = 1$. The last equation follows with (8) and (15).

Corollary 2. *The norms of traces of the Green kernel on the far boundary are bounded by the norms of traces of the scalar fundamental solution,*

$$|\gamma_{\mathrm{D}}^R G_p|_{L^2(\Gamma^R)}^{X'} \leq |\gamma_{\mathrm{D}}^R G_0|_{L^2(\Gamma^R)}^{X'}, \tag{59a}$$

$$|(\gamma_{\mathrm{N}}^R - \overline{ik}\gamma_{\mathrm{D}}^R) G_p|_{L^2(\Gamma^R)}^{X'} \leq |(\gamma_{\mathrm{N}}^R - \overline{ik}\gamma_{\mathrm{D}}^R) G_0|_{L^2(\Gamma^R)}^{X'} + |\mathrm{d}\gamma_{\mathrm{D}}^R G_0|_{L^2(\Gamma^R)}^{X'}. \tag{59b}$$

The inequality for the Neumann trace features an additional term, which involves tangential derivatives.

Proof. We denote the unit volume form on Γ^R by μ and consider

$$\begin{aligned}\big(|\gamma_{\mathrm{D}}^R G_p|_{L^2(\Gamma^R)}^{X'}\big)^2 &= \sup|\gamma_{\mathrm{D}}^R(\overline{g}_n\eta)|_{L^2(\Gamma^R)}^2 = \sup|(\gamma_{\mathrm{D}}^R\overline{g}_n)(\gamma_{\mathrm{D}}^R\eta)|_{L^2(\Gamma^R)}^2\\ &= \sup\int_{\Gamma^R}|\gamma_{\mathrm{D}}^R\overline{g}_n|^2\,|\gamma_{\mathrm{D}}^R\eta|^2\,\mu\\ &\le \int_{\Gamma^R}|\gamma_{\mathrm{D}}^R\overline{g}_n|^2\,\mu = \big(|\gamma_{\mathrm{D}}^R G_0|_{L^2(\Gamma^R)}^{X'}\big)^2,\end{aligned}\tag{60}$$

where we used $|\gamma_{\mathrm{D}}^R\eta|_X \le |\eta|_{\iota X} = 1$. This proves (59a).

To derive an estimate for the Neumann trace of the Green kernel, we first have to consider

$$\begin{aligned}\gamma_{\mathrm{N}}^R(\overline{g}_n\eta) &= \gamma_{\mathrm{D}}^R\mathrm{i}_{\mathbf{n}}\mathrm{d}(\overline{g}_n\eta) = \gamma_{\mathrm{D}}^R\mathrm{i}_{\mathbf{n}}(\mathrm{d}\overline{g}_n\wedge\eta)\\ &= \gamma_{\mathrm{D}}^R(\mathrm{i}_{\mathbf{n}}\mathrm{d}\overline{g}_n\wedge\eta - \mathrm{d}\overline{g}_n\wedge\mathrm{i}_{\mathbf{n}}\eta)\\ &= (\gamma_{\mathrm{N}}^R\overline{g}_n)(\gamma_{\mathrm{D}}^R\eta) - \mathrm{d}\gamma_{\mathrm{D}}^R\overline{g}_n\wedge\mathrm{n}^R\eta,\end{aligned}$$

where we used (41), and therefore

$$(\gamma_{\mathrm{N}}^R - \overline{ik}\gamma_{\mathrm{D}}^R)(\overline{g}_n\eta) = \big((\gamma_{\mathrm{N}}^R - \overline{ik}\gamma_{\mathrm{D}}^R)\overline{g}_n\big)(\gamma_{\mathrm{D}}^R\eta) - \mathrm{d}\gamma_{\mathrm{D}}^R\overline{g}_n\wedge\mathrm{n}^R\eta.$$

We now tackle

$$\begin{aligned}|(\gamma_{\mathrm{N}}^R - \overline{ik}\gamma_{\mathrm{D}}^R)G_p|_{L^2(\Gamma^R)}^{X'} &= \sup|(\gamma_{\mathrm{N}}^R - \overline{ik}\gamma_{\mathrm{D}}^R)(\overline{g}_n\eta)|_{L^2(\Gamma^R)}\\ &= \sup\big|\big((\gamma_{\mathrm{N}}^R - \overline{ik}\gamma_{\mathrm{D}}^R)\overline{g}_n\big)(\gamma_{\mathrm{D}}^R\eta) - \mathrm{d}\gamma_{\mathrm{D}}^R\overline{g}_n\wedge\mathrm{n}^R\eta\big|_{L^2(\Gamma^R)}\\ &\le \sup\big|\big((\gamma_{\mathrm{N}}^R - \overline{ik}\gamma_{\mathrm{D}}^R)\overline{g}_n\big)(\gamma_{\mathrm{D}}^R\eta)\big|_{L^2(\Gamma^R)} + \sup|\mathrm{d}\gamma_{\mathrm{D}}^R\overline{g}_n\wedge\mathrm{n}^R\eta|_{L^2(\Gamma^R)}.\end{aligned}$$

Recall that the supremum is taken over all covariantly constant p-forms $\eta \in \mathscr{F}^{\mathrm{const},p}(\Omega\cup\Omega^{\mathrm{c}})$ subject to $|\eta|_{X'} = 1$. Along the same line as in (60) we obtain for the first term

$$\sup\big|\big((\gamma_{\mathrm{N}}^R - \overline{ik}\gamma_{\mathrm{D}}^R)\overline{g}_n\big)(\gamma_{\mathrm{D}}^R\eta)\big|_{L^2(\Gamma^R)}^2 \le \big(|(\gamma_{\mathrm{N}}^R - \overline{ik}\gamma_{\mathrm{D}}^R)G_0|_{L^2(\Gamma^R)}^{X'}\big)^2.$$

For the second term,

$$\begin{aligned}\sup|\mathrm{d}\gamma_{\mathrm{D}}^R\overline{g}_n\wedge\mathrm{n}^R\eta|_{L^2(\Gamma^R)}^2 &= \sup\int_{\Gamma^R}|\mathrm{d}\gamma_{\mathrm{D}}^R\overline{g}_n\wedge\mathrm{n}^R\eta|_X^2\,\mu \le \sup\int_{\Gamma^R}|\mathrm{d}\gamma_{\mathrm{D}}^R\overline{g}_n|_X^2\,|\mathrm{n}^R\eta|_X^2\,\mu\\ &\le \int_{\Gamma^R}|\mathrm{d}\gamma_{\mathrm{D}}^R\overline{g}_n|_X^2\,\mu = \big(|\mathrm{d}\gamma_{\mathrm{D}}^R G_0|_{L^2(\Gamma^R)}^{X'}\big)^2,\end{aligned}$$

where we used that for a 1-form ν it holds that $|\nu\wedge\omega|_X \le |\nu|_X|\omega|_X$, and $|\mathrm{n}^R\eta|_X \le |\eta|_{\iota X} = 1$. This proves (59b). □

Proof (Lemma 6). It has been shown in [27, Lemma 7.11, Thms. 8.9 and 9.6] for the case $p=0$ that the asymptotic conditions (40) and (44) imply $M\omega=0$ for $R\to\infty$, and vice versa. In what follows we generalize the proof of the first implication to arbitrary p, i.e., we demonstrate that the representation formula works without extra terms due to the far boundary. For the converse implication see Remark 15.

To this end, we write (58) in a particular form. From (4) and (37b) we infer $\mathrm{t}\delta=-*^{-1}\gamma_{\mathrm{N}}*$. Taking this into account yields

$$\begin{aligned} M\omega = &\left\langle(\gamma_{\mathrm{N}}^R-ik\gamma_{\mathrm{D}}^R)\omega,\gamma_{\mathrm{D}}^R G_p\right\rangle_{L^2(\Gamma^R)}-\left\langle\gamma_{\mathrm{D}}^R\omega,(\gamma_{\mathrm{N}}^R-\overline{ik}\gamma_{\mathrm{D}}^R)G_p\right\rangle_{L^2(\Gamma^R)}\\ &+(*^{-1})'\left\langle(\gamma_{\mathrm{N}}^R-ik\gamma_{\mathrm{D}}^R)*\omega,\gamma_{\mathrm{D}}^R G_q\right\rangle_{L^2(\Gamma^R)}\\ &-(*^{-1})'\left\langle\gamma_{\mathrm{D}}^R*\omega,(\gamma_{\mathrm{N}}^R-\overline{ik}\gamma_{\mathrm{D}}^R)G_q\right\rangle_{L^2(\Gamma^R)}, \end{aligned} \tag{61}$$

where we used (11a), (28) and (35), i.e. $\gamma_{\mathrm{N}}^R*\omega=0$.

Consider an integral transformation of the form $\omega=\langle\hat{\omega},\gamma_{\mathrm{X}}^R G_p\rangle_{L^2(\Gamma^R)}$, and a covariantly constant p-form $\eta\in\mathscr{F}^{\mathrm{const},p}(\Omega\cup\Omega^{\mathrm{c}})$, subject to $|\eta|_{X'}=1$. Then it holds that

$$\begin{aligned} |\omega|_{X'} &= \sup\langle\omega,\eta\rangle_{X'}=\sup\left\langle\hat{\omega},\gamma_{\mathrm{X}}^R\langle G_p,\eta\rangle_{X'}\right\rangle_{L^2(\Gamma^R)}\\ &\le |\hat{\omega}|_{L^2(\Gamma^R)}\sup\left|\gamma_{\mathrm{X}}^R\langle G_p,\eta\rangle_{X'}\right|_{L^2(\Gamma^R)}=|\hat{\omega}|_{L^2(\Gamma^R)}\left|\gamma_{\mathrm{X}}^R G_p\right|_{L^2(\Gamma^R)}^{X'}, \end{aligned}$$

where we used the Cauchy-Schwarz inequality. The supremum is taken over all admissible η, compare Corollary 2. Then, from (61) with the triangle inequality it follows that

$$\begin{aligned} |M\omega|_{X'} \le &\left|(\gamma_{\mathrm{N}}^R-ik\gamma_{\mathrm{D}}^R)\omega\right|_{L^2(\Gamma^R)}\left|\gamma_{\mathrm{D}}^R G_p\right|_{L^2(\Gamma^R)}^{X'}\\ &+\left|\gamma_{\mathrm{D}}^R\omega\right|_{L^2(\Gamma^R)}\left|(\gamma_{\mathrm{N}}^R-\overline{ik}\gamma_{\mathrm{D}}^R)G_p\right|_{L^2(\Gamma^R)}^{X'}\\ &+\left|ik\mathrm{n}^R\omega\right|_{L^2(\Gamma^R)}\left|\gamma_{\mathrm{D}}^R G_q\right|_{L^2(\Gamma^R)}^{X'}\\ &+\left|\mathrm{n}^R\omega\right|_{L^2(\Gamma^R)}\left|(\gamma_{\mathrm{N}}^R-\overline{ik}\gamma_{\mathrm{D}}^R)G_q\right|_{L^2(\Gamma^R)}^{X'}, \end{aligned} \tag{62}$$

where we used $\mathrm{t}*=*\mathrm{n}$, see (28).

We will demonstrate that $|M\omega|_{X'}=o(1)$ for all $X'\in\Omega^{\mathrm{c}}\cap\Omega^R$ as $R\to\infty$. Since $M\omega$ is actually independent of the exact location and shape of Γ^R, this implies $M\omega=0$. We leverage this freedom and pick a large ball with radius R centered at a fixed point in Ω. Three cases need to be distinguished:

1. *Case $k\neq 0$.* It holds that

$$\left.\begin{aligned} \left|(\gamma_{\mathrm{N}}^R-ik\gamma_{\mathrm{D}}^R)\omega\right|_{L^2(\Gamma^R)}&=o(1),\\ \left|\gamma_{\mathrm{D}}^R\omega\right|_{L^2(\Gamma^R)}&=\mathscr{O}(1),\\ \left|\mathrm{n}^R\omega\right|_{L^2(\Gamma^R)}&=o(1), \end{aligned}\right\} \tag{63}$$

for $R \to \infty$, see (38) and (42), respectively. The scalar fundamental solution g_n enjoys the properties

$$\left.\begin{aligned} g_n &= \mathscr{O}(r^{-(n-1)/2}),\\ \left(\tfrac{\partial}{\partial r} - ik\right) g_n &= o(r^{-(n-1)/2}),\\ \tfrac{\partial}{\partial r} g_n &= \mathscr{O}(r^{-(n-1)/2}), \end{aligned}\right\} \tag{64a}$$

see [27, eq. (9.10), (9.13)]. Note that for $X \in \Gamma^R$ and fixed $X' \in \Omega^c \cap \Omega^R$

$$\begin{aligned} \left|\mathrm{d}\gamma_{\mathrm{D}}^R G_0\right|_X &= |\mathrm{d}R \wedge \mathrm{d}g_n|_{\iota X} = |\mathrm{d}R \wedge \mathrm{d}r|_{\iota X} \left|\tfrac{\partial}{\partial r} g_n\right| \\ &= \mathscr{O}(r^{-1})\mathscr{O}(r^{-(n-1)/2}) = o(r^{-(n-1)/2}). \end{aligned} \tag{64b}$$

We win one order of decay for the tangential derivatives by the spherical symmetry of the fundamental solution. In fact, if the ball Ω^R happened to be centered in X' we would have $r = R$ and $\mathrm{d}R \wedge \mathrm{d}r = 0$.[6]

By standard asymptotics for Hankel functions it can be confirmed that the asymptotic orders in (64) stay the same if we replace r by R. It follows then from (59) and (64) that

$$\left.\begin{aligned} \left|\gamma_{\mathrm{D}}^R G_p\right|^{X'}_{L^2(\Gamma^R)} &= \mathscr{O}(1),\\ \left|(\gamma_{\mathrm{N}}^R - \overline{ik}\gamma_{\mathrm{D}}^R) G_p\right|^{X'}_{L^2(\Gamma^R)} &= o(1), \end{aligned}\right\} \tag{65}$$

for $R \to \infty$. Finally, (63) and (65) in connection with (62) yield the assertion.

2. *Case $k = 0$, $n \geq 3$.* The asymptotic conditions for the traces of ω are given by (44) and (45), respectively. The decay behaviour of the fundamental solution with $k = 0$ is obvious from (14). While the third term on the right hand side of (62) vanishes, it is easy to see that the three remaining terms are of order $\mathscr{O}(R^{2-n})$ for $R \to \infty$.
3. *Case $k = 0$, $n = 2$.* For $p = 0$ see [27, Thm. 8.9]. For $p = 1$, there holds $b = 0$ in (44) and (45), respectively. We can argue like in the previous case. The first term in (62) is of order $\mathscr{O}(R^{-1} \ln R)$, the other two non-zero terms are of order $\mathscr{O}(R^{-1})$, for $R \to \infty$. □

Lemma 7. *The representation formula*

$$\omega = -\Psi_{\mathrm{SL}}\,\gamma + \Psi_{\mathrm{DL}}\,\beta - \mathrm{d}\,\Psi_{\mathrm{SL}}\,\varphi$$

is well defined for boundary data according to

$$\begin{aligned} \beta &= [\![\gamma_{\mathrm{D}}]\!]\,\omega \in H_{\perp}^{-1/2}\Lambda^p(\mathrm{d}, \Gamma),\\ \gamma &= [\![\gamma_{\mathrm{N}}]\!]\,\omega \in H_{\parallel}^{-1/2}\Lambda^p(\delta, \Gamma),\\ \varphi &= [\![\mathrm{n}]\!]\,\omega \in H_{\parallel}^{-1/2}\Lambda^{p-1}(\delta 0, \Gamma), \end{aligned}$$

where $\omega \in X^p(\Omega \cup \Omega^c)$ is a Maxwell solution.

[6] For $n = 3$, $p = 1$, the expression $\mathrm{d}R \wedge \mathrm{d}g_n$ corresponds to $\mathbf{n} \times \mathbf{grad}\, g_3$, see [14, p. 161].

Proof. Taking into account the regularity of the Green operator and the mapping properties of the trace operator, it can be shown along the same lines as in [18, eq. 5.5, Thm. 5.1] that Ψ_{SL} can be extended to a linear continuous operator

$$\Psi_{\mathrm{SL}} : H_{\|}^{-1/2}\Lambda^p(\Gamma) \to H^1_{\mathrm{loc}}\Lambda^p(M). \tag{66}$$

If we restrict its domain to $H_{\|}^{-1/2}\Lambda^p(\delta,\Gamma)$ then (23a) is well defined and yields that $\delta\Psi_{\mathrm{SL}}$ is in $H^1_{\mathrm{loc}}\Lambda^{p-1}(M) \subset H_{\mathrm{loc}}\Lambda^{p-1}(\mathrm{d},M)$. Therefore we know that Ψ_{SL} is then even in $H_{\mathrm{loc}}\Lambda^p(\mathrm{d}\delta,M)$. From (23b), which holds in Ω and Ω^{c} separately, we see that

$$\Psi_{\mathrm{SL}} : H_{\|}^{-1/2}\Lambda^p(\delta,\Gamma) \to H^1_{\mathrm{loc}}\Lambda^p(M) \cap H_{\mathrm{loc}}\Lambda^p(\delta\mathrm{d},\Omega\cup\Omega^{\mathrm{c}}) \tag{67}$$

is continuous. Moreover, from (67),

$$\mathrm{d}\,\Psi_{\mathrm{SL}} : H_{\|}^{-1/2}\Lambda^p(\delta 0,\Gamma) \to H_{\mathrm{loc}}\Lambda^{p+1}(\mathrm{d}0,M) \cap H_{\mathrm{loc}}\Lambda^{p+1}(\delta,\Omega\cup\Omega^{\mathrm{c}}). \tag{68}$$

The definition (21b) of the double layer potential, or, equivalently, (23c), extends to a linear and continuous operator

$$\Psi_{\mathrm{DL}} : H_{\perp}^{-1/2}\Lambda^p(\Gamma) \to H_{\mathrm{loc}}\Lambda^p(\delta,M).$$

If we restrict its domain to $H_{\perp}^{-1/2}\Lambda^p(\mathrm{d},\Gamma)$, then (23e) is well defined in Ω and Ω^{c} separately and yields that $\mathrm{d}\,\Psi_{\mathrm{DL}}$ is in $H_{\mathrm{loc}}\Lambda^{p+1}(\delta,M)$. From this we find that

$$\Psi_{\mathrm{DL}} : H_{\perp}^{-1/2}\Lambda^p(\mathrm{d},\Gamma) \to H_{\mathrm{loc}}\Lambda^p(\delta,M) \cap H_{\mathrm{loc}}\Lambda^p(\delta\mathrm{d},\Omega\cup\Omega^{\mathrm{c}}) \tag{69}$$

is continuous. We conclude that all boundary-integral operators in the representation formula are well defined for the respective boundary data. □

Proof (Theorem 1). The proof of Theorem 1 follows directly from the Lemmata 5, 6, and 7. □

Remark 13. If we dispense with the requirements $(\delta\mathrm{d}-k^2)\omega = 0$ and $\delta\omega = 0$, and the asymptotic condition, the most complete statement of the representation formula for forms in $H_{\mathrm{loc}}\Lambda^p(\delta\mathrm{d},\Omega\cup\Omega^{\mathrm{c}}) \cap H_{\mathrm{loc}}\Lambda^p(\delta,\Omega\cup\Omega^{\mathrm{c}})$ reads

$$\begin{aligned}\omega = &-\Psi_{\mathrm{SL}}\,\gamma + \Psi_{\mathrm{DL}}\,\beta - \mathrm{d}\,\Psi_{\mathrm{SL}}\,\varphi + M\omega \\ &+\langle(\delta\mathrm{d}-k^2)\omega, G_p\rangle_{L^2(\Omega)} + \mathrm{d}\,\langle\delta\omega, G_{p-1}\rangle_{L^2(\Omega)}.\end{aligned}$$

Both $(\delta\mathrm{d}-k^2)\omega$ and $\delta\omega$ have to be compactly supported. Then Ω can always be enlarged such that it contains their supports, which has been assumed in the above representation formula.

We proceed to show that individual terms of the representation formula lie in $X^p(\Omega\cup\Omega^{\mathrm{c}})$. This is a prerequisite for indirect methods, where some Maxwell solution is represented in terms of either single or double layer potential rather than

combining them into the representation formula. Lemma 8 shows that the relevant terms lie in $Y^p(\Omega \cup \Omega^c)$, and Lemma 9 proves the asymptotic properties.

Lemma 8. *Let* (β, γ, φ) *be boundary data according to* (46) *and fulfilling* (48). *For* $k \neq 0$ *it holds that* $(\Psi_{\mathrm{SL}}\gamma + \mathrm{d}\Psi_{\mathrm{SL}}\varphi)$ *and* $\Psi_{\mathrm{DL}}\beta$ *are each elements of* $Y^p(\Omega \cup \Omega^c)$. *For* $k = 0$ *it holds that* $\Psi_{\mathrm{SL}}\gamma$, $\mathrm{d}\Psi_{\mathrm{SL}}\varphi$, *and* $\Psi_{\mathrm{DL}}\beta$ *are each elements of* $Y^p(\Omega \cup \Omega^c)$.

Proof. From (69) it follows that (23d, g) are well defined, which shows that $\Psi_{\mathrm{DL}}\beta \in Y^p(\Omega \cup \Omega^c)$. We note in passing that also (23f) is well-defined provided that its domain is chosen as $H_\perp^{-1/2}\Lambda^p(\mathrm{d}, \Gamma)$. Consider now

$$\omega = \Psi_{\mathrm{SL}}\gamma + \mathrm{d}\Psi_{\mathrm{SL}}\varphi,$$

with $(\gamma, \varphi) \in H_\parallel^{-1/2}\Lambda^p(\delta, \Gamma) \times H_\parallel^{-1/2}\Lambda^{p-1}(\delta 0, \Gamma)$ obeying to (48). From (67) and (68) we know that $\omega \in H_{\mathrm{loc}}\Lambda^p(\delta, \Omega \cup \Omega^c) \cap H_{\mathrm{loc}}\Lambda^p(\delta \mathrm{d}, \Omega \cup \Omega^c)$. We can therefore calculate

$$\begin{aligned}
(\delta\mathrm{d} - k^2)\omega &= -\mathrm{d}\Psi_{\mathrm{SL}}\delta\gamma - \mathrm{d}\Psi_{\mathrm{SL}}k^2\varphi \\
&= -\mathrm{d}\Psi_{\mathrm{SL}}(\delta\gamma + k^2\varphi) = 0, \\
\delta\omega &= \Psi_{\mathrm{SL}}\delta\gamma + k^2\Psi_{\mathrm{SL}}\varphi - \mathrm{d}\Psi_{\mathrm{SL}}\delta\varphi \\
&= \Psi_{\mathrm{SL}}(\delta\gamma + k^2\varphi) - \mathrm{d}\Psi_{\mathrm{SL}}\delta\varphi = 0,
\end{aligned}$$

where we used (23a, b). We have thus shown that $\Psi_{\mathrm{SL}}\gamma + \mathrm{d}\Psi_{\mathrm{SL}}\varphi \in Y^p(\Omega \cup \Omega^c)$. The case $k = 0$ follows from the above formulae and (23a). □

Lemma 9. *Let* (β, γ, φ) *be boundary data according to* (46) *and fulfilling* (48). *For* $k \neq 0$ *it holds that* $(\Psi_{\mathrm{SL}}\gamma + \mathrm{d}\Psi_{\mathrm{SL}}\varphi)$ *and* $\Psi_{\mathrm{DL}}\beta$ *each satisfy the radiation condition* (40). *For* $k = 0$ *it holds that* $\Psi_{\mathrm{SL}}\gamma$, $\mathrm{d}\Psi_{\mathrm{SL}}\varphi$, *and* $\Psi_{\mathrm{DL}}\beta$ *each satisfy the decay condition* (44).

Proof.

1. *Case* $k \neq 0$. We rely on [21, Lemma 3.2], which tells us that $\omega = \Psi_{\mathrm{SL}}\gamma$ as well as its derivatives d and δ satisfy the following radiation condition

$$|\mathrm{i}_{\mathbf{n}}\mathrm{d}\omega + \mathrm{j}_{\mathrm{d}R}\delta\omega - ik\omega|_{\iota X'} = o(R^{-(n-1)/2}), \tag{70}$$

uniformly for $R \to \infty$. Note the extra term $\mathrm{j}_{\mathrm{d}R}\delta\omega$ that controls the coderivative, which is non-zero, in general. Let us define the linear maps that correspond to the conditions (40) and (70), respectively,

$$\begin{aligned}
f(\omega) &= \mathrm{i}_{\mathbf{n}}\mathrm{d}\omega - ik\omega, \\
g(\omega) &= \mathrm{i}_{\mathbf{n}}\mathrm{d}\omega + \mathrm{j}_{\mathrm{d}R}\delta\omega - ik\omega.
\end{aligned}$$

Both maps coincide on $Y^p(\Omega \cup \Omega^c)$. From Lemma 8 we know that $\Psi_{\mathrm{SL}}\gamma + \mathrm{d}\Psi_{\mathrm{SL}}\varphi$ and $\Psi_{\mathrm{DL}}\beta$ lie in $Y^p(\Omega \cup \Omega^c)$. Moreover, it is easy to see that $g(*\omega) = *g(\omega)$. We can therefore argue

$$
\begin{aligned}
|f(\Psi_{\mathrm{SL}}\gamma+\mathrm{d}\,\Psi_{\mathrm{SL}}\varphi)|_{\iota X'} &= |g(\Psi_{\mathrm{SL}}\gamma+\mathrm{d}\,\Psi_{\mathrm{SL}}\varphi)|_{\iota X'} \\
&\leq |g(\Psi_{\mathrm{SL}}\gamma)|_{\iota X'} + |g(\mathrm{d}\,\Psi_{\mathrm{SL}}\varphi)|_{\iota X'} \\
&= o(R^{-(n-1)/2}), \\
|f(\Psi_{\mathrm{DL}}\beta)|_{\iota X'} &= |g(\Psi_{\mathrm{DL}}\beta)|_{\iota X'} = |*\,g(\mathrm{d}\,\Psi_{\mathrm{SL}}*^{-1}\beta)|_{\iota X'} \\
&= |g(\mathrm{d}\,\Psi_{\mathrm{SL}}*^{-1}\beta)|_{\iota X'} = o(R^{-(n-1)/2}),
\end{aligned}
$$

where we used (21b). This completes the proof for $k \neq 0$.

2. *Case $k = 0$, except for $n = 2$, $p = 1$.* The boundary integral operators decay at least as fast as the fundamental solution, compare (14) with (44), for $k = 0$.
3. *Case $k = 0$, $n = 2$, $p = 1$.* Define the abbreviations $A = \Psi_{\mathrm{SL}}\gamma$, $B = \mathrm{d}\,\Psi_{\mathrm{SL}}\varphi$ and $C = \Psi_{\mathrm{DL}}\beta$. All terms obey at least condition (44), with $b \neq 0$, according to the previous case. Terms B and C can be expressed each in terms of the exterior derivative of a scalar single layer potential, which yields $\mathscr{O}(R^{-1})$ decay for $R \to \infty$, i.e. $b = 0$. It remains to deal with term A.

   As a corollary, we consider the more general case $k = 0$, $p = n-1$, and let $\omega = \Psi_{\mathrm{SL}}\gamma$. γ is required to be coclosed, $\delta\gamma = 0$, therefore $*\gamma$ is a closed 0-form, and must be constant on each connected component of Γ. Since we assumed a trivial topology, we can for linearity reasons simply set $\gamma = *^{-1}1$. Now it is a well-known result from potential theory that $\Psi_{\mathrm{DL}}1 = 0$ on the exterior domain Ω^{c}, taking into account (44), which prohibits a constant at infinity. But then with (21b)

$$
\begin{aligned}
0 &= -*^{-1}\Psi_{\mathrm{DL}}1 = \mathrm{d}\,\Psi_{\mathrm{SL}}(*^{-1}1) \\
&= \mathrm{d}\,\Psi_{\mathrm{SL}}\gamma = \mathrm{d}\omega.
\end{aligned} \tag{71}
$$

   Thus, with (23a) we have $\mathrm{d}\omega = \delta\omega = 0$ in Ω^{c}.

   Now returning to the case $n = 2$ we apply Stokes' theorem in the annulus $\Omega^{\mathrm{c}} \cap \Omega^R$ to $\mathrm{d}\omega$ and $\mathrm{d} * \omega$, respectively. We infer that the contour integrals of the tangential and radial components of ω along the circle Γ^R must be constant, as $R \to \infty$. This proves that neither of the components can involve a logarithmic singularity, nor can the modulus, thus $b = 0$ in (44) for term A as well. □

Remark 14. In 2-D electromagnetics, (71) has an intuitive interpretation. If γ is seen to model a surface current that flows in circumferential direction along Γ, then ω would be its vector potential. Equation (71) says that the magnetic flux density in the exterior domain vanishes. In other words, (71) states that the magnetostatic field of a densely wound cylindrical coil is entirely confined to its interior.

Remark 15. The converse of Lemma 6 states that $M\omega = 0$ for $R \to \infty$ implies that ω fulfills the asymptotic condition. This can be seen easily, since from $M\omega = 0$ it follows from (51) that ω can be represented solely in terms of the layer potentials. Then from Lemma 9 we know that ω satisfies the asymptotic condition.

Equation (34) encompasses the Helmholtz equation for $p = 0$ and the **curl curl** equation for $p = 1$. The following table lists the translation into classical calculus for $n = 3$, $p = 0, 1$.

p	Translation	$(\delta \mathrm{d} - k^2)\,\omega = 0$	$\gamma_{\mathrm{D}}\,\omega$	$\gamma_{\mathrm{N}}\,\omega$
0	$u = \Upsilon^0 \omega$	$(\Delta_{\mathrm{s}} + k^2)\,u = 0$	γu	$\gamma_n \mathbf{grad}\, u$
1	$\mathbf{u} = \Upsilon^1 \omega$	$(\mathbf{curl}\,\mathbf{curl} - k^2)\,\mathbf{u} = \mathbf{0}$	$\pi_\tau \mathbf{u}$	$\gamma_\tau \mathbf{curl}\,\mathbf{u}$

The representation formula (49) for $n = 3$ encompasses and generalizes the classical Kirchhoff ($p = 0$) and Stratton-Chu ($p = 1$, [32, Sect. 4.15]) representation formulae in three dimensions, which read in vector notation

$$u = \int_{\partial\Omega} \left(g_3 \frac{\partial u}{\partial n} - \frac{\partial g_3}{\partial n} u \right) \mathrm{d}\Gamma,$$

$$\mathbf{u} = \int_{\partial\Omega} g_3\, \mathbf{curl}\,\mathbf{u} \times \mathbf{n}\, \mathrm{d}\Gamma + \mathbf{curl}' \int_{\partial\Omega} g_3\, \mathbf{u} \times \mathbf{n}\, \mathrm{d}\Gamma + \mathbf{grad}' \int_{\partial\Omega} g_3\, \mathbf{u} \cdot \mathbf{n}\, \mathrm{d}\Gamma.$$

Note that for $p = 0$ the last term in (49) vanishes.

Equation (48) motivates the definition of the *Maxwell single layer potential* for $k \neq 0$

$$\boxed{\widetilde{\Psi}_{\mathrm{SL}} : H_{\parallel}^{-1/2} \Lambda^p(\delta, \Gamma) \to X^p(\Omega \cup \Omega^{\mathrm{c}}) : \gamma \mapsto (\Psi_{\mathrm{SL}} - \frac{1}{k^2} \mathrm{d}\, \Psi_{\mathrm{SL}} \delta)\gamma,} \tag{72}$$

so that the representation formula (47) can be written equivalently

$$\omega = -\widetilde{\Psi}_{\mathrm{SL}}\, \gamma + \Psi_{\mathrm{DL}}\, \beta. \tag{73}$$

From (23a) and (23b) it follows that the Maxwell single layer potential can also be written as $\widetilde{\Psi}_{\mathrm{SL}} = k^{-2} \delta \mathrm{d}\, \Psi_{\mathrm{SL}}$.

We proceed to show the mapping properties of $\widetilde{\Psi}_{\mathrm{SL}}$. From (67) and (68) it can be inferred that

$$\widetilde{\Psi}_{\mathrm{SL}} : H_{\parallel}^{-1/2} \Lambda^p(\delta, \Gamma) \to H_{\mathrm{loc}} \Lambda^p(\delta, \Omega \cup \Omega^{\mathrm{c}}) \cap H_{\mathrm{loc}} \Lambda^p(\delta \mathrm{d}, \Omega \cup \Omega^{\mathrm{c}}) \tag{74}$$

is continuous. The Maxwell single layer potential has the following properties, which are obvious from the proof of Lemma 7,

$$\delta \widetilde{\Psi}_{\mathrm{SL}} = 0, \tag{75a}$$

$$(\delta \mathrm{d} - k^2) \widetilde{\Psi}_{\mathrm{SL}} = 0. \tag{75b}$$

Moreover, from Lemma 9 it follows immediately that the Maxwell single layer potential satisfies the radiation condition (40). This confirms in connection with (74) and (75) the mapping property that is stated in definition (72).

Remark 16. Representation formula (73) without the extra Neumann data φ can also be derived following a different route. For $k \neq 0$, the Maxwell-type operator in (34) admits a fundamental solution, which is defined by the Maxwell Green kernel double p-form

$$\widetilde{G}_p = \big(1 - \frac{1}{k^2}\mathrm{d}\delta\big) G_p.$$

Plugging this kernel into Green's second identity (53) yields, after a few manipulations, directly the modified representation formula (73). The disadvantage of this derivation is that the case $k = 0$ is lost.

4.4 Jump Relations of the Layer Potentials

Lemma 10. *All relevant jump relations on the interface between Ω and Ω^{c} are collected in the subsequent table for data $\gamma \in H_{\parallel}^{-1/2}\Lambda^p(\delta,\Gamma)$, $\beta \in H_{\perp}^{-1/2}\Lambda^p(\mathrm{d},\Gamma)$, and $\varphi \in H_{\parallel}^{-1/2}\Lambda^p(\delta,\Gamma)$.*

Potential	$[\![\gamma_{\mathrm{N}}]\!]\cdot$	$[\![\gamma_{\mathrm{D}}]\!]\cdot$	$[\![\mathrm{n}]\!]\cdot$
$\Psi_{\mathrm{SL}}\gamma$	$-\gamma$	0	0
$\Psi_{\mathrm{DL}}\beta$	0	β	0
$\mathrm{d}\Psi_{\mathrm{SL}}\varphi$	0	0	$-\varphi$

Remark 17.

1. The mapping properties (67) and (69) of the layer potentials together with those of the trace operators (37) ensure that all combinations displayed in the table are well defined.
2. The top left 2x2 block of the table reveals that these jump relations coincide with those of the standard single and double layer potentials in the scalar case.
3. In the sequel we call $\mathrm{d}\Psi_{\mathrm{SL}}$ the exact potential, to distinguish it from single- and double-layer potentials.

Proof. The nine proofs are given below:

Dirichlet and normal traces of the single layer potential

Obvious, due to the H^1-regularity of the potential, see (67).

Neumann trace of the single layer potential

Write Green's second identity (53) for the domains Ω and Ω^{c} separately. Recall the extension of the L^2 inner product $\langle\cdot,\cdot\rangle_{L^2(\Gamma)}$ to the sesquilinear form $b(\cdot,\cdot)$ according to (31). Be aware that all boundary terms carry an additional minus sign in the case of Ω^{c}, because the boundary Γ was chosen to be consistently oriented with Ω. Assume $\eta = \Phi \in \mathscr{D}\Lambda^p(M)$, which renders all traces of Φ continuous. Adding both equations yields

$$\begin{aligned}\langle(\delta\mathrm{d}-k^2)\omega,\Phi\rangle_{L^2(\Omega\cup\Omega^{\mathrm{c}})} - \langle\omega,(\delta\mathrm{d}-\overline{k}^2)\Phi\rangle_{L^2(\Omega\cup\Omega^{\mathrm{c}})}\\ = -\overline{b(\gamma_{\mathrm{N}}\Phi,[\![\gamma_{\mathrm{D}}]\!]\omega)} + b([\![\gamma_{\mathrm{N}}]\!]\omega,\gamma_{\mathrm{D}}\Phi).\end{aligned} \tag{76}$$

In a similar way we obtain from Green's second identity (54)

$$\langle\mathrm{d}\delta\omega,\Phi\rangle_{L^2(\Omega\cup\Omega^{\mathrm{c}})} - \langle\omega,\mathrm{d}\delta\Phi\rangle_{L^2(\Omega\cup\Omega^{\mathrm{c}})} = -\overline{b(\mathrm{n}\Phi,[\![\mathrm{t}]\!]\delta\omega)} + b([\![\mathrm{n}]\!]\omega,\mathrm{t}\delta\Phi). \tag{77}$$

Add up (76) and (77),

$$\begin{aligned}&\langle(\Delta-k^2)\omega,\Phi\rangle_{L^2(\Omega\cup\Omega^{\mathrm{c}})} - \langle\omega,(\Delta-\overline{k}^2)\Phi\rangle_{L^2(\Omega\cup\Omega^{\mathrm{c}})}\\ &\quad= -\overline{b(\gamma_{\mathrm{N}}\Phi,[\![\gamma_{\mathrm{D}}]\!]\omega)} + b([\![\gamma_{\mathrm{N}}]\!]\omega,\gamma_{\mathrm{D}}\Phi) - \overline{b(\mathrm{n}\Phi,[\![\mathrm{t}]\!]\delta\omega)} + b([\![\mathrm{n}]\!]\omega,\mathrm{t}\delta\Phi).\end{aligned}$$

There are no contributions from the far boundary Γ^R, since Φ is compactly supported. Pick $\omega = \Psi_{\mathrm{SL}}\varphi$, $\varphi \in H_{\|}^{-1/2}\Lambda^p(\delta,\Gamma)$. We already know that $[\![\gamma_{\mathrm{D}}]\!]\omega = 0$ and $[\![\mathrm{n}]\!]\omega = 0$. From (23a) in connection with (66) it follows that $\delta\omega \in H^1_{\mathrm{loc}}\Lambda^{p-1}(M)$. The H^1-regularity implies $[\![\mathrm{t}]\!]\delta\omega = 0$. Eventually, (23b) eliminates the first domain integral. We are left with

$$-\langle\omega,(\Delta-\overline{k}^2)\Phi\rangle_{L^2(\Omega\cup\Omega^{\mathrm{c}})} = b([\![\gamma_{\mathrm{N}}]\!]\omega,\gamma_{\mathrm{D}}\Phi). \tag{78}$$

Check that

$$\langle(\Delta-\overline{k}^2)\Phi,\overline{G}_p\rangle_{L^2(\Omega\cup\Omega^{\mathrm{c}})} = \langle\Phi,\overline{(\Delta-\overline{k}^2)G_p}\rangle_{L^2(\Omega\cup\Omega^{\mathrm{c}})} = \widetilde{\Phi}.$$

The first equation is justified by the self adjointness of the Laplace-Beltrami operator, the second by (17). Note that $\widetilde{\Phi}$ is not defined on the boundary $\partial\Omega$, but can be continuously extended to yield Φ. Then

$$\begin{aligned}\langle\Psi_{\mathrm{SL}}\varphi,(\Delta-\overline{k}^2)\Phi\rangle_{L^2(\Omega\cup\Omega^{\mathrm{c}})} &= \langle b(\varphi,\mathrm{t}G_p),(\Delta-\overline{k}^2)\Phi\rangle'_{L^2(\Omega\cup\Omega^{\mathrm{c}})}\\ &= b\big(\varphi,\mathrm{t}\langle(\Delta-\overline{k}^2)\Phi,\overline{G}_p\rangle'_{L^2(\Omega\cup\Omega^{\mathrm{c}})}\big)\\ &= b(\varphi,\gamma_{\mathrm{D}}\Phi),\end{aligned}$$

and with (78)

$$b([\![\gamma_{\mathrm{N}}]\!]\omega+\varphi,\gamma_{\mathrm{D}}\Phi) = 0.$$

Density of $\mathrm{t}\mathscr{D}\Lambda^p(M)$ in $H_{\|}^{-1/2}\Lambda^p(\delta,\Gamma)$ completes the proof,

$$[\![\gamma_\mathrm{N}]\!]\Psi_\mathrm{SL}\varphi = -\varphi.$$

Dirichlet trace of the double layer potential

This jump can be related to the Neumann trace of the single layer potential. Consider

$$\gamma_\mathrm{D} * \mathrm{d} = \mathrm{t} * \mathrm{d} = * \mathrm{n}\,\mathrm{d} = * \gamma_\mathrm{N},$$

therefore

$$\gamma_\mathrm{D}\Psi_\mathrm{DL}\varphi = - * \gamma_\mathrm{N}\Psi_\mathrm{SL}(*^{-1}\varphi), \tag{79}$$

which is well defined for $\varphi \in H_{\perp}^{-1/2}\Lambda^p(\mathrm{d},\Gamma)$. The jump relation for the Neumann trace of the single layer potential gives us immediately the desired result,

$$[\![\gamma_\mathrm{D}]\!]\Psi_\mathrm{DL}\varphi = \varphi.$$

Neumann trace of the double layer potential

Consider

$$\begin{aligned}\gamma_\mathrm{N}\Psi_\mathrm{DL}\varphi &= *^{-1}\mathrm{t} * \mathrm{d}\,\Psi_\mathrm{DL}\varphi \\ &= *^{-1}\mathrm{t}\big((-1)^p \mathrm{d}\,\Psi_\mathrm{SL}(*\,\mathrm{d}\varphi) + k^2\Psi_\mathrm{SL}(*\varphi)\big) \\ &= -\delta\, *^{-1}\,\mathrm{t}\,\Psi_\mathrm{SL}(*\,\mathrm{d}\varphi) + k^2 *^{-1}\mathrm{t}\,\Psi_\mathrm{SL}(*\varphi),\end{aligned} \tag{80}$$

where (23f) has been used. For $\varphi \in H_{\perp}^{-1/2}\Lambda^p(\mathrm{d},\Gamma)$, we know that the tangential traces of the above single layer potentials are continuous. Thus we have shown

$$[\![\gamma_\mathrm{N}]\!]\Psi_\mathrm{DL}\varphi = 0.$$

Dirichlet trace of the exact potential

Because of $\mathrm{t}\,\mathrm{d} = \mathrm{d}\,\mathrm{t}$ the jump of the Dirichlet trace of the exact potential is related to the jump of the Dirichlet trace of the single layer potential, which yields

$$[\![\gamma_\mathrm{D}]\!]\mathrm{d}\Psi_\mathrm{SL}\varphi = 0$$

for $\varphi \in H_{\|}^{-1/2}\Lambda^p(\delta,\Gamma)$.

Normal trace of the double layer potential

Equation (23c) shows that the normal trace of the double layer potential is related to the Dirichlet trace of the exact potential as follows

$$\begin{aligned}\mathrm{n}\Psi_{\mathrm{DL}}\varphi &= *^{-1}\mathrm{t} * \Psi_{\mathrm{DL}}\varphi \\ &= (-1)^{p+1} *^{-1} \mathrm{t}\,\mathrm{d}\,\Psi_{\mathrm{SL}}(*\varphi).\end{aligned}$$

We therefore conclude

$$[\![\mathrm{n}]\!]\Psi_{\mathrm{DL}}\varphi = 0$$

for $\varphi \in H_{\perp}^{-1/2}\Lambda^p(\mathrm{d},\Gamma)$.

Neumann trace of the exact potential

Trivial, since this trace vanishes.

Normal trace of the exact potential

The normal trace of the exact potential coincides with the Neumann trace of the single layer potential. Therefore

$$[\![\mathrm{n}]\!]\,\mathrm{d}\Psi_{\mathrm{SL}}\varphi = -\varphi,$$

for $\varphi \in H_{\|}^{-1/2}\Lambda^p(\delta,\Gamma)$. This completes the proof of Lemma 10. □

5 Boundary Integral Operators

In this section, we introduce boundary-integral operators, and discuss their properties with respect to the sesquilinear form (31).

We denote the average of some trace γ_{X} of a form ω across Γ by

$$\{\gamma_{\mathrm{X}}\}\,\omega = \tfrac{1}{2}(\gamma_{\mathrm{X}}^{\mathrm{c}}\omega + \gamma_{\mathrm{X}}\omega),$$

and define the following boundary integral operators:

$$\begin{aligned}
V &= \gamma_{\mathrm{D}}\Psi_{\mathrm{SL}}: && H_{\|}^{-1/2}\Lambda^p(\delta,\Gamma) \to H_{\perp}^{-1/2}\Lambda^p(\mathrm{d},\Gamma), && && (81a)\\
\tilde{V} &= \gamma_{\mathrm{D}}\widetilde{\Psi}_{\mathrm{SL}}: && H_{\|}^{-1/2}\Lambda^p(\delta,\Gamma) \to H_{\perp}^{-1/2}\Lambda^p(\mathrm{d},\Gamma), && k \neq 0, && (81b)\\
K^{\dagger} &= \{\gamma_{\mathrm{N}}\}\Psi_{\mathrm{SL}}: && H_{\|}^{-1/2}\Lambda^p(\delta,\Gamma) \to H_{\|}^{-1/2}\Lambda^p(\delta,\Gamma), && && (81c)\\
K &= \{\gamma_{\mathrm{D}}\}\Psi_{\mathrm{DL}}: && H_{\perp}^{-1/2}\Lambda^p(\mathrm{d},\Gamma) \to H_{\perp}^{-1/2}\Lambda^p(\mathrm{d},\Gamma), && && (81d)\\
D &= -\gamma_{\mathrm{N}}\Psi_{\mathrm{DL}}: && H_{\perp}^{-1/2}\Lambda^p(\mathrm{d},\Gamma) \to H_{\|}^{-1/2}\Lambda^p(\delta,\Gamma), && && (81e)\\
W &= \mathrm{n}\Psi_{\mathrm{SL}}: && H_{\|}^{-1/2}\Lambda^p(\delta,\Gamma) \to H_{\|}^{-1/2}\Lambda^{p-1}(\delta,\Gamma), && && (81f)
\end{aligned}$$

where V denotes the single layer operator, $\tilde{V}$ the Maxwell single layer operator, K the double layer operator, $K^{\dagger}$ the conjugate adjoint double layer operator, and D the hypersingular operator. Inspecting the mapping properties of the trace operators and

of the layer potentials shows that the boundary integral operators are well defined and continuous.

Lemma 11. *The boundary integral operators have the following properties:*

$$(i) \qquad *K^\dagger = -K*, \tag{82a}$$

$$(ii) \quad \delta K^\dagger - K^\dagger \delta = -k^2 W, \tag{82b}$$

$$(iii) \quad \mathrm{d}K - K\mathrm{d} = (-1)^{p+1} k^2 *^{-1} W *, \tag{82c}$$

$$(iv) \qquad D = *^{-1}\mathrm{d}V\delta * - k^2 *^{-1} V *. \tag{82d}$$

For $k \neq 0$ it also holds that

$$(v) \qquad \tilde{V} = V - \frac{1}{k^2}\mathrm{d}V\delta, \tag{82e}$$

$$(vi) \qquad D = -k^2 *^{-1} \tilde{V} *. \tag{82f}$$

Remark 18.

1. Properties (ii) and (iii) show that the double-layer operator and its adjoint respect the respective de Rham sequence for $k = 0$.
2. Properties (iv) and (vi) connect the hypersingular operator D to the weakly singular operator V, by using integration by parts. For the Laplace case this goes back to MAUE [26, p. 604], and there is a paper by NÉDÉLEC [28] on related representations for different second order partial differential equations. This provides a way of avoiding the evaluation of hypersingular integrals in Galerkin boundary element methods. For example, from (iv) we find

$$b(D\omega, \eta) = \overline{b(\delta * \eta, V\delta * \omega)} - k^2 \overline{b(*\eta, V * \omega)},$$

$\omega, \eta \in H_\perp^{-1/2}\Lambda^p(\mathrm{d}, \Gamma)$.

Proof. Property (i) is an immediate consequence of (79). Property (ii) can be seen as follows:

$$\begin{aligned} \delta K^\dagger &= \delta \mathrm{n}\mathrm{d}\Psi_{\mathrm{SL}} = -\mathrm{n}\delta\mathrm{d}\Psi_{\mathrm{SL}} \\ &= -\mathrm{n}(k^2 - \mathrm{d}\delta)\Psi_{\mathrm{SL}} = \mathrm{n}\mathrm{d}\Psi_{\mathrm{SL}}\delta - k^2\mathrm{n}\Psi_{\mathrm{SL}} \\ &= K^\dagger\delta - k^2 W, \end{aligned}$$

where we used (23a), (23b), (30), (81c), and (81f). Equation (iii) can be seen as follows:

$$\begin{aligned} \mathrm{d}K &= -\mathrm{d} * K^\dagger *^{-1} = (-1)^q * \delta K^\dagger *^{-1} \\ &= (-1)^q * (K^\dagger\delta - k^2 W) *^{-1} = - * K^\dagger *^{-1} \mathrm{d} - (-1)^q k^2 * W *^{-1} \\ &= K\mathrm{d} - (-1)^p k^2 *^{-1} W *, \end{aligned}$$

where we used (4), (82a), and (82b). Eventually, (iv) follows from (80) with (4), and (81e). Properties (v) and (vi) follow from (72) with (27). □

The ordinary scalar and vectorial boundary integral operators in three dimensions follow from (81) by means of the translation isomorphisms. For the vectorial operators we adopt the conventions of [19, Thm. 9].

(81)	$p=0$, scalar operators	$p=1$, vectorial operators
V	V: $H^{-\frac{1}{2}}(\partial\Omega) \to H^{\frac{1}{2}}(\partial\Omega)$	A: $\mathbf{H}^{-\frac{1}{2}}(\mathrm{div}_\Gamma,\partial\Omega) \to \mathbf{H}^{-\frac{1}{2}}(\mathrm{curl}_\Gamma,\partial\Omega)$
$K^\dagger$	$\mathsf{K}^\dagger$: $H^{-\frac{1}{2}}(\partial\Omega) \to H^{-\frac{1}{2}}(\partial\Omega)$	B: $\mathbf{H}^{-\frac{1}{2}}(\mathrm{div}_\Gamma,\partial\Omega) \to \mathbf{H}^{-\frac{1}{2}}(\mathrm{div}_\Gamma,\partial\Omega)$
K	K: $H^{\frac{1}{2}}(\partial\Omega) \to H^{\frac{1}{2}}(\partial\Omega)$	$-\mathsf{C}$: $\mathbf{H}^{-\frac{1}{2}}(\mathrm{curl}_\Gamma,\partial\Omega) \to \mathbf{H}^{-\frac{1}{2}}(\mathrm{curl}_\Gamma,\partial\Omega)$
D	D: $H^{\frac{1}{2}}(\partial\Omega) \to H^{-\frac{1}{2}}(\partial\Omega)$	N: $\mathbf{H}^{-\frac{1}{2}}(\mathrm{curl}_\Gamma,\partial\Omega) \to \mathbf{H}^{-\frac{1}{2}}(\mathrm{div}_\Gamma,\partial\Omega)$

Equation (82d) yields for $p=0$ (compare [27, Thm. 9.15])

$$\mathsf{D}\beta = \mathrm{curl}_\Gamma\,\mathsf{A}\,\mathbf{curl}_\Gamma\beta - k^2\int_{\partial\Omega}\beta(X)g_3(X,X')\mathbf{n}(X)\cdot\mathbf{n}(X')\,\mathrm{d}\Gamma(X),$$

where the integral extends to $\beta\in H^{1/2}(\partial\Omega)$. For $p=1$, the same equation yields

$$\mathsf{N} = \mathbf{curl}_\Gamma\,\mathsf{V}\,\mathrm{curl}_\Gamma + k^2\mathsf{R}\,\mathsf{A}\,\mathsf{R},$$

where the rotation operator R was defined in (33). This generalizes Lemma 6.3 in [18][7].

We state some useful relations that stem from (i)–(iii) for $k=0$:

$$\begin{aligned}
\text{(i)}; p=1: &\quad \mathbf{n}\times\mathsf{B} = \mathsf{C}\,\mathbf{n}\times\cdot,\\
\text{(i), (ii)}; p=1: &\quad \mathrm{curl}_\Gamma\mathsf{C} = \mathsf{K}^\dagger\mathrm{curl}_\Gamma,\\
\text{(iii)}; p=0: &\quad \mathbf{grad}_\Gamma\mathsf{K} = -\mathsf{C}\,\mathbf{grad}_\Gamma,\\
\text{(i), (iii)}; p=0: &\quad \mathbf{curl}_\Gamma\mathsf{K} = -\mathsf{B}\,\mathbf{curl}_\Gamma.
\end{aligned}$$

5.1 Symmetry Properties

Lemma 12. *If $k\neq 0$, the boundary integral operators exhibit the following symmetry properties with respect to the sesquilinear form $b(\cdot,\cdot)$:*

[7] Be aware that the operators B, C, and N are defined slightly differently in [18] compared to [19]. In particular, N bears an additional minus sign.

$$\overline{b(\gamma, V\gamma')} = b(\gamma', \overline{V}\gamma), \tag{83a}$$

$$\overline{b(\gamma, \tilde{V}\gamma')} = b(\gamma', \tilde{\overline{V}}\gamma), \tag{83b}$$

$$\overline{b(D\beta', \beta)} = b(\overline{D}\beta, \beta'), \tag{83c}$$

$$b(K^{\dagger}\gamma, \beta) = b(\gamma, \overline{K}\beta), \tag{83d}$$

for all $\beta, \beta' \in H_{\perp}^{-1/2}\Lambda^p(\mathrm{d}, \Gamma)$ *and* $\gamma, \gamma' \in H_{\parallel}^{-1/2}\Lambda^p(\delta, \Gamma)$. *The single layer operators* V, $\tilde{V}$ *and the hypersingular operator* D *are complex symmetric, while* $K^{\dagger}$ *is the conjugate adjoint of* K. [8]

Relationships (i), (iii), and (iv) hold in the case $k = 0$ *as well, provided* γ, γ' *are restricted to the space* $H_{\parallel}^{-1/2}\Lambda^p(\delta 0, \Gamma)$. *The conjugations are just irrelevant, so that* V *and* D *are symmetric, and* $K^{\dagger}$ *is the adjoint of* K.

To prove Lemma 12, we need the following corollary.

Corollary 3. *We exclude the case* $k = 0$, $n = 2$, $p = 0$. *In all other cases, for* $\omega, \eta \in X^p(\Omega \cup \Omega^{\mathrm{c}})$, *we can use the following equality:*

$$b([\![\gamma_{\mathrm{N}}]\!]\omega, \{\gamma_{\mathrm{D}}\}\overline{\eta}) + b(\{\gamma_{\mathrm{N}}\}\omega, [\![\gamma_{\mathrm{D}}]\!]\overline{\eta}) = b([\![\gamma_{\mathrm{N}}]\!]\eta, \{\gamma_{\mathrm{D}}\}\overline{\omega}) + b(\{\gamma_{\mathrm{N}}\}\eta, [\![\gamma_{\mathrm{D}}]\!]\overline{\omega}). \tag{84}$$

Proof. Substituting ω by $\mathrm{d}\omega$, $\omega \in H\Lambda^p(\delta\mathrm{d}, \Omega)$, in (31) yields

$$b(\gamma_{\mathrm{N}}\omega, \gamma_{\mathrm{D}}\eta) = \langle \mathrm{d}\omega, \mathrm{d}\eta \rangle_{L^2(\Omega)} - \langle \delta\mathrm{d}\omega, \eta \rangle_{L^2(\Omega)}.$$

We may assume that $\omega \in X^p(\Omega)$ is a Maxwell solution, to obtain

$$b(\gamma_{\mathrm{N}}\omega, \gamma_{\mathrm{D}}\eta) = \langle \mathrm{d}\omega, \mathrm{d}\eta \rangle_{L^2(\Omega)} - k^2 \langle \omega, \eta \rangle_{L^2(\Omega)}. \tag{85}$$

The same arguments can be applied to the exterior domain $\Omega^{\mathrm{c}} \cap \Omega^R$, where $\omega \in X^p(\Omega^{\mathrm{c}} \cap \Omega^R)$, $\eta \in H\Lambda^p(\mathrm{d}, \Omega^{\mathrm{c}} \cap \Omega^R)$, from which we conclude

$$-b(\gamma_{\mathrm{N}}^{\mathrm{c}}\omega, \gamma_{\mathrm{D}}^{\mathrm{c}}\eta) + \langle \gamma_{\mathrm{N}}^{R}\omega, \gamma_{\mathrm{D}}^{R}\eta \rangle_{L^2(\Gamma^R)} = \langle \mathrm{d}\omega, \mathrm{d}\eta \rangle_{L^2(\Omega^{\mathrm{c}} \cap \Omega^R)} - k^2 \langle \omega, \eta \rangle_{L^2(\Omega^{\mathrm{c}} \cap \Omega^R)}. \tag{86}$$

Note that on the far boundary Γ^R we encounter sufficient regularity so to work with the L^2 inner product rather than the sesquilinear form $b(\cdot, \cdot)$. By combining (85) and (86) we find for $\omega \in X^p\big((\Omega \cup \Omega^{\mathrm{c}}) \cap \Omega^R\big)$

$$\begin{aligned} &b(\gamma_{\mathrm{N}}\omega, \gamma_{\mathrm{D}}\eta) - b(\gamma_{\mathrm{N}}^{\mathrm{c}}\omega, \gamma_{\mathrm{D}}^{\mathrm{c}}\eta) + \langle \gamma_{\mathrm{N}}^{R}\omega, \gamma_{\mathrm{D}}^{R}\eta \rangle_{L^2(\Gamma^R)} \\ &= \langle \mathrm{d}\omega, \mathrm{d}\eta \rangle_{L^2((\Omega \cup \Omega^{\mathrm{c}}) \cap \Omega^R)} - k^2 \langle \omega, \eta \rangle_{L^2((\Omega \cup \Omega^{\mathrm{c}}) \cap \Omega^R)}. \end{aligned} \tag{87}$$

[8] Compare with [19, Thm. 10]. Note that HIPTMAIR defines the rotation operator as $\mathsf{R} = -\mathbf{n} \times \cdot$ rather than $\mathsf{R} = \mathbf{n} \times \cdot$, which yields an additional minus sign in the definition of the double layer potential and consequently in HIPTMAIR's Thm. 10.

Rearranging terms and substituting η by $\overline{\eta}$ yields

$$\begin{aligned} &-b([\![\gamma_{\mathrm{N}}]\!]\omega,\{\gamma_{\mathrm{D}}\}\overline{\eta})-b(\{\gamma_{\mathrm{N}}\}\omega,[\![\gamma_{\mathrm{D}}]\!]\overline{\eta})+\langle\gamma_{\mathrm{N}}^R\omega,\gamma_{\mathrm{D}}^R\overline{\eta}\rangle_{L^2(\Gamma^R)}\\ &\quad=\langle \mathrm{d}\omega,\mathrm{d}\overline{\eta}\rangle_{L^2((\Omega\cup\Omega^{\mathrm{c}})\cap\Omega^R)}-k^2\langle\omega,\overline{\eta}\rangle_{L^2((\Omega\cup\Omega^{\mathrm{c}})\cap\Omega^R)}. \end{aligned} \tag{88}$$

We may assume that $\eta\in X^p(\Omega\cup\Omega^{\mathrm{c}})$ is a Maxwell solution as well, exchange the roles of ω and η, and subtract both equations. This eliminates the sesquilinear L^2 inner products over the domain. The sesquilinear L^2 inner products

$$x=\langle\gamma_{\mathrm{N}}^R\omega,\gamma_{\mathrm{D}}^R\overline{\eta}\rangle_{L^2(\Gamma^R)}-\langle\gamma_{\mathrm{N}}^R\eta,\gamma_{\mathrm{D}}^R\overline{\omega}\rangle_{L^2(\Gamma^R)}$$

over the far boundary Γ^R vanish for $R\to\infty$, which we show in the sequel. We need to distinguish three cases:

1. *Case $k\neq 0$.* Rewrite

$$x=\langle\gamma_{\mathrm{N}}^R\omega-ik\gamma_{\mathrm{D}}^R\omega,\gamma_{\mathrm{D}}^R\overline{\eta}\rangle_{L^2(\Gamma^R)}-\langle\gamma_{\mathrm{N}}^R\eta-ik\gamma_{\mathrm{D}}^R\eta,\gamma_{\mathrm{D}}^R\overline{\omega}\rangle_{L^2(\Gamma^R)}.$$

   From the triangle inequality we obtain

$$|x|\leq\left|\langle\gamma_{\mathrm{N}}^R\omega-ik\gamma_{\mathrm{D}}^R\omega,\gamma_{\mathrm{D}}^R\overline{\eta}\rangle_{L^2(\Gamma^R)}\right|+\left|\langle\gamma_{\mathrm{N}}^R\eta-ik\gamma_{\mathrm{D}}^R\eta,\gamma_{\mathrm{D}}^R\overline{\omega}\rangle_{L^2(\Gamma^R)}\right|,$$

   and from the Cauchy-Schwarz inequality

$$\left|\langle\gamma_{\mathrm{N}}^R\omega-ik\gamma_{\mathrm{D}}^R\omega,\gamma_{\mathrm{D}}^R\overline{\eta}\rangle_{L^2(\Gamma^R)}\right|\leq\left|\gamma_{\mathrm{N}}^R\omega-ik\gamma_{\mathrm{D}}^R\omega\right|_{L^2(\Gamma^R)}\left|\gamma_{\mathrm{D}}^R\overline{\eta}\right|_{L^2(\Gamma^R)}=o(1),$$

   where we used (38) and (42). Therefore, $|x|=o(1)$ for $R\to\infty$.
2. *Case $k=0$, $n\geq 3$.* From (44) and (45) we obtain

$$\left|\langle\gamma_{\mathrm{N}}^R\omega,\gamma_{\mathrm{D}}^R\overline{\eta}\rangle_{L^2(\Gamma^R)}\right|=\mathscr{O}(R^{2-n}). \tag{89}$$

   Together with the triangle inequality this yields $|x|=o(1)$ for $R\to\infty$.
3. *Case $k=0$, $n=2$, $p=1$.* Taking into account $b=0$, (44) and (45) yield

$$\left|\langle\gamma_{\mathrm{N}}^R\omega,\gamma_{\mathrm{D}}^R\overline{\eta}\rangle_{L^2(\Gamma^R)}\right|=\mathscr{O}(R^{-2}), \tag{90}$$

   for $R\to\infty$, and we can proceed like in the previous case.

We conclude that for $\omega,\eta\in X^p(\Omega\cup\Omega^{\mathrm{c}})$

$$b([\![\gamma_{\mathrm{N}}]\!]\omega,\{\gamma_{\mathrm{D}}\}\overline{\eta})+b(\{\gamma_{\mathrm{N}}\}\omega,[\![\gamma_{\mathrm{D}}]\!]\overline{\eta})=b([\![\gamma_{\mathrm{N}}]\!]\eta,\{\gamma_{\mathrm{D}}\}\overline{\omega})+b(\{\gamma_{\mathrm{N}}\}\eta,[\![\gamma_{\mathrm{D}}]\!]\overline{\omega}).$$

□

Proof (Lemma 12). The case $k=0$, $n=2$, $p=0$ is covered by the formally self-adjoint case in [27, eq. (7.3), (7.4)]. In all other cases we choose ω,η in (84) according to the representation formula (47) as

$$\begin{aligned} \omega&=-\Psi_{\mathrm{SL}}\gamma\ +\Psi_{\mathrm{DL}}\beta\ -\mathrm{d}\,\Psi_{\mathrm{SL}}\varphi,\\ \eta&=-\Psi_{\mathrm{SL}}\gamma'+\Psi_{\mathrm{DL}}\beta'-\mathrm{d}\,\Psi_{\mathrm{SL}}\varphi'. \end{aligned}$$

To prove (83a), we pick $\beta = \beta' = 0$. With Lemma 10, (48), and definition (81a) we obtain

$$\begin{aligned} b(\gamma, \overline{V\gamma' + \mathrm{d}V\varphi'}) &= b(\gamma', \overline{V\gamma + \mathrm{d}V\varphi}), \\ b(\gamma, \overline{V\gamma'}) + b(\delta\gamma, \overline{V\varphi'}) &= b(\gamma', \overline{V\gamma}) + b(\delta\gamma', \overline{V\varphi}), \\ b(\gamma, \overline{V\gamma'}) - k^2 b(\varphi, \overline{V\varphi'}) &= b(\gamma', \overline{V\gamma}) - k^2 b(\varphi', \overline{V\varphi}), \end{aligned}$$

which proves (83a) for $k = 0$. Otherwise restrict γ, γ' to $H_{\|}^{-1/2}\Lambda^p(\delta 0, \Gamma)$. This eliminates the second and forth terms, since (48) then implies $\varphi = \varphi' = 0$. From the remaining terms we can conclude that (83a) holds at least on $H_{\|}^{-1/2}\Lambda^p(\delta 0, \Gamma)$. From this we infer with $\varphi, \varphi' \in H_{\|}^{-1/2}\Lambda^{p-1}(\delta 0, \Gamma)$ that the second and forth terms always cancel, which means that the first and third terms imply (83a) even for $\gamma, \gamma' \in H_{\|}^{-1/2}\Lambda^p(\delta, \Gamma)$.

Property (83c) is seen setting $\gamma = \gamma' = 0$, $\varphi = \varphi' = 0$. With Lemma 10 and definition (81e) we obtain

$$b(D\beta, \overline{\beta'}) = b(D\beta', \overline{\beta}),$$

which proves (83c).

For (83d), we pick $\beta = 0$, $\gamma' = 0$, $\varphi' = 0$. With Lemma 10 and the definitions (81c), (81d) we obtain

$$b(\gamma, \overline{K\beta'}) - b(K^{\dagger}\gamma, \overline{\beta'}) = 0,$$

which proves (83d).

Finally, we have

$$\begin{aligned} \overline{b(\gamma, \tfrac{1}{k^2}\mathrm{d}V\delta\gamma')} &= \tfrac{1}{k^2}\overline{b(\delta\gamma, V\delta\gamma')} \\ &= \tfrac{1}{k^2} b(\delta\gamma', \overline{V}\delta\gamma) = b(\gamma', \overline{\tfrac{1}{k^2}\mathrm{d}V\delta}\gamma), \end{aligned}$$

where we used (83a). Together with (82e) this proves (83b). □

5.2 Ellipticity Properties

Lemma 13. *The boundary integral operators in connection with the sesquilinear form $b(\cdot,\cdot)$ exhibit the following ellipticity properties for $\Im m\, k > 0$:*

$$|b(\gamma, V\gamma)| \geq c\,\frac{\Im m\, k}{|k|}\min\Big(1, \frac{1}{|k|^2}\Big)|\gamma|^2_{H_{\|}^{-1/2}\Lambda^p(\delta,\Gamma)} \quad \forall \gamma \in H_{\|}^{-1/2}\Lambda^p(\delta 0, \Gamma), \tag{91a}$$

$$|b(\gamma, \tilde{V}\gamma)| \geq c\,\frac{\Im m\, k}{|k|}\min\Big(1, \frac{1}{|k|^2}\Big)|\gamma|^2_{H_{\|}^{-1/2}\Lambda^p(\delta,\Gamma)} \quad \forall \gamma \in H_{\|}^{-1/2}\Lambda^p(\delta, \Gamma), \tag{91b}$$

$$|b(D\beta, \beta)| \geq c\,\frac{\Im m\, k}{|k|}\min(1, |k|^2)\ |\beta|^2_{H_{\perp}^{-1/2}\Lambda^p(\mathrm{d},\Gamma)} \quad \forall \beta \in H_{\perp}^{-1/2}\Lambda^p(\mathrm{d}, \Gamma), \tag{91c}$$

with positive generic constants c, that depend only on the boundary.[9] *For* $k = 0$ *it holds that*

$$b(\gamma, V\gamma) \geq c\,|\gamma|^2_{H_{\|}^{-1/2}\Lambda^p(\delta,\Gamma)} \quad \forall \gamma \in H_{\|}^{-1/2}\Lambda^p(\delta 0,\Gamma), \tag{91d}$$

while $b(D\beta,\beta) \geq 0$ *on* $H_{\perp}^{-1/2}\Lambda^p(\mathrm{d},\Gamma)$. *In the case* $n = 2$, $p = 0$ *the parameter* r_0 *in the fundamental solution* (14) *has to be large enough, see [27, Thm. 8.16].*

Remark 19.

1. The estimates (91) are useful to establish well-posedness of boundary integral equations based on the above operators, by leveraging the Lax-Milgram theorem. This carries over to conforming Galerkin discretizations, and quasi-optimal error estimates in the norms of the trace spaces are available from Cea's lemma [18, 19].
2. For $k \in \mathbb{R}^+$, the estimates (91) become trivial. Still, the well-posedness of boundary integral equations based on the above operators can be established, based on a generalized Gårding inequality and Hodge decompositions [6, 10, 12, 13].

Proof. To show the ellipticity properties (91), we need to distinguish three cases:

1. *Case* $\Im m\, k > 0$. We proceed like in the derivation of (43), but consider the domain $(\Omega \cup \Omega^{\mathrm{c}}) \cap \Omega^R$ rather than $\Omega^{\mathrm{c}} \cap \Omega^R$. We find for $\omega \in X^p\big((\Omega \cup \Omega^{\mathrm{c}}) \cap \Omega^R\big)$

$$\begin{aligned}
&\Im\mathrm{m}\big(\overline{k}b([\![\gamma_{\mathrm{N}}]\!]\omega, \{\gamma_{\mathrm{D}}\}\omega) + \overline{k}b(\{\gamma_{\mathrm{N}}\}\omega, [\![\gamma_{\mathrm{D}}]\!]\omega)\big)\\
=&(\Im\mathrm{m}\, k)\big(|\mathrm{d}\omega|^2_{L^2((\Omega\cup\Omega^{\mathrm{c}})\cap\Omega^R)} + |k|^2|\omega|^2_{L^2((\Omega\cup\Omega^{\mathrm{c}})\cap\Omega^R)}\big)\\
&+ \tfrac{1}{2}\big(|\gamma^R_{\mathrm{N}}\omega|^2_{L^2(\Gamma^R)} + |k|^2|\gamma^R_{\mathrm{D}}\omega|^2_{L^2(\Gamma^R)}\big) + o(1).
\end{aligned}$$

   Pick $\omega = \Psi_{\mathrm{DL}}\beta$ and let $R \to \infty$, which yields

$$-\Im\mathrm{m}\big(\overline{k}b(D\beta,\beta)\big) \geq (\Im\mathrm{m}\, k)\big(|\mathrm{d}\omega|^2_{L^2(\Omega\cup\Omega^{\mathrm{c}})} + |k|^2|\omega|^2_{L^2(\Omega\cup\Omega^{\mathrm{c}})}\big) \geq 0,$$

   where we used Lemma 10 and definition (81e). Next, consider

$$|k|^2|b(D\beta,\beta)|^2 = |\overline{k}b(D\beta,\beta)|^2 \geq \Im\mathrm{m}\,\big(\overline{k}b(D\beta,\beta)\big)^2,$$

   and therefore

$$\begin{aligned}
|k|\,|b(D\beta,\beta)| &\geq -\Im\mathrm{m}\big(\overline{k}b(D\beta,\beta)\big)\\
&\geq (\Im\mathrm{m}\, k)\big(|\mathrm{d}\omega|^2_{L^2(\Omega\cup\Omega^{\mathrm{c}})} + |k|^2|\omega|^2_{L^2(\Omega\cup\Omega^{\mathrm{c}})}\big).
\end{aligned}$$

[9] Estimates for the real part instead of the modulus can be derived as well [19], under the prerequisite $\Re\mathrm{e}\, k^2 \leq 0$. When comparing with [19], $\kappa^2 = -k^2$ has to be taken into account.

Finally,

$$|b(D\beta,\beta)| \geq \frac{\Im\mathrm{m}\,k}{|k|}\min(1,|k|^2)\big(|\mathrm{d}\omega|^2_{L^2(\Omega\cup\Omega^\mathrm{c})}+|\omega|^2_{L^2(\Omega\cup\Omega^\mathrm{c})}\big)$$
$$\geq \frac{1}{2}\frac{\Im\mathrm{m}\,k}{|k|}\min(1,|k|^2)|\omega|^2_{H\Lambda^p(\mathrm{d},\Omega\cup\Omega^\mathrm{c})}, \tag{92}$$

where we used $a^2+b^2 \geq (a+b)^2/2$.

On the other hand, from the continuity of the tangential trace operator we have

$$|\beta|_{H_\perp^{-1/2}\Lambda^p(\mathrm{d},\Gamma)} = |[\![\mathrm{t}]\!]\omega|_{H_\perp^{-1/2}\Lambda^p(\mathrm{d},\Gamma)} \leq c|\omega|_{H\Lambda^p(\mathrm{d},\Omega\cup\Omega^\mathrm{c})}, \tag{93}$$

with $c>0$ that depends only on Γ. Combining (92) with (93) proves (91c).

Equation (91b) follows immediately with (82f), if we let $\gamma = *\beta$. For $k\neq 0$ (91a) is obvious, since V coincides with $\tilde{V}$ on $H_\parallel^{-1/2}\Lambda^p(\delta 0,\Gamma)$.

2. *Case $k=0$, $n=2$, $p=0$.* See [27, Thm. 8.16] for V and [27, Thm. 8.21] for D.
3. *Case $k=0$, all other n and p.* Consider the same domain as in the case $k\neq 0$, but with (87) as starting point. We rearrange as in (88), with $\eta=\omega$, $k=0$, let $R\to\infty$ and take into account (89) or (90), respectively,

$$-b([\![\gamma_\mathrm{N}]\!]\omega,\{\gamma_\mathrm{D}\}\omega)-b(\{\gamma_\mathrm{N}\}\omega,[\![\gamma_\mathrm{D}]\!]\omega) = \langle \mathrm{d}\omega,\mathrm{d}\omega\rangle_{L^2(\Omega\cup\Omega^\mathrm{c})}. \tag{94}$$

Pick $\omega=\Psi_\mathrm{SL}\,\gamma$, $\gamma\in H_\parallel^{-1/2}\Lambda^p(\delta 0,\Gamma)$, which yields

$$b(\gamma,V\gamma) = |\mathrm{d}\omega|^2_{L^2(\Omega\cup\Omega^\mathrm{c})}, \tag{95}$$

where we used Lemma 10 and definition (81a). On the other hand, from the continuity of the normal trace operator we have

$$|\gamma|_{H_\parallel^{-1/2}\Lambda^p(\delta,\Gamma)} = |[\mathrm{n}]\mathrm{d}\omega|_{H_\parallel^{-1/2}\Lambda^p(\delta,\Gamma)} \leq c|\mathrm{d}\omega|_{H\Lambda^{p+1}(\delta,\Omega\cup\Omega^\mathrm{c})}, \tag{96}$$

with $c>0$ that depends only on Γ. Since $\delta\mathrm{d}\omega=0$ in $\Omega\cup\Omega^\mathrm{c}$ it holds that $|\mathrm{d}\omega|_{H\Lambda^{p+1}(\delta,\Omega\cup\Omega^\mathrm{c})} = |\mathrm{d}\omega|_{L^2(\Omega\cup\Omega^\mathrm{c})}$, and combining (95) and (96) yields (91d).

Finally, if we pick $\omega=\Psi_\mathrm{DL}\,\beta$, (94) yields the positive semidefiniteness

$$b(D\beta,\beta) = |\mathrm{d}\omega|^2_{L^2(\Omega\cup\Omega^\mathrm{c})} \geq 0,$$

where we used Lemma 10 and definition (81e). □

Remark 20. The proof of (91d) critically hinges on the fact that $\delta\mathrm{d}\omega=0$. In the light of (23a) and (23b), this requires $\gamma\in H_\parallel^{-1/2}\Lambda^p(\delta 0,\Gamma)$ rather than $\gamma\in H_\parallel^{-1/2}\Lambda^p(\delta,\Gamma)$.

6 Boundary Integral Equations

In this section we discuss Calderón projectors and their properties under dual transformations. To study the case $k = 0$ we introduce quotient spaces with respect to exact forms on the space of Maxwell solutions and the space of Dirichlet data, respectively. In a slight abuse of notation, we work with representatives of the equivalence classes as if they were actual elements of the quotient spaces.

6.1 Calderón Projector for Interior and Exterior Problems

Up to now, we have considered the representation formula for the domain $\Omega \cup \Omega^{\mathrm{c}}$. The boundary data have been defined in terms of the jumps on Γ of Dirichlet, Neumann, and normal traces, respectively. In this section, we treat the interior domain Ω and the exterior domain Ω^{c} separately.

An *interior problem* is a Maxwell-type problem with the additional requirement that $\omega = 0$ in Ω^{c}. The solution space effectively reduces to $X(\Omega)$. For an *exterior problem* we require that $\omega = 0$ in Ω, and its solutions therefore lie in $X(\Omega^{\mathrm{c}})$. Hence the boundary data acquire status of *Cauchy data* for the respective problem.

Applying the Dirichlet trace γ_{D} and the Neumann trace γ_{N}, respectively, to the representation formula (47) yields the *Calderón equations*

$$\begin{pmatrix} \gamma_{\mathrm{D}} \\ \gamma_{\mathrm{N}} \end{pmatrix} \omega = P \begin{pmatrix} \gamma_{\mathrm{D}} \\ \gamma_{\mathrm{N}} \\ \mathrm{n} \end{pmatrix} \omega \tag{97}$$

for the interior problem, where

$$P = \tfrac{1}{2} I + A.$$

For the exterior problem, all traces in (97) have to be replaced by the exterior traces, and P reads

$$P = \tfrac{1}{2} I - A.$$

We have

$$I = \begin{pmatrix} \mathrm{Id} & 0 & 0 \\ 0 & \mathrm{Id} & 0 \end{pmatrix},$$

$$A = \begin{pmatrix} \{\gamma_{\mathrm{D}}\} \\ \{\gamma_{\mathrm{N}}\} \end{pmatrix} \begin{pmatrix} -\Psi_{\mathrm{DL}} & \Psi_{\mathrm{SL}} & \mathrm{d}\Psi_{\mathrm{SL}} \end{pmatrix} = \begin{pmatrix} -K & V & \mathrm{d}V \\ D & K^{\dagger} & 0 \end{pmatrix}.$$

To arrive at the usual square form of P, the extra Neumann data $\mathrm{n}\omega$ needs to be eliminated. P is then called the *Calderón projector*. We distinguish two cases:

1. *Case* $k \neq 0$. The goal is achieved by leveraging (48) and using the Maxwell single layer potential. With $Z = H_{\perp}^{-1/2}\Lambda^p(\mathrm{d},\Gamma) \times H_{\parallel}^{-1/2}\Lambda^p(\delta,\Gamma)$ we obtain

$$A = \begin{pmatrix} -K & \tilde{V} \\ D & K^\dagger \end{pmatrix} : Z \to Z. \tag{98}$$

2. *Case* $k = 0$. We eliminate the extra Neumann data by projecting the first Calderón equation onto the quotient space

$$[H_\perp^{-1/2}\Lambda^p(\mathrm{d},\Gamma)] = H_\perp^{-1/2}\Lambda^p(\mathrm{d},\Gamma)/\mathrm{d}H_\perp^{-1/2}\Lambda^{p-1}(\mathrm{d},\Gamma). \tag{99}$$

Exact forms are mapped to zero, therefore the term containing the extra Neumann data vanishes. Inspection of (82c) and (82d) reveals that K and D are well defined on the quotient space. Moreover, from (48) we know that $\gamma \in H_\parallel^{-1/2}\Lambda^p(\delta 0,\Gamma)$. Let $Z^0 = [H_\perp^{-1/2}\Lambda^p(\mathrm{d},\Gamma)] \times H_\parallel^{-1/2}\Lambda^p(\delta 0,\Gamma)$, to obtain

$$A^0 = \begin{pmatrix} -K & V \\ D & K^\dagger \end{pmatrix} : Z^0 \to Z^0. \tag{100}$$

The mapping property of the second equation can be seen from (82b) and (82d).

Galerkin boundary element methods are based on a variational formulation of the Calderón projector. Again, we distinguish the two cases:

1. *Case* $k \neq 0$. Following [12, Sect. 3.4][10], we introduce the *antisymmetric bilinear* form

$$B : Z \times Z \to \mathbb{C} : \left(\begin{pmatrix}\beta\\ \gamma\end{pmatrix}, \begin{pmatrix}\beta'\\ \gamma'\end{pmatrix}\right) \mapsto \frac{1}{k}\big(b(\gamma,\overline{\beta}') - b(\gamma',\overline{\beta})\big),$$

where the factor $1/k$ is conventional. The related variational form of the boundary integral operator A is

$$\mathscr{A} : Z \times Z \to \mathbb{C} : (\alpha,\alpha') \mapsto B(A\alpha,\alpha').$$

As a consequence of (83) we note that

$$\mathscr{A}(\alpha,\alpha') = \mathscr{A}(\alpha',\alpha)$$

holds, which generalizes [12, Thm. 3.9].

2. *Case* $k = 0$. We introduce the symmetric form

$$B^0 : Z^0 \times Z^0 \to \mathbb{C} : \left(\begin{pmatrix}\beta\\ \gamma\end{pmatrix}, \begin{pmatrix}\beta'\\ \gamma'\end{pmatrix}\right) \mapsto b(\gamma,\beta') + b(\gamma',\beta),$$

which is non degenerate, since $[H_\perp^{-1/2}\Lambda^p(\mathrm{d},\Gamma)]$ and $H_\parallel^{-1/2}\Lambda^p(\delta 0,\Gamma)$ are dual spaces with respect to the sesquilinear form $b(\cdot,\cdot)$. The related variational form of the boundary integral operator A^0 is

$$\mathscr{A}^0 : Z^0 \times Z^0 \to \mathbb{C} : (\alpha,\alpha') \mapsto B^0(A^0\alpha,\alpha').$$

[10] When comparing with [12], the following identifications hold: $\gamma_\mathrm{D} \to *\gamma_\mathrm{D}$, $k\gamma_\mathrm{N} \to -\gamma_\mathrm{N}$, $b(\mathbf{v},\mathbf{w}) \to -b(\nu, *\overline{\omega})$, $M \to K^\dagger$, $C \to -k*\tilde{V}$, $\mathbf{m} \to *\beta$, $k\mathbf{j} \to -\gamma$.

It holds that

$$\mathscr{A}^0(\alpha,\alpha) \geq c\big(|\mathrm{d}\beta|^2_{H_\perp^{-1/2}\Lambda^{p+1}(\mathrm{d},\Gamma)} + |\gamma|^2_{H_\parallel^{-1/2}\Lambda^p(\delta,\Gamma)}\big) \quad \forall \alpha = \begin{pmatrix}\beta\\ \gamma\end{pmatrix} \in Z^0,$$

as a consequence of (83) and (91), which is useful for establishing coercivity. The boundary integral operator in its variational form $\mathscr{A}^0$ is a major building block for the Galerkin boundary element methods presented in [18, 19].

6.2 Equivalent Maxwell-Type Problems, Dual Transformations

There is an inherent symmetry in the solution set $X^p(\Omega \cup \Omega^c)$ that can be exploited by so-called dual transformations. To show this, we need to distinguish the cases $k \neq 0$ and $k = 0$:

1. *Case $k \neq 0$.* The *dual transformation for $k \neq 0$* is defined by

$$\Phi : \omega \mapsto \tfrac{1}{ik} * \mathrm{d}\omega. \tag{101}$$

Lemma 14. *The dual transformation* (101) *constitutes an isomorphism $X^p(\Omega \cup \Omega^c) \to X^{q-1}(\Omega \cup \Omega^c)$.*

Proof. We first show that $\Phi : X^p(\Omega \cup \Omega^c) \to Y^{q-1}(\Omega \cup \Omega^c)$ is injective, and then, that the image of Φ fulfills the radiation condition and hence lies in $X^{q-1}(\Omega \cup \Omega^c)$.

Let $\tilde{\omega} = \Phi\omega$. Since $\omega \in X^p(\Omega \cup \Omega^c)$ we know at least that $\tilde{\omega} \in H_{\mathrm{loc}}\Lambda^{q-1}(\mathrm{d}, \Omega \cup \Omega^c)$ and can compute

$$(-1)^{p+1} *^{-1} \mathrm{d}\tilde{\omega} = \tfrac{1}{ik}\delta\mathrm{d}\omega = -ik\omega \in H_{\mathrm{loc}}\Lambda^p(\delta\mathrm{d}, \Omega \cup \Omega^c). \tag{102}$$

We are therefore entitled to apply $*\mathrm{d}$ to find

$$\delta\mathrm{d}\tilde{\omega} = k^2\tilde{\omega},$$

which implies $\tilde{\omega} \in Y^{q-1}(\Omega \cup \Omega^c)$. From (102) we read off

$$\omega = (-1)^{p(q-1)}\tfrac{1}{ik} * \mathrm{d}\tilde{\omega},$$

which shows that

$$\Phi^2\omega = (-1)^{p(q-1)}\omega, \quad \omega \in X^p(\Omega \cup \Omega^c),$$

that is, Φ is injective.

It is of advantage to introduce a slightly different form of the radiation condition in connection with the above dual transformation. The condition is stated in terms of both, ω and $\tilde{\omega}$, and reads [29, Def. 3.2 (iii)][11]

[11] When comparing with [29], the correct identifications are $(\omega, \tilde{\omega}) = (E, -*H)$. Moreover, $\omega \in L^{2,p}_{>-\frac{1}{2}}(\Omega)$ is a weak version of $|\omega|_{\imath X} = o(R^{-(n-1)/2})$.

$$\left.\begin{aligned} |\mathrm{i}_{\mathbf{n}} *^{-1} \tilde{\omega} - \omega|_{\imath X} &= o(R^{-(n-1)/2}), \\ |\mathrm{i}_{\mathbf{n}} * \omega - (-1)^p \tilde{\omega}|_{\imath X} &= o(R^{-(n-1)/2}). \end{aligned}\right\} \tag{103}$$

X denotes an arbitrary point on Γ^R. The condition is invariant under dual transformations. Indeed, if we replace $(\omega, \tilde{\omega})$ by $\Phi(\omega, \tilde{\omega}) = \big(\tilde{\omega}, (-1)^{p(q-1)}\omega\big)$, and p by $q-1$, then the equations (103) just exchange their roles.
The first equation in connection with (101) is identical to (40). To investigate the second equation let us study its tangential and normal traces on Γ^R, more specifically

$$\begin{aligned} (-1)^{p+1} ik *^{-1} \mathrm{t}^R \big(\mathrm{i}_{\mathbf{n}} * \omega - (-1)^p \tilde{\omega}\big) &= (\gamma_{\mathrm{N}}^R - ik\gamma_{\mathrm{D}}^R)\omega, \quad \text{and} \\ ik *^{-1} \mathrm{n}^R \big(\mathrm{i}_{\mathbf{n}} * \omega - (-1)^p \tilde{\omega}\big) &= \mathrm{d}\gamma_{\mathrm{D}}^R \omega. \end{aligned}$$

While the tangential part is equivalent to the first equation of (39), the normal part gives an additional condition. We have thus shown that (103) is equivalent to (39) plus

$$|\mathrm{d}\gamma_{\mathrm{D}}^R \omega|_X = o(R^{-(n-1)/2}), \tag{104}$$

which fixes the asymptotic behaviour of the tangential derivatives. However, it can be shown that solutions of the Maxwell-type equation subject to radiation condition (40) necessarily fulfill (104), so that we see that no additional constraint has been introduced. This is related to the asympotic behavior (64b) of the fundamental solution.[12]

It follows from the equivalence of (103) and (40) and from the invariance of (103) under dual transformations, that Φ maps to $X^{q-1}(\Omega \cup \Omega^{\mathrm{c}})$. □

Remark 21. For $n = 3$, $p = 1$, the dual transformation (101) describes the symmetry between electric and magnetic fields encountered in the propagation of harmonic waves in simple media.

Let $(\mathbf{E}, \mathbf{H})$ denote the vector proxies of the 1-forms $(\omega, \tilde{\omega})$. Then (101) and (103) read

$$\mathbf{H} = \frac{1}{ik}\mathbf{curl}\,\mathbf{E}$$

and

$$\begin{aligned} |\mathbf{H} \times \mathbf{n} - \mathbf{E}|_{\imath X} &= o(R^{-1}), \\ |\mathbf{E} \times \mathbf{n} + \mathbf{H}|_{\imath X} &= o(R^{-1}), \end{aligned}$$

respectively, compare [14, Thm. 6.4, Def. 6.5]. This is yet another way to state the Silver-Müller radiation conditions.

[12] Compare also [14, p. 163], which says that both equations (103) are equivalent for $n = 3$, $p = 1$.

We introduce an adapted set of trace operators

$$\widetilde{\gamma}_{\mathrm{D}} = ik\gamma_{\mathrm{D}} : H\Lambda^p(\mathrm{d},\Omega) \quad \to H_{\perp}^{-1/2}\Lambda^p(\mathrm{d},\Gamma),$$
$$\widetilde{\gamma}_{\mathrm{N}} = *\gamma_{\mathrm{N}} : \; H\Lambda^p(\delta\mathrm{d},\Omega) \to H_{\perp}^{-1/2}\Lambda^{q-1}(\mathrm{d},\Gamma).$$

It is easy to see from the definitions that these trace operators fulfill

$$\widetilde{\gamma}_{\mathrm{D}} = (-1)^{p(q-1)}\widetilde{\gamma}_{\mathrm{N}}\Phi, \tag{105a}$$
$$\widetilde{\gamma}_{\mathrm{N}} = \widetilde{\gamma}_{\mathrm{D}}\Phi. \tag{105b}$$

In sum, Φ maps Maxwell solutions onto Maxwell solutions and interchanges the roles of the adapted boundary data, up to sign.

This symmetry can be exploited to render (98) in the following symmetric form

$$\tfrac{1}{2}\begin{pmatrix}\widetilde{\gamma}_{\mathrm{D}}\omega\\ \widetilde{\gamma}_{\mathrm{N}}\omega\end{pmatrix} = \begin{pmatrix}-K & (-1)^{p(q-1)}C\\ C & -K\end{pmatrix}\begin{pmatrix}\widetilde{\gamma}_{\mathrm{D}}\omega\\ \widetilde{\gamma}_{\mathrm{N}}\omega\end{pmatrix}, \tag{106}$$

where we introduced a boundary integral operator C according to

$$C = ik\tilde{V}* : H_{\perp}^{-1/2}\Lambda^p(\mathrm{d},\Gamma) \to H_{\perp}^{-1/2}\Lambda^{q-1}(\mathrm{d},\Gamma), \quad k \neq 0,$$

and used (82a) and (82f).
From (105) it can be inferred that the Calderón equation (106) is invariant under dual transformations (101), up to sign.

Remark 22

1. This result implies that electric field and magnetic field based formulations share the same Calderón equation (106), up to sign of the off-diagonal elements.
2. The analysis of Maxwell transmission problems in Lipschitz domains in [12, p. 468] is essentially based on the Calderón projector in (106). [13]

2. *Case $k = 0$.* We first define a quotient space on $X^p(\Omega \cup \Omega^{\mathrm{c}})$ by

$$X_0^p(\Omega \cup \Omega^{\mathrm{c}}) = X^p(\Omega \cup \Omega^{\mathrm{c}}) \cap \mathrm{d}H\Lambda^{p-1}(\mathrm{d},\Omega \cup \Omega^{\mathrm{c}}),$$
$$[X^p(\Omega \cup \Omega^{\mathrm{c}})] = X^p(\Omega \cup \Omega^{\mathrm{c}})/X_0^p(\Omega \cup \Omega^{\mathrm{c}}). \tag{107}$$

The *dual transformation for $k = 0$*

$$\Phi^0 : [X^p(\Omega \cup \Omega^{\mathrm{c}})] \to [X^{q-2}(\Omega \cup \Omega^{\mathrm{c}})] : \omega \mapsto \tilde{\omega}$$

[13] The formulation in [12] can be stated in $H_{\|}^{-1/2}\Lambda^1(\delta,\Gamma)$ with the help of the translation isomorphisms. The following identifications hold: $ik\gamma_{\mathrm{D}} \to *\widetilde{\gamma}_{\mathrm{D}}$, $k\gamma_{\mathrm{N}} \to *\widetilde{\gamma}_{\mathrm{N}}$, $C \to i*C*^{-1}$, $M \to -*^{-1}K*$.

can be defined implicitly, in two equivalent ways:

1. The dual transformation fulfills

$$\mathrm{d}\tilde{\omega} = *\mathrm{d}\omega. \tag{108}$$

Extend the definition (46) of the boundary data (β,γ) to the quotient spaces (99) and (107). Applying $[\![\mathrm{t}]\!]$ and $[\![\mathrm{n}]\!]$, and using (27) and (28), it can be seen that (108) implies a transformation

$$\begin{aligned}&[H_{\perp}^{-1/2}\Lambda^{p}(\mathrm{d},\Gamma)]\times H_{\parallel}^{-1/2}\Lambda^{p}(\delta 0,\Gamma)\\ \to\ &[H_{\perp}^{-1/2}\Lambda^{q-2}(\mathrm{d},\Gamma)]\times H_{\parallel}^{-1/2}\Lambda^{q-2}(\delta 0,\Gamma):\\ &(\beta,\gamma)\mapsto(\tilde{\beta},\tilde{\gamma})\end{aligned}$$

so that

$$\left.\begin{aligned}\mathrm{d}\tilde{\beta} &= *\gamma,\\ \tilde{\gamma} &= (-1)^{p+1} * \mathrm{d}\beta.\end{aligned}\right\} \tag{109}$$

2. Building on (109), we may also define the dual transformation by

$$\tilde{\omega} = \Psi_{\mathrm{SL}}\tilde{\gamma} - \Psi_{\mathrm{DL}}\tilde{\beta}. \tag{110}$$

Lemma 15. *The two definitions* (108) *and* (110) *of the dual transformation are well defined; they are equivalent and constitute an isomorphism.*

Proof. We first show that (110) is well defined and implies (108). Check that for $\omega \in [X^{p}(\Omega\cup\Omega^{\mathrm{c}})]$ the boundary data (β,γ) in (109) are well defined. Since $*\gamma$ is closed, it can be represented by a potential $\tilde{\beta}$. In general, there might be a contribution from cohomology as well, which can be discarded, since we restricted ourselves to trivial topology. Existence of the potential is guaranteed from the exact sequence property (26). The potential is defined up to exact forms, so it corresponds to exactly one element of the quotient space $[H_{\perp}^{-1/2}\Lambda^{q-2}(\mathrm{d},\Gamma)]$.[14] The last equation in (109) poses no further difficulties.

Equation (110) results from the representation formula (47), when applied to $(\tilde{\beta},\tilde{\gamma})$ and projected onto the quotient spaces. The exact potential $\mathrm{d}\Psi_{\mathrm{SL}}\varphi$ lies in the zero class and therefore does not appear in (110). In the light of (23e), a different choice of the representative $\tilde{\beta}$ in (109) leads to a different representative $\tilde{\omega}$ in (110). However, the map is well defined in terms of the quotient spaces. The definition via the representation formula ensures that $\tilde{\omega}\in[X^{q-2}(\Omega\cup\Omega^{\mathrm{c}})]$. We have thus shown that the dual transformation Φ^{0} based on (109) and (110) is well defined.

[14] We consider (109) as a mere theoretical device, but it has also profound practical implications. For $n=3$, $p=1$ $\tilde{\beta}$ is a scalar potential. In [18, Ch. 8], a scalar stream function $\tilde{\beta}_h$ is employed on the discrete level to span solenoidal surface Raviart-Thomas covector fields γ_h. This provides a discrete subspace of $H_{\parallel}^{-1/2}\Lambda^{1}(\delta 0,\Gamma)$.

To show that $\tilde{\omega}$ fulfills (108) we first represent ω in terms of its boundary data (β,γ), in analogy to (110), and apply $*\mathrm{d}$. We obtain

$$\begin{aligned} *\mathrm{d}\omega &= *\mathrm{d}\Psi_{\mathrm{SL}}\gamma - *\mathrm{d}\Psi_{\mathrm{DL}}\beta \\ &= -\Psi_{\mathrm{DL}} * \gamma + (-1)^{p+1}\mathrm{d}\Psi_{\mathrm{SL}} * \mathrm{d}\beta, \end{aligned}$$

where we used (21b) and (23f). When we plug in (109) this yields

$$*\mathrm{d}\omega = \mathrm{d}(\Psi_{\mathrm{SL}}\tilde{\gamma} - \Psi_{\mathrm{DL}}\tilde{\beta}) = \mathrm{d}\tilde{\omega},$$

which proves the assertion.

Next we show that (108) is well defined and implies (110). Existence of $\tilde{\omega}$ is guaranteed from the first part of the proof. Uniqueness can be seen as follows: We know that (108) implies (109). If there were several solutions for $\tilde{\omega}$, their boundary data $(\tilde{\beta},\tilde{\gamma})$ had to coincide, because we know from the first part of the proof that (109) fixes $(\tilde{\beta},\tilde{\gamma})$ for given (β,γ). But from Theorem 1 we know that elements of $[X^{q-2}(\Omega\cup\Omega^{\mathrm{c}})]$ can be uniquely represented in terms of their boundary data. Therefore $\tilde{\omega}$ is unique and coincides with the solution obtained from (110).

It remains to show that Φ^0 constitutes an isomorphism. To that end we apply the map (109) to the boundary data twice, which yields

$$(\tilde{\tilde{\beta}},\tilde{\tilde{\gamma}}) = (-1)^{(p+1)(q-1)}(\beta,\gamma).$$

Arguing like in the second part reveals

$$(\Phi^0)^2\omega = (-1)^{(p+1)(q-1)}\omega, \quad \omega\in[X^p(\Omega\cup\Omega^{\mathrm{c}})], \tag{111}$$

which concludes the proof. □

We introduce yet another set of trace operators

$$\begin{aligned} \tilde{\gamma}_{\mathrm{D}}^0 = \mathrm{d}\gamma_{\mathrm{D}}: &\qquad H\Lambda^p(\mathrm{d},\Omega) \to H_{\perp}^{-1/2}\Lambda^{p+1}(\mathrm{d},\Gamma), \\ \tilde{\gamma}_{\mathrm{N}}^0 = \tilde{\gamma}_{\mathrm{N}} = *\gamma_{\mathrm{N}}: &\, H\Lambda^p(\delta\mathrm{d},\Omega) \to H_{\perp}^{-1/2}\Lambda^{q-1}(\mathrm{d},\Gamma). \end{aligned}$$

Note that $\tilde{\gamma}_{\mathrm{D}}^0$ and $\tilde{\gamma}_{\mathrm{N}}^0$ are well defined on $[X^p(\Omega)]$. From (108) and (111) it is immediate that these trace operators fulfill

$$\tilde{\gamma}_{\mathrm{D}}^0 = (-1)^{(p+1)(q-1)}\tilde{\gamma}_{\mathrm{N}}^0\Phi^0, \tag{112a}$$

$$\tilde{\gamma}_{\mathrm{N}}^0 = \tilde{\gamma}_{\mathrm{D}}^0\Phi^0. \tag{112b}$$

Equation (100) can be rearranged in the following symmetric form

$$\tfrac{1}{2}\begin{pmatrix}\widetilde{\gamma}_{\mathrm{D}}^{0}\omega\\ \widetilde{\gamma}_{\mathrm{N}}^{0}\omega\end{pmatrix}=\begin{pmatrix}-K & (-1)^{(p+1)(q-1)}B\\ B & -K\end{pmatrix}\begin{pmatrix}\widetilde{\gamma}_{\mathrm{D}}^{0}\omega\\ \widetilde{\gamma}_{\mathrm{N}}^{0}\omega\end{pmatrix},\tag{113}$$

$p=\deg\omega$, where we introduced a boundary integral operator B according to

$$B=(-1)^{p}\mathrm{d}V*:H_{\perp}^{-1/2}\Lambda^{p}(\mathrm{d},\Gamma)\to H_{\perp}^{-1/2}\Lambda^{q}(\mathrm{d},\Gamma),$$

and used (82a), (82c) and (82d). From (112) it can be inferred that Calderón equation (113) is invariant under dual transformations (108), up to sign.

For $n=3$, $p=1$ this invariance means that magnetostatic vector-potential and scalar-potential formulations share basically the same Calderón equation (113). This confirms the observation in [18, Sect. 9] which states that the boundary integral operators associated with the **curlcurl** equation are structurally equal to those of scalar second order elliptic problems.
Let $\gamma_n\mathbf{B}\in H^{-1/2}(\partial\Omega)$ be the normal trace of the magnetic flux density, and $\gamma_\tau\mathbf{H}\in\mathbf{H}^{-1/2}(\mathrm{div}_\Gamma 0,\partial\Omega)$ the tangential trace of the magnetic field. Equation (113) translates for $n=3$, $p=1$ into

$$\tfrac{1}{2}\begin{pmatrix}\gamma_n\mathbf{B}\\ \gamma_\tau\mathbf{H}\end{pmatrix}=\begin{pmatrix}\mathsf{K}^{\dagger} & \mathrm{curl}_\Gamma\mathsf{A}\\ \mathbf{curl}_\Gamma\mathsf{V} & \mathsf{B}\end{pmatrix}\begin{pmatrix}\gamma_n\mathbf{B}\\ \gamma_\tau\mathbf{H}\end{pmatrix}.\tag{114}$$

The flux density can be represented by a magnetic vector potential $\mathbf{A}$, where $\pi_\tau\mathbf{A}\in\mathbf{H}^{-1/2}(\mathrm{curl}_\Gamma,\partial\Omega)$, $\gamma_n\mathbf{B}=\gamma_n\mathbf{curlA}=\mathrm{curl}_\Gamma\pi_\tau\mathbf{A}$. Moreover, for a trivial topology, the magnetic field can be represented by a magnetic scalar potential ψ, where $\gamma\psi\in H^{1/2}(\partial\Omega)$, $\gamma_\tau\mathbf{H}=\gamma_\tau\mathbf{grad}\psi=\mathbf{curl}_\Gamma\gamma\psi$. Equation (114) may be expressed in terms of these potentials in different ways. The operators curl_Γ and $\mathbf{curl}_\Gamma$ inherit L^2 adjointness from d and δ, which is useful to proceed to variational forms of the equations.
All the formulations have in common that they are built upon the scalar and vectorial single and double layer operators, plus straightforward surface curl operators. Hence only this set of boundary-integral operators needs to be implemented to cover both, scalar and vector potential formulations.

7 Conclusions

We have shown that the theory of boundary-integral equations for Maxwell-type problems can be formulated entirely in the framework of differential-form calculus. The basic toolkit is given by Sobolev spaces on the problem domain and their traces on the domain's Lipschitz boundary, as well as by integral transformations and fundamental solutions of Maxwell-type equations. The presented proofs concerning the representation formula, layer potentials, and boundary-integral operators

follow the strategies of classical vector-analysis literature. Their scope, however, extends beyond scalar- or vector-potential formulations in dimensions two and three. Nonetheless, it is the authors' opinion that the main advantage of employing differential-form calculus in this field of applied mathematics does not lie in the prospect of extending the theory beyond three dimensions; it lies in the emphasis that is put on structural considerations and abstract viewpoints. For instance consider the properties of layer potentials and boundary integral operators that are presented in Lemmata 3 and 11, respectively. As a further example, we have presented the invariance of the Calderón projectors under dual transformations, which not only strikes us by its elegance, but also has a direct impact on our implementation of the boundary-element method for magnetostatics: in three dimensions, a single set of boundary integral operators covers both, the scalar- and the vector-potential case.

Acknowledgements. The authors would like to thank Ralf Hiptmair for feedback and valuable suggestions.

References

[1] Ammari, H., Buffa, A., Nédélec, J.C.: A justification of eddy currents model for the Maxwell equations. SIAM J. Appl. Math. 60(5), 1805–1823 (2000)
[2] Arnold, D.N., Falk, R.S., Winther, R.: Finite element exterior calculus, homological techniques, and applications. Acta Numerica 15, 1–155 (2006)
[3] Bossavit, A.: On the representation of differential forms by potentials in dimension 3. In: van Rienen, U., Günther, M., Hecht, D. (eds.) Scientific Computing in Electrical Engineering. LNCSE, vol. 18, pp. 97–104. Springer, Berlin (2001)
[4] Buffa, A.: Hodge decompositions on the boundary of a polyhedron: The non-simply connected case. Math. Models Meth. Appl. Sciences 11(9), 1491–1503 (2001)
[5] Buffa, A.: Trace theorems on non-smooth boundaries for functional spaces related to Maxwell equations: an overview. In: Carstensen, C., et al. (eds.) Computational Electromagnetics. LNCSE, vol. 28, pp. 23–34. Springer, Heidelberg (2003)
[6] Buffa, A.: Remarks on the discretization of some nonpositive operators with application to heterogeneous Maxwell problems. SIAM J. Numer. Anal. 43(1), 1–18 (2005)
[7] Buffa, A., Christiansen, S.: A dual finite element complex on the barycentric refinement. Math. Comp. 76(260), 1743–1769 (2007)
[8] Buffa, A., Ciarlet Jr., P.: On traces for functional spaces related to Maxwell's equations Part I: An integration by parts formula in Lipschitz polyhedra. Math. Meth. Appl. Sci. 24, 9–30 (2001)
[9] Buffa, A., Ciarlet Jr., P.: On traces for functional spaces related to Maxwell's equations Part II: Hodge decompositions on the boundary of Lipschitz polyhedra and applications. Math. Meth. Appl. Sci. 24, 31–48 (2001)
[10] Buffa, A., Costabel, M., Schwab, C.: Boundary element methods for Maxwell equations in non-smooth domains. Numer. Math. 92(4), 679–710 (2002)
[11] Buffa, A., Costabel, M., Sheen, D.: On traces for $\mathbf{H}(\mathbf{curl}, \Omega)$ in Lipschitz domains. J. Math. Anal. Appl. 276, 845–867 (2002)
[12] Buffa, A., Hiptmair, R., von Petersdorff, T., Schwab, C.: Boundary element methods for Maxwell transmission problems in Lipschitz domains. Numer. Math. 95, 459–485 (2003)

[13] Christiansen, S.: Mixed boundary element method for eddy current problems. Tech. Rep. 2002-16, Seminar für Angewandte Mathematik, ETH Zürich (2002)
[14] Colton, D., Kress, R.: Inverse acoustic and electromagnetic scattering theory. Springer, Berlin (1998)
[15] Greub, W.: Multilinear Algebra. Springer, Berlin (1967)
[16] Hehl, F., Obukhov, Y.: Foundations of Classical Electrodynamics. Birkhäuser, Boston (2003)
[17] Hiptmair, R.: Finite elements in computational electromagnetism. Acta Numerica 11, 237–339 (2002)
[18] Hiptmair, R.: Symmetric coupling for eddy current problems. SIAM J. Numer. Anal. 40(1), 41–65 (2003)
[19] Hiptmair, R.: Boundary element methods for eddy current computation. In: Boundary Element Analysis. LNACM, vol. 29, pp. 213–248. Springer, Berlin (2007)
[20] Jänich, K.: Vector Analysis. Springer, Berlin (2001)
[21] Jawerth, B., Mitrea, M.: Higher dimensional electromagnetic scattering theory on C^1 and Lipschitz domains. American J. Math. 117(4), 929–963 (1995)
[22] Kotiuga, R.: Weitzenböck identities and variational formulations in nanophotonics and micromagnetics. IEEE Trans. Magn. 43(4), 1669–1672 (2007)
[23] Kress, R.: Potentialtheoretische Randwertprobleme bei Tensorfeldern beliebiger Dimension und beliebigen Ranges. Arch. Ration. Mech. Anal. 47, 59–80 (1972)
[24] Kurz, S., Auchmann, B., Flemisch, B.: Dimensional reduction of field problems in a differential-form framework. COMPEL 28(4), 907–921 (2009)
[25] Kythe, P.K.: Fundamental Solutions for Differential Operators and Applications. Birkhäuser, Boston (1996)
[26] Maue, A.W.: Zur Formulierung eines allgemeinen Beugungsproblems durch eine Integralgleichung. Z. Physik A 126, 601–618 (1949)
[27] McLean, W.: Strongly Elliptic Systems and Boundary Integral Equations. Cambridge University Press, Cambridge (2000)
[28] Nédélec, J.C.: Integral equations with non integrable kernels. Integral Eqn. Oper. Th. 5, 562–572 (1982)
[29] Pauly, D.: Low frequency asymptotics for time-harmonic generalized Maxwell equations in nonsmooth exterior domains. Adv. Math. Sci. Appl. 16(2), 591–622 (2006)
[30] de Rham, G.: Differentiable Manifolds. Springer, Berlin (1984)
[31] Rota, G.C.: Indiscrete Thoughts. Birkhäuser, Boston (2000)
[32] Stratton, J.: Electromagnetic Theory. McGraw-Hill Book Company, New York (1941)
[33] Tai, C.T.: Dyadic Green's functions in electromagnetic theory. IEEE Press, Piscataway (1994)
[34] Tucker, R.W.: Differential form valued forms and distributional electromagnetic sources. J. Math. Phys. 50(3) (2009)
[35] Warnick, K., Arnold, D.: Electromagnetic Green functions using differential forms. J. Electromagn. Waves Appl. 10(3), 427–438 (1996)
[36] Weck, N.: Traces of differential forms on Lipschitz boundaries. Internat. Math. J. Anal. Appl. 24(2), 147–169 (2004)
[37] Weck, N., Witsch, K.: Generalized spherical harmonics and exterior differentiation in weighted Sobolev spaces. Math. Meth. Appl. Sci. 17(13), 1017–1043 (1994)
[38] Weyl, H.: Die natürlichen Randwertaufgaben im Außenraum für Strahlungsfelder beliebiger Dimension und beliebigen Ranges. Math. Z. 56(2), 105–119 (1952)

Discrete Electromagnetism with Shape Forms of Higher Polynomial Degree

Marvin Fleck and Sergej Rjasanow

Abstract. The classical Discrete Electromagnetism (DEM) uses a set of discrete differential forms and associated discrete operators for treatment of electromagnetic PDEs. The operators originate from a differential form representation and can be classified as metric-dependent and metric-independent ones. The appearance of the discretised operators depends on the underlying shape functions. While the lowest order version using Whitney elements is well known for its simple structure, a "natural" extension to higher polynomial degrees has yet to be found. We present a higher order Discrete Electromagnetism using a hierarchical set of shape forms. Our focus of interest lies on the magneto(quasi)static formulation of Maxwell's equations.

1 Introduction

The Discrete Electromagnetism (DEM) introduces discrete fields and operators which are derived from a differential form representation of electromagnetic PDEs. Discrete fields are represented by vectors of their degrees of freedom. In the low order case they coincide with co-chains, i.e. there is one degree of freedom per element. The discrete operators can be classified as metric-dependent material Hodge operators and metric-independent derivative and trace operators. Problems are treated on an oriented cell complex and its topologically dual complex. Degrees of freedom are localized on either of these complexes according to Tonti's diagram (Fig. 1). This localization coincides with the distinction of ordinary (Faraday complex) and twisted (Ampère-Maxwell complex) differential forms [7]. However, explicit construction of dual complexes can be avoided by making use of so-called pairing matrices [2, 13] which convert degrees of freedom on the primal complex to d.o.f.'s on its dual. We will limit ourselves to simplicial complexes and their barycentric duals.

Marvin Fleck · Sergej Rjasanow
Universität des Saarlandes, Fachrichtung Mathematik, 66123 Saarbrücken, Germany
e-mail: fleck@num.uni-sb.de, rjasanow@num.uni-sb.de

U. Langer et al. (Eds.): Fast Boundary Element Methods, LNACM 63, pp. 63–92.
springerlink.com

The classical (low order) DEM is based on Whitney forms [3, 24], which are a realization of Nédélec elements of first kind and Raviart-Thomas-Nédélec elements respectively [16]. Whitney forms of higher polynomial order should also fall in that category. Criteria for the spaces of higher order Whitney forms and suited degrees of freedom were discussed in [14]. A realization can be found by reordering shape functions presented in [22, 25], which originally resemble Nédélec elements of second kind [17]. An alternative concept for degrees of freedom was presented by BOSSAVIT [6, 20].

We are interested in the magneto(quasi)static approximation of Maxwell's equations on a domain $\Omega \subset \mathbb{R}^3$ with time parameter τ:

$$\begin{aligned} \operatorname{curl}\frac{1}{\mu}\operatorname{curl} A(\tau,x) + \kappa\frac{\partial}{\partial\tau}A(\tau,x) &= j(\tau,x), && x\in\Omega,\ \tau>0,\\ (\gamma_N A)(\tau,x) &= \gamma(\tau,x), && x\in\partial\Omega,\ \tau>0,\\ A(0,x) &= A_0(x), && x\in\Omega \end{aligned} \tag{1}$$

with the vector potential A, the imprinted electric current density j, the magnetic permeability μ, the electric conductivity κ and the Neumann trace γ_N (see Table 4). Note that we are interested in $B = \operatorname{curl} A$ rather than in A itself. The magnetostatic case corresponds to $\kappa = 0$ and time-independent quantities A, j and γ.

In terms of differential forms this equation and the boundary and initial conditions have the shape:

$$\begin{aligned} d *_{\frac{1}{\mu}} d\bar{A} + *_\kappa \frac{\partial}{\partial\tau}\bar{A} &= \bar{j},\\ t * d\bar{A} &= \bar{\gamma},\\ \bar{A}|_{\tau=0} &= \bar{A}_0, \end{aligned} \tag{2}$$

where $\bar{A}$ and $\bar{j}$ are 1- and 2-forms respectively on Ω and $\bar{\gamma}$ is a 1-form on $\partial\Omega$. A description of the exterior derivative operator d, the Hodge operator $*$ and the trace operator t is given in Sect. 2.2. However, the actual quantity of interest is not $\bar{A}$ but $\bar{B} = d\bar{A}$. Other problems, like electrostatics, can be treated analogously.

In real-life applications often there are ferromagnetic materials involved, which have non-constant magnetic permeability μ. Unfortunately, in general this parameter is only available in the form of tables of (relatively few) measurements. Therefore approximation of material parameters is an important issue. While standard spline interpolation methods are widely used, some more sophisticated versions have been presented, e.g. [18].

In Sect. 2 we derive the magnetoquasistatic approximation of Maxwell's equations. This is done in terms of vectors as well as differential forms. For the latter we provide a brief introduction to the corresponding calculus. Sect. 3 gives a brief

description of the low order DEM based upon Whitney forms. A description of pairing matrices is included. The problem of localizing the degrees of freedom for higher order forms is discussed in Sect. 4 along with an example for shape forms, where d.o.f.'s of p-forms are restricted to chains of p-simplices. The higher order DEM introduced in Sect. 5 includes degrees of freedom localized on simplices of higher dimension. This localization on manifolds of different dimension leads to a block structure of the discrete operators. Sect. 6 deals with the approximation of non-constant material parameters and the resulting non-linearity of the equations. In Sect. 7 we present some numerical examples for the static and the quasistatic equations.

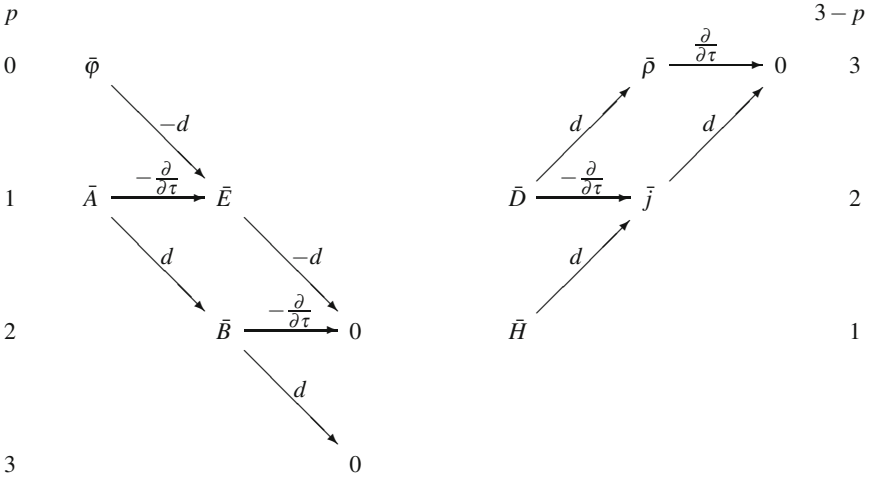

Fig. 1 Tonti diagram with Faraday complex on the left-hand side and Ampère-Maxwell complex on the right-hand side. Physical quantities are represented by p- and $3-p$-forms respectively

Ω is approximated by a simplicial complex, i.e. a mesh consisting of tetrahedra, triangles, edges and nodes. We denote this complex by C. It can be described locally by means of barycentric coordinates and their interpretation as nodal functions respectively. We use the common notation λ_i for the barycentric coordinate associated with vertex i as well as for the corresponding nodal function.

For clarity, in some examples we tag differential forms with a prefix, e.g., ${}^1\bar{\omega}$ to point out that $\bar{\omega}$ is a 1-form. In similar fashion we may write t_S for the trace operator restricting forms to the manifold S.

2 The Magnetoquasistatic Approximation of Maxwell's Equations

The interrelation between electric and magnetic fields is described by Maxwell's equations (James Clerk Maxwell; 1831-1879). However, for many problems it is sufficient to treat a reduced system of equations. In this section we describe the derivation of the magneto(quasi)static formulations of Maxwell's equations, which are well-suited for treating electromagnetic problems in accelerator magnets.

2.1 Classical Derivation

We take a look at the full system of Maxwell's equations:

$$\operatorname{curl} H = j + \frac{\partial D}{\partial \tau}, \tag{3}$$

$$\operatorname{div} B = 0, \tag{4}$$

$$\operatorname{curl} E = -\frac{\partial B}{\partial \tau}, \tag{5}$$

$$\operatorname{div} D = \rho, \tag{6}$$

completed by the material interrelations

$$B = \mu H, \tag{7}$$

$$D = \sigma E, \tag{8}$$

$$j = \kappa E + j_S. \tag{9}$$

These equations contain a total of 16 unknowns, which are of varying importance to us. The quantities which are most interesting to us are the magnetic induction B, the electric field E, the electric current density j. The material parameters which are most important to us are the magnetic permeability μ and the electric conductivity κ. For an explanation and the units of all physical quantities involved see Table 1.

In order to derive a reduced system, we rewrite the equations in a scaled form which involves characteristic time T and length L for a certain problem [19, 1]. In addition one chooses characteristic values for the magnetic induction B_0 as well as for the electric field E_0. Characteristic values μ_c, κ_c and σ_c for the material parameters are also required. The scaled physical quantities can then be written in a unit-free way:

$$\tilde{B} = \frac{B}{B_0}, \quad \tilde{H} = \frac{\mu_c H}{B_0}, \quad \tilde{j} = \frac{j}{\kappa_c E_0},$$
$$\tilde{E} = \frac{E}{E_0}, \quad \tilde{D} = \frac{D}{\sigma_c E_0}, \quad \tilde{\rho} = \frac{L\rho}{\sigma_c E_0},$$
$$\tilde{\kappa} = \frac{\kappa}{\kappa_c}, \quad \tilde{\mu} = \frac{\mu}{\mu_c}, \quad \tilde{\sigma} = \frac{\sigma}{\sigma_c}.$$

Table 1 Physical quantities and their units

quantity	description	unit
B	magnetic induction	Vs/m^2
H	magnetizing field	A/m
D	electric displacement field	As/m^2
E	electric field	V/m
j	electric current density	A/m^2
ρ	electric charge density	As/m^3
A	magnetic vector potential	Vs/m
φ	electric scalar potential	V
j_S	imprinted electric current density	A/m^2
μ	magnetic permeability	Vs/Am
σ	permittivity	As/Vm
κ	electric conductivity	A/Vm

The scaled differential operators are given by:

$$\tilde{\text{curl}} = L\,\text{curl}, \quad \tilde{\text{div}} = L\,\text{div}, \quad \frac{\partial}{\partial\tilde{\tau}} = T\frac{\partial}{\partial\tau}.$$

In addition we introduce the relaxation time T_R, the propagation speed c, i.e. the speed of light in the respective material, and the unit-free time parameter $\tilde{\tau}$:

$$T_R = \frac{\sigma_c}{\kappa_c}, \quad c = \frac{1}{\sqrt{\mu_c\sigma_c}}, \quad \tilde{\tau} = \frac{\tau}{T}.$$

Incorporating these we arrive at the scaled Maxwell equations:

$$\tilde{\text{curl}}\,\tilde{H} = \left[\frac{L}{cT_R}\frac{E_0}{cB_0}\right]\tilde{j} + \left[\frac{L}{cT}\frac{E_0}{cB_0}\right]\frac{\partial}{\partial\tilde{\tau}}\tilde{D}, \tag{10}$$

$$\tilde{\text{div}}\,\tilde{B} = 0, \tag{11}$$

$$\tilde{\text{curl}}\,\tilde{E} = -\left[\frac{L}{T}\frac{B_0}{E_0}\right]\frac{\partial}{\partial\tilde{\tau}}\tilde{B}, \tag{12}$$

$$\tilde{\text{div}}\,\tilde{D} = \tilde{\rho}. \tag{13}$$

The tilde-version of the material interrelations has the same shape as the original one. If the requirement

$$\frac{L}{cT}\frac{E_0}{cB_0} \ll 1 \tag{14}$$

is fulfilled, the system is regarded as being dominantly magnetic. If also

$$\frac{T_R}{T} \ll 1$$

is valid, the second term in (10) becomes very small in comparison to the first one and can therefore be neglected.

Remark 1. An alternative approach is to set $\sigma = 0$, which corresponds to the absence of the electrical component of field energy. By doing this, given sufficiently small values for the electric field E, we also arrive at the magnetoquasistatic approximation: From (8) it follows that $D = 0$ and therefore $\rho = 0$ due to (6).

We now can neglect the second term in (10). Equation (13) is not needed in order to obtain a complete system of equations for $\tilde{E}$, $\tilde{B}$, $\tilde{H}$ and $\tilde{j}$. Our reduced system is:

$$\tilde{\text{curl}}\, \tilde{H} = \tilde{\tilde{j}} \left(= \left[\frac{L}{cT_R} \frac{E_0}{cB_0} \right] \tilde{j} \right), \tag{15}$$

$$\tilde{\text{div}}\, \tilde{B} = 0, \tag{16}$$

$$-\frac{\partial \tilde{B}}{\partial \tilde{\tau}} = \tilde{\text{curl}}\, \tilde{\tilde{E}} \left(= \left[\frac{TE_0}{LB_0} \right] \tilde{\text{curl}} \tilde{E} \right) \tag{17}$$

with the material interrelations

$$\tilde{B} = \tilde{\mu} \tilde{H}, \tag{18}$$

$$\tilde{\tilde{j}} = \tilde{\tilde{\kappa}} \tilde{\tilde{E}} + \tilde{\tilde{j}}_S = \left[\frac{L}{cT_R} \frac{L}{cT} \right] \tilde{\kappa} \left[\frac{TE_0}{LB_0} \right] \tilde{E} + \left[\frac{L}{cT_R} \frac{E_0}{cB_0} \right] \tilde{j}_S. \tag{19}$$

This formulation accounts for eddy currents, while neclecting wave phenomena. In the following we will omit the tilde notation, keeping in mind the necessary scaling of physical quantities.

We are interested in the electromagnetics of accelerator magnets, such as used in the Large Hadron Collider (LHC) at CERN[1]. Characteristic values for this application are [1]:

$$B_0 = 1Vs/m^2, \quad c^2 = 8.98754957212 \cdot 10^{13} (m/s)^2$$
$$T = 10^{-1}s, \quad L = 10^{-1}m.$$

In order for (14) to be fulfilled also for critical values $B_c = 10^{-4}Vs/m^2$, we must require that

$$E_0 \ll 10^9 V/m,$$

which is practically always the case. Typical values for the electric field are about $E_0 = 10^{-3}V/m$.

[1] Conseil Européen pour la Recherche Nucléaire (European Organization for Nuclear Research); Geneva, Switzerland.

Potential Formulations

In order to create an equation for a single vector-valued unknown, we introduce the magnetic vector potential A as well as the electric scalar potential φ.

Lemma 1. *On a contractible domain, i.e. a domain containing no holes, for any solenoidal vector field B there is a (non-unique) vector field A such that $B = curl\, A$. Also for each vector field V, which is irrotational on such a domain, there is a (non-unique) scalar field φ such that $V = \nabla\varphi$.*

The lemma can be expressed in an elegant way in terms of differential forms (see Sect. 2.2.4). For the proof, also in terms of differential forms, see [11]. Since the lemma is not valid on domains which are topologically non-trivial, we must not exclude any cavities (non-conducting parts of the magnet) from our domain. However, if we mind this, we may reformulate (16):

$$B = \operatorname{curl} A. \tag{20}$$

The Maxwell-Faraday equation (17) now transforms to:

$$\operatorname{curl}\left(E + \frac{\partial A}{\partial \tau}\right) = 0. \tag{21}$$

Applying the lemma once more we get:

$$E = -\frac{\partial A}{\partial \tau} - \nabla\varphi. \tag{22}$$

Plugging (20) and (22) into (15)-(19) we obtain the equation

$$\operatorname{curl}\frac{1}{\mu}\operatorname{curl} A + \kappa\left(\frac{\partial A}{\partial \tau} + \nabla\varphi\right) = j_S. \tag{23}$$

However, this equation does not offer unique solutions for A and φ. For any continuously differentiable scalar field ψ the potentials can be modified without altering the fields E and B:

$$A = A' + \nabla\psi, \tag{24}$$

$$\varphi = \varphi' - \frac{\partial \psi}{\partial \tau}. \tag{25}$$

In order to obtain unique solutions, we have to introduce a gauging condition. For Finite Element Methods it is convenient to choose the so-called topological gauging $\varphi = 0$, which leads to the reduced equation:

$$\operatorname{curl}\frac{1}{\mu}\operatorname{curl} A + \kappa\frac{\partial A}{\partial \tau} = j_S. \tag{26}$$

However, note that this equation is only uniquely solvable on domains of conducting materials ($\kappa > 0$). On non-conducting subdomains we will make use of a regularization, applied to the discretized equation, that does not alter curl A.

2.2 Differential Forms

The calculus of differential forms can be utilized to express differential equations in a generalized way, which reveals geometrical invariants at play. For example the classical differential operators ∇, curl and div are pooled in a single operator, the so-called exterior derivative d. In the same manner the theorems of Green, Gauss and Stokes are expressed by the more general Stokes' theorem for differential forms:

$$\int_S d\bar{\omega} = \int_{\partial S} \bar{\omega}. \tag{27}$$

In addition to a formal definition of differential forms, in order to allow for a better acclimatization to this concept, we offer a more intuitive version [9].

2.2.1 Intuitive Definition

Informally speaking, a differential form is an integrand, i.e. an entity which can be integrated. For example, consider a smooth function $F : \mathbb{R} \to \mathbb{R}$ and its derivative

$$f = \frac{dF}{dx}.$$

Abusing notation for the sake of simplicity, we rewrite this equation, which leads to:

$$\int_{[a,b]} f dx = \int_{[a,b]} dF = \int_{\partial[a,b]} F = F(b) - F(a).$$

The integrand $f dx$ is called a 1-form, since it can be integrated over one-dimensional intervals only. In the same tenor F is a 0-form, which can be evaluated pointwise. Similarly, for a three-dimensional scalar-field $\varphi : \mathbb{R}^3 \to \mathbb{R}$ we have

$$d\varphi = \frac{\partial \varphi}{\partial x} dx + \frac{\partial \varphi}{\partial y} dy + \frac{\partial \varphi}{\partial z} dz,$$

which is a 1-form resembling $\nabla \varphi$ and can be integrated over 1D curves in $\mathbb{R}^3$. Generally speaking, a p-form is an entity, which is meant to be integrated over a p-dimensional manifold.

Keeping in mind that most physical measurements are of integral nature, we see that differential forms are a meaningful representation for physical quantities.

2.2.2 Formal Definition

Consider an n-dimensional manifold, i.e. a topological space $\mathscr{M} \subset \mathbb{R}^n$, which can locally be mapped to $\mathbb{R}^n$ by homeomorphisms. These mappings, which are named charts, determine the local structure of the manifold.

The vector space $T_x\mathscr{M}$ consists of all vectors tangent to $\mathscr{M}$ at point $x \in \mathscr{M}$:

$$T_x\mathscr{M} = \{y \in \mathbb{R}^n \mid \exists \gamma : [-1,1] \to \mathscr{M},\ \gamma(0) = x,\ \gamma'(0) = y\}. \tag{28}$$

It can therefore be identified with $\mathbb{R}^n$ itself. The definition (28) is a geometric one. There also is a popular alternative, describing tangential vectors by directional derivatives (see, e.g.,[11]). These concepts can be identified with each other. They lead to two different definitions of differential forms, which again can be identified. We will stick to the geometric description here.

A p-form $\bar{\omega}$ is an antisymmetric tensor field of rank p over $\mathscr{M}$. At each point $x \in \mathscr{M}$ it evaluates to a multi-linear mapping taking p tangential vectors (more precisely: a p-multivector composed of tangential vectors) as input and returning a real number:

$$\bar{\omega}(x) : T_x\mathscr{M} \times \ldots \times T_x\mathscr{M} \to \mathbb{R}.$$

Odd permutations of the arguments result in a change of sign. We will denote the space of (differentiable) p-forms on a manifold $\mathscr{M}$ by $\mathscr{F}^p(\mathscr{M})$. An explanation of derivatives of differential forms will follow in Sect. 2.2.4. Considering a submanifold $\mathscr{N} \subset \mathscr{M}$, a p-form on $\mathscr{N}$ is naturally induced by restricting the linear maps to the product of tangent spaces of the submanifold.

We are not bound to Cartesian coordinates to express differential forms. A change of coordinates locally induces a linear mapping in the space of tangential vectors. The coordinates of a differential form transform covariantly to the basis of this space [15]. We will make use of barycentric coordinates later on.

2.2.3 Integration of Differential Forms

In order to explain the integral of a p-form over a p-dimensional manifold, we need some definitions first.

Definition 1 (Multivectors and wedge product). Let $u, v \in V$ be two vectors in some arbitrary n-dimensional vector space V. The wedge product, or exterior product, assigns a 2-vector $u \wedge v$ to the pair $(u,v) \in V \times V$. The wedge product is linear in each factor:

$$u \wedge (\alpha v + \beta w) = \alpha(u \wedge v) + \beta(u \wedge w), \tag{29}$$

$$(\alpha u + \beta v) \wedge w = \alpha(u \wedge w) + \beta(v \wedge w), \quad \forall u, v, w \in V,\ \forall \alpha, \beta \in \mathbb{R}. \tag{30}$$

Also it is anti-symmetric

$$u \wedge v = -(v \wedge u). \tag{31}$$

From (29)-(31) it follows that the wedge product vanishes, if its factors are linearly dependent. In particular it follows that $u \wedge u = 0$. The 2-vectors span a vector space of dimension

$$\binom{n}{2} = \frac{n(n-1)}{2}, \tag{32}$$

which we will denote $\bigwedge^2 V$. In the same fashion we can construct general multivectors. Again, the wedge product is assumed to be linear in each factor. Under odd permutations of its arguments it changes sign. 0-vectors are defined as scalar values.

The wedge product can be expanded to a product acting on multivectors:

$$\wedge : \bigwedge^p V \times \bigwedge^q V \to \bigwedge^{p+q} V, \quad p,q \in \mathbb{N} \tag{33}$$

$$(u_1 \wedge \ldots \wedge u_p) \wedge (v_1 \wedge \ldots \wedge v_q) = u_1 \wedge \ldots \wedge u_p \wedge v_1 \wedge \ldots \wedge v_q. \tag{34}$$

Since differential forms are dual to fields of tangent multivectors, there is an analogous definition for the wedge product acting on differential forms:

$$\wedge : \mathscr{F}^p(\mathscr{M}) \times \mathscr{F}^q(\mathscr{M}) \to \mathscr{F}^{p+q}(\mathscr{M}), \quad p,q \in \mathbb{N}. \tag{35}$$

If fact, each p-form, $p > 1$, is a linear combination of wedge products of 1-forms. However, it is a common convention on notation to omit the wedges.

We will now introduce a concept that illustrates the connection between differential forms and scalar/vector fields. Strictly speaking this is not part of the calculus of differential forms, but rather auxiliary.

Definition 2 (Vector proxies). If $n \leq 3$, the dimension of a multivector space $\bigwedge^p V$, $0 \leq p \leq 3$, and therefore also the dimension of a space of differential forms $\mathscr{F}^p(\mathscr{M})$ on an n-dimensional manifold $\mathscr{M}$ is either 1 or n. This allows for a bijective, linear mapping between differential forms and scalar/vector fields. For a three-dimensional manifold $\mathscr{M} \subset \mathbb{R}^3$ the natural mappings are:

$$\zeta_0 : \quad 1 \quad \mapsto 1, \tag{36}$$

$$\zeta_1 : \quad dx_i \quad \mapsto e_i, \tag{37}$$

$$\zeta_2 : \quad dx_i dx_j \quad \mapsto e_k, \tag{38}$$

$$\zeta_3 : \quad dx_i dx_j dx_k \mapsto 1, \tag{39}$$

where x_i, x_j, x_k are the space coordinates up to even permutations and e_i, e_j, e_k are the associated canonical unit vectors. We call $\zeta_p(\bar{\omega})$ the vector (or scalar) proxy of the differential form $\bar{\omega}$. By duality we also obtain a version for (tangent) multivectors, which offers an extrinsic description of manifolds, in contrast to the intrinsic description offered by the tangent multivectors themselves.

Definition 3 (Simplices and barycentric coordinates). Consider the n-dimensional Euclidean space $\mathbb{R}^n$. A p-dimensional simplex S, $0 \leq p \leq n$, is defined as the non-degenerated convex hull of $p+1$ points $x_i \in \mathbb{R}^n$, $i = 1, \ldots, p+1$. If $p > 0$, its boundary is composed of $p-1$-dimensional simplices. The volume of S is given by

$$Vol(S) = \frac{|\zeta_p((x_2 - x_1) \wedge \ldots \wedge (x_{p+1} - x_1))|}{p!}. \tag{40}$$

Here ζ_p denotes the proxy for a tangent p-vector. A special attribute of simplices is, that they offer a canonical coordinate system, namely barycentric coordinates. Each point inside the simplex is uniquely determined by

$$x = \sum_{i=1}^{p+1} \lambda_i(x) x_i, \tag{41}$$

with linear coordinate functions determined by $\lambda_i(x_j) = \delta_{ij}$. As a consequence the $p+1$ coordinate functions sum up to 1 everywhere inside the simplex. For convenience one can limit oneself to the first p coordinates, keeping in mind the relation

$$\lambda_{p+1} = 1 - \sum_{i=1}^{p} \lambda_i \tag{42}$$

and its consequence (cf. Definition 5 in the next section):

$$d\lambda_{p+1} = -\sum_{i=1}^{p} d\lambda_i. \tag{43}$$

We will now explain the integration of a p-form $\bar{\omega}$ over a p-dimensional manifold $\mathscr{M}$. We will pursue the following strategy [15]:

- The manifold is partitioned by p-simplices S_i on $\mathscr{M}$, strictly speaking by domains which are mapped to p-simplices on $\mathbb{R}^p$ by the manifold's charts.
- For each simplex a point P_i in its interior is selected.
- We choose an arbitrary vertex x_j of the simplex and compose a p-vector v_{P_i} out of the p vectors $x_k - x_j$, $k \neq j$, in a way that the orientation of v_{P_i} coincides with the orientation of the simplex. The simplex will be represented by $(v_{P_i}/p!)$. This turns out to be a linear approximation to the simplex.
- By evaluating $\bar{\omega}$ in P_i we obtain a p-covector $\bar{\omega}(P_i)$ and $\bar{\omega}(P_i)|v_{P_i}$ is a real number.
- The integral is approximated by summing up the contribution of all simplices:

$$\int_{\mathscr{M}} \bar{\omega} \approx \frac{1}{p!} \sum_i \bar{\omega}(P_i)|v_{P_i}. \tag{44}$$

- If we refine the partitioning mesh, and thus the grid size of the approximation by tangent vectors, the sum on the right-hand side converges towards the actual integral value.

Remark 2. Integration of differential forms over manifolds is often explained by mapping the integrals to a parameter space and treating them in a classical way. When doing this, one should keep in mind, that the integration of differential forms is in principle a metric-free concept.

2.2.4 Equation in Terms of Differential Forms

In order to obtain a formulation of our problem in terms of exterior calculus (2), we need to introduce some important operators acting on differential forms.

The trace operator t maps p-forms on a manifold $\mathscr{M}$ to p-forms on its boundary, i.e. on a submanifold of $\mathscr{M}$. As mentioned in Sect. 2.2.2, this is done by a simple restriction to the space of tangent vectors of the submanifold. However, the trace operator can also be seen as a special case of a more general operator:

Definition 4 (Pullback). Let $\mathscr{M}$ be an m-dimensional manifold, $\mathscr{N}$ an n-dimensional manifold and $\varphi : \mathscr{M} \to \mathscr{N}$ a smooth mapping. We define the pullback operator φ^* by

$$\varphi^* : \mathscr{F}^p(\mathscr{N}) \to \mathscr{F}^p(\mathscr{M}), \tag{45}$$

$$\bar{\omega} \mapsto \bar{\omega} \circ \varphi. \tag{46}$$

Note that the thus created differential forms $\varphi^*(\bar{\omega})$ take tangential vector fields of $\mathscr{M}$ as arguments. The name pullback results from the fact, that φ^* transports forms from $\mathscr{N}$ to $\mathscr{M}$, i.e. the "opposite" direction of the original mapping. The pullback can be used to express changes of coordinates, if $\mathscr{M} = \mathscr{N}$.

Remark 3. For an embedding $\varphi : \partial\mathscr{M} \hookrightarrow \mathscr{M}$ we obtain the trace operator t. This operator can be seen as a generalized Dirichlet trace acting differently on forms of varying order. For an example in $\mathbb{R}^3$ see Table 3. Other types of traces can be constructed by combining t with other operators (see Table 4 for the example of 1-forms).

The exterior derivative d has already appeared in several places, e.g. in Stokes' theorem (27).

Definition 5 (Exterior derivative). The exterior derivative maps p-forms on an n-dimensional manifold $\mathscr{M}$ to $p+1$-forms on the same manifold:

$$d : \mathscr{F}^p(\mathscr{M}) \to \mathscr{F}^{p+1}(\mathscr{M}). \tag{47}$$

A formal definition of d is given by

$$d = \sum_{i=1}^{n} dx_i \wedge \frac{\partial}{\partial x_i}, \tag{48}$$

where the x_i are the coordinates on $\mathscr{M}$. It becomes obvious, that d is a linear operator. As we have mentioned before, the exterior derivative resembles classical differential operators of vector calculus (see Table 2); strictly speaking these operators can be described by $\zeta_{p+1} \circ d \circ \zeta_p^{-1}$.

Example 1. Consider a 1-form $\bar{\omega} = adx + bdy + cdz$. Applying the exterior derivative we get:

Table 2 Vector proxies of the exterior derivative

p	differential forms	vector calculus
0	$d^{\,0}\bar{\omega}$	$\nabla\omega$
1	$d^{\,1}\bar{\alpha}$	curl α
2	$d^{\,2}\bar{\eta}$	div η

$$\begin{aligned} d\bar{\omega} &= \left(\frac{\partial a}{\partial x}dxdx+\frac{\partial a}{\partial y}dydx+\frac{\partial a}{\partial z}dzdx\right)+\left(\frac{\partial b}{\partial x}dxdy+\frac{\partial b}{\partial y}dydy+\frac{\partial b}{\partial z}dzdy\right)\\ &+\left(\frac{\partial c}{\partial x}dxdz+\frac{\partial c}{\partial y}dydz+\frac{\partial c}{\partial z}dzdz\right)\\ &=\left(\frac{\partial c}{\partial y}-\frac{\partial b}{\partial z}\right)dydz+\left(\frac{\partial a}{\partial z}-\frac{\partial c}{\partial x}\right)dzdx+\left(\frac{\partial b}{\partial x}-\frac{\partial a}{\partial y}\right)dxdy. \end{aligned}$$

One recognizes the curl-structure of the result and indeed $\zeta_2(d\bar{\omega}) = \text{curl}\ \zeta_1(\bar{\omega})$.

Theorem 1. *The exterior derivative commutes with the pullback:*

$$d(\varphi^*\bar{\omega}) = \varphi^*(d\bar{\omega}). \tag{49}$$

In particular this property holds for changes of coordinates and trace operators. The former means, that the exterior derivative is independent of the coordinate system in which it is computed.

Proof. This property can easily be checked for monomials. □

The calculus of differential forms, as treated so far, is a metric-free concept. We will now add metric information with help of the so-called Hodge operator $*$.

Definition 6 (Hodge operator). The Hodge operator linearly maps p-forms to $(n-p)$-forms. It can be described by the way it acts on monomials, e.g., in two-dimensional Cartesian coordinates:

$$*: \begin{cases} 1 \mapsto dx_1dx_2 \mapsto 1, \\ dx_1 \mapsto -dx_2 \mapsto -dx_1, \end{cases} \tag{50}$$

and in three-dimensional Cartesian coordinates:

$$*: \begin{cases} 1 \mapsto dx_idx_jdx_k \mapsto 1, \\ dx_i \mapsto dx_jdx_k \mapsto dx_i, \quad (i,j,k) \in \{(1,2,3),(2,3,1),(3,1,2)\}. \end{cases} \tag{51}$$

The explicit construction of general Hodge operators is explained in [11]. In general, for any monomial p-form $\bar{\omega}$ there is a n-form $\bar{\omega}\wedge *\bar{\omega}$, which coincides with the orientation of the manifold and $\zeta_n(\bar{\omega}\wedge *\bar{\omega}) = \langle\omega,\omega\rangle$. Here $\langle .,. \rangle$ denotes the scalar

product, which determines the metric introduced by the Hodge operator. The scalar product of two vectors u and v can be expressed in terms of differential forms:

$$\langle u, v\rangle = \zeta_3(\zeta_1^{-1}(u) \wedge *\zeta_1^{-1}(v)) = \zeta_3(\zeta_1^{-1}(v) \wedge *\zeta_1^{-1}(u)) = \langle v, u\rangle. \tag{52}$$

For a positive definite metric the Hodge operator is self-inverse up to a possible change of sign:

$$** \bar{\omega} = (-1)^{p(n-p)}\bar{\omega}. \tag{53}$$

Often the Hodge operator is supplemented with a scaling factor, in applications typically a material parameter, which is indicated by a subindex, e.g., $*_\kappa$.

Table 3 Dirichlet traces from a 3-dimensional manifold to its boundary. Here $\tilde{x} \in \Omega$ for interior traces, $\mathbf{n}(x)$ denotes the outer unit normal vector to the boundary Γ at $x \in \Gamma$.

p	differential forms	vector calculus
0	$t^{\,0}\bar{\omega}$	$(\gamma_0\omega)(x) = \lim_{\tilde{x}\to x\in\partial\Omega} \omega(\tilde{x})$
1	$t^{\,1}\bar{\alpha}$	$\mathbf{n}(x) \times ((\gamma_0\alpha)(x) \times \mathbf{n}(x))$
2	$t^{\,2}\bar{\eta}$	$(\gamma_0\eta)(x) \cdot \mathbf{n}(x)$
3	$t^{\,3}\bar{f}$	0

Table 4 Traces for 1-forms/$H(\mathrm{curl})$-conforming functions (from a 3-dimensional manifold to its boundary).

trace	differential forms	vector calculus
$\gamma_D\alpha$	$t^{\,1}\bar{\alpha}$	$\mathbf{n}(x) \times ((\gamma_0\alpha)(x) \times \mathbf{n}(x))$
$\gamma_N\alpha$	$t*d^{\,1}\bar{\alpha}$	$\mathbf{n}(x) \times ((\gamma_0 \mathrm{curl}\ \alpha)(x) \times \mathbf{n}(x))$
$\tilde{\gamma}_D\alpha$	$t*^{\,1}\bar{\alpha}$	$(\gamma_0\alpha)(x) \cdot \mathbf{n}(x)$
$\tilde{\gamma}_N\alpha$	$t*d*^{\,1}\bar{\alpha}$	$(\gamma_0 \mathrm{div}\ \alpha)(x)$

In order to justify the potential formulation we need the converse of the Poincaré lemma (Lemma 1).

Lemma 2 (Converse of Poincaré lemma). *Let $\mathscr{M} \subset \mathbb{R}^3$ be a contractible domain. Let $\bar{\omega}$ be a $p+1$-form on $\mathscr{M}$ with $d\bar{\omega} = 0$. Then there exists a p-form $\bar{\alpha}$, such that $d\bar{\alpha} = \bar{\omega}$.*

Proof. A constructive proof can be found in [11]. □

We can now translate (26) to an equivalent equation for differential forms. The curl corresponds to an exterior derivative applied to a 1-form. Since curl A corresponds to a 2-form, it has to be mapped to a 1-form. This is done by means of the Hodge operator, while incorporating the material parameters. We arrive at

$$d *_{\frac{1}{\mu}} d\bar{A} + *_{\kappa} \frac{\partial}{\partial \tau} \bar{A} = \bar{j}_S, \tag{54}$$

where $\bar{A}$ is a 1-form and $\bar{j}_S$ is a 2-form. The time parameter τ stands out due to the fact, that it is not incorporated into the differential form formulation. While this would be possible by means of a four-dimensional space-time manifold, it would lead to a space-time boundary value problem. Separate treatment of time allows for a initial value problem with respect to time.

3 The Low Order Version

The principal idea of DEM is to discretize not only the differential forms themselves, but also the operators occuring in the differential form representation (2). This is done in a way that projects the equation to the space spanned by the shape forms used for approximation. In contrast to Finite Element Methods no weak formulation is used here. The appearance of discrete operators depends on the corresponding set of shape forms. In low order DEM classical Whitney forms are used. These make for a simple structure of the metric-independent operators.

We denote the space of Whitney p-forms of polynomial degree ϑ on a simplex T, typically a tetrahedron, by $\mathscr{W}^p_\vartheta(T)$. The polynomial degree is to be understood in the sense that

$$\mathscr{P}^p_\vartheta(T) \subset \mathscr{W}^p_\vartheta(T),$$

where $\mathscr{P}^p_\vartheta(T)$ is the space of all polynomial p-forms of degree ϑ on T. Moreover $\mathscr{W}^p_\vartheta(T)$ contains additional p-forms of polynomial degree $\vartheta+1$, so that the space of corresponding vector proxies resembles Nédélec elements of first kind and Raviart-Thomas-Nédélec elements respectively. The well-known low order space is abbreviated with $\mathscr{W}^p(T) = \mathscr{W}^p_0(T)$.

3.1 Dual Complex

Classical Whitney forms are defined for simplicial complexes. Their degrees of freedom are given by the values of their integrals over the corresponding simplices. The continuity of Whitney forms across faces is limited to tangential continuity for 1-forms and normal continuity for 2-forms respectively. Therefore the Hodge operator applied to a Whitney-1-form $\bar{\omega}$ generally results in a 2-form $*\bar{\omega}$ without normal continuity across certain faces. Since it is not possible to

assign a degree of freedom to $*\bar{\omega}$ for concerned faces, $*\bar{\omega}$ is no proper discrete differential form on the given complex [13]. Thus a topologically dual complex is introduced [4]. We will construct a barycentric dual complex, which is always possible for simplicial primal complexes.

Definition 7 (Barycentric dual complex). Let C be a simplicial complex, S a p-dimensional simplex and T a tetrahedron, both elements of the complex, with $S \subset \bar{T}$. Without loss of generality we can assume that S is described by the barycentric coordinates

$$\{\lambda : \sum_{i=1}^{p+1} \lambda_i = 1; \lambda_i = 0,\ i = p+2, \ldots, n+1\}.$$

We denote the dual element of S by $\tilde{S}$. Its intersection $\tilde{S} \cap \bar{T}$ with the tetrahedron is for $p < n$ given by the barycentric coordinates

$$\{\lambda :\ \lambda_i = a,\ i = 1, \ldots, p+1;\ \lambda_j < a,\ j = p+2, \ldots, n+1;\ \sum_{i=1}^{n+1} \lambda_i = 1\}. \tag{55}$$

We have $n - p$ degrees of freedom for the coordinates, thus the dimension of $\tilde{S}$ is $n - p$. The (inner) orientation of S induces an outer orientation for $\tilde{S}$. We name the complex composed of all dual elements $\tilde{S}$ the dual complex $\tilde{C}$.

In general the dual complex is no simplicial one. Its elements may even have irregularities at the boundaries of the primal tetrahedra, e.g., broken edges are allowed. A two-dimensional example is sketched in Fig. 2.

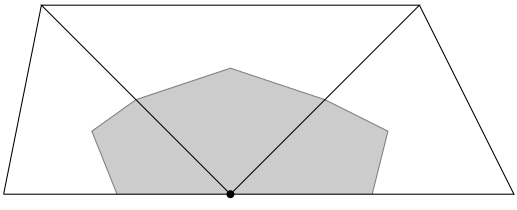

Fig. 2 Parts of the dual face, associated with marked vertex, in primal triangles

3.2 Derivative and Trace Operators

Since $d\mathscr{W}^p(C) \subset \mathscr{W}^{p+1}(C)$ we can construct a discrete exterior derivative, that is exact in the space spanned by Whitney forms. We are looking for an operator, which maps degrees of freedom of p-forms to d.o.f. of $(p+1)$-forms, which resemble the derived form. Regarding Stokes' theorem on a $(p+1)$-dimensional simplex S

$$\int_S d\bar{\omega} = \int_{\partial S} \bar{\omega} \tag{56}$$

and recalling, that the d.o.f. of Whitney forms are their integral values over simplices, i.e. co-chains, we recognize the relation of the discrete exterior derivative to the topology of the complex. In fact the incidence matrix describing the topology between p- and $(p+1)$-simplices can also be used to map the degrees of freedom for Whitney-p-forms to those of Whitney-$(p+1)$-forms in the correct way. Keeping this relation in mind, the fact that a boundary itself is boundary-free shows, that the property

$$d \circ d \equiv 0$$

is also valid for the discrete derivatives. For a set of $(p+1)$-dimensional simplices $\{S_i\}$ and a set of p-dimensional simplices $\{s_j\}$ the entries of the corresponding incidence matrix are given by

$$d_{ij}^p = \begin{cases} 0: & s_j \nsubseteq \partial S_i, \\ 1: & s_j \subset \partial S_i, \text{ orientations of } s_j \text{ and } S_i \text{ match}, \\ -1: & s_j \subset \partial S_i, \text{ orientations of } s_j \text{ and } S_i \text{ do not match.} \end{cases} \tag{57}$$

The incidence matrices for the dual complex are given by $\tilde{D}^{n-p-1} = (-1)^{p+1}(D^p)^\top$.

The construction of the discrete Dirichlet trace operator is even more simple. Whitney forms defined on the boundary complex are themselves traces of those Whitney forms not vanishing on the boundary and thus have the same d.o.f.'s. Therefore the discrete trace operator simply eliminates those degrees of freedom which are not located on the boundary.

While the trace operator corresponds to Dirichlet traces, other traces are assembled from trace-, derivative- and Hodge-operators (see Tables 3 and 4).

3.3 Hodge Operators

Hodge operators are the only metric-dependent operators in DEM. On an n-dimensional manifold they map primal p-forms to dual $(n-p)$-forms. In addition material parameters can be incorporated. For the formulation of the quasistatic problem we will need Hodge operators of varying dimension. The discrete Hodge operators resemble mass matrices as in Finite Element Methods [5]:

$$[M_\nu^p]_{ij} = \int_C \nu \bar{w}_j^p \wedge * \bar{w}_i^p, \tag{58}$$

where $\bar{w}_i^p$ denotes the Whitney p-form associated with the i-th p-dimensional simplex, ν is a material parameter. For simplicity reasons, one can assume parameters to be constant on each cell of the complex. For globally vanishing parameters, e.g. electric parameters in the magnetostatic case, the whole matrix vanishes. The integration is performed over the whole complex C. Nevertheless, the shape forms

used have compact support, which leads to sparse matrices. In fact, low order DEM is equivalent to FEM making use of Whitney elements[2].

3.4 Pairing Matrices

Pairing matrices take on a special position, since they occur in the discretized equation only. They map degrees of freedom representing primal p-forms to d.o.f.'s resembling dual p-forms, i.e. degrees of freedom localized on the dual complex. Therefore quantities associated with the barycentric dual complex can be discretized on the primal one instead. The pairing matrices for a complex C and its boundary ∂C have the general shape:

$$[P^p]_{ij} = \int_C \bar{w}_j^p \wedge \bar{w}_i^{3-p}, \quad i = 1,\ldots,N_{3-p},\ j = 1,\ldots,N_p, \tag{59}$$

$$[P_b^p]_{ij} = \int_{\partial C} t\bar{w}_j^p \wedge t\bar{w}_i^{2-p}, \quad i = 1,\ldots,N_{2-p},\ j = 1,\ldots,N_p \tag{60}$$

where N_k is the number of simplices of dimension k in the complex. Note that the $\wedge$-product does not resemble a scalar product. Since the integrand does not contain a Hodge operator, the entries do not depend on the shape of simplices in the complex, in contrast to those of the Hodge matrix.

The derivation of pairing matrices is related to the construction of the elements inside the dual complex by chains of primal simplices [2]. We recall, that the relation between the two complexes is a topological one. Due to this independence from metrics the entries can be calculated a priori. In low order DEM all non-zero entries of a single pairing matrix have the same absolute value, e.g. $\frac{1}{12}$ for $[P^1]$ in three-dimensional spaces.

3.5 Discrete Equation

We can now assemble a discrete version of (2) using the discretized operators. The general discrete equation for time step $k+1$ is:

$$\begin{aligned}(-1)^{3-p}[D^p]^\top[M_{\frac{1}{\mu}}^{p+1}][D^p]\{A_{k+1}\} + [M_\beta^p]\{A_{k+1}\} \\ = [P^{3-p}]\{j\} + [M_\beta^p]\{A_k\} - [T^p]^\top[P_b^{2-p}]\{\gamma\}, \quad \beta = \frac{\kappa}{\Delta\tau},\end{aligned} \tag{61}$$

where β contains the electric conductivity κ and the step size $\Delta\tau$ from an implicit Euler scheme for time discretization. For field-dependent permeability μ an additional nonlinear iteration is needed for each time step. For our problem we have $p = 1$; one can see, that for example the Helmholtz equation ($p = 0$) has the same shape. As mentioned before, this discrete formulation is equivalent to a finite

[2] Outside the calculus of differential forms we speak of Whitney elements rather than forms.

element formulation, which means that FEM actually features pairing matrices and therefore implicitly defined dual meshes [2].

For the magnetostatic case $\beta = 0$ the system matrix is singular. Keeping in mind the discrete exact sequence property

$$\mathrm{Im}(D^{p-1}) = \mathrm{Ker}(D^p), \tag{62}$$

we can define a regularization matrix $R = c[D^{p-1}][D^{p-1}]^\top$ with a scaling factor $c > 0$. The kernel of this regularization matrix is orthogonal to $\mathrm{Ker}(D^p)$ and

$$\mathrm{rank}(R) = \dim(\mathrm{Ker}(D^p)).$$

Therefore we can add it to the system matrix without altering

$$\{B\} = [D^p]\{A\} \tag{63}$$

and obtain a regular matrix.

4 Localization of Degrees of Freedom

Common higher order FEM shape functions feature degrees of freedom localized not only on edges, but also on faces and cells. Although this concept can also be used for the Discrete Electromagnetism, it does not seem natural[3] to locate d.o.f.'s of p-forms on simplices of dimensions other than p. Several attempts have been made to avoid this inconsistency [6, 20].

4.1 Small Simplices

An idea proposed by Alain Bossavit is to increase the polynomial degree of Whitney forms by multiplying them by barycentric coordinate functions. In addition their corresponding simplices are transformed into sets of so-called small simplices via the $\tilde{k}$-map [20].

Definition 8 ($\tilde{k}$-map). Let S be a d-dimensional simplex, $\mathbf{k} = (k_0, \ldots, k_d) \in \mathbb{N}^{d+1}$. Then we can define the map $\tilde{\mathbf{k}} = (\tilde{k}_0, \ldots, \tilde{k}_d)$ component-wise on $[0,1]$:

$$\tilde{k}_i(x) = (x + k_i)/(1 + |\mathbf{k}|).$$

The small simplex $S_{\mathbf{k}}$, originating from S, is defined by its barycentric coordinates $\tilde{k}_i(\lambda_i)$, $i = 0, \ldots, d$, where λ_i are the barycentric coordinates of S. The corresponding higher-order form is given by

[3] Integration of p-forms over p-manifolds is related to the physical process of measuring a field.

$$\bar{w}_{S,\mathbf{k}} = \bar{w}_S \prod_{i=0}^{d} \bar{\lambda}_i^{k_i},$$

where $\bar{w}_S$ is the low order form associated with S. Orientations are preserved for simplices and forms.

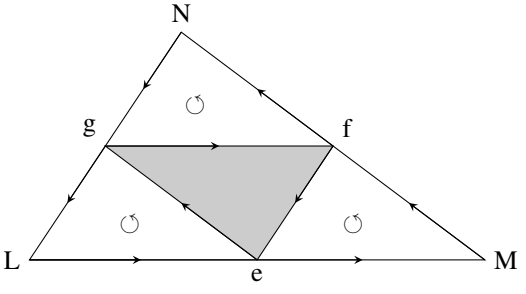

Fig. 3 Small simplices originating from a single triangle and its subsimplices for $|\mathbf{k}| = 1$. Note that the upside down triangle is a hole that does not belong to the complex of small simplices.

Theorem 2. *The spaces spanned by thus modified Whitney forms fulfill the three requirements for spaces of higher order Whitney forms postulated in [14]:*

$$\{\bar{\omega} \in \mathscr{W}_\vartheta^p(T), d\bar{\omega} = 0\} = d\mathscr{W}_\vartheta^{p-1}(T),\ 1 \le p \le 3, \tag{64}$$

$$t_S \mathscr{W}_\vartheta^p(T) = \mathscr{W}_\vartheta^p(S), \quad \text{if } S \text{ is a subsimplex of } T, \tag{65}$$

$$\mathscr{P}_\vartheta^p(T) \subset \mathscr{W}_\vartheta^p(T) \subset \mathscr{P}_{\vartheta+1}^p(T), \tag{66}$$

where the first requirement states a local exact sequence property. These forms can therefore be seen as a realization of Nédélec elements of first kind and Raviart-Thomas-Nédélec elements respectively [16].

Proof. $\mathscr{W}_\vartheta^p(T)$ is spanned by the forms

$$\bar{w}_{\tilde{S},\mathbf{k}} = \bar{w}_{\tilde{S}} \prod_{i=0}^{d} \bar{\lambda}_i^{k_i},\ \vartheta = |\mathbf{k}|.$$

Since (65) holds true for lowest order Whitney forms and the vertices of S are a subset of the vertices of T, it follows by construction, that $\mathscr{W}_\vartheta^p(S)$ is spanned by

$$t_S\{\bar{w}_{\tilde{S},\mathbf{k}} | \tilde{S} \subset S\ p\text{-dim subsimplex}, k_i = 0 \text{ for all vertices not contained in } S\}.$$

If $\tilde{S} \not\subseteq S$ or $k_i > 0$ for at least one vertex not contained in S, it follows that

$$t_S \bar{w}_{\tilde{S},\mathbf{k}} = 0 \in \mathscr{W}_\vartheta^p(S).$$

Since (66) is fulfilled by the lowest order Whitney forms and the barycentric coordinate functions locally span the space of linear polynomials, its validity for arbitrary $\vartheta \ge 0$ follows by induction.

We postpone the proof of the exact sequence property until the end of the section. □

Degrees of freedom of higher order Whitney forms can be localized on the small simplices.

However, this approach has some shortcomings. In general the thus constructed higher order forms are linearly dependent. This can be dealt with by eliminating superfluous forms, and the small simplices associated with them, at the cost of symmetry.

Another point is that, although there exists exactly one (small) simplex for each shape form, degrees of freedom are not located on these simplices themselves, but rather on nontrivial chains (linear combinations) of them. In order to use them in the given theory of DEM, one has to introduce additional transformation matrices, which translate coefficients of shape forms to their integrals over small simplices and vice versa.

Table 5 Number of 1-forms corresponding to small simplices on a tetrahedron and dimension of spaces spanned [14]

$\lvert\mathbf{k}\rvert$	$\dim(\mathscr{W}^1_{\lvert\mathbf{k}\rvert})$	$\#forms$
0	6	6
1	20	24
2	45	60
3	84	120

For the proof of the exact sequence property we will need an additional lemma:

Lemma 3. *For uniform polynomial degree ϑ the exterior derivative maps from the space of modified Whitney p-forms to the space of modified Whitney $(p+1)$-forms: $d\mathscr{W}^p_\vartheta(T) \subset \mathscr{W}^{p+1}_\vartheta(T)$.*

Proof. This property is known for the usual Whitney forms ($\vartheta = 0$). We will prove it for higher polynomial degree by induction. It is sufficient to do this for the shape forms. Let $\bar{w} \in \mathscr{W}^p_\vartheta(T)$ be a shape form with $\vartheta > 0$. Then $\bar{w} = \bar{\lambda}_i \bar{v}$ with $\bar{v} \in \mathscr{W}^p_{\vartheta-1}(T)$, i.e. the polynomial degree of $\bar{v}$ is ϑ at most. It is $d\bar{w} = d\bar{\lambda}_i \bar{v} + \bar{\lambda}_i d\bar{v}$. Since the statement is valid for $\vartheta - 1$, the second term lies in $\mathscr{W}^{p+1}_\vartheta(T)$. Since the mapping

$$\bar{v} \mapsto d\bar{\lambda}_i \bar{v}$$

does not increase the polynomial degree of $\bar{v}$, the first term is also in $\mathscr{W}^{p+1}_\vartheta(T)$, which in particular contains all $(p+1)$-forms of polynomial degree ϑ. □

Proof (Exact sequence property). Let $\bar{\omega} \in \mathscr{W}^p_\vartheta(T)$, $1 \le p \le 3$, with $d\bar{\omega} = 0$. Since T is contractible to a point, there exists a $(p-1)$-form $\bar{\alpha} \in \mathscr{F}^{p-1}(T)$ with $\bar{\omega} = d\bar{\alpha}$. Let $\bar{\alpha}_W \in \mathscr{W}^{p-1}_\vartheta(T)$ be the interpolant of $\bar{\alpha}$ sharing the same degrees of freedom

(on nontrivial chains of small simplices). Then $\bar{\omega}_W = d\alpha_W \in \mathscr{W}^p_\vartheta(T)$ according to the lemma and by construction the degrees of freedom of $\bar{\omega}$ and $\bar{\omega}_W$ are equal and therefore $\bar{\omega} = \bar{\omega}_W$. □

4.2 Higher-Dimensional Simplices

Degrees of freedom of p-forms on p-simplices are determined by simple integration. On higher-dimensional simplices this direct approach is not feasible.

In [8, 25] higher order degrees of freedom are defined for $H(\mathrm{curl})$- and $H(\mathrm{div})$-conforming functions on edges, faces and cells separately. In terms of differential forms they can be pooled in two types of d.o.f.'s for p-forms $\bar{u}$ on m-dimensional simplices S:

$$N_i^S(\bar{u}) = \begin{cases} \int\limits_S td\bar{u} \wedge *td\bar{v}_i & \text{for h.o. } S\text{-based } p\text{-shape forms } \bar{v}_i \notin \ker(d), m > p, \\ \int\limits_S t\bar{u} \wedge *t\bar{v}_i & \text{for h.o. } S\text{-based } p\text{-shape forms } \bar{v}_i \in \ker(d), m \geq p. \end{cases} \tag{67}$$

Note that the correct trace and Hodge operators depend on the dimension m of S. The trace for $m = 3$ equals the identity. The low order d.o.f.'s are included in (67) for $m = p$, $*t\bar{v}_i \equiv 1$.

These definitions exploit orthogonality of fitting higher order shape forms and do not require additional geometrical help concepts, like small simplices. However, the physical meaning of the degrees of freedom is hard to decipher.

5 Higher Order DEM

A hierarchical set of shape functions, which uses the d.o.f. concept described in Sect. 4.2, was presented in [22, 25]. Whitney elements are included as low order functions. Higher order forms for simplices are defined by means of barycentric coordinate functions and Legendre polynomials. In this section we will analyse their impact on discrete operators, when used as shape forms for DEM.

Legendre Polynomials

For defining the higher order forms, we need several versions of Legendre polynomials.

Definition 9 (Legendre polynomials). For $0 \leq i \leq \vartheta$ the Legendre polynomials $l_i(x)$ are $L_2([-1,1])$-orthogonal polynomials spanning $P^\vartheta([-1,1])$. They satisfy the orthogonality relation

$$\int_{-1}^{1} l_i(x) l_j(x) dx = \frac{2}{2i+1} \delta_{ij}. \tag{68}$$

Legendre polynomials can be evaluated via the recurrence relation:

$$l_0(x) = 1, \tag{69}$$
$$l_1(x) = x, \tag{70}$$
$$(n+1)l_{n+1}(x) = (2n+1)l_n(x)x - nl_{n-1}(x), \quad n \geq 1. \tag{71}$$

Definition 10 (Integrated and scaled Legendre polynomials).
Let $l_i(x)$, $x \in [-1,1]$, $i \geq 0$ be the common Legendre polynomials. We define the integrated Legendre polynomials:

$$L_i(x) = \int_{-1}^{x} l_{i-1}(\xi)d\xi, \quad i \geq 2. \tag{72}$$

In addition, for a scaling parameter $r \in (0,1]$, we define the scaled Legendre polynomials and the scaled integrated Legendre polynomials by:

$$l_i^S(x,r) = r^i l_i\left(\frac{x}{r}\right),\ x \in [-r,r], \tag{73}$$
$$L_i^S(x,r) = r^i L_i\left(\frac{x}{r}\right),\ x \in [-r,r]. \tag{74}$$

In the following we define shape forms, which make use of the different types of Legendre polynomials as well as barycentric coordinate functions of the tetrahedron, both interpreted as 0-forms.

Shape 1*-Forms on the Tetrahedron*

Edge-based forms
For $m = 1,\ldots,6$ we describe the edges E_m by their vertices $E_m = [e_{m_1}, e_{m_2}]$.
For lowest order we have the Whitney forms:

$$\bar{w}_m^1 = \bar{\lambda}_{e_{m_1}} d\bar{\lambda}_{e_{m_2}} - \bar{\lambda}_{e_{m_2}} d\bar{\lambda}_{e_{m_1}}. \tag{75}$$

Higher order edge-based forms (resembling gradient fields) are given by:

$$\bar{\varphi}_i^{E_m} = d(\bar{L}_{i+2}^S(\bar{\lambda}_{e_{m_1}} - \bar{\lambda}_{e_{m_2}}, \bar{\lambda}_{e_{m_1}} + \bar{\lambda}_{e_{m_2}})), \quad 0 \leq i \leq \vartheta_{E_m} - 1. \tag{76}$$

Face-based forms
For $m = 1,\ldots,4$ we describe the faces F_m by their vertices $F_m = [f_{m_1}, f_{m_2}, f_{m_3}]$.
For $0 \leq i + j \leq \vartheta_{F_m} - 2$ we define the help forms:

$$\bar{u}_i = \bar{L}_{i+2}^S(\bar{\lambda}_{f_{m_1}} - \bar{\lambda}_{f_{m_2}}, \bar{\lambda}_{f_{m_1}} + \bar{\lambda}_{f_{m_2}}),$$
$$\bar{v}_j = \bar{\lambda}_{f_{m_3}} \bar{l}_j^S(2\bar{\lambda}_{f_{m_3}} - \bar{\lambda}_{F_m}, \bar{\lambda}_{F_m}),$$

where $\bar{\lambda}_{F_m} = \bar{\lambda}_{f_{m_1}} + \bar{\lambda}_{f_{m_2}} + \bar{\lambda}_{f_{m_3}}$.

Using these, we define a basis of face-based 1-forms:

$$\begin{aligned}\bar{\varphi}^{F_m,1}_{(i,j)} &= d(\bar{u}_i\bar{v}_j),\\ \bar{\varphi}^{F_m,2}_{(i,j)} &= (d\bar{u}_i)\bar{v}_j - \bar{u}_i(d\bar{v}_j),\\ \bar{\varphi}^{F_m,3}_{(0,j)} &= (\bar{\lambda}_{f_{m_2}} d\bar{\lambda}_{f_{m_1}} - \bar{\lambda}_{f_{m_1}} d\bar{\lambda}_{f_{m_2}})\bar{v}_j,\end{aligned} \tag{77}$$

where $\bar{\varphi}^{F_m,1}_{(i,j)}$ resemble gradient fields.

Cell-based forms
For $0 \le i+j+k \le \vartheta_C - 3$ we define the help forms:

$$\begin{aligned}\bar{u}_i &= \bar{L}^S_{i+2}(\bar{\lambda}_1 - \bar{\lambda}_2, \bar{\lambda}_1 + \bar{\lambda}_2),\\ \bar{v}_j &= \bar{\lambda}_3\, \bar{l}^S_j(2\bar{\lambda}_3 - (1-\bar{\lambda}_4), 1-\bar{\lambda}_4),\\ \bar{w}_k &= \bar{\lambda}_4 \bar{l}_k(2\bar{\lambda}_4 - 1).\end{aligned}$$

Using these, we define a basis of cell-based 1-forms:

$$\begin{aligned}\bar{\varphi}^{C,1}_{(i,j,k)} &= d(\bar{u}_i\bar{v}_j\bar{w}_k),\\ \bar{\varphi}^{C,2}_{(i,j,k)} &= (d\bar{u}_i)\bar{v}_j\bar{w}_k - \bar{u}_i(d\bar{v}_j)\bar{w}_k + \bar{u}_i\bar{v}_j(d\bar{w}_k),\\ \bar{\varphi}^{C,2}_{\vartheta_C+(i,j,k)} &= (d\bar{u}_i)\bar{v}_j\bar{w}_k + \bar{u}_i(d\bar{v}_j)\bar{w}_k - \bar{u}_i\bar{v}_j(d\bar{w}_k),\\ \bar{\varphi}^{C,3}_{(0,j,k)} &= (\bar{\lambda}_2 d\bar{\lambda}_1 - \bar{\lambda}_1 d\bar{\lambda}_2)\bar{v}_j\bar{w}_k,\end{aligned} \tag{78}$$

where $\bar{\varphi}^{C,1}_{(i,j,k)}$ resemble gradient fields.

Shape 2*-Forms on the tetrahedron*

Face-based forms
For $m = 1,\dots,4$ we describe the faces F_m by their vertices $F_m = [f_{m_1}, f_{m_2}, f_{m_3}]$.
For lowest order we have the Whitney forms:

$$\bar{w}^2_m = 2(\bar{\lambda} f_{m_1} d\bar{\lambda}_{f_{m_2}} d\bar{\lambda}_{f_{m_3}} + \bar{\lambda}_{f_{m_2}} d\bar{\lambda}_{f_{m_3}} d\bar{\lambda}_{f_{m_1}} + \bar{\lambda}_{f_{m_3}} d\bar{\lambda}_{f_{m_1}} d\bar{\lambda}_{f_{m_2}}) \tag{79}$$

For $0 \le i+j \le \vartheta_{F_m} - 2$ we define the help forms:

$$\begin{aligned}\bar{u}_i &= \bar{L}^S_{i+2}(\bar{\lambda}_{f_{m_1}} - \bar{\lambda}_{f_{m_2}}, \bar{\lambda}_{f_{m_1}} + \bar{\lambda}_{f_{m_2}}),\\ \bar{v}_j &= \bar{\lambda}_{f_{m_3}}\, \bar{l}^S_j(2\bar{\lambda}_{f_{m_3}} - \bar{\lambda}_{F_m}, \bar{\lambda}_{F_m}).\end{aligned}$$

Using these, we define a basis of face-based 2-forms (resembling divergence-free vector fields):

$$\begin{aligned}\bar{\psi}^{F_m}_{(i,j)} &= -2d\bar{u}_i d\bar{v}_j,\\ \bar{\psi}^{F_m}_{(0,j)} &= -(\bar{\lambda}_{f_{m_2}} d\bar{\lambda}_{f_{m_1}} - \bar{\lambda}_{f_{m_1}} d\bar{\lambda}_{f_{m_2}})d\bar{v}_j - 2\bar{v}_j d\bar{\lambda}_{f_{m_1}} d\bar{\lambda}_{f_{m_2}}.\end{aligned} \tag{80}$$

Cell-based forms

For $0 \le i+j+k \le \vartheta_C - 3$ we define the help forms:

$$\begin{aligned}\bar{u}_i &= \bar{L}^S_{i+2}(\bar{\lambda}_1 - \bar{\lambda}_2, \bar{\lambda}_1 + \bar{\lambda}_2),\\ \bar{v}_j &= \bar{\lambda}_3\, \bar{l}^S_j(2\bar{\lambda}_3 - (1-\bar{\lambda}_4), 1-\bar{\lambda}_4),\\ \bar{w}_k &= \bar{\lambda}_4\, \bar{l}_k(2\bar{\lambda}_4 - 1).\end{aligned}$$

Using these, we define a basis of cell-based 2-forms:

$$\begin{aligned}\bar{\psi}^{C,1}_{(i,j,k)} &= 2\bar{u}_i d\bar{v}_j d\bar{w}_k - 2\bar{w}_k d\bar{u}_i d\bar{v}_j,\\ \bar{\psi}^{C,1}_{\vartheta_C+(i,j,k)} &= 2\bar{v}_j d\bar{w}_k d\bar{u}_i - 2\bar{u}_i d\bar{v}_j d\bar{w}_k,\\ \bar{\psi}^{C,1}_{2\vartheta_C+(i,j,k)} &= -(\bar{\lambda}_2 d\bar{\lambda}_1 - \bar{\lambda}_1 d\bar{\lambda}_2)d(\bar{v}_j\bar{w}_k) - 2\bar{v}_j\bar{w}_k d\bar{\lambda}_1 d\bar{\lambda}_2,\\ \bar{\psi}^{C,2}_{(i,j,k)} &= \bar{u}_i d\bar{v}_j d\bar{w}_k,\\ \bar{\psi}^{C,2}_{(0,j,k)} &= \bar{v}_j(\bar{\lambda}_2 d\bar{\lambda}_1 - \bar{\lambda}_1 d\bar{\lambda}_2)d\bar{w}_k,\\ \bar{\psi}^{C,3}_{(0,0,k)} &= \bar{w}_k(\bar{\lambda}_1 d\bar{\lambda}_2 d\bar{\lambda}_3 + \bar{\lambda}_2 d\bar{\lambda}_3 d\bar{\lambda}_1 + \bar{\lambda}_3 d\bar{\lambda}_1 d\bar{\lambda}_2),\end{aligned} \tag{81}$$

where $\bar{\psi}^{C,1}_{(i,j,k)}$, $\bar{\psi}^{C,1}_{\vartheta_C+(i,j,k)}$ and $\bar{\psi}^{C,1}_{2\vartheta_C+(i,j,k)}$ resemble divergence-free vector fields.

Properties

The polynomial degrees ϑ of the shape forms can be chosen for each simplex seperately. For uniform polynomial degree $\vartheta_{E_l} = \vartheta_{F_m} = \vartheta_C$, $\forall l,m$, these forms span complete polynomial spaces (resembling Nédélec elements of second kind [17]). However, these do not coincide with the spaces of higher order Whitney forms according to [14] (resembling Nédélec elements of first kind and Raviart-Thomas-Nédélec elements respectively [16]). In order to get a basis for $\mathscr{W}^p_\vartheta(T)$ one has to omit the shape forms of polynomial degree $\vartheta+1$, which lie in $\ker(D^p)$.

In order for the d.o.f. to be dual to the shape forms normalization is required:

$$\tilde{N}^S_i(\bar{u}) = \frac{N^S_i(\bar{u})}{\|\bar{v}_i\|_{L_2(S)}} \text{ and } \tilde{N}^S_i(\bar{u}) = \frac{N^S_i(\bar{u})}{\|d\bar{v}_i\|_{L_2(S)}} \text{ respectively.}$$

In our case it is sufficient to use a reduced basis on $\Omega \setminus \partial\Omega$ by dropping the gradient fields, since they do not contribute to $\bar{B} = d\bar{A}$. One has to keep in mind, that approximation of the Neumann data, which are discretized using 1-forms as well, in general depends on gradient fields. Therefore a reduction of the basis should leave out boundary simplices.

Discrete Operators

Assuming corresponding ordering of shape forms, due to the localization of degrees of freedom on simplices of different dimension, the discrete higher order operators have a distinct block structure best visible in the metric-independent ones.

The forms are chosen in a way, that for a p-shape form $\bar{\varphi}$ there is a $(p+1)$-shape form $d\bar{\varphi}$. Then again these forms span the kernel of the proximate derivative operator. Therefore the exact sequence (62) is fulfilled. Due to the two versions of $\tilde{N}_i^S$ those degrees of freedom associated with the aforementioned p-shape forms are preserved under the exterior derivative. The appropriate discrete operator is composed of its low order version and additional zero and identity blocks:

$$[D_{HO}^p] = \begin{pmatrix} D_{LO}^p & 0 & 0 \\ 0 & 0 & I \\ 0 & 0 & 0 \end{pmatrix}, \tag{82}$$

and fulfill $[D_{HO}^{p+1}][D_{HO}^p] \equiv 0$.

Dirichlet traces of shape forms on tetrahedra are shape forms on triangles (except for cell-based forms which vanish on the cell boundary). This leads to a simple shape of the trace operator similar to that of the low order case. Also property (65) is fulfilled.

On the other hand the structure of higher order pairing matrices becomes rather complex compared to the low order case. Although entries can be calculated in advance, there is quite a variety of possible entries due to a lack of symmetry in the set of trial forms. For example triangle-based forms have a distinguished vertex and do not neccessarily depend on the ordering of the remaining vertices. Therefore in matrix blocks associated with shape forms, based upon simplices of different dimension, the simplices' relative position as well as their relative orientation have to be taken into account. One can assemble the pairing matrices in a simple but not very efficient way by using numerical integration.

As in the low order case discrete Hodge operators resemble FEM mass matrices.

6 Nonlinear Materials

Applications often involve ferromagnetic materials, whose magnetic permeabilities vary with the magnetic field. Since this renders our equation nonlinear, an additional iteration is required during each time step. Also, the material parameters are generally available only as a rather small set of data often suffering from measurement errors. It is therefore helpful to reduce noise by smoothing or to use schemes that enforce physical properties of the B-H curves, e.g. monotonicity. However, since the parameters have to be recalculated in each iteration step, efficient approximation methods are required.

The simplified model, we use here, is isotropic and neglects hysteresis. The measured data reflects the relation $|H|(|B|) = |B|/\mu(|B|)$. The parameters required for

the nonlinear iteration are $\nu(|B|) = 1/\mu(|B|)$ and for the Jacobian of the system matrix $|H|'(|B|)$.

Linear interpolation of the corresponding B-H curve is the most simple way of approximating magnetic permeability. It is often used due to its efficiency and good results in noncritical parts of the material curve. Also, monotonicity of the data is preserved. In the middle part densely distributed measuring points are recommended. Anyway, in order to use Newton iteration schemes for dealing with the nonlinearity a C^1-approximation is needed.

More evolved approximation methods are usually based on higher order splines. A general framework for shape-preserving interpolation and approximation is presented in [10]. Specialized techniques for interpolation [12] or approximation [21] of B-H curves usually feature preservation of monotonicity. An approach which aims at the preservation of additional physical properties was presented in [18].

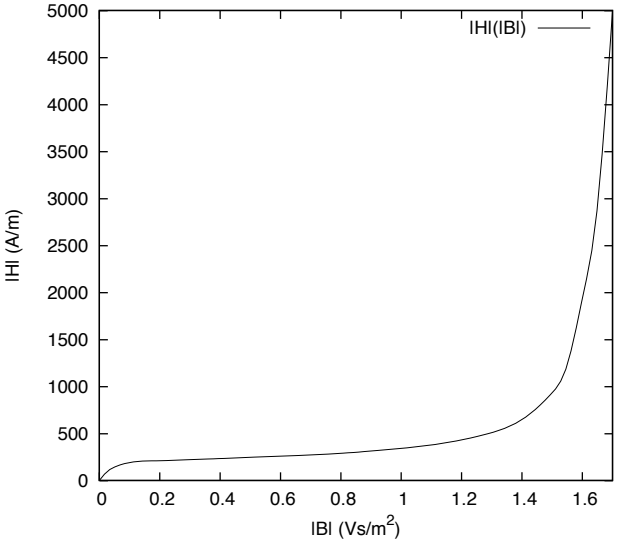

Fig. 4 BH curve for steel interpolated with cubic splines

7 Numerical Results

We illustrate the convergence behaviour of DEM with the help of numerical examples. We start by a comparison of the use of $\mathscr{W}_0^p$- and $\mathscr{W}_1^p$-forms in magnetostatics on a cube $[-0.5, 0.5]^3$ composed of linear material. The experimental rate of convergence is given by

$$\mathrm{eoc} = \frac{\log \|B - B_{h_l}\| - \log \|B - B_{h_{l+1}}\|}{\log h_l - \log h_{l+1}},$$

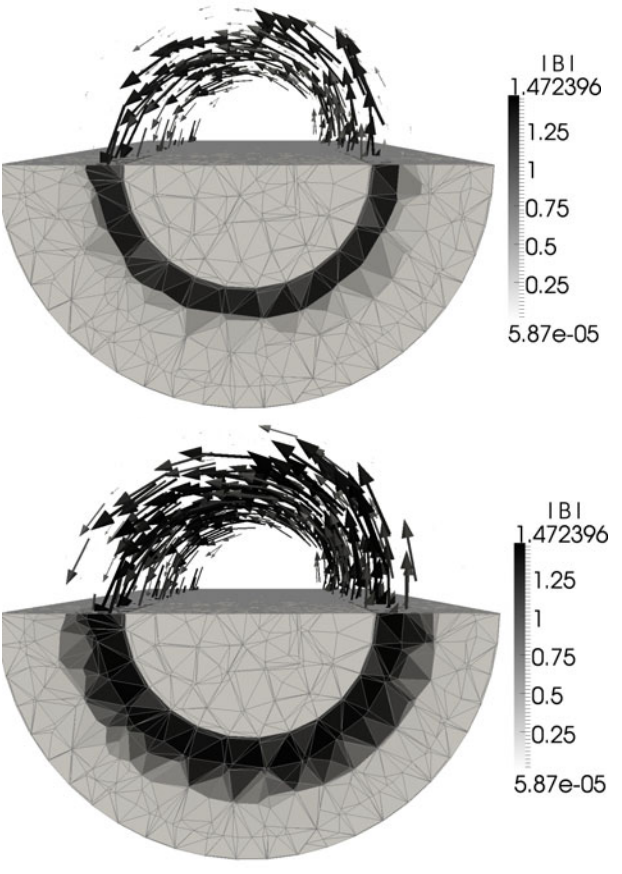

Fig. 5 Magnetoquasistatic example on a hollow cylinder made of nonlinear material. The upper parts of the images show the field of magnetic induction B, the lower parts show its magnitude. Top: after 50 timesteps ($10s$); Bottom: after 150 timesteps ($30s$).

where h_l denotes the grid size at the l-th refinement step. We use a uniform refinement with $h_l = 2h_{l+1}$. Due to the non-uniqueness of $\bar{A}$ we need the regularization mentioned in Sect. 3.5. As can be seen in Table 6, the rate of convergence coincides with that of an FEM, which makes use of the corresponding shape functions. The apparent loss of one order is due to the fact that we examine $d\bar{A}$ (curl A) instead of $\bar{A}$.

Another numerical experiment has been performed for the magnetoquasistatic equation (54). Time discretization has been realized by an implicit Euler scheme with time step size $\tau = 0.2s$ for the time interval $[0s, 35s]$. Fig. 5 illustrates the evolution of a magnetic field, approximated with $\mathscr{W}_1^p$-forms, in a hollow steel cylinder ($D^2(\mathbf{0}, 1) \times [-5, 5]$ with cavity $D^2(\mathbf{0}, 0.5) \times [-5, 5]$) under influence of a direct current in the center. Since we require a trivial topology, the cavity is included in the

computational domain. The simplicial complex describing the cylinder consists of 126123 tetrahedra. We have to implement a localized version of the regularization, we used before.

Measurements of the magnetic permeability were taken from T.E.A.M. [23], problem 13, and are interpolated by cubic splines. Inside the cavity, the permeability is that of air: $\mu = 1.2566375 \cdot 10^{-6} Vs/Am$. For the scaling of the problem we choose the characteristic values $B_0 = 1 Vs/m^2$, $L = 10^{-1} m$ and $\mu_c = 10^{-5} Vs/Am$. We perform Newton iterations until an accuracy of 10^{-3} with respect to the residual norm is reached. The number of steps required varies over the computation.

Table 6 Absolute L_2-errors and orders of convergence for the B-field (magnetostatic example)

# tetrahedra	$\vartheta = 0$: abs. L_2-error	eoc	$\vartheta = 1$: abs. L_2-error	eoc
12	0.059508	-	0.046127	-
96	0.026550	1.16	0.012083	1.93
768	0.011509	1.21	0.002815	2.10
6144	0.005558	1.05	0.000665	2.08
49152	0.002779	1.00	0.000160	2.06
393216	0.001397	0.99	0.000039	2.04

8 Conclusions

As we have seen, the calculus of differential forms offers a different angle of view to known problems. While being equivalent to Finite Element Methods the Discrete Electromagnetism reveals some of their hidden details, e.g. the implicit use of dual meshes.

The d.o.f. used in higher order FEM methods also work well for DEM and can be formulated in a more general way. Degrees of freedom located on simplices of appropriate dimension may also be used, but increase complexity significantly.

From the viewpoint of application one can observe that the DEM for magnetoquasistatics makes use of exterior derivatives and Hodge operators of different degrees. One can imagine to expand a correspondent code to a toolset which is also able to treat more general second-order PDE's, like e.g. electrostatic problems.

Acknowledgements. This work was financially supported by the DFG (German Research Foundation), project RJ 2/14.

References

[1] Auchmann, B.: Private communication (2008)
[2] Auchmann, B., Kurz, S.: The Pairing Matrix in Discrete Electromagnetism - On the Geometry of Discrete de Rham Currents. oai:cds.cern.ch:1048822. Tech. Rep. CERN-AT-2007-017, CERN, Geneva (2007)

[3] Bossavit, A.: Computational electromagnetism. Electromagnetism. Academic Press Inc., San Diego (1998)
[4] Bossavit, A.: Computational electromagnetism and geometry (1): Network equations. J. Japan Soc. Appl. Electromagn. & Mech. 7, 150–159 (1999)
[5] Bossavit, A.: Computational electromagnetism and geometry (2): Network constitutive laws. J. Japan Soc. Appl. Electromagn. & Mech. 7, 294–301 (1999)
[6] Bossavit, A.: Generating Whitney forms of polynomial degree one and higher. IEEE Trans. Magn. 38(2), 341–344 (2002)
[7] Burke, W.L.: Applied differential geometry. Cambridge University Press, Cambridge (1986)
[8] Demkowicz, L., Monk, P., Vardapetyan, L., Rachowicz, W.: De Rham diagram for hp finite element spaces. Comput. Math. Appl. 39(7-8), 29–38 (2000)
[9] Desbrun, M., Kanso, E., Tong, Y.: Discrete differential forms for computational modeling. In: SIGGRAPH 2005: ACM SIGGRAPH 2005 Courses. ACM, New York (2005)
[10] Dierckx, P.: Curve and surface fitting with splines. Monographs on Numerical Analysis. The Clarendon Press, Oxford University Press, New York (1993)
[11] Flanders, H.: Differential Forms with Applications to the Physical Sciences. Dover Publications, New York (1989)
[12] Heise, B.: Analysis of a fully discrete finite element method for a nonlinear magnetic field problem. SIAM J. Numer. Anal. 31(3), 745–759 (1994)
[13] Hiptmair, R.: Discrete Hodge operators. Numer. Math. 90(2), 265–289 (2001)
[14] Hiptmair, R.: Higher order Whitney forms. PIER 32, 271–299 (2001)
[15] Kurz, S.: Kontinuierliche und diskrete Darstellung der Elektrodynamik mit Differentialformen und ihre Anwendung zur numerischen Lösung elektromagnetischer Feldprobleme. Kontinuierliche Differentialformen, Entwurf Teil I (2002)
[16] Nédélec, J.C.: Mixed finite elements in $\mathbb{R}^3$. Numer. Math. 35(3), 315–341 (1980)
[17] Nédélec, J.C.: A new family of mixed finite elements in $\mathbb{R}^3$. Numer. Math. 50(1), 57–81 (1986)
[18] Pechstein, C., Jüttler, B.: Monotonicity-preserving interproximation of *B*-*H*-curves. J. Comput. Appl. Math. 196(1), 45–57 (2006)
[19] Prechtl, A.: Vorlesung über die Grundlagen der Elektrotechnik, Band 2. Springer, Wien (1995)
[20] Rapetti, F., Bossavit, A.: Geometrical localisation of the degrees of freedom for Whitney elements of higher order. IET Science, Measurement & Technology 1(1), 63–66 (2007)
[21] Reitzinger, S., Kaltenbacher, B., Kaltenbacher, M.: A note on the approximation of B-H curves for nonlinear computations. Tech. Rep. 02-30, SFB013, Johannes Kepler University Linz (2002)
[22] Schöberl, J., Zaglmayr, S.: High order Nédélec elements with local complete sequence properties. COMPEL 24(2), 374–384 (2005)
[23] TEAM, Testing electromagnetic analysis methods (since 1986), `http://www.compumag.org/jsite/team.html`
[24] Whitney, H.: Geometric integration theory. Princeton University Press, Princeton (1957)
[25] Zaglmayr, S.: High Order Finite Element Methods for Electromagnetic Field Computation. PhD thesis, Johannes Kepler University Linz (2006)

Additive Schwarz Methods for the *hp* Version of the Boundary Element Method in $\mathbb{R}^3$

Florian Leydecker and Ernst P. Stephan

Abstract. For the Galerkin matrices of the hypersingular and weakly singular first kind integral equations on plane surfaces we present preconditioners obtained by additive Schwarz methods. When those integral equations are solved numerically by the Galerkin boundary element method the resulting matrices become ill-conditioned. Hence, for an efficient solution procedure appropriate preconditioners are necessary to reduce the number of CG-iterations. We consider the *hp* version of the boundary element method and show how to decompose the boundary element spaces such that the resulting preconditioned Galerkin matrices have in the worst case condition numbers which are only polylogarithmically growing with respect to the discretization parameters, i.e. the mesh size h and the polynomial degree p.

1 Introduction

In this article we review additive Schwarz methods for first kind integral equations on plane surfaces in $\mathbb{R}^3$. We demonstrate with the benchmarks of Dirichlet and Neumann screen problems how to perform the *hp* version of the boundary element method and how to precondition the corresponding Galerkin matrices by suitable decompositions of the ansatz spaces with the tool of the additive Schwarz operator. For the *h* version, where accuracy of the Galerkin solution is achieved by reducing the mesh size, suitable additive Schwarz methods give preconditioned stiffness matrices with bounded condition numbers; whereas in the *p* version where accuracy is achieved by increasing the polynomial degree the use of suitable Schwarz preconditioners leads to only polylogarithmically growing condition numbers.

Florian Leydecker · Ernst P. Stephan
Leibniz Universität Hannover, Institut für Angewandte Mathematik,
Welfengarten 1, 30167 Hannover, Germany
e-mail: leydecker@ifam.uni-hannover.de,
stephan@ifam.uni-hannover.de

U. Langer et al. (Eds.): Fast Boundary Element Methods, LNACM 63, pp. 93–109.
springerlink.com

For the hypersingular integral equation resulting from the Neumann screen problem we distinguish between rectangular and triangular meshes. For rectangular meshes we describe a substructuring technique originally derived for the h version BEM in [4] and for the hp version in [6]. For triangular meshes as originally analyzed in [9] we present an additive Schwarz method for the p version BEM where the boundary element space is decomposed into a global wire basket space (consisting of nodal and side basis functions) and into a sum of local spaces given by the bubble functions in the triangles. The p version of the Galerkin method on the triangular mesh is done by using special low energy basis functions [18] together with suitable polynomial extensions of vertex and edge functions into triangles [1, 3].

For the weakly singular integral equation with the single layer potential resulting from the Dirichlet screen problem the p version of the Galerkin method is performed by use of affine images of Legendre polynomials as boundary elements on a uniform mesh. We present a splitting (introduced by HEUER in [2]) of the ansatz space (where the latter consists of piecewise polynomials of degree p on a mesh of size h) by introducing a coarse mesh of size $H \geq h$. When subtracting the piecewise constant functions on the coarse mesh this gives local subspaces of piecewise polynomials living only on elements of size h. This decomposition yields an additive Schwarz preconditioner which bounds the spectral condition number of the stiffness matrix by $\mathcal{O}(\log \frac{H}{h} p)^2$.

The problems under consideration are: the Dirichlet and the Neumann screen problems of the Laplacian in $\mathbb{R}^3 \backslash \overline{\Gamma}$, where Γ is a planar surface piece with polygonal boundary. That is, given g or h on Γ find $u \in H^1_{loc}(\mathbb{R}^3 \backslash \overline{\Gamma})$ satisfying

$$\Delta u = 0 \quad \text{in } \Omega := \mathbb{R}^3 \setminus \bar{\Gamma}, \qquad u = \mathcal{O}(r^{-1}) \quad \text{as } r := |x| \to \infty,$$

$$u = g \quad \text{on } \Gamma \quad (\textbf{Dirichlet}) \quad \text{or} \qquad \frac{\partial u}{\partial n} = h \quad \text{on } \Gamma \quad (\textbf{Neumann}).$$

The above problems can be converted into first kind integral equations on the screen Γ which are amenable for numerical solution procedures such as the Galerkin boundary element method. Since for these first kind integral equations the Galerkin stiffness matrices are ill-conditioned one needs good preconditioners for fast numerical simulations. In order to derive bounds for the additive Schwarz preconditioner one needs besides the mapping properties of the integral operator in fractional Sobolev spaces a detailed analysis of these norms.

As shown in [19] u solves the **Dirichlet** screen problem if and only if $\phi := \left[\frac{\partial u}{\partial n}\right]_\Gamma$ solves

$$V\phi(x) := \frac{1}{4\pi} \int_\Gamma \phi(y) \frac{1}{|x-y|} \, dS_y = g(x) \quad (x \in \Gamma). \tag{1}$$

Furthermore there holds, see [19], u solves the **Neumann** screen problem if and only if $\phi := [u]_\Gamma$ solves

$$D\phi(x) := -\frac{1}{4\pi} \frac{\partial}{\partial n_x} \int_\Gamma \phi(y) \frac{\partial}{\partial n_y} \frac{1}{|x-y|} \, dS_y = h(x) \quad (x \in \Gamma). \tag{2}$$

The above integral operators

$$D:\ \tilde{H}^{1/2}(\Gamma) \to H^{-1/2}(\Gamma), \qquad V:\ \tilde{H}^{-1/2}(\Gamma) := \left(H^{1/2}(\Gamma)\right)' \to H^{1/2}(\Gamma)$$

are continuous mappings and lead to positive definite bilinear forms, with the interpolation space $\tilde{H}^{1/2}(\Gamma) = H_{00}^{1/2}(\Gamma) = \left[L_2(\Gamma), H_0^1(\Gamma)\right]_{1/2}$ and the trace space $H^{1/2}(\Gamma)$ with the norms

$$\|v\|^2_{\tilde{H}^{1/2}(\Gamma)} = \int_0^\infty K(t,v)^2 \frac{\mathrm{d}t}{t^2} \quad \forall v \in \tilde{H}^{1/2}(\Gamma), \tag{3}$$

$$K(t,v)^2 = \inf_{v=v_0+v_1} \left(\|v_0\|^2_{L^2(\Gamma)} + t^2 \, |v_1|^2_{H^1(\Gamma)} \right)$$

and

$$\|v\|_{H^{1/2}(\Gamma)} = \inf_{w \in H^1_{loc}(\Omega), w|_\Gamma = v} \left(\|w\|_{H^1_{loc}(\Omega)} \right), \quad \Omega = \mathbb{R}^3 \backslash \overline{\Gamma}.$$

In concise form we rewrite the above integral equations (1) and (2) as

$$Au = f \text{ on } \Gamma \tag{4}$$

where $A:\ \tilde{H}^{\alpha/2}(\Gamma) \to H^{-\alpha/2}(\Gamma)$ with $\alpha = 1$ when $A = D$ and $\alpha = -1$ when $A = V$.

The boundary element Galerkin method for the above integral equations is now formulated as: *Find* $u_N \in X_N \subset \tilde{H}^{\alpha/2}(\Gamma)$ *such that*

$$a(u_N, \psi) := \langle Au_N, \psi \rangle = \langle f, \psi \rangle \quad \forall \psi \in X_N. \tag{5}$$

It is well-known that the Galerkin matrices of the above first-kind integral equations are ill-conditioned. When $X_N = \mathrm{span}\{\psi_1, \ldots, \psi_N\}$ is the boundary element space of an hp-version on a quasi-uniform mesh, then the stiffness matrix $A_N := (\langle A\psi_i, \psi_j \rangle)_{ij}$ has a spectral condtion number κ depending on the parameters of mesh size h and polynomial degree p like $\kappa(A_N) = O(h^{-|\alpha|} p^{2|\alpha|})$.

As the above integral operators V and D are building blocks in the symmetric finite element/boundary element coupling one can obtain also efficient preconditioners for the FE/BE coupling by using the additive Schwarz strategy, as described below, for both the integral operators on the coupling interface and the differential operators in the FEM-domain (see e.g. [5, 8]). The additive Schwarz method considered here was originally introduced for integral equations on curves in a series of papers by TRAN and STEPHAN [7, 12, 22, 20, 23, 24]. For the use of multiplicative Schwarz methods to obtain preconditioners for first kind integral equations see [13, 14, 21].

2 Additive Schwarz Method – General Setting

In order to find efficient preconditioners for the Galerkin matrices in (5) we use the framework of the additive Schwarz method. It can be shortly described as follows.

Given a subspace decomposition $X_N = \text{span}\{H_0 \cup H_1 \cup \cdots \cup H_n\}$ and projections $P_j : X_N \to H_j$ which are defined with the help of bilinear forms

$$b_j(P_j\phi, \psi) = a(\phi, \psi) \quad \forall \psi \in H_j, \tag{6}$$

then the additive Schwarz method for the Galerkin scheme (5) consists in solving, by an iterative method, the equation

$$P\phi_N := (P_0 + \cdots + P_n)\,\phi_N = \tilde{g}_N, \tag{7}$$

where the right-hand side $\tilde{g}_N$ is given by $\tilde{g}_N = \sum_{j=0}^{n} g_j$ with g_j being solutions of

$$b_j(g_j, w_j) = \langle f, w_j \rangle \qquad \text{for all } w_j \in H_j,$$

see [22].

Note that (7) is the preconditioned form of the equation (5). Here the additive Schwarz operator P is given in matrix form as $P = BA_N$ with the preconditioner B resulting from the specific subspace decomposition. Of course, the quality of the preconditioner is reflected by the condition number of the preconditioned system. To estimate this condition number the following estimates are commonly used [17].

$$a(\phi,\phi) \le C \sum_{j=0}^{n} b_j(\phi_j,\phi_j) \quad \forall \phi = \sum_{j=0}^{n} \phi_j \qquad \Rightarrow \quad \lambda_{\max}(P) \le C,$$

$$\forall \phi \; \exists \phi = \sum_{j=0}^{n} \phi_j : \quad a(\phi,\phi) \ge c \sum_{j=0}^{n} b_j(\phi_j,\phi_j) \qquad \Rightarrow \quad \lambda_{\min}(P) \ge c,$$

and one is interested on the dependence of the bounds C, c on the discretisation parameters.

3 Additive Schwarz Method for the *hp*-Version BEM for the Hypersingular Integral Equation on Rectangular Meshes

Now we consider the hypersingular integral equation (2). First we decompose the screen Γ into patches Γ_j which are further decomposed into quasi-uniform rectangular pieces Γ_{ji}, $\bar{\Gamma} := \bigcup_{j=1}^{J} \bar{\Gamma}_j$, $\quad \bar{\Gamma}_j := \bigcup_{i=1}^{I_j} \bar{\Gamma}_{ji}$. This induces a locally quasi-uniform, non-overlapping decomposition of the boundary element space of continuous piecewise polynomials vanishing on the boundary γ of the screen Γ, namely

$$X_N := S^1_{h,p}(\Gamma) := \{v \in C^0(\Gamma);\; v|_{\Gamma_{ji}} \in \mathbb{P}_p(\Gamma_{ji}),\, v = 0 \text{ on } \gamma\}$$

as follows. We have the building blocks

- **a coarse mesh** of shape regular, non-uniform subdomains (triangles/quadrilaterals) Γ_j of diameter H_j,
- **a fine mesh** of shape regular quadrilaterals Γ_{ji} of diameter h_j which are uniform on subdomains Γ_j,
- a locally quasi-uniform p**-distribution** on the elements where p_j denotes the maximal polynomial degree on Γ_j.

In order to obtain an efficient substructuring one has to consider also a splitting of the ansatz functions in piecewise linear functions and polynomials of higher polynomial degrees. If we use the standard basis functions consisting of antiderivatives of Legendre polynomials then there is a strong coupling between side and interior functions. This can be avoided by using the so-called discretely harmonic basis functions, see [6], where a locally quasi-uniform hp-version of the boundary element method for the hypersingular integral equation is analyzed. In [6] the following splitting is used

- **nodal** basis functions: tensor products of the pth degree polynomial φ_0 with $\varphi_0(-1) = 0$ and $\varphi_0(1) = 1$ such that

$$\|\varphi_0\|_{L^2(-1,1)} = \min_{\psi:\, \deg \psi = p} \|\psi\|_{L^2(-1,1)}, \tag{8}$$

- **side** basis functions: tensor products of arbitrary polynomials along sides vanishing at the end points and φ_0 (perpendicular to the rectangular sides),
- **interior** basis functions: tensor product polynomials that vanish at sides and nodes.

Altogether this defines a decomposition of the hp-ansatz space in

- a **coarse level** of bilinear functions on subdomains Γ_j (then interpolation to piecewise bilinears on the fine mesh consisting of subsubdomains Γ_{ji}),
- a **fine level** of piecewise bilinears on the fine mesh consisting of
  - a subspace of functions on the coarse wire basket $\mathcal{W}$, the boundaries of subdomains Γ_j,
  - subspaces of functions on subsubdomains Γ_{ji},
- a **level of high degree polynomials** consisting of
  - a subspace of functions on the fine wire basket W, the boundary of the Γ_{ji}'s,
  - subspaces of interior functions on elements Γ_{ji}.

Note that the wire basket consists of all basis functions which are associated to the nodes and the edges of the mesh.

This splitting of the boundary element space induces a splitting of the Galerkin matrix for the hypersingular operators D into various sub-blocks which corresponds to the additive Schwarz operator. We can put it into the abstract framework of Sect. 2 if we introduce bilinear forms $b_j(\cdot,\cdot)$ as follows:

- **on coarse level**: $b_j(\cdot,\cdot) = \langle D\cdot,\cdot\rangle_{L^2(\Gamma)}$,
- **on fine level**:
  - on coarse wire basket $\mathscr{W}$: $b_j(\cdot,\cdot) = \langle\cdot,\cdot\rangle_{L^2(\mathscr{W})}$
  - on subdomains Γ_j: $b_j(\cdot,\cdot) = \langle D\cdot,\cdot\rangle_{L^2(\Gamma_j)}$
- **on high degrees level**:
  - on fine wire basket W: $b_j(\cdot,\cdot) = \langle\cdot,\cdot\rangle_{L^2(W)}$
  - on elements Γ_{ji}: $b_j(\cdot,\cdot) = \langle D\cdot,\cdot\rangle_{L^2(\Gamma_{ji})}$

Since the operator D defines a positive definite and continuous bilinear form $\langle D\cdot,\cdot\rangle_{L^2(\Gamma)}$ on the screen Γ, where the L^2-inner product is understood as duality between $\tilde{H}^{1/2}(\Gamma)$ and $H^{-1/2}(\Gamma)$, the above subspace splitting corresponds to a domain decomposition in $\tilde{H}^{1/2}(\Gamma)$. Making use of the definition of the norm (3) one can show that the above subspace decomposition fits into the abstract framework of Sect. 2 yielding for the corresponding additive Schwarz operator a condition number $\kappa(P)$ which grows only polylogarithmically with respect to the discretization parameters H_j, h_j and p_j.

Theorem 1 ([6]). $\kappa(P) \le C \max_j (1 + \log \frac{H_j p_j}{h_j})^2$ *with a constant C, independent of* H_j, h_j, p_j.

We emphasize that the boundary element method produces stiffness matrices which are in general fully occupied which means that even functions with disjoint supports are coupled via the integral operator. Therefore, when performing a domain decomposition to create a preconditioner, one not only decouples adjacent subdomains but also neglects the coupling of functions in subdomains which are not adjacent. The latter coupling is not present in the finite element method. However, this coupling is always present in the boundary element method, and therefore the theoretical bounds for the extremum eigenvalues are most often just asymptotically obtained from the experimental results and are not obvious as in the finite element method.

The numerical experiments in [6] are carried out by computing the entries of the stiffness matrices by analytical recurrence formulas, see MAISCHAK [11]. The condition numbers are computed by reducing the matrices to tridiagonal form and by calculating the minimum and maximum eigenvalues via the QR-algorithm. For this we use standard LAPACK routines.

For our model problem we choose Γ to be the square plate $(-1/2,1/2)^2 \times \{0\}$ and we use uniform meshes of squares of size h. For the polynomial degree distribution in Table 1 we consider a uniform method (for a locally uniform and a non-uniform method, see [6]). For the uniform method the same polynomial degree is used everywhere.

Table 1 presents the number of iterations of the conjugate gradient method which are necessary to reduce the initial residual by a factor of 10^{-6}. The results demonstrate the efficiency of the additive Schwarz preconditioner as the iteration numbers

Table 1 Iteration numbers for the hypersingular integral equation

$1/h$	p	N	CG (SB)	CG(DH)	PCG	$1/h$	p	N	CG (SB)	CG(DH)	PCG
2	2	9	3	3	3	3	2	25	6	6	6
4	2	49	10	10	10	3	3	64	11	10	9
6	2	121	25	16	12	3	4	121	40	27	10
8	2	225	40	20	13	3	5	196	67	43	11
10	2	361	49	24	13	3	6	289	118	65	12
12	2	529	56	27	13	3	7	400	161	89	13
14	2	729	58	29	13						
16	2	961	64	32	13						

in columns PCG are substantially reduced. It appears that the iteration numbers depend only slightly on the ratio $1/h$ and on p. This all holds for the uniform h- and p-versions. We use the basis functions as introduced directly after (8). For our implementation we use antiderivatives of Legendre polynomials on the sides that vanish at the endpoints of the sides. The basis functions given above are specifically chosen to ensure the efficiency of our preconditioner. In a standard hp-boundary element method, where the convergence does not depend on the basis functions (only on the approximation space), one would use simpler basis functions. These basis functions are referred to as the standard basis functions (SB). They differ from the basis functions above (used in the preconditioned conjugate gradient method PCG) in replacing the φ_0^p components by affine functions. That means, on the reference interval $(-1,1)$, we use for the standard basis (SB) the affine functions $\varphi_0^1(x)$ and $\varphi_0^1(-x)$ instead of the polynomials $\varphi_0^p(x)$ and $\varphi_0^p(-x)$ of full degree. The corresponding results in Table 1 are indicated by (SB).

As Table 1 shows discretely harmonic polynomials (DH) already reduce the iteration numbers significantly compared to the case of standard basis functions (SB) where antiderivatives of Legendre polynomials are used as edge functions and their tensor products as bubble functions. In Fig. 1 we display examples of discretely harmonic polynomials (originally introduced by PAVARINO and WIDLUND [18]) of degree 8 for vertex, edge and interior of the rectangles. They are tensor products of the following functions:

- nodal components $\varphi_0 \in \mathbb{P}_p(-1,1)$ as in (8):

$$\|\varphi_0\|_{L^2(-1,1)} = \min_{\varphi} \|\varphi\|_{L^2(-1,1)}, \quad \varphi_0(1) = 1,\ \varphi_0(-1) = 0.$$

- inner components $\Phi_i \in \mathbb{P}_p^0(-1,1)$ $(i = 1,\dots,p-1)$:

$$\int_{-1}^{1} \Phi_i'(x)v'(x)\,dx = \lambda_i^{(p)} \int_{-1}^{1} \Phi_i(x)v(x)\,dx \quad \forall v \in \mathbb{P}_p^0(-1,1)$$

- edge components $\varphi_i \in \mathbb{P}_p(-1,1)$ $(i = 1,\dots,p-1)$ $\varphi_i(-1) = 0,\ \varphi_i(1) = 1$):

$$\int_{-1}^{1} \varphi_i'(x)v'(x)\,dx + \frac{\lambda_i^{(p)}}{2}\int_{-1}^{1} \varphi_i(x)v(x)\,dx = 0 \quad \forall v \in \mathbb{P}_p^0.$$

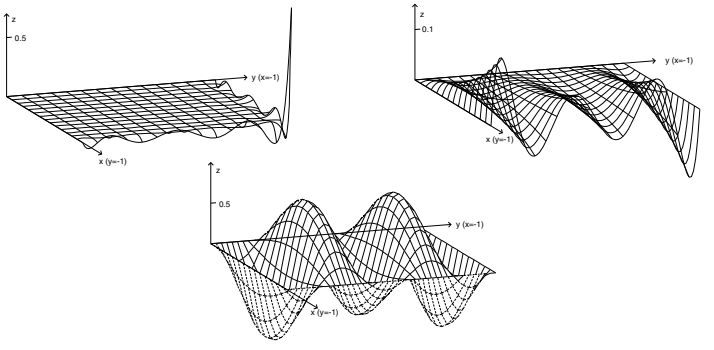

Fig. 1 Discretely harmonic basis functions (nodal, edge, interior) for $p = 8$.

4 Additive Schwarz Method for the p-Version BEM for the Hypersingular Integral Equation on Triangles

Let us consider on the screen Γ a quasi-uniform mesh of shape-regular triangles Γ_i, $i = 1,\dots,n$. Commonly in the p-version one uses piecewise polynomials on triangles as follows. Let $T = \{(x,y) : 0 \le y \le 1-x, 0 \le x \le 1\}$ denote the reference triangle given in Fig. 2 and let $\mathscr{L}_n$ be the antiderivatives of the Legendre polynomials L_{n-1},

$$\mathscr{L}_0(x) = \frac{1-x}{2}, \quad \mathscr{L}_1(x) = \frac{1+x}{2}, \quad x \in [-1,1]$$

$$\mathscr{L}_n(x) = \frac{L_n(x) - L_{n-2}(x)}{2n-1} = \int_{-1}^{x} L_{n-1}(y)\,dy.$$

Then standard basis functions on the reference triangle for the p-version are

$$\begin{aligned}
&\phi_{00}(x,y) = 1-x-y && \text{in lower left corner}\\
&\phi_{10}(x,y) = x && \text{in lower right corner}\\
&\phi_{01}(x,y) = y && \text{in upper left corner}\\
&\phi_{k0}(x,y) = \tilde{\mathscr{L}}_k(x) - y\overline{\mathscr{L}}_k(x),\ 2 \le k \le p && \text{on lower edge}\\
&\phi_{0l}(x,y) = \tilde{\mathscr{L}}_l(y) - x\overline{\mathscr{L}}_l(y),\ 2 \le l \le p && \text{on left edge}\\
&\phi_{k1}(x,y) = \overline{\mathscr{L}}_{k+1}(x)y,\ 1 \le k \le p-1 && \text{on right edge}\\
&\phi_{kl}(x,y) = \overline{\mathscr{L}}_{k+1}(x)\overline{\mathscr{L}}_l(y)(1-x-y),\ 1 \le k,\ 2 \le l, k+l \le p && \text{in interior}
\end{aligned}$$

with the transformed antiderivatives

$$\mathscr{L}_k(x) = \mathscr{L}_k(2x-1),\ \overline{\mathscr{L}}_k(x) = \mathscr{L}_k(x)/(1-x), k \geq 2,\ \ x \in [0,1].$$

As in the case of rectangles also on triangles there is a strong coupling between vertex/side functions and interior functions. To reduce this coupling one uses again low energy functions and polynomial extensions from the triangle sides into the interior of the triangle. On the interval $[0,1]$ the low energy functions of degree p are defined as $\phi_0 \in \mathbb{P}_p(0,1)$ with $\phi_0(0) = 1$, $\phi_0(1) = 0$ and

$$\|\phi_0\|_{L^2(0,1)} = \min_{\phi \in \mathbb{P}_p(0,1)} \|\phi\|_{L^2(0,1)}, \quad \phi(0) = 1, \phi(1) = 0.$$

In the following we describe the construction of the basis functions for the triangles. An essential tool are polynomial extension operators from one side of a triangle into its interior. To construct vertex and edge basis functions the extension operators have to have the property to preserve zeros in the vertices.

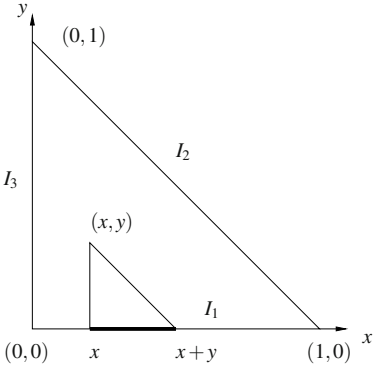

Fig. 2 The reference triangle T

For $f \in \mathbb{P}_p(I_1)$ we define extension operators (see also [1, 10, 16]) from I_1 by (cf. Fig. 2)

$$E_1^1 f(x,y) := \frac{x}{y} \int_x^{x+y} \frac{f(t)}{t}\, dt, \quad \text{if } f(0) = 0,$$

$$E_2^1 f(x,y) := \frac{1-x-y}{y} \int_x^{x+y} \frac{f(t)}{1-t}\, dt, \quad \text{if } f(1) = 0,$$

$$E^1 f(x,y) := \frac{x(1-x-y)}{y} \int_x^{x+y} \frac{f(t)}{t(1-t)}\, dt, \quad \text{if } f(0) = f(1) = 0.$$

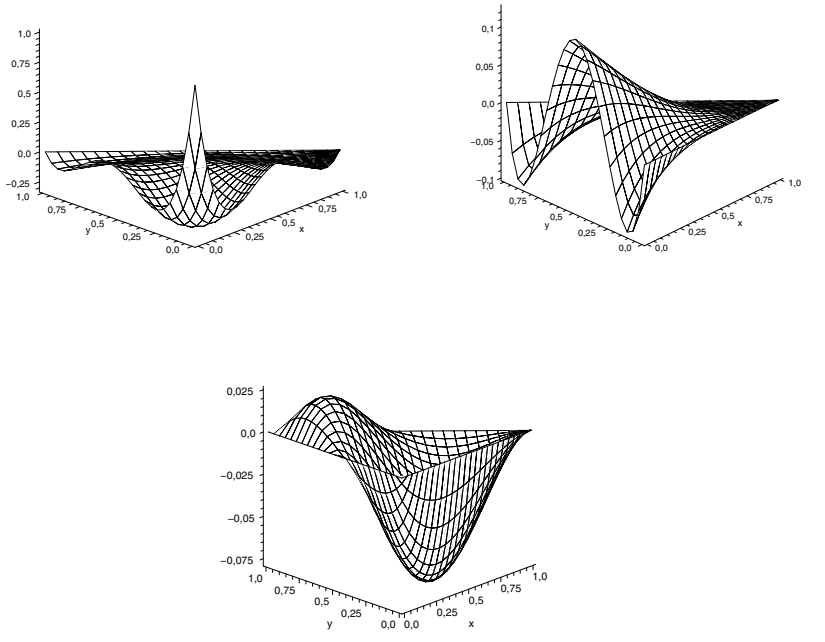

Fig. 3 Low energy basis functions (nodal, edge, interior) for $p = 4$.

All these extensions are polynomials of degree p on T and there holds $E_1^1 f = f$ on I_1, $E_1^1 f = 0$ on I_3; $E_2^1 f = f$ on I_1, $E_2^1 f = 0$ on I_2; $E^1 f = f$ on I_1, $E^1 f = 0$ on I_2 and I_3.

Analogously one can define extension operators for the other edges of the reference triangle.

For the construction of a vertex function we perform the following steps (here for the vertex $V_1 = (0,0)$). First we use the above defined low energy functions and set $u|_{I_1} = u|_{I_3} = \phi_0$ and $u|_{I_2} = 0$ and extend it into the interior of T, that is $u_1 := E_2^1 \phi_0$, $g_2 := u_1|_{I_3}$, $u_2 := E^3(g_2 - \phi_0)$, $u := u_1 - u_2$. The other vertex functions are defined analogously.

For the construction of edge basis functions we extend the antiderivatives of Legendre polynomials by E^1. As interior (bubble) functions we use as above

$$\phi_{k,l}(x,y) = \frac{\mathscr{L}_{k+1}(2x-1)}{1-x} \frac{\mathscr{L}_l(2y-1)}{1-y}(1-x-y), \quad 1 \le k, 2 \le l, k+l \le p.$$

An example of such low energy basis functions created by the above extension procedure is plotted for $p = 4$ in Fig. 3.

Finally we modify the space of wire basket functions to contain the constant function. We redefine the vertex and edge functions as follows. Let $u \in \mathbb{P}_p(T)$ be

decomposed as $u = \sum_{i=1}^{3} \tilde{u}_{V_i} + \sum_{i=1}^{3} \tilde{u}_{I_i} + \tilde{u}_T$. This splitting defines an interpolation operator $\tilde{I}^W$ from $\mathbb{P}_p(T)$ onto the space of wire basket functions by

$$\tilde{I}^W u = \sum_{i=1}^{3} \tilde{u}_{V_i} + \sum_{i=1}^{3} \tilde{u}_{I_i}.$$

As the vertex and edge functions do not contain the constants a further interpolation operator is needed, namely

$$I^W u = \tilde{I}^W u + \mathscr{F}\overline{u}_W, \quad \text{where } \mathscr{F} := 1 - \tilde{I}^W 1 \text{ and } \overline{u}_W = \frac{\int_{\partial T} u}{\int_{\partial T} 1}.$$

Note that, I^W maps a constant function onto itself. By applying this map to the edge and vertex functions (defined above with the specific extension operators) we obtain a new basis where $u_{V_i} = I^W \tilde{u}_{V_i}$ and $u_{I_i} = I^W \tilde{u}_{I_i}$, $i = 1 \ldots 3$, whereas the bubble functions are not changed.

With these special basis functions we perform in [9] on a triangular mesh a subspace decomposition of the p-version boundary element space $S_n^p(\Gamma) = \{u; u|_{\Gamma_i} \in \mathbb{P}_p(\Gamma_i)\}$ where the screen Γ is the union of triangles Γ_i. Our decomposition is

$$S_n^p(\Gamma) = H_0 + H_1 + \cdots + H_n \tag{9}$$

with the space of wire basket functions H_0, i.e. all basis functions which are associated to the nodes and the edges of the mesh, and the space H_j of interior functions on Γ_j ($j = 1, \ldots, n$), i.e. functions that are zero on all edges (triangle sides).

For the interior spaces $H_1, \ldots, H_n$ we set $b_j(v,w) := \langle Dv, w\rangle_{L^2(\Gamma)} \quad \forall v, w \in H_j$, $j = 1, \ldots, n$. For the wire basket space H_0 we take $b_0(v,w) := \langle Dv, w\rangle_{L^2(\Gamma)}, v, w \in H_0$ or $b_0(v,w) := \hat{a}_W(v,w), v, w \in H_0$ where the L^2-bilinear form $\hat{a}_W$ is defined as

$$\hat{a}_W(v,w) := (1 + \log p)^3 \sum_{i=1}^{n} \inf_{c_i \in \mathbb{R}} \langle v - c_i, w - c_i\rangle_{L^2(W_i)}.$$

Using these bilinear forms we prove in [9] the following theorem.

Theorem 2 ([9]). *With the splitting $u = u_W + \sum_{i=1}^{n} u_{\Gamma_i} \in S_n^p(\Gamma)$ where $u_W \in H_0$ and $u_{\Gamma_i} \in H_i$ there exist constants C_0, C_1 independent of h, p and u such that*

$$C_0(1 + \log p)^{-4} \left(b_0(u_W, u_W) + \sum_{j=1}^{n} \langle Du_{\Gamma_i}, u_{\Gamma_i}\rangle_{L^2(\Gamma_i)} \right) \leq \langle Du, u\rangle_{L^2(\Gamma)}$$

$$\leq C_1 \left(b_0(u_W, u_W) + \sum_{j=1}^{n} \langle Du_{\Gamma_i}, u_{\Gamma_i}\rangle_{L^2(\Gamma_i)} \right).$$

In terms of Sect. 2 the additive Schwarz operator is defined by the subspace splitting (9) together with the projections $P_j : S_n^p(\Gamma) \to H_j (j = 0, \ldots, n)$ defined for $v \in S_n^p(\Gamma)$ by $b_j(P_j v, \varphi) = \langle Dv, \varphi\rangle_{L^2(\Gamma)} \quad \forall \varphi \in H_j$.

Thus Theorem 2 implies for the minimum and the maximal eigenvalues of the additive Schwarz operator P_{AS} that

$$\lambda_{min}(P_{AS}) \geq C_0(1+\log p)^{-4}, \quad \lambda_{max}(P_{AS}) \leq C_1$$

yielding for its condition number with a constant $C > 0$, independent of h and p,

$$\kappa(P_{AS}) = \frac{\lambda_{\max}(P_{AS})}{\lambda_{\min}(P_{AS})} \leq C\,(1+\log p)^4.$$

The main tool of the proof of Theorem 2 are the special polynomial extension operators E_1^1, E_1 etc., introduced above. Concerning these operators there hold the following bounds:

Theorem 3 ([3]). *For $f \in \mathbb{P}_p(I)$ with $f(0) = 0$ there holds*

$$\|E_1^1(f)\|_{\tilde{H}^{1/2}(T,I_3)} \leq C\,(1+\log p)^{1/2}\,\|f\|_{L^2(I)}. \tag{10}$$

For $f \in \mathbb{P}_p(I)$ with $f(1) = 0$ there holds

$$\|E_2^1(f)\|_{\tilde{H}^{1/2}(T,I_2)} \leq C\,(1+\log p)^{1/2}\,\|f\|_{L^2(I)}. \tag{11}$$

For $f \in \mathbb{P}_p(I)$ with $f(0) = f(1) = 0$ there holds

$$\|E^1(f)\|_{\tilde{H}^{1/2}(T,I_2\cup I_3)} \leq C\,(1+\log p)^{1/2}\,\|f\|_{L^2(I)}. \tag{12}$$

The constant C above is independent of p and f.

Application of these bounds implies the following extension theorem.

Theorem 4 ([3]). *Let $\tilde{T}$ be a triangle and let γ be one of its sides or the union of two. Then, for a given continuous function f on $\partial\tilde{T}$ which is a polynomial of degree up to p on each of the sides and which vanishes on γ, there exists an extension U on $\tilde{T}$ such that U is a polynomial of total degree up to p, $U = f$ on $\partial\tilde{T}$ and*

$$\|U\|_{\tilde{H}^{1/2}(\tilde{T},\gamma)} \leq C\,(1+\log p)^{1/2}\,\|f\|_{L^2(\partial\tilde{T})}. \tag{13}$$

Here, the constant $C > 0$ is independent of f and p.

Further ingredients of the proof of Theorem 2 are the use of special norms on triangles already introduced in[1]. On the reference triangle T, for $u = 0$ on edge I_i we take

$$\|u\|^2_{\tilde{H}^{1/2}(T,I_i)} := |u|^2_{H^{1/2}(T)} + \|\rho_i^{-1/2}u\|^2_{L^2(T)}$$

where

$$|v|^2_{H^{1/2}(T)} := \int_T \int_T \frac{|v(x)-v(y)|^2}{|x-y|^3}\,dS_x\,dS_y.$$

When $u = 0$ on the edges I_i and I_j then

$$\|u\|^2_{\tilde{H}^{1/2}(T,I_i,I_j)} := |u|^2_{H^{1/2}(T)} + \|\rho_i^{-1/2}u\|^2_{L^2(T)} + \|\rho_j^{-1/2}u\|^2_{L^2(T)}$$

where ρ_i, ρ_j denote the distance to I_i, I_j, respectively. Furthermore there holds the norm equivalence

$$\langle Dv, v\rangle_{L^2(\Gamma)} \simeq \|v\|^2_{\tilde{H}^{1/2}(\Gamma)} = |v|^2_{H^{1/2}(\Gamma)} + \int_\Gamma \frac{|v(x)|^2}{\operatorname{dist}(x, \partial\Gamma)}\, dS_x.$$

As a model problem we choose the scaled domain $\Gamma = (-1/2, 1/2)^2$, take a uniform mesh consisting of 8 right-angled triangles and perform the Galerkin scheme (5) with the right hand side $h \equiv 1$ in (2). The uniform polynomial degrees are increased from 1 to 6.

In Fig. 4 the condition numbers of the Galerkin matrix with preconditioner are plotted. Here we consider only the preconditioner using the modified L^2-bilinear form $\hat{a}_W$ for the wire basket space. This is the practically relevant case and the other preconditioner (using the energy bilinear form) behaves analogously. In the plot we also give the curve of $(1 + \log p)^4$, and the numerical results behave similarly in the given range of p. Exact numbers are listed in Table 2 together with the condition numbers of the un-preconditioned stiffness matrix. We also give the iteration numbers of the conjugate gradient method that are needed to reduce the l_2-norm of the initial residuals of the preconditioned/un-preconditioned linear systems by a factor of 10^{-8}. The zero vector is taken as initial guess. As expected the iteration numbers increase only moderately when one of the preconditioners is used and grow substantially without preconditioner.

In Fig. 5 we present from [9] condition numbers of the preconditioned matrix for the h-version using uniform meshes and different polynomial degrees. The results confirm the asymptotic independence of the condition numbers on h.

Table 2 Condition numbers and iteration numbers for the p-version without and with preconditioning (using the L^2- and the energy bilinear form) [9]

p	DOF	cond(w/o)	niter	cond(pre, L^2)	niter	cond(pre, $\tilde{H}^{1/2}$)	niter
1	1	0.100E+01	1	0.100E+01	1	0.100E+01	1
2	9	0.781E+01	6	0.561E+01	7	0.100E+01	1
3	25	0.734E+02	29	0.443E+02	18	0.547E+01	11
4	49	0.739E+03	100	0.745E+02	34	0.796E+01	17
5	81	0.102E+05	315	0.112E+03	44	0.103E+02	22
6	121	0.189E+06	993	0.150E+03	56	0.124E+02	27

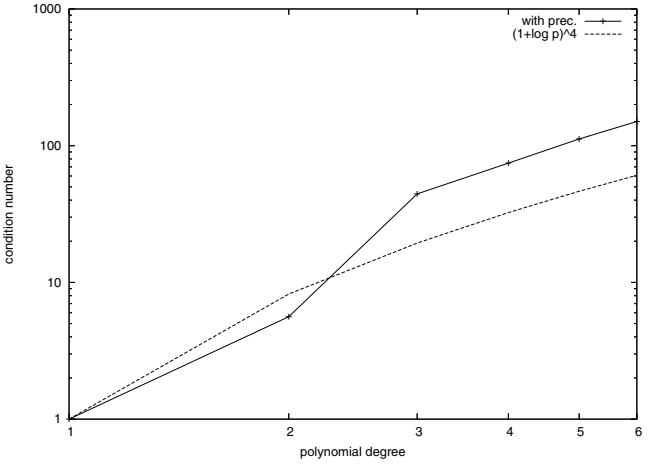

Fig. 4 Condition number of the preconditioned Galerkin matrix, p-version

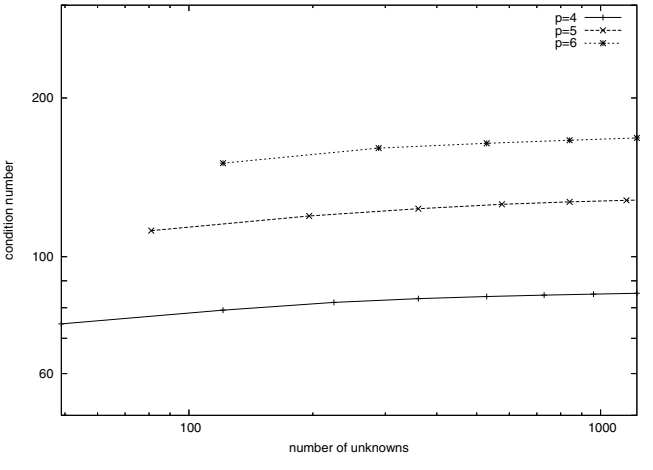

Fig. 5 Condition number of the preconditioned Galerkin matrix, h-version

5 Additive Schwarz Method for the hp-Version BEM for the Weakly Integral Equation

Now we consider the first kind integral equation (1). For simplicity we introduce a quasi-uniform mesh as indicated in Fig. 6 and take polynomials of degree p on the subsquares Γ_j where $\bar{\Gamma} = \cup_{j=1}^{J} \bar{\Gamma}_j$. The boundary element space of globally discontinuous polynomials $X_N := S^0_{h,p}(\Gamma) := \{\phi \in L^2(\Gamma);\ \phi|_{\Gamma_j} \in \mathbb{P}_p(\Gamma_j)\}$ is further decomposed via the patches G_i with $\bar{\Gamma} = \cup_{i=1}^{n} \bar{G}_i$ as

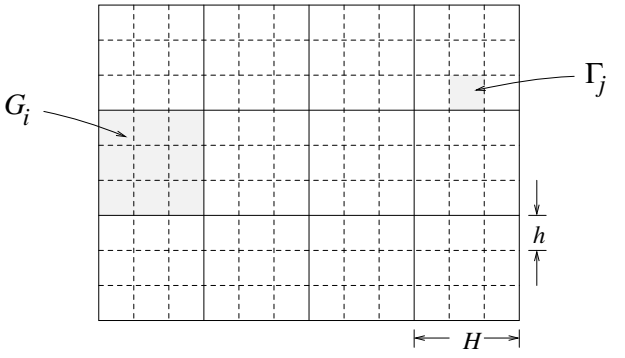

Fig. 6 Mesh for the weakly singular operator

$$X_N = \operatorname{span}\left\{S^0_{H,0}(\Gamma) \oplus H_1 \oplus \cdots \oplus H_n\right\} \tag{14}$$

where

$$H_i = \{\phi \in X_N \setminus H_0;\ \operatorname{supp}(\phi) \subset \bar{G}_i, \int_{G_i} \phi = 0\}, \quad H_0 := S^0_{H,0}(\Gamma).$$

For the corresponding additive Schwarz operator there holds the following result by HEUER [2] where $S^0_{H,0}(\Gamma)$ is the space of constants on the patches.

Theorem 5 (Heuer, 2001). *For the condition number of the additive Schwarz operator belonging to the subspace decomposition* (14) *of the boundary element space of the single layer potential there holds*

$$\kappa(P) \le C(1 + \log \frac{H}{h}(p+1))^2$$

where the constant C is independent of H, h and p.

The proof in [2] uses the following building blocks. Here

$$a(\phi, \phi) = \langle V\phi, \phi \rangle_\Gamma$$

is equivalent to $\|\phi\|^2_{\tilde{H}^{-1/2}(\Gamma)}$. Thus giving in terms of Sect. 2 bounds for the minimal and maximal eigenvalues of P via the inequalities

$$\|\phi\|^2_{\tilde{H}^{-1/2}(\Gamma)} \le C \sum_{j=1}^{n} \|\phi|_{G_j}\|^2_{\tilde{H}^{-1/2}(G_j)} \quad \left(\phi|_{G_j} \in \tilde{H}^{-1/2}(G_j)\right),$$

$$\sum_{j=1}^{n} \|\phi|_{G_j}\|^2_{H^{-1/2}(G_j)} \le c\|\phi\|^2_{H^{-1/2}(\Gamma)} \quad \left(\phi \in H^{-1/2}(\Gamma)\right).$$

Furthermore the following relations are used

$$H^{-1/2}(G_j) = \left(\tilde{H}^{1/2}(G_j)\right)' = \left(H_{00}^{1/2}(G_j)\right)' \quad (0 < s < 1/2),$$

and

$$\|\phi\|^2_{\tilde{H}^s(G_j)} \simeq \|\phi\|^2_{H^s(G_j)} + \left\| \frac{\phi(x)}{\operatorname{dist}(x, \partial G_j)} \right\|^2_{L^2(G_j)} \leq \frac{c}{\left(1/2 - |s|\right)^2} \|\phi\|^2_{H^s(G_j)}.$$

For the piecewise polynomial ϕ there holds

$$\|\phi\|_{\tilde{H}^{-1/2}(G_j)} \leq \|\phi\|_{\tilde{H}^{-1/2+\varepsilon}(G_j)} \leq \frac{c}{\varepsilon} \|\phi\|_{H^{-1/2+\varepsilon}(G_j)} \leq \frac{c}{\varepsilon} h^{-\varepsilon} p^{2\varepsilon} \|\phi\|_{H^{-1/2}(G_j)}.$$

Thus setting $\varepsilon := \frac{1}{\log \frac{p^2}{h}}$ yields

$$\|\phi\|_{\tilde{H}^{-1/2}(G_j)} \leq c(1 + \log \frac{p+1}{h}) \|\phi\|_{H^{-1/2}(G_j)}$$

which gives the assertion.

Remark 1. For the pure h-version we also refer to [15] where a two-level method has been investigated. There, a bound $\mathcal{O}((H/h)^2)$ for the spectral condition number of the additive Schwarz operator has been proved. Taking $p = 0$ the above result by Heuer gives here an improved bound for the spectral condition number like $\mathcal{O}(\log H/h)^2$.

References

[1] Bică, I.: Iterative substructuring algorithms for the p-version finite element method for elliptic problems. PhD thesis. Courant Institute of Mathematical Sciences, New York University (1997)

[2] Heuer, N.: Additive Schwarz method for the p-version of the boundary element method for the single layer potential operator on a plane screen. Numer. Math. 88(3), 485–511 (2001)

[3] Heuer, N., Leydecker, F.: An extension theorem for polynomials on triangles. Calcolo 45(2), 69–85 (2008)

[4] Heuer, N., Stephan, E.P.: Iterative substructuring for hypersingular integral equations in $\mathbb{R}^3$. SIAM J. Sci. Comput. 20(2), 739–749 (1998)

[5] Heuer, N., Stephan, E.P.: Preconditioners for the p-version of the Galerkin method for a coupled finite element/boundary element system. Num. Methods Part Diff. Eq. 14(1), 47–61 (1998)

[6] Heuer, N., Stephan, E.P.: An additive Schwarz method for the h-p version of the boundary element method for hypersingular integral equations in $\mathbb{R}^3$. IMA J. Numer. Anal. 21(1), 265–283 (2001)

[7] Heuer, N., Stephan, E.P., Tran, T.: Multilevel additive Schwarz method for the h-p version of the Galerkin boundary element method. Math. Comp. 67(222), 501–518 (1998)

[8] Heuer, N., Maischak, M., Stephan, E.P.: Preconditioned minimum residual iteration for the *h*-*p* version of the coupled FEM/BEM with quasi-uniform meshes. Numer. Linear Algebra Appl. 6(6), 435–456 (1999)
[9] Heuer, N., Leydecker, F., Stephan, E.P.: An iterative substructuring method for the *hp*-version of the BEM on quasi-uniform triangular meshes. Num. Methods Part Diff. Eq. 23(4), 879–903 (2007)
[10] Maday, Y.: Relèvements de traces polynomiales et interpolations hilbertiennes entre espaces de polynômes. C R Acad. Sci. Paris Sér. I Math. 309(7), 463–468 (1989)
[11] Maischak, M.: The analytical computation of the Galerkin elements for the Laplace, Lamé and Helmholtz equation in 3d-bem. Preprint, Institute of Applied Mathematics, Hannover University, Germany (1995)
[12] Maischak, M., Stephan, E.P., Tran, T.: Domain decomposition methods for boundary integral equations of the first kind: numerical results. Appl. Anal. 63(1-2), 111–132 (1996)
[13] Maischak, M., Stephan, E.P., Tran, T.: Multiplicative Schwarz algorithms for the Galerkin boundary element method. SIAM J. Numer. Anal. 38(4), 1243–1268 (2000)
[14] Maischak, M., Stephan, E.P., Tran, T.: A multiplicative Schwarz algorithm for the Galerkin boundary element approximation of the weakly singular integral operator in three dimensions. Int. J. Pure Appl. Math. 12(1), 1–21 (2004)
[15] Mund, P., Stephan, E.P., Weiße, J.: Two-level methods for the single layer potential in $\mathbb{R}^3$. Computing 60(3), 243–266 (1998)
[16] Muñoz-Sola, R.: Polynomial liftings on a tetrahedron and applications to the *h*-*p* version of the finite element method in three dimensions. SIAM J. Numer. Anal. 34(1), 282–314 (1997)
[17] Oswald, P.: Multilevel finite element approximation. B. G. Teubner, Stuttgart (1994)
[18] Pavarino, L.F., Widlund, O.B.: A polylogarithmic bound for an iterative substructuring method for spectral elements in three dimensions. SIAM J. Numer. Anal. 33(4), 1303–1335 (1996)
[19] Stephan, E.P.: Boundary integral equations for screen problems in $\mathbb{R}^3$. Integral. Eq. Oper. Theory 10(2), 236–257 (1987)
[20] Stephan, E.P., Tran, T.: Domain decomposition algorithms for indefinite hypersingular integral equations: the *h* and *p* versions. SIAM J. Sci. Comput. 19(4), 1139–1153 (1998)
[21] Stephan, E.P., Maischak, M., Leydecker, F.: Some Schwarz methods for integral equations on surfaces—*h* and *p* versions. Comput. Vis. Sci. 8(3-4), 211–216 (2005)
[22] Tran, T., Stephan, E.P.: Additive Schwarz methods for the *h*-version boundary element method. Appl. Anal. 60(1-2), 63–84 (1996)
[23] Tran, T., Stephan, E.P.: Additive Schwarz algorithms for the *p* version of the Galerkin boundary element method. Numer. Math. 85(3), 433–468 (2000)
[24] Tran, T., Stephan, E.P.: Two-level additive Schwarz preconditioners for the *h*-*p* version of the Galerkin boundary element method for 2-d problems. Computing 67(1), 57–82 (2001)

Fast Boundary Element Methods for Industrial Applications in Magnetostatics

Zoran Andjelic, Günther Of, Olaf Steinbach, and Peter Urthaler

Abstract. For the solution of magnetostatic field problems with industrial applications we consider several boundary integral formulations for a scalar potential ansatz. The presented fast boundary element methods are capable to deal with simply and multiple connected domains, large jumps in the magnetic permeabilities, and real–world examples. We compare the formulations on the basis of several numerical examples taking into account accuracy, efficiency, and robustness.

1 Introduction

One of the challenging problems in engineering and industry is the efficient, accurate, and robust numerical simulation of magnetostatic field problems. This covers a robust handling of complex real–world single or multiple connected structures with geometrical singularities at corners and edges, the treatment of small gaps and jumping material parameters, nonlinearities, and the coupling with other physical fields.

The magnetostatic field equations are considered as a model problem, where some magnetic material is placed within a bounded domain, and where a prescribed source of magnetisation (current carrying conductor or permanent magnet) is applied in the surrounding unbounded air domain. Compared to finite element methods, see, e.g., [4, 8, 9, 20, 22], there are several boundary element methods around, see for example [5, 11, 13, 16, 19, 21, 23, 24, 30], for the numerical solution in particular for linear magnetostatics in unbounded domains. This paper aims to present a unified approach for the solution of magnetostatic field problems by using a scalar

Zoran Andjelic
Corporate Research, ABB Switzerland Ltd., 5405 Baden–Dättwil, Switzerland
e-mail: zoran.andjelic@ch.abb.com

Günther Of · Olaf Steinbach · Peter Urthaler
Institut für Numerische Mathematik, TU Graz, Steyrergasse 30, 8010 Graz, Austria
e-mail: of@tugraz.at, o.steinbach@tugraz.at, urthaler@tugraz.at

U. Langer et al. (Eds.): Fast Boundary Element Methods, LNACM 63, pp. 111–143.
springerlink.com

potential and Galerkin boundary element methods for the discretization of different related boundary integral equations. In fact, we will consider several direct approaches which result either in first or second kind boundary integral equations. While on the continuous level all boundary integral formulations are equivalent to each other, this does not remain true in the discrete case. By comparison we will rate the different boundary element approaches with respect to their accuracy, efficiency, and robustness to deal with multiple connected computational domains, complicated structures with small gaps, and large jumps in the magnetic permeablity.

This paper is organized as follows: In Sect. 2, we derive the transmission problem of a scalar potential ansatz for the linear magnetostatic field equations, and we present a choice of four boundary integral formulations to solve this transmission problem. Based on the interior and exterior representation formulae and related boundary integral equations, the Steklov–Poincaré operator interface equation is derived to determine the unknown scalar magnetostatic potential on the interface. A linear combination of the interior and exterior representation formulae results in a representation of the scalar potential by the single layer potential. The related second kind boundary integral equation is based on the adjoint double layer integral operator. Another linear combination of the interior and exterior boundary integral equations results in a second kind boundary integral equation with the double layer integral operator. We present a direct and an indirect approach to solve the involved auxiliary problem to include the prescribed current density. The unique solvability and the equivalence of all boundary integral equations on the continuous level are highlighted and some modifications are described for the particular case of a simply connected domain.

In Sect. 3, we describe the boundary element discretization of all considered formulations in detail. We use Galerkin variational formulations and data–sparse approximations of the boundary element matrices implemented by the fast multipole method [12, 26]. In addition, we explain the evaluation of the magnetic field for the presented formulations.

Finally, all considered approaches are evaluated for several numerical examples in Sect. 4. Starting with two academic examples, a sphere and a cube, to check for the asymptotic convergence behaviour, a simply connected and a multiple connected domain are considered for the interior point evaluation. An example of industrial interest, a controllable reactor, shows the same effects, which were observed in the previous examples, but to extremer extent. Finally, we give some conclusions in Sect. 5.

2 Boundary Integral Formulations for Transmission Problems

In this section we present several boundary integral equations to solve the linear magnetostatic field equations based on a scalar potential ansatz. While one formulation is motivated by a domain decomposition framework, the others are based on global represention of the solution by boundary potentials. Although, at a first

glance, the latter can be considered as indirect approaches, we derive these formulations based on a direct approach for both the interior and exterior subproblem, see, e.g., [21].

2.1 Model Problem

As a model problem, we consider the magnetostatic field equations

$$\operatorname{curl}\mathbf{H}(x)=\mathbf{j}(x),\quad \operatorname{div}\mathbf{B}(x)=0,\quad \mathbf{B}(x)=\mu(x)\mathbf{H}(x)\quad \text{for } x\in\mathbb{R}^3, \tag{1}$$

where $\mathbf{j}$ is a prescribed current density; $\mathbf{B}$ and $\mathbf{H}$ denote the magnetic flux density and the magnetic field intensity, respectively. For simplicity in the presentation, we consider just one magnetic material occupying a bounded Lipschitz domain $\Omega\subset\mathbb{R}^3$ and surrounded by the unbounded air domain $\Omega^c:=\mathbb{R}^3\setminus\overline{\Omega}$. In particular, we assume a piecewise constant magnetic permeability

$$\mu(x)=\mu_1=\mu_0\mu_r\quad \text{for } x\in\Omega,\quad \mu(x)=\mu_0\quad \text{for } x\in\Omega^c,\quad 0<\mu_0<\mu_1,$$

with a relative permeability μ_r, and μ_0 is the permeability of vacuum. In addition, the transmission conditions

$$[\mathbf{B}(x)\cdot n_x]_{|x\in\Gamma}=0,\quad [\mathbf{H}(x)\times n_x]_{|x\in\Gamma}=0 \tag{2}$$

have to be satisfied where n_x denotes the exterior normal vector for $x\in\Gamma=\partial\Omega$ almost everywhere.

We apply a scalar potential ansatz to solve the magnetostatic field equations (1). The magnetic field $\mathbf{H}$ is splitted into a particular solution $\mathbf{H}_j$ and a potential field to obtain the representations

$$\mathbf{H}(x)=\mathbf{H}_j(x)-\nabla\varphi(x),\quad \mathbf{B}(x)=\mu(x)[\mathbf{H}_j(x)-\nabla\varphi(x)]\quad \text{for } x\in\mathbb{R}^3. \tag{3}$$

We assume that the support V of the current $\mathbf{j}$ is located somewhere in the exterior domain Ω^c. A particular solution is then given by the Biot–Savart integral

$$\mathbf{H}_j(x)=\operatorname{curl}_x\int_V\frac{1}{4\pi}\frac{\mathbf{j}(y)}{|x-y|}dy=\frac{1}{4\pi}\int_V\mathbf{j}(y)\times\frac{x-y}{|x-y|^3}dy\quad \text{for } x\in\mathbb{R}^3. \tag{4}$$

By construction there holds

$$\operatorname{curl}\mathbf{H}_j(x)=\mathbf{j}(x),\quad \operatorname{div}\mathbf{H}_j(x)=0\quad \text{for } x\in\mathbb{R}^3.$$

The remaining vector field $\mathbf{H}_0:=\mathbf{H}-\mathbf{H}_j$ satisfies

$$\operatorname{curl}\mathbf{H}_0(x)=0,\quad \operatorname{div}\mathbf{B}(x)=0,\quad \mathbf{B}(x)=\mu(x)[\mathbf{H}_0(x)+\mathbf{H}_j(x)]\quad \text{for } x\in\mathbb{R}^3, \tag{5}$$

which can be represented by the scalar potential

$$\mathbf{H}_0(x) = -\nabla\varphi(x) \quad \text{for } x \in \mathbb{R}^3.$$

The homogeneous problem (5) is then converted to the potential equation

$$-\operatorname{div}[\mu(x)\nabla\varphi(x)] = 0 \quad \text{for } x \in \mathbb{R}^3.$$

Thus, the local restrictions $\varphi_1 = \varphi_{|\Omega}$ and $\varphi_0 = \varphi_{|\Omega^c}$ are solutions of the local partial differential equations

$$-\Delta\varphi_1(x) = 0 \quad \text{for } x \in \Omega, \quad -\Delta\varphi_0(x) = 0 \quad \text{for } x \in \Omega^c \tag{6}$$

satisfying the radiation condition

$$\varphi_0(x) = \mathcal{O}\Big(\frac{1}{|x|}\Big) \quad \text{as } |x| \to \infty \tag{7}$$

and the transmission boundary condition

$$\varphi_1(x) = \varphi_0(x) \quad \text{for } x \in \Gamma. \tag{8}$$

From the continuity (2) of the normal component of the magnetic flux $\mathbf{B}$ we conclude a second transmission boundary condition, i.e.,

$$\mu_1 \frac{\partial}{\partial n_x}\varphi_1(x) - \mu_0 \frac{\partial}{\partial n_x}\varphi_0(x) = (\mu_1 - \mu_0)\,\mathbf{H}_j(x)\cdot n_x \quad \text{for } x \in \Gamma. \tag{9}$$

2.2 Steklov–Poincaré Operator Interface Equation

We briefly describe the representation formulae and the related boundary integral equations of the exterior and of the interior Laplace equation (6). For the mapping properties of the involved boundary integral operators, see, e.g., [15, 25, 31, 34]. Finally, we derive a Steklov–Poincaré operator interface equation to solve the considered transmission problem.

2.2.1 Interior Steklov–Poincaré Operator

In a direct approach, the solution of the interior Laplace equation in (6) is given by the representation formula

$$\varphi_1(x) = \frac{1}{4\pi}\int_\Gamma \frac{1}{|x-y|} t_1(y)\,ds_y - \frac{1}{4\pi}\int_\Gamma \frac{\partial}{\partial n_y}\frac{1}{|x-y|}\varphi_1(y)\,ds_y \quad \text{for } x \in \Omega \tag{10}$$

where t_1 denotes the interior conormal derivative

$$t_1(x) := \lim_{\Omega \ni \tilde{x} \to x} n_x \cdot \nabla_{\tilde{x}}\varphi_1(\tilde{x}) \quad \text{for almost all } x \in \Gamma.$$

When considering the limit $x \to \Gamma$ of the representation formula (10), we obtain the weakly singular boundary integral equation

$$(Vt_1)(x) = (\sigma I + K)\varphi_1(x) \quad \text{for } x \in \Gamma, \tag{11}$$

where for $x \in \Gamma$

$$(Vt_1)(x) = \frac{1}{4\pi} \int_\Gamma \frac{1}{|x-y|} t_1(y) ds_y \tag{12}$$

is the single layer boundary integral operator and

$$(K\varphi_1)(x) = \frac{1}{4\pi} \int_\Gamma \frac{\partial}{\partial n_y} \frac{1}{|x-y|} \varphi_1(y) ds_y \tag{13}$$

is the double layer integral operator. In addition we have, due to the jump relation of the double layer potential, the solid angle

$$\sigma(x) := \lim_{\varepsilon \to 0} \frac{1}{4\pi\varepsilon^2} \int_{y \in \Omega : |y-x| = \varepsilon} ds_y.$$

Since the single layer potential V in (11) is invertible, the interior Steklov–Poincaré operator S_1 defines a unique Dirichlet to Neumann map by

$$t_1(x) = V^{-1}(\sigma I + K)\varphi_1(x) =: (S_1\varphi_1)(x) \quad \text{for } x \in \Gamma. \tag{14}$$

When considering the interior conormal derivative of the representation formula (10), we end up with the hypersingular boundary integral equation

$$t_1(x) = (D\varphi_1)(x) + (\sigma I + K')t_1(x) \quad \text{for } x \in \Gamma, \tag{15}$$

where in addition to the adjoint double layer integral operator

$$(K't_1)(x) = \frac{1}{4\pi} \int_\Gamma \frac{\partial}{\partial n_x} \frac{1}{|x-y|} \varphi_1(y) ds_y \quad \text{for } x \in \Gamma, \tag{16}$$

we use the hypersingular boundary integral operator

$$(Dv)(x) = -\frac{1}{4\pi} \frac{\partial}{\partial n_x} \int_\Gamma \frac{\partial}{\partial n_y} \frac{1}{|x-y|} v(y) ds_y \quad \text{for } x \in \Gamma.$$

Plugging the Dirichlet to Neumann map (14) into the hypersingular boundary integral equation (15) admits an alternative representation of the interior Steklov–Poincaré operator

$$S_1 = V^{-1}(\sigma I + K) = D + (\sigma I + K')V^{-1}(\sigma I + K) \tag{17}$$

which results in a symmetric approximation of the self-adjoint operator S_1 after a suitable boundary element discretization, see Sect. 3.1.

2.2.2 Exterior Steklov–Poincaré Operator

Similar to the interior problem, the solution φ_0 of the exterior Laplace equation in (6) is given by the representation formula

$$\varphi_0(x) = -\frac{1}{4\pi}\int_\Gamma \frac{1}{|x-y|} t_0(y)ds_y + \frac{1}{4\pi}\int_\Gamma \frac{\partial}{\partial n_y}\frac{1}{|x-y|}\varphi_0(y)ds_y \quad \text{for } x \in \Omega^c \tag{18}$$

where t_0 denotes the exterior conormal derivative

$$t_0(x) := \lim_{\Omega^c \ni \tilde{x} \to x} n_x \cdot \nabla_{\tilde{x}} \varphi_0(\tilde{x}) \quad \text{for almost all } x \in \Gamma.$$

The corresponding boundary integral equation reads as

$$(Vt_0)(x) = ((\sigma - 1)I + K)\varphi_0(x) \quad \text{for } x \in \Gamma, \tag{19}$$

and therefore the related exterior Dirichlet to Neumann map is given by

$$t_0(x) = -V^{-1}((1-\sigma)I - K)\varphi_0(x) =: -(S_0\varphi_0)(x) \quad \text{for } x \in \Gamma. \tag{20}$$

Again, the conormal derivative of the representation formula (18) results in a hypersingular boundary integral equation

$$t_0(x) = -(D\varphi_1)(x) + ((1-\sigma)I - K')t_0(x) \quad \text{for } x \in \Gamma. \tag{21}$$

Thus, the exterior Steklov–Poincaré operator S_0 admits an alternative representation

$$S_0 = V^{-1}((1-\sigma)I - K) = D + ((1-\sigma)I - K')V^{-1}((1-\sigma)I - K). \tag{22}$$

2.2.3 Steklov–Poincaré Operator Interface Equation

The interior and exterior Dirichlet to Neumann maps (14) and (20), respectively, correspond to the computation of the conormal derivative of solutions of the interior and exterior Dirichlet boundary value problems of the partial differential equations (6) taking into account the radiation condition (7). To satisfy the Dirichlet transmission condition (8), we set $\varphi(x) = \varphi_1(x) = \varphi_0(x)$ for $x \in \Gamma$. Utilizing both Dirichlet to Neumann maps, the remaining Neumann transmission condition (9) is rewritten as a boundary integral equation to find the scalar potential $\varphi \in H^{1/2}(\Gamma)$ such that

$$\mu_1(S_1\varphi)(x) + \mu_0(S_0\varphi)(x) = (\mu_1 - \mu_0)\mathbf{H}_j(x) \cdot n_x \qquad \text{for } x \in \Gamma. \tag{23}$$

This equation is called Steklov–Poincaré operator interface equation in the context of domain decomposition methods [33]. Note that this concept is applicable to the case of more than one magnetic material by assigning a subdomain to each magnetic material.

2.3 Single Layer Potential Formulation

Based on the partial differential equations (6), we can summarize the representation formulae (10) and (18) as well as the boundary integral equations (11) and (19) for $x \in \mathbb{R}^3$ as

$$\sigma(x)\varphi_1(x) = \frac{1}{4\pi}\int_\Gamma \frac{1}{|x-y|}t_1(y)ds_y - \frac{1}{4\pi}\int_\Gamma \frac{\partial}{\partial n_y}\frac{1}{|x-y|}\varphi_1(y)ds_y, \quad (24)$$

$$(1-\sigma(x))\varphi_0(x) = -\frac{1}{4\pi}\int_\Gamma \frac{1}{|x-y|}t_0(y)ds_y + \frac{1}{4\pi}\int_\Gamma \frac{\partial}{\partial n_y}\frac{1}{|x-y|}\varphi_0(y)ds_y. \quad (25)$$

For $x \in \Gamma$, the two equations correspond to the boundary integral equations (11) and (19). For $x \in \Omega$, i.e., $\sigma(x) = 1$, equation (24) is the interior representation formula (10) and (25) holds true due to Green's formula. On the other hand, equation (25) is the exterior representation formula (18) for $x \in \Omega^c$, i.e., $\sigma(x) = 0$, while (24) holds true.

Next we want to find a global representation of φ in $\mathbb{R}^3$ by just a single boundary potential. Taking into account the continuity $\varphi_1 = \varphi_0$ on Γ, the sum of (24) and (25) results in the representation

$$\varphi(x) = \frac{1}{4\pi}\int_\Gamma \frac{1}{|x-y|}[t_1(y)-t_0(y)]ds_y = \frac{1}{4\pi}\int_\Gamma \frac{1}{|x-y|}w(y)ds_y \text{ for all } x \in \mathbb{R}^3 \quad (26)$$

with $w := t_1 - t_0$. Using the Neumann transmission condition (9), we get an alternative representation for this density function based on t_1 and $\mathbf{H}_j$,

$$w(x) = \frac{\mu_1 - \mu_0}{\mu_0}[\mathbf{H}_j(x)\cdot n_x - t_1(x)] \quad \text{for } x \in \Gamma. \quad (27)$$

Note that w is not only a density function within an indirect approach but also the jump of the interior and exterior fluxes t_1 and t_0 within a direct approach.

To derive a boundary integral equation for the computation of w, we take the sum of the interior and exterior hypersingular boundary integral equations (15) and (21),

$$t_1(x) = (\frac{1}{2}I + K')t_1(x) + (D\varphi_1)(x),$$
$$t_0(x) = (\frac{1}{2}I - K')t_0(x) - (D\varphi_0)(x),$$

where we used $\sigma = 1/2$ for almost all $x \in \Gamma$, to end up with

$$\frac{1}{2}(t_1 + t_0)(x) - K'(t_1 - t_0)(x) = 0 \qquad \text{for almost all } x \in \Gamma$$

taking into account $\varphi_0 = \varphi_1$ on Γ. After substituting $w = t_1 - t_0$ and, by using (27),

$$t_1 + t_0 = 2t_1 - w = 2\left[\mathbf{H}_j \cdot n_x - \frac{\mu_0}{\mu_1 - \mu_0} w\right] - w = 2\,\mathbf{H}_j \cdot n_x - \frac{\mu_1 + \mu_0}{\mu_1 - \mu_0} w,$$

the unknown function w can be determined from the boundary integral equation

$$\frac{1}{2}(\mu_1 + \mu_0) w(x) + (\mu_1 - \mu_0)(K'w)(x) = (\mu_1 - \mu_0)\mathbf{H}_j(x) \cdot n_x \tag{28}$$

for almost all $x \in \Gamma$.

Note that this formulation, which was derived as a direct approach, coincides with an indirect single layer potential ansatz

$$\varphi(x) = \frac{1}{4\pi} \int_\Gamma \frac{1}{|x - y|} w(y)\, ds_y \quad \text{for } x \in \mathbb{R}^3 \backslash \Gamma,$$

as we will explain next. This indirect ansatz defines a solution of the partial differential equations (6) and guarantees the continuity (8) of the potential φ. The interior and exterior conormal derivatives of φ read as

$$\frac{\partial}{\partial n_x} \varphi_1(x) = \frac{1}{2} w(x) + (K'w)(x), \quad \frac{\partial}{\partial n_x} \varphi_0(x) = -\frac{1}{2} w(x) + (K'w)(x)$$

for almost all $x \in \Gamma$. Thus, the jump condition (9) results in the boundary integral equation (28). Summarizing, the presented approach can be derived as a direct formulation or starting from an indirect ansatz. In both cases, the unknown density functions φ and w, respectively, allow some physical interpretation. However, the boundary integral equation (28) has to be seen in a weak sense, i.e., $w \in H^{-1/2}(\Gamma)$ is a solution of the boundary integral equation (28) in $H^{-1/2}(\Gamma)$. This may result in a more complicated numerical realization. Hence we are interested in an alternative formulation of a second kind boundary integral equation in $H^{1/2}(\Gamma)$.

2.4 Double Layer Potential Formulation

The intension of this section is to derive a second kind boundary integral equation which is based on a double layer potential ansatz. First we multiply (24) by μ_1 and (25) by μ_0. Second we we sum up the results and we get, due to $\varphi = \varphi_0 = \varphi_1$ on Γ,

$$[\mu_1\sigma(x)+\mu_0(1-\sigma(x))]\varphi(x)$$
$$= \frac{1}{4\pi}\int_\Gamma \frac{1}{|x-y|}[\mu_1 t_1(y)-\mu_0 t_0(y)]ds_y - (\mu_1-\mu_0)\frac{1}{4\pi}\int_\Gamma \frac{\partial}{\partial n_y}\frac{1}{|x-y|}\varphi(y)ds_y$$

for $x \in \mathbb{R}^3$, and by using the transmission condition (9)

$$[\mu_1\sigma(x)+\mu_0(1-\sigma(x))]\varphi(x) + (\mu_1-\mu_0)\frac{1}{4\pi}\int_\Gamma \frac{\partial}{\partial n_y}\frac{1}{|x-y|}\varphi(y)ds_y$$
$$= (\mu_1-\mu_0)\frac{1}{4\pi}\int_\Gamma \frac{1}{|x-y|}\mathbf{H}_j(y)\cdot n_y ds_y \tag{29}$$

follows for $x \in \mathbb{R}^3$.

Since we would like to use only double layer potentials for the representation of the scalar potential φ, we may consider the interior Neumann boundary value problem

$$-\Delta\varphi_j(x) = 0, \quad \text{for } x \in \Omega, \quad \frac{\partial}{\partial n_x}\varphi_j(x) = \mathbf{H}_j(x)\cdot n_x \quad \text{for } x \in \Gamma, \tag{30}$$

where we have the representation formula

$$\sigma(x)\varphi_j(x) = \frac{1}{4\pi}\int_\Gamma \frac{1}{|x-y|}\mathbf{H}_j(y)\cdot n_y ds_y - \frac{1}{4\pi}\int_\Gamma \frac{\partial}{\partial n_y}\frac{1}{|x-y|}\varphi_j(y)ds_y \quad \text{for } x \in \mathbb{R}^3.$$

Recall that $\sigma(x) = 1$ for $x \in \Omega$, and $\sigma(x) = 0$ for $x \in \Omega^c$. Note that any additive constant in φ_j is eliminated due to the kernel properties of the double layer potential and does not effect the final formulation. In particular we have

$$\frac{1}{4\pi}\int_\Gamma \frac{1}{|x-y|}\mathbf{H}_j(y)\cdot n_y ds_y = \sigma(x)\varphi_j(x) + \frac{1}{4\pi}\int_\Gamma \frac{\partial}{\partial n_y}\frac{1}{|x-y|}\varphi_j(y)ds_y \tag{31}$$

for $x \in \mathbb{R}^3$. Substituting (31) into (29), we get for $x \in \mathbb{R}^3$

$$[\mu_1\sigma(x)+\mu_0(1-\sigma(x))]\varphi(x) + (\mu_1-\mu_0)\frac{1}{4\pi}\int_\Gamma \frac{\partial}{\partial n_y}\frac{1}{|x-y|}\varphi(y)ds_y$$
$$= (\mu_1-\mu_0)\sigma(x)\varphi_j(x) + (\mu_1-\mu_0)\frac{1}{4\pi}\int_\Gamma \frac{\partial}{\partial n_y}\frac{1}{|x-y|}\varphi_j(y)ds_y,$$

and by introducing

$$v := (\mu_1-\mu_0)(\varphi-\varphi_j)$$

we obtain

$$[\mu_1\sigma(x)+\mu_0(1-\sigma(x))]\varphi(x)+\frac{1}{4\pi}\int_\Gamma \frac{\partial}{\partial n_y}\frac{1}{|x-y|}v(y)ds_y=(\mu_1-\mu_0)\sigma(x)\varphi_j(x) \tag{32}$$

for $x\in\mathbb{R}^3$. In particular for almost all $x\in\Gamma$ we conclude

$$\frac{1}{2}(\mu_1+\mu_0)\varphi(x)+\frac{1}{4\pi}\int_\Gamma \frac{\partial}{\partial n_y}\frac{1}{|x-y|}v(y)ds_y=\frac{1}{2}(\mu_1-\mu_0)\varphi_j(x).$$

By using

$$\varphi=\varphi_j+\frac{1}{\mu_1-\mu_0}v$$

we finally obtain the boundary integral equation

$$\frac{1}{2}\frac{\mu_1+\mu_0}{\mu_1-\mu_0}v(x)+(Kv)(x)=-\mu_0\varphi_j(x)\quad\text{for almost all } x\in\Gamma. \tag{33}$$

The same boundary integral equation can be derived from the indirect double layer potential ansatz

$$\varphi_1(x):=-\frac{1}{\mu_1}\frac{1}{4\pi}\int_\Gamma \frac{\partial}{\partial n_y}\frac{1}{|x-y|}v(y)ds_y+\frac{\mu_1-\mu_0}{\mu_1}\varphi_j(x)\quad\text{for } x\in\Omega,$$

$$\varphi_0(x):=-\frac{1}{\mu_0}\frac{1}{4\pi}\int_\Gamma \frac{\partial}{\partial n_y}\frac{1}{|x-y|}v(y)ds_y\qquad\text{for } x\in\Omega^c,$$

where v is an unknown density function, and φ_j is a solution of the auxiliary boundary value problem (30). Both φ_1 and φ_0 are solutions of the partial differential equations (6). φ_1 is chosen such that the Neumann transmission condition (9) is satisfied implicitly, as there holds

$$\mu_1 t_1-\mu_0 t_0=Dv+(\mu_1-\mu_0)\frac{\partial}{\partial n_x}\varphi_j-Dv=(\mu_1-\mu_0)\mathbf{H}_j\cdot n_x\quad\text{on }\Gamma$$

by definition. Thus, it remains to satisfy the Dirichlet transmission condition (8), i.e., for almost all $x\in\Gamma$ we have, by taking into account the jump relations of the double layer potential,

$$\begin{aligned}0&=\mu_0\mu_1[\varphi_1(x)-\varphi_0(x)]\\&=\mu_1(\frac{1}{2}I+K)v(x)-\mu_0\left[(-\frac{1}{2}I+K)v(x)-(\mu_1-\mu_0)\varphi_j(x)\right]\\&=\frac{1}{2}(\mu_1+\mu_0)v(x)+(\mu_1-\mu_0)(Kv)(x)+\mu_0(\mu_1-\mu_0)\varphi_j(x),\end{aligned}$$

which is equivalent to the boundary integral equation (33).

Recall, that φ_j can be determined when considering (31) for $x \in \Gamma$ which results in the boundary integral equation

$$\frac{1}{2}\varphi_j(x) + (K\varphi_j)(x) = (V(\mathbf{H}_j \cdot n))(x) \quad \text{for almost all } x \in \Gamma.$$

Alternatively, we can define φ_j by the indirect single layer potential ansatz

$$\varphi_j(x) = \frac{1}{4\pi} \int_\Gamma \frac{1}{|x-y|} w_j(y) ds_y \quad \text{for } x \in \Omega \tag{34}$$

where the related density function w_j is determined from the boundary integral equation

$$(\sigma I + K')w_j(x) = \mathbf{H}_j(x) \cdot n_x \quad \text{for } x \in \Gamma.$$

As for the direct formulation, the quantity v is determined from (33) but we use φ_j for the right hand side.

2.5 Equivalence and Unique Solvability of the Boundary Integral Equations

In the previous subsections, we have presented several boundary integral formulations to solve the transmission problem (6)–(9) which admits a unique solution. All presented formulations represent this solution and must be equivalent. In particular, there holds [1, Theorem 3.1]

$$\varphi(x) = (Vw)(x) = -\frac{1}{\mu_0}(\frac{1}{2}I + K)v(x) \quad \text{for almost all } x \in \Gamma, \tag{35}$$

where φ is the solution of the Steklov–Poincaré operator interface equation (23), w is the solution of the the single layer integral operator equation (28), and v is the solution of the double layer integral operator formulation (33). Note that the first equation corresponds to the single layer potential representation (26). The other equality is a direct consequence of the boundary integral equation (32) and of the equality $v = (\mu_1 - \mu_0)(\varphi - \varphi_j)$.

The unique solvability of the single and double layer integral operator equations (28) and (33) in $H^{-1/2}(\Gamma)$ and in $H^{1/2}(\Gamma)$, respectively, can be concluded from contraction properties of the involved double layer potentials [1, Theorem 3.2]. The unique solvability of the Steklov–Poincaré operator interface equation (23) can be deduced by the Lemma of Lax–Milgram from the ellipticity of $\mu_1 S_1 + \mu_0 S_0$, see, e.g., [1, Theorem 3.3].

2.6 Evaluation of the Magnetic Field

The magnetic field $\mathbf{H}$ is the quantity of interest and can be computed by using the representation (3), i.e.,

$$\mathbf{H}(x) = \mathbf{H}_j(x) - \nabla\varphi(x) \quad \text{for } x \in \mathbb{R}^3, \tag{36}$$

based on the different formulations presented to determine the scalar potential φ as the solution of the transmission problem (6)–(7).

A special situation is given in the particular case of a simply connected domain Ω. In this case, it is well known that

$$\mathbf{H}(x) = \mathbf{H}_j(x) - \nabla\varphi_1(x) \to 0 \quad \text{for } x \in \Omega \quad \text{as } \mu_1 \to \infty.$$

In particular for large μ_1 there holds

$$\nabla\varphi_1(x) \approx \mathbf{H}_j(x) \quad \text{for } x \in \Omega.$$

For small relative errors of the numerical approximation of $\nabla\varphi_1$ we observe large relative errors for the approximation of $\mathbf{H}$, see Sect. 4.1. Therefore we are interested in an alternative approach to compute the magnetic field in Ω more robustly.

We consider the more general case that there exists a simply connected domain Ω_s such that $\Omega \subset \Omega_s$ and $\operatorname{supp}\mathbf{j} \cap \Omega_s = \emptyset$. Since Ω_s is simply connected and $\operatorname{curl}\mathbf{H}_j(x) = 0$ for $x \in \Omega_s$, $\mathbf{H}_j$ can be represented as a gradient field in Ω_s. In particular, there holds

$$\mathbf{H}_j(x) = \nabla\varphi_j(x) \quad \text{for } x \in \Omega, \tag{37}$$

where φ_j is a solution of the Neumann boundary value problem (30).

Many approaches which are based on boundary integral equations are restricted to the case of a simply connected domain. However, the presented formulations overcome this restriction. The potential φ_j can be defined in any case, but its gradient coincides with $\mathbf{H}_j$ only in the case of a simply connected domain Ω.

Next, we will utilize the relation (37) to setup more robust evaluations of $\mathbf{H}$ in the case of a simply connected domain.

2.6.1 Steklov–Poincaré Operator Interface Equation

In general, the magnetic field $\mathbf{H}$ is evaluated by (36) using the interior representation formula (10) and the exterior representation formula (18), respectively. For the representation formulae, we need to have the complete Cauchy data. Thus, we compute the Neumann datum

$$\frac{\partial}{\partial n_x}\varphi_k(x) = (S_k\varphi_k)(x) \quad \text{for } x \in \Gamma$$

locally for $k = 0, 1$ after solving the global problem (23).

In the case of a simply connected domain Ω, we additionally solve the auxiliary Neumann boundary value problem (30) by considering the Steklov–Poincaré operator equation

$$(S_1\varphi_j)(x) = \mathbf{H}_j(x) \cdot n_x \quad \text{for } x \in \Gamma. \tag{38}$$

Finally the excitation field $\mathbf{H}_j$ can be evaluated as the gradient of a representation formula for $\varphi_j(x)$, $x \in \Omega$. The projection of $\mathbf{H}_j$ to the same spaces as $\mathbf{H}_0$ provides a more accurate evaluation of $\mathbf{H}$ in Ω, for the discrete approximation, see, e.g. [19], and Sect. 4.1.

2.6.2 Single Layer Potential Formulation

In general, the magnetic field is evaluated by

$$\mathbf{H}(x) = \mathbf{H}_j(x) - \nabla\varphi(x) = \mathbf{H}_j(x) - \frac{1}{4\pi}\nabla_x \int_\Gamma \frac{1}{|x-y|} w(y) ds_y \quad \text{for } x \in \mathbb{R}^3.$$

In the case of a simply connected domain, the excitation field $\mathbf{H}_j = \nabla\varphi_j$ is represented by an indirect single layer potential ansatz, see (34). After determining the solution of the boundary integral equation

$$\frac{1}{2} w_j(x) + (K' w_j)(x) = \mathbf{H}_j(x) \cdot n_x \quad \text{for } x \in \Gamma, \tag{39}$$

the evaluation reads

$$\mathbf{H}(x) = \frac{1}{4\pi}\nabla_x \int_\Gamma \frac{1}{|x-y|} (w_j(y) - w(y)) ds_y \quad \text{for } x \in \Omega.$$

2.6.3 Double Layer Potential Formulation

For the evaluation of the magnetic field $\mathbf{H}$, we get from the general relation (32)

$$\mathbf{H}(x) = \mathbf{H}_j(x) + \frac{1}{\mu_0}\frac{1}{4\pi}\nabla_x \int_\Gamma \frac{\partial}{\partial n_y}\frac{1}{|x-y|} v(y) ds_y$$

for $x \in \Omega^c$ ($\sigma = 0$) and

$$\mathbf{H}(x) = \mathbf{H}_j(x) + \frac{1}{\mu_1}\nabla_x \int_\Gamma \frac{\partial}{\partial n_y}\frac{1}{|x-y|} v(y) ds_y - \frac{\mu_1 - \mu_0}{\mu_1}\nabla\varphi_j(x)$$

for $x \in \Omega$ ($\sigma = 1$). For the evaluation of $\nabla\varphi_j$, one has to distinguish between the direct and the indirect approach for the solution of the local Neumann problem (30).

In the case of a simply connected domain, we apply relation (37) to get a representation

$$\mathbf{H}(x) = \frac{\mu_0}{\mu_1}\mathbf{H}_j(x) + \frac{1}{\mu_1}\frac{1}{4\pi}\nabla_x \int_\Gamma \frac{\partial}{\partial n_y}\frac{1}{|x-y|} v(y) ds_y \quad \text{for } x \in \Omega,$$

which is more stable for large μ_1 in the discretized version, see Sect. 4.1.

3 Boundary Element Methods

In this section, we describe boundary element discretizations of the presented boundary integral formulations. The resulting discrete systems and the related approximate computations of the magnetic field **H** are used in the numerical examples presented in Sect. 4. In all cases, we use Galerkin variational formulations to solve the boundary integral equations under consideration. For more details on boundary element methods see, e.g., [29, 31, 34].

In general, we consider admissible triangulations of the boundary $\Gamma = \partial\Omega$ with N plane triangles and M nodes. We use lowest order elements for the discrete ansatz spaces, i.e.,

$$S_h^0(\Gamma) = \operatorname{span}\{\psi_k^0\}_{k=1}^N \subset H^{-1/2}(\Gamma)$$

of piecewise constant basis functions ψ_ℓ^0 for the fluxes, which are one on a single element τ_ℓ and zero else, and

$$S_h^1(\Gamma) = \operatorname{span}\{\psi_m^1\}_{m=1}^M \subset H^{1/2}(\Gamma)$$

of piecewise linear and continuous hat functions ψ_m^1 for the potentials. In particular, $t_h \in S_h^0(\Gamma)$ and $u_h \in S_h^1(\Gamma)$ are linear combinations of the basis functions, i.e.,

$$t_h(x) = \sum_{k=1}^N t_k \psi_k^0(x), \quad u_h(x) = \sum_{m=1}^M u_m \psi_m^1(x).$$

The coefficients t_k and u_m define vectors $\underline{t} \in \mathbb{R}^N$ and $\underline{u} \in \mathbb{R}^M$. Thus, we identify the functions t_h and u_h with the related vectors $\underline{t}$ and $\underline{u}$, respectively.

We use the fast multipole method [12] for a data–sparse approximation of the occurring boundary element matrices and for a fast evaluation of all boundary integral operators. For details, see [26] and the references therein. The computation of all matrix entries is based on the 7–point cubature rule for triangles [28] and analytic evaluations of the boundary integral operators as presented in [29]. The evaluation of the boundary integral operators for the computation of the magnetic field **H** is based on the analytic formulae only. In particular, the gradient of the single layer potential is computed analytically as well as the gradient of the double layer potential after integration by parts, see, e.g., [34, p. 135],

$$\frac{1}{4\pi}\nabla_x \int_\Gamma \frac{\partial}{\partial n_y}\frac{1}{|x-y|}u(y)ds_y = \frac{1}{4\pi}\int_\Gamma \left(\mathbf{curl}_{\Gamma,y}u(y) \times \nabla_x \frac{1}{|x-y|}\right) ds_y \tag{40}$$

for $x \in \Omega \cup \Omega^c$, where the surface curl is defined by

$$\mathbf{curl}_{\Gamma,y}u(y) := n(y) \times \nabla\tilde{u}(y)$$

for a suitable extension $\tilde{u}$ of the function u into a three–dimensional neighborhood of Γ.

3.1 Steklov–Poincaré Operator Interface Equation

According to the Steklov–Poincaré operator interface equation (23), we solve the global system of linear equations

$$\left(\mu_1 \widetilde{S}_{1,h} + \mu_0 \widetilde{S}_{0,h}\right) \underline{\varphi} = (\mu_1 - \mu_0)\underline{f}^1, \tag{41}$$

where

$$f_k^1 = \int_\Gamma (\mathbf{H}_j(x) \cdot n_x)\, \psi_k^1(x) ds_x \quad \text{for } k = 1, \ldots, M.$$

Due to the involved inverse single layer potential operator, a direct discretization of the Steklov–Poincaré operators S_0 and S_1 is not possible in general. But the approximations

$$\widetilde{S}_{1,h} = D_h + (\frac{1}{2}M_h^\top + K_h^\top)V_h^{-1}(\frac{1}{2}M_h + K_h),$$
$$\widetilde{S}_{0,h} = D_h + (\frac{1}{2}M_h^\top - K_h^\top)V_h^{-1}(\frac{1}{2}M_h - K_h)$$

preserve the optimal order of convergence, see e.g. [33]. The Galerkin matrices are given by

$$D_h[m,n] = \langle D\psi_n^1, \psi_m^1\rangle_\Gamma, \qquad K_h[k,n] = \langle K\psi_n^1, \psi_k^0\rangle_\Gamma,$$
$$M_h[k,n] = \langle \psi_n^1, \psi_k^0\rangle_\Gamma, \qquad V_h[k,\ell] = \langle V\psi_\ell^0, \psi_k^0\rangle_\Gamma$$

for $m,n = 1,\ldots,M$ and $k,\ell = 1,\ldots,N$. Possible difficulties in the evaluation of the hypersingular operator D can be overcome by using integration by parts. In particular, there holds

$$\langle Du, v\rangle_\Gamma = \frac{1}{4\pi}\int_\Gamma \int_\Gamma \frac{\mathbf{curl}_\Gamma u(y) \cdot \mathbf{curl}_\Gamma v(x)}{|x-y|} ds_y ds_x,$$

i.e., a matrix times vector product $D_h\underline{u}$ is realized by three matrix times vector products of V_h. Thus the matrix D_h is never assembled.

The inversion of the matrix V_h and the solving of the linear system (41) are implemented by the preconditioned CG method. We use an artificial multilevel preconditioner [32] as preconditioner for V_h, and the technique of operators of opposite order [35] for the global system (41).

For the evaluation of the magnetic field, we first determine the approximate Neumann data $t_{1,h}$ and $t_{0,h}$ from

$$V_h\underline{t}_1 = (\frac{1}{2}M_h + K_h)\underline{\varphi}, \quad \text{and} \quad V_h\underline{t}_0 = (\frac{1}{2}M_h - K_h)\underline{\varphi}.$$

Thus, an approximation $\widetilde{\mathbf{H}}$ of the magnetic field $\mathbf{H}$ is computed by the discrete version of the representation formulae (10) and (18), i.e.,

$$\widetilde{\mathbf{H}}(x) = \mathbf{H}_j(x) + \frac{1}{4\pi}\nabla_x \int_\Gamma \frac{1}{|x-y|} t_{0,h}(y) ds_y - \frac{1}{4\pi}\nabla_x \int_\Gamma \frac{\partial}{\partial n_y}\frac{1}{|x-y|}\varphi_h(y) ds_y,\ x \in \Omega^c,$$

$$\widetilde{\mathbf{H}}(x) = \mathbf{H}_j(x) - \frac{1}{4\pi}\nabla_x \int_\Gamma \frac{1}{|x-y|} t_{1,h}(y) ds_y + \frac{1}{4\pi}\nabla_x \int_\Gamma \frac{\partial}{\partial n_y}\frac{1}{|x-y|}\varphi_h(y) ds_y,\ x \in \Omega.$$

In the case of a simply connected domain Ω, we evaluate

$$\widetilde{\mathbf{H}}(x) = \frac{1}{4\pi}\nabla_x \int_\Gamma \frac{1}{|x-y|}(t_{j,h}(y) - t_{1,h}(y)) ds_y - \frac{1}{4\pi}\nabla_x \int_\Gamma \frac{\partial}{\partial n_y}\frac{1}{|x-y|}(\varphi_{j,h}(y) - \varphi_h(y)) ds_y$$

for $x \in \Omega$ where we use additional approximations $\varphi_{j,h}$ and $t_{j,h}$ to represent the field $\mathbf{H}_j$ which results in better results in our numerical examples, see [19] and Sect. 4.1. For this purpose, we compute an approximation of the potential φ_j of the auxiliary Neumann boundary value problem (38) by solving

$$(\widetilde{S}_{1,h} + \underline{b}\underline{b}^\top)\underline{\varphi}_j = \underline{f}^1 \tag{42}$$

where for $k = 1, \ldots, M$

$$f_k^1 = \int_\Gamma (\mathbf{H}_j(x) \cdot n_x)\, \psi_k^1(x) ds_x, \quad b_k = \int_\Gamma \psi_k^1(x) ds_x.$$

The rank one term $\underline{b}\underline{b}^\top$ corresponds to an orthogonalization to the constant homogeneous solutions, which is used to define a unique solution $\underline{\varphi}_j$, see, e.g., [34] for details. $t_{j,h}$ corresponds to the solution of the linear system

$$V_h \underline{t}_j = (\frac{1}{2} M_h + K_h)\underline{\varphi}_j.$$

Both systems of linear equations are solved by the conjugate gradient method and the previously described preconditioning techniques.

In any case, we use the linear combination, see e.g. [15],

$$\mathbf{H}(\bar{x}_k) = \mathbf{H}_j(\bar{x}_k) - \big(t_{0,h}(\bar{x}_k) n_k + \nabla_\Gamma \varphi_h(\bar{x}_k)\big) \tag{43}$$

on the transmission interface Γ to evaluate the magnetic field in the centers $\bar{x}_k$ of the triangles τ_k with normal direction n_k. The tangential derivative $\nabla_\Gamma \varphi$ is given by

$$\nabla_\Gamma \varphi(x) = \nabla \varphi(x) - (n_x \cdot \nabla \varphi(x)) n_x = n_x \times (\nabla \varphi(x) \times n_x) \quad \text{for } x \in \Gamma \tag{44}$$

in the case that all derivatives and the exterior normal derivative are well defined. In particular, we have to exclude that x is a geometric corner point or lies on a

geometric edge. The use of linear combination (43), which also holds true for the continuous case, avoids evaluations of boundary integral operators to compute the solution on the interfaces and is one of the advantages of such direct methods.

3.2 Single Layer Potential Formulation

Based on the boundary integral equation (28), we compute a piecewise constant approximation $w_h \in S_h^0(\Gamma)$ from the system of linear equations,

$$\left(\frac{1}{2}\frac{\mu_1+\mu_0}{\mu_1-\mu_0}\widetilde{M}_h + \widetilde{K}_h'\right)\underline{w} = \underline{f}^0$$

where for $k,\ell = 1,\ldots,N$

$$\begin{aligned}
\widetilde{M}_h[k,\ell] &= \int_\Gamma \psi_\ell^0(x)\psi_k^0(x)ds_x,\\
\widetilde{K}_h'[k,\ell] &= \int_\Gamma \psi_\ell^0(x)(K\psi_k^0)(x)ds_x,\\
f_k^0 &= \int_\Gamma (\mathbf{H}_j(x)\cdot n_x)\psi_k^0(x)ds_x.
\end{aligned}$$

The linear system is solved by the GMRES method with a simple diagonal preconditioning, which is sufficient to get reasonable iteration numbers.

For the evaluation of the magnetic field, we use the ideas as presented in Sect. 2.6.2. In general, the approximation $\widetilde{\mathbf{H}}$ of the magnetic field $\mathbf{H}$ is computed by

$$\widetilde{\mathbf{H}}(x) = \mathbf{H}_j(x) - \frac{1}{4\pi}\nabla_x \int_\Gamma \frac{1}{|x-y|} w_h(y)ds_y \quad \text{for } x \in \mathbb{R}^3 \setminus \Gamma. \tag{45}$$

Next, we consider the approximate evaluation of $\mathbf{H}$ on the interface Γ. If the tangential and the normal derivative of the single layer potential operator as well as the normal direction are well defined, the gradient of the single layer potential can be defined by the splitting (44). In the case of a smooth boundary and a smooth density function, the gradient of the single layer potential has the same jump terms as its normal derivative, see, e.g., [6]. Therefore, we have to restrict the evaluation to the interior of any element τ_ℓ for $\ell = 1,\ldots,N$. Thus, we evaluate the approximate magnetic field $\widetilde{\mathbf{H}}$ by

$$\widetilde{\mathbf{H}}(x) = \mathbf{H}_j(x) - \frac{1}{2}w_h(x)n_x - \frac{1}{4\pi}\nabla_x \int_\Gamma \frac{1}{|x-y|} w_h(y)ds_y \quad \text{for almost all } x \in \Gamma \tag{46}$$

from the interior and by

$$\widetilde{\mathbf{H}}(x) = \mathbf{H}_j(x) + \frac{1}{2} w_h(x)\, n_x - \frac{1}{4\pi} \nabla_x \int_\Gamma \frac{1}{|x-y|} w_h(y) ds_y \quad \text{for allmost all } x \in \Gamma \quad (47)$$

from the exterior.

In the case of a simply connected domain, we use, as described in Sect. 2.6.2, an indirect single layer approach to represent the excitation field $\mathbf{H}_j$. We solve the system of linear equations

$$\left(\frac{1}{2} \widetilde{M}_h + \widetilde{K}'_h + \underline{a}\,\underline{a}^\top \right) \underline{w}_j = \underline{f}^0 \quad (48)$$

to compute an approximation $w_{j,h} \in S_h^0(\Gamma)$ of the density function w_j according to the boundary integral equation (39). The constraint

$$\int_\Gamma w_j(x) ds_x = 0$$

is used to define a unique solution of the auxiliary Neumann boundary value problem (30). This constraint corresponds to the rank one term $\underline{a}\,\underline{a}^\top$ with coefficients

$$a_k = \int_\Gamma \psi_k^0(x) ds_x \quad \text{for } k = 1, \ldots, N.$$

Again, the system (48) is solved by a diagonal preconditioned GMRES method. Finally, the approximation $\widetilde{\mathbf{H}}$ of the magnetic field is computed by

$$\widetilde{\mathbf{H}}(x) = \frac{1}{4\pi} \nabla_x \int_\Gamma \frac{1}{|x-y|} (w_{j,h}(y) - w_h(y)) ds_y \quad \text{for } x \in \Omega$$

and by (45) for $x \in \Omega^c$. On the interface Γ, we have to take into account the jump terms according to (46) and (47), respectively.

3.3 Direct Double Layer Potential Formulation

First, we determine an approximate solution $\varphi_{j,h} \in S_h^1(\Gamma)$ of the interior Neumann boundary value problem (30), in particular of the boundary integral equation (31). For this we solve the system of linear equations

$$\left(\frac{1}{2} \widehat{M}_h + \widehat{K}_h + \underline{b}\,\underline{b}^\top \right) \underline{\varphi}_j = \widehat{V}_h \underline{g}$$

where for $m, n = 1, \ldots, M$, $\ell = 1, \ldots, N$

$$\widehat{M}_h[m,n] = \int_\Gamma \psi_n^1(x) \psi_k^1(x) ds_x, \qquad \widehat{K}_h[m,n] = \int_\Gamma (K \psi_n^1)(x) \psi_m^1(x) ds_x,$$

$$\widehat{V}_h[m,\ell] = \int_\Gamma (V\psi_\ell^0)(x)\psi_m^1(x)ds_x, \qquad b_m = \int_\Gamma \psi_m^1(x)ds_x.$$

The rank one term $\underline{b}\,\underline{b}^\top$ is used to fix the solution which is orthogonal to the constant homogeneous solutions. Again, the linear system is solved by the GMRES method with diagonal preconditioning. $\underline{g} \in \mathbb{R}^M$ is the vector of the L_2 projection $g_h \in S_h^0(\Gamma)$ defined by

$$\int_\Gamma g_h(x)\tau_h(x)ds_x = \int_\Gamma (\mathbf{H}_j(x)\cdot n_x)\tau_h(x)ds_x \quad \text{for all } \tau_h \in S_h^0(\Gamma).$$

Next, we compute a piecewise linear and continuous approximation $v_h \in S_h^1(\Gamma)$ of the density function v of the boundary integral equation (33) from the system of linear equations

$$\left(\frac{1}{2}\frac{\mu_1+\mu_0}{\mu_1-\mu_0}\widehat{M}_h + \widehat{K}_h\right)\underline{v} = -\mu_0\widehat{M}_h\underline{\varphi}_j \tag{49}$$

which is again solved by a GMRES method with diagonal preconditioning.

Now we are in the position to compute the magnetic field $\widetilde{\mathbf{H}}$ based on the approximations as considered in Sect. 2.6.3. $\widetilde{\mathbf{H}}$ is evaluated by

$$\widetilde{\mathbf{H}}(x) = \mathbf{H}_j(x) + \frac{1}{\mu_0}\frac{1}{4\pi}\nabla_x \int_\Gamma \frac{\partial}{\partial n_y}\frac{1}{|x-y|}v_h(y)ds_y \quad \text{for } x \in \Omega^c. \tag{50}$$

For $x \in \Omega$, we distinguish between

$$\widetilde{\mathbf{H}}(x) = \frac{\mu_0}{\mu_1}\mathbf{H}_j(x) + \frac{1}{\mu_1}\frac{1}{4\pi}\nabla_x \int_\Gamma \frac{\partial}{\partial n_y}\frac{1}{|x-y|}v_h(y)ds_y \tag{51}$$

in the case of a simply connected domain Ω, and else

$$\begin{aligned}\widetilde{\mathbf{H}}(x) = \mathbf{H}_j(x) &+ \frac{1}{\mu_1}\frac{1}{4\pi}\nabla_x \int_\Gamma \frac{\partial}{\partial n_y}\frac{1}{|x-y|}v_h(y)ds_y \\ &- \frac{\mu_1-\mu_0}{\mu_1}\left(\frac{1}{4\pi}\nabla_x \int_\Gamma \frac{1}{|x-y|}g_h(y)ds_y - \frac{1}{4\pi}\nabla_x \int_\Gamma \frac{\partial}{\partial n_y}\frac{1}{|x-y|}\varphi_{j,h}(y)ds_y\right)\end{aligned}$$

using the representation formula for φ_j. On the interface Γ, we have to take into account jump terms, see, e.g., [6]. Again, we restrict the evaluation points to the interior of each element τ_ℓ. Therefore, we can compute the approximate magnetic field $\mathbf{H}$ on the interface Γ from the exterior by

$$\widetilde{\mathbf{H}}(x) = \mathbf{H}_j(x) + \frac{1}{\mu_0}\frac{1}{2}\nabla_\Gamma v_h(x) + \frac{1}{\mu_0}\frac{1}{4\pi}\int_\Gamma \mathbf{curl}_{\Gamma,y}v_h(y)\times\nabla_x\frac{1}{|x-y|}ds_y \tag{52}$$

for almost all $x \in \Gamma$. For the interior trace we evaluate

$$\widetilde{\mathbf{H}}(x) = \frac{\mu_0}{\mu_1}\mathbf{H}_j(x) - \frac{1}{\mu_1}\frac{1}{2}\nabla_\Gamma v_h(x) + \frac{1}{\mu_1}\frac{1}{4\pi}\int_\Gamma \mathbf{curl}_{\Gamma,y} v_h(y) \times \nabla_x \frac{1}{|x-y|} ds_y \quad (53)$$

for almost all $x \in \Gamma$ in the case of a simply connected domain Ω, and else

$$\widetilde{\mathbf{H}}(x) = \mathbf{H}_j(x) - \frac{1}{\mu_1}\frac{1}{2}\nabla_\Gamma v_h(x) + \frac{1}{\mu_1}\frac{1}{4\pi}\int_\Gamma \mathbf{curl}_{\Gamma,y} v_h(y) \times \nabla_x \frac{1}{|x-y|} ds_y$$

$$-\frac{\mu_1-\mu_0}{\mu_1}\left(\frac{1}{2}g_h(x)n_x + \frac{1}{4\pi}\nabla_x \int_\Gamma \frac{1}{|x-y|} g_h(y) ds_y + \frac{1}{2}\nabla_\Gamma \varphi_{j,h}(x) - \nabla(K\varphi_{j,h})(x)\right)$$

for almost all $x \in \Gamma$.

3.4 Indirect Double Layer Potential Formulation

In contrast to the direct version, we now find a representation of φ_j by using the indirect single layer potential. Therefore, we compute an approximation $w_{j,h}$ from the linear system (48) as in the case of the single layer potential formulation.

Accordingly, the approximation $v_h \in S_h^1(\Gamma)$ is determined from the system of linear equations

$$\left(\frac{1}{2}\frac{\mu_1+\mu_0}{\mu_1-\mu_0}\widehat{M}_h + \widehat{K}_h\right)\underline{v} = -\mu_0 \widehat{V}_h^\top \underline{w}_j \quad (54)$$

instead of from the system (49).

For the evaluation of the magnetic field, we follow the lines of the direct double layer potential formulation. We use (50) for $x \in \Omega^c$ and (51) for $x \in \Omega$ in the case of a simply connected domain. For a multiple connected domain, the evaluation for Ω reads as

$$\widetilde{\mathbf{H}}(x) = \mathbf{H}_j(x) + \frac{1}{\mu_1}\frac{1}{4\pi}\nabla_x \int_\Gamma \frac{\partial}{\partial n_y}\frac{1}{|x-y|} v_h(y) ds_y - \frac{\mu_1-\mu_0}{\mu_1}\frac{1}{4\pi}\nabla_x \int_\Gamma \frac{1}{|x-y|} w_{j,h}(y) ds_y.$$

For the interior trace in the case of a simply connected domain and for the exterior trace, the approximate gradient field $\widetilde{\mathbf{H}}(x)$ for almost all $x \in \Gamma$ is computed by (53) and (52), respectively. Just for the case of a multiple connected domain, the interior trace changes to

$$\widetilde{\mathbf{H}}(x) = \mathbf{H}_j(x) - \frac{1}{\mu_1}\frac{1}{2}\nabla_\Gamma v_h(x) + \frac{1}{\mu_1}\frac{1}{4\pi}\int_\Gamma \mathbf{curl}_{\Gamma,y} u(y) \times \nabla_x \frac{1}{|x-y|} ds_y$$

$$-\frac{\mu_1-\mu_0}{\mu_1}\left(\frac{1}{2}w_{j,h}(x)n_x + \frac{1}{4\pi}\nabla_x \int_\Gamma \frac{1}{|x-y|} w_{j,h}(y) ds_y\right)$$

for almost all $x \in \Gamma$.

4 Numerical Examples

In this section, we compare and discuss the presented single layer potential formulation (SL) of Sect. 3.2, the indirect version of the double layer potential formulation (IDL) of Sect. 3.4, the direct version of the double layer potential formulation (DL) of Sect. 3.3, and the Steklov–Poincaré operator interface formulation (SP) of Sect. 3.1 for several test examples. We try to elaborate the advantages and the drawbacks of the discussed approaches. For the details of the computations, see Sect. 3. In all examples, we consider $\mu_0 = 4\pi \cdot 10^{-7}$ and $\mu_1 = \mu_0 \mu_r$ with different values of the relative permeability μ_r.

4.1 Sphere

To show the effect of the modified evaluation methods in the case of simply connected domains, as presented in Sect. 2.6, we start with a numerical example where Ω is a sphere of diameter 10^{-3}, and where the analytic solution is known. The excitation field is given as $\mathbf{H}_j = (0,0,17)^\top$, which results in the magnetic field $\mathbf{H} = (0,0,51/(\mu_r+2))^\top$, see [19]. In Fig. 1, the relative $L_2(\Gamma)$ errors of the approximate solutions $\widetilde{\mathbf{H}}$ of the magnetic field $\mathbf{H}$ are given for several values of μ_r, and for an approximation of the sphere by 288 plane triangles. Since the sphere is simply connected, approximation problems appear for a higher relative permeability μ_r. To investigate this behavior we consider values $\mu_r = 5 \cdot 10^s$ for $s \in \{0,1,\ldots,13\}$. This problem has been discussed in Sect. 2.6. We observe the same effects also for finer meshes. We compare the straightforward evaluations with their modified versions, which were presented in Sect. 2.6.1 to 2.6.3 to overcome these problems.

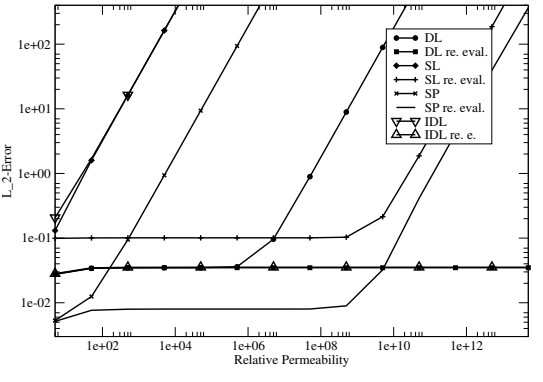

Fig. 1 L_2-error of the magnetic field plotted versus the relative permeability for all formulations

Almost instantly, the errors for most approaches without the modified evaluation increases dramatically for increasing μ_r. The only exception seems to be the direct double layer formulation (DL), which stays accurate up to a relative permeability of $5 \cdot 10^6$. However, the accuracy decreases dramatically for higher permeabilities. The rewritten evaluations certainly improve the accuracy for all approaches. For the single layer potential ansatz (SL) and for the Steklov–Poincaré operator formulation (SP) the rewritten evaluation is feasible up to a relative permeability of about $5 \cdot 10^9$. For higher permeabilities the error of the evaluation increases again. However, the accuracy of the rewritten evaluation of the indirect (IDL) and of the direct double layer potential formulation (DL) seems to be stable even up to the maximal computed $\mu_r = 5 \cdot 10^{19}$. When using the rewritten evaluation, there seems to be little difference between the two double layer potential approaches. This is however due to the absence of edges and corners, which will be considered in Sect. 4.2 for the particular case when Ω is a cube.

Comparing the accuracy of the four methods in the stable region, the Steklov–Poincaré operator formulation gives better results than the two double layer potential formulations which in turn are more accurate than the single layer potential formulation. From here on, we always use the modified evaluations in the case of a simply connected domain.

4.2 Cube

As an academic example with corner and edges, the cube $\Omega = (0,1)^3$ is chosen and the initial mesh (level 0) of 24 triangles is refined uniformly several times. The excitation field is induced by a conductor loop with the center at $(0.5, 0.5, 0.5)^\top$ and a radius of one. We use

$$\|\widetilde{\mathbf{H}}_L - \widetilde{\mathbf{H}}_7^{\mathrm{DL}}\|_V / \|\widetilde{\mathbf{H}}_7^{\mathrm{DL}}\|_V, \quad \text{where } \|w\|_V^2 = \frac{1}{4\pi} \int_\Gamma w(x) \int_\Gamma \frac{1}{|x-y|} w(y) ds_y ds_x,$$

as an error indicator for the approximation $\widetilde{\mathbf{H}}_L$ on the Lth refinement level. This error indicator approximates the relative $H^{-1/2}(\Gamma)$ error, as the single layer boundary integral operator V induces an equivalent norm. The solution of the considered transmission problem is not known analytically. Therefore, the approximation $\widetilde{\mathbf{H}}_7^{\mathrm{DL}}$ of the direct double layer potential approach at the refinement level seven is chosen as reference solution, as this approach seems to be the most accurate one for this example. Thus the order of convergence at level six of the direct double layer potential formulation is too high and not reliable. In Tables 1 and 2, the single layer potential ansatz (SL) is compared with the Steklov–Poincaré operator formulation (SP), the indirect (IDL) and the direct (DL) double layer potential formulations and for $\mu_r = 5000$ and $\mu_r = 5$, respectively.

The single layer potential formulation (SL) shows the largest errors and the lowest experimental order of convergence (eoc) of all approaches. The indirect double layer approach (IDL) also seems to have a lower convergence order for $\mu_r = 5$,

Table 1 Approximate $H^{1/2}(\Gamma)$ error and convergence order for the cube and $\mu_r = 50000$

L	SL	eoc	IDL	eoc	DL	eoc	SP	eoc
0	6.37e-01		2.02e-01	0.93	1.27e-01	1.06	1.51e-01	0.82
2	2.69e-01	0.60	1.15e-01	0.82	6.80e-02	0.90	7.94e-02	0.93
3	1.79e-01	0.59	6.60e-02	0.80	3.86e-02	0.82	4.64e-02	0.77
4	1.20e-01	0.58	3.83e-02	0.79	2.18e-02	0.82	2.71e-02	0.78
5	8.38e-02	0.51	2.16e-02	0.83	1.14e-02	0.93	1.50e-02	0.85
6	5.27e-02	0.67	1.12e-02	0.94	4.80e-03	1.25	7.24e-03	1.05

Table 2 Approximate $H^{1/2}(\Gamma)$ error and convergence order for the cube and $\mu_r = 5$

L	SL	eoc	IDL	eoc	DL	eoc	SP	eoc
0	5.23e-01		2.58e-01		1.66e-01		1.58e-01	
1	3.06e-01	0.77	1.31e-01	0.98	7.35e-02	1.18	8.97e-02	0.82
2	1.91e-01	0.68	7.06e-02	0.89	3.25e-02	1.18	3.50e-02	1.36
3	1.22e-01	0.64	3.99e-02	0.82	1.62e-02	1.00	1.78e-02	0.98
4	8.02e-02	0.61	2.33e-02	0.78	8.42e-03	0.94	9.67e-03	0.88
5	5.28e-02	0.60	1.36e-02	0.77	4.16e-03	1.02	5.09e-03	0.93
6	3.47e-02	0.60	7.84e-03	0.80	1.67e-03	1.32	2.35e-03	1.11

whereas for $\mu_r = 50000$ the convergence order seems to be comparable to the direct double layer potential formulation and to the Steklov–Poincaré operator formulation (SP), but nevertheless its errors are larger. In general, density functions of indirect approaches show a lower regularity than the quantities of direct approaches, see, e.g., [7, 27]. In such a case, the convergence order of the approximation is reduced. The direct double layer potential formulation (DL) seems to have the highest order of convergence for both permeabilities, however the Steklov–Poincaré operator formulation gives comparable results. For none of the formulations the optimal order of convergence is obtained, as the solution of the transmission problem does not provide the necessary regularity due to the reentrant corners with respect to the exterior domain, see again [27].

In the case of $\mu_r = 50000$ and the single layer potential ansatz, the accuracy of the fast multipole method and thus the computational times had to be increased dramatically to reach the shown convergence rates. For the other approaches, such an additional adjustment of the parameters of the fast multipole method was not necessary. It was observed that the result of the single layer ansatz was very sensitive especially at corners. The behavior of the method at corners and edges will be discussed in more details in Sect. 4.3.

4.3 Ring

As a multi–connected domain, a three–dimensional ring with a square as cross section, as depicted in Fig. 2, is considered. The radius of the ring is 0.1 and the length and height of the cross section are 0.05. Again, a relative permeability $\mu_r = 50000$

is considered. The excitation field is created by a conductor loop with radius 0.1 and an induced current of 500A. The ring is approximated by several surface meshes of 560, 2024, 8096, 32384, and 128832 plane triangles.

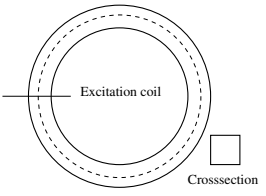

Fig. 2 2D projection of the ring and dotted line of evaluation points

Again, we consider all four presented methods. First, we compare the evaluated magnetic field $\widetilde{\mathbf{H}}$ on the surface for the mesh of 2024 triangles. In Fig. 3 and 4, the approximate magnetic field $\widetilde{\mathbf{H}}$ on the interior of the boundary is plotted in the centers of each triangle for all discussed methods.

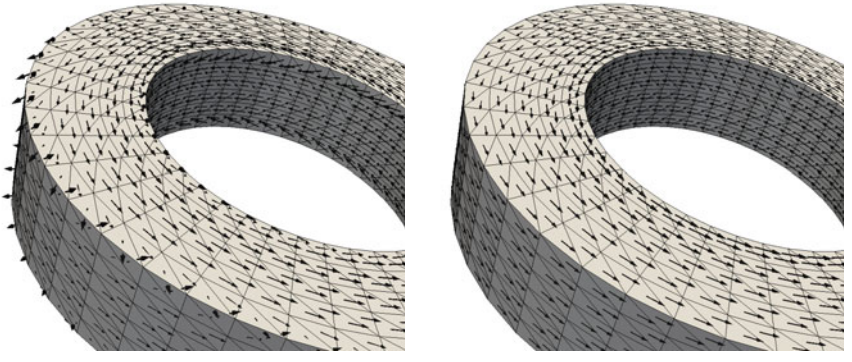

Fig. 3 Approximate magnetic field $\widetilde{\mathbf{H}}$ for the single layer potential ansatz (left) and the direct double layer potential formulation (right) for $\mu_r = 50000$ and 2024 triangles

Apart from the edges the results look alike, whereas close to geometric edges the vector fields $\widetilde{\mathbf{H}}$ differ significantly. There we observe two good and two bad approximate solutions. The Steklov–Poincaré operator formulation and the direct double layer potential formulation provide good approximations of the magnetic field. But the approximations by the single layer potential ansatz and the indirect double layer potential ansatz are non–physical in the last two elements towards the geometrical edges. Nevertheless, if we fix such an observation point and consider finer meshes, the magnetic fields of these two approaches converge towards the result of the Steklov–Poincaré operator approach and the direct double layer potential

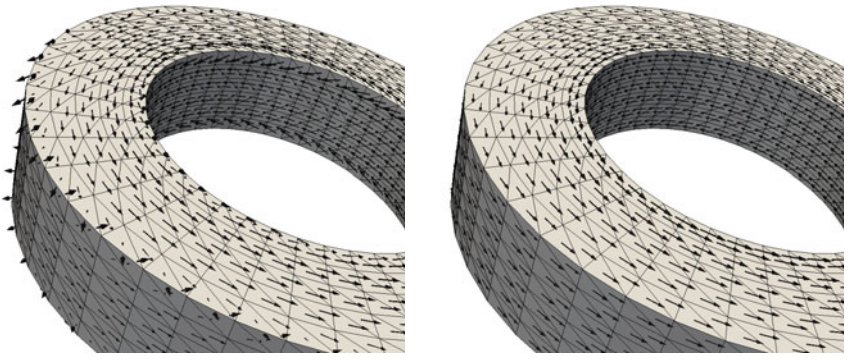

Fig. 4 Approximations of $\widetilde{\mathbf{H}}$ for the indirect double layer potential ansatz (left) and for the Steklov–Poincaré operator formulation (right) for $\mu_r = 50000$ and 2024 triangles

formulation at that observation point. The same effects were observed for all tested values of μ_r in all examples with edges. We conclude that the approximations of the magnetic field close to geometrical edges for the single layer potential formulation and for the indirect double layer potential ansatz have a very low accuracy. While the direct double layer potential gives good approximations, the indirect version suffers from these effects, which are introduced by the low accuracy of the indirect approximation of the interior Neumann boundary value problem.

Next, all formulations are compared with respect to the accuracy of interior point evaluations. Therefore, the magnetic field is evaluated along the dotted line in the center of the cross section as depicted in Fig. 2 for a relative permeability $\mu_r = 50000$. It is well known that for $\mu_r \to \infty$ the magnitude of the magnetic field tends towards an uniform distribution along this line. In Fig. 5, the magnitudes of the magnetic field are plotted for three subsequent refinement levels with 560 (L1), 2024 (L2), and 8096 (L3) boundary elements.

For the coarsest mesh the geometrical approximation dominates the errors for all four approaches, After one refinement step, the geometry seems to be dissolved fine enough, as the Steklov–Poincaré operator approach (SP) already provides a suitable approximation. The curves of the second and third level of the Steklov–Poincaré operator formulation do not differ much and are already quite close to the almost uniform distribution. The direct double layer potential (DL) offers reasonable approximations even if they are worse than those of the Steklov–Poincaré operator formulation. Obviously, the approximations of the single layer potential ansatz (SL) and of the indirect double potential ansatz (IDL) are significantly worse than those of the two other methods, in particular, close to the excitation coil.

We extend the comparison by the computational times, which are given in seconds in Table 3. The computational times include the setup and solving of the linear systems as well as the evaluation in the interior points and the computation of the gradient on the surface.

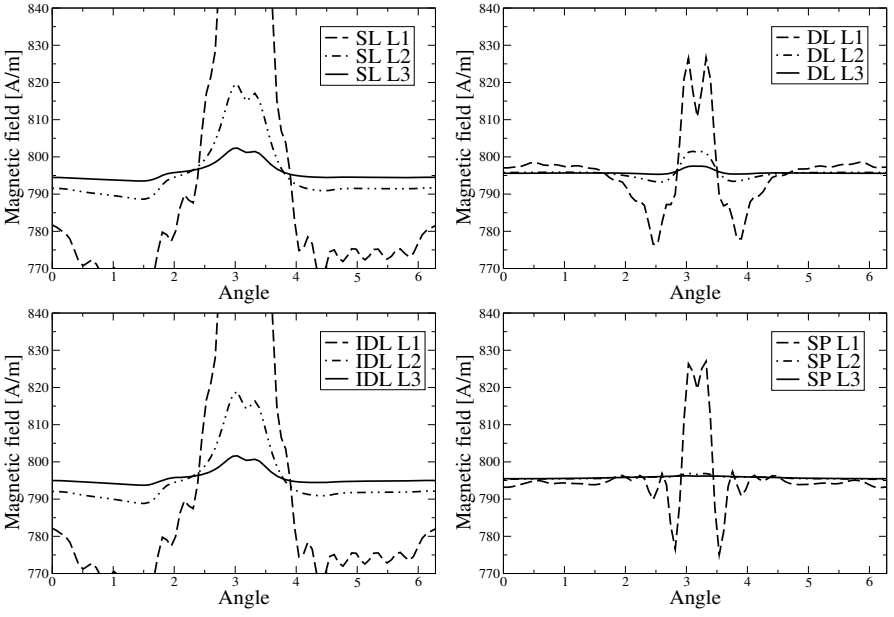

Fig. 5 Magnetic field along the dotted line of the ring

Table 3 Solution time for the ring in seconds

L	# Elements	SL	DL	IDL	SP
1	560	1	5	5	13
2	2024	5	46	26	81
3	8096	14	87	82	268
4	32384	75	448	459	1443
5	128832	248	1623	1610	4832

For a fixed level L, the increase in the computational times from the single layer potential ansatz to the double layer potential approaches is mainly due to the setup of the additional matrices, to the higher polynomial degree of the ansatz and test functions, and to the solution of a second system of linear equations. As the indirect double layer potential ansatz requires approximately the same amount of time as the direct version, and the results are always worse, there is no benefit to use the indirect version. The Steklov–Poincaré operator formulation requires the largest amount of computational times because all boundary integral operators as well as the preconditioners are computed, and local Dirichlet boundary value problems have to be solved in each iteration step of the global system (41).

But such a comparison of computational times has to take into account the accuracy of the approximations, too. In Table 4, the computational times of the formulations are compared with respect to matchable relative errors in the discrete l_2 norm

$$\left(\sum_{k=1}^{P} |\widetilde{\mathbf{H}}_L(y_k) - \widetilde{\mathbf{H}}_5^{\mathrm{SP}}(y_k)|^2\right)^{\frac{1}{2}} \left(\sum_{k=1}^{P} |\widetilde{\mathbf{H}}_5^{\mathrm{SP}}(y_k)|^2\right)^{-\frac{1}{2}}$$

with P evaluation points y_k along the dotted line in the center of the cross section, see Fig. 2. The solution of the Steklov–Poincaré operator formulation at level five was chosen as a reference solution, as it seems to be the most accurate one.

Table 4 Comparison of the methods for different refinement levels of the ring

Method	level L	# Elements	Solution Time	rel. l_2-error
DL	3	8096	87	5.25e-4
SL	5	128832	248	4.40e-4
IDL	5	128832	1610	4.40e-4
SP	2	2024	81	2.45e-4
DL	5	128832	1623	7.79e-5
SP	3	8096	268	3.24e-5

The error of the single layer potential ansatz (SL) and the error of the indirect double layer potential ansatz (IDL) at level five are both about $4.4 \cdot 10^{-4}$. The direct double layer potential formulation and the Steklov–Poincaré operator approach give comparable errors at level three and two, respectively. They require almost the same computational time and outperform the other two approaches by a factor of three. Still the accuracy of the Steklov–Poincaré operator approach is twice as high. Comparing the last level of the direct double layer potential formulation to level three of the Steklov–Poincaré operator formulation, the latter is clearly faster and yields a higher accuracy.

Overall, the indirect double layer potential ansatz and the single layer potential ansatz give similar results for this example, as we observed a bad approximation towards edges, and an overall poor accuracy of the approximate solutions. The Steklov–Poincaré operator approach outperforms the other approaches as far as accuracy of interior point evaluations is concerned.

Remark 1. The presented computational times depend highly on the details of the implementation of the boundary element method. The fast multipole method is optimal suited for a low number of matrix times vector multiplications like for the single and double layer potential formulations. Our integration routines are based on the use of semi–analytic integration formulae [29] and exploit the lowest order elements in K_h' as well as the large blocks of zero entries in K_h and K_h'. Overall, our implementation is more favorable for the potential approaches than for the Steklov–Poincaré operator formulation.

The use of integration routines based on the Duffy transformation [10] would not give the potential approaches such an advantage. The use of the adaptive cross approximation [2] would increase the setup and evaluation times in general, but the times for solving a linear system of equations would be reduced significantly. The Steklov–Poincaré operator formulation would benefit in comparison to the potential

approaches, due to the realization of the inverse single layer potential operator in each iteration step of the global solution algorithm.

4.4 Ring with Gap

As another example of a simply connected domain, a ring with gap, see Fig. 6, was chosen. The initial discretization consists of 552 boundary elements. The boundary was further discretized with 2096 elements on level two, 8394 elements on level three, 33536 elements on level four, and 107264 elements on level five. All computations are based on the modified formulations as discussed in Sect. 2.6.

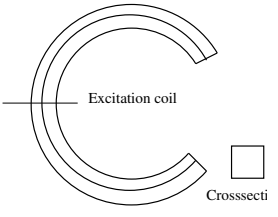

Fig. 6 2D projection of the ring with gap and dotted line of evaluation points

The magnetic flux density **B** is evaluated along the center line of the ring, depicted in Fig. 6, and plotted in Fig. 7 for relative permeabilities $\mu_r = 5$ and $\mu_r = 50000$. We use the same evaluation formulae as for the magnetic field **H** but take care of the additional scaling. As the indirect version of the double layer potential formulation showed to be worse than the direct version in all our examples, we restrict our investigations to the direct formulation only.

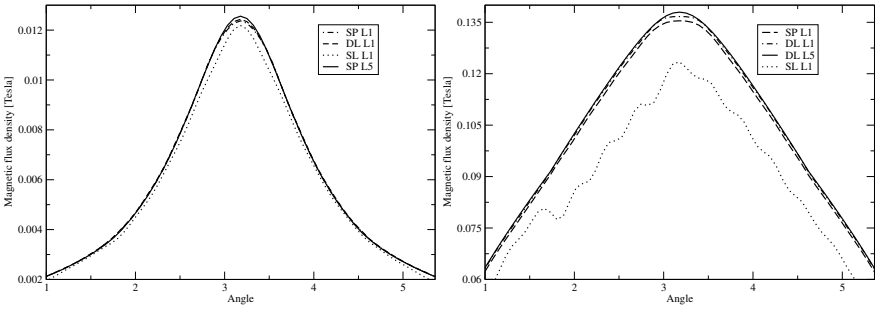

Fig. 7 Magnetic flux density **B** along the dotted line of the ring for $\mu_r = 5$ (left) and $\mu_r = 50000$ (right)

For $\mu_r = 5$, the magnetic flux $\mathbf{B}$ computed by the Steklov–Poincaré operator formulation (SP) was chosen as reference solution and for $\mu_r = 50000$ the $\mathbf{B}$ field computed by the direct double layer potential formulation (DL) was chosen as a reference solution. Those methods turned out to be the most accurate ones. Additionally, the respective relative l_2 errors for the interior point evaluation along the dotted line as shown in Fig. 6 are given in Tables 5 and 6.

It can be observed that the accuracy of the single layer potential ansatz (SL) is already considerably worse at the first level. This is especially visible in Fig. 7 for $\mu_r = 50000$. Furthermore, due to lower rates of convergence, the discrepancy gets even higher for finer levels.

For $\mu_r = 5$ the Steklov–Poincaré operator formulation (SP) results in the highest accuracy. For levels three and four, the error is about half the error of the direct double layer potential formulation. For $\mu_r = 50000$, however, the direct double layer potential approach results in half the error of the Steklov–Poincaré operator formulation. The Steklov–Poincaré operator formulation starts out with a higher error for both cases but tends to have a higher convergence rate. It has to be noted that the convergence rate of the direct double layer potential formulation for level four for $\mu_r = 50000$ is not reliable, since the direct double layer potential formulation at level five was chosen as a reference solution. Overall, the direct double layer potential formulation and the Steklov–Poincaré operator approach give comparable good results for this example.

Table 5 Relative l_2 error and order of convergence for the ring with gap and $\mu_r = 5$

L	SL	eoc	DL	eoc	SP	eoc
1	5.97e-02		6.29e-03		8.03e-03	
2	2.08e-02	1.52	1.68e-03	1.91	1.31e-03	2.62
3	5.38e-03	1.96	4.00e-04	2.07	2.61e-04	2.33
4	1.32e-03	2.03	8.64e-05	2.21	4.23e-05	2.62

Table 6 Relative l_2 error and order of convergence for the ring with gap and $\mu_r = 50000$

L	SL	eoc	DL	eoc	SP	eoc
1	3.96e-03		1.04e-04		3.64e-04	
2	1.38e-03	1.52	5.71e-05	0.86	1.17e-04	1.64
3	4.24e-04	1.70	2.19e-05	1.38	3.73e-05	1.64
4	1.26e-04	1.75	4.97e-06	2.14	1.03e-05	1.86

4.5 Controllable Reactor

Finally, we consider a controllable reactor as an example of an industrial application. Controllable reactors, sometimes called shunt reactors, are important components in Extra/Ultra High Voltage power systems used for voltage regulation issues. Typically fixed shunt reactors are used to compensate the reactive power. New concepts

are based on controllable reactors. Fig. 8 shows the typical structure of a controllable reactor. The cylindric structure in the middle, which is wrapped by the main winding in the complete setup, consists of alternating layers of iron discs and control discs. By modifying the current in the windings wound around the control discs, the saturation level of the magnetic core can be adjusted and thus the total inductance, i.e., the reluctance of the reactor can be controlled interactively.

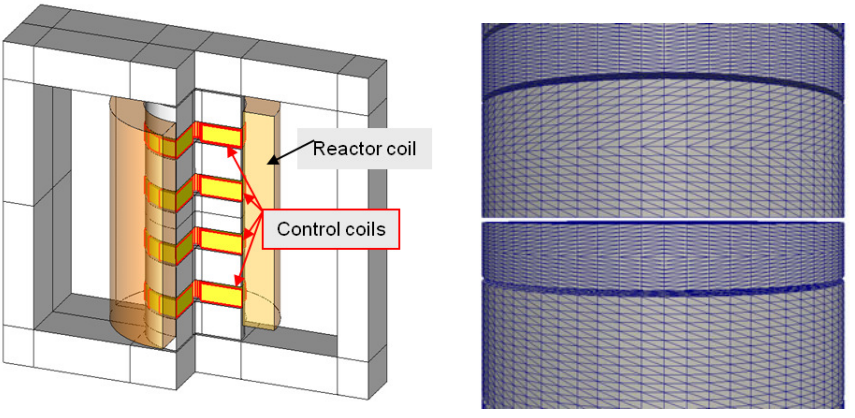

Fig. 8 Controllable reactor and a closeup of the small gaps

For the purpose of this paper, we assume a linear and isotropic behavior of the magnetic material with a relative permeability of $\mu_r = 200$. The surface of the reactor is approximated by 122880 triangular boundary elements. The calculated magnetic fields $\widetilde{\mathbf{H}}$ of the three different approaches are plotted on the surface of one of the iron discs in Fig. 9.

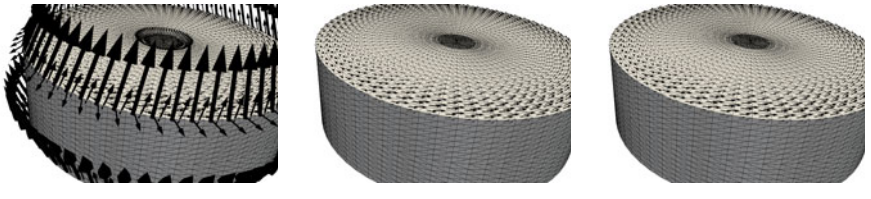

Fig. 9 Magnetic field of the single layer potential ansatz (left), the direct double layer potential formulation (middle), and the Steklov–Poincaré operator formulation (right) for $\mu_1 = 200$

As expected, the approximate magnetic field of the single layer potential ansatz shows the same non–physical phenomena at corners and edges as in the example of the ring in Sect. 4.3. Additionally, the result differs close to the center of the smooth surface of the disc because the gap to the next control disc is very small and these

control discs have a small hole in the middle. Thus a corner is very close to these elements, which seems to disrupt the solution on the iron disc. As for the previous examples, the double layer potential ansatz (DL) and the Steklov–Poincaré operator formulation (SP) provide good approximations of the magnetic field.

5 Conclusions

We considered several boundary integral equations for the solution of the transmission problem of a scalar potential ansatz in the context of linear magnetostatics. In contrast to other formulations in the literature, all presented formulation are not only applicable to simply connected domains but to multiple connected domains, too. While the formulations are equivalent in the continuous setting, their discretized versions are diverse. Therefore, we presented an in–depth comparison of the considered approaches. Based on plenty of numerical examples, we are able to rate these approaches.

The presented discrete version of the single layer potential approach is maybe the most easiest to implement and seems to be the fastest method at a first glance, but it provides extremely poor approximations of the variables of interest for non academic examples. Similarly, the indirect version of the double layer potential formulation yields bad approximate solutions, as the auxiliary indirect problem is solved in the same way as the single layer potential approach.

The direct double layer potential formulation and the Steklov–Poincaré operator approach both provide excellent computational results and are the methods of choice. The direct double layer potential formulation features a natural stabilization for the evaluation of the field values in the case of a simply connected domain. In most of our examples, the Steklov–Poincaré operator approach offers more accurate results. In addition, the Steklov–Poincaré operator formulation is applicable to the cases of more subdomains with several different permeabilities and provides a straightforward parallelization. The final performance of the direct double layer formulation and of the Steklov–Poincaré operator approach depends highly on the implementation.

Acknowledgements. This work was supported by the Euorpean Union within the framework of the FP7 Marie Curie IAPP Project CASOPT (Controlled Component and Assembly Level Optimization of Industrial Devices, www.casopt.com).

References

[1] Andjelic, Z., Of, G., Steinbach, O., Urthaler, P.: Boundary element methods for magnetostatic field problems: A critical view. Comput. Visual. Sci. 14, 117–130 (2011)
[2] Bebendorf, M., Rjasanow, S.: Adaptive low–rank approximation of collocation matrices. Computing 70(1), 1–24 (2003)
[3] Beuchler, S., Eibner, T., Langer, U.: Primal and dual interface concentrated iterative substructuring methods. SIAM J. Numer. Anal. 46, 2818–2842 (2008)

[4] Bossavit, A.: A rationale for 'edge–elements' in 3-d fields computations. IEEE Trans. Magn. 24(1), 74–79 (1988)
[5] Buchau, A., Rucker, W.M., Rain, O., Rischmüller, V., Kurz, S., Rjasanow, S.: Comparison between different approaches for fast and efficient 3-D BEM computations. IEEE Trans. Magn. 39(3), 1107–1110 (2003)
[6] Colton, D.L., Kress, R.: Integral equation methods in scattering theory. Pure and Applied Mathematics. John Wiley & Sons Inc., New York (1983)
[7] Costabel, M., Stephan, E.P.: Boundary integral equations for mixed boundary value problems in polygonal domains and Galerkin approximation. In: Mathematical Models and Methods in Mechanics, vol. 15, pp. 175–251. Banach Center Publ., PWN, Warsaw (1985)
[8] Coulomb, J.L.: Finite elements three dimensional magnetic field computation. IEEE Trans. Magn. 17(6), 3241–3246 (1981)
[9] Demkowicz, L., Kurtz, J., Pardo, D., Paszynski, M., Rachowicz, W., Zdunek, A.: Computing with hp–adaptive finite elements. Frontiers: three–dimensional elliptic and Maxwell problems with applications, vol. 2. Chapman & Hall/CRC, Boca Raton (2008)
[10] Erichsen, S., Sauter, S.A.: Efficient automatic quadrature in 3-D Galerkin BEM. Comput. Methods Appl. Mech. Eng. 157(3-4), 215–224 (1998)
[11] Forster, H., Schrefl, T., Dittrich, R., Scholz, W., Fidler, J.: Fast boundary methods for magnetostatic interactions in micromagnetics. IEEE Trans. Magn. 39(5), 2513–2515 (2003)
[12] Greengard, L., Rokhlin, V.: A fast algorithm for particle simulations. J. Comput. Phys. 73, 325–348 (1987)
[13] Hafla, W., Groh, F., Buchau, A., Rucker, W.M.: Magnetostatic field computations by an integral equation method using a difference field concept and the fast multipole method. In: Proceedings of the 10th International IGTE Symposium on Numerical Field Calculation in Electrical Engineering, pp. 262–266 (2002)
[14] Hofreither, C., Langer, U., Pechstein, C.: Analysis of a non–standard finite element method based on boundary integral operators. Electr. Trans. Numer. Anal. 436, 413–436 (2010)
[15] Hsiao, G.C., Wendland, W.L.: Boundary integral equations. Applied Mathematical Sciences, vol. 164. Springer, Berlin (2008)
[16] Ishibashi, K., Andjelic, Z.: Nonlinear magnetostatic BEM formulation using one unknown double layer charge. In: Proceedings of the 14th International IGTE Symposium 2010 (2010)
[17] Khoromskij, B.N., Melenk, J.M.: Boundary concentrated finite element methods. SIAM J. Numer. Anal. 41, 1–36 (2003)
[18] Khoromskij, B.N., Wittum, G.: Numerical Solution of Elliptic Differential Equations by Reduction to the Interface. LNCSE, vol. 36. Springer, Heidelberg (2004)
[19] Krstajic, B., Andelic, Z., Milojkovic, S., Babic, S., Salon, S.: Nonlinear 3D magnetostatic field calculation by the integral equation method with surface and volume magnetic charges. IEEE Trans. Magn. 28(2), 1088–1091 (1992)
[20] Kuhn, M., Langer, U., Schöberl, J.: Scientific computing tools for 3D magnetic field problems. In: The Mathematics of Finite Elements and Applications, pp. 239–258. Elsevier (2000)
[21] Lindholm, D.: Notes on boundary integral equations for three–dimensional magnetostatics. IEEE Trans. Magn. 16(6), 1409–1413 (1980)
[22] Magele, C., Stogner, H., Preis, K.: Comparison of different finite element formulations for 3D magnetostatic problems. IEEE Trans. Magn. 24(1), 31–34 (1988)

[23] Mayergoyz, I., Chari, M., D'Angelo, J.: A new scalar potential formulation for three–dimensional magnetostatic problems. IEEE Trans. Magn. 23(6), 3889–3894 (1987)
[24] Mayergoyz, I.D., Andrei, P., Dimian, M.: Nonlinear magnetostatic calculations based on fast multipole method. IEEE Trans. Magn. 39(3), 1103–1106 (2003)
[25] McLean, W.: Strongly Elliptic Systems and Boundary Integral Equations. Cambridge University Press, Cambridge (2000)
[26] Of, G., Steinbach, O., Wendland, W.L.: The fast multipole method for the symmetric boundary integral formulation. IMA J. Numer. Anal. 26(2), 272–296 (2006)
[27] von Petersdorff, T., Schwab, C.: Wavelet approximations for first kind boundary integral equations on polygons. Numer. Math. 74(4), 479–516 (1996)
[28] Radon, J.: Zur mechanischen Kubataur. Monatshefte Math. 52, 286–300 (1948)
[29] Rjasanow, S., Steinbach, O.: The fast solution of boundary integral equations. Mathematical and Analytical Techniques with Applications to Engineering. Springer, New York (2007)
[30] Rucker, W.M., Richter, K.R.: Three–dimensional magnetostatic field calculation using boundary element method. IEEE Trans. Magn. 24(1), 23–26 (1988)
[31] Sauter, S.A., Schwab, C.: Boundary Element Methods. Springer Series in Computational Mathematics, vol. 39. Springer, Heidelberg (2011)
[32] Steinbach, O.: Artificial multilevel boundary element preconditioners. Proc. Appl. Math. Mech. 3, 539–542 (2003)
[33] Steinbach, O.: Stability estimates for hybrid coupled domain decomposition methods. LNM, vol. 1809. Springer, Berlin (2003)
[34] Steinbach, O.: Numerical approximation methods for elliptic boundary value problems. Finite and boundary elements. Springer, New York (2008)
[35] Steinbach, O., Wendland, W.L.: The construction of some efficient preconditioners in the boundary element method. Adv. Comput. Math. 9(1-2), 191–216 (1998)

Wave Propagation Problems Treated with Convolution Quadrature and BEM

Lehel Banjai and Martin Schanz

Abstract. Boundary element methods for steady state problems have reached a state of maturity in both analysis and efficient implementation and have become an ubiquitous tool in engineering applications. Their time-domain counterparts, however, in particular for wave propagation phenomena, still present many open questions related to the analysis of the numerical methods and their algorithmic implementation. In recent years many exciting results have been achieved in this area. In this review paper, a particular type of methods for treating time-domain boundary integral equations (TDBIE), the *convolution quadrature*, is described together with application areas and most recent improvements to the analysis and efficient implementation. An important attraction of these methods is their intrinsic stability, often a problem with numerical methods for TDBIE of wave propagation. Further, since convolution quadrature, though a time-domain method, uses only the kernel of the integral operator in the Laplace domain, it is widely applicable also to problems such as viscoelastodynamics, where the kernel is known only in the Laplace domain. This makes convolution quadrature for TDBIE an important numerical method for wave propagation problems, which requires further attention.

1 Introduction – State of the Art

The Boundary Element Method (BEM) in time domain is especially important for treating wave propagation problems in semi-infinite or infinite domains. In this

Lehel Banjai
Max-Planck Institute for Mathematics in the Sciences, Inselstrasse 22,
04103 Leipzig, Germany
e-mail: banjai@mis.mpg.de

Martin Schanz
Graz University of Technology, Institute of Applied Mechanics,
Technikerstr. 4, 8010 Graz, Austria
e-mail: m.schanz@tugraz.at

U. Langer et al. (Eds.): Fast Boundary Element Methods, LNACM 63, pp. 145–184.
springerlink.com

application the main advantage of this method becomes obvious, i.e., its ability to model the radiation condition correctly. Certainly this is not the only advantage of a time domain BEM but very often the main motivation as, e.g., in earthquake engineering or scattering problems. The mathematical background of time-dependent boundary integral equations is summarized by COSTABEL [27].

Scattering problems have been treated very early with integral equations where some solution techniques may be seen as a BEM in time domain, e.g., [37]. For elastodynamics the first boundary integral formulation was published by CRUSE and RIZZO [28]. However, this formulation performs in Laplace domain with a subsequent inverse transformation to time domain to achieve results for the transient behavior. The corresponding formulation in Fourier domain, i.e., frequency domain, was presented by DOMÍNGUEZ [35]. The first boundary element formulation directly in the time domain was developed by MANSUR for the scalar wave equation and for elastodynamics with zero initial conditions [56]. The extension of this formulation to non-zero initial conditions was presented by ANTES [5]. A completely different approach to handle dynamic problems utilizing static fundamental solutions is the so-called dual reciprocity BEM. This method was introduced by NARDINI and BREBBIA [62] and details may be found in the monograph of PARTRIDGE, BREBBIA, and WROBEL [64]. A very detailed review of elastodynamic boundary element formulations and a list of applications can be found in two articles of BESKOS [15, 16]. Fast formulations for elastodynamics based on a plane wave expansion has been published by OTANI et. al. [63] and TAKAHASHI et. al. [80].

An important area of applications of time (and frequency) domain boundary integral equations is electrodynamics. Variational methods initiated for acoustics [9] have been extended to electromagnetism in [81, 83, 7, 66] and also to FEM-BEM coupling in the time domain [8]. Collocation methods are also here of great importance in applications [34]. There has been a very important development in fast methods for electrodynamics [77, 85, 25] where fast multipole methods for high-frequency problems [25, 24] have been extended to the time-domain. All these methods have been known to experience stability problems in longer time computations [30, 32, 76], but various remedies have over the years been developed [30, 32, 33, 31, 76]. In particular, as in the frequency domain case, the combined integral equations give rise to more stable methods [76].

The above listed methodologies to treat time dependent problems with the BEM can be split in two main groups: direct computation in time domain or inverse transformation combined with computation in Laplace domain. Not only due to the dependency of numerical inverse transformations on some sophisticated parameter, but also due to physical reasons it is more natural to work in the real time domain and observe the phenomenon as it evolves. But, as all time-stepping procedures, such a formulation requires an adequate choice of the time step size. An improperly chosen time step size leads to instabilities or numerical damping. An improved and stable version of the underlying integral equation has been published by BAMBERGER and HA-DUONG [9] and AIMI and DILIGENTI [3]. Both rely on an energy principle and require two temporal integrations. The instabilities of the usual time-stepping

algorithm have been analysed by BIRGISSON et. al. [19]. Four procedures to improve the stability of the classical dynamic time-stepping BE formulation can be quoted: the first employs modified numerical time marching procedures, e.g., [6] for acoustics, [65] for elastodynamics; the second employs a modified fundamental solution, e.g., [67] for elastodynamics; the third employs an additional integral equation for velocities [57]; and the last uses weighting methods, e.g., [87] for elastodynamics and [88] for acoustics.

Beside these improved approaches there exist the possibility to solve the convolution integral in the boundary integral equation with the so-called Convolution Quadrature Method (CQM) proposed by LUBICH [51, 52]. Applications to hyperbolic and parabolic integral equations can be found in [55, 53]. The CQM utilizes the Laplace domain fundamental solution and results not only in a more stable time stepping procedure but also damping effects in case of visco- or poroelasticity can be taken into account (see [73, 74, 71]). The motivation to use the CQM in these engineering applications is that only the Laplace domain fundamental solutions are required. This fact is also used for BE formulations in cracked anisotropic elastic [89] or piezoelectric materials [39]. Another aspect is the better stability behavior compared with the above mentioned formulation. For acoustics this may be found in [1, 2] and in elastodynamics in [72]. Recently work has begun in investigating CQM for electromagnetism [83]. In the framework of fast BE formulations the CQM is used in a Panel-clustering formulation for the Helmholtz equation by HACKBUSCH et. al. [46]. Recently, some newer mathematical aspects of the CQM have been published by LUBICH [54]. Further, interest in high order Runge-Kutta based CQM has lately increased due to its good performance in applications, see [10] for numerical experiments in acoustics and [12, 14, 22] for convergence results.

In this paper, both, the linear multistep and Runge-Kutta based CQM is described together with most recent theoretical results on convergence, the application to various linear hyperbolic problems is explained, and the paper ends with a numerical experiment for an elastodynamic problem. Important for the paper at hand are different approaches to the implementation of CQM. The originally proposed construction of convolution weights by fast Fourier transform (FFT) [52] is described, also the recent decoupling approach promoted in [13], and the recursive method of [10], a modification of [48].

Throughout this paper, vectors and tensors are denoted by bold symbols and matrices by sans serif and upright symbols. The Laplace transform of a function $f(t)$ is denoted by $\hat{f}(s)$ with the complex Laplace parameter $s \in \mathbb{H}$ and $\mathbb{H} = \{s \in \mathbb{C} | \Re s > 0\}$.

2 Time Dependent Boundary Integral Equations

In this work linear hyperbolic differential equations are considered. The most simple equation is the scalar wave equation. However, vectorial problems will also be

tackled and, hence, the basic equations are described for the simplest vectorial problem, for elastodynamics.

2.1 Governing Equations

Describing with $\mathbf{x}$ and t the position in the three-dimensional Euclidean space $\mathbb{R}^3$ and the time point from the interval $(0,\infty)$ the hyperbolic initial value problem for the displacement field $\mathbf{u}(\mathbf{x},t)$ is (see, e.g., [41])

$$\begin{aligned} c_1^2\nabla\nabla\cdot\mathbf{u}(\mathbf{x},t) - c_2^2\nabla\times\nabla\times\mathbf{u}(\mathbf{x},t) &= \frac{\partial^2\mathbf{u}}{\partial t^2}(\mathbf{x},t) \quad && (\mathbf{x},t)\in\Omega\times(0,\infty) \\ \mathbf{u}(\mathbf{y},t) &= \mathbf{g}_D(\mathbf{y},t) && (\mathbf{y},t)\in\Gamma_D\times(0,\infty) \\ \mathbf{t}(\mathbf{y},t) &= \mathbf{g}_N(\mathbf{y},t) && (\mathbf{y},t)\in\Gamma_N\times(0,\infty) \\ \mathbf{u}(\mathbf{x},0) = \frac{\partial\mathbf{u}}{\partial t}(\mathbf{x},0) &= \mathbf{0} && (\mathbf{x},t)\in\Omega\times(0)\,. \end{aligned} \tag{1}$$

The material properties of the solid are represented by the wave speeds

$$c_1 = \sqrt{\frac{K+\frac{4}{3}G}{\rho}} \qquad c_2 = \sqrt{\frac{G}{\rho}}\,,$$

with the material data compression modulus K, shear modulus G, and the mass density ρ. The first statement in (1) requires the fulfillment of the partial differential equation in the spatial domain Ω for all times $0<t<\infty$. This spatial domain Ω has the boundary Γ which is subdivided into two disjoint sets Γ_D and Γ_N at which boundary conditions are prescribed. The Dirichlet boundary condition is the second statement of (1) and assigns a given datum $\mathbf{g}_D$ to the displacement $\mathbf{u}$ on the part Γ_D of the boundary. Similarly, the Neumann boundary condition is the third statement in which the datum $\mathbf{g}_N$ is assigned to the surface traction $\mathbf{t}$, which is defined by (see, e.g., [41])

$$\begin{aligned} \mathbf{t}(\mathbf{y},t) &= (\mathscr{T}\mathbf{u})(\mathbf{y},t) \\ &= \lim_{\Omega\ni\mathbf{x}\to\mathbf{y}\in\Gamma}\left[\left(G\left(\nabla\mathbf{u}+(\nabla\mathbf{u})^\top\right)+\left(K-\frac{2}{3}G\right)\nabla\cdot\mathbf{u}\,\mathbf{I}\right)(\mathbf{x},t)\cdot\mathbf{n}(\mathbf{y})\right] \\ &= \lim_{\Omega\ni\mathbf{x}\to\mathbf{y}\in\Gamma}\left[\boldsymbol{\sigma}(\mathbf{x},t)\cdot\mathbf{n}(\mathbf{y})\right]. \end{aligned} \tag{2}$$

In (2), $\boldsymbol{\sigma}$ is the stress tensor depending on the displacement field $\mathbf{u}$ according to the linear strain-displacement relationship and Hooke's law and $\mathbf{n}$ denotes the outward normal at the boundary. For later purposes the traction operator $\mathscr{T}$ is defined, which maps the displacement field $\mathbf{u}$ to the surface traction $\mathbf{t}$. The boundary conditions have to hold for all times and may be also prescribed in each direction by different

types, e.g., roller bearings. Finally, in the last statement of (1) the condition of a quiescent past is given which implies homogeneous initial conditions.

Beside the elastodynamic problem, a number of other wave propagation problems describing different physical phenomena can be treated similarly. The respective governing differential equations are listed next.

2.1.1 Acoustics – Scalar Wave Equation

The hyperbolic differential equation for waves traveling in a non-viscous fluid is (see, e.g., [61])

$$c^2\nabla^2 p\,(\mathbf{x},t) = \frac{\partial^2 p}{\partial t^2}\,(\mathbf{x},t) \quad (\mathbf{x},t) \in \Omega \times (0,\infty)\,, \tag{3}$$

with boundary conditions defined analogously to (1) and also vanishing initial conditions. The wave velocity is defined by

$$c = \sqrt{\frac{K}{\rho}}$$

with the compressibility K of the fluid. The traction operator (2) degenerates to the normal derivative to define the normal flux

$$q_n\,(\mathbf{y},t) = (\mathscr{T} p)\,(\mathbf{y},t) = \lim_{\Omega \ni \mathbf{x} \to \mathbf{y} \in \Gamma} [\nabla p(\mathbf{x},t) \cdot \mathbf{n}(\mathbf{y})]\,. \tag{4}$$

2.1.2 Viscoelastodynamics

This extension of the elastodynamic case to materials with damping can be easily performed with the elastic-viscoelastic correspondence principle [26]. This principle says that in Laplace domain the material data has simply to be exchanged with the viscoelastic material data which are dependent on the Laplace variable s, i.e., they are time dependent. Consequently, the governing differential equation is the Laplace transform of (1) to Laplace domain

$$c_{1v}^2(s)\nabla\nabla\cdot\hat{\mathbf{u}}(\mathbf{x},s) - c_{2v}^2(s)\nabla\times\nabla\times\hat{\mathbf{u}}(\mathbf{x},s) = s^2\hat{\mathbf{u}}(\mathbf{x},s), \quad (\mathbf{x},s) \in \Omega \times \mathbb{H}, \tag{5}$$

with the viscoelastic wave speeds

$$c_{1v}(s) = \sqrt{\frac{\hat{K}(s) + \frac{4}{3}\hat{G}(s)}{\rho}}, \qquad c_{2v} = \sqrt{\frac{\hat{G}(s)}{\rho}}\,. \tag{6}$$

The material data $\hat{K}(s)$ and $\hat{G}(s)$ can be given, for most materials, as rational functions of s, e.g., for the simplest causal model - the three parameter model - it holds

$$\hat{K}(s) = K\frac{1+q^H s}{1+p^H s}, \qquad \hat{G}(s) = G\frac{1+q^D s}{1+p^D s}\,, \tag{7}$$

with the compression modulus K and the shear modulus G from elasticity. The parameters q^H, q^D, p^H, and p^D are further material data. More details on viscoelastic constitutive equations may be found in [26] and their implementation in BEM in [40, 72].

The traction operator is defined as in elastodynamics where Hooke's law has now the material data from (7), i.e., the constitutive equation in time domain is a convolution integral. This and also the structure of (5) shows that a formulation of the problem in time domain yields an integro-differential equation.

2.1.3 Poroelastodynamics

The wave propagation in saturated two-phase media as, e.g., soil is governed by a coupled set of differential equations for the solid displacements $\mathbf{u}$ and the pore pressure p. Beside mixture theory based approaches (see, e.g., the theory of porous media [20] or the simple mixture theory [86]), Biot's theory is widely used in practice and will also be used here. The basic formulation for wave propagation problems can be found in the two papers [17, 18]. The set of governing equations in Laplace domain is

$$\begin{aligned} G\nabla^2\hat{\mathbf{u}}(\mathbf{x},s) + \left(K+\frac{1}{3}G\right)\nabla\nabla\cdot\hat{\mathbf{u}}(\mathbf{x},s) - (\alpha-\beta(s))\nabla\hat{p} &= s^2\left(\rho-\beta(s)\rho_f\right)\hat{\mathbf{u}}(\mathbf{x},s), \\ \frac{\beta(s)}{s\rho_f}\nabla^2\hat{p}(\mathbf{x},s) - \frac{\phi^2 s}{R}\hat{p}(\mathbf{x},s) - (\alpha-\beta(s))s\nabla\cdot\hat{\mathbf{u}}(\mathbf{x},s) &= 0\,, \\ & (\mathbf{x},s)\in\Omega\times\mathbb{H} \end{aligned} \tag{8}$$

with the bulk material data shear modulus G and compression modulus K, Biot's coefficients α and R, and the porosity ϕ. The bulk density is denoted by $\rho = (1-\phi)\rho_s + \phi\rho_f$, composed by the partial densities of the solid ρ_s and the fluid ρ_f. The complex valued parameter $\beta(s)$ is an abbreviation and defined as

$$\beta(s) = \frac{\kappa\rho_f\phi^2 s^2}{\phi^2 s + s^2\kappa(\rho_a+\phi\rho_f)}$$

with the permeability κ and the apparent mass density ρ_a. As in viscoelasticity, this set of governing equations can not be formulated as a pure differential equation in time domain because the coefficients depend on s. The wave velocities, due to the incorporated friction between the solid and the fluid, are time dependent. The respective wave numbers, defined as usual $\lambda = \frac{s}{c}$, are

$$\lambda_{1,2}^2 = \frac{s^2}{2}\left[\frac{\phi^2\rho_f}{\beta(s)R} + \frac{\rho-\beta(s)\rho_f}{K+\frac{4}{3}G} + \frac{\rho_f(\alpha-\beta(s))^2}{\beta(s)(K+\frac{4}{3}G)} \pm \sqrt{\left(\frac{\phi^2\rho_f}{\beta(s)R} + \frac{\rho-\beta(s)\rho_f}{K+\frac{4}{3}G} + \frac{\rho_f(\alpha-\beta(s))^2}{\beta(s)(K+\frac{4}{3}G)}\right)^2 - 4\frac{\phi^2\rho_f(\rho-\beta(s)\rho_f)}{\beta(s)R(K+\frac{4}{3}G)}}\right],$$

$$\lambda_3^2 = \frac{s^2(\rho-\beta(s)\rho_f)}{G}.$$

Compared to the above given models in poroelasticity three waves, a fast and slow compressional wave and a shear wave, exist.

The traction operator has to be seen in a generalized way and has obviously two parts. It is composed of the definition of the total stress and the flux governed by Darcy's law

$$\begin{bmatrix}\hat{\mathbf{t}}\\ \hat{q}\end{bmatrix}(\mathbf{y},s) = (\mathscr{T}\begin{bmatrix}\hat{\mathbf{u}}\\ \hat{p}\end{bmatrix})(\mathbf{y},s) = \lim_{\Omega\ni\mathbf{x}\to\mathbf{y}\in\Gamma}\begin{bmatrix}[\hat{\sigma}-\alpha\hat{p}\mathbf{I}](\mathbf{x},s)\cdot\mathbf{n}(\mathbf{y})\\ \left[-\frac{\beta}{s\rho_f}\left(\nabla\hat{p}+\rho_f s^2\hat{\mathbf{u}}\right)\right](\mathbf{x},s)\cdot\mathbf{n}(\mathbf{y})\end{bmatrix}. \quad (9)$$

2.1.4 Electromagnetism – Maxwell Equations

The system of Maxwell equations in a homogeneous and isotropic medium is given by

$$\begin{aligned}\mu\frac{\partial\mathbf{H}}{\partial t}(\mathbf{x},t) + \nabla\times\mathbf{E}(\mathbf{x},t) &= 0\\ \varepsilon\frac{\partial\mathbf{E}}{\partial t}(\mathbf{x},t) - \nabla\times\mathbf{H}(\mathbf{x},t) &= 0,\end{aligned} \quad (10)$$

with $\mathbf{E}$ and $\mathbf{H}$ being the electric and magnetic fields, respectively, and ε and μ respectively electric permittivity and magnetic permeability. Boundary conditions are obtained by a combination of tangential traces of the two fields: $\mathbf{n}\times\mathbf{E}$ and $\mathbf{n}\times\mathbf{H}$, e.g., $\mathbf{n}\times\mathbf{E}=0$ for a perfectly conducting surface and the impedance boundary condition $\mathbf{n}\times\mathbf{H}-\alpha(\mathbf{n}\times\mathbf{E})\times\mathbf{n}=0$, $\alpha\geq 0$, for an imperfectly conducting surface [60].

The relationship to wave equations can be made more visible by rewriting the first order system (10) as a second order system. This can be done by, for example, eliminating the magnetic field $\mathbf{H}$ and thereby obtaining the equation

$$-c^2\nabla\times\nabla\times\mathbf{E}(\mathbf{x},t) = \frac{\partial^2\mathbf{E}}{\partial t^2}(\mathbf{x},t), \quad (11)$$

with the wave speed $c=\frac{1}{\sqrt{\varepsilon\mu}}$.

2.2 Integral Equations

For all of the governing equations given above, a representation formula can be derived (see, e.g., for acoustics [61], for elastodynamics [84], for viscoelastodynamics [42], for poroelastodynamics [72], and for electromagnetism [78, Chapter 25]). Representation formula for Maxwell equations does not fit the general framework of the other equations, therefore it is presented separately.

Taking $\mathbf{u}$ as representative for the unknowns in the governing equations (1), (3), (5), and (8) the representation formula is

$$\mathbf{u}(\mathbf{x},t) = \int_0^t \int_\Gamma \mathbf{U}(\mathbf{x}-\mathbf{y},t-\tau)\mathbf{t}(\mathbf{y},\tau)\mathrm{d}\Gamma_\mathbf{y}\mathrm{d}\tau - \int_0^t \int_\Gamma (\mathscr{T}_\mathbf{y}\mathbf{U})(\mathbf{x}-\mathbf{y},t-\tau)\mathbf{u}(\mathbf{y},\tau)\mathrm{d}\Gamma_\mathbf{y}\mathrm{d}\tau, \quad \mathbf{x}\in\Omega. \tag{12}$$

The surface measure $\mathrm{d}\Gamma_\mathbf{y}$ carries its subscript in order to emphasize that the integration variable is $\mathbf{y}$. Similarly, $\mathscr{T}_\mathbf{y}$ indicates that the derivatives involved in the computation of the surface traction are taken with respect to the variable $\mathbf{y}$. The function $\mathbf{U}(\mathbf{x}-\mathbf{y},t-\tau)$ denotes the fundamental solution of the respective governing equation. In the Laplace domain, the fundamental solutions of all of the above given problems can be formulated in 3-d as

$$\hat{\mathbf{U}}(\mathbf{x}-\mathbf{y},s) = \sum_{i=1}^{w} \mathbf{A}^{(i)}(r,s)\frac{e^{-\lambda_i r}}{4\pi r} \qquad \text{with} \quad r=|\mathbf{x}-\mathbf{y}|\,, \tag{13}$$

using the wave number $\lambda_i = \frac{s}{c_i}$ instead of the wave velocities c_i. The upper limit w of the sum in (13) is the amount of body waves in the model. The coefficients $\mathbf{A}^{(i)}(r,s)$ are listed in the Appendix. In 2-d, the structure of the fundamental solution is the same, however, the exponential function has to be replaced by the modified Bessel functions of zero or first order. Time dependent fundamental solutions are only available for acoustics, elastodynamics, and electromagnetism, but even here, for example for elastodynamics and the dissipative wave equation in acoustics, the time domain fundamental solution can become very complex. In the following, this problem is overcome by using the CQM for time discretisation.

By means of equation (12), the unknown $\mathbf{u}$ is given at any point $\mathbf{x}$ inside the domain Ω and at any time $0<t<\infty$, if the boundary data $\mathbf{u}(\mathbf{y},\tau)$ and $\mathbf{t}(\mathbf{y},\tau)$ are known for all points $\mathbf{y}$ of the boundary Γ and times $0<\tau<t$. The first boundary integral equation is obtained by taking the expression (12) to the boundary. Using operator notation, this boundary integral equation reads

$$(\mathscr{V}\mathbf{t})(\mathbf{x},t) = \mathscr{C}(\mathbf{x})\mathbf{u}(\mathbf{x},t) + (\mathscr{K}\mathbf{u})(\mathbf{x},t), \quad (\mathbf{x},t)\in\Gamma\times(0,\infty)\,. \tag{14}$$

The introduced operators are the single layer operator $\mathscr{V}$, the integral-free term $\mathscr{C}$, and the double layer operator $\mathscr{K}$ which are defined as

$$(\mathscr{V}\mathbf{t})(\mathbf{x},t) = \int_0^t \int_\Gamma \mathbf{U}(\mathbf{x}-\mathbf{y},t-\tau)\mathbf{t}(\mathbf{y},\tau)\mathrm{d}\Gamma_\mathbf{y}\mathrm{d}\tau, \tag{15a}$$

$$\mathscr{C}(\mathbf{x}) = \mathscr{I} + \lim_{\varepsilon\to 0} \int_{\partial B_\varepsilon(\mathbf{x})\cap\Omega} (\mathscr{T}_\mathbf{y}\mathbf{U}_{\text{static}})^\top(\mathbf{x}-\mathbf{y})\mathrm{d}\Gamma_\mathbf{y}, \tag{15b}$$

$$(\mathscr{K}\mathbf{u})(\mathbf{x},t) = \lim_{\varepsilon\to 0}\int_0^t \int_{\Gamma\setminus B_\varepsilon(\mathbf{x})} (\mathscr{T}_\mathbf{y}\mathbf{U})^\top(\mathbf{x}-\mathbf{y},t-\tau)\mathbf{u}(\mathbf{y},\tau)\mathrm{d}\Gamma_\mathbf{y}\mathrm{d}\tau\,. \tag{15c}$$

In these expressions, $B_\varepsilon(\mathbf{x})$ denotes a ball of radius ε centered at $\mathbf{x}$ and $\partial B_\varepsilon(\mathbf{x})$ is its surface. In (15b), the integral free term is only determined by the static counterpart of each operator, i.e., the index $_{\text{static}}$ denotes the respective fundamental solution. E.g., in elastodynamics $\mathbf{U}_{\text{static}}$ is the elastostatic fundamental solution. Note that the single layer operator (15a) involves a weakly singular integral over Γ and the double layer operator (15c) has to be understood in the sense of a principal value. Further, it should be remarked that the operator notation in (15a) and (15c) includes the convolution operator in time.

Application of the traction operator $\mathscr{T}_x$ to the dynamic representation formula (12) yields the second boundary integral equation

$$(\mathscr{D}\mathbf{u})(\mathbf{x},t) = (\mathscr{I}-\mathscr{C}(\mathbf{x}))\,\mathbf{t}(\mathbf{x},t) - (\mathscr{K}'\mathbf{t})(\mathbf{x},t), \quad \mathbf{x}\in\Gamma\,. \tag{16}$$

The newly introduced operators are the adjoint double layer operator $\mathscr{K}'$ and the hyper-singular operator $\mathscr{D}$. They are defined as

$$(\mathscr{K}'\mathbf{t})(\mathbf{x},t) = \lim_{\varepsilon\to 0}\int_0^t \int_{\Gamma\setminus B_\varepsilon(\mathbf{x})} (\mathscr{T}_\mathbf{x}\mathbf{U})(\mathbf{x}-\mathbf{y},t-\tau)\mathbf{t}(\mathbf{y},\tau)\mathrm{d}\Gamma_\mathbf{y}\mathrm{d}\tau, \tag{17a}$$

$$(\mathscr{D}\mathbf{u})(\mathbf{x},t) = -\lim_{\varepsilon\to 0}\int_0^t \mathscr{T}_\mathbf{x} \int_{\Gamma\setminus B_\varepsilon(\mathbf{x})} (\mathscr{T}_\mathbf{y}\mathbf{U})^\top(\mathbf{x}-\mathbf{y},t-\tau)\mathbf{u}(\mathbf{y},\tau)\mathrm{d}\Gamma_\mathbf{y}\mathrm{d}\tau\,. \tag{17b}$$

The hyper-singular operator has to be understood in the sense of a finite part.

For the solution of mixed initial boundary value problems, a non-symmetric formulation by means of the first boundary integral equation (14) in combination with a collocation technique will be used. A symmetric formulation is obtained using both the first and the second boundary integral equations, (14) and (16) in combination with a Galerkin technique.

Symmetric Formulation

First, the Dirichlet datum $\mathbf{u}$ and the Neumann datum $\mathbf{t}$ are decomposed into

$$\mathbf{u} = \tilde{\mathbf{u}} + \tilde{\mathbf{g}}_D \qquad \text{and} \qquad \mathbf{t} = \tilde{\mathbf{t}} + \tilde{\mathbf{g}}_N\,, \tag{18}$$

with arbitrary but fixed extensions, $\tilde{\mathbf{g}}_D$ and $\tilde{\mathbf{g}}_N$, of the given Dirichlet and Neumann data, $\mathbf{g}_D$ and $\mathbf{g}_N$. They are introduced such that

$$\begin{aligned} \tilde{\mathbf{g}}_D(\mathbf{x},t) &= \mathbf{g}_D(\mathbf{x},t)\,, \qquad (\mathbf{x},t) \in \Gamma_D \times (0,\infty), \\ \tilde{\mathbf{g}}_N(\mathbf{x},t) &= \mathbf{g}_N(\mathbf{x},t)\,, \qquad (\mathbf{x},t) \in \Gamma_N \times (0,\infty) \end{aligned} \tag{19}$$

holds. The extension $\tilde{\mathbf{g}}_D$ of the given Dirichlet datum has to be continuous due to regularity requirements [79].

In order to establish a symmetric formulation, the first boundary integral equation (14) is used only on the Dirichlet boundary Γ_D whereas the second one (16) is used only on the Neumann part Γ_N. Taking the prescribed boundary conditions in (1) into account and inserting the decompositions (18) into both integral equations leads to the symmetric formulation for the unknowns $\tilde{\mathbf{u}}$ and $\tilde{\mathbf{t}}$

$$\begin{aligned} \mathscr{V}\tilde{\mathbf{t}} - \mathscr{K}\tilde{\mathbf{u}} &= \mathbf{f}_D, \quad (\mathbf{x},t) \in \Gamma_D \times (0,\infty), \\ \mathscr{D}\tilde{\mathbf{u}} + \mathscr{K}'\tilde{\mathbf{t}} &= \mathbf{f}_N, \quad (\mathbf{x},t) \in \Gamma_N \times (0,\infty) \end{aligned} \tag{20}$$

with the abbreviations

$$\begin{aligned} \mathbf{f}_D &= \mathscr{C}\tilde{\mathbf{g}}_D + \mathscr{K}\tilde{\mathbf{g}}_D - \mathscr{V}\tilde{\mathbf{g}}_N\,, \\ \mathbf{f}_N &= (\mathscr{I} - \mathscr{C})\tilde{\mathbf{g}}_N - \mathscr{K}'\tilde{\mathbf{g}}_N - \mathscr{D}\tilde{\mathbf{g}}_D\,. \end{aligned}$$

Representation Formula for Maxwell Equations

The representation formula has the following form for the electric field

$$\begin{aligned} \mathbf{E}(\mathbf{x},t) = &-\mu \int_0^t \int_\Gamma \mathbf{U}(\mathbf{x}-\mathbf{y},t-\tau)\frac{\partial \mathbf{j}}{\partial t}(\mathbf{y},\tau)\mathrm{d}\Gamma_{\mathbf{y}}\mathrm{d}\tau \\ &+ \frac{1}{\varepsilon}\nabla \int_0^t \int_\Gamma \mathbf{U}(\mathbf{x}-\mathbf{y},t-\tau)\partial_t^{-1}\nabla_\Gamma \cdot \mathbf{j}(\mathbf{y},\tau)\mathrm{d}\Gamma_{\mathbf{y}}\mathrm{d}\tau \\ &- \nabla \times \int_0^t \int_\Gamma \mathbf{U}(\mathbf{x}-\mathbf{y},t-\tau)\mathbf{m}(\mathbf{y},\tau)\mathrm{d}\Gamma_{\mathbf{y}}\mathrm{d}\tau \end{aligned}$$

and the following for the magnetic field

$$\begin{aligned}\mathbf{H}(\mathbf{x},t) = &-\varepsilon \int_0^t \int_\Gamma \mathbf{U}(\mathbf{x}-\mathbf{y},t-\tau)\frac{\partial \mathbf{m}}{\partial t}(\mathbf{y},\tau)\mathrm{d}\Gamma_{\mathbf{y}}\mathrm{d}\tau \\ &+ \frac{1}{\mu}\nabla \int_0^t \int_\Gamma \mathbf{U}(\mathbf{x}-\mathbf{y},t-\tau)\partial_t^{-1}\nabla_\Gamma \cdot \mathbf{m}(\mathbf{y},\tau)\mathrm{d}\Gamma_{\mathbf{y}}\mathrm{d}\tau \\ &+ \nabla \times \int_0^t \int_\Gamma \mathbf{U}(\mathbf{x}-\mathbf{y},t-\tau)\mathbf{j}(\mathbf{y},\tau)\mathrm{d}\Gamma_{\mathbf{y}}\mathrm{d}\tau,\end{aligned}$$

where $\mathbf{j} = \mathbf{H} \times \mathbf{n}$ and $\mathbf{m} = \mathbf{n} \times \mathbf{E}$ are, respectively, the surface current and surface charge density. The symbol ∂_t^{-1} denotes integration on the interval $[0,t]$, this is consistent with the operational notation introduced in the next section. The fundamental solution $\hat{\mathbf{U}}(\mathbf{x},s)$ still has the form (13) and is in fact the same as the fundamental solution for the acoustic wave equation, showing the close relationship between the two sets of equations. Taking tangential traces one obtains boundary integral formulations of boundary value problems. Since the formalism using the four integral operators introduced for other governing equations does not directly translate to the Maxwell system, for further information the reader is referred to literature, see [78, Chapter 25].

3 Convolution Quadrature

All of the time domain integral operators of the previous section have the form of a time convolution

$$u(t) = \int_0^t k(t-\tau)g(\tau)\mathrm{d}\tau. \tag{21}$$

The difficulty in computing such convolutions comes from the fact that the kernel $k(t)$ is often distributional and in many cases of practical interest, e.g., viscoelasticity and poroelasticity, even not known explicitly. However, the Laplace transform of the kernel

$$K(s) = \hat{k}(s) = \mathscr{L}k(s) := \int_0^\infty k(t)e^{-st}\mathrm{d}t$$

is always explicitly known and simpler. For this reason it is essential to be able to compute (21) by using only the Laplace transformed kernel $K(s)$. To make this dependence on the Laplace transformed kernel explicit, operational notation, going back to Heaviside and standard in papers on convolution quadrature [53],

$$\left(K(\partial_t)g\right)(t) := \int_0^t k(t-\tau)g(\tau)\mathrm{d}\tau, \tag{22}$$

is used in this paper. The rationale behind this notation comes from identities of the type $K(\partial_t)g = g'$ for $K(s) = s$ and the composition rule $K_2K_1(\partial_t)g = K_2(\partial_t)K_1(\partial_t)g$. Convolution quadrature time discretization will be explained and convergence results given with the following assumption on the operator $K(s)$:

$$\begin{gathered} K(s) \text{ is analytic for } \Re s > 0 \text{ and bounded as} \\ |K(s)| \leq C(\sigma_0)\frac{|s|^\mu}{(\Re s)^\nu}, \text{ for } \Re s \geq \sigma_0 > 0. \end{gathered} \tag{23}$$

To make the connection to the previous section explicit, note that in this notation the single layer operator of (15a) can be written as

$$(\mathscr{V}\mathbf{t})(\mathbf{x},t) = (V(\partial_t)\mathbf{t})(\mathbf{x},t)$$

where V is the single layer operator in the Laplace domain:

$$(V(s)\phi)(\mathbf{x}) := \int_\Gamma \hat{\mathbf{U}}(\mathbf{x}-\mathbf{y},s)\phi(\mathbf{y})\mathrm{d}s_y \tag{24}$$

and $\hat{\mathbf{U}}$ is the explicitly known fundamental solution in the Laplace domain, see (13).

3.1 Linear Multistep Based Convolution Quadrature

For $\Delta t > 0$ let $t_j = j\Delta t$ be the discrete time steps at which (22) is to be computed. Convolution quadrature approximation of (22) at $t = t_n$ is given by

$$\left(K(\partial_t^{\Delta t})g\right)(t_n) := \sum_{j=0}^{n} \omega_{n-j}^{\Delta t}(K)g(t_j). \tag{25}$$

Here the convolution weights $\omega_j^{\Delta t}(K)$ are defined implicitly by

$$K\left(\frac{\gamma(\zeta)}{\Delta t}\right) = \sum_{j=0}^{\infty} \omega_j^{\Delta t}(K)\zeta^j, \tag{26}$$

where $\gamma(\zeta)$ is the quotient of the generating polynomials of a linear multistep method of order p. For hyperbolic problems only A-stable methods are admissible, the most often used methods being the backward difference formulas of order 1 (BDF1/backward Euler) and order 2 (BDF2) for which

$$\gamma(\zeta) = 1-\zeta \quad \text{(BDF1)}, \quad \gamma(\zeta) = \frac{3}{2} - 2\zeta + \frac{1}{2}\zeta^2 \quad \text{(BDF2)}.$$

An important property of convolution quadrature is that the composition rule is preserved. Namely, $K_2K_1(\partial_t^{\Delta t})g = K_2(\partial_t^{\Delta t})K_1(\partial_t^{\Delta t})g$. Further, for $K(s) = s$, $K(\partial_t^{\Delta t})g = \partial_t^{\Delta t} g$ is the linear multistep approximation of the derivative g'.

A brief motivation for the approximation (25) is in order. Making use of the extension $g(t) \equiv 0$ for $t \leq 0$, the approximation (25) can be defined for all t: $\left(K(\partial_t^{\Delta t})g\right)(t) = \sum_{j=0}^{\infty} \omega_j^{\Delta t}(K) g(t - t_j)$. Taking the Laplace transformation of this expression gives

$$\mathscr{L}\left(K(\partial_t^{\Delta t})g\right)(s) = \left(\sum_{j=0}^{\infty} \omega_j^{\Delta t}(K) e^{-s\Delta t j}\right) \mathscr{L}g(s) = K\left(\frac{\gamma\left(e^{-s\Delta t}\right)}{\Delta t}\right) \mathscr{L}g(s).$$

Since $\mathscr{L}(K(\partial_t)g)(s) = K(s)\mathscr{L}g(s)$, the convolution quadrature manifests itself through the approximation $s \approx \frac{\gamma(e^{-s\Delta t})}{\Delta t} = s + sO((s\Delta t)^p)$, p being the order of the multistep method. The restriction to A-stable methods comes from the requirement $\Re\gamma(e^{-s\Delta t}) > 0$ for $\Re s > 0$.

Next, a result on convergence of the linear multistep based convolution quadrature is given, the proof of which can be found in [53].

Theorem 1 (Lubich 1994). *Let* (23) *hold,* $g(0) = g'(0) = \cdots = g^{(m-1)}(0) = 0$ *for* m *such that* $m \geq \max(p+2+\mu, p)$*, and let* $u_n = \left(K(\partial_t^{\Delta t})g\right)(t_n)$ *be the approximation obtained by convolution quadrature* (25) *based on BDF formula of order* $p = 1, 2$*. Then there exists* $\bar{t} > 0$ *such that for all* $0 < \Delta t < \bar{t}$ *and* $n = 0, 1, \ldots, N = T/\Delta t$ *it holds*

$$|u_n - u(t_n)| \leq C\Delta t^p \int_0^{t_n} |g^{(m)}(\tau)| d\tau.$$

The constant C *is independent of* Δt *and* N*, but depends on* T *and constant* $C(\sigma_0)$ *in* (23)*.*

The result proved in [53] covers a larger class of A-stable linear multistep methods. The statement here has been restricted to BDF methods in order to shorten the exposition. The trapezoid rule does not satisfy the assumptions of the general theory given in [53] if $\mu > 0$. Recently, in [10] the convergence of the trapezoid rule has been proved for this case and successful numerical experiments have been performed for acoustic scattering applications.

Because of the restriction to A-stable linear multistep methods, the highest order attainable is $p = 2$. To achieve higher orders of convergence one has to turn to Runge-Kutta methods. Further reasons to prefer Runge-Kutta methods are highlighted later in the paper, see Sect. 4.3.

3.2 Runge-Kutta Based Convolution Quadrature

Let a Runge-Kutta method of (classical) order p and stage order q be given by its Butcher tableau $\begin{array}{c|c} c & A \\ \hline & b^\top \end{array}$ where $A \in \mathbb{R}^{m\times m}$, $b, c \in \mathbb{R}^m$; for a detailed introduction to

Runge-Kutta methods see [21, 47, 49]. A Runge-Kutta method is said to be A-stable if the stability function

$$R(z) = 1 + zb^\top (I - zA)^{-1} \quad , \qquad := (1,1,\dots,1)^\top, \tag{27}$$

is bounded as

$$|R(z)| \le 1, \quad \text{for } \Re z \le 0 \text{ and } I - zA \text{ is non-singular for all } \Re z \le 0. \tag{28}$$

To simplify expressions assume further that $b^\top A^{-1} = (0,0,\dots,1)$, i.e., that the method is stiffly accurate [47]; this in turn implies that $c_m = 1$. A further technical assumption is needed

$$|R(\mathrm{i}y)| < 1, \qquad \text{for all } |y| > 0.$$

Radau IIA and Lobatto IIIC are examples of Runge-Kutta methods satisfying all of the above conditions.

In a Runge-Kutta method computations are done not only at the equally spaced points $t_j = j\Delta t$ but also at the stages $t_j + c_\ell \Delta t$, $\ell = 1,2,\dots,m$. Note that $c_m = 1$ implies $t_j + c_m \Delta t = t_{j+1}$. The Runge-Kutta based convolution quadrature approximation to $u(t_n + c_\ell \Delta t)$, $\ell = 1,\dots,m$, is then given by

$$\begin{pmatrix} u_{n1} \\ \vdots \\ u_{nm} \end{pmatrix} = \left(K(\underline{\partial_t}^{\Delta t}) g \right)_n := \sum_{j=0}^{n} W_{n-j}^{\Delta t}(K) \begin{pmatrix} g(t_j + c_1 \Delta t) \\ \vdots \\ g(t_j + c_m \Delta t) \end{pmatrix}. \tag{29}$$

Here, the matrix convolution weights $W_j^{\Delta t}(K)$ are defined implicitly through a generating function

$$K\left(\frac{\Delta(\zeta)}{\Delta t} \right) = \sum_{j=0}^{\infty} W_j^{\Delta t}(K) \zeta^j, \tag{30}$$

with

$$\Delta(\zeta) = A^{-1} - \zeta A^{-1} \quad b^\top A^{-1}. \tag{31}$$

The solution at t_{n+1} is given simply by $u_{n+1} = u_{nm} = b^\top A^{-1} (u_{n\ell})_{\ell=1}^m$, i.e.,

$$u_{n+1} := b^\top A^{-1} \left(K(\underline{\partial_t}^{\Delta t}) g \right)_n .$$

The composition rule still holds for the stage approximation, that is, $K_2 K_1 (\underline{\partial_t}^{\Delta t}) g = K_2 (\underline{\partial_t}^{\Delta t}) K_1 (\underline{\partial_t}^{\Delta t}) g$. This is however not true for the approximation $b^\top A^{-1} K (\underline{\partial_t}^{\Delta t}) g$, whence we refrain from using the operational quadrature notation here.

First convergence results under the assumption (23) with $\nu = 0$ have been proved in [12]. Subsequently it has been noticed that, unlike in the linear multistep case, a more favourable result can be proved if $\nu > 0$. This result has been proved in [14]

and is stated next. It shows that for sufficiently smooth and compatible data an order of convergence $O(\Delta t^{q+1-\mu+\nu})$ is obtained; recall that q is the *stage* order of the Runge-Kutta method.

Theorem 2. *Assume* (23)*, with* $\nu \geq 0$*. Let* $r > \max(p+\mu+1, p, q+1)$ *and* $g \in C^r([0,T])$ *satisfy* $g(0) = g'(0) = \cdots = g^{(r)}(0) = 0$*. Then, under the above conditions on the Runge-Kutta method there exists* $\bar{t} \geq 0$ *such that for* $0 < \Delta t < \bar{t}$ *and* $t \in [0,T]$*,*

$$|u_n - u(t_n)| \leq C(\Delta t^p + \Delta t^{q+1-\mu+\nu}) \int_0^t |g^{(r+1)}(\tau)| d\tau\,.$$

The constant C is independent of Δt *and g, but does depend on the Runge-Kutta method,* $\bar{t}$*, and T.*

3.3 Implementation

The implicitly defined convolution weights $\omega_j^{\Delta t}(K)$ can be computed by numerical quadrature of the Cauchy integral formula, as proposed in [52],

$$\omega_j^{\Delta t}(K) = \frac{1}{2\pi \mathrm{i}} \oint_C K\left(\frac{\gamma(\zeta)}{\Delta t}\right) \zeta^{-j-1} \mathrm{d}\zeta \approx \frac{\mathscr{R}^{-j}}{N+1} \sum_{\ell=0}^{N} K\left(\frac{\gamma(\mathscr{R}\zeta_{N+1}^{-\ell})}{\Delta t}\right) \zeta_{N+1}^{\ell j}, \quad (32)$$

where $\zeta_{N+1} = e^{\frac{2\pi \mathrm{i}}{N+1}}$ and $0 < \mathscr{R} < 1$. The computational cost using the fast Fourier transform (FFT) to compute the sum for all $j = 0, 1, \ldots, N$, is $O(N \log N)$ and the error is $O(\mathscr{R}^{N+1})$. Due to finite precision arithmetic the accuracy is restricted to $\sqrt{\text{eps}}$, where eps is the machine precision and the parameter $\mathscr{R}$ is chosen as $\mathscr{R} = \text{eps}^{\frac{1}{2(N+1)}}$; see [52].

In applications it is of interest to solve a discrete convolutional system:

$$\text{Find } u_n, \text{ such that} \qquad g_n = \sum_{j=0}^{n} \omega_{n-j}^{\Delta t}(K) u_j, \quad n = 0, 1, \ldots, N, \quad (33)$$

or the equivalent system in the Runge-Kutta case. Due to the composition rule $K_2 K_1(\partial_t^{\Delta t}) g = K_2(\partial_t^{\Delta t}) K_1(\partial_t^{\Delta t}) g$ solving this system is equivalent to computing the convolution with the operator K^{-1}:

$$u_n = \sum_{j=0}^{n} \omega_{n-j}^{\Delta t}(K^{-1}) g_j = \sum_{j=0}^{N} \omega_{n-j}(K^{-1}) g_j, \quad n = 0, 1, \ldots, N, \quad (34)$$

with the definition, $\omega_j = 0$ for $j < 0$, which is compatible with (26). Two approaches to implementation are presented next. The first one uses the representation (34), whereas the second uses (33), but both avoid constructing the weights $\omega_j^{\Delta t}$

explicitly. The presentation is done for the linear multistep based convolution quadrature. Modifications needed in the Runge-Kutta case are explained at the end of the subsection.

3.3.1 Solving the Convolutional System by Computing a Discrete Convolution with K^{-1}

Next an efficient method for computing (34) is presented. The method has been introduced in [13] but bears similarities with Method iii) of [52].

Substituting the approximation (32), this time with K^{-1} instead of K, into (34) and after rearranging the terms the following expression is obtained

$$u_n \approx \frac{\mathscr{R}^{-n}}{N+1} \sum_{\ell=0}^{N} K^{-1}\left(\frac{\gamma(\mathscr{R}\zeta_{N+1}^{-\ell})}{\Delta t}\right)\left[\sum_{j=0}^{N} \mathscr{R}^j g_j \zeta_{N+1}^{-\ell j}\right]\zeta_{N+1}^{\ell n}. \tag{35}$$

The term in the square bracket is the discrete Fourier transform of the vector $(g_0, \mathscr{R}g_1, \ldots, \mathscr{R}^N g_N)^\top$ and, hence, can be computed in $O(N\log N)$ time using FFT. The outer sum represents the inverse discrete Fourier transform also computable in $O(N\log N)$ time using FFT. Thus, the whole computation can be performed in $O(N\log N)$ time and the convolution weights need never be computed explicitly. In [13], it is shown that the error of this approximation is still $O(\mathscr{R}^{N+1})$ with the accuracy again restricted to $\sqrt{\text{eps}}$ by the finite precision arithmetic.

Since computing $K^{-1}(s)$ is usually a significantly more complex and expensive operation than the computation of $K(s)$, this method can become expensive [58]. For this reason a recursive procedure is presented in the next section that requires the inversion of $K(s)$ only at the single frequency $s = \gamma(0)/\Delta t$.

3.3.2 Solving the Discrete Convolutional System Recursively

In [10], a modification of the recursive procedure of [48] is introduced which allows the solution of (33) without ever constructing the convolution weights. This method is presented next.

First, assume that

$$\sum_{j=0}^{n} \omega_{n-j}^{\Delta t}(K) u_j = g_n,$$

has already been solved for $n = 0, 1, \ldots, N_{1/2} < N$. Then, it remains to solve

$$\sum_{j=N_{1/2}+1}^{n} \omega_{n-j}^{\Delta t}(K) u_j = g_n - \sum_{j=0}^{N_{1/2}} \omega_{n-j}^{\Delta t}(K) u_j, \quad n = N_{1/2}+1, \ldots, N. \tag{36}$$

Once the history $\sum_{j=0}^{N_{1/2}} \omega_{n-j}^{\Delta t}(K) u_j$ is computed, the above system can be computed recursively. The expensive part is hence the computation of the history, but it can be computed efficiently using the fast Fourier transform (FFT). In order to avoid

constructing the weights $\omega_j^{\Delta t}(K)$ explicitly, a scaled FFT can be used, as explained next.

Define

$$\tilde{g}_n := \sum_{j=0}^{N_{1/2}} \omega_{n-j}^{\Delta t}(K) u_j = \mathscr{R}^{-n} \sum_{j=0}^{N_{1/2}} \mathscr{R}^{n-j} \omega_{n-j}^{\Delta t}(K) \mathscr{R}^j u_j, \quad n = N_{1/2}+1, \ldots, N,$$

for a fixed $0 < \mathscr{R} < 1$. Let $\tilde{\mathbf{g}}_{\mathscr{R}}$ be the vector obtained by a matrix-vector multiplication of the circulant matrix, whose first column is given by

$$\mathbf{c}_{\mathscr{R}}(K) := (\omega_0^{\Delta t}(K), \mathscr{R}\omega_1^{\Delta t}(K), \cdots, \mathscr{R}^N \omega_N^{\Delta t}(K))^\top,$$

with the vector

$$\mathbf{u}_{\mathscr{R}} := (u_0, \mathscr{R}u_1, \cdots, \mathscr{R}^{N_{1/2}} u_{N_{1/2}}, 0, \cdots, 0)^\top.$$

It is not difficult to check that

$$\mathscr{R}^{-n}(\tilde{\mathbf{g}}_{\mathscr{R}})_n = \tilde{g}_n, \quad \text{for } n = N_{1/2}+1, \ldots, N;$$

here it is implicitly assumed that the numbering of elements in a vector begin with 0. Therefore, if $\tilde{\mathbf{g}}_{\mathscr{R}}$ can be computed efficiently and without explicitly constructing the convolution weights, then so can the history required for (36). Since circulant matrices are diagonalized by the discrete Fourier transform, in the following denoted by $\mathscr{F}_{N+1}$, it holds

$$\tilde{\mathbf{g}}_{\mathscr{R}} = \mathscr{F}_{N+1}^{-1} \mathrm{diag}(\mathscr{F}_{N+1}\mathbf{c}_{\mathscr{R}}(K)) \mathscr{F}_{N+1}\mathbf{u}_{\mathscr{R}}. \tag{37}$$

The definition of $\mathscr{F}_{N+1}$ that will be used in the following is

$$(\mathscr{F}_{N+1}\mathbf{u})_\ell = \sum_{j=0}^{N} u_j \zeta_{N+1}^{-\ell j}, \quad \text{with } \zeta_{N+1} = e^{\frac{2\pi \mathrm{i}}{N+1}}.$$

The definition of convolution weights (26) then gives

$$\begin{aligned}(\mathscr{F}_{N+1}\mathbf{c}_{\mathscr{R}}(K))_\ell &= \sum_{j=0}^{N} \mathscr{R}^j \omega_j^{\Delta t} \zeta_{N+1}^{-\ell j} = K\left(\frac{\gamma(\mathscr{R}\zeta_{N+1}^{-\ell})}{\Delta t}\right) - \sum_{j=N+1}^{\infty} \mathscr{R}^j \omega_j^{\Delta t} \zeta_{N+1}^{-\ell j} \\ &= K\left(\frac{\gamma(\mathscr{R}\zeta_{N+1}^{-\ell})}{\Delta t}\right) - \sum_{k=1}^{\infty} \mathscr{R}^{k(N+1)} \left[\sum_{j=0}^{N} \mathscr{R}^j \omega_{j+k(N+1)}^{\Delta t}(K) \zeta_{N+1}^{-\ell j}\right].\end{aligned}$$

Since the term in square brackets is again a discrete Fourier transform, considering (37) and applying $\mathscr{F}_{N+1}^{-1}$ to both sides in the above equation gives

$$\tilde{\mathbf{g}}_{\mathscr{R}} = \mathscr{F}_{N+1}^{-1}\mathrm{diag}\left[K\left(\frac{\gamma(\mathscr{R})}{\Delta t}\right),\cdots,K\left(\frac{\gamma(\mathscr{R}\zeta_{N+1}^{-N})}{\Delta t}\right)\right]\mathscr{F}_{N+1}\mathbf{u}_{\mathscr{R}}$$
$$-\sum_{k=1}^{\infty}\mathscr{R}^{k(N+1)}\mathrm{diag}\left[\omega_{k(N+1)}^{\Delta t},\mathscr{R}\omega_{1+k(N+1)}^{\Delta t},\cdots,\mathscr{R}^{N}\omega_{N+k(N+1)}^{\Delta t}\right]\mathscr{F}_{N+1}\mathbf{u}_{\mathscr{R}}.$$

Scaling both sides with $R^{-1} := \mathrm{diag}(1,\mathscr{R}^{-1},\ldots,\mathscr{R}^{-N})$ finally gives

$$\tilde{\mathbf{g}} = R^{-1}\mathscr{F}_{N+1}^{-1}\mathrm{diag}\left[K\left(\frac{\gamma(\mathscr{R})}{\Delta t}\right),\cdots,K\left(\frac{\gamma(\mathscr{R}\zeta_{N+1}^{-N})}{\Delta t}\right)\right]\mathscr{F}_{N+1}\mathbf{u}_{\mathscr{R}} \tag{38}$$
$$-\sum_{k=1}^{\infty}\mathscr{R}^{k(N+1)}\mathrm{diag}\left[\omega_{k(N+1)}^{\Delta t}(K),\cdots,\omega_{N+k(N+1)}^{\Delta t}(K)\right]\mathscr{F}_{N+1}\mathbf{u}_{\mathscr{R}}.$$

Therefore, the vector $\tilde{\mathbf{g}}$, containing the update due to the history, can be computed to an accuracy $O(\mathscr{R}^{N+1})$ by using only evaluations of the Laplace domain operator $K(s)$. Further, the computational cost is only $O(N\log N)$. The error is however restricted by finite precision eps of computations of $K(s)$ and the FFT. Therefore, the total error for computation of the correction $\tilde{g}_n$ is $\mathscr{R}^{N+1}+\mathscr{R}^{-n}\mathrm{eps}$, $n = N_{1/2},\ldots,N$. Hence, the best accuracy $\sqrt{\mathrm{eps}}$ is obtained with the choice $\mathscr{R} = \mathrm{eps}^{1/2N}$.

This procedure can be continued recursively. Thereby no convolution weights $\omega_j^{\Delta t}(K)$ need to be computed except for the first one

$$\omega_0^{\Delta t}(K) = K\left(\frac{\gamma(0)}{\Delta t}\right).$$

It is also the only operator that needs to be inverted if the recursion is performed until a 1×1 system is reached. In practice it is more common to stop the recursion once a small sized system is reached and then solve the small system using the method of Section 3.3.1. See Algorithm 1 for the structure of such an approach. In order to solve (33) the algorithm is called with arguments SolveCQ(0, N, g, u, J), where a constant J defines the size of the "small" system. The cost of such a recursive procedure is $O(N\log^2 N)$ [48] since there are $\log N$ levels in the recursion and at each level an FFT is computed.

Remark 1 (Parallelization). Algorithm 1 can easily gain from the availability of a parallel architecture. In applications, the expensive part of the computation is the evaluation of the operator $K(s)$. Due to the diagonalization of the (block) circulant matrices, in both methods, this part of the computation is trivially parallel and, therefore, appropriate also for distributed memory parallel architecture.

3.3.3 A Few Remarks Regarding the Implementation of Runge-Kutta Based Convolution Quadrature

The same procedure as explained above for the linear multistep case can also be used to implement the Runge-Kutta based convolution quadrature. Again, it is only necessary to be able to evaluate operators

Algorithm 1. SolveCQ(N_0,N_1,g,u,J)

% Solves convolutional system $\sum_{j=N_0}^{n} \omega_{n-j}^{\Delta t}(K)u_j = g_n, \quad n = N_0,\ldots,N_1$

if $N_1 - N_0 \geq J$ **then**

$N_{1/2} = \lceil (N_1+N_0)/2 \rceil$

SolveCQ(N_0, $N_{1/2}$, g, u, J)

update right-hand side

$$g_n = g_n - \sum_{j=N_0}^{N_{1/2}} \omega_{n-j}^{\Delta t}(K)u_j, \quad n = N_{1/2}+1,\ldots,N_1$$

using (38).

SolveCQ($N_{1/2}+1$, N_1, g, u, J)

else

compute

$$u_n = \sum_{j=N_0}^{n} \omega_{n-j}^{\Delta t}(K^{-1})g_j, \quad n = N_0,\ldots,N_1,$$

using (35).

end if

$$K\left(\frac{\Delta(\mathscr{R}\zeta_{N+1}^{-\ell})}{\Delta t}\right) \quad \text{and} \quad K\left(\frac{\Delta(0)}{\Delta t}\right) = K\left(\frac{A^{-1}}{\Delta t}\right).$$

If $\Delta(\mathscr{R}\zeta_{N+1}^{-\ell})$ has a full basis of eigenvectors, i.e., if there exist an invertible matrix X and a diagonal matrix $\Lambda = \mathrm{diag}(\lambda_1,\lambda_2,\cdots,\lambda_m)^\top$ such that $\Delta(\mathscr{R}\zeta_{N+1}^{-\ell}) = X\Lambda X^{-1}$, then the matrix valued operator is easily computed by

$$K\left(\frac{\Delta(\mathscr{R}\zeta_{N+1}^{-\ell})}{\Delta t}\right) = X\mathrm{diag}(K(\lambda_1/\Delta t),\cdots,K(\lambda_m/\Delta t))X^{-1}.$$

In [10], it has been shown that there is only a single value of $\mathscr{R}\zeta_{N+1}^{-\ell}$, respectively two such values, for which $\Delta(\mathscr{R}\zeta_{N+1}^{-\ell})$ is not diagonalizable in the case of the 2-stage Radau IIA method, and respectively, the 3-stage Radau IIA method. These particular values are very unlikely to be hit during a computation, still the condition number of the basis of eigenvectors X should, as a precaution, be examined.

4 Convolution Quadrature Applied to Hyperbolic Initial Value Problems

In the notation of Sect. 3, the time domain integral operators $\mathscr{V},\mathscr{K},\mathscr{K}'$, and $\mathscr{D}$ can be written as $V(\partial_t),K(\partial_t),K'(\partial_t)$, and $D(\partial_t)$ where V,K,K', and D are the corresponding Laplace domain operators

$$(V\mathbf{t})(\mathbf{x},s) = \int_\Gamma \hat{\mathbf{U}}(\mathbf{x}-\mathbf{y},s)\mathbf{t}(\mathbf{y})\mathrm{d}\Gamma_\mathbf{y}, \tag{39a}$$

$$(K\mathbf{u})(\mathbf{x},s) = \lim_{\varepsilon\to 0} \int_{\Gamma\setminus B_\varepsilon(\mathbf{x})} (\mathscr{T}_\mathbf{y}\hat{\mathbf{U}})^\top(\mathbf{x}-\mathbf{y},s)\mathbf{u}(\mathbf{y})\mathrm{d}\Gamma_\mathbf{y}, \tag{39b}$$

$$(K'\mathbf{t})(\mathbf{x},s) = \lim_{\varepsilon\to 0} \int_{\Gamma\setminus B_\varepsilon(\mathbf{x})} (\mathscr{T}_\mathbf{x}\hat{\mathbf{U}})(\mathbf{x}-\mathbf{y},s)\mathbf{t}(\mathbf{y})\mathrm{d}\Gamma_\mathbf{y}, \tag{39c}$$

$$(D\mathbf{u})(\mathbf{x},s) = -\lim_{\varepsilon\to 0} \mathscr{T}_\mathbf{x} \int_{\Gamma\setminus B_\varepsilon(\mathbf{x})} (\mathscr{T}_\mathbf{y}\hat{\mathbf{U}})^\top(\mathbf{x}-\mathbf{y},s)\mathbf{u}(\mathbf{y})\mathrm{d}\Gamma_\mathbf{y}, \quad \text{for } \mathbf{x}\in\Gamma. \tag{39d}$$

Once the Cauchy data are computed, the representation formula (12) can be used to evaluate the solution inside the domain Ω. The single and double layer potentials used in the representation formula are denoted by $\widetilde{V}$ and $\widetilde{K}$, i.e.,

$$(\widetilde{V}\mathbf{t})(\mathbf{x},s) = \int_\Gamma \hat{\mathbf{U}}(\mathbf{x}-\mathbf{y},s)\mathbf{t}(\mathbf{y})\mathrm{d}\Gamma_\mathbf{y}, \tag{40a}$$

$$(\widetilde{K}\mathbf{u})(\mathbf{x},s) = \int_\Gamma (\mathscr{T}_\mathbf{y}\hat{\mathbf{U}})^\top(\mathbf{x}-\mathbf{y},s)\mathbf{u}(\mathbf{y})\mathrm{d}\Gamma_\mathbf{y}, \quad \text{for } \mathbf{x}\in\Omega. \tag{40b}$$

The linear multistep method based convolution quadrature of the symmetric formulation (20) is given by

$$\begin{aligned} (V(\partial_t^{\Delta t})\tilde{\mathbf{t}})(\mathbf{x},t_n) - (K(\partial_t^{\Delta t})\tilde{\mathbf{u}})(\mathbf{x},t_n) &= \mathbf{f}_D(\mathbf{x},t_n), \quad \mathbf{x}\in\Gamma_D,\\ (D(\partial_t^{\Delta t})\tilde{\mathbf{u}})(\mathbf{x},t_n) + (K'(\partial_t^{\Delta t})\tilde{\mathbf{t}})(\mathbf{x},t_n) &= \mathbf{f}_N(\mathbf{x},t_n), \quad \mathbf{x}\in\Gamma_N \end{aligned} \tag{41}$$

for $n = 0,1,\ldots,N$ and with the abbreviations

$$\begin{aligned} \mathbf{f}_D &= \mathscr{C}\tilde{\mathbf{g}}_D + K(\partial_t^{\Delta t})\tilde{\mathbf{g}}_D - V(\partial_t^{\Delta t})\tilde{\mathbf{g}}_N,\\ \mathbf{f}_N &= (\mathscr{I}-\mathscr{C})\tilde{\mathbf{g}}_N - K'(\partial_t^{\Delta t})\tilde{\mathbf{g}}_N - D(\partial_t^{\Delta t})\tilde{\mathbf{g}}_D. \end{aligned}$$

Once (41) is solved for the boundary data, the solution $\mathbf{u}$ inside the domain Ω is obtained by discretizing the representation formula as

$$\mathbf{u}_n(\mathbf{x}) = (\widetilde{V}(\partial_t^{\Delta t})\mathbf{t})(\mathbf{x},t_n) - (\widetilde{K}(\partial_t^{\Delta t})\mathbf{u})(\mathbf{x},t_n), \quad \mathbf{x}\in\Omega. \tag{42}$$

For the Runge-Kutta based convolution quadrature, $\partial_t^{\Delta t}$ is replaced by $\underline{\partial_t}^{\Delta t}$.

4.1 Bounds in the Laplace Domain

In order to be able to apply Theorem 1 and Theorem 2 to show convergence and stability of the semi-discretized symmetric formulation (41), estimates in the Laplace domain of the form (23) are needed. That is, considering the symmetric formulation in Laplace domain

$$\begin{aligned}(V(s)\hat{\mathbf{t}})(\mathbf{x},s)-(K(s)\hat{\mathbf{u}})(\mathbf{x},s)&=\hat{\mathbf{f}}_D(\mathbf{x},s),\quad \mathbf{x}\in\Gamma_D,\\ (D(s)\hat{\mathbf{u}})(\mathbf{x},s)+(K'(s)\hat{\mathbf{t}})(\mathbf{x},s)&=\hat{\mathbf{f}}_N(\mathbf{x},s),\quad \mathbf{x}\in\Gamma_N\end{aligned}\tag{43}$$

with

$$\begin{aligned}\hat{\mathbf{f}}_D&=\mathscr{C}\hat{\mathbf{g}}_D+K(s)\hat{\mathbf{g}}_D-V(s)\hat{\mathbf{g}}_N,\\ \hat{\mathbf{f}}_N&=(\mathscr{I}-\mathscr{C})\hat{\mathbf{g}}_N-K'(s)\hat{\mathbf{g}}_N-D(s)\hat{\mathbf{g}}_D,\end{aligned}$$

a s-dependent bound in an appropriate norm of the solution operator

$$T(s):(\hat{\mathbf{g}}_D,\hat{\mathbf{g}}_N)\mapsto(\hat{\mathbf{u}},\hat{\mathbf{t}})$$

is needed. Since the kernel functions of the integral operators involved in (43) are analytic in the right half complex plane as functions of s, so are the integral operators themselves, and consequently, if it exists, the solution operator T also. If the problem is well-posed, the solution operator must be polynomially bounded in appropriate norms, but determining the degree of such a polynomial bound, μ in (23), and ν in (23), is in general difficult and for the symmetric formulation only known in the acoustic case, see [50], with the results extendible to the elastic case. For the linear multistep based convolution quadrature, see Theorem 1, the value of μ gives the smoothness of the data required for optimal convergence rate to be reached. For the Runge-Kutta method, see Theorem 2, this constant, in fact $\mu-\nu$, influences the optimal convergence rate however smooth the data may be. Accordingly, for the Runge-Kutta method it is of an extra importance to know this constant.

Bounds for various formulations with explicit dependance on s, have so far been computed for acoustics and electromagnetism. For the acoustic case, in the pioneering work of BAMBERGER and HA-DUONG [9] estimates

$$\|V(s)\|_{H^{-1/2}(\Gamma)\to H^{1/2}(\Gamma)}\le C\frac{|s|}{\Re s}\quad\text{and}\quad\|V^{-1}(s)\|_{H^{1/2}(\Gamma)\to H^{-1/2}(\Gamma)}\le C\frac{|s|^2}{\Re s},\tag{44}$$

have been proved. Therefore, according to Theorem 2, the expected rate of convergence to the exact densities is $\mathscr{O}(\Delta t^q)$, i.e., stage order q. More favourable bounds have been shown in [14] for the operator $\widetilde{V}(s)$, these imply that the rate of convergence to $\mathbf{u}(\mathbf{x},t)$ for a fixed $\mathbf{x}\in\Omega$ is $\mathscr{O}(\Delta t^p)$, that is the full (classical) order of the Runge-Kutta method; this result is likely to extend to all of the other wave propagation problems.

In the recent work by LALIENA and SAYAS [50], various formulations, the symmetric coupling, FEM-BEM coupling, transmission problems, etc., have also been investigated in the acoustics case. As stated by the authors of [50] all these results are extendible to the elastic case. The bound obtained in [50] for the solution operator of the symmetric formulation is

$$\|T(s)\|\le C\frac{|s|^{5/2}}{\Re s}.\tag{45}$$

For the electric field integral equation (EFIE) formulation of the problem of scattering of electromagnetic waves by a perfect conductor, the corresponding bound has been given in [66, 81].

Note that for the analysis of the fully discretized problem, i.e., discretized both in time *and* space, bounds of the type (44) are needed also for the spatially discretized integral operators [53].

4.2 Properties of Convolution Weights

It is instructive to investigate the shape of the convolution weights for the various boundary integral operators. In this section, the single layer operator convolution weights $\omega_j^{\Delta t}(V)$ and $W_j^{\Delta t}(V)$ for the acoustic and viscoelastodynamic equations are investigated.

These have the form

$$\omega_j^{\Delta t}(V)\mathbf{t} = \int_\Gamma \widetilde{\omega}_j^{\Delta t}(\mathbf{x}-\mathbf{y})\mathbf{t}(\mathbf{y})\mathrm{d}\Gamma_\mathbf{y} \quad \text{and} \quad W_j^{\Delta t}(V)\mathbf{t} = \int_\Gamma \widetilde{W}_j^{\Delta t}(\mathbf{x}-\mathbf{y})\mathbf{t}(\mathbf{y})\mathrm{d}\Gamma_\mathbf{y},$$

the kernels being given by the generating functions

$$\hat{\mathbf{U}}(\mathbf{z},\gamma(\zeta)/\Delta t) = \sum_{j=0}^{\infty} \widetilde{\omega}_j^{\Delta t}(\mathbf{z})\zeta^j \quad \text{and} \quad \hat{\mathbf{U}}(\mathbf{z},\Delta(\zeta)/\Delta t) = \sum_{j=0}^{\infty} \widetilde{W}_j^{\Delta t}(\mathbf{z})\zeta^j.$$

For the backward Euler method and the acoustic wave equation, the kernels $\widetilde{\omega}_j^{\Delta t}(V)$ can be given explicitly:

$$\widetilde{\omega}_j^{\Delta t}(\mathbf{z}) = \frac{e^{-\frac{|\mathbf{z}|}{c\Delta t}}}{4\pi|\mathbf{z}|}\left(\frac{|\mathbf{z}|}{c\Delta t}\right)^j \frac{1}{j!}, \qquad \text{BDF1 for the wave equation.}$$

From this formula and Stirling's approximation of $j!$ it is not difficult to see that $\widetilde{\omega}_j^{\Delta t}(\mathbf{z})$ is close to zero except for $|\mathbf{z}|/c \approx j\Delta t$. This is not surprising since the kernel function in this case approximates, in a certain sense, the Dirac delta distribution $\frac{\delta(t_j-|\mathbf{z}|/c)}{4\pi|\mathbf{z}|}$. Explicit formulas for $\widetilde{\omega}_j^{\Delta t}(\mathbf{z})$ in the case of BDF2 can be given in terms of Hermite polynomials [46]. The width of the intervals to which $|\mathbf{z}|$ needs to belong to in order that $|\widetilde{\omega}_j^{\Delta t}(\mathbf{z})| > \varepsilon$ for some $\varepsilon > 0$ have been investigated in [46]. For Runge-Kutta methods such estimates do not exist as yet, but numerical experiments [10], suggest that the width of this band is considerably smaller for high-order Runge-Kutta methods.

Because of the increased complexity of viscoelastodynamics compared to acoustics it is particularly of interest to investigate the shape of the kernel functions in this case. In Fig. 1, the shapes are compared for different choices of Δt and the underlying linear multistep or Runge-Kutta method. For the Runge-Kutta method the sum of the last row of $\widetilde{W}_j^{\Delta t}(\mathbf{z}) \in \mathbb{R}^{m\times m}$ is plotted; in fact each component has a similar

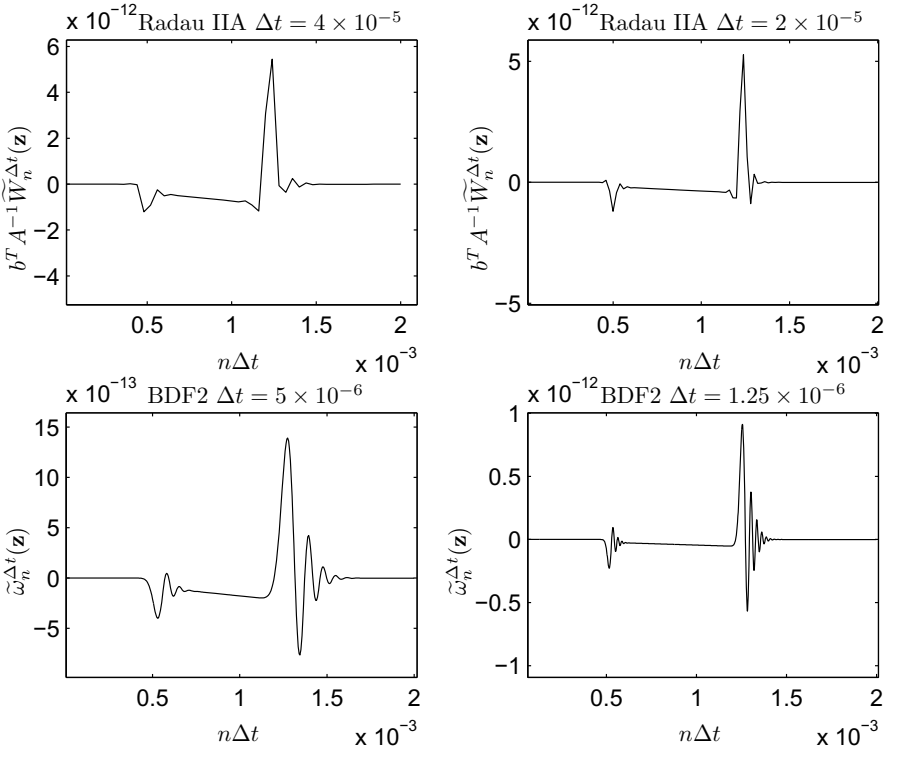

Fig. 1 Plots of the $i = 1$ and $j = 2$ entry of the tensors $\widetilde{\omega}_n^{\Delta t}(\mathbf{z})$ and $b^\top A^{-1}\widetilde{W}_n^{\Delta t}(\mathbf{z}) = \sum_{l=1}^{m}\left(\widetilde{W}_n^{\Delta t}(\mathbf{z})\right)_{ml}$ with $\mathbf{z} = (1,1,0)^\top$ for 3-stage Radau IIA and BDF2 methods

shape. For this plot, the measured material data of a Perspex (PMMA) are used, i.e., the material constants in (6) and (7), are set with

$$K = 6.2 \times 10^9\,\mathrm{N/m^2}, \quad G = 1.33 \times 10^9\,\mathrm{N/m^2}, \quad \rho = 1184\,\mathrm{kg/m^3}$$
$$q^H = q^D = 0.0023\,1/\mathrm{s}, \quad p^H = p^D = 0.002\,1/\mathrm{s}.$$

The two waves, with different speeds of propagation, can nicely be seen in these plots. It is also seen that for the Runge-Kutta method the fronts are much better localised and with less non-physical oscillation for considerably larger Δt than for the BDF2 kernels. This suggests that the higher order brings also qualitative advantages, that is, that the results should be closer to the physical reality earlier as Δt is decreased. This observation is explained more thoroughly in the next section.

4.3 Dissipation and Dispersion

It is often possible to say more about the numerical solution of a problem than just the assymptotic convergence order. Certain qualitative properties of the numerical solution can be quantified by the notions of numerical dissipation and dispersion, see [82].

An important fact, in this respect, is that the convolution quadrature of the time-domain boundary integral equation is equivalent to a boundary integral formulation of the semi-discretization of the underlying partial differential equation. Namely, the solution of the semi-discrete problem (41) and (42) satisfies the linear multistep, respectively Runge-Kutta discretization, of the underlying partial differential equation (1). For example in the case of viscoelastodynamics, see (5), the solution $\mathbf{u}_n$, $n = 0, 1, \ldots, N$, of (41) will satisfy the semi-discrete PDE

$$c_{1v}^2(\partial_t^{\Delta t})\Delta\mathbf{u} - c_{2v}^2(\partial_t^{\Delta t})\nabla\times\nabla\times\mathbf{u} = (\partial_t^{\Delta t})^2\mathbf{u}, \tag{46}$$

whereas in the case of the acoustic wave equation the solution u_n, $n = 0, 1, \ldots, N$, of (41) satisfies the semi-discrete PDE

$$c^2\Delta u = (\partial_t^{\Delta t})^2 u \tag{47}$$

in the domain Ω. For the method of proof of this fact, see [53, Theorem 5.2] and the introduction of [10]. To perform dispersion and dissipation analysis, one assumes (46) or (47) to hold in the whole space $\mathbb{R}^3$ and investigates the shape of plane wave solutions. Such an analysis is classical, but has first been performed in the context of convolution quadrature in [23].

For simplicity only the scalar wave equation (47) is investigated here. The non-discretized wave equation (3) admits plane-wave solutions of the form $e^{\mathrm{i}(\frac{\xi}{c}\cdot\mathbf{x}+\omega t)}$ with $\omega^2 = |\xi|^2$. The semi-discrete equation (47) also admits plane wave solutions $u_n(\mathbf{x}) = e^{\mathrm{i}(\frac{\xi}{c}\cdot\mathbf{x}+\omega_{\Delta t}t_n)}$, but, the relationship between $\omega_{\Delta t}$ and ξ is considerably more involved and constitutes the dissipation and dispersion analysis. For linear multistep methods the relationship is given by

$$|\xi|^2 = \left(\frac{\gamma(e^{-\mathrm{i}\omega_{\Delta t}\Delta t})}{\mathrm{i}\Delta t}\right)^2. \tag{48}$$

In the case of a backward Euler discretization, i.e., $\gamma(\zeta) = 1-\zeta$, solving this equation for $\omega_{\Delta t}$ the following relationship is obtained

$$\omega_{\Delta t} = \pm|\xi| + \frac{\mathrm{i}}{2}\Delta t|\xi|^2 \mp \frac{1}{3}\Delta t^2|\xi|^3\cdots, \qquad \text{Backward Euler.}$$

This shows that plane waves satisfying the semi-discrete wave equation discretized by first order BDF method are of size $\mathcal{O}(e^{-\frac{1}{2}\Delta t|\xi|^2})$, i.e., the solutions are significantly damped unless $\Delta t|\xi|^2 \ll 1$. This is a much stronger condition than the sampling condition of a few degrees of freedom per wavelength, i.e., $\Delta t|\xi| \ll 1$. In

general, it is seen from (48) and the approximation property $\gamma(e^{-z}) = z + \mathscr{O}(z^{p+1})$, that for a p-th order linear multistep based discretization to give an accurate result, Δt must satisfy the condition $\Delta t^p |\xi|^{p+1} \ll 1$. Since the order of A-stable multistep methods is restricted to $p \leq 2$, this condition on Δt is always significantly more stringent than the sampling condition.

For Runge-Kutta methods consider the plane wave $u_{n\ell} = e^{\mathrm{i}(\frac{\zeta}{c}\cdot\mathbf{x} + \omega_{\Delta t} t_n + \omega_{\ell,\Delta t} c_\ell \Delta t)}$. Since $c_m = 1$, $\omega_{m,\Delta t} = \omega_{\Delta t}$ must hold, but in general it is not possible to require $\omega_{\ell,\Delta t} = \omega_{\Delta t}$ for all ℓ. For the analysis the following result proved in [10] will be used.

Lemma 1. *Let* (28) *hold,* $|\zeta| \neq 1$*, and* λ *be an eigenvalue of* $\Delta(\zeta)$*, but not of* A^{-1}*. Then* $R(\lambda) = \zeta^{-1}$*.*

A similar calculation as for the linear multistep methods gives the relationship

$$|\xi|^2 \begin{pmatrix} u_{n1} \\ \vdots \\ u_{nm} \end{pmatrix} = \left(\frac{\Delta(e^{-\mathrm{i}\omega_{\Delta t}\Delta t})}{\mathrm{i}\Delta t} \right)^2 \begin{pmatrix} u_{n1} \\ \vdots \\ u_{nm} \end{pmatrix}. \tag{49}$$

A solution $\omega_{l,\Delta t}$ of the following equation also satisfies (49)

$$|\xi| \begin{pmatrix} u_{n1} \\ \vdots \\ u_{nm} \end{pmatrix} = \left(\frac{\Delta(e^{-\mathrm{i}\omega_{\Delta t}\Delta t})}{\mathrm{i}\Delta t} \right) \begin{pmatrix} u_{n1} \\ \vdots \\ u_{nm} \end{pmatrix}. \tag{50}$$

Therefore, $\mathrm{i}\Delta t|\xi|$ is an eigenvalue of $\Delta(e^{-\mathrm{i}\omega_{\Delta t}\Delta t})$ and for small enough $\Delta t|\xi|$ cannot be an eigenvalue of A^{-1}. Consequently, due to Lemma 1,

$$R(\mathrm{i}\Delta t|\xi|) = e^{\mathrm{i}\omega_{\Delta t}\Delta t}.$$

Recalling the approximation property of the stability function $R(z) = e^z + \mathscr{O}(z^{p+1})$, it is seen that

$$\omega_{\Delta t} = |\xi| + |\xi|\mathscr{O}(|\xi\Delta t|^p). \tag{51}$$

Since for the 2-stage Radau IIA method $p = 3$ and for the 3-stage method $p = 5$, it is seen from the last equation that these methods are significantly less dissipative and dispersive than the A-stable linear multistep formulas. Furthermore, the constant implicit in (51) is very favourable in the case of Radau IIA methods, it is $C = 1/216$ for the 2-stage and $C = 1/7200$ for the 3-stage method.

5 Space Discretization

Space discretization, in the context of convolution quadratures, poses no extra difficulty compared to the space discretization of boundary integral operators of elliptic, in particular Helmholtz, problems. It is merely necessary to replace the Laplace domain integral operators in (41) by their discretized counterparts.

5.1 Galerkin and Collocation in Space

When using Galerkin discretization in space, finite element bases on boundaries Γ_D and Γ_N are used to construct the approximation spaces

$$X_D = \mathrm{Span}\{\varphi_1, \varphi_2, \ldots, \varphi_{M_1} \mid \varphi_j \equiv 0 \text{ on } \Gamma_N\},$$
$$X_N = \mathrm{Span}\{\psi_1, \psi_2, \ldots, \psi_{M_2} \mid \psi_j \equiv 0 \text{ on } \Gamma_D\}.$$

The unknowns $(\tilde{\mathbf{u}})_n$ and $(\tilde{\mathbf{t}})_n$ at time $t = t_n$ are approximated by a linear combination of functions in X_D and X_N

$$(\tilde{\mathbf{u}}_h)_n = \sum_{\ell=1}^{M_1} \alpha_\ell^{(n)} \varphi_\ell \quad \text{and} \quad (\tilde{\mathbf{t}}_h)_n = \sum_{k=1}^{M_2} \beta_k^{(n)} \psi_k, \quad n = 0, 1, \ldots, N. \tag{52}$$

Inserting this ansatz into (41) and testing by functions from X_D and X_N gives the fully discrete system

$$\int_\Gamma V(\partial_t^{\Delta t})\tilde{\mathbf{t}}_h(\mathbf{x}, t_n)\psi_k(\mathbf{x})\mathrm{d}\Gamma_\mathbf{x} - \int_\Gamma K(\partial_t^{\Delta t})\tilde{\mathbf{u}}_h(\mathbf{x}, t_n)\psi_k(\mathbf{x})\mathrm{d}\Gamma_\mathbf{x} = \int_\Gamma \mathbf{f}_D(\mathbf{x}, t_n)\psi_k(\mathbf{x})\mathrm{d}\Gamma_\mathbf{x},$$
$$\int_\Gamma D(\partial_t^{\Delta t})\tilde{\mathbf{u}}_h(\mathbf{x}, t_n)\varphi_\ell(\mathbf{x})\mathrm{d}\Gamma_\mathbf{x} + \int_\Gamma K'(\partial_t^{\Delta t})\tilde{\mathbf{t}}_h(\mathbf{x}, t_n)\varphi_\ell(\mathbf{x})\mathrm{d}\Gamma_\mathbf{x} = \int_\Gamma \mathbf{f}_N(\mathbf{x}, t_n)\varphi_\ell(\mathbf{x})\mathrm{d}\Gamma_\mathbf{x},$$

for $n = 0, 1, \ldots, N$, $\ell = 1, 2, \ldots, M_1$, and $k = 1, 2, \ldots, M_2$.

When solving this convolutional linear system of equations using the techniques of Sect. 3.3, quadrature required to implement these equations can be done solely in Laplace domain. More specifically, the Galerkin discretization of the operators $V(s_\ell)$, $K(s_\ell)$, $K'(s_\ell)$, and $D(s_\ell)$ for all the frequencies s_ℓ occurring in the algorithms described in Section 3.3 are needed. For example, the Galerkin discretization of the single layer potential requires the computation of the following integrals

$$\int_\Gamma (V(s_\ell)\psi_j)(\mathbf{x})\psi_k(\mathbf{x})\mathrm{d}\Gamma_\mathbf{x} = \int_\Gamma \int_\Gamma \hat{\mathbf{U}}(\mathbf{x} - \mathbf{y}, s_\ell)\psi_j(\mathbf{y})\psi_k(\mathbf{x})\mathrm{d}\Gamma_\mathbf{y}\mathrm{d}\Gamma_\mathbf{x}.$$

Numerical quadrature routines for kernels $\hat{\mathbf{U}}(\mathbf{x} - \mathbf{y}, s_\ell)$ have been extensively investigated and are readily available, see for example [36, 45, 75]. In fact, one of the main advantages of convolution quadrature lies in the fact that numerical quadrature of the difficult/unknown distributional kernel function is not necessary.

It has to be mentioned that the right-hand sides $\mathbf{f}_D$ and $\mathbf{f}_N$ are not immediately available, but have to be first computed by applying time-domain integral operators to the data $\tilde{\mathbf{g}}_D$ and $\tilde{\mathbf{g}}_N$. This is usually done by first projecting the data onto boundary element bases defined on Γ; note that since it is not necessarily true that $\tilde{\mathbf{g}}_D \equiv 0$ on Γ_N and $\tilde{\mathbf{g}}_N \equiv 0$ on Γ_D it is not possible here to re-use spaces X_D and X_N.

To avoid double integration in space, it is of interest to use collocation in space instead of Galerkin discretization. Here the unknown functions are again approximated by a linear combination of basis functions as in (52) and this approximation is substituted in (41). To arrive at a system of linear equations, the resulting equations are evaluated at *collocation* points on the boundary.

Stability and convergence analysis of the fully discrete symmetric system has not yet appeared in literature in any of the applications covered in this paper. The linear multistep convolution quadrature with Galerkin discretization in space for the indirect boundary integral formulation of the Dirichlet problem of acoustics has been fully analysed in [53].

5.2 Fast Data-Sparse Methods in Frequency Domain

Using Algorithm 1 to solve the fully discrete system it is necessary to discretize operators $V(s_\ell)$, $K(s_\ell)$, $K'(s_\ell)$, and $D(s_\ell)$. Galerkin or collocation discretizations of such operators result in dense $M_j \times M_k$ matrices, $j,k = 1,2$. Therefore, direct computation and storage of such matrices has cost $\mathscr{O}(M^2)$ with $M = \max(M_1, M_2)$. Fortunately, so called data sparse techniques have been developed in the past couple of decades that can in almost linear cost, i.e., $\mathscr{O}(M \log^a M)$ for some $a > 0$, compute approximations of these matrices. Two main classes of such data sparse methods are hierarchical matrices ($\mathscr{H}$-matrices) [43, 44] and the fast multipole methods (FMM) [24, 68].

The difficulty of computing a data sparse representation of space discretizations of integral operators is directly related to the wavenumbers s_ℓ. The kernel functions have the form

$$\hat{\mathbf{U}}(\mathbf{x}, s) = \sum_{i=1}^{w} \mathbf{A}^{(i)}(r, s) \frac{e^{-\frac{s}{c_i(s)} r}}{4\pi r}, \qquad r = |\mathbf{x}|,$$

with $c_i(s) \to const > 0$ for $|s| \to \infty$, and hence if $|\Im s_\ell| \gg 1$ the kernel is highly oscillatory and consequently difficult to discretize efficiently, on the other hand if $\Re s \gg 1$ the operator is practically diagonal and easy to efficiently discretize.

The evaluation of integral operators at different wavenumbers occurs in two places in Algorithm 1 where a discrete convolutional system of size J is solved by solving a decoupled set of linear systems in Laplace domain, and where a matrix-vector product with discretized integral operators in Laplace domain needs to be computed. In [10], it is shown that if J is chosen as a constant independent of Δt the frequencies arising in solving the small system (last block) all satisfy $|\Im s|/\Re s \leq const$. This in turn implies that the integral operators in Laplace domain can be approximated by an $\mathscr{H}$-matrix with computational and storage complexity $\mathscr{O}(M \log M)$. Furthermore, an (approximate) LU-decomposition in $\mathscr{H}$-matrix format can be computed in $\mathscr{O}(N \log^2 N)$ time, which can be used as a very good preconditioner for solving the linear systems by an iterative method, such as GMRES.

Wavenumbers occurring in the line *update right hand side* can have $|\Im s| \sim \Delta t^{-1}$. If $\Delta t / c_i$, with c_i the speed of the wave, is much smaller than the size of the computational domain Ω, high-frequency problems occur for which $\mathscr{H}$-matrices lose their

efficiency [58]. Fortunately, the highly-oscillatory operators need not be inverted, but only a single matrix-vector product needs to be computed. This is an ideal task for the so called fast multipole methods. Here the advantage of the recursive procedure from Sect. 3.3.2 can best be seen.

Many fast-multipole like methods for high-frequency Helmholtz integral operators have been developed since the early 1990s [4, 11, 29, 69, 70]. These have dealt with cases of purely real and purely imaginary wavenumbers. They can be adapted to the present case of the whole range of complex frequencies, still, to do this optimally more work is needed.

6 Numerical Example

In this section, the solution procedure of Sect. 3.3.1 is tested for elastodynamics with different Runge-Kutta and multistep methods. In order to show the validity of the results only benchmark examples, whose analytical solutions are known, are treated. All computations were performed by using the HyENA C++ library for the numerical solution of partial differential equations using the boundary element method [59]. For the Fourier like transformations the FFTW routines [38] are taken.

A 3-d rod of size $\ell_1 = 3.0\,\mathrm{m}$ and $\ell_2 = \ell_3 = 1.0\,\mathrm{m}$, as depicted in Fig. 2, is considered. It is fixed on one end and the other end is excited by a pressure jump $t_1 = -1.0H(t)\,\mathrm{N/m^2}$. $H(t)$ denotes the unit step function. The material parameters of steel ($\rho = 7850\,\mathrm{kg/m^3}$, $G = 1.055 \times 10^{11}\,\mathrm{N/m^2}$, $K = 7.03 \times 10^{10}\,\mathrm{N/m^2}$) are taken. Poisson ratio is chosen to be zero, such that the results can be compared with the analytical solution of longitudinal waves in a 1-d elastodynamic rod (see [41]).

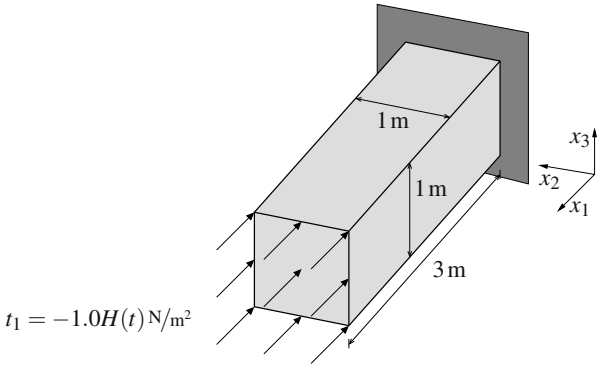

Fig. 2 System and boundary conditions

The rod shown in Fig. 2 is discretised with two different meshes, the coarse with 565 triangular boundary elements of uniform mesh size $h = 0.2\,\mathrm{m}$ and the fine with 2176 triangular boundary elements of uniform mesh size $h = 0.1\,\mathrm{m}$. Both are depicted in Fig. 3.

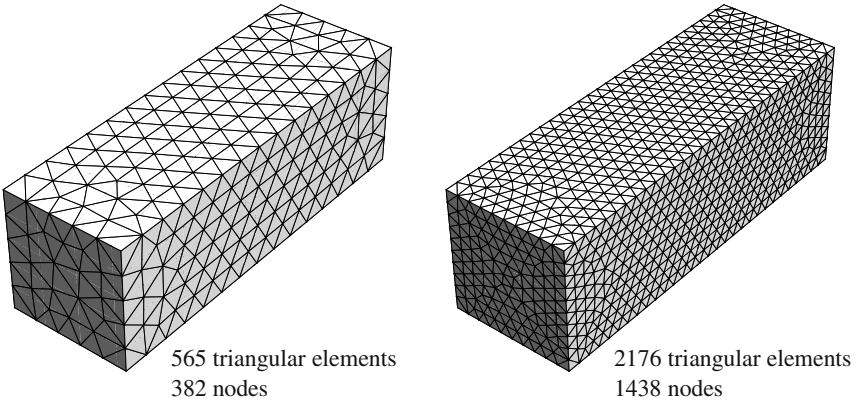

(a) coarse mesh: $h = 0.2m$ (b) fine mesh: $h = 0.1m$

Fig. 3 Uniform meshes used for the calculations

The tractions and displacements are approximated by piecewise constant and continuous linear polynomials, respectively. In order to compare different time discretizations the dimensionless value

$$\beta = \frac{c_1 \Delta t}{h} \tag{53}$$

is introduced. This value depends on the velocity of the compression wave c_1, the time step size Δt, and the average mesh size h. For the Runge-Kutta methods the time step size Δt is taken that of the stages and not of one step to have a fair comparison with the multistep method.

In the following, results are presented to show the influence of the different time discretisations, i.e., the chosen methods are BDF2, Radau IIA (2-stage), and Radau IIA (3-stage). It is studied how these different methods work in relation to the spatial discretisation and the time step size.

First, the displacement in the middle of the top and the tractions in the middle of the bottom of the bar are displayed in Fig. 4 versus time for the different Runge-Kutta methods listed above and the BDF2.

A collocation technique with $\beta = 0.3$ and the fine mesh is used. The displacement results are more or less equal and coincide well with the analytical solution. The traction solution is overall good as well. The differences between the Runge-Kutta methods and the BDF2 are visible in the oscillations at the jumps. There, the Runge-Kutta methods show less pronounced effects and as well a better representation of the straight lines. This is in accordance with the observations made for the integration weights in Sect. 4 (see Fig. 1). The Runge-Kutta methods have represented the wave fronts much sharper than the BDF2. Hence, here the oscillations must be smaller. Nevertheless, also the results for the BDF2 are good. As the

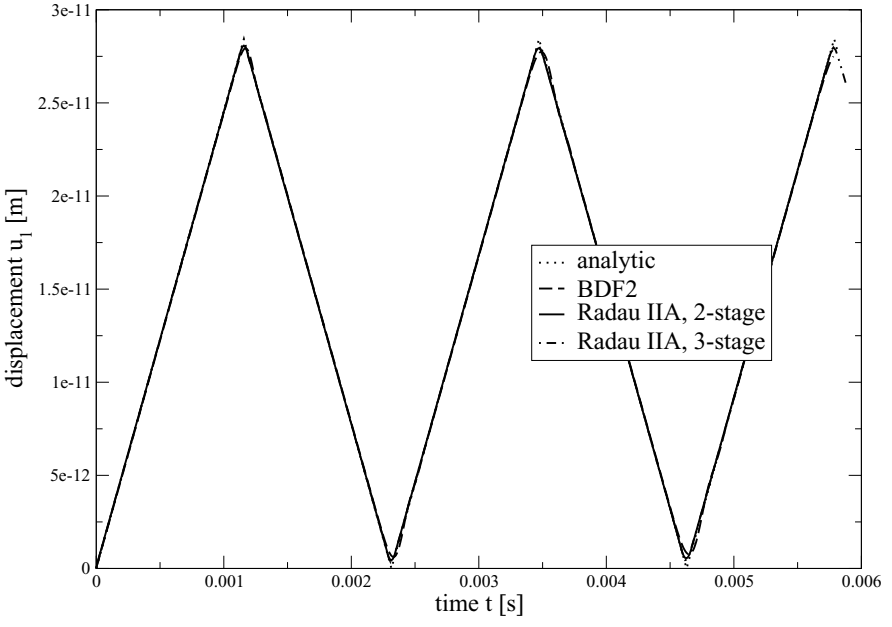

(a) Displacements at the top

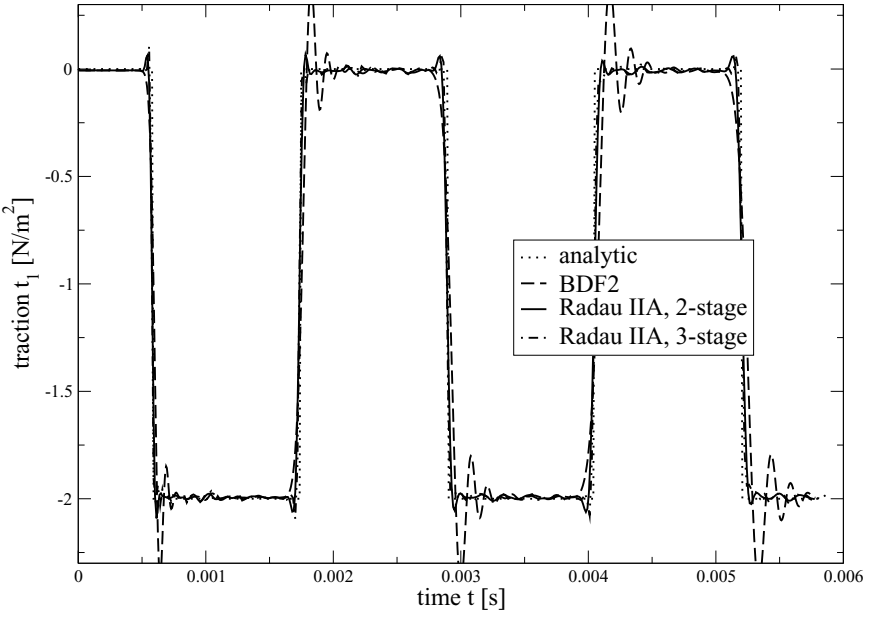

(b) Tractions at the bottom

Fig. 4 Results for different Runge-Kutta methods and the BDF2 versus time

different displacement results are nearly not distinguishable, in the following only traction results will be presented.

The next study shows the influence of the mesh size where the traction results using a Radau IIA (2-stage) are compared. In Fig. 5, the results are displayed versus time for both discretisations of Fig. 3 and for a collocation (denoted by 'collo') and a symmetric Galerkin BEM (denoted by 'SGBEM').

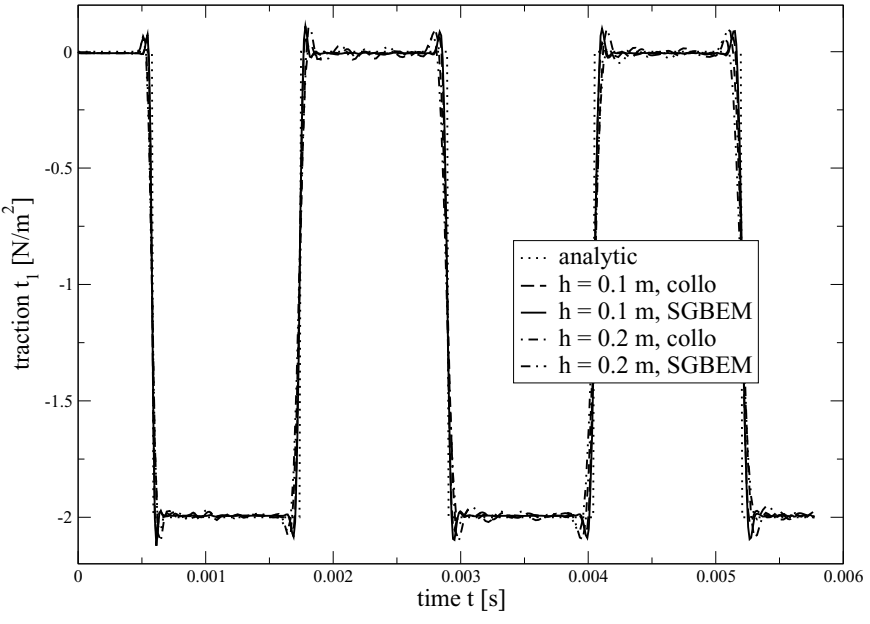

Fig. 5 Influence of mesh size using a Radau IIA (2-stage) method

As expected the finer mesh yields better results. The difference between collocation and the SGBEM is not observable. Similar plots can be made with the other time discretisations, which yield qualitatively the same. One difference can be observed. The 3-stage Radau IIA method tends to instabilities for the chosen $\beta = 0.3$.

The sensitivity on the times step size is studied in Fig. 6. The traction results are computed with the finer mesh for all three multistep methods for different β-values. For $\beta = 0.1$ the 3-stage Radau IIA method shows clearly an instability. These results are truncated after $t \approx 0.0033\,\mathrm{s}$, not to destroy the whole picture. With a coarser mesh also the other methods would show instabilities. Overall, the numerical tests confirm that a finer mesh moves the instabilities to smaller values of β. Comparing to the mathematics in Sect. 3 this behavior is not obvious. But, it must be remarked that all proofs require some smoothness of the given data which is in the example by the Heaviside function clearly violated. However, for engineering applications such loadings are necessary and, therefore, the numerical tests has been made with this right hand side.

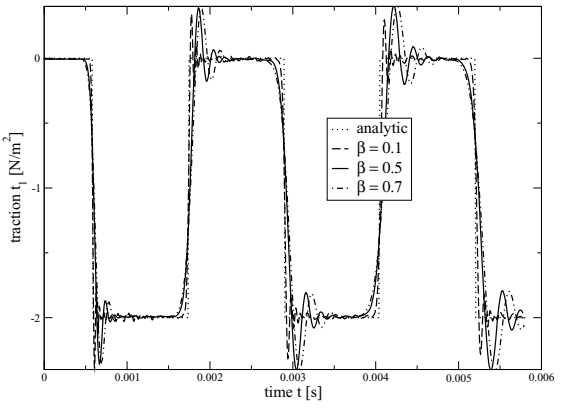

(a) BDF2

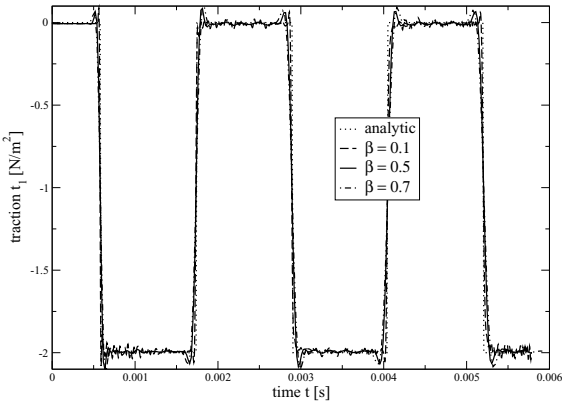

(b) Radau IIA (2-stage)

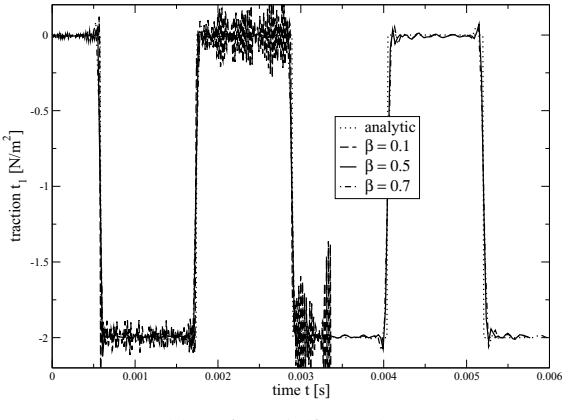

(c) Radau IIA (3-stage)

Fig. 6 Influence of time step size for the different multistep methods

The last study concerns the long time behavior, because a lot of time domain BE formulations suffer from either strong numerical damping or instabilities in the long time range. The proposed method shows a very nice behavior as presented in Fig. 7. The collocation and the SGBEM results are given for both meshes using a 3-stage Radau IIA method.

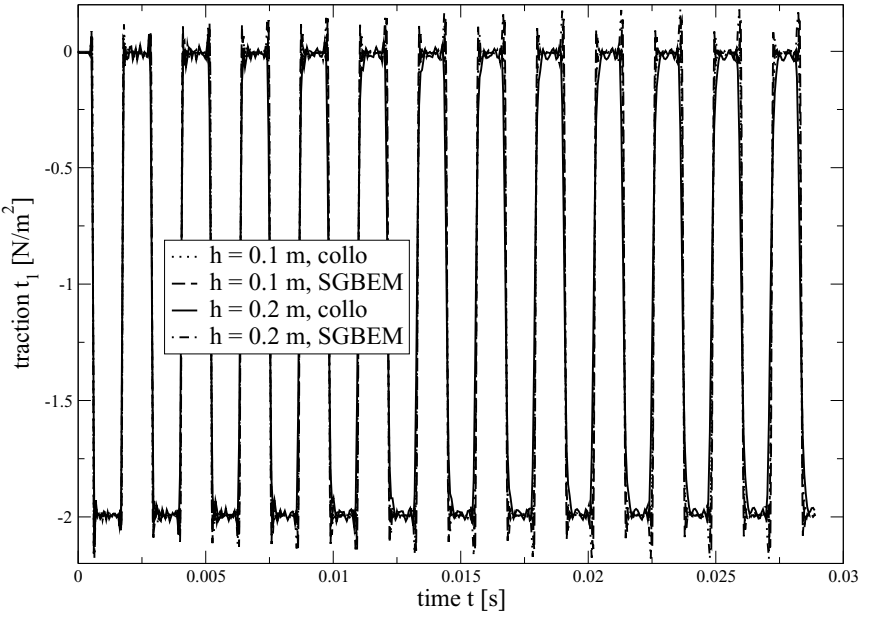

Fig. 7 Long time behavior using a Radau IIA (3-stage) method

Nearly no numerical damping is observed and no instabilities. The time step size is chosen according to $\beta = 0.5$. The other Runge-Kutta or multistep methods produce comparable results. Hence, it can be concluded that the long time behavior is satisfactory.

Overall, the presented results show that the method is robust with respect to the time and the spatial discretisation if the mesh is sufficiently fine and the time step size not too small.

Appendix

The general form of the fundamental solutions for the operators given in Sect. 2 can be found in (13). For better readability it is recalled

$$\hat{\mathbf{U}}(\mathbf{x}-\mathbf{y},s) = \sum_{i=1}^{w} \mathbf{A}^{(i)}(r,s)\frac{e^{-\lambda_i r}}{4\pi r} \qquad \text{with} \quad r = |\mathbf{x}-\mathbf{y}| \,.$$

In the following, the coefficients $\mathbf{A}^{(i)}(r,s)$ are listed. For the vectorial problems the fundamental solutions are tensors. For them the indical notation is used where $r_{,i} = \frac{x_i - y_i}{r}$ stands for the directional derivative and δ_{ij} for the Kronecker delta.

Acoustics

The respective equations are presented in Sect. 2.1.1. In (3), the homogeneous form of the differential equation is given. For the definition of the fundamental solution a source of Dirac type has to be added. As in acoustics only one compressional wave appears and the sum in (13) has only one term, i.e., $w = 1$ holds. Further, it is a scalar problem, hence, the tensor of fundamental solutions degenerates to a scalar value. The coefficient is

$$A^{(1)} = 1 \qquad \text{with} \quad \lambda_1 = \frac{s}{c} = s\sqrt{\frac{\rho}{K}}\,.$$

Visco- and Elastodynamics

The governing equations for viscoelasticity are given in Sect. 2.1.2 as an extension of the elastodynamic case (1). Only the wave velocities have to be replaced by (6). The excitation in the definition of the fundamental solutions is a force of Dirac type. Two waves, the compression and the shear wave, exist and, therefore, the sum in (13) has two terms, i.e., $w = 2$ holds. The coefficients are

$$A_{ij}^{(1)} = \frac{1}{\rho s^2}\left\{\frac{3r_{,i}r_{,j} - \delta_{ij}}{r^2}(\lambda_1 r + 1) + \lambda_1^2 r_{,i}r_{,j}\right\},$$
$$A_{ij}^{(2)} = \frac{1}{\rho s^2}\left\{\frac{3r_{,i}r_{,j} - \delta_{ij}}{r^2}(\lambda_2 r + 1) + \lambda_2^2 r_{,i}r_{,j}\right\}$$

with the complex wave numbers

$$\lambda_1 = \frac{s}{c_1}, \qquad \lambda_2 = \frac{s}{c_2} \qquad \text{in elastodynamics and}$$
$$\lambda_1 = \frac{s}{c_{1v}}, \qquad \lambda_2 = \frac{s}{c_{2v}} \qquad \text{in viscoelastodynamics.}$$

Poroelastodynamics

The governing equation of poroelastodynamics (8) is a coupled set of differential equations for the unkowns solid displacement $\mathbf{u}$ and the pore pressure p. Consequently, the fundamental solution is a matrix

$$\hat{\mathbf{G}} = \begin{pmatrix} \hat{U}_{ij}^s & \hat{U}_i^f \\ \hat{P}_j^s & \hat{P}^f \end{pmatrix} \qquad \text{with} \quad \hat{U}_i^f = s\hat{P}_i^s\,.$$

The single entries are composed as given in (13) and have either three waves, i.e., $w = 3$ or only two compressional waves, i.e., $w = 2$. The respective coefficients of the sum are for the solid displacements due to a bulk body forc of Dirac type in the solid, i.e., $\hat{U}^s_{ij}$

$$A^{(1)}_{ij} = \frac{1}{(\rho - \beta(s)\rho_f)s^2} R_1 \frac{\lambda_4^2 - \lambda_2^2}{\lambda_1^2 - \lambda_2^2},$$
$$A^{(2)}_{ij} = \frac{-1}{(\rho - \beta(s)\rho_f)s^2} R_2 \frac{\lambda_4^2 - \lambda_1^2}{\lambda_1^2 - \lambda_2^2},$$
$$A^{(3)}_{ij} = \frac{1}{(\rho - \beta(s)\rho_f)s^2} (\delta_{ij}\lambda_3^2 - R_3)$$

with

$$R_k = \frac{3r_{,i}r_{,j} - \delta_{ij}}{r^2} + \lambda_k \frac{3r_{,i}r_{,j} - \delta_{ij}}{r} + \lambda_k^2 r_{,i}r_{,j} \quad \text{and} \quad \lambda_4^2 = s^2 \frac{\rho - \beta(s)\rho_f}{K + 4/3G}.$$

The pressure caused by the same load is, i.e., $\hat{P}^s_j$

$$A^{(1)}_{ij} = \frac{(\alpha - \beta(s))s\rho_f r_{,j}}{\beta(s)(K + \frac{4}{3}G)(\lambda_1^2 - \lambda_2^2)} \left(\lambda_1 + \frac{1}{r}\right),$$
$$A^{(2)}_{ij} = \frac{-(\alpha - \beta(s))s\rho_f r_{,j}}{\beta(s)(K + \frac{4}{3}G)(\lambda_1^2 - \lambda_2^2)} \left(\lambda_2 + \frac{1}{r}\right).$$

The remaining one is the pressure due to a source of Dirac type in the fluid, i.e., $\hat{P}^f$

$$A^{(1)}_{ij} = \frac{s\rho_f}{\beta(s)} \frac{\lambda_1^2 - \lambda_4^2}{\lambda_1^2 - \lambda_2^2}, \qquad A^{(2)}_{ij} = \frac{-s\rho_f}{\beta(s)} \frac{\lambda_2^2 - \lambda_4^2}{\lambda_1^2 - \lambda_2^2}.$$

Electromagnetism

The fundamental solution is the same as for the acoustic wave equation, i.e.,

$$A^{(1)} = 1 \qquad \text{with} \quad \lambda_1 = \frac{s}{c} = s\sqrt{\varepsilon\mu}\,.$$

References

[1] Abreu, A.I., Carrer, J.A.M., Mansur, W.J.: Scalar wave propagation in 2D: a BEM formulation based on the operational quadrature method. Eng. Anal. Bound Elem. 27, 101–105 (2003)

[2] Abreu, A.I., Mansur, W.J., Carrer, J.A.M.: Initial conditions contribution in a BEM formulation based on the convolution quadrature method. Int. J. Numer. Methods Engrg. 67, 417–434 (2006)

[3] Aimi, A., Diligenti, M.: A new space-time energetic formulation for wave propagation analysis in layered media by BEMs. Int. J. Numer. Methods Engrg. 75(9), 1102–1132 (2008)
[4] Amini, S., Profit, A.T.J.: Multi-level fast multipole solution of the scattering problem. Eng. Anal. Bound Elem. 27(5), 547–564 (2003)
[5] Antes, H.: A boundary element procedure for transient wave propagations in two-dimensional isotropic elastic media. Finite Elem. Anal. Des. 1, 313–322 (1985)
[6] Antes, H., Jäger, M.: On stability and efficiency of 3d acoustic BE procedures for moving noise sources. In: Atluri, S., Yagawa, G., Cruse, T. (eds.) Computational Mechanics, Theory and Applications, vol. 2, pp. 3056–3061. Springer, Heidelberg (1995)
[7] Bachelot, A., Lange, V.: Time dependent integral method for Maxwell's system. In: Mathematical and Numerical Aspects of Wave Propagation (Mandelieu-La Napoule, 1995), pp. 151–159. SIAM, Philadelphia (1995)
[8] Bachelot, A., Bounhoure, L., Pujols, A.: Couplage éléments finis–potentiels retardés pour la diffraction électromagnétique par un obstacle hétérogène. Numer. Math. 89(2), 257–306 (2001)
[9] Bamberger, A., Ha-Duong, T.: Formulation variationelle espace-temps pour le calcul par potentiel retardé d'une onde acoustique. Math. Meth. Appl. Sci. 8, 405–435, 598–608 (1986)
[10] Banjai, L.: Multistep and multistage convolution quadrature for the wave equation: Algorithms and experiments. SIAM J. Sci. Comput. 32, 2964–2994 (2010)
[11] Banjai, L., Hackbusch, W.: Hierarchical matrix techniques for low and high frequency Helmholtz equation. IMA J. Numer. Anal. 28(1), 46–79 (2008)
[12] Banjai, L., Lubich, C.: An error analysis of Runge-Kutta convolution quadrature. BIT Num. Math. 51(3), 483–496 (2011)
[13] Banjai, L., Sauter, S.: Rapid solution of the wave equation in unbounded domains. SIAM J. Numer. Anal. 47(1), 227–249 (2009)
[14] Banjai, L., Lubich, C., Melenk, J.M.: Runge-Kutta convolution quadrature for operators arising in wave propagation. Numer. Math. 119(1), 1–20 (2011)
[15] Beskos, D.E.: Boundary element methods in dynamic analysis. AMR 40(1), 1–23 (1987)
[16] Beskos, D.E.: Boundary element methods in dynamic analysis: Part II (1986-1996). AMR 50(3), 149–197 (1997)
[17] Biot, M.A.: Theory of propagation of elastic waves in a fluid-saturated porous solid. I. Low-frequency range. J. Acoust. Soc. Am. 28(2), 168–178 (1956)
[18] Biot, M.A.: Theory of propagation of elastic waves in a fluid-saturated porous solid. II. Higher frequency range. J. Acoust. Soc. Am. 28(2), 179–191 (1956)
[19] Birgisson, B., Siebrits, E., Peirce, A.P.: Elastodynamic direct boundary element methods with enhanced numerical stability properties. Int. J. Numer. Methods Engrg. 46, 871–888 (1999)
[20] de Boer, R.: Theory of Porous Media. Springer, Berlin (2000)
[21] Butcher, J.C.: The numerical analysis of ordinary differential equations. A Wiley-Interscience Publication, John Wiley & Sons Ltd., Chichester (1987)
[22] Calvo, M.P., Cuesta, E., Palencia, C.: Runge-Kutta convolution quadrature methods for well-posed equations with memory. Numer. Math. 107(4), 589–614 (2007)
[23] Chen, Q., Monk, P., Wang, X., Weile, D.: Analysis of convolution quadrature applied to the time-domain electric field integral equation (2010) (submitted)

[24] Cheng, H., Crutchfield, W.Y., Gimbutas, Z., Greengard, L.F., Ethridge, J.F., Huang, J., Rokhlin, V., Yarvin, N., Zhao, J.: A wideband fast multipole method for the Helmholtz equation in three dimensions. J. Comput. Phys. 216(1), 300–325 (2006)
[25] Chew, W.C., Jin, J.M., Michielssen, E., Song, J.M.: Fast and Efficient Algorithms in Computational Electromagnetics. Artech House, Boston (2001)
[26] Christensen, R.M.: Theory of Viscoelasticity. Academic Press, New York (1971)
[27] Costabel, M.: Time-dependent problems with the boundary integral equation method. In: Stein, E., de Borst, R., Hughes, T.J.R. (eds.) Encyclopedia of Computational Mechanics. Fundamentals, ch. 25, vol. 1, John Wiley & Sons, New York (2005)
[28] Cruse, T.A., Rizzo, F.J.: A direct formulation and numerical solution of the general transient elastodynamic problem, I. Aust. J. Math. Anal. Appl. 22(1), 244–259 (1968)
[29] Darve, E., Havé, P.: Efficient fast multipole method for low-frequency scattering. J. Comput. Phys. 197(1), 341–363 (2004)
[30] Davies, P.J.: On the stability of time-marching schemes for the general surface electric-field integral equation. IEEE Trans. Antenn. Propag. 44(11), 1467–1473 (1996)
[31] Davies, P.J.: Averaging techniques for time marching schemes for retarded potential integral equations. Appl. Numer. Math. 23, 291–310 (1997)
[32] Davies, P.J.: A stability analysis of a time marching scheme for the general surface electric field integral equation. Appl. Numer. Math. 27(1), 33–57 (1998)
[33] Davies, P.J., Duncan, D.B.: Stability and convergence of collocation schemes for retarded potential integral equations. SIAM J. Numer. Anal. 42(3), 1167–1188 (2004)
[34] Davies, P.J., Duncan, D.B., Zubik-Kowal, B.: The stability of numerical approximations of the time domain current induced on thin wire and strip antennas. Appl. Numer. Math. 55(1), 48–68 (2005)
[35] Domínguez, J.: Dynamic stiffness of rectangular foundations. Report no. R78-20, Department of Civil Engineering, MIT, Cambridge, MA (1978)
[36] Erichsen, S., Sauter, S.A.: Efficient automatic quadrature in 3-d Galerkin BEM. Comput. Methods Appl. Mech. Engrg. 157(3-4), 215–224 (1998)
[37] Friedman, M.B., Shaw, R.: Diffraction of pulses by cylindrical obstacles of arbitrary cross section. J. Appl. Mech. 29(1), 40–46 (1962)
[38] Frigo, M., Johnson, S.G.: The design and implementation of FFTW3. Proceedings of the IEEE 93(2), 216–231 (2005)
[39] García-Sánchez, F., Zhang, C., Sáez, A.: 2-d transient dynamic analysis of cracked piezoelectric solids by a time-domain BEM. Comput. Methods Appl. Mech. Engrg. 197(33-40), 3108–3121 (2008)
[40] Gaul, L., Schanz, M.: A comparative study of three boundary element approaches to calculate the transient response of viscoelastic solids with unbounded domains. Comput. Methods Appl. Mech. Engrg. 179(1-2), 111–123 (1999)
[41] Graff, K.F.: Wave Motion in Elastic Solids. Oxford University Press (1975)
[42] Gurtin, M.E., Sternberg, E.: On the Linear Theory of Viscoelasticity. Arch. Rational Mech. Anal. 11, 291–356 (1962)
[43] Hackbusch, W.: Hierarchische Matrizen. Springer, Heidelberg (2009)
[44] Hackbusch, W., Nowak, Z.P.: On the fast matrix multiplication in the boundary element method by panel clustering. Numer. Math. 54(4), 463–491 (1989)
[45] Hackbusch, W., Sauter, S.A.: On the Efficient Use of the Galerkin Method to Solve Fredholm Integral Equations. Appl. Math. 38(4-5), 301–322 (1993)

[46] Hackbusch, W., Kress, W., Sauter, S.A.: Sparse convolution quadrature for time domain boundary integral formulations of the wave equation by cutoff and panel-clustering. In: Schanz, M., Steinbach, O. (eds.) Boundary Element Analysis: Mathematical Aspects and Applications. LNACM, vol. 29, pp. 113–134. Springer, Heidelberg (2007)
[47] Hairer, E., Wanner, G.: Solving ordinary differential equations. II. Springer Series in Computational Mathematics, vol. 14. Springer, Berlin (1996)
[48] Hairer, E., Lubich, C., Schlichte, M.: Fast numerical solution of nonlinear Volterra convolution equations. SIAM J. Sci. Stat. Comput. 6(3), 532–541 (1985)
[49] Hairer, E., Nørsett, S.P., Wanner, G.: Solving ordinary differential equations. I. Springer Series in Computational Mathematics, vol. 8. Springer, Berlin (1993)
[50] Laliena, A.R., Sayas, F.J.: Theoretical aspects of the application of convolution quadrature to scattering of acoustic waves. Numer. Math. 112(4), 637–678 (2009)
[51] Lubich, C.: Convolution quadrature and discretized operational calculus. I. Numer. Math. 52(2), 129–145 (1988)
[52] Lubich, C.: Convolution quadrature and discretized operational calculus. II. Numer. Math. 52(4), 413–425 (1988)
[53] Lubich, C.: On the multistep time discretization of linear initial-boundary value problems and their boundary integral equations. Numer. Math. 67, 365–389 (1994)
[54] Lubich, C.: Convolution quadrature revisited. BIT Num. Math. 44(3), 503–514 (2004)
[55] Lubich, C., Schneider, R.: Time discretization of parabolic boundary integral equations. Numer. Math. 63, 455–481 (1992)
[56] Mansur, W.J.: A time-stepping technique to solve wave propagation problems using the boundary element method. PhD Thesis, University of Southampton (1983)
[57] Mansur, W.J., Carrer, J.A.M., Siqueira, E.F.N.: Time discontinuous linear traction approximation in time-domain BEM scalar wave propagation. Int. J. Numer. Methods Engrg. 42(4), 667–683 (1998)
[58] Messner, M., Schanz, M.: An accelerated symmetric time-domain boundary element formulation for elasticity. Eng. Anal. Bound Elem. 34(11), 944–955 (2010)
[59] Messner, M., Messner, M., Rammerstorfer, F., Urthaler, P.: Hyperbolic and elliptic numerical analysis BEM library (HyENA) (2010), `http://www.mech.tugraz.at/HyENA` (Online; accessed January 22, 2010)
[60] Monk, P.: Finite element methods for Maxwell's equations. Numerical Mathematics and Scientific Computation. Oxford University Press, New York (2003)
[61] Morse, P.M., Ingard, K.U.: Theoretical Acoustics. Princeton University Press (1986)
[62] Nardini, D., Brebbia, C.A.: A new approach to free vibration analysis using boundary elements. In: Brebbia, C.A. (ed.) Boundary Element Methods, pp. 312–326. Springer, Berlin (1982)
[63] Otani, Y., Takahashi, T., Nishimura, N.: A fast boundary integral equation method for elastodynamics in time domain and its parallelisation. In: Schanz, M., Steinbach, O. (eds.) Boundary Element Analysis: Mathematical Aspects and Applications. LNACM, vol. 29, pp. 161–185. Springer, Heidelberg (2007)
[64] Partridge, P.W., Brebbia, C.A., Wrobel, L.C.: The Dual Reciprocity Boundary Element Method. Computational Mechanics Publication, Southampton (1992)
[65] Peirce, A., Siebrits, E.: Stability analysis and design of time-stepping schemes for general elastodynamic boundary element models. Int. J. Numer. Methods Engrg. 40(2), 319–342 (1997)

[66] Pujols, A.: Time dependent integral method for Maxwell equations. In: Mathematical and Numerical Aspects of Wave Propagation Phenomena (Strasbourg, 1991), pp. 118–126. SIAM, Philadelphia (1991)
[67] Rizos, D.C., Karabalis, D.L.: An advanced direct time domain BEM formulation for general 3-D elastodynamic problems. Comput. Mech. 15, 249–269 (1994)
[68] Rokhlin, V.: Rapid solution of integral equations of classical potential theory. J. Comput. Phys. 60(2), 187–207 (1985)
[69] Rokhlin, V.: Rapid solution of integral equations of scattering theory in two dimensions. J. Comput. Phys. 86(2), 414–439 (1990)
[70] Rokhlin, V.: Diagonal forms of translation operators for the Helmholtz equation in three dimensions. Appl. Comput. Harmon Anal. 1(1), 82–93 (1993)
[71] Schanz, M.: Application of 3-d Boundary Element formulation to wave propagation in poroelastic solids. Eng. Anal. Bound Elem. 25(4-5), 363–376 (2001)
[72] Schanz, M.: Wave Propagation in Viscoelastic and Poroelastic Continua: A Boundary Element Approach. LNAM, vol. 2. Springer, Heidelberg (2001)
[73] Schanz, M., Antes, H.: Application of 'operational quadrature methods' in time domain boundary element methods. Meccanica 32(3), 179–186 (1997)
[74] Schanz, M., Antes, H.: A new visco- and elastodynamic time domain boundary element formulation. Comput. Mech. 20(5), 452–459 (1997)
[75] Schwab, C., Wendland, W.L.: On numerical cubatures of singular surface integrals in boundary element methods. Numer. Math. 62(3), 343–369 (1992)
[76] Shanker, B., Ergin, A.A., Aygün, K., Michielssen, E.: Analysis of transient electromagnetic scattering from closed surfaces using a combined field integral equation. IEEE Trans. Antenn. Propag. 48(7), 1064–1074 (2000)
[77] Shanker, B., Ergin, A.A., Lu, M.Y., Michielssen, E.: Fast analysis of transient electromagnetic scattering phenomena using the multilevel plane wave time domain algorithm. IEEE Trans. Antenn. Propag. 51, 628–641 (2003)
[78] Stein, E., de Borst, R., Hughes, T.J.R. (eds.): Encyclopedia of computational mechanics, vol. 1. John Wiley & Sons Ltd., Chichester (2004)
[79] Steinbach, O.: Numerical Approximation Methods for Elliptic Boundary Value Problems. Finite and Boundary Elements. Springer, New York (2008)
[80] Takahashi, T., Nishimura, N., Kobayashi, S.: A fast BIEM for three-dimensional elastodynamics in time domain. Eng. Anal. Bound Elem. 28, 165–180 (2004); erratum in EABEM 28, 165–180 (2004)
[81] Terrasse, I.: Résolution mathmatique et numérique des équations de Maxwell instationnaires par une méthode de potentiels retardés. PhD Thesis, Ecole Polytechnique (1993)
[82] Trefethen, L.N.: Finite difference and spectral methods for ordinary and partial differential equations (1996), Unpublished text available at
`http://www.comlab.ox.ac.uk/nick.trefethen/pdetext.html`
[83] Wang, X., Wildman, R.A., Weile, D.S., Monk, P.: A finite difference delay modeling approach to the discretization of the time domain integral equations of electromagnetics. IEEE Trans. Antenn. Propag. 56, 2442–2452 (2008)
[84] Wheeler, L.T., Sternberg, E.: Some theorems in classical elastodynamics. Arch. Rational Mech. Anal. 31, 51–90 (1968)
[85] Wildman, R.A., Pisharody, G., Weile, D.S., Shanker, B., Michielssen, E.: An accurate scheme for the solution of the time-domain integral equations of electromagnetics using higher order vector bases and bandlimited extrapolation. IEEE Trans. Antenn. Propag. 52, 2973–2984 (2004)

[86] Wilmanski, K.: A thermodynamic model of compressible porous materials with the balance equation of porosity. Transp. Porous Media 32(1), 21–47 (1998)
[87] Yu, G., Mansur, W.J., Carrer, J.A.M., Gong, L.: Time weighting in time domain BEM. Eng. Anal. Bound Elem. 22(3), 175–181 (1998)
[88] Yu, G., Mansur, W.J., Carrer, J.A.M., Gong, L.: Stability of Galerkin and Collocation time domain boundary element methods as applied to the scalar wave equation. Comput. & Structures 74(4), 495–506 (2000)
[89] Zhang, C.: Transient elastodynamic antiplane crack analysis in anisotropic solids. Internat. J. Solids Structures 37(42), 6107–6130 (2000)

Fast Nyström Methods for Parabolic Boundary Integral Equations

Johannes Tausch

Abstract. Time dependence in parabolic boundary integral operators appears in form of an integral over the previous time evolution of the problem. The kernels are singular only at the current time and get increasingly smooth for contributions that are further back in time. The thermal layer potentials can be regarded as generalized Abel operators where the kernel is a parameter dependent surface integral operator. This special form implies that discretization methods and fast evaluation methods must be significantly changed from the familiar elliptic case. After a brief review of recent developments in the area we discuss the different options to discretize Abel integral operators in time. These methods are combined with standard surface quadrature rules to obtain a Nyström method for parabolic integral equations. The method is explicit and we will show how a version of the fast multipole method in space and time can be used to evaluate the time stepping scheme efficiently.

1 Introduction

The solution of parabolic problems by boundary integral techniques is a well known alternative to the finite element or finite difference method and has a long history, beginning in the 1960's [31, 33]. However, the application of integral equation methods to realistic, three dimensional problems was hampered by the high computational expense of evaluating parabolic boundary integral operators. This stems from fact that these operators involve integrals over time in addition to integrals over the boundary surface. Furthermore, the computation of the influence matrix involves integration of singular or nearly singular integrals on the boundary surface and time, adding to the overall computational cost.

Johannes Tausch
Department of Mathematics, Southern Methodist University, Dallas, TX, 75275, USA
e-mail: tausch@smu.edu

U. Langer et al. (Eds.): Fast Boundary Element Methods, LNACM 63, pp. 185–219.
springerlink.com

Because of this computational burden, integral equation methods were performed either in Laplace domain, or were applied to the elliptic equation that arises after time discretization of the parabolic PDE. True boundary element methods that evaluate the time convolution numerically have also been considered by several authors, for instance [11, 18, 28], but are typically limited to two dimensional problems, or fairly coarse discretizations.

The thermal single layer operator is coercive in an appropriate anisotropic Sobolev space [1, 7]. Likewise, the thermal double layer operator is compact in the proper setting [7, 22]. This result is the background for the analysis of the Galerkin method in both space and time. Spline collocation methods for two dimensional domains where Fourier series techniques can be used have been discussed as well, see [21, 9]. Another discretization approach is the convolution quadrature method for the time discretization [27, 34]. This method is combined with a Galerkin or collocation method for the space discretization of the Laplace transformed integral operators. All the above methods involve the computation of multi-dimensional and possibly weakly singular influence coefficients. The different discretization options for parabolic integral equation methods and their theoretical foundations of are surveyed in [8].

The focus here is on Nyström discretizations. The method is based on the observation that thermal layer potentials can be viewed as generalized Abel integral operators with smooth operator-valued kernels. The quadrature rule in time is a desingularized version of the trapezoidal rule. The time discretization results in a series of spatial integral operators with kernel, which can be treated with standard surface quadrature rules. The resulting scheme is explicit in time, and does not require the computation of an influence matrix. The convergence analysis draws heavily on the compactness of the layer potentials in the space of continuous functions. Thus the arguments will, of course, break down if the the surface is not smooth. For the Laplace equation it is possible to show stability and convergence rates of the Nyström method on non-smooth domains [32], although it is not clear yet whether similar results can be obtained for the heat equation as well.

Since integral operators are non-local, discretizations lead to dense matrices and therefore fast methods are important to handle large scale problems. This is well known for elliptic equations, and is true even more so for parabolic equations. One can distinguish three approaches to obtain efficient representations of integral operators: Multiscale (wavelet) discretizations, fast Fourier methods and clustering techniques.

Wavelets lead to asymptotically optimal algorithms in very general settings, we refer to the survey [10]. Recently, they have attracted considerable interest for solving parabolic PDEs because of their good scaling properties in high dimensions [30]. On the other hand, it appears that very little has been done in the context of parabolic boundary integral equations. The author is only aware of the preprint [3] that derives some optimal convergence results.

Fourier techniques suggest themselves because of the convolutional nature of the heat kernel. The underlying principle is that convolutions turn to multiplications in Fourier domain. The first paper in this direction is [15], which considers expanding

the Green's function for the heat equation a bounded domain by a Fourier series. In the more natural setting of an unbounded domain the kernel appears as a continuous Fourier transform which requires special care to obtain discrete spectral approximations [14]. An application of this approach to evaluate thermal potentials is reported in [24].

Clustering techniques, which include the fast multipole method, H-matrices, and adaptive cross approximations, have proved to be extremely successful to solve elliptic problems with complicated geometries.

The fast Gauss transform [16] can be seen as a precursor of clustering methods for parabolic integral equations, because the heat kernel with frozen time is a Gaussian in space. In [35] this algorithm is applied to handle the elliptic problem that arises after time discretization of the heat equation. The original version of the fast Gauss transform is based on Hermite expansions of the heat kernel. Since the spatial variables of the kernel separate, the translation operator appear in tensor product form, which can be exploited to reduce the computational cost associated with translation operators [36]. Recently, more efficient approximations have been considered, in particular exponential expansions which result in diagonal translation operators [17] and Chebyshev expansions [41], which allow global approximations of the Gaussian.

We will concentrate on space-time clustering methods for discretizations of thermal layer potentials, which was first introduced in [38]. The algorithm relies on a hierarchic subdivision of space and time and uses a truncated Chebyshev expansion of the heat kernel to evaluate interactions of well separated spatio-temporal clusters efficiently. Here we will present the method together with some background material on the discretization and fast evaluation of Abel integral operators and on the approximation theory of the heat kernel. We will also include some new unpublished developments including results obtained with an improved implementation of our method.

2 Heat Potentials as Abel Integral Operators

Green's formula relates the Dirichlet and Neumann data on the boundary surface S. For the heat equation $u_t = \Delta u$ with homogeneous initial conditions it can be stated as

$$\pm\frac{1}{2}u(x,t) = \mathscr{K}u(x,t) - \mathscr{V}\frac{\partial u}{\partial n}(x,t), \quad x \in S,\ t > 0. \tag{1}$$

Here, the plus sign applies for an exterior and the minus sign for an interior problem. The single- and double layer potentials are given by

$$\mathscr{V}g(x,t) = \int_0^t \int_S G(x-y,t-\tau)g(y,\tau)\,ds(y)d\tau,$$

$$\mathscr{K}g(x,t) = \int_0^t \int_S \frac{\partial}{\partial n_y} G(x-y,t-\tau) g(y,\tau)\, ds(y) d\tau,$$

respectively. The Green's function of the heat equation in d spatial dimensions is

$$G(r,\delta) = \frac{1}{(4\pi\delta)^{\frac{d}{2}}} \exp\left(-\frac{|r|^2}{4\delta}\right).$$

Green's formula will include additional volume integral operators if nontrivial initial conditions and source terms are present. Moreover, many problems of physical interest deal with geometries that evolve in time, in which case the normal velocity of the surface must be added to the normal derivative of the solution, see, e.g. [4]. In principle, it is possible to extend the methodology discussed below in these more general settings. However, in the interest of conciseness, we will keep the focus on the numerical solution of problems that are governed by (1).

For $\delta > 0$, the Green's function is a Gaussian in space that becomes increasingly peaked as δ gets smaller. In the limit as $\delta \to 0$, it converges to the delta function. This follows from the well-known Poisson-Weierstrass integral, which states that

$$\lim_{\delta \to 0} \int_{\mathbb{R}^d} G(x-y,\delta)\phi(y) dy = \phi(x).$$

When the Green's formula is applied to a problem in three dimensions, the layer potentials involve integrals over two dimensional manifolds. To apply the the Poisson-Weierstrass integral in this case one must factor $(4\pi\delta)^{-\frac{1}{2}}$ out to obtain the two-dimensional Green's function. This motivates us to define the time-dependent surface integral operators

$$[V(\delta)\phi](x) = \frac{1}{4\pi\delta} \int_S \exp\left(-\frac{|x-y|^2}{4\delta}\right) \phi(y)\, ds(y), \tag{2}$$

$$[K(\delta)\phi](x) = \frac{1}{4\pi\delta} \int_S \frac{\partial}{\partial n_y} \exp\left(-\frac{|x-y|^2}{4\delta}\right) \phi(y)\, ds(y), \tag{3}$$

and thus the single and double layer potentials appear in the form

$$\mathscr{V}g(t) = \frac{1}{\sqrt{4\pi}} \int_0^t \frac{1}{\sqrt{t-\tau}} V(t-\tau) g(\tau)\, d\tau, \tag{4}$$

$$\mathscr{K}g(t) = \frac{1}{\sqrt{4\pi}} \int_0^t \frac{1}{\sqrt{t-\tau}} K(t-\tau) g(\tau)\, d\tau. \tag{5}$$

This representation clearly exposes the $(t-\tau)^{-\frac{1}{2}}$- singularity because $V(t-\tau)$ and $K(t-\tau)$ can be regarded as smooth operator-valued functions on the triangle

$$\Delta_T = \{(t,\tau) : 0 \le \tau \le t \le T\},$$

where T is the last time of interest. This observation is made more precise the following version of the Poisson-Weierstrass integral formula. The proof can be found in [39].

Theorem 1. *If S is smooth and $\phi \in C^{2p}(S)$, then the functions $V\phi$ and $K\phi$ are smooth functions in $S\times(0,\infty)$. Furthermore, the derivatives $\partial_\delta^m V\phi$ and $\partial_\delta^m K\phi$ have continuous extensions to $S\times[0,\infty)$ when $m \le p$. For $x \in S$ and $q \le p$ the expansions*

$$\begin{aligned}[V(\delta)\phi](x) &= \phi(x) + \delta v_1(x) + \cdots + \delta^{q-1} v_{q-1}(x) + \delta^q \tilde{v}_q(x,\delta)\\ [K(\delta)\phi](x) &= H(x)\phi(x) + \delta w_1(x) + \cdots + \delta^{q-1} w_{q-1}(x) + \delta^q \tilde{w}_q(x,\delta)\end{aligned}$$

hold, where $H(x)$ is the mean curvature of S, $v_m, w_m \in C^{2(p-m)}(S)$ and $\tilde{v}_q, \tilde{w}_q \in C^{2(p-q)}(S\times[0,T])$.

Here and in the following we write $g(t) := g(\cdot,t)$ to denote the function of the spatial variable with frozen time variable. The representation (4) and (5) shows that the thermal layer potentials may be regarded as generalized Abel integral operators time where kernels are smooth layer potentials. This view is helpful for their discretization and the design of fast methods for their evaluation.

3 Time Dependent Integral Operators

A generalized Abel integral operator has the form

$$Kg(t) = \int_0^t \frac{k(t,\tau)}{\sqrt{t-\tau}}\, g(\tau)\, d\tau \tag{6}$$

where the kernel $k(\cdot,\cdot)$ is a smooth function on the triangle Δ_T and $k(t,t) \ge k_0 > 0$.

We call this operator causal because the potential $Kg(t)$ at time t depends only on the function $g(\tau)$ for times $\tau \le t$. Abel integral operators arise in the context of singular Volterra integral equations

$$\lambda g(t) + Kg(t) = f(t), \quad t \in [0,T]. \tag{7}$$

If $\lambda \neq 0$ the equation is of the second kind, otherwise of the first kind.

We have seen that integral equations of the heat equation are also of this form, where the kernel in (6) is a time-dependent boundary integral operator. Many of the ideas to treat the time dependence in parabolic integral equations can be better exposed by considering operators that only depend on time, which is what we will do in the following two sections.

The remainder of this section will briefly review the various options of discretizing (6). It is not our intention to give a complete account of the vast literature in this field as it can be found, e.g., in the monographs [25, 5]. Instead, we will focus our attention on how these methods can be combined with the fast evaluation methods introduced in section 4.

While Abel integral operators are causal, discretization methods may or may not preserve this property. In the discrete case, causality means that the operator is replaced by a lower triangular matrix and solving (7) amounts to a simple forward substitution.

In the case of equations in time the computational cost of nontrivial super diagonals may not be significant. On the other hand, the complexity of the analogous scheme for a parabolic integral equation will be significantly increased, therefore we will look for schemes that preserve causality in order to apply them to parabolic equations.

3.1 Projection Methods

In a projection method the solution of the integral equation is approximated by a function g_h selected from a finite dimensional function space S_h. Typically, S_h is a piecewise polynomial spline space with certain regularity conditions.

In the Galerkin method the approximation is the function g_h whose residual is orthogonal to the space S_h. This is equivalent to

$$\int_0^T \phi_h(t)\big(\lambda g_h(t) + Kg_h(t)\big)\,dt = \int_0^T \phi_h(t) f(t)\,dt,$$

for all $\phi_h \in S_h$. A natural choice for S_h is a spline space subject to the partition

$$P_h = \{0 = t_0 < \tau_1 < \tau_2 < \cdots < \tau_N = T\}.$$

A set of basis function is denoted by χ_j, $0 \le j \le N$. The discretized integral operator is a matrix with coefficients

$$K^g_{i,j} = \int_0^T \int_0^t \frac{k(t,\tau)}{\sqrt{t-\tau}} \chi_i(t)\chi_j(\tau)\,d\tau dt.$$

It is easy to see that in the case of piecewise linear splines this matrix is a lower Hessenberg matrix, i.e., lower triangular with an additional non-zero super-diagonal. If higher order splines are considered, more non-zero diagonals will appear. Causality is preserved only with piecewise constant elements.

A different way to seek an approximate $g_h \in S_h$ is the collocation method. This involves a set of nodes X_h of cardinality $\dim S_h = N+1$ which is selected such that the interpolation problem

$$g_h(t_i) = g_i, \quad 0 \le i \le N,$$

has a unique solution $g_h \in S_h$ for all $g_i \in \mathbb{R}$. The collocation discretization of (7) is

$$\lambda g_h(t_i) + K g_h(t_i) = f(t_i), \quad t_i \in X_h.$$

If g_h is represented by the basis functions χ_j of S_h, then the coefficients of discretized operator are

$$K^c_{i,j} = \int_0^{t_i} \frac{k(t_i,\tau)}{\sqrt{t_i - \tau}} \chi_j(\tau)\, d\tau$$

In the case of piecewise linears the node points are $t_i = \tau_i$ and the matrix K^c is lower triangular. However, higher order spaces will again generate non vanishing super diagonals.

Since Abel integral equations may be regarded as weakly singular Fredholm integral equations with the additional property that the kernel vanishes outside the triangle Δ_T, the standard convergence results apply. More on this can be found in the introductory texts to integral equations, e.g., [2, 5, 19, 23].

3.2 Product Integration Methods

Historically, product integration methods have received the most interest and have been reviewed in, e.g., [25]. They can be regarded as a special case of a Nyström method. That is, the integral operator in (7) is replaced by a quadrature rule, and the equation is enforced on the quadrature nodes. Since the integrand is singular at the right endpoint, some care must be taken to select a rule that handles the singularity with sufficient accuracy.

To derive such a quadrature rule the *kernel* is replaced by a piecewise polynomial interpolate and the singularity is integrated exactly. For example, a piecewise linear interpolant

$$k(t_n,\tau)g(\tau) \approx \begin{cases} \sum_j k(t_n,t_j)g(t_j)\chi_j(\tau), & \text{if } \tau \le t_n, \\ 0, & \text{otherwise,} \end{cases}$$

leads to the approximation

$$Kg(t_n) \approx \sum_{j=0}^{n} k(t_n,t_j) w_{n,j} g(t_j), \tag{8}$$

where $w_{n,j}$ are quadrature weights

$$w_{n,j} = \int_0^{t_n} \frac{1}{\sqrt{t_n - \tau}} \chi_j(\tau)\, d\tau,$$

which can be found in closed form by elementary means. Thus the discretization of the Abel integral operator is a lower triangular matrix K^p with coefficients

$$K^p_{n,j} = k(t_n, t_j) w_{n,j}.$$

The numerical analysis of product integration methods involve an estimate of the quadrature error and some stability argument. For integral equations of the second kind stability can be derived from a Gronwall lemma [19]. Stability for Abel integral equations of the first kind is considerably more subtle. The case where the kernel is replaced by a piecewise linear has quadratic convergence and been discussed by Eggermont [12]. Unfortunately, the order cannot be increased beyond three, as the schemes become unstable [25, 26].

3.3 Convolution Quadrature

The limitations of product or desingularized integration methods for first-kind equations can be overcome with the convolution quadrature, an idea introduced in the paper [26]. There it is shown that the Abel integral operator can be discretized in the form

$$K^{cq} g(t_n) = h_t^\alpha \sum_{m=0}^{n} \omega_{n-m} k(t_n, t_m) g(t_m), \tag{9}$$

where the quadrature weights ω_n are derived from a linear multistep method with generating polynomials $\rho(z) = a_0 + z a_1 + \cdots + z^p a_p$ and $\sigma(z) = b_0 + z b_1 + \cdots + z^p b_p$, with $a_p, b_p \neq 0$. The weights are the Maclaurin series coefficients of

$$\sum_{k=0}^{\infty} \omega_k z^k = \left(\frac{\sigma(1/z)}{\rho(1/z)} \right)^{\frac{1}{2}}.$$

The stability and consistency of this method is directly related to the properties of the underlying multistep method. Unlike product integration methods, it is possible to obtain stable schemes of arbitrary order.

3.4 Desingularized Quadrature

Another way to handle the singularity in the Abel operator is singularity subtraction. The regularized integral can then be treated with the trapezoidal rule. The derivation is quite simple

$$Kg(t) = \int_0^t \frac{1}{\sqrt{t-\tau}} \big(k(t,\tau) g(\tau) - k(t,t) g(t) \big)\, d\tau + 2\sqrt{t} k(t,t) g(t).$$

The new integrand vanishes at the right endpoint. In fact, if $g(t)$ and k are smooth the intgrand is $O(\sqrt{t-\tau})$ and the trapezoidal rule converges at rate $O(h_t^{3/2})$. Thus

$$\begin{aligned}\mathscr{K}_h g(t_n) &= h_t \sum_{m=0}^{n-1}{}' \frac{1}{\sqrt{t_n - t_m}} \big(k(t_n,t_m)g(t_m) - k(t_n,t_n)g(t_n)\big) + 2\sqrt{t_n}k(t_n,t_n)g(t_n) \\ &= h \sum_{m=0}^{n-1}{}' \frac{k(t_n,t_m)}{\sqrt{t_n - t_m}} g(t_m) + \hat{w}_n k(t_n,t_n)g(t_n), \end{aligned} \tag{10}$$

where

$$\hat{w}_n = h_t \sum_{m=0}^{n-1}{}' \frac{1}{\sqrt{t_n - t_m}} - 2\sqrt{t_n}.$$

Here, the prime at the summation sign indicates that the $m = 0$ term must be multiplied by the factor $1/2$. The advantage of the desingularized quadrature method over the product integration and convolution quadrature is that all except for the last term in (10) have the same quadrature weight. In (8) and (9) the weights depend on the row and column index. While this is not very significant for the direct solution of the discretized equation with forward substitution, it will play an important role when designing fast summation methods described below. Higher order methods can be obtained easily by subtracting more terms of the Taylor expansion of the kernel.

The arguments used in the analysis of desingularized quadrature methods is similar to the product quadrature. A form of the Gronwall lemma that is suitable to show stability for second-kind equations is given in [37]. As in the case of the product integration method, the schemes become unstable for higher orders when they are applied for first-kind equations . The maximal stable order is $O(h_t^{5/2})$, see [40].

4 The Fast Multipole Method in Time Domain

Discretizations of Abel integral operators lead to essentially lower triangular matrices with quadratic complexity in the number of unknowns. While for one-dimensional problems this may be still acceptable, the quadratic scaling will be prohibitive when parabolic problems in three space dimensions are considered. Therefore it is worthwhile to understand how to accelerate the evaluation of Abel integral operators, as these techniques can be easily extended to parabolic problems.

When the kernel is a convolution, several of the discussed discretization methods preserve this structure which suggests to use fast Fourier transforms for efficient numerics. However, a straight forward application of Fourier methods enables the fast application of the operator to a vector, but does not facilitate solving a lower triangular system by forward elimination. The latter can be accomplished by a hierarchic splitting of the matrix into smaller blocks, where local FFTs are employed.

An $O(N_t \log^2 N_t)$ scheme based on such ideas has been introduced in [20] to solve nonlinear Volterra equations. Here and in the following N_t denotes the number of time steps in the interval $[0,T]$.

Unfortunately, many interesting problems are not convolutional. For instance, this happens in parabolic problems when surfaces are time dependent. Therefore we focus on extending the fast multipole method for elliptic problems to parabolic problems.

Although the multipole expansion is specific to the Laplace kernel, it has become customary to refer to a fast algorithm that is based on a hierarchic decomposition of the problem domain and some form of kernel expansions as a fast multipole method, see, e.g., [42]. We will follow this slight misuse of terminology. A one-dimensional FMM that can be applied to very general operators was discussed in the afore mentioned paper. Instead of approximating the kernel in a truncated series, we will consider an interpolation approximation of the kernel. This has the advantage that only the kernel, and not its derivatives must be computed. In the context of elliptic problems, this approach is used in [13, 29].

In the following we will summarize the basic ideas in the fast multipole algorithm for fast evaluations of discretized Abel integral operators. A straight forward application of the FMM is not causal and hence not very useful in the context of Volterra or Abel equations. Therefore we introduce a causal version of the FMM in section 4.5 that enables fast forward substitutions.

4.1 Separation of Variables

The first idea is the separation of variables in the kernel of the integral operator. Since the kernel is singular on the diagonal $\tau = t$ this will succeed only locally, in a rectangular region $(t,\tau) \in I \times J$ where the intervals I and J are sufficiently separated. If this is the case, an approximation of the form

$$\frac{k(t,\tau)}{\sqrt{t-\tau}} \approx \sum_{i,j} k_{i,j} L_i(t) L_j(\tau) \tag{11}$$

can be achieved with few terms in the summation on the right hand side. An example is the truncated Taylor expansion of the kernel. Here the L_i's are monomials and the $k_{i,j}$'s are partial derivatives of the kernel at the centroid of $I \times J$. This may not be the optimal choice as the Taylor polynomials may converge slowly and derivatives are often difficult to compute. A more straight forward approximation is a two-variate polynomial interpolation. To this end, let I and J be intervals of same length 2δ with centers $\bar{t}$ and $\bar{\tau}$, respectively. We introduce local variables with the transform

$$t = \bar{t} + \delta t', \tau = \bar{\tau} + \delta \tau', \quad -1 \le t', \tau' \le 1.$$

and select interpolation nodes $\{\omega_0^p, \ldots, \omega_p^p\} \subset [-1,1]$. Then

$$\frac{k(t,\tau)}{\sqrt{t-\tau}} \approx \sum_{i,j=0}^{p} \frac{k(t_i,\tau_j)}{\sqrt{t_i-\tau_j}} L_i(t') L_j(\tau') \tag{12}$$

where

$$t_i = \bar{t} + \delta\omega_i^p, \quad \tau_i = \bar{\tau} + \delta\omega_i^p,$$

and L_i is a Lagrange polynomial

$$L_i(t') = \prod_{k \neq i} \frac{t' - \omega_k^p}{\omega_i^p - \omega_k^p}. \tag{13}$$

Because of their well-known suitability for interpolation, we let ω_k^p be the roots of the $(p+1)$-st Chebyshev polynomial

$$\omega_k^p = \cos\left(\frac{\pi}{2}\frac{2k+1}{p+1}\right). \tag{14}$$

The coefficients of the expansion (11) follow from the interpolation property

$$k_{i,j} = \frac{k(t_i,t_j)}{\sqrt{t_i - t_j}}, \quad 0 \leq i,j \leq p.$$

If the kernel is sufficiently smooth it is possible to show that the interpolation error can be bounded independently of δ provided that $|\bar{t} - \bar{\tau}| > r\delta$ for some fixed $r > 2$. This will motivate the subdivision scheme in Sect. 4.2.

4.2 Hierarchy of Intervals

The second idea of the Fast Multipole Method is to evaluate potentials using a hierarchical subdivision of the time interval $[0,T]$. The coarsest level is the interval itself, which is subdivided into two finer intervals of equal length. These intervals are divided into two equal subinterval each and the process is repeated until the finest intervals contain a small pre-determined number of time steps. The result is a tree of intervals. The coarsest level is level L, the finest is level zero. The l-th level consists of the intervals

$$I_k^l = \frac{T}{2^{L-l}}[k, k+1), \quad k \in \{0, \ldots, K_l\}.$$

where $K_l = 2^{L-l} - 1$. Each interval I_k^l above level zero has two children which are given by

$$\mathscr{K}_k^l = \{I_{2k}^{l-1}, I_{2k+1}^{l-1}\}.$$

The binary representation of an integer is

$$k = (\sigma_R \dots \sigma_1 \sigma_0)_2 = \sigma_R 2^R + \dots + 2\sigma_1 + \sigma_0$$

where $\sigma_i \in \{0,1\}$, $0 \le i < R$ and $\sigma_R = 1$. The level-l parent of interval I_k^0 is the interval $I_{k_l}^l$ where the binary representation of k_l is

$$k_l = (\sigma_R \dots \sigma_{l+1} \sigma_l)_2 = \sigma_R 2^{R-l} + \dots + 2\sigma_{l+1} + \sigma_l$$

The neighbors of I_k^l are the intervals in the same level that are near to the given interval including the interval itself. Since the kernel vanishes for $\tau > t$ it suffices to consider only intervals with a smaller or equal k-index. Here we define the interval to be a neighbor if it shares at least one endpoint, thus the set of neighbors is

$$\mathcal{N}(I_k^l) = \begin{cases} \{I_0^l\}, & \text{if } k = 0, \\ \{I_{k-1}^l, I_k^l\}, & \text{else.} \end{cases}$$

Related to the neighbors is the concept of the interaction list of an interval. It consists of intervals whose parents are neighbors but which are not neighbors themselves, i.e.,

$$\mathcal{I}(I_k^l) = \begin{cases} \emptyset, & \text{if } k \in \{0,1\}, \\ \{I_{k-2}^l\}, & \text{if } k \ge 2, \text{ even}, \\ \{I_{k-3}^l, I_{k-2}^l\}, & \text{if } k > 2, \text{ odd}. \end{cases}$$

Because of the singularity at $t = \tau$ approximation (11) of the kernel in the Abel integral operator is valid only if the source and evaluation intervals are sufficiently separated and holds for larger intervals if their separation is larger. The interaction lists provide a systematic way to split a time interval into well separated intervals of increasing size

$$\bigcup_{j=0}^{k-2} I_j^0 = \bigcup_{l=0}^{R-2} \bigcup_{J \in \mathcal{I}(I_{k_l}^l)} J.$$

The right hand side consists of the union of the interaction lists of all parents of I_k^0.

For the evaluation point $t_n \in I_k^0$, the sum in the desingularized quadrature rule (10) is written as

$$(\mathcal{K}_h g)(t_n) = \hat{w}_n k(t_n, t_n) g(t_n) + h_t \sum_{\tilde{t} \le t_m < t_n} \frac{k(t_n, t_m)}{\sqrt{t_n - t_m}} g(t_m) + \phi_{\mathrm{sm}}(t_n) \tag{15}$$

where $\tilde{t}$ is the left endpoint of interval I_{k-1}^l and ϕ_{sm} is the smooth potential given by

$$\phi_{\mathrm{sm}}(t_n) = h_t \sum_{l=0}^{R-2} \sum_{J \in \mathcal{I}(I_{k_l}^l)} {\sum_{t_m \in J}}' \frac{k(t_n, t_m)}{\sqrt{t_n - t_m}} g(t_m). \tag{16}$$

The first terms in (15) make up the local part. Since the finest level intervals contain a fixed number of quadrature points the cost for the evaluation of the local part is independent of the total number of time steps. If evaluated directly, the cost for the smooth potential dominates if n is large. The fast multipole method accelerates the computation of ϕ_{sm} by replacing the kernels in the smooth potential by expansion (11). The details are described in the following.

4.3 Translation Operators

4.3.1 Moment-to-Local Operator

We now consider the contribution of a certain interval J in the smooth potential evaluated in interval I, which is a parent of I_k^0 in the same level as J. If I and J are sufficiently separated then the kernel can be replaced by its interpolation (11), which results in a low-rank approximation of the operator. This follows from the calculation

$$\sum_{t_m\in J}{}' \frac{k(t_n,t_m)}{\sqrt{t_n-t_m}}g(t_m) \approx \sum_{i=0}^{p} k_{i,j}\left(\sum_{j=0}^{p}\sum_{t_m\in J}{}' L_j(t_m)g(t_m)\right)L_i(t_n), \quad t_n\in I.$$

Thus the potential due to interval J is approximated by a combination of the L_i's in interval I

$$h_t\sum_{t_m\in J}\frac{k(t_n,t_m)}{\sqrt{t_n-t_m}}g(t_m) \approx \sum_{i=0}^{p}\lambda_i(I)L_i(t_n), \quad t_n\in I,$$

where

$$\lambda_i(I) = \sum_{j=0}^{p} k_{i,j}\mu_j(J) \tag{17}$$

and

$$\mu_j(J) = h_t\sum_{t_m\in J}{}' L_j(t_m)g(t_m). \tag{18}$$

The λ_i's are the local expansion coefficients, which depend on the moments μ_j defined in (18) and the moment-to-local (MtL) transformation (17). If the intervals I and J contain sufficiently many points, then computing the potential via this process can be much more efficient than computing the potential directly. The fundamental principle behind the Fast Multipole Method is to compute the potentials of all interactions in the smooth potential in this manner.

In (16) J is in the interaction list of I and thus both intervals are in the same level and are separated by either one or two intervals. That is,

$$I = I_k^l \quad \text{and} \quad J = I_{k-d}^l, \quad d\in\{2,3\}.$$

In matrix notation, we write (17) in the form

$$\boldsymbol{\lambda}_k^l = MtL\,\boldsymbol{\mu}_{k-d}, \quad d \in \{2,3\}, \tag{19}$$

where $\boldsymbol{\mu}_{k-r}^l$ is a vector of moments in the interval I_{k-r}^l and $\boldsymbol{\lambda}_k^l$ is the vector of expansion coefficients for the interval I_k^l and MtL is a matrix with coefficients $k_{i,j}$. Of course, the matrix depends on the direction d, but our notations suppress this dependence, because it is implied by the input and output vectors.

4.3.2 Source-to-Moment and Local-to-Potential Operators

In matrix notation, the source-to-moment operation (18) is written as

$$\boldsymbol{\mu}_k^l = QtM\,\boldsymbol{g}_k^l,$$

where $\boldsymbol{\mu}_k^l$ is the vector of moments of interval I_k^l and $\boldsymbol{g}_k^l$ is the vector of nodal values of the function g in I_k^l.

Once the expansion coefficients for every parent of I_k^0 have been determined, the smooth potential is evaluated by the series expansion (17). We call this the local-to-potential translation and write it as

$$\boldsymbol{\Phi}_k^l = LtP\,\boldsymbol{\lambda}_k^l,$$

where $\boldsymbol{\Phi}_k^l$ is the vector of nodal values of the function ϕ_{sm} in I_k^l. The matrices QtM and LtP have coefficients $L_j(t_m)$ and are transposes of each other.

At first glance, one might consider computing all moments in all levels using QtM transformations. Since every time step contributes to a moment in any level, the complexity of computing all moments is order pNL.

Likewise, after all expansion coefficients in all levels have been computed, the total potential at a point can be obtained by adding the LtP transformations of the interval and all its parents where the point is located. This type of potential evaluation is also order pNL.

A great deal of the computations can be saved if the moments and expansion coefficients are computed in a systematic manner, exploiting the hierarchy of the intervals. Such a hierarchic scheme can reduce the complexity of the moment and potential evaluations to order pN. This is based on the observation that the moments in an interval only depend on the moments of the interval's children. Likewise, the expansion coefficients depend on the coefficients of the parent. This will be described below in more detail.

4.3.3 Moment-to-Moment Operator

The moments in the coarser levels are computed in an upward pass, where the moments of a given interval are computed from the moments of the children. Likewise, the expansion coefficients a computed in a downward pass, where the coefficients of a given interval are computed from the parent's coefficients.

The translation formulas are derived from a linear relationship between the local coordinates of the parent and its children. It is given by

$$\tau' = \frac{1}{2}\tau'' \pm \frac{1}{2}.$$

Here the plus sign is for the right and the minus sign for the left child of I_k^l. Since the local variables are affinely related, a polynomial in the parent's coordinates remains a polynomial of the same degree in the child's coordinates. Thus the Lagrange polynomials satisfy the addition theorem

$$L_i\left(\frac{1}{2}\tau'' \pm \frac{1}{2}\right) = \sum_{j=0}^{p} q_{i,j}^{\pm} L_j(\tau''), \tag{20}$$

where the coefficients follow from the interpolation property

$$q_{i,j}^{\pm} = L_i\left(\frac{1}{2}\omega_k^p \pm \frac{1}{2}\right).$$

We begin with the translation of the moments. Consider a moment in interval I_k^l in some level $l > 0$

$$\begin{aligned}\mu^i(I_k^l) &= h_t \sum_{t_m \in I_{2k}^{l-1}} L_i(t'_m) g(t_m) + h_t \sum_{t_m \in I_{2k+1}^{l-1}} L_i(t'_m) g(t_m) \\ &= h_t \sum_{t_m \in I_{2k}^{l-1}} L_i\left(\frac{1}{2}t''_m - \frac{1}{2}\right) g(t_m) + h_t \sum_{t_m \in I_{2k+1}^{l-1}} L_i\left(\frac{1}{2}t''_m + \frac{1}{2}\right) g(t_m)\end{aligned}$$

where I_{2k}^{l-1} and I_{2k+1}^{l-1} are the two children and t'_m and t''_m are local coordinates of t_m. From the addition theorem it follows that

$$\mu^i(I_k^l) = \sum_{j=0}^{p} q_{i,j}^{-} \mu^j(I_{2k}^{l-1}) + \sum_{j=0}^{p} q_{i,j}^{+} \mu^j(I_{2k+1}^{l-1}).$$

We also write the last relation in matrix-vector notation as

$$\boldsymbol{\mu}_k^l = MtM\boldsymbol{\mu}_{2k}^{l-1} + MtM\boldsymbol{\mu}_{2k+1}^{l-1}.$$

where MtM is the matrix with coefficients $q_{i,j}^{\pm}$. Our notations omit the dependence on the direction because it is implied by the input and output vectors.

4.3.4 Local-to-Local Operator

We turn to the translation of the local expansion coefficients. Suppose the polynomial $f_p(t)$ is given in terms of the Lagrange polynomials of I_k^l. That is,

$$f_p(t) = \sum_{i=0}^{p} \lambda^i(I_k^l) L_i(t'),$$

where t' is the local coordinate of I_k^l and $\lambda^i(I_k^l)$ is the function value of f_p at the i-th interpolation node of I_k^l. The same polynomial can also be expressed in terms of the Lagrange polynomials of I_k^l's children. For instance, the addition theorem gives for the left child

$$\begin{aligned} f_p(t) &= \sum_{i=0}^{p} \lambda^i(I_k^l) L_i\left(\frac{1}{2}t'' - \frac{1}{2}\right) \\ &= \sum_{i=0}^{p} \lambda^i(I_k^l) \sum_{j=0}^{p} q_{i,j}^{-} L_j(t'') \\ &= \sum_{j=0}^{p} \lambda^j(I_{2k}^{l-1}) L_j(t'') \end{aligned}$$

The new expansion coefficients are given by the local-to-local (LtL) translation

$$\lambda^j(I_{2k}^{l-1}) = \sum_{i=0}^{p} q_{i,j}^{-} \lambda^i(I_k^l).$$

The translation to the right child is completely analogous. In matrix vector notations we write

$$\boldsymbol{\lambda}_{\tilde{k}}^{l-1} = LtL\, \boldsymbol{\lambda}_k^l, \qquad \tilde{k} \in \{2k, 2k+1\},$$

where the LtL operators are the transposes of the MtM operators.

4.4 The Standard FMM

The standard FMM is an efficient scheme to compute the smooth potential using the splitting (16). It proceeds by computing all moments in all levels, then all expansion coefficients and finally the potentials by evaluating the expansion coefficients. The details are given in Algorithm 2.

To compute the discrete integral operator in (15) the local potential must be added in each time step. This version of the FMM can be regarded as the fast application of a vector g to a lower triangular matrix. In particular, the vector g must be known in all time steps *before* the potential can be computed at any time step. Thus this algorithm is useful only if the linear system is solved by an iterative procedure. Of course it is more natural to solve lower triangular systems by forward substitution, taking advantage of the causality of the Abel integral operator. This can be accomplished by rearranging the order in which moments and expansion coefficients are computed. We call the resulting method the causal FMM and describe it in the following section.

Algorithm 2. The Standard Fast Multipole Algorithm

% Moment Calculation.
for $k = 0$ to K_0 **do**
  $\boldsymbol{\mu}_k^0 = QtM\,\mathbf{g}_k^0$
end for

% Upward Pass.
for $l = 1$ to $L-2$ **do**
  for $k = 0$ to K_l **do**
    $\boldsymbol{\mu}_k^l = MtM\boldsymbol{\mu}_{2k}^{l-1} + MtM\boldsymbol{\mu}_{2k+1}^{l-1}$
  end for
end for

% Interaction Phase.
for $l = 0$ to $L-2$ **do**
  for $k = 2$ to K_l **do**
    if k even **then**
      $\boldsymbol{\lambda}_k^l = MtL\,\boldsymbol{\mu}_{k-2}^l$
    else
      $\boldsymbol{\lambda}_k^l = MtL\,\boldsymbol{\mu}_{k-2}^l + MtL\,\boldsymbol{\mu}_{k-3}^l$
    end if
  end for
end for

% Downward Pass.
for $l = L-2$ down to 1 **do**
  for $k = 0$ to K_l **do**
    $\boldsymbol{\lambda}_{2k}^{l-1} = \boldsymbol{\lambda}_{2k}^{l-1} + LtL\boldsymbol{\lambda}_k^l$
    $\boldsymbol{\lambda}_{2k+1}^{l-1} = \boldsymbol{\lambda}_{2k+1}^{l-1} + LtL\boldsymbol{\lambda}_k^l$
  end for
end for

% Potential evaluation.
for $k = 0$ to K_0 **do**
  $\Phi_k^0 = LtP\,\boldsymbol{\lambda}_k^0$
end for

4.5 The Causal FMM

To enable the fast computation of g_n from the g_m, $m < n$, the order in which moments, expansion coefficients and potentials are computed must be changed. In particular, the outermost loop is over all time steps, and moments and expansion coefficients are computed as soon as they become available as time progresses.

To describe how this process works we introduce further notations

R: Index of the highest digit in the binary representation of k.
S: Index of the lowest non-zero digit in the binary representation of k.

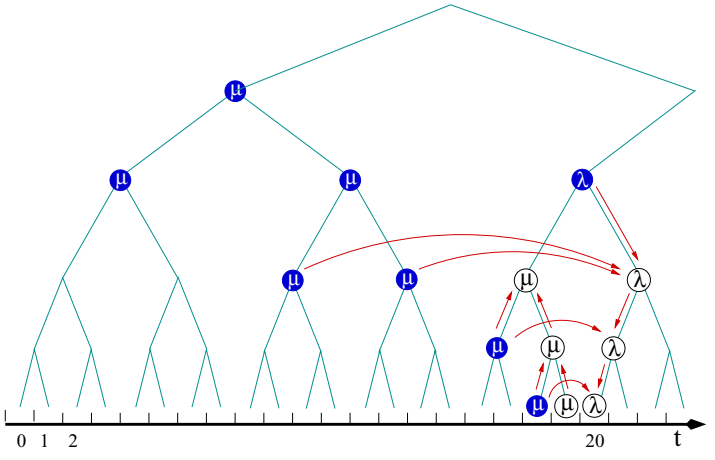

Fig. 1 Operations for the 20th interval. Quantities on white ground are computed in this time step. Quantities on dark ground have been computed in earlier time steps

For example, the binary representation of the number 20 is $(10100)_2$ which implies that $R = 4$ and $S = 2$.

Suppose now that the forward substitution process has moved to interval I_k^0. Hence $\mathbf{g}_{\hat{k}}^0$, where $\hat{k} = k - 1$, has been computed and the moment $\boldsymbol{\mu}_{\hat{k}}^0$ can be determined by a QtM transform. Furthermore, there may be moments in the parents of $I_{\hat{k}}^0$ that also become available at this time step. These are exactly the levels where the binary representation changes bits as $\hat{k}$ is increased to k. This happens exactly in levels 1 to S. Consider, for instance, the case $k = 20$, which is illustrated in Fig. 1. The moment $\boldsymbol{\mu}_{19}^0$ is new and can be computed by a QtM. Since $\hat{k} = 19 = (10011)_2$ and $k = 20 = (10100)_2$ the bits in levels 0, 1 and 2 have change. Therefore the moments in the coarser levels $\boldsymbol{\mu}_9^1$ and $\boldsymbol{\mu}_4^2$ are are also new and can be computed by MtMs. Note that the moments that are necessary to do that have been computed in earlier time steps. The parent moments in levels above S will be computed in a later time step.

The expansion coefficients are always computed for all parents of the current interval. Thus the coefficients above level S are known as the time stepping moves into interval I_k^0, and we only need to compute the coefficients $\boldsymbol{\lambda}_k^0$ to $\boldsymbol{\lambda}_{ks}^S$ by MtL transformations. Since MtLs always go back in time, the moments that are necessary to do that are already known. Finally, the contributions of the parents to the children is added in levels S down to 0. In the previous example, we compute $\boldsymbol{\lambda}_5^2$,$\boldsymbol{\lambda}_{10}^1$ and $\boldsymbol{\lambda}_{20}^0$. The coefficient $\boldsymbol{\lambda}_2^3$ was already computed when k was 16. The coefficients in the higher levels are all zero because the interaction lists are empty.

Algorithm 3. The Causal Fast Multipole Algorithm

for $k = 0$ to K_0 **do**
  Compute S and R in the binary representation of k.
  Set $\hat{k} = k - 1$.

  % Moment Calculation.
  $\boldsymbol{\mu}_{\hat{k}}^0 = QtM\,\mathbf{g}_{\hat{k}}^0$

  % Upward Pass.
  for $l = 1$ to S **do**
    $\boldsymbol{\mu}_{\hat{k}_l}^l = MtM\,\boldsymbol{\mu}_{2\hat{k}_l}^{l-1} + MtM\,\boldsymbol{\mu}_{2\hat{k}_l+1}^{l-1}$
  end for

  % Interaction Phase.
  $\boldsymbol{\lambda}_{k_S}^S = MtL\,\boldsymbol{\mu}_{k_S-2}^S + MtL\,\boldsymbol{\mu}_{k_S-3}^S$
  for $l = S-1$ down to 0 **do**
    $\boldsymbol{\lambda}_{k_l}^l = MtL\,\boldsymbol{\mu}_{k_l-2}^l$
  end for

  % Downward Pass.
  for $l = S$ down to 0 **do**
    $\boldsymbol{\lambda}_{k_l}^l = \boldsymbol{\lambda}_{k_l}^l + LtL\,\boldsymbol{\lambda}_{k_{l+1}}^{l+1}$
  end for

  % Potential evaluation.
  $\Phi_k^0 = LtP\,\boldsymbol{\lambda}_k^0$

  % Compute $\mathbf{g}_k^0$ using the smooth potential Φ_k^0 and the local part.
end for

Since only the order is changed in which quantities are evaluated, the causal FMM has the same complexity as the standard FMM. Unlike the standard FMM, it is not necessary to store all moments and expansion coefficients in all levels. In fact, it is easy to see that in Algorithm 3 we only need to keep three moment vectors and one coefficient vector per level. It is possible to rearrange computations such that only two moments per level must be stored. This was described in [38].

5 The Parabolic FMM

5.1 Discretization of Thermal Layer Potentials

For the time discretization we take the view that thermal layer potentials are generalized Abel integral operators with operator-valued kernels. Hence the desingularized quadrature rule (10) applied to the thermal single layer operator leads to

$$\mathscr{V}_{h_t} g(t_n) := \frac{h_t}{\sqrt{4\pi}} \sum_{m=0}^{n-1}{}' \frac{1}{\sqrt{t_n - t_m}} V(t_n - t_m) g(t_m) \;+\; \hat{w}_n g(t_n). \tag{21}$$

The surface integral operators in the above quadrature rule have smooth kernels, thus the Nyström method can also be used for the spatial discretization. Quadrature rules for smooth surface integrals are usually constructed in a triangulation of the parameter space and lifted on the surface. Details of the derivation with error estimates can be found in ATKINSON [2] and CHIEN [6]. We write the rule as

$$\int_S f(x)\,ds(x) \approx \sum_{l=1}^{N_S} f(x_l) w_l. \tag{22}$$

where $x_l \in S$ are the nodes and w_l are the quadrature weights.

All kernels of the surface integral operators in (21) are smooth, but for values of the summation index m near n they become very peaked. To resolve this behavior the mesh width of the surface triangulation must be decreased as the temporal time step is decreased. The relationship between h_t and h_s should be

$$\frac{h_s}{\sqrt{h_t}} \to 0 \quad \text{as} \quad h_t \to 0, \tag{23}$$

to preserve the asymptotic convergence rate of the time discretization scheme, see [39].

Combining (21) and (22) leads to the quadrature rules

$$\mathscr{V}_{h_s,h_t} g(x_k,t_n) := h_t \sum_{m=0}^{n-1}{}' \sum_{l=1}^{N_s} G(x_k - x_l, t_n - t_m) w_l g(x_l,t_m) + \hat{w}_n g(x_k,t_n),$$

$$\mathscr{K}_{h_s,h_t} g(x_k,t_n) := h_t \sum_{m=0}^{n-1}{}' \sum_{l=1}^{N_s} \frac{\partial}{\partial n_l} G(x_k - x_l, t_n - t_m) w_l g(x_l,t_m) + \hat{w}_n H(x_k) g(x_k,t_n).$$

The Nyström discretization of the Green's formula replaces the thermal layer potentials by their discrete counterparts. This results in an *explicit* scheme for the unknown boundary data in every time step.

For the Neumann problem on a smooth surface Green's formula is an integral equation of the second kind with compact operator. In this setting it is possible to prove stability and convergence at same rate as the temporal discretization provided that assumption (23) holds [39]. Of course, it is hard to extend these results to first-kind equations and non smooth geometries.

Because of its simplicity, the Nyström discretization is an effective method to solve the heat equation. However, the refinement of the mesh that can be used is severely limited by the $O(N_t^2 N_s^2)$ complexity of the direct evaluation of $\mathscr{V}_{h_s,h_t}$ and $\mathscr{K}_{h_s,h_t}$. Fortunately, the causal FMM can be easily modified to rapidly evaluate the discrete thermal potentials. We call this extension parabolic FMM and describe the details in the following section.

5.2 Approximation Theory for the Heat Kernel

We have seen that integral operators can be evaluated efficiently if the kernel is approximated by a truncated series expansion to achieve separation of variables. By definition, Abel integral operators are singular for $t = \tau$. Therefore the approximation can be accomplished only locally, for rectangular regions in the (τ, t) plane that are sufficiently separated from the diagonal.

In addition to the two temporal variables, the heat kernel depends on six spatial variables. When $t > \tau$, the heat kernel is smooth, which somewhat simplifies the approximation scheme in space. However, when τ is near t the heat kernel is peaked near $x = y$ and decays rapidly as x and y separate. In this range space must be subdivided into small clusters, but only nearby cluster interactions must be considered. When τ and t are farther separated, the heat kernel is more smooth, but decays more slowly. In this range space is subdivided into larger clusters. Since the clusters are bigger, it suffices again to consider only neighboring cluster interactions.

Before we discuss the subdivision scheme of space and time in more detail, we consider different possibilities to approximate the heat kernel. To that end, let ν be a cube in $\mathbb{R}^3$ with center $\bar{x}$ side length $2h_x$ and $\tilde{\nu}$ be a cube with same side length and center $\tilde{x}$, furthermore let I and $\tilde{I}$ be non overlapping intervals of $\mathbb{R}$ with length $2h_t$ and centers $\bar{t}$ and $\tilde{t}$, respectively. For $x \in \nu$, $y \in \tilde{\nu}$, $t \in I$ and $\tau \in \tilde{I}$ we introduce local variables with the transformation

$$\begin{aligned} x &= \bar{x} + x' h_x,\ y = \tilde{x} + y' h_x, && -1 \le x'_\sigma, y'_\sigma \le 1,\ \sigma \in \{1,2,3\} \\ t &= \bar{t} + t' h_t,\ \tau = \tilde{t} + \tau' h_t, && -1 \le t', \tau' \le 1. \end{aligned}$$

In the local variables, the heat kernel is

$$\begin{aligned} G_{\mathrm{loc}}(x', y', t', \tau') &= \frac{1}{[4\pi(t-\tau)]^{\frac{3}{2}}} \exp\left(-\frac{|x-y|^2}{4(t-\tau)}\right) \\ &= \frac{1}{[(4\pi h_t)(d' + t' - \tau')]^{\frac{3}{2}}} \exp\left(-\rho \frac{|r' + x' - y'|^2}{d + t' - \tau'}\right). \end{aligned} \tag{24}$$

The constants $d' > 0$, $r' \in \mathbb{R}^3$ and $\rho > 0$ are given by

$$d' = (\bar{t} - \bar{\tau})/h_t, \tag{25}$$

$$r' = (\bar{x} - \bar{y})/h_x, \tag{26}$$

$$\rho = \frac{h_x^2}{4h_t}. \tag{27}$$

The fast evaluation of potentials is based on separation of variables of the heat kernel in (24). Unfortunately, the multivariate interpolation approximation results in a very large number of terms: For order p polynomials in time and order q polynomials in space the multivariate version of (11) has $(p+1)^2(q+1)^6$ terms, which is prohibitively large even for moderate values of p and q. We will show below that a

more efficient approximation can be obtained if the spatial variables are expanded in Chebyshev instead of Lagrange polynomials.

For the temporal variables it is still more efficient to use the Lagrange form. Although this leads to more terms, the benefit is that the tensor product form of the heat kernel is preserved. Thus we begin by approximating (24) in time as follows

$$G_{\mathrm{loc}}(x',y',t,\tau') \approx \frac{1}{(4\pi h_t)^{\frac{3}{2}}} \sum_{i,j=0}^{p} \frac{1}{(d'+\omega_i^p-\omega_j^p)^{\frac{3}{2}}} \exp\left(-\rho\frac{|r'+x'-y'|^2}{d'+\omega_i^p-\omega_j^p}\right) L_i(t')L_j(\tau'). \quad (28)$$

Since the heat kernel is analytic in the local variables, the convergence rate of the approximation is exponential in p. Each term in the sum is a Gaussian. Before we discuss how the multivariate Gaussian can be approximated we will first focus on the one dimensional case in the following section.

5.3 Chebyshev Expansion of the Gauss Kernel

It is well known that Chebyshev polynomials have distinct advantages for the approximation of functions. In the interval $[-1,1]$ they are defined by

$$T_n(x) = \cos(n \arccos(x)).$$

The functions T_n are polynomials of degree n which are $L^2_w[-1,1]$-orthogonal with weight function $w(x) = (1-x^2)^{-\frac{1}{2}}$. That is,

$$\int_{-1}^{1} T_n(x)T_m(x)w(x)\,dx = \frac{\pi}{\gamma_n}\delta_{n,m},$$

where $\gamma_0 = 1$ and $\gamma_n = 2$ for $n \geq 1$. The roots of T_{p+1} are given by (14). By orthogonality, the expansion of the one-dimensional Gauss Kernel is

$$\exp\left(-\frac{(r+x-y)^2}{\delta}\right) = \sum_{k,l=0}^{\infty} E_{k,l}(r,\delta)T_k(x)T_l(y), \quad x,y \in [-1,1], \quad (29)$$

where

$$E_{k,l}(r,\delta) = \frac{\gamma_k\gamma_l}{\pi^2}\int_{-1}^{1}\int_{-1}^{1} \exp\left(-\frac{(r+x-y)^2}{\delta}\right) T_k(x)T_l(y)w(x)w(y)\,dxdy. \quad (30)$$

Separation of variables is accomplished by truncating the expansion (29) Since the magnitude of the Chebyshev polynomials bounded by unity, the approximation

error depends on how rapidly the coefficients $E_n(r,\delta)$ approach zero. The following bound can be derived.

Lemma 1. *For every $a > 0$ and $n = k + l$ the bound*

$$\left|E_{k,l}(r,\delta)\right| \leq \frac{\gamma_k \gamma_l}{a^n} \exp\left(\frac{4}{\delta}\left(a - \frac{1}{a}\right)^2\right)$$

holds.

Note that $a > 0$ is a free parameter, which means that the geometric progression can be made arbitrarily fast by increasing the value of a. The trade off is that a larger a implies that the constant factor is also larger. For given k and l the optimal a can be determined by simple calculus. This leads to an estimate of the form

$$\left|E_{k,l}(r,\delta)\right| \leq \gamma_k \gamma_l \exp\Big(-\kappa(\delta n) n\Big)$$

where $\kappa(t) \sim \ln(4t)/4$. The super exponential behavior has to do with the fact that the Gaussian is not only analytic but also entire. This becomes evident from the following proof, which follows a similar argument as in [41].

Proof. After changing variables $x = \cos\theta$, $y = \cos\phi$ and using the symmetry properties integral (30) becomes

$$\begin{aligned} E_{k,l}(r,\delta) &= \frac{\gamma_k \gamma_l}{\pi^2} \int_0^{\pi}\int_0^{\pi} \exp\left(-\frac{(r+\cos\theta-\cos\phi)^2}{\delta}\right) \cos(k\theta)\cos(l\phi)\, d\theta d\phi \\ &= \frac{\gamma_k \gamma_l}{(2\pi)^2} \int_0^{2\pi}\int_0^{2\pi} \exp\left(-\frac{(r+\cos\theta-\cos\phi)^2}{\delta}\right) \exp(-ik\theta)\exp(-il\phi)\, d\theta d\phi. \end{aligned}$$

The integrand is analytic and periodic in θ and ϕ. By Cauchy's theorem, we can shift both intervals into the complex plane without changing the integral. For any $\tilde{a} > 0$ we obtain

$$\begin{aligned} &E_{k,l}(r,\delta) \\ &= \frac{\gamma_k \gamma_l}{(2\pi)^2} \frac{1}{a^n} \int_0^{2\pi}\int_0^{2\pi} \exp\left(-\frac{(r+\cos(\theta+i\tilde{a})-\cos(\phi+i\tilde{a}))^2}{\delta}\right) \exp(-i(k\theta+l\phi))\, d\theta d\phi, \end{aligned}$$

where $a = \exp(\tilde{a})$. The magnitude of the integral is determined by the real part of the argument to the exponential function. We find that

$$\begin{aligned}
&\mathrm{Re}\Big[(r+\cos(\theta+i\tilde{a})-\cos(\phi+i\tilde{a}))^2\Big] \\
&\quad = \Big[r+(\cos(\theta)-\cos(\phi))\cosh\tilde{a}\Big]^2 - \Big[(\sin(\theta)-\sin(\phi))\sinh\tilde{a}\Big]^2 \\
&\quad \geq -4\sinh^2\tilde{a} = -4\left(a-\frac{1}{a}\right)^2.
\end{aligned}$$

From this the assertion follows easily. □

The estimate of the coefficient $E_{k,l}(r,\delta)$ depends only on the *sum* of the coefficients. This suggests to retain only terms in expansion (29) that are indexed by the triangular region

$$S_q^2 = \{(k,l) : 0 \leq k+l \leq q\},$$

where q is the expansion order for the space variable. The truncation error

$$R_q(x,y) = \exp\left(-\frac{(r+x-y)^2}{\delta}\right) - \sum_{(k,l)\in S_q^2} E_n(r,\delta)T_k(x)T_l(y)$$

can be estimated by

$$\big|R_q(x,y)\big| \leq \sum_{n=q+1}^{\infty}\sum_{k+l=n}\big|E_{k,l}(r,\delta)\big| \leq (2+q)\left(\frac{1}{a-1}\right)^{q+1}\exp\left(\frac{4}{\delta}\left(a-\frac{1}{a}\right)^2\right).$$

Since a is arbitrary the convergence is super exponential. The approximation has about half as many terms as the corresponding interpolation approximation (12).

The effect is more pronounced in the three dimensional case. From the properties of the exponential function we have that

$$\exp\left(-\frac{1}{\delta}\big|r'+x'-y'\big|^2\right) = \sum_{\alpha,\beta} E_{\alpha,\beta}(\delta,r)T_\alpha(x')T_\beta(y'). \tag{31}$$

Here α and β are multi-indices, $\alpha=(\alpha_1,\alpha_2,\alpha_3)$, $|\alpha|=\alpha_1+\alpha_2+\alpha_3$ and $T_\alpha(x') = T_{\alpha_1}(x'_1)T_{\alpha_2}(x'_2)T_{\alpha_3}(x'_3)$. Because of the basic properties of the exponential function the coefficients of the three dimensional Gauss kernel are products of the one-dimensional coefficients

$$E_{\alpha,\beta}(\delta,r) = E_{\alpha_1,\beta_1}(\delta,r_1)E_{\alpha_2,\beta_2}(\delta,r_2)E_{\alpha_3,\beta_3}(\delta,r_3).$$

Thus it suffices to retain the terms in (31) whose indices add up to the given expansion order q. These indices are in the set

$$S_q^6 = \{(\alpha,\beta) : 0 \leq |\alpha+\beta| \leq q\}.$$

with cardinality

$$\#S_q^6 = \binom{q+6}{q} \sim \frac{q^6}{6!} \text{ as } q\to\infty.$$

Even for small expansion orders this number is much less than the $(q+1)^6$ terms in the interpolation approximation.

The truncation error can be bounded by

$$\left|R_p(x,y)\right| \leq \exp\left(\frac{12}{\delta}\left(a-\frac{1}{a}\right)^2\right)\sum_{n=q+1}^{\infty}\binom{n+5}{n}\frac{1}{a^n} \leq q^6 C(a,\delta)\left(\frac{1}{a-1}\right)^{q+1}$$

where $C(a,\delta)$ is independent of q. This shows that the error is super exponential.

Replacing the Gaussians in (28) by the truncation of (31) leads to

$$G_{\mathrm{loc}}(x',y',t,\tau') \approx \frac{1}{(4\pi h_t)^{\frac{3}{2}}}\sum_{i,j=0}^{p}\sum_{|\alpha+\beta|\leq q} E_{i\alpha,j\beta}T_\alpha(x')T_\beta(y')L_i(t')L_j(\tau'), \qquad (32)$$

where

$$E_{i\alpha,j\beta} = \frac{1}{(d'+\omega_i^p-\omega_j^p)^{\frac{3}{2}}}E_{\alpha_1,\beta_1}\left(\frac{\rho}{d'+\omega_i^p-\omega_j^p},r_1\right)\cdot\cdots\cdot E_{\alpha_3,\beta_3}\left(\frac{\rho}{d'+\omega_i^p-\omega_j^p},r_3\right).$$

The integrals in (30) are not available in closed form and must be computed by quadrature. The most natural way to do this is to apply the Gauss-Chebyshev quadrature rule

$$E_{k,l}(\delta,r') \approx \left(\frac{2}{q+1}\right)^2\sum_{\substack{0\leq n\leq q\\ 0\leq m\leq q}} T_k(\omega_n^q)T_l(\omega_m^q)\exp\left(-\frac{(r'+\omega_n^q-\omega_m^q)^2}{\delta}\right).$$

5.4 Space-Time Subdivision

The parabolic FMM relies on a hierarchic subdivision of time and space. The temporal subdivision into intervals was already described in section 4.2, we now turn our attention to the spatial subdivision into cubes. Its construction is familiar from the elliptic FMM: The coarsest cube of the spatial tree contains the entire boundary surface. This cube is refined into eight cubes of half the side length. The process is repeated until the finest cubes contain at most a predetermined number of surface quadrature points. Since the boundary is a surface of dimension two, most cubes in the finer levels will be empty and do not have to be considered in a fast algorithm.

With a parabolic operator every temporal interaction involves calculating a surface potential with a smooth kernel. In the parabolic FMM these interactions are agglomerated in the cubes of the spatial tree. The level where the agglomeration takes place is selected such that the truncation error of an MtL translation is independent of the level of the temporal tree.

Lemma 1 and the form of the local kernel in (28) show how this can be done. It follows that the spatial truncation error depends on the variance δ of the Gauss kernel, which are given by

$$\delta = \frac{d' + \omega_i^p - \omega_j^p}{\rho}. \tag{33}$$

A smaller value of δ implies a larger truncation error. Since the Gauss kernel is smooth, the approximation (28) is valid even when the source and destination cubes are close or identical.

The interaction list of a temporal interval I_k^l in any level consists of the interval I_{k-2}^l and, if k is odd, also of I_{k-3}^l. Thus the value of d' is either four or six and hence the numerator in (33) is bounded below by two. To ensure uniform error bounds, the factor ρ in (27) must be bounded independently of the level of the temporal tree. This suggests to compute MtL translations in the spatial level

$$l_s = \min\Big(\mathrm{trunc}(l/2), L_s\Big), \tag{34}$$

where l is the temporal level. To see this, let $h_t^{(l)}$ be the half-length of a temporal interval in the l-th level and $h_s^{(l_s)}$ be the half-length of a cube in the l_s-th spatial level. Then

$$\rho = \frac{(h_s^{(l_s)})^2}{4h_t^{(l)}} = \frac{2^{2l_s}(h_s^{(0)})^2}{4\cdot 2^l h_t^{(0)}} \le \frac{(h_s^{(0)})^2}{4h_t^{(0)}}.$$

Hence ρ is indeed bounded.

The variance also determines the decay rate of the Gauss kernel in space. Interactions of cubes can be neglected when they are sufficiently well separated in space and only a certain number N of neighboring cubes in a linear direction must be included in the spatial interaction lists. Condition (34) implies that N is always the same in every level.

Since the spatial level is coarsened only in every second temporal level there will be translation operators that will either go in space and time or only in time. To simplify their description we introduce the following notations. The nonempty cubes that must be considered in a temporal level are

$$\mathscr{C}(l) = \big\{\text{nonempty cubes in level } l_s\big\}.$$

For a cube $\nu \in \mathscr{C}(l)$ the neighbors are defined as

$$\mathscr{N}(\nu) = \big\{\tilde\nu \in \mathscr{C}(l) \,:\, \|\nu - \tilde\nu\|_\infty \le N\big\}.$$

MtM and LtL translations always go from children to parents of time intervals but may stay within a spatial cube. Thus we extend the concept of the child of a cube $\nu \in \mathscr{C}(l)$ as

$$\mathscr{K}(\nu) = \begin{cases} \big\{\text{nonempty spatial children of } \nu\big\} & \text{if } l_s \ne (l-1)_s, \\ \big\{\nu\big\} & \text{if } l_s = (l-1)_s. \end{cases}$$

Likewise, the definition of a parent of $\nu \in \mathscr{C}(l-1)$ is extended as

$$\pi(\nu) = \begin{cases} \{\text{spatial parent of } \nu\} & \text{if } l_s \neq (l-1)_s, \\ \{\nu\} & \text{if } l_s = (l-1)_s. \end{cases}$$

5.5 Space-Time Translation Operators

We proceed by describing the translation operators of the parabolic FMM. This is analogous to the temporal FMM except for the fact that the spatial dependence significantly adds to the complexity.

5.5.1 Moment-to-Local Translations

Similar to what we had done in Sect. 4.3.1 we consider the influence of one time interval on another in the interaction list. We set

$$\Phi(x,t) = \sum_{\substack{t_m \in J, \\ x_P \in S}}{}' G(x - x_P, t - t_m) g(x_P, t_m) w_P h_t, \quad x \in S, t \in I. \tag{35}$$

For $J \in \mathscr{I}(I)$ the heat kernel is smooth, but may be very peaked if the intervals are close to each other, which happens if they are in a low level of the temporal tree. Thus we cannot expect that the heat kernel can be approximated with low degree polynomials. Towards that goal we break up the surface into pieces that intersect with the cubes of the spatial tree and choose the level according to formula (34), because this will lead to uniform error bounds in any level. We write

$$S = \bigcup_{\nu \in \mathscr{C}(l_s)} S_\nu.$$

where S_ν is the piece of the surface that intersects with cube ν. Since the heat kernel decays exponentially only the neighboring cubes contribute in a significant way. For $x \in S_\nu$ the potential in (35) is approximated by

$$\Phi(x,t) \approx \sum_{\tilde{\nu} \in \mathscr{N}(\nu)} \sum_{\substack{t_m \in J, \\ x_P \in S_{\tilde{\nu}}}}{}' G(x - x_P, t - t_m) g(x_P, t_m) w_P h_t, \quad t \in I, x \in S_\nu. \tag{36}$$

We proceed by replacing the heat kernel in each term of (36) by expansion (32). Because of the scaling we have $r' = 2(\nu - \tilde{\nu})$ and obtain for the potential generated by $S_{\tilde{\nu}}$

$$\Phi_{\tilde{\nu}}(x,t) \approx \sum_{i=0}^{p} \sum_{|\alpha| \leq q} \lambda^{i\alpha}(I \times S_\nu) L_i(t') T_\alpha(x'), \quad t \in I, x \in S_\nu,$$

where

$$\lambda^{i\alpha}(I \times S_\nu) = \sum_{j=0}^{p} \sum_{|\alpha+\beta| \leq q} E_{i\alpha,j\beta} \mu^{j\beta}(J \times S_{\tilde{\nu}}) \tag{37}$$

and $\mu^{j\beta}(J \times S_{\tilde{\nu}})$ are the moments, given by

$$\mu^{j\beta}(J \times S_{\tilde{\nu}}) = \sum_{\substack{t_m \in J, \\ x_P \in S_{\tilde{\nu}}}} {}'L_j(t'_m) T_\beta(x'_P) g(x_P, t_m)\, w_P h_t .$$

The MtL translation of (37) does not have tensor product structure. To understand that, re-write on term in (37) more explicitly as

$$\lambda_j^{i\alpha} = \sum_{\beta_3=0}^{q-|\alpha|} E^{(3)}_{\alpha_3,\beta_3} \sum_{\beta_2=0}^{q-|\alpha|-\beta_3} E^{(2)}_{\alpha_2,\beta_2} \sum_{\beta_1=0}^{q-|\alpha|-\beta_2-\beta_3} E^{(1)}_{\alpha_1,\beta_1} \mu^{i\beta}.$$

The inner summations depend on the order of index α and thus the tensor form is lost. However, it can be easily restored by including *more* terms of the expansion

$$\tilde{\lambda}_j^{i\alpha} = \sum_{\beta_3=0}^{q-\alpha_1-\alpha_3} E^{(3)}_{\alpha_3,\beta_3} \sum_{\beta_2=0}^{q-\alpha_2-\beta_3} E^{(2)}_{\alpha_2,\beta_2} \sum_{\beta_1=0}^{q-\beta_2-\beta_3} E^{(1)}_{\alpha_1,\beta_1} \mu^{i\beta}.$$

This sum can be evaluated in three stages, working from the inside to the outside

$$\begin{aligned}
\lambda^{(1)}_{\alpha_1,\beta_2,\beta_3} &= \sum_{\beta_1=0}^{q-\beta_2-\beta_3} E^{(1)}_{\alpha_1,\beta_1} \mu_{i,\beta_1,\beta_2,\beta_3}\,, \\
\lambda^{(2)}_{\alpha_1,\alpha_2,\beta_3} &= \sum_{\beta_2=0}^{q-\alpha_1-\beta_3} E_{\alpha_2,\beta_2} \lambda^{(1)}_{\alpha_1,\beta_2,\beta_3}\,, \\
\lambda^{(3)}_{\alpha_1,\alpha_2,\alpha_3} &= \sum_{\beta_3=0}^{q-\alpha_1-\alpha_2} E_{\alpha_3,\beta_3} \lambda^{(2)}_{\alpha_1,\alpha_2,\beta_3}\,.
\end{aligned}$$

At the end of this computation $\lambda^{(3)}_\alpha = \tilde{\lambda}_j^{i\alpha}$ holds. Inspection of the upper bound in the summation shows that in every step we only need to compute coefficients that are indexed by the set S^3_q. This algorithm entails $3 \cdot \# S^3_q$ multiplications and additions which is much less than the cost to evaluate (37).

5.5.2 Moment-to-Moment Translations

From (34) it follows that the spatial level is coarsened only in every other temporal level. Thus there are two types of MtM translations, depending on whether the spatial level of the parent interval is the same or different from the child's level. To derive the actual form of the MtM matrix recall that the temporal translation follows from the addition theorem for Lagrange polynomials (20). For space translations we need the analogous formula for Chebyshev polynomials. It is given by

$$T_k\left(\frac{1}{2}x' \pm \frac{1}{2}\right) = \sum_{l=0}^{k} a_{k,l} T_l(x'), \tag{38}$$

where

$$a_{k,l} = \frac{2}{p+1} \sum_{k=0}^{p} T_l(\omega_k^p) T_k \left(\frac{1}{2}\omega_k^p \pm \frac{1}{2} \right),$$

and p is any integer greater than k. This formula follows from the discrete orthogonality of Chebyshev polynomials, see, e.g. [38].

Equipped with the addition theorems, the MtM translation operator can be derived in a similar manner as in Sect. 4.3.3. If the translation involves space and time then

$$\mu^{j\beta}(I \times S_\nu) = \sum_{\substack{\tilde{I} \in \mathscr{K}(I) \\ \tilde{\nu} \in \mathscr{K}(\nu)}} \sum_{\substack{0 \le i \le p \\ |\alpha| \le \beta}} q_{j,i} a_{\beta,\alpha} \mu^{j\alpha}(\tilde{I} \times S_{\tilde{\nu}}).$$

Here, the coefficients depend on direction of the translation from the child to the parent. This computation can be tensorized in a similar manner as the MtL translations.

If there is only a temporal translation we have

$$\mu^{j\beta}(I \times S_\nu) = \sum_{\tilde{I} \in \mathscr{K}(I)} \sum_{\substack{0 \le i \le p \\ |\beta| \le \alpha}} q_{j,i} \mu^{i\beta}(\tilde{I} \times S_\nu).$$

Using matrix notations, and the extended definition of a child, both cases can be written as

$$\boldsymbol{\mu}_{k_l,\nu}^{l} = \sum_{\tilde{\nu} \in \mathscr{K}(\nu)} MtM\, \boldsymbol{\mu}_{2k_l,\tilde{\nu}}^{l-1} + MtM\, \boldsymbol{\mu}_{2k_l+1,\tilde{\nu}}^{l-1}.$$

where $\boldsymbol{\mu}_{k,\nu}^{l}$ is the moment vector of cube ν and time interval I_k^l.

5.5.3 Local-to-Local Translations

As in the temporal FMM, the LtL translations in the parabolic case are the transposes of the MtM translations. Their derivation is completely analogous and is omitted here to avoid repetition. We only state the resulting translation formulas. In the case of a spatio-temporal translation we have

$$\lambda^{i\alpha}(\tilde{I} \times S_{\tilde{\nu}}) = \sum_{\substack{0 \le j \le p \\ |\beta| \le \alpha}} q_{j,i} a_{\beta,\alpha} \lambda^{j\beta}(I \times S_\nu),$$

where $\tilde{I} \in \mathscr{K}(I)$ and $\tilde{\nu}$ is a child of ν.

In the case of a time-only translation the formula simplifies to

$$\lambda^{i\alpha}(\tilde{I} \times S_\nu) = \sum_{0 \le j \le p} q_{j,i} \lambda^{j\alpha}(I \times S_\nu).$$

In matrix notation, both cases can be written as

$$\boldsymbol{\lambda}_{\tilde{k},\pi(\nu)}^{l-1} = LtL\, \boldsymbol{\lambda}_{k,\nu}^{l}, \qquad \tilde{k} \in \{2k, 2k+1\}.$$

5.6 The Parabolic FMM

The general structure of the parabolic FMM is the same as the causal FMM, with the exception that translations are in time and space. The details are given in Algorithm 4.

6 A Numerical Example

To illustrate the convergence properties of the method we solve the Dirichlet and the Neumann problem of the heat equation in the exterior of the unit sphere for the time interval $[0,1]$. The boundary conditions are chosen such that the solution is $u(x,t) = G(x-x_0,t)$ where $x_0 = (0.5,0,0)$. Hence the initial condition vanishes and the numerical results can be compared with the given analytical solution.

Green's formula (1) is an integral equation of the first kind for the Dirichlet and of the second kind for the Neumann problem. The sphere is triangulated and the weights in the spatial quadrature rule are selected to obtain degree of precision two. The resulting rule has nodes on the midpoints of the edges, see equation (5.1.44) in [2]. The coarsest refinement has 288 quadrature nodes, and is four times uniformly refined. From relation (23) it follows that $h_s \sim h_t^{1/2}$ is not sufficient to maintain the asymptotic convergence of the time discretization method. We therefore adjust the space and time mesh according to $h_s \sim h_t^{\lambda}$, with $\lambda = \ln(10)/\ln(4) \approx 0.6021$. Table 1 shows the discretization parameters and the expansion orders for the parabolic FMM.

Table 1 Mesh parameters and expansion orders for the different refinements

Mesh	1	2	3	4
N_t	25	80	250	800
N_s	288	1152	4608	18432
$N_s N_t$	7,200	92,160	1,252,000	14,745,600
p/q	3/12	4/22	5/16	6/24

The errors as a function of time are shown in Fig. 2 and the overall errors in Fig. 4. It is apparent that the results obtained with both integral formulations reproduce the theoretical $O(h_t^{3/2})$ estimate well. The integral equation of the first kind shows some minor oscillations in the finest meshes which are caused by the truncation error of the fast method.

The CPU time per time step and the total times are shown in Fig. 3 and 4, respectively. Because of the fast method, the CPU time in a time step mainly depends on how many translation operators must be evaluated, but not so much on how far the computation has progressed in time.

Algorithm 4. The Parabolic Fast Multipole Algorithm

for $k = 0$ to K_0 **do**
Compute S and R in the binary representation of k.
Set $\hat{k} = k - 1$.

% Moment Calculation.
for $v \in \mathscr{C}(0)$ **do**
$\boldsymbol{\mu}^0_{\hat{k},v} = QtM\,\mathbf{g}^0_{\hat{k},v}$
end for

% Upward Pass.
for $l = 1$ to S **do**
for $v \in \mathscr{C}(l)$ **do**
$$\boldsymbol{\mu}^l_{\hat{k}_l} = \sum_{\tilde{v}\in\mathscr{K}(v)} MtM\,\boldsymbol{\mu}^{l-1}_{2\hat{k}_l,\tilde{v}} + MtM\,\boldsymbol{\mu}^{l-1}_{2\hat{k}_l+1,\tilde{v}}$$
end for
end for

% Interaction Phase.
for $v \in \mathscr{C}(S)$ **do**
$$\boldsymbol{\lambda}^S_{k_S,v} = \sum_{\tilde{v}\in\mathscr{N}(v)} MtL\,\boldsymbol{\mu}^S_{k_S-2,\tilde{v}} + MtL\,\boldsymbol{\mu}^S_{k_S-3,\tilde{v}}$$
end for
for $l = S-1$ down to 0 **do**
for $v \in \mathscr{C}(l)$ **do**
$$\boldsymbol{\lambda}^l_{k_l,v} = \sum_{\tilde{v}\in\mathscr{N}(v)} MtL\,\boldsymbol{\mu}^l_{k_l-2,\tilde{v}}$$
end for
end for

% Downward Pass.
for $l = S$ down to 0 **do**
for $v \in \mathscr{C}(l)$ **do**
$$\boldsymbol{\lambda}^l_{k_l,v} = \boldsymbol{\lambda}^l_{k_l,v} + LtL\,\boldsymbol{\lambda}^{l+1}_{k_{l+1},\pi(v)}$$
end for
end for

% Potential evaluation.
for $v \in \mathscr{C}(0)$ **do**
$\boldsymbol{\Phi}^0_{k,v} = LtP\,\boldsymbol{\lambda}^0_{k,v}$
end for

% Compute $\mathbf{g}^0_{k,v}$'s using the smooth potential $\boldsymbol{\Phi}^0_{k,v}$ and the local part.
end for

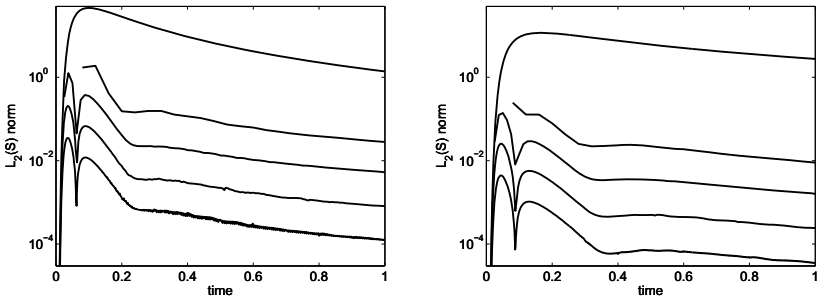

Fig. 2 Computational results as a function of time for the integral equation of the first kind (left) and second kind (right). The top curve is the $L_2(S)$ norm of the solution, the curves below are the $L_2(S)$-errors for meshes 1 to 4 of Table 1

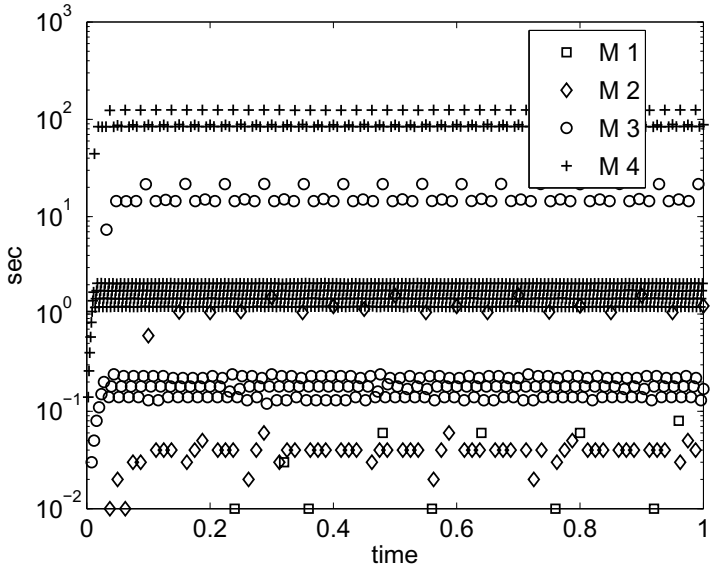

Fig. 3 CPU time per time step for the four meshes of Table 1

The overall computational complexity is strongly dependent on the choice of the expansion orders of the fast method. The values of p and q in Table 1 have been determined experimentation such that the error of the fast method is negligible compared with the discretization error. The total complexity of the scheme is $O(p^2q^4N_tN_s)$, see [38]. Since the expansion orders also depend on the discretization, the timings are, except for logarithmic terms, linear in the number of quadrature points. Our numerical experiments are in good agreement with this observation.

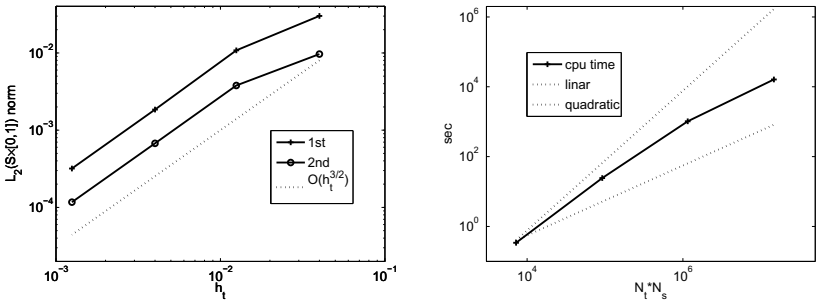

Fig. 4 Left: $L_2(S\times[0,1])$ errors versus temporal step length. Right: Total CPU time versus number of quadrature nodes

Acknowledgements. The work of Johannes Tausch is in part funded by the National Science Foundation under grant number 0915222.

References

[1] Arnold, D., Noon, P.: Coercivity of the single layer heat potential. J. Comput. Math. 7, 100–104 (1989)
[2] Atkinson, K.E.: The Numerical Solution of Integral Equations of the Second Kind. Cambridge University Press (1997)
[3] Bourgeois, C., Schneider, R.: Biorthogonal wavelets for the direct integral formulation of the heat equation. Tech. Rep. SFB393/00-14, Technical University Chemnitz (2000)
[4] Brattkus, K., Meiron, D.: Numerical simulations of unsteady crystal growth. SIAM J. Appl. Math. 52, 1303–1320 (1992)
[5] Brunner, H.: Collocation Methods for Volterra Integral and Related Functional Differential Equations, Cambridge (2004)
[6] Chien, D.: Numerical evaluation of surface integrals in three dimensions. Math. Comp. 64, 727–743 (1995)
[7] Costabel, M.: Boundary integral operators for the heat equation. Integral. Eq. Oper. Theory 13(4), 498–552 (1990)
[8] Costabel, M.: Time-dependent problems with the boundary integral equation method. In: Stein, E., de Borst, R., Hughes, T. (eds.) Encyclopedia of Computational Mathematics. Wiley (2004)
[9] Costabel, M., Saranen, J.: The spline collocation method for parabolic boundary integral equations on smooth curves. Numer. Math. 93(3), 549–562 (2003)
[10] Dahmen, W.: Wavelet and multiscale methods for operator equations. Acta Numerica 6, 55–228 (1997)
[11] Dargush, G., Banerjee, P.: Application of the boundary element method to transient heat conduction. Internat. J. Numer. Methods Engrg. 31, 1231–1247 (1991)
[12] Eggermont, P.: A new analysis of the trapezoidal - discretization method for the numerical solution of Abel-type integral equations. J. Integral Equations 3, 317–332 (1981)
[13] Giebermann, K.: Multilevel approximation of boundary integral operators. Computing 67, 183–207 (2001)

[14] Greengard, L., Lin, P.: Spectral approximation of the free-space heat kernel. Appl. Comput. Harmonic Anal. 9, 83–97 (1999)
[15] Greengard, L., Strain, J.: A fast algorithm for the evaluation of heat potentials. Comm. Pure Appl. Math. XLIII, 949–963 (1990)
[16] Greengard, L., Strain, J.: The fast Gauss transform. SIAM J. Sci. Comput. 12, 79–94 (1991)
[17] Greengard, L., Sun, X.: A new version of the fast Gauss transform. Doc Math J DMV Extra Volume ICM 1998 III, 575–584 (1998)
[18] Grigoriev, M., Dargush, G.: Higher-order boundary element methods for transient diffusion problems. part I: Bounded flux formulation. Internat. J. Numer. Methods Engrg. 55, 1–40 (2002)
[19] Hackbusch, W.: Integral Equations: Theory and Numerical Treatment. Birkhäuser, Basel (1994)
[20] Hairer, E., Lubich, C., Schlichte, M.: Fast numerical solution of nonlinear Volterra integral equations. SIAM J. Sci. Comput. 6(3), 532–541 (1985)
[21] Hamina, M., Saranen, J.: On the spline collocation method for the single-layer heat operator equation. Math. Comp. 62, 41–64 (1994)
[22] Hsiao, G., Saranen, J.: Boundary integral solution of the two-dimensional heat equation. Math. Methods Appl. Sci. 16(2), 87–114 (1993)
[23] Kress, R.: Linear Integral Equations, Applied Mathematical Sciences, vol. 82. Springer, Heidelberg (1989)
[24] Li, J., Greengard, L.: High order accurate methods for the evaluation of layer heat potentials. SIAM J. Sci. Comput. 31(5), 3847–3860 (2009)
[25] Linz, P.: Analytical and Numerical Methods for Volterra Equations. Studies in Applied Mathematics. SIAM (1985)
[26] Lubich, C.: Fractional linear multistep methods for Abel-Volterra integral equations of the first kind. IMA J. Numer. Anal. 7, 97–106 (1987)
[27] Lubich, C., Schneider, R.: Time discretization of parabolic boundary integral equations. Numer. Math. 63(1), 455–481 (1992)
[28] McIntyre, E.: Boundary integral solutions of the heat equation. Math. Comp. 46(173), 71–79 (1986)
[29] Melenk, J., Boerm, S., Loehndorf, M.: Approximation of integral operators by variable-order interpolation. Numer. Math. 99(4), 605–643 (2005)
[30] von Petersdorff, T., Schwab, C.: Numerical solution of parabolic equations in high dimensions. Math. Model Numer. Anal. 38(1), 93–128 (2004)
[31] Pogorzelski, W.: Integral equations and their applications. Pergamon (1966)
[32] Rathsfeld, A.: Nyström's method and iterative solvers for the solution of the double-layer potential equation over polyhedral boundaries. SIAM J. Numer. Anal. 32(3), 924–951 (1995)
[33] Rizzo, F., Shippy, D.: A method of solution for certain problems of transient heat conduction. AIAA J. 8, 2004 (1971)
[34] Schanz, M., Antes, H.: Application of operational quadrature methods in time domain boundary element methods. Meccanica 32(3), 179–186 (1997)
[35] Strain, J.: Fast adaptive methods for the free-space heat equation. SIAM J. Sci. Comput. 15(1), 185–206 (1994)
[36] Sun, X., Bao, Y.: A Kronecker product representation of the fast Gauss transform. SIAM J. Matrix Anal. Appl. 24(3), 768–786 (2003)

[37] Tao, L., Yong, H.: A generalization of discrete Gronwall inequality and its application to weakly singular Volterra integral equation of the second kind. J. Math. Anal. Appl. 282, 56–62 (2003)
[38] Tausch, J.: A fast method for solving the heat equation by layer potentials. J. Comput. Phys. 224, 956–969 (2007)
[39] Tausch, J.: Nystrom discretization of parabolic boundary integral equations. Appl. Numer. Math. 59(11), 2843–2856 (2009)
[40] Tausch, J.: The generalized Euler-Maclaurin formula for the numerical solution of Abel-type integral equations. J. Integral. Eqns. Appl. 22(1), 115–140 (2010)
[41] Tausch, J., Weckiewicz, A.: Multidimensional fast Gauss transforms by Chebyshev expansions. SIAM J. Sci. Comput. 31(5), 3547–3565 (2009)
[42] Yarvin, N., Rokhlin, V.: An improved fast multipole algorithm for potential fields on the line. SIAM J. Numer. Anal. 36(2), 629–666 (1999)

Fast Stokes Solvers for MEMS

Attilio Frangi

Abstract. Providing an estimate of gas damping in MEMS is a complex task since MEMS are fully three dimensional micro-structures which cannot in general be reduced to simple 1D or 2D models and since the gas cannot be treated as a continuum medium at the microscale. This issue is here addressed, focusing on high pressure applications, by means of integral equations and fast solvers implementing a linear incompressible Stokes formulation with slip boundary conditions. Numerical results are validated with experimental data. Extensions to high working frequencies and low pressures are discussed.

1 Introduction

Estimating mechanical dissipation in air-packaged MEMS (Micro Electro Mechanical Systems) seems, for several reasons, to be an ideal application for the now maturing fast integral equation methods [5, 18, 20, 24, 27, 33, 40]. First, the micromechanical structures (see e.g. Fig. 5), are innately three-dimensional and too geometrically complicated to analyze analytically. Therefore, a numerical approach is needed. Second, the mechanical dissipation is primarily due to pressure and drag forces generated by the air surrounding the mechanical structure. Hence, even though the exterior domain is effectively infinite in extent, the only quantities of interest are velocities and forces on the structure surface. Surface-only integral equations, if they can be formulated, have a dimensional advantage over volume methods in such a setting. Third, the velocities and displacements for many MEMS of interest are small enough, and the surrounding air is viscous enough, that the flow can be described by a spatially invariant linearization. Therefore, surface-only integral equations can be formulated.

Attilio Frangi
Politecnico di Milano, Piazza L. da Vinci 32, 20133 Milano, Italy
e-mail: attilio.frangi@polimi.it

U. Langer et al. (Eds.): Fast Boundary Element Methods, LNACM 63, pp. 221–240.
springerlink.com

For the above reasons, there have been a number of experimentally-verified successes in evaluating gas damping for air-package MEMS using fast integral equation solvers, though considerable algorithmic development was required [12, 13, 38]. Much of the past effort was on improving the efficiency and robustness of quasi-static-Stokes based fast solvers, but now the focus has shifted to addressing more challenging physics. Newer MEMS use higher operating frequencies and finer dimensions, and therefore the effects of unsteady flow, gas compression, and rarefaction can no longer be ignored.

In the next sections we review many of the issues associated with integral formulation, discretization and fast solution of the incompressible, quasi-static Stokes equations. In Section 3 the formulation is adapted to slip boundary conditions and validated with the experiments performed on two inertial resonators. Section 4 describes methods for including unsteady effects.

In this chapter focus is set on fast multipole techniques. It is however worth mentioning that alternative accelerators for BEM, like the Precorrected-FFT technique [30], are available. Unlike the FMM, the key technique employed in the precorrected FFT method is the Fast Fourier Transformation. To compute the far-field interaction, the first step in the precorrected-FFT technique is to enclose the meshed problem domain with a 3D uniform grid which serves for two purposes: first, it distinguishes the near- and far-field interactions; second, it forms the basis for the FFT. Successful applications have been reported, e.g., in [30, 37, 38].

2 Classical Quasi-static Stokes Flow

The most mature and best validated of the fast solvers for estimating gas damping in MEMS are based on solving integral formulations of the 3D incompressible quasi-static Stokes equations [13, 36, 38]. For quasi-static Stokes to be a good model of the gas surrounding a micromachined structure, the gas should be incompressible, sufficiently viscous, moving slowly, and not be too rarified. This list of assumptions hold, at least loosely, for air-packaged MEMS like arrays of electrostatically positioned micromirrors [36], inertial sensors like accelerometers, gyroscopes and magnetometers, and structures like the Tang resonator of Fig. 5. In this background section the quasi-static Stokes model is given, and the standard integral formulation and the common numerical discretizations described. In later sections, the quasi-static Stokes assumptions will be revisited, and techniques for extending the model to include the effects of unsteady flow will be described.

2.1 Governing Equations

For an isotropic Newtonian fluid, if the fluid velocity, $\mathbf{u}$, is divergence-free, then the relation between $\mathbf{u}$ and the stress tensor, σ, is given by [32]

$$\sigma(\mathbf{x}) = -p(\mathbf{x}) \quad + \eta \left(\nabla \mathbf{u}(\mathbf{x}) + \nabla^{\top} \mathbf{u}(\mathbf{x}) \right) \tag{1}$$

where η is the fluid viscosity and $\nabla \mathbf{u}$ denotes a matrix of velocity partial derivatives whose elements are given by

$$(\nabla \mathbf{u})_{ij} = \frac{\partial u_i}{\partial x_j}.$$

The quasi-static Stokes equations are derived from combining incompressibility, conservation of mass, and conservation of momentum yielding the well-known quasi-static Stokes equations

$$\nabla p(\mathbf{x}) - \eta \Delta(\mathbf{x}) = \mathbf{0}, \qquad \nabla \cdot \mathbf{u}(\mathbf{x}) = 0 \quad \text{in} \quad \Omega \tag{2}$$

where Ω denotes the volume occupied by the fluid.

The standard boundary conditions for the classical quasi-static Stokes equation are no-slip conditions. In a later section, generalizations of the no-slip boundary condition will be used to model rarefaction effects. For the case of several interacting micromachined structures surrounded by fluid, the no-slip condition implies that for each structure surface point, the fluid velocity must match the structure's velocity. More precisely, for the MEMS problem, the domain of the fluid, Ω, is defined as the domain exterior to the micromachined structures. For each point $\mathbf{x}$ on surface S, where S is defined to be the union the structure surfaces,

$$\mathbf{u}(\mathbf{x}) = \mathbf{g}(\mathbf{x}) \tag{3}$$

where $\mathbf{g}(\mathbf{x})$ is the velocity of the micromachined structure at point $\mathbf{x}$. Note also that typically the velocity distant from the micromachined structures is assumed to approach zero. Nonzero background velocities can be treated by perturbation.

Given $\mathbf{u}$ which satisfies Eqs. (2) and (3), the vector force density the structure exerts on the fluid can be computed from the product of the stress tensor with the surface normal pointing out of Ω. That is, at each structure surface point $\mathbf{x}$,

$$\mathbf{t}(\mathbf{x}) = \sigma(\mathbf{x}) \cdot \mathbf{n}(\mathbf{x})$$

where $\mathbf{n}(\mathbf{x})$ is the surface normal pointing outside the fluid domain. Note that $\mathbf{t}$ is the negative of force per unit area exerted by the fluid on the structure surface. In a modest abuse of terminology, we refer to the vector $\mathbf{t}$ as a traction force density even though it contains components which act in a direction normal to the surface.

2.2 Integral Formulation

Either Greens identities [31] or Lorentz reciprocity [32] can be used to derive an integral formulation that relates the Stokes flow generated traction forces to the surface velocities. Specifically, if $\mathbf{x}$ is a point on a smooth region in S,

$$\frac{1}{2}\mathbf{u}(\mathbf{x}) = \int_S \{\mathscr{V}(\mathbf{r}) \cdot \mathbf{t}(\mathbf{y}) - [\mathscr{K}(\mathbf{r}) \cdot \mathbf{n}(\mathbf{y})] \cdot \mathbf{u}(\mathbf{y})\}\, dS_y \tag{4}$$

where $\mathbf{r} \equiv \mathbf{x} - \mathbf{y}$, $r = \|\mathbf{r}\|$, the kernels (also referred to as Greens functions) $\mathscr{V}$ and $\mathscr{K}$ are given by

$$V_{ik}(\mathbf{r}) = \frac{1}{8\pi\eta}\left(\frac{\delta_{ik}}{r} + \frac{r_i r_k}{r^3}\right),$$
$$K_{iqk}(\mathbf{r}) = -\frac{3}{4\pi}\frac{1}{r^5} r_i r_q r_k,$$

and the integrals of the strongly singular kernel, $\mathscr{K}$, should be interpreted in the Cauchy principal value sense. The kernels $\mathscr{V}$ and $\mathscr{K}$ are often interpreted as generating the velocities associated with stokeslet and stresslet point sources [31], but these kernels also coincide with the Kelvin kernels used in the displacement equation for incompressible elasticity [4].

Combining the no-slip boundary conditions with Eq. (4) yields a first kind integral equation which relates the known structure velocities to the unknown fluid traction forces

$$\frac{1}{2}\mathbf{g}(\mathbf{x}) = \int_S \{\mathscr{V}(\mathbf{r}) \cdot \mathbf{t}(\mathbf{y}) - [\mathscr{K}(\mathbf{r}) \cdot \mathbf{n}(\mathbf{y})] \cdot \mathbf{g}(\mathbf{y})\}\, dS_y. \tag{5}$$

In the common case where the structure velocities correspond to rigid body motions, the second integral in Eq. (5) vanishes, resulting in

$$\frac{1}{2}\mathbf{g}(\mathbf{x}) = \int_S \mathscr{V}(\mathbf{r}) \cdot \mathbf{t}(\mathbf{y})\, dS_y. \tag{6}$$

The formulation in (6) is common in the literature on integral equations for Stokes flow, but there are alternatives that can have superior properties. For example, the above formulation is a vector integral equation with matrix kernels that are non-diagonal. Of more immediate concern is the fact that (6) does not have a unique solution, an issue that will be addressed in the next section.

2.3 Null Space Problem

The differential form of Stokes equation (2) only involves the gradient of the pressure and is therefore insensitive to spatially constant shifts in pressure. Since the pressure is a component of $\mathbf{t}$, and $\mathbf{t}$ is the unknown, Eq. (6) can not have a unique solution. The matter is even more problematic when the surface S corresponds to N unconnected structures. In that case,

$$[\mathscr{V}\mathbf{t}] = \int_S \mathscr{V}(\mathbf{r}) \cdot \mathbf{t}(\mathbf{y})\, dS_y$$

has null space $\mathcal{N}(\mathcal{V})$ of dimension N whose basis is given by

$$\mathbf{t}^{\alpha}(\mathbf{x}) = \begin{cases} \mathbf{n}(\mathbf{x}), & \mathbf{x} \in S^{\alpha}, \\ 0 & \text{elsewhere}, \end{cases} \qquad 1 \leq \alpha \leq N. \tag{7}$$

Many techniques exist for dealing with the null space of (6) [31]. Unfortunately, standard BEM approaches are ill-conditioned when applied to complex structures even if the null space is filtered out exactly.

In order to cure the issue of ill-conditioning, a new boundary element method, the Mixed Velocity Traction approach (MVT), has been recently proposed [12] and extended to large scale problems [13] using fast solvers.

The second tool required for setting up the MVT is the traction integral equation, an integral identity which can be obtained through careful differentiation of (4), for a smooth $\mathbf{x} \in S$:

$$\frac{1}{2}\mathbf{t}(\mathbf{x}) = \int_S \left\{ -\left[\mathbf{n}(\mathbf{x}) \cdot \mathscr{K}(\mathbf{r})\right] \cdot \mathbf{t}(\mathbf{y}) - \left[\mathbf{n}(\mathbf{x}) \cdot \mathscr{W}(\mathbf{r}) \cdot \mathbf{n}(\mathbf{y})\right] \cdot \mathbf{u}(\mathbf{y}) \right\} dS_y \tag{8}$$

where $\mathscr{W}$ is a fourth order two-point kernel with components

$$W_{qiks}(\mathbf{r}) = \frac{\eta}{4\pi}\frac{1}{r^3}\left[2\delta_{sk}\delta_{iq} + \frac{3}{r^2}\left(\delta_{ik}r_q r_s + \delta_{kq}r_i r_s + \delta_{is}r_k r_q + \delta_{sq}r_i r_k\right) - 30\frac{r_i r_k r_q r_s}{r^4}\right]$$

Equation (8) also contains an hypersingular integral interpreted here in the finite-part sense. Again, when the structure velocities correspond to rigid body motion the integral of $\left[\mathbf{n}(\mathbf{x}) \cdot \mathscr{W}(\mathbf{r}) \cdot \mathbf{n}(\mathbf{y})\right] \cdot \mathbf{g}(\mathbf{y})$ over a closed surface vanishes. The MVT simply consists in enforcing a linear combination of Eqs. (6) and (8):

$$\mathbf{g}(\mathbf{x}) - \frac{\gamma}{\eta}\frac{1}{2}\mathbf{t}(\mathbf{x}) = \int_S \left\{ \mathscr{V}(\mathbf{r}) \cdot \mathbf{t}(\mathbf{y}) + \frac{\gamma}{\eta}\left[\mathbf{n}(\mathbf{x}) \cdot \mathscr{K}(\mathbf{r})\right] \cdot \mathbf{t}(\mathbf{y}) \right\} dS_y \tag{9}$$

where γ is a length scale to be calibrated. The benefits of this formulation have been pointed out in [12] where it has been shown that the mixed formulation is well posed when $\gamma > 0$ and that not only does it filter out automatically all the exact null space of the velocity equation, but also considerably improves the condition number which is crucial for the iterative solvers employed.

3 Extension to the Slip Flow Regime and Implementation

Working pressures of MEMS are spread over a large range (1 bar – 10^{-6} bar). This issue, associated to the micro-scale at hand, promotes rarefaction effects which, at low pressures, have to be dealt with using techniques of rarefied gas-dynamics [16].

A measure of rarefaction is provided by the Knudsen number $\mathrm{Kn} = \lambda/L$, where λ is the molecular mean free path and L is a typical dimension of the flux, e.g., the gap between plates in Poiseuille (squeeze) flow. As a rule of thumb, when $\mathrm{Kn} < 0.01$ classical tools of macroscale fluid flow can be applied, (e.g., Navier–Stokes solvers). In the range $0.01 < \mathrm{Kn} < 0.1$ an accurate prediction of the flow properties can be obtained by applying a continuum approach with slip boundary conditions (slip BC). Since the dimensions typical of MEMS are of a few microns, the flow mainly develops in the slip regime even at ambient pressure. For larger values of Kn the flows enters the so called transition regime which can be analysed only by means of kinetic theories, (e.g., Boltzmann equation).

Let $\mathbf{t}^S$ denote the surface components of tractions:

$$\mathbf{t}^S(\mathbf{x}) = [\quad -\mathbf{n}(\mathbf{x}) \otimes \mathbf{n}(\mathbf{x})] \cdot \mathbf{t}(\mathbf{x}),$$

where $\quad -\mathbf{n}(\mathbf{x}) \otimes \mathbf{n}(\mathbf{x})$ is the surface projector tensor. As pointed out recently [13], first order boundary slip conditions should be expressed in terms of $\mathbf{t}^S$:

$$\mathbf{u}(\mathbf{x}) = \mathbf{g}(\mathbf{x}) - c_t \mathbf{t}^S(\mathbf{x}), \qquad c_t := \frac{2-\sigma}{\sigma}\frac{\lambda}{\eta} \tag{10}$$

where σ is the tangential momentum accommodation coefficient.

Since Eq. (10) operates linearly on $\mathbf{t}$, the BEM formulation Eq. (9) can be easily adapted, yielding [13] (see Eq. (8) for the definition of $\mathscr{W}$):

$$\mathbf{g}(\mathbf{x}) - \frac{c_t}{2}\mathbf{t}^S(\mathbf{x}) - \frac{\gamma}{\eta}\frac{1}{2}\mathbf{t}(\mathbf{x}) = \int_S \Big\{ \mathscr{V}(\mathbf{r}) \cdot \mathbf{t}(\mathbf{y}) + c_t \left[\mathscr{K}(\mathbf{r}) \cdot \mathbf{n}(\mathbf{y})\right] \cdot \mathbf{t}^S(\mathbf{y}) + \frac{\gamma}{\eta}\left(\left[\mathbf{n}(\mathbf{x}) \cdot \mathscr{K}(\mathbf{r})\right] \cdot \mathbf{t}(\mathbf{y}) - c_t \left[\mathbf{n}(\mathbf{x}) \cdot \mathscr{W}(\mathbf{r}) \cdot \mathbf{n}(\mathbf{y})\right] \cdot \mathbf{t}^S(\mathbf{y}) \right) \Big\} dS_y. \tag{11}$$

3.1 Numerical Implementation

The numerical solution of Eq. (11) requires, as usual, the discretization of S (in this case we choose a triangulation $\mathscr{T}$ with M flat triangles) and the choice of the space X_h to which the interpolation of $\mathbf{t}$ belongs. Since $\mathbf{t}$ represents tractions which are typically discontinuous along edges and corners, we choose X_h as the space of piecewise constant functions. At this stage, different alternative procedures can be employed. In the Galerkin approach Eq. (11) is contracted with a traction test field $\tilde{\mathbf{t}} \in X_h$, integrated over S and enforced for any choice of $\tilde{\mathbf{t}} \in X_h$: Let τ_β and τ_γ be generic triangles of the mesh with $\mathbf{x} \in \tau_\beta$ and $\mathbf{y} \in \tau_\gamma$, and let A_β be the area of τ_β. If $\mathbf{T}_\gamma$ and $\mathbf{T}^S_\gamma$ are the tractions on τ_γ, the discretized Galerkin approach yields the linear system:

$$\int_{\tau_\beta} \mathbf{g}(\mathbf{x})\, dS_x - A_\beta \left(\frac{c_t}{2}\mathbf{T}^S_\beta + \frac{\gamma}{2\eta}\mathbf{T}_\beta \right) \qquad \forall \beta = \{1 : M\} \tag{12}$$

$$= \sum_{\gamma=1}^{M} \left[\int_{\tau_\beta} \int_{\tau_\gamma} \left(\mathscr{V}(\mathbf{r}) + \frac{\gamma}{\eta} \mathbf{n}(\mathbf{x}) \cdot \mathscr{K}(\mathbf{r}) \right) dS_y \, dS_x \right] \cdot \mathbf{T}_\gamma$$

$$+ \sum_{\gamma=1}^{M} \left[c_t \int_{\tau_\beta} \int_{\tau_\gamma} \left(\mathscr{K}(\mathbf{r}) \cdot \mathbf{n}(\mathbf{y}) - \frac{\gamma}{\eta} \mathbf{n}(\mathbf{x}) \cdot \mathscr{W}(\mathbf{r}) \cdot \mathbf{n}(\mathbf{y}) \right) dS_y \, dS_x \right] \cdot \mathbf{T}_\gamma^S.$$

However, though accurate, this approach requires the evaluation of lengthy double surface integrals. This issue has been studied at length, but still represents a considerable obstacle when computing time becomes an issue and hence, typically, in large scale problems.

The classical and faster collocation approach consists in enforcing Eq. (11) at the center of each triangle:

$$\mathbf{g}(\mathbf{x}_\beta) - \frac{c_t}{2} \mathbf{T}_\beta^S - \frac{\gamma}{2\eta} \mathbf{T}_\beta \qquad \forall \beta = \{1 : M\} \tag{13}$$

$$= \sum_{\gamma=1}^{M} \left[\int_{\tau_\gamma} \left(\mathscr{V}(\mathbf{y} - \mathbf{x}_\beta) + \frac{\gamma}{\eta} \mathbf{n}(\mathbf{x}_\beta) \cdot \mathscr{K}(\mathbf{y} - \mathbf{x}_\beta) \right) dS_y \right] \cdot \mathbf{T}_\gamma$$

$$+ \sum_{\gamma=1}^{M} \left[c_t \int_{\tau_\gamma} \left(\mathscr{K}(\mathbf{y} - \mathbf{x}_\beta) \cdot \mathbf{n}(\mathbf{y}) - \frac{\gamma}{\eta} \mathbf{n}(\mathbf{x}_\beta) \cdot \mathscr{W}(\mathbf{y} - \mathbf{x}_\beta) \cdot \mathbf{n}(\mathbf{y}) \right) dS_y \right] \cdot \mathbf{T}_\gamma^S$$

where $\mathbf{x}_\beta$ represents the center of mass of the τ_β triangle.

3.1.1 Evaluation of Integrals

The numerical evaluation of singular and hypersingular integrals for a generic choice of shape functions and geometry discretization can be addressed with techniques developed at length during last decade for fracture mechanics applications.

Here, however, thanks to the simplifying hypotheses detailed in the previous section, an analytical approach can be adopted for both singular and near singular integrals. All the integrals in Eq. (13) can be computed analytically exploiting formulas available in [25], but for the terms with the $\mathscr{W}$ kernel, which are analysed in this section.

The task is greatly simplified by the introduction of some identities developed in the context of Galerkin boundary element methods [4]. Using the indicial notation, for the sake of clarity:

$$n_q(\mathbf{x}) W_{qiks}(\mathbf{r}) n_s(\mathbf{y}) = R_q^x R_s^y Q_{ikqs}(\mathbf{r}) \tag{14}$$

where:

$$Q_{ikqs}(\mathbf{r}) = -\frac{\eta}{8\pi} e_{iep} e_{kgr} \left[2\delta_{pq}\delta_{rs} + (\delta_{pr}\delta_{qs} + \delta_{ps}\delta_{qr}) \right] \mathbf{r}_{,eg} \tag{15}$$

and R_q^y denotes the q^{th} component of the surface curl operator with respect to the coordinate y (see, e.g., [13]).

The integral over any open surface S can be transformed into an integral along the outer contour ∂S of S. Let us focus, for instance, on one triangle τ_γ. Then

$$\int_{\tau_\gamma} n_q(\mathbf{x}) W_{qiks}(\mathbf{r}) n_s(\mathbf{y}) \, dS_y = \int_{\partial\tau_\gamma} R_q^x Q_{ikqs}(\mathbf{r}) \tau_s(\mathbf{y}) ds_y \,. \tag{16}$$

Finally, the regular line integrals can be evaluated analytically as detailed in [13].

3.1.2 Multipole Expansions

While in classical FE based methods each element interacts only with neighbours ("local" field interaction), it is apparent that integral equations also entail "far field" interactions. As a matter of fact, when the problem size N increases, storage and computing-time problems stem mainly from "far field" interactions, their cost being roughly proportional to N^2 for each matrix-vector product. This issue is often dealt with by multipole based methods, their aim being to provide an approximate but fast technique to evaluate far field interactions, eventually limiting their cost to $\sim N$. Fast multipole accelerators represent nowadays a well established technique applied successfully in different fields of mechanics. A review of BE accelerated formulations can be found in [29, 23]. A complete explanation of FMM is however beyond the scope of this chapter and reference is made to [18] for details. While the construction of the hierarchical octree structure with the associated upward and downward swap procedures is almost problem independent, at least in static applications (and can be taken from the literature as is), the form of multipoles strongly depends on the formulation at hand and will be detailed in the sequel. Similar results have been presented in the context of elasticity in [28] and are exploited at length herein. The fundamental identity for our developments is the expansion for the inverse radius [11]:

$$\frac{1}{r} = \sum_{b=0}^{\infty} \sum_{a=-b}^{a=b} \overline{S_a^b}(\mathbf{Ox}) R_a^b(\mathbf{Oy}) \tag{17}$$

where $\mathbf{O}$ is a properly chosen pole such that $|\mathbf{Oy}| < |\mathbf{Ox}|$, the bar denotes complex conjugate and S_a^b, R_a^b are solid harmonics which can be computed by means of simple and fast algebraic recursive formulae (see, e.g., [28]):

$$R_n^m(\mathbf{r}) = \frac{1}{(n+m)!} P_n^m(\cos\theta) e^{\mathrm{i}m\phi} r^n,$$

$$S_n^m(\mathbf{r}) = (n-m)! P_n^m(\cos\theta) e^{\mathrm{i}m\phi} \frac{1}{r^{n+1}},$$

and satisfying

$$R_n^{-m} = (-1)^m \overline{R}_n^m, \qquad S_n^{-m} = (-1)^m \overline{S}_n^m.$$

If ϕ is a generic vector function and we define the eight multipoles:

$$\begin{aligned}
M_i^{ab}(\mathbf{O},\mathbf{y}) &= R_a^b(\mathbf{O}\mathbf{y})\phi_i(\mathbf{y}),\\
M_0^{ab}(\mathbf{O},\mathbf{y}) &= M_i^{ab}(\mathbf{O},\mathbf{y})y_i,\\
N_i^{ab}(\mathbf{O},\mathbf{y}) &= R_{a,k}^b(\mathbf{O}\mathbf{y})\phi_k(\mathbf{y})n_i(\mathbf{y}) + R_{a,k}^b(\mathbf{y})n_k(\mathbf{y})\phi_i(\mathbf{y}),\\
N_0^{ab}(\mathbf{O},\mathbf{y}) &= N_i^{ab}(\mathbf{O},\mathbf{y})y_i,
\end{aligned}$$

it can be shown that:

$$V_{ik}(\mathbf{r})\phi_k(\mathbf{y}) = \frac{1}{8\pi\eta}\sum_{b=0}^{\infty}\sum_{a=-b}^{a=b}\left[S_a^b M_i^{ab} - x_k S_{a,i}^b M_k^{ab} + S_{a,i}^b M_0^{ab}\right], \quad (18)$$

$$\begin{aligned}
n_q(\mathbf{x})K_{qik}(\mathbf{r})\phi_k(\mathbf{y}) &= \qquad (19)\\
&= \frac{1}{8\pi}\sum_{b=0}^{\infty}\sum_{a=-b}^{a=b}\left[2\left(n_i S_{a,j}^b - S_{a,iq}^b n_q x_j\right)M_j^{ab} + (2S_{a,iq}^b n_q)M_0^{ab}\right],
\end{aligned}$$

$$K_{ikq}(\mathbf{r})n_q(\mathbf{y})\phi_k(\mathbf{y}) = \frac{1}{8\pi}\sum_{b=0}^{\infty}\sum_{a=-b}^{a=b}\left[(S_a^b\delta_{ms} - S_{a,m}^b X_s)Nab_s + S_{a,m}^b N_0^{ab}\right] \quad (20)$$

$$\begin{aligned}
n_q(\mathbf{x})W_{qiks}(\mathbf{r})n_s(\mathbf{y})\phi_k(\mathbf{y}) &= \qquad (21)\\
&= \frac{\eta}{8\pi}\sum_{b=0}^{\infty}\sum_{a=-b}^{a=b}\left[2S_{a,s}^b n_i N_s^{ab} - 2x_j S_{a,im}^b n_m N_j^{ab} + 2S_{a,im}^b n_m N_0^{ab}\right].
\end{aligned}$$

The main consequences of these identities is that both velocity and traction equations can be expressed in terms of the same eight multipoles. The results presented depend only on the kernels of the continuum formulation and hence apply to both collocation and Galerkin schemes. Indeed, by inspection of equations (18-21) it is apparent that any expression to integrate can be recast in the form $F(\mathbf{O},\mathbf{x})G(\mathbf{O},\mathbf{y})$. Now, let us suppose that the double surface integral of $F(\mathbf{O},\mathbf{x})G(\mathbf{O},\mathbf{y})$ is evaluated in the context of a Galerkin approach. By means of the multipole expansions developed above the integration with respect to $\mathbf{x}$ and $\mathbf{y}$ can be decoupled:

$$\int_{\tau_\beta}\sum_{\gamma}\int_{\tau_\gamma} F(\mathbf{O},\mathbf{x})G(\mathbf{O},\mathbf{y})\,dS_x\,dS_y = \left(\int_{\tau_\beta} F(\mathbf{O},\mathbf{x})\,dS_x\right)\left(\sum_{\gamma}\int_{\tau_\gamma} G(\mathbf{O},\mathbf{y})\,dS_y\right)$$

independently of the Gauss-Hammer rules to be applied. As pointed out before, collocation can be recovered from the Galerkin scheme by employing a one point rule for the inner and outer integrals (integrations over $\mathbf{y}$ and $\mathbf{x}$, respectively) so that no formal difference exists between the two approaches.

4 Extension to High Frequency Oscillatory Flow

The results presented in previous sections hold under specific assumptions. Three non-dimensional parameters are generally identified as crucial: the Mach number M; the Reynolds number $\mathrm{R}e = UL/\nu$ and the Stokes number $\mathrm{St} = fL^2/\nu$. U is the flow velocity, ν is the kinematic viscosity, L is a typical flow length and f is the frequency of oscillation. If all these parameters are small compared to unity, the proposed linear quasi-static approach is deemed acceptable and compares very well with experiments. When f increases, these conditions may fail. Taking into account inertia effects, the governing equations for oscillatory flows [37, 38] change to

$$\nabla p(\mathbf{x}) - \eta \Delta \mathbf{u}(\mathbf{x}) = i\omega\rho\mathbf{u}, \qquad \nabla \cdot \mathbf{u}(\mathbf{x}) = 0 \quad \text{in} \quad \Omega \tag{22}$$

and the corresponding integral equation is the same as (9) with the following kernel functions:

$$\begin{aligned} V_{ik}(\mathbf{r}) &= \frac{1}{4\pi\eta}\left(A(kr)\frac{\delta_{ik}}{r} + B(kr)\frac{r_i r_k}{r^3}\right), \\ K_{iqk}(\mathbf{r}) &= -\frac{\delta_{ij}r_k + \delta_{kj}r_i}{4\pi r^3}[e^{ikr}(-ikr+1) - B] - \frac{\delta_{ik}r_j(1-B)}{4\pi r^3} \\ &\quad -\frac{r_i r_j r_k}{4\pi r^5}[5B - 2e^{ikr}(-ikr+1)] \end{aligned}$$

where $\mathbf{r} = \mathbf{y} - \mathbf{x}$, $r = \|\mathbf{y} - \mathbf{x}\|$ and

$$\begin{aligned} A &= e^{ikr}\left(1 + \frac{i}{kr} - \frac{1}{k^2r^2}\right) + \frac{1}{k^2r^2}, \\ B &= -e^{ikr}\left(1 + \frac{3i}{kr} - \frac{3}{k^2r^2}\right) - \frac{3}{k^2r^2}, \\ k &= (-1+i)\sqrt{\frac{\rho}{\eta}\frac{\omega}{2}}. \end{aligned}$$

The numerical implementation of this model using integral equations becomes more involved, but can be addressed with the same techniques described above.

Adapting a result presented in [41] for elasticity problems, the $\mathscr{V}$ kernel (and similarly all the other kernels in the MVT formulation) can be expressed in terms of the classical Helmholtz kernel:

$$V_{ik}(\mathbf{r}) = \frac{1}{4\pi\eta}\left(\frac{e^{ikr}}{r}\delta_{ij} + \frac{1}{k^2}\frac{\partial^2}{\partial y_i \partial y_j}\left(\frac{e^{ikr}}{r} - \frac{1}{r}\right)\right). \tag{23}$$

As a consequence, in the following we will focus on the performance of the FMM of $V(\mathbf{r}) = \exp(\mathrm{i}kr)/4\pi r$. Indeed, its interest goes well beyond Stokes applications, since many physical problems are governed by equations of Helmholtz type which arise, e.g., in linear acoustics, in electromagnetics, or for elastic waves. All cases involve integral equations whose (scalar or tensorial) kernels are defined, for

three-dimensional formulations, in terms of the fundamental solution $V(\mathbf{r})$ and its derivatives.

For real values of the wavenumber k, which correspond to wave propagation problems in lossless media, FMMs based on either type of expansion have been extensively studied and implemented. These studies have in particular established that multipole expansions of $V(\mathbf{r})$ are too costly except at low frequencies (because the expansion truncation threshold increases with k), while plane-wave expansions are well-suited to higher frequencies but break down in the low-wavenumber limit. It is also known that in the zero-wavenumber (i.e. static) limit an a priori indication is usually available on the number N of multipoles to be employed in truncated expansions in order to obtain a prescribed accuracy in $K(\mathbf{r})$ and N is unaffected by the dimensions of the cells in the octree. This nice feature (which ensures a $O(n_{\mathrm{dof}})$ complexity per iteration for multi-level FMMs applied to static problems) is no longer present in frequency-domain formulations [7, 8, 9, 34], whose implementation thus becomes substantially complicated by the need to adapt the truncation order to the level of the octree (resulting in a $O(n_{\mathrm{dof}} \log n_{\mathrm{dof}})$ complexity per iteration).

In contrast, only scattered efforts have so far been devoted to FMMs for Helmholtz-type problems involving *complex* wavenumbers k, see, e.g., [17] for electromagnetic waves in lossy media or [39] for acoustic wave propagation in porous media. Such formulations involve wavenumbers of the form $k = (\alpha + \mathrm{i}\beta)\vartheta$ (where ϑ is a real nonnegative parameter related to frequency and α, β are real constants). The paucity of available studies notwithstanding, complex-wavenumber FMMs arise for a number of different physical problems.

First, such equations and kernels arise naturally upon considering wave propagation in lossy media (e.g. soils) in which mechanical or electromagnetic waves are damped. Such materials (e.g. viscoelastic materials) may be described, within frequency-domain approaches, in terms of linear constitutive relations involving complex moduli. This leads to complex-valued wavenumbers such that $0 < \beta < \alpha$, often with a small imaginary part, i.e. such that $\beta/\alpha \ll 1$, and represents the most direct generalization of Helmholtz-type equations with real wavenumbers.

Another class of such problems correspond to parabolic problems involving elliptic partial differential operators in the space variables and first-order time derivatives, upon using Fourier transform in time or applying excitations at a prescribed frequency. They include heat conduction, transient Stokes flows, and eddy currents, and the associated Green's functions or tensors involve $K(\mathbf{r})$ with $|\alpha| = \beta = 1$. Also amenable to the general framework of Helmholtz-type equations is the computation of Casimir forces, which are attractive force arising between uncharged conductive surfaces in vacuum, a remarkable consequence of quantum electrodynamics first realized by [6]. Finally, one may mention that optical tomography [42] also leads to a Helmholtz equation with complex wavenumber (defined in terms of modulation frequency of light and optical parameters of the medium), this time such that $\beta < 0 < \alpha$ and $|\beta| < |\alpha|$.

The above-summarized wealth of different applications has stimulated in [14] an investigation of the Fast Multipole Methods for this class of problems. Currently,

little is known about, e.g., the appropriate non-dimensional frequency ranges of applicability of either multipole-based or plane wave-based expansions, or the choice of truncation order. An empirical study of multipole expansions of $K(\mathbf{r})$, of the kind known to be suitable for low real wavenumbers, is conducted for complex wavenumbers of the form $k = (\alpha + \mathrm{i}\beta)\vartheta$, so as to estimate ranges of applicability in terms of ϑd (d denoting a characteristic cell size) and suitable settings for the truncation order N according to the values of α, β.

4.1 Multipole Expansion

Let us consider the full-space Green's function $V(\mathbf{r})$ for the Helmholtz equation:

$$V(\mathbf{r}) = \frac{e^{\mathrm{i}(\alpha+\mathrm{i}\beta)\vartheta r}}{4\pi r} = \frac{e^{\mathrm{i}kr}}{4\pi r}, \qquad k = (\alpha + \mathrm{i}\beta)\vartheta. \tag{24}$$

For a given pole $\mathbf{O}$, let $\mathbf{r}_x = \mathbf{Ox}$ and $\mathbf{r}_y = \mathbf{Oy}$ and $r_x = \|\mathbf{r}_x\|$, $r_y = \|\mathbf{r}_y\|$. The Gegenbauer addition theorem [1] states that, for $r_x > r_y$

$$\frac{e^{\mathrm{i}kr}}{4\pi r} = \frac{\mathrm{i}k}{4\pi} \sum_{n=0}^{\infty} \sum_{m=-n}^{n} (2n+1)(-1)^m \mathscr{I}_n^{-m}(k, \mathbf{r}_y) \mathscr{O}_n^m(k, \mathbf{r}_x) \tag{25}$$

where, setting $\hat{\mathbf{r}} = \mathbf{r}/r$,

$$\mathscr{O}_n^m(k, \mathbf{r}) = h_n(kr) Y_n^m(\hat{\mathbf{r}}), \tag{26}$$

$$\mathscr{I}_n^m(k, \mathbf{r}) = j_n(kr) Y_n^m(\hat{\mathbf{r}}). \tag{27}$$

In Eq. (27) j_n is the spherical Bessel function of the first kind [1], h_n is the spherical Hankel function of the first kind:

$$h_n(z) = h_n^{(1)}(z) = j_n(z) + \mathrm{i}y_n(z)$$

while the spherical harmonics $Y_n^m(\hat{\mathbf{r}})$ are given in terms of the angular spherical coordinates θ, ϕ of a unit vector $\hat{\mathbf{r}}$ by:

$$Y_n^m(\hat{\mathbf{r}}) = \sqrt{\frac{(n-m)!}{(n+m)!}} P_n^m(\cos\theta) e^{\mathrm{i}m\phi}.$$

In [11, 28, 41] it is shown that a more efficient implementation can be achieved if solid harmonics R_n^m and S_n^m (see Sect. 3.1.2) are employed instead of spherical harmonics in Eq. (27), to obtain:

$$\mathscr{O}_n^m(k, \mathbf{r}) = h_n(kr) \frac{1}{\sqrt{(n-m)!(n+m)!}} S_n^m(\hat{\mathbf{r}}), \tag{28}$$

$$\mathscr{I}_n^m(k, \mathbf{r}) = j_n(kr) \sqrt{(n-m)!(n+m)!} R_n^m(\hat{\mathbf{r}}). \tag{29}$$

In any numerical implementation, the summation over n in expansion Eq. (25) is truncated at level N, yielding an approximation $V_N(\mathbf{r})$ of the kernel $V(\mathbf{r})$:

$$V_N(\mathbf{r}) = \frac{\mathrm{i}k}{4\pi} \sum_{n=0}^{N} \sum_{m=-n}^{n} (2n+1)(-1)^m \mathscr{I}_n^{-m}(k, \mathbf{r}_y) \mathscr{O}_n^m(k, \mathbf{r}_x). \tag{30}$$

The accuracy of Eq. (30) has been analysed, e.g., by [34] for the specific case of real wavenumbers ($\alpha = 1, \beta = 0$), $r_x \gg r_y$ and $\hat{\mathbf{r}}_x \cdot \hat{\mathbf{r}}_y = 1$. Empirical formulas for the choice of N have been proposed in order to guarantee a chosen level of accuracy on the evaluation of $K(\mathbf{r})$. For instance, it is found that

$$N = \vartheta r_y + M \log(\pi + \vartheta r_y) \tag{31}$$

should guarantee a relative error $E = |V - V_N|/|V| = 10^{-3}$ with $M = 3$, and $E = 10^{-6}$ with $M = 5$. Numerical evaluation of the truncation error E, displayed in Fig. 1 as isovalues of $\log(E)$ in a $(\vartheta r_y, N)$-plane, leads to essentially the same conclusions as Eq. (31). On the basis of such results it is generally concluded and accepted that the expansion Eq. (30) is not suited for efficient numerical implementations in the presence of moderate to high frequencies, for which a plane-wave expansion of $V(\mathbf{r})$ in diagonal form is usually preferred [7, 8, 9].

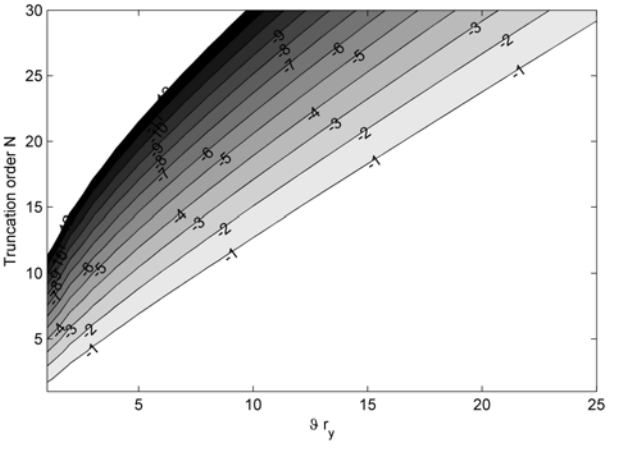

Fig. 1 Isovalues of $\log(E)$, case $|\alpha| = 1, \beta = 0$ (real frequency)

In the case of complex wavenumbers of interest herein, the situation somewhat improves, as the truncation level N needed to reach a given kernel accuracy E is seen to decrease with increasing β. However, Fig. 2 also shows that N still should be adjusted as a function of ϑd.

The foregoing analysis, however, does not take into account that $V(\mathbf{r})$ decays exponentially with $\|\mathbf{r}\|$ if $\beta > 0$. For this reason, the relative accuracy E achieved

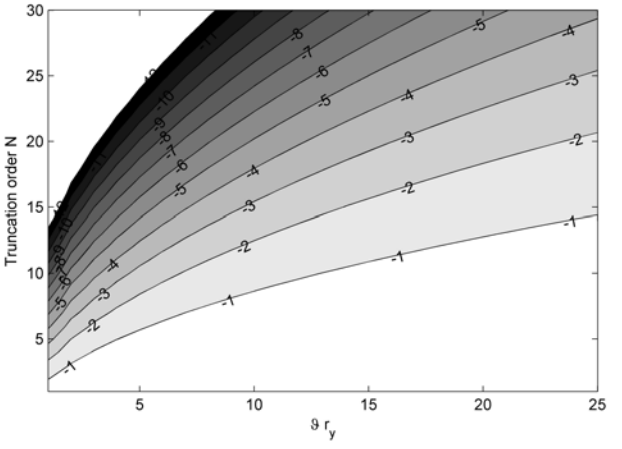

Fig. 2 Isovalues of $\log(E)$, case $|\alpha| = 1, \beta = 1$

on $V(\mathbf{r})$ may not be the most useful indicator, as it does not take into account the absolute relevance of the contribution of field points far from the collocation in the presence of dissipative terms. For this reason, an alternative line of reasoning is now proposed. Since for large values of $\beta\vartheta r$ the decaying term dominates in Eq. (24), it is natural to investigate the relative kernel error in a way that takes into account the absolute contribution of the kernel to the overall evaluation of integral operators. This suggests to consider the pointwise weighted error

$$E_M = E \exp^{-\beta\theta 2d} \tag{32}$$

instead of the standard relative error E. Besides, it is also useful to exploit the observation, commonly made about FMM implementations, that the most severe errors in the application of Eq. (30) occur when the collocation point lies in a cell $\mathscr{C}_x$ and the integration element lies in a cell $\mathscr{C}_y$ of the interaction list of $\mathscr{C}_x$ closest to $\mathscr{C}_x$ (as in Fig. 3).

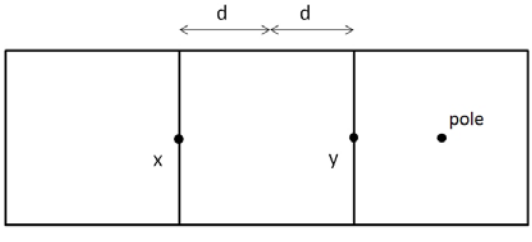

Fig. 3 Choice of pole, source point, integration point

Accordingly, this worst-case cell and source/collocation point configuration is now considered. Placing the expansion origin **O** at the origin of Cartesian coordinates, let $\mathbf{x} = (-3d, 0, 0)$ and $\mathbf{y} = (-d, 0, 0)$, where $2d$ denotes the length of a cell side.

In what follows, the truncated series Eq. (24) is computed for different values of parameters d and N (with $\vartheta d \leq 25$, $N \leq 30$), and the weighted error E_M is numerically evaluated. In [14] several specific values of α and β have been tested, chosen so as to be representative of the main physical models employing the kernel $V(\mathbf{r})$. For $|\alpha| \leq \beta$ the largest weighted error occurs at $\vartheta d = 0$ and, for instance, $N = 12$ guarantees $\log(E_M) = -6$ while $N = 8$ is sufficient for ensuring $\log(E_M) = -4$. For $\beta < |\alpha|$, one can still identify the truncation order N such that E_M is controlled and less than a prescribed amount, independently of ϑd, but this threshold now depends on β.

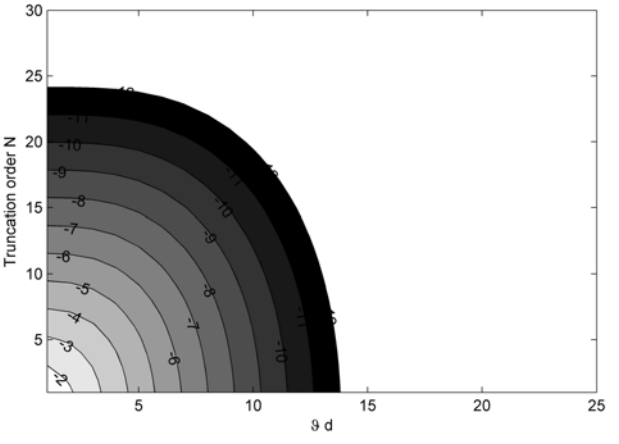

Fig. 4 Isovalues of $\log(E_M)$ for $|\alpha| = 1, \beta = 1$

For instance, consider the case $\alpha = -1, \beta = 1$ which occurs for, e.g., oscillatory Stokes flows or eddy currents. The weighted point-wise error E_M for this case is plotted in Fig. 4 and a maximum value of $\log(E_M) \approx -3.5, -5.3, -7.1$ is predicted for $N = 6, 10, 14$, respectively. Since E_M is a decreasing function of ϑ (apart from small oscillations for small ϑ), the values of E_M predicted from Fig. 4 for $\vartheta d = 0$ should overestimate the actual relative error encountered in real analyses. Similar findings are made for the non-oscillatory exponential kernel ($\alpha = 0, \beta = 1$). The most important practical conclusion for the two cases $\alpha = 0$ or -1, $\beta = 1$ is that the classical FMM based on expansion Eq. (30) with a *fixed* truncation order N, say $N = 10$, is expected to work satisfactorily.

5 Numerical Results

As a validation of the working assumptions, the academic Tang resonator of Fig. 5 has been analysed and tested.

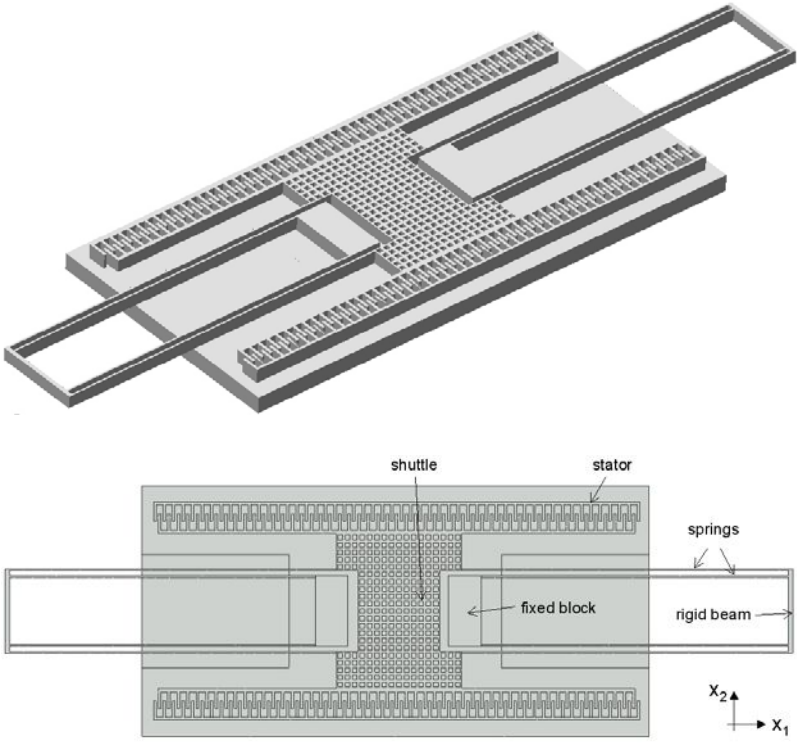

Fig. 5 Comb finger resonator: 3D view and 2D layout

The main components of the resonator consist of two folded beams (springs), two comb drives, each with two sets of fingers, one moving and one fixed, and a shuttle connecting folded beams and moving fingers. When a bias AC voltage is applied to one comb drive, the electrostatic force moves the moving fingers and thus the shuttle and the folded beam towards the fixed fingers while the mechanical restoring force of the beams brings them back to their equilibrium position, resulting in an oscillating motion.

The length of each finger is $20\,\mu$m, the in-plane width is $3.2\,\mu$m, and the air gaps are $2.6\,\mu$m wide; the length of each spring is $405\,\mu$m, while its width is $2.2\,\mu$m. The out-of-plane dimension of the whole structure is $15\,\mu$m. The gap between the shuttle and the substrate is $1.8\,\mu$m. Also this structure has a first resonating frequency

of approximately 4400 Hz. In these working conditions the accelerometer can be effectively represented by a linearized 1D model

$$M\ddot{y} + C\dot{y} + Ky = F\cos\omega t \qquad \text{or} \quad \ddot{y} + 2\xi\omega_0\dot{y} + \omega_0^2 y = \frac{F}{M}\cos\omega t \tag{33}$$

where M denotes the mass of the structure, K the equivalent stiffness due to springs and C the damping coefficient. Since the amplitude of the oscillation is small with respect to the plate gap, C, K, F can be reasonably taken as independent of y.

Sensing is achieved by means of electrostatic capacitors embedded in the MEMS. These data are used to identify the "experimental" values of ξ in the associated 1D model.

This example has been analysed by means of the FFM MVT quasi static ormulation (detailed in Section 3) in order to provide an estimate of the damping coefficient C. It is indeed worth recalling that the MVT employed herein is based on a linear quasi-static Stokes formulation and that the damping force depends linearly on the input-velocity of the shuttle which can be hence taken as unity. In this case, the force exerted by the fluid on the rotor directly yields the desired damping coefficient C.

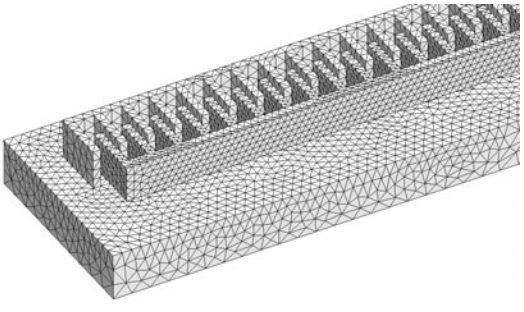

Fig. 6 Comb finger resonator: detail of the finest mesh adopted

The BEM formulation has been suitably modified to account for the deformability of the structure which is essential to capture squeeze film effects between the springs which are very close in this unusual layout. Several meshes have been tested, and the results presented in the sequel refer to the finest mesh adopted (see Fig. 6) containing $\simeq 342000$ elements, which amount to $\simeq 1388000$ unknowns.

The iterative GMRES solver employed [15] rapidly converges. It has been empirically remarked that: i) the rate of convergence remains virtually unchanged down to relative residuums of $10^{-8} \simeq 10^{-9}$; ii) the error on the global force, with respect to its value at convergence of the iterative procedure, is of the same order as the relative residuum. Hence a very mild stopping condition can be employed for the GMRES solver.

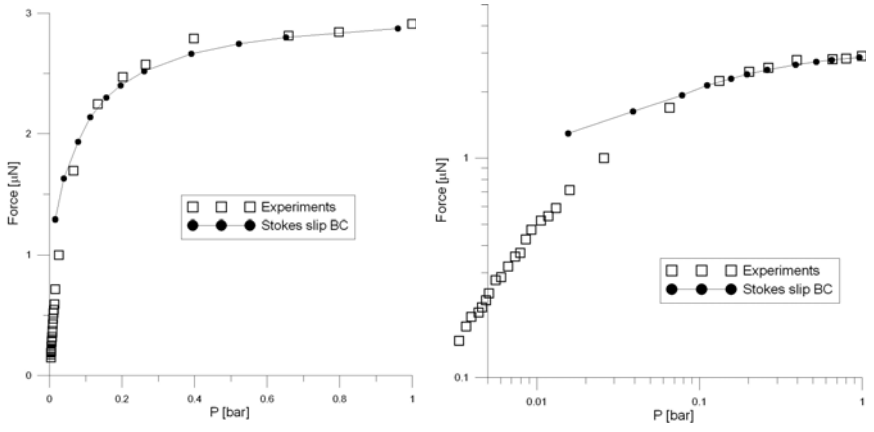

Fig. 7 BEM results with slip BC: comparison with experiments in linear and log-scale

Considering the gaps between the structure and the substrate and between fingers, the transition region starts at approximately $p = 0.1$ bar. At higher pressures, the code with slip-boundary conditions is thus expected to be accurate. This is confirmed by the results plotted in Fig. 7 where the linear scale on the left shows good agreement at high pressures, while the log scale on the right puts in evidence the divergence at low pressures. This is largely expected since the working conditions are entering the transition regime which should be addressed by different techniques (see e.g. [16]).

Acknowledgements. The author wishes to thank Marc Bonnet, Jacob White, Johannes Tausch and Wenjing Ye for their precious contributions.

References

[1] Abramowitz, M., Stegun, I.: Handbook of Mathematical Functions with Formulas, Graphs, and Mathematical Tables. Dover, New York (1964)
[2] Aluru, N.R., White, J.: A fast integral equation technique for analysis of microflow sensors based on drag force calculations. In: Proc. MSM, Santa Clara, CA, pp. 283–286 (1998)
[3] Barnes, J., Hut, P.: A hierarchical $O(N \log N)$ force-calculation algorithm. Nature 324, 446–449 (1986)
[4] Bonnet, M.: Boundary Integral Equation Methods for Solids and Fluids. Wiley, Chichester (1999)
[5] Borup, D.T., Gandhi, O.P.: Calculation of high-resolution SAR distributions in biological bodies using the FFT algorithm and conjugate gradient method. IEEE Trans. Microwave Theor. Techn. 33, 417–419 (1985)
[6] Casimir, H.B.G.: On the attraction between two perfectly conducting plates. Proc. K Ned Akad Wet 60, 793–795 (1948)

[7] Chaillat, S., Bonnet, M., Semblat, J.F.: A multi-level fast multipole BEM for 3-D elastodynamics in the frequency domain. Comput Methods Appl. Mech. Engrg. 197, 4233–4249 (2008)
[8] Darve, E.: The Fast Multipole Method: Numerical Implementation. J. Comp. Phys. 160, 195–240 (2000)
[9] Darve, E.: The fast multipole method: I. Error analysis and asymptotic complexity. SIAM J. Numer. Anal. 38, 98–128 (2000)
[10] Ding, J., Ye, W.: A fast integral approach for drag force calculations to to oscillatory slip Stokes flows. Int. J. Num. Meth. Engng. 60, 1535–1567 (2004)
[11] Epton, M.A., Dembart, B.: Multipole translation theory for three-dimensional Laplace and Helmholtz equations. SIAM J. Sci. Comp. 16, 865–897 (1995)
[12] Frangi, A., Tausch, J.: A qualocation enhanced approach for the Dirichlet problem of exterior Stokes flow. Engng. Anal. Boundary Elem. 29, 886–893 (2005)
[13] Frangi, A., Spinola, G., Vigna, B.: On the evaluation of damping in MEMS in the slip-flow regime. Int. J. Num. Meth. Engng. 68, 1031–1051 (2006)
[14] Frangi, A., Bonnet, M.: On the fast multipole method for the Helmholtz equation with complex frequency. CMES 58, 271–291 (2010)
[15] Frayssé, V., Giraud, L., Gratton, S., Langou, J.: A set of GMRES routines for real and complex arithmetics on high performance computers. CERFACS technical report TR/PA/03/3 (2003)
[16] Gad-el-Hak, M. (ed.): The MEMS handbook. CRC Press (2002)
[17] Geng, N., Sullivan, A., Carin, L.: Fast multipole method for scattering from an arbitrary PEC target above or buried in a lossy half space. IEEE Trans. Antennas Propag. 49, 740–748 (2001)
[18] Greengard, L., Rokhlin, V.: A new version of the fast multipole algorithm for the Laplace equation in three dimensions. Acta Numerica 6, 229–269 (1997)
[19] Greengard, L., Rokhlin, V.: A fast algorithm for particle simulations. J. Comput. Phys. 73, 325–348 (1987)
[20] Hackbusch, W., Nowak, Z.P.: On the fast matrix multiplication in the boundary element method by panel clustering. Numer. Math. 54, 463–491 (1989)
[21] Greengard, L., Kropinski, M.C.: An integral equation approach to the incompressible Navier-Stokes equation in two dimensions. SIAM J. Sci. Comput. 20, 318–336 (1998)
[22] Hockney, R.W., Eastwood, J.W.: Computer simulation using particles. Adam Hilger, New York (1988)
[23] Liu, Y.J.: Fast Multipole Boundary Element Method - Theory and Applications in Engineering. Cambridge University Press, Cambridge (2009)
[24] Lu, C.C., Chew, W.C.: Fast algorithms for solving hybrid integral equations. IEEE Proceedings-H 140, 455–460 (1993)
[25] Milroy, J.S., Hinduja, S., Davey, K.: The elastostatic three dimensional boundary element method: analytical integration for linear isoparametric triangular elements. Appl. Math. Modelling 21, 763–782 (1997)
[26] Mukherjee, S., Telekunta, S., Mukherjee, Y.X.: BEM modeling of damping forces on MEMS with thin plates. Engng. Anal. Boundary Elem. 29, 1000–1007 (2005)
[27] Nabors, K., Korsmeyer, F.T., Leighton, F.T., White, J.: Preconditioned, adaptive, multipole-accelerated iterative methods for three-dimensional first-kind integral equations of potential theory. SIAM J. Sci. Statist Comput 15, 713–735 (1994)
[28] Nishimura, N., Yoshida, K., Kobayashi, S.: Application of fast multipole Galerkin boundary integral equation method to elastostatic crack problems in 3D. Int. J. Num. Meth. Engng. 50, 525–547 (2001)

[29] Nishimura, N.: Fast multipole accelerated boundary integral equation methods. Appl. Mech. Reviews 55, 299–324 (2002)
[30] Phillips, J.R., White, J.: A precorrected-FFT method for electrostatic analysis of complicated 3D structures. IEEE Trans. Comput. Aided Devices 16, 1059–1072 (1997)
[31] Power, H., Wrobel, L.: Boundary Integral Methods in Fluid Mechanics. Computational Mechanics Publications, Southampton (1995)
[32] Pozrikidis, C.: Boundary Integral and Singularity Methods for Linearized Viscous Flows. Cambridge Univeristy Press, Cambridge (1992)
[33] Rokhlin, V.: Rapid solution of integral equation of classical potential theory. J. Comput. Phys. 60, 187–207 (1985)
[34] Song, J., Lu, C.C., Chew, W.C.: Multilevel fast multipole algorithm for electromagnetic scattering by large complex objects. IEEE Trans. Antennas Propag. 45, 1488–1493 (1997)
[35] Tausch, J., White, J.: Second kind integral formulations of the capacitance problem. Adv. Comput. Math. 9, 217–232 (1998)
[36] Wang, X., Judy, M., White, J.: Validating fast simulation of air damping in micromachined devices. In: Proceedings of MEMS 2002 (2002)
[37] Wang, X.: FastStokes: A Fast 3D Fluid Simulation Program for Micro-Electro-Mechanical Systems. PhD Thesis, MIT (2002)
[38] Ye, W., Wang, X., Hemmert, W., Freeman, D., White, J.: Air damping in lateral oscillating micro-resonators: a numerical and experimental study. Journal of MEMS 12, 557–566 (2003)
[39] Yasuda, Y., Sakuma, T.: Analysis of sound fields in porous materials using the fast multipole BEM. In: 37th International Congress and Exposition on Noise Control, Internoise 2008, Shanghai (2008)
[40] Ying, L., Biros, G., Zorin, D.: A kernel-independent adaptive fast multipole algorithm in two and three dimensions. J. Comp. Physics 196, 591–626 (2004)
[41] Yoshida, K.: Applications of Fast Multipole Method to Boundary Integral Equation Method. PhD Thesis, Kyoto University (2001)
[42] Zacharopoulos, A.D., Arridge, S.R., Dorn, O., Kolehmainen, V., Sikora, J.: Three dimensional reconstruction of shape and piecewise constant region values for optical tomography using spherical harmonic parameterisation and a boundary element method. Inverse Problems 22, 1509–1532 (2006)

Engineering Multibody Contact Problems Solved by Scalable TBETI

Marie Sadowská, Zdeněk Dostál, Tomáš Kozubek,
Alexandros Markopoulos, and Jiří Bouchala

Abstract. We review our recent results in the development of scalable total BETI (TBETI) based domain decomposition algorithms for the solution of multibody contact problems of linear elastostatics. We report the scalability of our algorithms for the frictionless problems and the problems with a given (Tresca) friction. Our main tool is the preconditioning by a natural coarse grid of the rigid body motions combined with the BETI methodology and with our in a sense optimal algorithms for the minimization of strictly convex quadratic function subject to separable inequality and linear equality constraints. The analysis admits floating bodies. The theoretical results are verified by numerical experiments, where we also use our algorithms to implement effectively the fixed point iterations for the solution of problems with the Coulomb friction. The power of the method is demonstrated on a real world problem.

1 Introduction

Solving large multibody contact problems of linear elastostatics is complicated by the non-interpenetration boundary conditions, which make them strongly nonlinear, and, if the system of bodies includes "floating" bodies, by the positive semidefinite stiffness matrices resulting from the discretization of such bodies. The task is even more involved when a friction is considered. Taking the above characteristics

Marie Sadowská · Zdeněk Dostál · Tomáš Kozubek · Jiří Bouchala
Department of Applied Mathematics, FEECS, VŠB–TU Ostrava,
17. listopadu 15, 70833 Ostrava, Czech Republic
e-mail: marie.sadowska@vsb.cz, zdenek.dostal@vsb.cz,
tomas.kozubek@vsb.cz, jiri.bouchala@vsb.cz

Alexandros Markopoulos
Department of Mechanics, FME, VŠB–TU Ostrava,
17. listopadu 15, 70833 Ostrava, Czech Republic
e-mail: alexandros.markopoulos@vsb.cz

U. Langer et al. (Eds.): Fast Boundary Element Methods, LNACM 63, pp. 241–269.
springerlink.com

into account, it is only natural to anticipate the solution of contact problems to be more costly than the solution of related linear problems with the classical boundary conditions.

Here we are interested in the development of a scalable domain decomposition algorithm for the solution of contact problems with a given (Tresca) friction. Let us recall that a domain decomposition algorithm is *(numerically) scalable* if its rate of convergence does not deteriorate when the number of subdomains grows (see [57], Definition 3.1), and it enjoys the *parallel scalability* if the cost of the solution can be reduced nearly proportionally to the number of available processors. If the cost of the solution of auxiliary subdomain problems is nearly fixed, then the scalable algorithm enjoys asymptotically linear complexity as long as the cost of its initialization is a proportional part of the overall costs. Since the cost of the solution of any problem increases at least linearly with the number of the unknowns, it follows that the development of a scalable algorithm for contact problems is a challenging task which requires to identify the contact conditions in a sense for free.

In spite of this, there has been made a considerable effort in this direction and a number of interesting results have been obtained. Most of the results, either experimental or theoretical, were obtained for the problems discretized by the Finite Element Method (FEM), either in the framework of the domain decomposition methods, see, e.g., SCHÖBERL [53], DUREISSEIX and FARHAT [23], AVERY and FARHAT [1], or by the multigrid methods, see, e.g., KORNHUBER [34], KORNHUBER and KRAUSE [35], and WOHLMUTH and KRAUSE [59]. Most recently, a theoretically supported algorithm for both coercive and semi-coercive contact problems was presented by DOSTÁL et al. [18, 19, 21].

A number of researchers developed effective algorithms also for the solution of contact problems by Boundary Element Method (BEM), including problems with friction [25], problems discretized by mortars [43], or semi-coercive problems [15]. The main benefit of the application of the BEM, as compared with the more popular FEM, is that the formulation of the problem is reduced to the boundary of the underlying domain which yields a significant dimension reduction. In particular, BEM is desirable, e.g., when dealing with large or unbounded domains [39, 49] or shape optimization problems [8]. However, since BEM requires the explicit knowledge of a fundamental solution of a given partial differential operator, it is applicable only to the problems involving materials with rather simple properties.

The point of this paper is to review our recent results in the development of scalable total BETI (TBETI) based domain decomposition algorithms for the solution of multibody contact problems of linear elastostatics. We consider the frictionless problems, the problems with a given (Tresca) friction, and the problems with the Coulomb friction. The scalability is reported for the frictionless problems, for the problems with the Tresca friction, and for the fixed point iterations which implement the Coulomb friction. We use the direct approach, which reformulates the boundary value problem in terms of the Boundary Integral Equations (BIEs) and the unknown Cauchy data (trace of the solution and its corresponding conormal derivative) are

found by solving these BIEs. We combine the direct method with the Galerkin discretization; though we have to handle double boundary integrals instead of a single boundary integration that arises from the application of the collocation method, we get the stiffness matrices that are closely related to the Schur complements of the matrices arising from FEM.

For the frictionless problems, our main tools are our in a sense optimal quadratic programming algorithms [11] and the Boundary Element Tearing and Interconnecting (BETI) method – a combination of the symmetric Galerkin BEM with the duality based Domain Decomposition (DD) approach – as it was originally introduced by LANGER and STEINBACH [40]. The essential idea behind DD methods is splitting the original boundary value problem into local problems on smaller subdomains that decompose the underlying domains which correspond to the bodies involved in the problem. The local problems are then coupled by suitable transmission conditions introduced on the artificial interfaces between subdomains. We use the "All Floating" or "Total" variant of the BETI method introduced independently by OF [45, 46, 47] and DOSTÁL, HORÁK, and KUČERA [17], respectively. This approach enforces the Dirichlet boundary conditions by additional Lagrange multipliers, so that the kernels of the stiffness matrices of all the subdomains are a priori known. After the application of duality, we use preconditioning by the projectors to the natural coarse subspace with the solution that was originally proposed by FARHAT et al. [27] for preconditioning of their FETI method. Since LANGER and STEINBACH showed in [40] that the discrete approximate Steklov–Poincaré operators generated by the FETI and BETI methods are spectrally equivalent, we can exploit the analysis of FARHAT et al. [27] to get the bounds on the spectrum of the preconditioned dual stiffness matrix independent of the discretization and decomposition parameters h and H, respectively. Let us point out that although our method is based on that introduced by LANGER and STEINBACH [40], we cannot use their preconditioning strategy, since their preconditioner transforms the bound constraints into more general inequalities, which prevents the application of our optimal algorithms.

To generalize our results to the problems with the Tresca friction, we use the dualization technique to reduce the conditions of equilibrium to the minimization of the same type cost function as in the frictionless case, but on a smaller feasible set that is specified by additional circular constraints. Since we have recently proposed modification of our quadratic programming algorithms (see DOSTÁL and KUČERA [13] or DOSTÁL and KOZUBEK [12]) so that they can solve the separable QPQC problems with the same optimality properties, it simply follows that we can use them to get scalable algorithms also for the problems with a given friction. The theoretical results are illustrated by the results of numerical solution of simple problems of academic interest. We also show the results for the problems with the Coulomb friction computed by plugging our optimal Tresca solver into the fixed point iterations for the solution of the problems with the Coulomb friction [32]. The power of the methods presented here is illustrated also by numerical solution of a real world problem.

2 Steklov–Poincaré Operator for 3D Linear Elastostatics

Let us briefly recall several well-known results concerning boundary integral operators. Note that more details can be found, e.g., in [9, 44, 50, 52, 56].

Let $\Omega \subset \mathbb{R}^3$ be a bounded Lipschitz domain with the boundary Γ which is filled with a homogeneous isotropic material and consider the elliptic partial differential operator $\mathscr{L}$ defined by

$$(\mathscr{L}\underline{u})_i(x) := -\sum_{j=1}^{3} \frac{\partial}{\partial x_j}\sigma_{ij}(\underline{u},x) \quad \text{for } x \in \Omega,\ i = 1,2,3,$$

where the stress tensor σ satisfies Hooke's law

$$\sigma_{ij}(\underline{u},x) := \frac{E\nu}{(1+\nu)(1-2\nu)}\delta_{ij}\sum_{k=1}^{3} e_{kk}(\underline{u},x) + \frac{E}{1+\nu}e_{ij}(\underline{u},x) \quad \text{for } i,j = 1,2,3$$

with the linearized strain tensor e given by

$$e_{ij}(\underline{u},x) := \frac{1}{2}\left(\frac{\partial}{\partial x_i}u_j(x) + \frac{\partial}{\partial x_j}u_i(x)\right) \quad \text{for } i,j = 1,2,3,$$

Young's modulus $E \in \mathbb{R}^+$, and Poisson's ratio $\nu \in (0,1/2)$. Both E and ν are constants.

Let us recall the standard interior trace and boundary traction operators

$$\gamma_0 :\ [H^1(\Omega)]^3 \mapsto [H^{1/2}(\Gamma)]^3 \quad \text{and} \quad \gamma_1 :\ [H^1_{\mathscr{L}}(\Omega)]^3 \mapsto [H^{-1/2}(\Gamma)]^3,$$

respectively, where $H^{1/2}(\Gamma)$ denotes the trace space of $H^1(\Omega)$, $H^{-1/2}(\Gamma)$ is the dual space to $H^{1/2}(\Gamma)$ with respect to the $L^2(\Gamma)$ scalar product, and

$$[H^1_{\mathscr{L}}(\Omega)]^3 := \left\{\underline{v} \in [H^1(\Omega)]^3 :\ \mathscr{L}\underline{v} \in [L^2(\Omega)]^3\right\}.$$

It is well-known [9, 44, 56] that for any $\underline{u} \in [H^1_{\mathscr{L}}(\Omega)]^3$ there exists the Dirichlet–Neumann map

$$\gamma_1\underline{u}(x) = (S\gamma_0\underline{u})(x) - (N\mathscr{L}\underline{u})(x) \quad \text{for } x \in \Gamma$$

with the Steklov–Poincaré operator

$$S := (\sigma I + K')V^{-1}(\sigma I + K) + D :\ [H^{1/2}(\Gamma)]^3 \mapsto [H^{-1/2}(\Gamma)]^3, \tag{1}$$

where $\sigma(x) = 1/2$ for almost all $x \in \Gamma$, and the Newton operator

$$N := V^{-1}N_0 :\ [L^2(\Omega)]^3 \mapsto [H^{-1/2}(\Gamma)]^3. \tag{2}$$

In (1) and (2) we use the single layer potential operator V, double layer potential operator K, adjoint double layer potential operator K', hypersingular integral operator

D given for $x \in \Gamma$ and $i = 1,2,3$ by

$$(V\underline{t})_i(x) := \int_\Gamma (\underline{t}(y), \underline{U}_i(x,y))\,\mathrm{d}s_y, \quad V:\ [H^{-1/2}(\Gamma)]^3 \mapsto [H^{1/2}(\Gamma)]^3,$$

$$(K\underline{u})_i(x) := \int_\Gamma (\underline{u}(y), \gamma_{1,y}\underline{U}_i(x,y))\,\mathrm{d}s_y, \quad K:\ [H^{1/2}(\Gamma)]^3 \mapsto [H^{1/2}(\Gamma)]^3,$$

$$(K'\underline{t})_i(x) := \int_\Gamma (\underline{t}(y), \gamma_{1,x}\underline{U}_i(x,y))\,\mathrm{d}s_y, \quad K':\ [H^{-1/2}(\Gamma)]^3 \mapsto [H^{-1/2}(\Gamma)]^3,$$

$$(D\underline{u})_i(x) := -\gamma_{1,x}\int_\Gamma (\underline{u}(y), \gamma_{1,y}\underline{U}_i(x,y))\,\mathrm{d}s_y, \quad D:\ [H^{1/2}(\Gamma)]^3 \mapsto [H^{-1/2}(\Gamma)]^3,$$

and the Newton potential operator N_0 given for $x \in \Gamma$ and $i = 1,2,3$ by

$$(N_0\underline{f})_i(x) := \int_\Omega \big(\underline{f}(y), \underline{U}_i(x,y)\big)\,\mathrm{d}y, \qquad N_0:\ [L^2(\Omega)]^3 \mapsto [H^{1/2}(\Gamma)]^3.$$

By U we mean the fundamental solution of $\mathscr{L}$ called the Kelvin tensor that is given for $x, y \in \mathbb{R}^3$ and $i, j = 1,2,3$ by

$$U_{ij}(x,y) := \frac{1+\nu}{8\pi E(1-\nu)}\left((3-4\nu)\frac{\delta_{ij}}{\|x-y\|} + \frac{(x_i-y_i)(x_j-y_j)}{\|x-y\|^3}\right).$$

Moreover, $\underline{U}_j := (U_{1j}, U_{2j}, U_{3j})$ and by $(\cdot,\cdot)$ and $\|\cdot\|$ we denote the Euclidean scalar product and norm, respectively. The mapping properties of the above integral operators are well-known [9, 56], in particular, the single layer potential operator V is $[H^{-1/2}(\Gamma)]^3$–elliptic, so its inversion exists. In what follows, these two lemmas are useful:

Lemma 1 ([56]). *The Steklov–Poincaré operator S is linear, bounded, symmetric, and semi–elliptic on $[H^{1/2}(\Gamma)]^3$. Moreover, the kernel of S is equal to the space of the linearized rigid body motions, i.e.,*

$$\mathrm{Ker}\, S = \mathrm{span}\left\{\begin{pmatrix}1\\0\\0\end{pmatrix}, \begin{pmatrix}0\\1\\0\end{pmatrix}, \begin{pmatrix}0\\0\\1\end{pmatrix}, \begin{pmatrix}-x_2\\x_1\\0\end{pmatrix}, \begin{pmatrix}0\\-x_3\\x_2\end{pmatrix}, \begin{pmatrix}x_3\\0\\-x_1\end{pmatrix}\right\}.$$

Lemma 2 ([56]). *The Newton operator N is linear and bounded on $[L^2(\Omega)]^3$.*

3 Multibody Contact Problem without Friction

We consider a system of s homogeneous isotropic elastic bodies whose reference configurations occupy bounded Lipschitz domains

$$\Omega^p \subset \mathbb{R}^3, \quad p = 1, 2, \ldots, s$$

with the boundaries

$$\Gamma^p := \partial\Omega^p, \quad p = 1, 2, \ldots, s,$$

each of which comprises three non-overlapping parts

$$\Gamma_d^p,\ \Gamma_n^p, \text{ and } \Gamma_c^p, \quad p = 1, 2, \ldots, s,$$

denoting the Dirichlet, Neumann, and contact boundary of the pth body, respectively. In particular, we denote by Γ_c^{pq} a part of Γ_c^p that is allowed to be in contact with the body Ω^q. The mechanical properties of Ω^p are characterized by the Young modulus $E^p \in \mathbb{R}^+$ and the Poisson ratio $\nu^p \in (0, 1/2)$ which are assumed to be constant for each Ω^p. An example of a reference configuration of a multibody contact problem can be seen in Fig. 1. To enable the contact with rigid obstacles, we admit the bodies with a priori defined zero displacements on the whole boundary as it can be seen in Fig. 1.

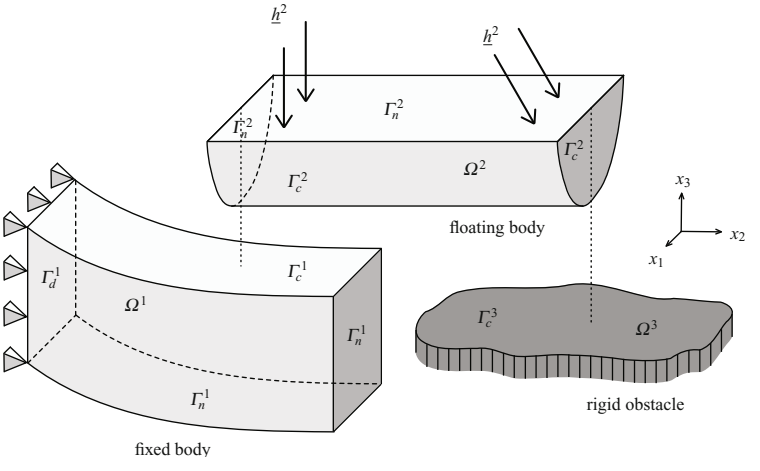

Fig. 1 Multibody contact problem

In the following, we denote by $\underline{u}^p : \Gamma^p \mapsto \mathbb{R}^3$ the boundary displacements corresponding to the pth body. Moreover, the imposed boundary displacements, boundary tractions, and the volume forces acting inside Ω^p are denoted by

$$\underline{g}^p \in [H^{1/2}(\Gamma_d^p)]^3, \quad \underline{h}^p \in [L^2(\Gamma_n^p)]^3, \quad \text{and} \quad \underline{f}^p \in [L^2(\Omega^p)]^3,$$

respectively.

To describe the linearized non-interpenetration conditions, let us define for each $p < q$ and non-empty Γ_c^{pq} a one-to-one continuous mapping

$$\underline{\mathscr{O}}^{pq} : \Gamma_c^{pq} \mapsto \Gamma_c^{qp},$$

so that $\underline{\mathscr{O}}^{pq}(x) \in \Gamma_c^{qp}$ is a "near" point to $x \in \Gamma_c^{pq}$. Now for each $p < q$ the linearized non-interpenetration condition is given by

$$(\underline{u}^p(x) - \underline{u}^q(\underline{\mathscr{O}}^{pq}(x)), \underline{n}^p(x)) \leq (\underline{\mathscr{O}}^{pq}(x) - x, \underline{n}^p(x)) \quad \text{for } x \in \Gamma_c^{pq}, \tag{3}$$

where $\underline{n}^p(x)$ is the outer unit normal vector to Ω^p at x; see Fig. 2. More details can also be found in [33, 60].

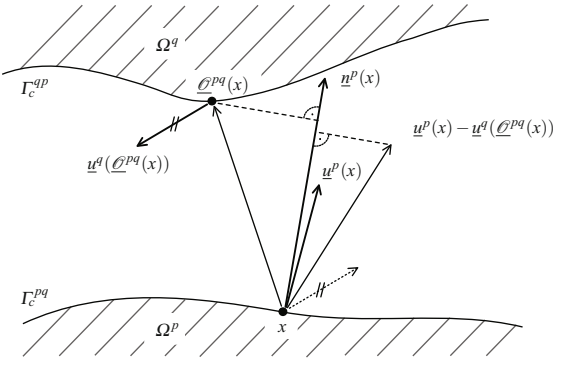

Fig. 2 The linearized non-interpenetration in 2D

Now let us introduce the Sobolev product space

$$\mathscr{V} := [H^{1/2}(\Gamma^1)]^3 \times \cdots \times [H^{1/2}(\Gamma^s)]^3$$

equipped with the norm

$$\|\underline{v}\|_{\mathscr{V}} := \left(\sum_{p=1}^{s} \|\underline{v}^p\|^2_{[H^{1/2}(\Gamma^p)]^3} \right)^{1/2} \quad \text{for } \underline{v} = (\underline{v}^1, \ldots, \underline{v}^s) \in \mathscr{V}.$$

For any displacement $\underline{u} = (\underline{u}^1, \ldots, \underline{u}^s) \in \mathscr{V}$ let us define the so-called energy functional by

$$\mathscr{J}_E(\underline{u}) := \frac{1}{2}\mathscr{A}(\underline{u}, \underline{u}) - \mathscr{F}(\underline{u}),$$

where $\mathscr{A}$ is a bilinear form on $\mathscr{V}$ defined by

$$\mathscr{A}(\underline{u}, \underline{v}) := \sum_{p=1}^{s} \langle S^p \underline{u}^p, \underline{v}^p \rangle_{\Gamma^p}$$

and $\mathscr{F}$ is a linear functional on $\mathscr{V}$ given by

$$\mathscr{F}(\underline{v}) := \sum_{p=1}^{s} \left\{ \langle N^p \underline{f}^p, \underline{v}^p \rangle_{\Gamma^p} + \langle \underline{h}^p, \underline{v}^p \rangle_{\Gamma_n^p} \right\}$$

with

$$\langle \underline{w}, \underline{y} \rangle_{\Gamma^p} := \sum_{i=1}^{3} \langle w_i, y_i \rangle_{L^2(\Gamma^p)}.$$

By

$$S^p : \ [H^{1/2}(\Gamma^p)]^3 \mapsto [H^{-1/2}(\Gamma^p)]^3 \quad \text{and} \quad N^p : \ [L^2(\Omega^p)]^3 \mapsto [H^{-1/2}(\Gamma^p)]^3$$

we denote the (local) Steklov–Poincaré and Newton operators, respectively, whose properties are shortly discussed in Sect. 2. Furthermore, let

$$\mathscr{K}_d := \left\{ \underline{v} = (\underline{v}^1, \ldots, \underline{v}^s) \in \mathscr{V} : \ \underline{v}^p = \underline{g}^p \quad \text{on } \Gamma_d^p \quad \text{for } p = 1, \ldots, s \right\},$$

$$\mathscr{K}_c := \left\{ \underline{v} = (\underline{v}^1, \ldots, \underline{v}^s) \in \mathscr{V} : \ (\underline{v}^p(x) - \underline{v}^q(\underline{\mathscr{O}}^{pq}(x)), \underline{n}^p(x)) \ \leq \right.$$
$$\left. (\underline{\mathscr{O}}^{pq}(x) - x, \underline{n}^p(x)) \quad \text{for } x \in \Gamma_c^{pq}, \ p, q = 1, \ldots, s, \text{ and } p < q \right\},$$

and

$$\mathscr{K} := \mathscr{K}_d \cap \mathscr{K}_c.$$

Note that $\mathscr{K}$ is a non-empty, closed, and convex subset of $\mathscr{V}$.

A potential energy minimization problem now reads: find the displacement $\underline{u} \in \mathscr{K}$ such that

$$\mathscr{J}_E(\underline{u}) = \min\{ \mathscr{J}_E(\underline{v}) : \ \underline{v} \in \mathscr{K} \}. \tag{4}$$

Due to Lemmas 1 and 2, the bilinear form $\mathscr{A}$ is bounded, symmetric, and semi-elliptic on $\mathscr{V}$ and the linear functional $\mathscr{F}$ is bounded on $\mathscr{V}$. Thus $\mathscr{J}_E$ is a convex quadratic functional on $\mathscr{V}$. The remaining conditions that guarantee the existence and uniqueness of the solution of (4), in particular, the coercivity of $\mathscr{J}_E$ on $\mathscr{K}$, may be found, for instance, in [32].

4 Multibody Contact Problem with Tresca Friction

To enhance the *Tresca friction law* into the variational formulation of the conditions of equilibrium, we introduce the functional $\mathscr{J}_T$ on $\mathscr{V}$ that describes the work of friction forces in the weak formulation of the problem (see, e.g., DUVAUT and LIONS [24]). It is defined by

$$\mathscr{J}_T(\underline{u}) := \sum_{p<q} \int_{\Gamma_c^{pq}} \xi^{pq}(x) \|\underline{u}_t^{pq}(x)\| \mathrm{d}s_x \quad \text{for } \underline{u} = (\underline{u}^1, \ldots, \underline{u}^s) \in \mathscr{V}, \tag{5}$$

where $\xi^{pq} : \ \Gamma_c^{pq} \mapsto \mathbb{R}^+$ is the non-negative slip bound and $\underline{u}_t^{pq}(x)$ represents the jump in the tangential displacements at x on Γ^{pq} and $\underline{\mathscr{O}}^{pq}(x)$ on Γ^{qp}, $p < q$. In order to describe $\underline{u}_t^{pq}$ effectively, let us define for any $x \in \Gamma_c^{pq}$ an orthonormal basis $\{\underline{t}_1^p(x), \underline{t}_2^p(x), \underline{n}^p(x)\}$ of $\mathbb{R}^3$ with the origin at x. Then

$$\underline{u}_t^{pq} = u_{t_1}^{pq} \underline{t}_1^p + u_{t_2}^{pq} \underline{t}_2^p,$$

where

$$u_{t_i}^{pq}(x) := \big(\underline{u}^p(x) - \underline{u}^q(\underline{\mathscr{O}}^{pq}(x)), \underline{t}_i^p(x)\big) \quad \text{for } i = 1,2,$$

and so

$$\|\underline{u}_t^{pq}(x)\| = \big\{(u_{t_1}^{pq}(x))^2 + (u_{t_2}^{pq}(x))^2\big\}^{1/2} \quad \text{for } x \in \Gamma_c^{pq}.$$

Notice that $\mathscr{J}_T$ is not differentiable.

For any displacement $\underline{u} = (\underline{u}^1, \ldots, \underline{u}^s) \in \mathscr{V}$ let us define the energy functional $\mathscr{J}$ with the dissipative term $\mathscr{J}_T$ by

$$\mathscr{J}(\underline{u}) := \mathscr{J}_E(\underline{u}) + \mathscr{J}_T(\underline{u}) = \frac{1}{2}\mathscr{A}(\underline{u},\underline{u}) - \mathscr{F}(\underline{u}) + \mathscr{J}_T(\underline{u}).$$

The condition of equilibrium in terms of a potential energy minimization problem now reads: find the displacement $\underline{u} \in \mathscr{K}$ such that

$$\mathscr{J}(\underline{u}) = \min\{\mathscr{J}(\underline{v}) : \underline{v} \in \mathscr{K}\} \tag{6}$$

with $\mathscr{K}$ being the same as in (4).

Due to Lemmas 1 and 2, the bilinear form $\mathscr{A}$ is bounded, symmetric, and semi-elliptic on $\mathscr{V}$ and the linear functional $\mathscr{F}$ is bounded on $\mathscr{V}$. Thus the energy functional $\mathscr{J}$ is continuous and convex on $\mathscr{V}$. The remaining conditions that guarantee the existence and uniqueness of the solution of (6), in particular, the coercivity of $\mathscr{J}$ on $\mathscr{K}$, may be found, for instance, in [32].

5 TBETI Domain Decomposition

First notice that the frictionless contact problem is a special case of the problem with the Tresca friction with zero slip bounds. Thus we can restrict our exposition to the problem with the Tresca friction except the solution algorithms which can benefit from the specific structure of the frictionless contact problems.

To enable efficient parallel solution of our problem, let us first "tear" each body from the part of the boundary with the Dirichlet boundary condition, and then decompose each body into non-overlapping Lipschitz subdomains, assign each subdomain a unique number, and introduce new "gluing" conditions on the artificial intersubdomain boundaries and on the boundaries with imposed Dirichlet condition. Furthermore, let Γ_g^p and Γ_g^{pq} denote the part of Γ^p that is glued to the other subdomains and the part of Γ^p that is glued to Ω^q, respectively. A decomposition of the problem in Fig. 1 with renumbered subdomains and artificial intersubdomain boundaries can be seen in Fig. 3. The gluing conditions require continuity of the boundary displacements and boundary tractions across the intersubdomain boundaries. From now on, s means the number of all subdomains after the decomposition.

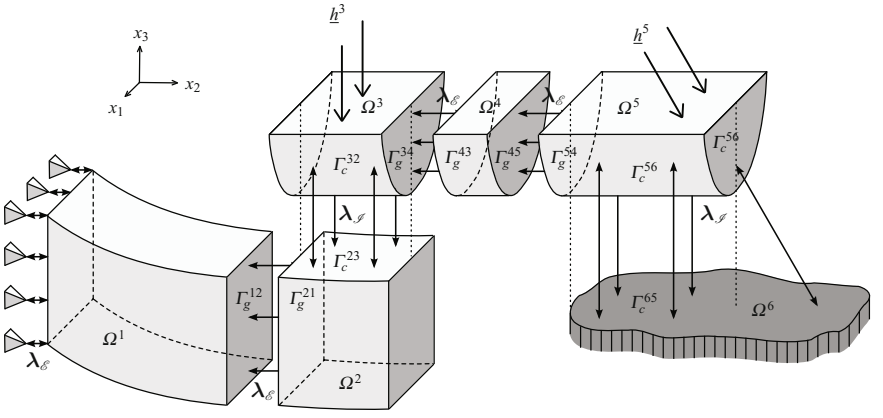

Fig. 3 TBETI domain decomposition of the problem in Fig. 1 with renumbering

In what follows, we use the symbols $\mathscr{I}$ and $\mathscr{E}$ to distinguish between the sets of indices corresponding to the non-interpenetration and equality constraints, respectively. After introducing suitable approximations $\widetilde{S}^p$ and $\widetilde{N}^p$ of the operators S^p and N^p, respectively, by using the boundary element method [40, 55], we apply the boundary element discretization of Γ^p into L^p plane triangles and M^p boundary nodes, $p = 1, \ldots, s$, that results in the quadratic programming problem

$$\text{minimize} \quad J(\mathbf{v}) \quad \text{subject to} \quad \mathsf{B}_{\mathscr{I}}\mathbf{v} \le \mathbf{c}_{\mathscr{I}} \quad \text{and} \quad \mathsf{B}_{\mathscr{E}}\mathbf{v} = \mathbf{c}_{\mathscr{E}}, \tag{7}$$

where

$$J(\mathbf{v}) := \frac{1}{2}\mathbf{v}^\top \widetilde{\mathsf{S}}\mathbf{v} - \widetilde{\mathbf{r}}^\top \mathbf{v} + J_T(\mathbf{v}),$$

$$\widetilde{\mathsf{S}} := \begin{pmatrix} \widetilde{\mathsf{S}}^1 & \mathsf{O} & \mathsf{O} \\ \mathsf{O} & \ddots & \mathsf{O} \\ \mathsf{O} & \mathsf{O} & \widetilde{\mathsf{S}}^s \end{pmatrix}, \quad \mathbf{v} := \begin{pmatrix} \mathbf{v}^1 \\ \vdots \\ \mathbf{v}^s \end{pmatrix}, \quad \mathbf{v}^p := \begin{pmatrix} \mathbf{v}_1^p \\ \mathbf{v}_2^p \\ \mathbf{v}_3^p \end{pmatrix}, \quad \widetilde{\mathbf{r}} := \begin{pmatrix} \widetilde{\mathbf{r}}^1 \\ \vdots \\ \widetilde{\mathbf{r}}^s \end{pmatrix},$$

and $J_T(\mathbf{v})$ denotes the discretized dissipative term.

In the above, $\widetilde{\mathsf{S}}^p \in \mathbb{R}^{3M^p \times 3M^p}$ represents the discrete approximate Steklov–Poincaré operator

$$\widetilde{\mathsf{S}}^p := \mathsf{D}^p + (\frac{1}{2}\mathsf{M}^p + \mathsf{K}^p)^\top (\mathsf{V}^p)^{-1} (\frac{1}{2}\mathsf{M}^p + \mathsf{K}^p), \tag{8}$$

and $\widetilde{\mathbf{r}}^p \in \mathbb{R}^{3M^p}$ represents the discretized forces. Here, V^p, K^p, and D^p denote the discrete single layer, double layer, and hypersingular operators, respectively. Details about suitable representations of these discrete operators can be found in [31, 38, 50, 56]. Note that V^p, K^p, and D^p are all fully populated. Moreover, the matrices V^p and D^p are symmetric positive definite and semi-definite, respectively.

To evaluate the entries of the boundary element matrices we have to calculate (possibly singular) double surface integrals. To do this, one can use several different approaches. One method is the so-called semi-analytical approach introduced by RJASANOW and STEINBACH in [50], where the inner integral is calculated analytically and the outer one is approximated by using a suitable numerical scheme. Another possibility is to use the quadrature formulae based on the Duffy transformation that removes the kernel singularity, as shown by SAUTER and SCHWAB in [52]. However, both these approaches lead to asymptotically quadratic space and time complexities when evaluating the matrices. To avoid this drawback, we decompose the domains into many small subdomains. Though the corresponding subdomain matrices are full, they are of small size. In our experiments, we keep the number of elements L^p less than 2000. Alternatively, one can use other fast techniques such as Adaptive Cross Approximation (ACA) [4, 3] or Fast Multipole Method (FMM) [29, 30, 48, 42] which accelerate the evaluation of the matrices and the consequent matrix–vector multiplication and lead to asymptotically nearly linear space and time complexities.

The mass matrix M^p corresponds to the discretized identity and the discrete approximate Newton operator $\widetilde{\mathbf{r}}^p$ is given by

$$\widetilde{\mathbf{r}}^p := (\mathsf{M}^p)^\top \left[(\mathsf{V}^p)^{-1} \mathbf{n}_0^p + \widehat{\mathbf{h}}^p \right].$$

The vector $\mathbf{n}_0^p$ denotes the discrete Newton potential whose evaluation requires the computation of $N_0^p \underline{f}^p$. This can be done by using an indirect approach, as it is introduced in [54, 55], or another possibility is the direct evaluation of $N_0^p \underline{f}^p$ requiring, however, a 3D mesh of Ω^p.

Finally, let us consider the zero extension $\widehat{\underline{h}}^p$ of the imposed boundary traction $\underline{h}^p$ from Γ_n^p to Γ^p. Typically, we approximate the components of $\widehat{\underline{h}}^p$ by piecewise constant trial functions and the element values of the approximated components of $\widehat{\underline{h}}^p$ then correspond to the entries of the vector $\widehat{\mathbf{h}}^p \in \mathbb{R}^{3L^p}$.

It remains to describe the constraining matrices $\mathsf{B}_{\mathscr{I}} \in \mathbb{R}^{m_{\mathscr{I}} \times n}$, $\mathsf{B}_{\mathscr{E}} \in \mathbb{R}^{m_{\mathscr{E}} \times n}$, $n := \sum_{p=1}^{s} 3M^p$, and vectors $\mathbf{c}_{\mathscr{I}} \in \mathbb{R}^{m_{\mathscr{I}}}$, $\mathbf{c}_{\mathscr{E}} \in \mathbb{R}^{m_{\mathscr{E}}}$ arising in (7). First, note that both matrices $\mathsf{B}_{\mathscr{I}}$ and $\mathsf{B}_{\mathscr{E}}$ are constructed as full rank matrices. The matrix $\mathsf{B}_{\mathscr{I}}$ and the vector $\mathbf{c}_{\mathscr{I}}$ correspond to the linearized non-interpenetration conditions. The rows $\mathbf{b}_{\mathscr{I},i}$ of $\mathsf{B}_{\mathscr{I}}$ are formed by zeros and appropriately placed multiples of coordinates of the outer unit normals, so that the change of the normal distance due to the displacement $\mathbf{v}$ is given by $\mathbf{b}_{\mathscr{I},i}\mathbf{v}$, and the entry $\mathbf{c}_{\mathscr{I},i}$ describes the gap in the normal direction between the ith couple of the corresponding nodes on the contact interface in the reference configuration.

The matrix $\mathsf{B}_{\mathscr{E}}$ with the rows $\mathbf{b}_{\mathscr{E},i}$ and the vector $\mathbf{c}_{\mathscr{E}}$ with the entries $\mathbf{c}_{\mathscr{E},i}$ enforce the prescribed displacements on the part of the boundary with imposed Dirichlet condition and the continuity of the displacements across the auxiliary interfaces. The rows $\mathbf{b}_{\mathscr{E},i}$ of $\mathsf{B}_{\mathscr{E}}$ are vectors with zero entries except 1 and -1 at appropriate positions. Moreover, note that the continuity condition requires that $\mathbf{b}_{\mathscr{E},i}\mathbf{v} = \mathbf{c}_{\mathscr{E},i} = 0$.

To define the non-differentiable term $J_T(\mathbf{v})$, let us introduce an $m_{\mathscr{J}} \times 1$ block and full rank matrix T whose blocks $\mathsf{T}_i = \mathsf{T}_i(\mathbf{x}_i) \in \mathbb{R}^{2\times n}$ are formed by appropriately placed multiples of the unit tangential vectors $\mathbf{t}_1(\mathbf{x}_i)$ and $\mathbf{t}_2(\mathbf{x}_i)$ so that the jump in the tangential displacements at $\mathbf{x}_i$ and $\underline{\mathscr{O}}^{pq}(\mathbf{x}_i)$ is given by $\mathsf{T}_i\mathbf{v} \in \mathbb{R}^2$. Note that $\mathbf{x}_i$ denotes a node located on Γ_c^{pq} and $\underline{\mathscr{O}}^{pq}(\mathbf{x}_i)$ on Γ_c^{qp}, $p < q$. After applying a numerical integration to (5), we get

$$J_T(\mathbf{v}) = \sum_{i=1}^{m_{\mathscr{J}}} \xi_i \|\mathsf{T}_i\mathbf{v}\|, \tag{9}$$

where ξ_i denotes the slip bound associated with T_i. Using the standard procedure (see, e.g., [32]) to modify the non-differentiable term $J_T(\mathbf{v})$ given by (9), we get

$$J_T(\mathbf{v}) = \sum_{i=1}^{m_{\mathscr{J}}} \max_{\|\boldsymbol{\tau}_i\| \le \xi_i} \boldsymbol{\tau}_i^\top \mathsf{T}_i\mathbf{v},$$

where $\boldsymbol{\tau}_i \in \mathbb{R}^2$ can be considered as a Lagrange multiplier.

6 Dual Formulation

Problem (7) is not suitable for numerical computations since its stiffness matrix $\widetilde{\mathsf{S}}$ is typically ill-conditioned and singular, and the feasible set is in general so complex that projections into it can hardly be effectively computed. Thus it would be very difficult to achieve a fast identification of the active set at the solution and a fast solution of the auxiliary linear problems.

The complications mentioned above may be essentially reduced by applying the duality theory of convex programming [2, 11]. First, let us define three types of Lagrange multipliers: $\boldsymbol{\lambda}_{\mathscr{J}} \in \mathbb{R}^{m_{\mathscr{J}}}$ corresponding to the non-interpenetration condition, $\boldsymbol{\lambda}_{\mathscr{E}} \in \mathbb{R}^{m_{\mathscr{E}}}$ associated with the "gluing" and imposed Dirichlet conditions, and

$$\boldsymbol{\tau} := (\boldsymbol{\tau}_1^\top, \boldsymbol{\tau}_2^\top, \ldots, \boldsymbol{\tau}_{m_{\mathscr{J}}}^\top)^\top \in \mathbb{R}^{2m_{\mathscr{J}}}$$

regularizing the non-differentiability. The Lagrangian associated with problem (7) is given as

$$L(\mathbf{v}, \boldsymbol{\lambda}_{\mathscr{J}}, \boldsymbol{\lambda}_{\mathscr{E}}, \boldsymbol{\tau}) := \frac{1}{2}\mathbf{v}^\top \widetilde{\mathsf{S}}\mathbf{v} - \widetilde{\mathbf{r}}^\top\mathbf{v} + \boldsymbol{\tau}^\top\mathsf{T}\mathbf{v} + \boldsymbol{\lambda}_{\mathscr{J}}^\top(\mathsf{B}_{\mathscr{J}}\mathbf{v} - \mathbf{c}_{\mathscr{J}}) + \boldsymbol{\lambda}_{\mathscr{E}}^\top(\mathsf{B}_{\mathscr{E}}\mathbf{v} - \mathbf{c}_{\mathscr{E}}).$$

Note that the both cost function and constraints are convex, so that we can use the classical duality theory [2] to reformulate problem (7) to obtain

$$\inf_{\mathbf{v}} \sup_{\substack{\boldsymbol{\lambda}_{\mathscr{E}} \in \mathbb{R}^{m_{\mathscr{E}}},\ \boldsymbol{\lambda}_{\mathscr{J}} \ge \mathbf{0} \\ \|\boldsymbol{\tau}_i\| \le \xi_i,\ i=1,\ldots,m_{\mathscr{J}}}} L(\mathbf{v}, \boldsymbol{\lambda}_{\mathscr{J}}, \boldsymbol{\lambda}_{\mathscr{E}}, \boldsymbol{\tau}) = \sup_{\substack{\boldsymbol{\lambda}_{\mathscr{E}} \in \mathbb{R}^{m_{\mathscr{E}}},\ \boldsymbol{\lambda}_{\mathscr{J}} \ge \mathbf{0} \\ \|\boldsymbol{\tau}_i\| \le \xi_i,\ i=1,\ldots,m_{\mathscr{J}}}} \inf_{\mathbf{v}} L(\mathbf{v}, \boldsymbol{\lambda}_{\mathscr{J}}, \boldsymbol{\lambda}_{\mathscr{E}}, \boldsymbol{\tau})$$

Introducing the notation

$$\boldsymbol{\lambda} := \begin{pmatrix} \boldsymbol{\lambda}_{\mathscr{I}} \\ \boldsymbol{\lambda}_{\mathscr{E}} \\ \boldsymbol{\tau} \end{pmatrix}, \quad \mathsf{B} := \begin{pmatrix} \mathsf{B}_{\mathscr{I}} \\ \mathsf{B}_{\mathscr{E}} \\ \mathsf{T} \end{pmatrix}, \quad \mathbf{c} := \begin{pmatrix} \mathbf{c}_{\mathscr{I}} \\ \mathbf{c}_{\mathscr{E}} \\ \mathbf{0} \end{pmatrix}$$

and

$$\Lambda(\xi) := \left\{ (\boldsymbol{\lambda}_{\mathscr{I}}^\top, \boldsymbol{\lambda}_{\mathscr{E}}^\top, \boldsymbol{\tau}^\top)^\top \in \mathbb{R}^{m_{\mathscr{E}}+3m_{\mathscr{I}}} : \boldsymbol{\lambda}_{\mathscr{I}} \geq \mathbf{0},\ \|\boldsymbol{\tau}_i\| \leq \xi_i,\ i = 1, \ldots, m_{\mathscr{I}} \right\},$$

one can write the Lagrangian briefly as

$$L(\mathbf{v}, \boldsymbol{\lambda}) = \frac{1}{2}\mathbf{v}^\top \widetilde{\mathsf{S}}\mathbf{v} - \widetilde{\mathbf{r}}^\top \mathbf{v} + \boldsymbol{\lambda}^\top (\mathsf{B}\mathbf{v} - \mathbf{c})$$

and problem (7) is equivalent [11] to the saddle point problem

$$L(\mathbf{u}, \widehat{\boldsymbol{\lambda}}) = \max_{\boldsymbol{\lambda} \in \Lambda(\xi)} \min_{\mathbf{v}} L(\mathbf{v}, \boldsymbol{\lambda}). \tag{10}$$

For a fixed $\boldsymbol{\lambda}$, the Lagrange function $L(\cdot, \boldsymbol{\lambda})$ is convex in the first variable and the minimizer $\mathbf{u}$ of $L(\cdot, \boldsymbol{\lambda})$ satisfies

$$\widetilde{\mathsf{S}}\mathbf{u} - \widetilde{\mathbf{r}} + \mathsf{B}^\top \boldsymbol{\lambda} = \mathbf{0}. \tag{11}$$

Note that equation (11) has essentially the same structure as the dual FETI formulation in [27] and the next steps basically follow the literature. Equation (11) has a solution iff

$$\widetilde{\mathbf{r}} - \mathsf{B}^\top \boldsymbol{\lambda} \in \operatorname{Im} \widetilde{\mathsf{S}}, \tag{12}$$

which can be expressed more conveniently by means of a full column matrix $\mathsf{R} \in \mathbb{R}^{n \times 6s}$ whose columns span the null space of $\widetilde{\mathsf{S}}$ as

$$\mathsf{R}^\top (\widetilde{\mathbf{r}} - \mathsf{B}^\top \boldsymbol{\lambda}) = \mathbf{0}.$$

Recall that the blocks $\widetilde{\mathsf{S}}^p$ of $\widetilde{\mathsf{S}}$ are positive semi-definite with the known kernel of the dimension six. Thus the matrix R may be formed directly by using any basis of the rigid body modes of the subdomains, i.e.,

$$\mathsf{R} := \begin{pmatrix} \mathsf{R}^1 & \mathsf{O} & \mathsf{O} \\ \mathsf{O} & \ddots & \mathsf{O} \\ \mathsf{O} & \mathsf{O} & \mathsf{R}^s \end{pmatrix}, \quad \mathsf{R}^p := \begin{pmatrix} \mathbf{1} & \mathbf{0} & \mathbf{0} & -\mathbf{x}_2^p & \mathbf{0} & \mathbf{x}_3^p \\ \mathbf{0} & \mathbf{1} & \mathbf{0} & \mathbf{x}_1^p & -\mathbf{x}_3^p & \mathbf{0} \\ \mathbf{0} & \mathbf{0} & \mathbf{1} & \mathbf{0} & \mathbf{x}_2^p & -\mathbf{x}_1^p \end{pmatrix} \in \mathbb{R}^{3M^p \times 6},$$

and $\mathbf{x}_i^p$ is a vector of the ith coordinates of all nodes located on Γ^p.

Now assume that $\boldsymbol{\lambda}$ satisfies (12) and denote by $\widetilde{\mathsf{S}}^+$ any left generalized inverse matrix to $\widetilde{\mathsf{S}}$, i.e.,

$$\widetilde{\mathsf{S}}\widetilde{\mathsf{S}}^{+}\widetilde{\mathsf{S}} = \widetilde{\mathsf{S}}.$$

Note that if we denote by $\widetilde{\mathsf{S}}^{p,+}$ a left generalized inverse to $\widetilde{\mathsf{S}}^{p}$, then the matrix

$$\widetilde{\mathsf{S}}^{+} := \begin{pmatrix} \widetilde{\mathsf{S}}^{1,+} & \mathsf{O} & \mathsf{O} \\ \mathsf{O} & \ddots & \mathsf{O} \\ \mathsf{O} & \mathsf{O} & \widetilde{\mathsf{S}}^{s,+} \end{pmatrix}$$

is a left generalized inverse to $\widetilde{\mathsf{S}}$. The action of $\widetilde{\mathsf{S}}^{+}$ can be evaluated in many ways [7, 26]. In the numerical experiments, we use our modification of the Cholesky factorization of $\widetilde{\mathsf{S}}^{p}$, $p = 1, \ldots, s$ [7, 22]. It may be verified directly that if $\mathbf{u}$ solves (11), then there is a vector $\alpha \in \mathbb{R}^{6s}$ such that

$$\mathbf{u} = \widetilde{\mathsf{S}}^{+}(\widetilde{\mathbf{r}} - \mathsf{B}^{\top}\boldsymbol{\lambda}) + \mathsf{R}\alpha. \tag{13}$$

After substituting expression (13) into problem (10), changing the signs, and omitting the constant term, we get that $\boldsymbol{\lambda}$ solves the minimization problem

$$\text{minimize} \quad \Theta(\boldsymbol{\lambda}) \quad \text{subject to} \quad \boldsymbol{\lambda} \in \Lambda(\xi) \quad \text{and} \quad \mathsf{G}\boldsymbol{\lambda} = \mathbf{e}, \tag{14}$$

where

$$\Theta(\boldsymbol{\lambda}) := \frac{1}{2}\boldsymbol{\lambda}^{\top}\mathsf{F}\boldsymbol{\lambda} - \boldsymbol{\lambda}^{\top}\widetilde{\mathbf{d}}$$

and

$$\mathsf{F} := \mathsf{B}\widetilde{\mathsf{S}}^{+}\mathsf{B}^{\top}, \quad \widetilde{\mathbf{d}} := \mathsf{B}\widetilde{\mathsf{S}}^{+}\widetilde{\mathbf{r}} - \mathbf{c}, \quad \mathsf{G} := \mathsf{R}^{\top}\mathsf{B}^{\top}, \quad \mathbf{e} := \mathsf{R}^{\top}\widetilde{\mathbf{r}}.$$

Once the solution $\widehat{\boldsymbol{\lambda}}$ of (14) is known, the solution $\mathbf{u}$ of (7) may be calculated by (13) with

$$\alpha = (\mathsf{R}^{\top}\mathsf{B}_{*}^{\top}\mathsf{B}_{*}\mathsf{R})^{-1}\mathsf{R}^{\top}\mathsf{B}_{*}^{\top}(\mathbf{c}_{*} - \mathsf{B}_{*}\widetilde{\mathsf{S}}^{+}(\widetilde{\mathbf{r}} - \mathsf{B}^{\top}\widehat{\boldsymbol{\lambda}})),$$

where the matrix B_{*} and the vector $\mathbf{c}_{*}$ are formed by the rows of B and $\mathbf{c}$ corresponding to the all the free (not active) Lagrange multipliers in $\Lambda(\xi)$.

7 Preconditioning by the Projector to the Rigid Body Modes

Even though by the application of the duality in Sect. 6 we obtained problem (14) that is much more suitable for computations than (7) and was used for efficient solution of contact problems [16], further improvement may be achieved by adapting some simple observations and the results of FARHAT, MANDEL, and ROUX [27].

Let Z denote a non–singular matrix that defines the orthonormalization of the rows of G, so that the matrix

$$\overline{\mathsf{G}} := \mathsf{Z}\mathsf{G}$$

satisfies $\overline{\mathsf{G}}\,\overline{\mathsf{G}}^{\top} = \mathsf{I}$, where I denotes a unit matrix. After putting $\overline{\mathbf{e}} := \mathsf{Z}\mathbf{e}$, problem (14) reads

$$\text{minimize} \quad \Theta(\boldsymbol{\lambda}) \quad \text{subject to} \quad \boldsymbol{\lambda} \in \Lambda(\xi) \quad \text{and} \quad \overline{\mathsf{G}}\boldsymbol{\lambda} = \overline{\mathbf{e}}. \tag{15}$$

Next we shall transform the problem of minimization on the subset of the affine space to that on the subset of the vector space by means of arbitrary $\boldsymbol{\lambda}_0$ that satisfies

$$\overline{\mathsf{G}}\boldsymbol{\lambda}_0 = \overline{\mathbf{e}}.$$

Having such a $\boldsymbol{\lambda}_0$, we can look for the solution of (15) in the form $\boldsymbol{\lambda} = \widetilde{\boldsymbol{\lambda}} + \boldsymbol{\lambda}_0$.

A natural choice for $\boldsymbol{\lambda}_0$ is the least square solution of $\overline{\mathsf{G}}\boldsymbol{\lambda} = \overline{\mathbf{e}}$ given by

$$\boldsymbol{\lambda}_0 = \overline{\mathsf{G}}^{\top}\overline{\mathbf{e}}.$$

Though this choice of $\boldsymbol{\lambda}_0$ works well in practical applications, it turns out that it is difficult to find a feasible initial approximation which is not too far from the solution. To avoid solving this rather theoretical problem and to simplify the reference to the relevant optimality results for the quadratic programming algorithms, we shall use in our analysis $\boldsymbol{\lambda}_0$ which satisfies an additional constraint $\boldsymbol{\lambda}_0 \in \Lambda(\xi)$. To see that such a $\boldsymbol{\lambda}_0$ exists, it is enough to notice that the feasible set of the minimization problem (15) is non–empty. We can find it effectively by the solution of the non–linear least square problem

$$\text{minimize} \quad \frac{1}{2}\|\boldsymbol{\lambda}\|^2 \quad \text{subject to} \quad \boldsymbol{\lambda} \in \Lambda(\xi) \quad \text{and} \quad \overline{\mathsf{G}}\boldsymbol{\lambda} = \overline{\mathbf{e}}. \tag{16}$$

Since we put $\boldsymbol{\lambda} = \widetilde{\boldsymbol{\lambda}} + \boldsymbol{\lambda}_0$, it holds

$$\Theta(\boldsymbol{\lambda}) = \frac{1}{2}\boldsymbol{\lambda}^{\top}\mathsf{F}\boldsymbol{\lambda} - \boldsymbol{\lambda}^{\top}\widetilde{\mathbf{d}} = \frac{1}{2}\widetilde{\boldsymbol{\lambda}}^{\top}\mathsf{F}\widetilde{\boldsymbol{\lambda}} - \widetilde{\boldsymbol{\lambda}}^{\top}(\widetilde{\mathbf{d}} - \mathsf{F}\boldsymbol{\lambda}_0) + \frac{1}{2}\boldsymbol{\lambda}_0^{\top}\mathsf{F}\boldsymbol{\lambda}_0 - \boldsymbol{\lambda}_0^{\top}\widetilde{\mathbf{d}},$$

and we can consider (in minimization) the dual function Θ without the last two constant terms. Now let us denote $\widetilde{\Lambda}(\xi) := \Lambda(\xi) - \boldsymbol{\lambda}_0$, return to the old notation before the homogenization of the equality constraints (except $\widetilde{\Lambda}(\xi)$) and reformulate problem (15) equivalently as:

$$\text{minimize} \quad \Xi_0(\boldsymbol{\lambda}) \quad \text{subject to} \quad \boldsymbol{\lambda} \in \widetilde{\Lambda}(\xi) \quad \text{and} \quad \overline{\mathsf{G}}\boldsymbol{\lambda} = \mathbf{0}, \tag{17}$$

where

$$\Xi_0(\boldsymbol{\lambda}) := \frac{1}{2}\boldsymbol{\lambda}^{\top}\mathsf{F}\boldsymbol{\lambda} - \boldsymbol{\lambda}^{\top}\mathbf{d}$$

and $\mathbf{d} := \widetilde{\mathbf{d}} - \mathsf{F}\boldsymbol{\lambda}_0$.

Our final step is based on the observation that problem (17) is equivalent to

$$\text{minimize} \quad \Xi(\boldsymbol{\lambda}) \quad \text{subject to} \quad \boldsymbol{\lambda} \in \widetilde{\Lambda}(\xi) \quad \text{and} \quad \overline{\mathsf{G}}\boldsymbol{\lambda} = \mathbf{0}, \tag{18}$$

where

$$\Xi(\boldsymbol{\lambda}) := \frac{1}{2}\boldsymbol{\lambda}^\top (F^{-1}\mathsf{PFP} + \rho\,\mathsf{Q})\boldsymbol{\lambda} - F^{-1}\boldsymbol{\lambda}^\top \mathsf{P}\mathbf{d} \quad \text{with} \quad F \approx \|\mathsf{PFP}\|,$$

ρ is a positive penalty factor, and

$$\mathsf{Q} := \overline{\mathsf{G}}^\top \overline{\mathsf{G}} \quad \text{and} \quad \mathsf{P} := \mathsf{I} - \mathsf{Q}$$

denote the orthogonal projectors on the image space of $\overline{\mathsf{G}}^\top$ and on the kernel of $\overline{\mathsf{G}}$, respectively. The expression $F \approx \|\mathsf{PFP}\|$ here means that there are positive constants F_1 and F_2 independent of h and H such that

$$F_1 \le F^{-1}\|\mathsf{PFP}\| \le F_2. \tag{19}$$

For convenience, let us denote the Hessian matrix of Ξ by

$$\mathscr{H} := F^{-1}\mathsf{PFP} + \rho\,\mathsf{Q}.$$

Let us note that if $[a,b] \subset \mathbb{R}_+$ is an interval containing non-zero elements of the spectrum $\sigma(\mathsf{PFP})$ of PFP, then $\sigma(\mathscr{H}) \subset [F^{-1}a, F^{-1}b] \cup \{\rho\}$, so that $\mathscr{H}$ is non-singular. In our numerical experiments we use $\rho := 1 \approx F^{-1}\|\mathsf{PFP}\|$. Our choice of ρ is motivated by an effort to use the maximal regularization parameter which does not increase the norm of $\mathscr{H}$. The regularization term is introduced in order to enable the application of the results of quadratic and QPQC programming that assume regularity of the Hessian matrix of the quadratic form. Problem (18) turns out to be a suitable starting point for the development of an efficient algorithm for variational inequalities due to the classical estimates of the extreme eigenvalues. To formulate them, we shall denote by $\lambda_{\min}(\mathsf{A})$ and $\lambda_{\max}(\mathsf{A})$ the smallest and the largest eigenvalues of a given symmetric matrix A, respectively.

Theorem 1. *Let there be constants $b, B > 0$ independent of the discretization parameter h and the decomposition parameter H such that*

$$b \le \lambda_{\min}(\mathsf{B}\mathsf{B}^\top) \le \lambda_{\max}(\mathsf{B}\mathsf{B}^\top) \le B$$

and let the elements and the subdomains have regular shape and size. Then there are constants $C_1, C_2 > 0$ independent of the discretization parameter h and the decomposition parameter H such that

$$C_1 \frac{h}{H} \le \lambda_{\min}(\mathscr{H}) \le \lambda_{\max}(\mathscr{H}) = \|\mathscr{H}\| \le C_2.$$

To prove the above theorem, it is enough to use the definition of $\mathscr{H}$, the bounds on the condition number of $\mathsf{PFP}|\mathrm{Im}\mathsf{P}$ for the FETI case by FARHAT, MANDEL, and ROUX [27], and the observation of LANGER and STEINBACH [40] that the boundary element stiffness matrix $\widetilde{\mathsf{S}}^p$ is spectrally equivalent to some Schur complement of the corresponding finite element stiffness matrix. See also [5].

Theorem 1 states that if we refine the mesh and increase the number of subdomains so that the ratio H/h is kept bounded, we have still the same upper bound on the spectral condition number of the Hessian $\mathscr{H}$. LANGER and STEINBACH [40] give stronger polylogarithmic bounds for the preconditioned F, but we cannot use their result since such preconditioning transforms the bound constraints to more general ones.

8 Optimality

First observe that in case of the frictionless contact problem, the only inequality constraints in (18) are the bound constraints in the multipliers $\boldsymbol{\lambda}_i$, $i \in \mathscr{I}$, where $\mathscr{I}$ is the set of indices of the multipliers for the non-interpenetration conditions. Such problems can be solved effectively by our semi-monotonic augmented Lagrangian method SMALBE-M [11] (or its variant SMALBE) [10, 11]. Unlike the standard augmented Lagrangian algorithm [28], the SMALBE-M method generates approximations for the Lagrange multipliers μ for the equality constraints in the outer loop, with any algorithm for the solution of the bound constrained problems in the inner loop. A specific feature of SMALBE-M is an effective precision control of the auxiliary problems in the inner loop. This precision control uses the gradual decrease of the balancing parameter M, keeping the regularization parameter fixed. The bound constrained problems in the inner loop are solved by the MPRGP algorithm proposed by DOSTÁL and SCHÖBERL [14].

The augmented Lagrangian L corresponding to (18) is defined by

$$L(\boldsymbol{\lambda},\mu,\rho) := \Xi(\boldsymbol{\lambda}) + \mu^\top \overline{\mathsf{G}}\boldsymbol{\lambda} \tag{20}$$

and its gradient with respect to the first variable is given by

$$\mathbf{g}(\boldsymbol{\lambda},\mu,\rho) := \nabla_{\boldsymbol{\lambda}} L(\boldsymbol{\lambda},\mu,\rho) = \left(F^{-1}\mathsf{PFP} + \rho\mathsf{Q}\right)\boldsymbol{\lambda} - F^{-1}\mathsf{P}\mathbf{d} + \overline{\mathsf{G}}^\top \mu.$$

Recall that $\mathscr{E}$ denotes a set of indices corresponding to the equality constraints. The *projected gradient* $\mathbf{g}^P = \mathbf{g}^P(\boldsymbol{\lambda},\mu,\rho)$ of L at $\boldsymbol{\lambda}$ *for the frictionless case* is then given component-wise by

$$\mathbf{g}^P_i := \begin{cases} \mathbf{g}_i & \text{for } \boldsymbol{\lambda}_i > -\boldsymbol{\lambda}_{0,i} \quad \text{and} \quad i \in \mathscr{I}, \quad \text{or} \quad i \in \mathscr{E}, \\ \mathbf{g}_i^- & \text{for } \boldsymbol{\lambda}_i = -\boldsymbol{\lambda}_{0,i} \quad \text{and} \quad i \in \mathscr{I}, \end{cases}$$

where $\mathbf{g}_i^- := \min\{\mathbf{g}_i, 0\}$. SMALBE-M is unique in that it is capable of finding an approximate solution of problem (18) for the frictionless case in a number of steps which is uniformly bounded in terms of the bounds on the spectrum of the Hessian $\mathscr{H}$. To get a bound on the number of matrix–vector multiplications, it is necessary to have an algorithm which is able to solve the problem

$$\text{minimize} \quad L(\boldsymbol{\lambda},\mu,\rho) \quad \text{with respect to} \quad \boldsymbol{\lambda} \quad \text{subject to} \quad \boldsymbol{\lambda}_{\mathscr{I}} \geq -\boldsymbol{\lambda}_{0,\mathscr{I}} \tag{21}$$

with the rate of convergence of the projected gradient $\mathbf{g}^P = \mathbf{g}^P(\boldsymbol{\lambda}, \mu, \rho)$ in terms of the bounds on the spectrum of $\mathscr{H}$. This property has been proved for the MPRGP (modified proportioning with the reduced gradient projection) algorithm [14]. More about the properties and implementation of SMALBE-M and MPRGP algorithms may be found in [10, 11, 14, 20]. Applications to the frictionless contact problems discretized either by finite or boundary elements can be found in [5, 6, 19, 51].

For the solution of the separable and equality constrained problem (18) arising from the discretization of the problem with the Tresca friction (6), we use our in a sense natural modification of SMALBE-M coined SMALSE-M (semi-monotonic augmented Lagrangians for separable and equality constraints) with the inner loop implemented by the MPGP algorithm [12].

SMALSE-M has similar properties as the algorithm SMALBE-M reported above. To get a bound on the number of matrix–vector multiplications, it is necessary to have an algorithm which is able to solve the problem

$$\text{minimize} \quad L(\boldsymbol{\lambda}, \mu, \rho) \quad \text{with respect to} \quad \boldsymbol{\lambda} \quad \text{subject to} \quad \boldsymbol{\lambda} \in \widetilde{\Lambda}(\xi), \tag{22}$$

where L is given by (20), with the rate of convergence of the *natural generalization of the projected gradient* $\mathbf{g}^P = \mathbf{g}^P(\boldsymbol{\lambda}, \mu, \rho)$ of L [12] in terms of the bounds on the spectrum of $\mathscr{H}$. More about the properties and implementation of SMALSE-M and closely related SMALBE and SMALBE-M algorithms may be found in [10, 11, 13, 21].

To guarantee the optimality, the inner loop of SMALSE-M [13, 21] (i.e., the solution of (22) to a precision that is adaptively controlled) can be implemented by means of a modification of the MPRGP algorithm, e.g., the MPGP algorithm by DOSTÁL and KOZUBEK [12] or the KPRGP algorithm proposed by KUČERA [37].

To formulate the optimality results, let $\overline{\mathscr{I}}$ denote the set of all indices corresponding to inequality constraints and write the inequality constraints in the unified form

$$h_i(\boldsymbol{\lambda}) = h_i(\boldsymbol{\lambda}_i) \le 0 \quad \text{for } i \in \overline{\mathscr{I}}.$$

For instance, if i is an index of a non-interpenetration constraint, then

$$h_i(\boldsymbol{\lambda}) := -\boldsymbol{\lambda}_i - \boldsymbol{\lambda}_{0,i}.$$

To show that the SMALSE-M algorithm with the inner loop implemented by means of MPGP is optimal for the solution of problem (18) provided $h_i(\mathbf{0}) \le 0$ for $i \in \overline{\mathscr{I}}$, we introduce a new notation that complies with that used in [12]. First, let us consider a system of elastic bodies in contact with the Tresca friction that can be discretized by a regular grid with the stepsize h and decomposed with the decomposition parameter H. We use

$$\mathscr{T} := \{(H,h) \in \mathbb{R}^2 : \ 2h \le H \text{ and } H/h \in \mathbb{N}\}$$

as the index set. Given a constant $C \ge 2$, let $\mathscr{T}_C$ be a subset of $\mathscr{T}$ defined by

$$\mathscr{T}_C := \{(H,h) \in \mathscr{T} : \ H/h \le C\}. \tag{23}$$

For any $t \in \mathscr{T}$, we define

$$\mathsf{A}_t := \mathscr{H}_t, \quad \mathbf{b}_t := F_t^{-1}\mathsf{P}_t\mathbf{d}_t, \quad \mathsf{C}_t := \overline{\mathsf{G}}_t$$

by the vectors and matrices generated with the discretization and decomposition parameters H and h, respectively, so that problem (18) is equivalent to the problem

$$\text{minimize} \quad \Xi_t(\boldsymbol{\lambda}_t) \quad \text{subject to} \quad \mathsf{C}_t\boldsymbol{\lambda}_t = \mathbf{0} \quad \text{and} \quad h_{t,i}(\boldsymbol{\lambda}_t) \le 0 \quad \text{for } i \in \overline{\mathscr{I}} \tag{24}$$

with

$$\Xi_t(\boldsymbol{\lambda}_t) := \frac{1}{2}\boldsymbol{\lambda}_t^\top \mathsf{A}_t\boldsymbol{\lambda}_t - \mathbf{b}_t^\top\boldsymbol{\lambda}_t.$$

By using these definitions and $\overline{\mathsf{G}}_t\,\overline{\mathsf{G}}_t^\top = \mathsf{I}$, we get

$$\|\mathsf{C}_t\| \le 1 \quad \text{and} \quad h_{t,i}(\mathbf{0}) \le 0 \quad \text{for } i \in \overline{\mathscr{I}}. \tag{25}$$

Moreover, it follows by Theorem 1 that for any $C \ge 2$ in (23) there are constants $a^C_{\max} \ge a^C_{\min} > 0$ such that

$$a^C_{\min} \le \lambda_{\min}(\mathsf{A}_t) \le \lambda_{\max}(\mathsf{A}_t) \le a^C_{\max} \tag{26}$$

for any $t \in \mathscr{T}_C$. In particular, it follows that the assumptions of Theorem 3 (i.e., the inequalities in (25) and (26)) of [12] are satisfied for any set of indices $\mathscr{T}_C$, $C \ge 2$, so that we have the following result:

Theorem 2 ([12]). *Let $C \ge 2$ and $\varepsilon > 0$ denote given constants, let $\{\boldsymbol{\lambda}_t^k\}, \{\mu_t^k\}$, and $\{M_{t,k}\}$ be generated by the SMALSE-M algorithm for (24) with the parameters*

$$\|\mathbf{b}_t\| \ge \eta_t > 0,\ \beta > 1,\ M_{t,0} := M_0 > 0,\ \rho > 0, \text{ and } \mu_t^0 := \mathbf{0}.$$

Let $s \ge 0$ denote the smallest integer such that

$$\beta^{2s}\rho \ge M_0^2/a^C_{\min}$$

and assume that Step 1 of SMALSE-M is implemented by means of the MPGP algorithm with the parameters

$$\Gamma > 0 \quad \text{and} \quad \overline{\alpha} \in (0, 2/a^C_{\max})$$

that guarantee the R-linear convergence of MPGP, so that it generates the iterates $\boldsymbol{\lambda}_t^{k,0}, \boldsymbol{\lambda}_t^{k,1}, \ldots, \boldsymbol{\lambda}_t^{k,l} =: \boldsymbol{\lambda}_t^k$ for the solution of the auxiliary problem (22) starting from $\boldsymbol{\lambda}_t^{k,0} := \boldsymbol{\lambda}_t^{k-1}$ with $\boldsymbol{\lambda}_t^{-1} := \mathbf{0}$, where $l = l_{t,k}$ is the first index satisfying

$$\|\mathbf{g}^P(\boldsymbol{\lambda}_t^{k,l}, \mu_t^k, \rho)\| \le M_{t,k}\|\mathsf{C}_t\boldsymbol{\lambda}_t^{k,l}\|$$

or

$$\|\mathbf{g}^P(\boldsymbol{\lambda}_t^{k,l}, \mu_t^k, \rho)\| \le \varepsilon\|\mathbf{b}_t\| \quad \text{and} \quad \|\mathsf{C}_t\boldsymbol{\lambda}_t^{k,l}\| \le \varepsilon\|\mathbf{b}_t\|.$$

Then for any $t \in \mathcal{T}_C$ and problem (24), SMALSE-M generates an approximate solution $\boldsymbol{\lambda}_t^{k_t}$ which satisfies

$$\|\mathbf{g}^P(\boldsymbol{\lambda}_t^{k_t}, \mu_t^{k_t}, \rho)\| \le \varepsilon \|\mathbf{b}_t\| \quad \text{and} \quad \|C_t \boldsymbol{\lambda}_t^{k_t}\| \le \varepsilon \|\mathbf{b}_t\|$$

at $\mathcal{O}(1)$ matrix–vector multiplications by the Hessian of the augmented Lagrangian for (24) and

$$M_{t,k}^2 \ge \min\{M_0^2, \rho a_{\min}^C / \beta^2\}.$$

Theorem 2 holds true also if we replace the MPGP algorithm by KPRGP with $\overline{\alpha} \in (0, 1/a_{\max}^C)$ [13]. In our experiments, we use $M_0 = \rho := 1$.

9 Numerical Experiments

The described algorithms are implemented in the `MatSol` library [36] developed in a Matlab environment and tested on the solution of two benchmarks comprising 3D contact problems. In the first benchmark, we vary the decomposition and discretization parameters in order to demonstrate the scalability of our method. In the second one, we illustrate the ability of our algorithms to solve some real world problems. For these computations we use the HP Blade system, model BLc7000 with one master node and eight computational nodes, each with two dual core CPUs AMD Opteron 2210 HE. The maximum number of parallel processes is limited by 48 due to the number of available licences of Matlab Distributed Computing Engine which is used as the parallel programming environment. All the computations are carried out with the parameters: $M_0 := 1$, $\eta := F^{-1}\|\mathsf{Pd}\|$, $\rho := 1 \approx F^{-1}\|\mathsf{PFP}\|$, $\overline{\alpha} := 2/\rho$, $\Gamma := 1$, $\beta := 10$, $\mu^0 := \mathbf{0}$, and the relative stopping tolerance $\varepsilon := 10^{-4}$. We estimated F by a few iterations of the Lanczos method.

9.1 Demonstration of Scalability on Two Cantilever Beams in Mutual Contact

The first problem is a 3D semicoercive contact problem of two cantilever beams in mutual contact and 75% overlap. Each beam is represented by a box $2000 \times 1000 \times 1000$ [mm]. We consider 3 friction models: a frictionless case, the Tresca friction with the slip bound $\Psi := 80$ [MPa] and the Coulomb friction with the coefficient of friction 0.1. The geometry with prescribed boundary conditions and material properties is shown in Fig. 4.

To demonstrate the scalability of our algorithms, we resolve the problem with varying discretizations and decompositions defined by the discretization parameter h and the decomposition parameter H, respectively. For each h and H, the bodies are discretized by structured grids decomposed into the subdomains (see Fig. 5). We keep $H/h = 10$. The results for all friction models are reported in Tables 1, 2, and 3. We can observe that the number of matrix–vector multiplications increases only mildly in agreement with the theory in all cases.

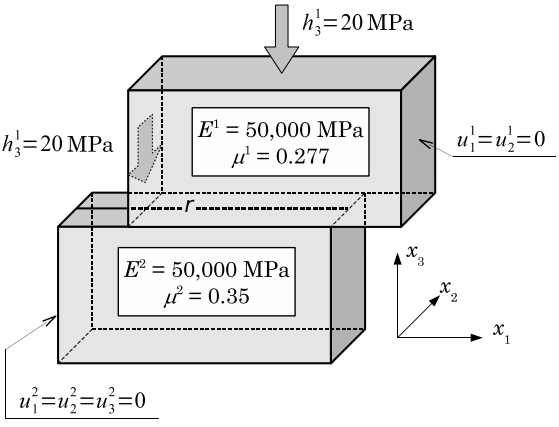

Fig. 4 Model specification

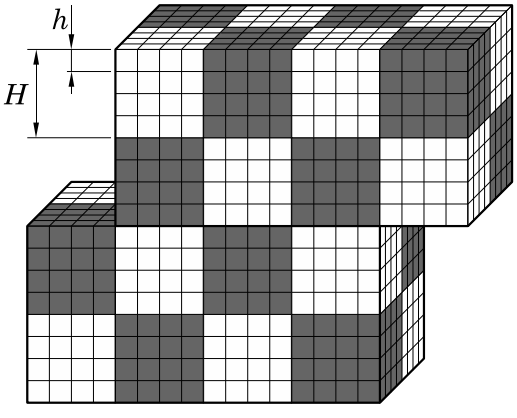

Fig. 5 Uniform domain decomposition

Table 1 Frictionless case: numerical scalability

Number of subdomains	108	500	1372	2916
Number of CPUs	48	48	48	48
Primal variables	195,048	903,000	2,477,830	5,266,300
Dual variables	88,601	444,927	1,261,493	2,728,955
Null space dimension	648	3000	8232	17,496
Hessian multiplications	87	76	124	195
SMALSE-M iterations	9	12	13	16
Solution time [s]	68	364	2206	7573
Total time [s]	224	1136	5645	11,221

The corresponding parallel scalability of our algorithms is depicted in Figs. 6, 7, and 8. In this case, we fix the number of primal variables in the subdomains and increase the number of partitions into subdomains accordingly to the number of used CPUs. The performance agrees with the theoretical results.

Table 2 Tresca friction: numerical scalability

Number of subdomains	108	500	1372	2916
Number of CPUs	48	48	48	48
Primal variables	195,048	903,000	2,477,830	5,266,300
Dual variables	88,601	444,927	1,261,493	2,728,955
Null space dimension	648	3000	8232	17,496
Hessian multiplications	107	108	107	207
SMALSE-M iterations	7	8	9	9
Solution time [s]	46	301	2211	7950
Total time [s]	127	656	3454	11,673

Table 3 Coulomb friction

Number of subdomains	108	500	1372	2916
Number of CPUs	48	48	48	48
Primal variables	195,048	903,000	2,477,830	5,266,300
Dual variables	88,601	444,927	1,261,493	2,728,955
Null space dimension	648	3000	8232	17,496
Hessian multiplications	221	191	400	687
SMALSE-M iterations	21	15	36	53
Solution time [s]	76	398	3206	13,817
Total time [s]	157	754	4447	17,542

The normal and tangent contact pressures along the line r lying in the middle of the contact interface (see Fig. 4) for all cases are depicted in Figs. 9, 10, and 11.

9.2 Mechanical Engineering Problem: Yielding Clamp Connection

The second example is a stress analysis in the yielding clamp connection of steel arched supports depicted in Fig. 12, where we see only a half of the whole structure because of the symmetry with respect to the x_2x_3 plane. This type of construction is used to support the mining openings. It is a typical multibody contact, where the yielding connection plays the role of the mechanical protection against destruction, i.e., against the total deformation of the supporting arches. We consider two contact models: a frictionless contact and contact with the Coulomb friction, where the coefficient of friction is 0.5. The problem is decomposed into 250 subdomains using METIS (see Fig. 13) and discretized by 713,751 and 261,553 primal and dual variables, respectively.

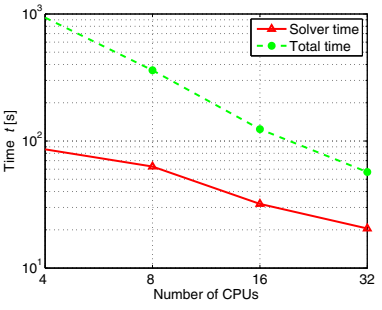

Fig. 6 Frictionless case: parallel scalability

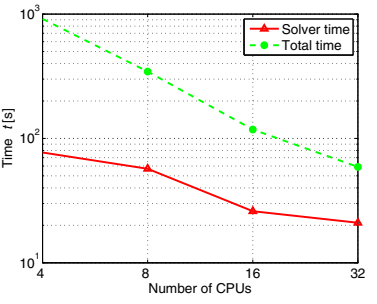

Fig. 7 Tresca friction: parallel scalability

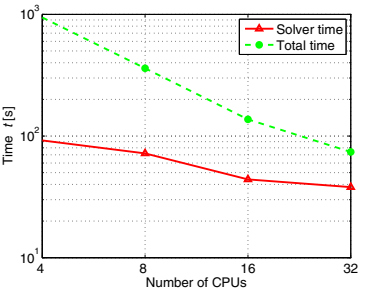

Fig. 8 Coulomb friction: parallel scalability

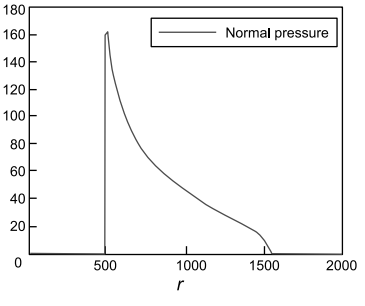

Fig. 9 Frictionless case: normal contact pressure along the line r [MPa]

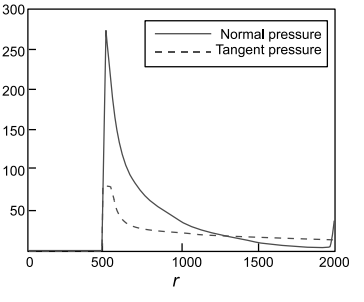

Fig. 10 Tresca friction: normal and tangent contact pressures along the line r [MPa]

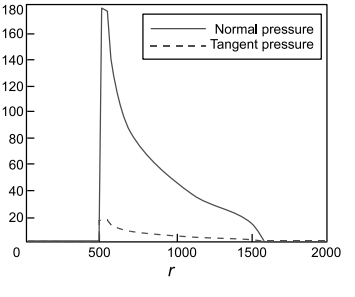

Fig. 11 Coulomb friction: normal and tangent contact pressures along the line r [MPa]

The total displacement for both contact models are depicted in Figs. 14 and 15. We see the significant difference. In the frictionless case, it requires 1745 matrix–vector multiplications and takes 7884 seconds. In the friction case, it requires 2479 matrix–vector multiplications and takes 11,169 seconds to find the solution. For all computations we use 24 CPUs. Finally, we depict the contact pressure for both cases in Figs. 16-19.

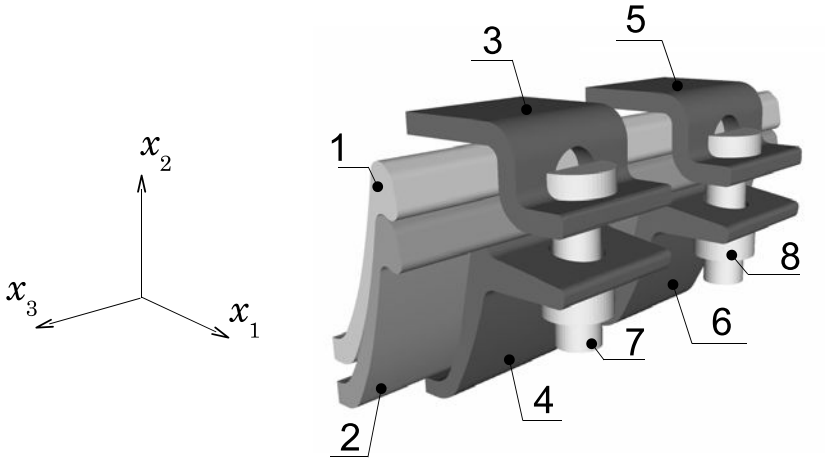

Fig. 12 Yielding clamp connection: 1-2 steel supports, 3-6 clamps, and 7-8 bolts with nuts

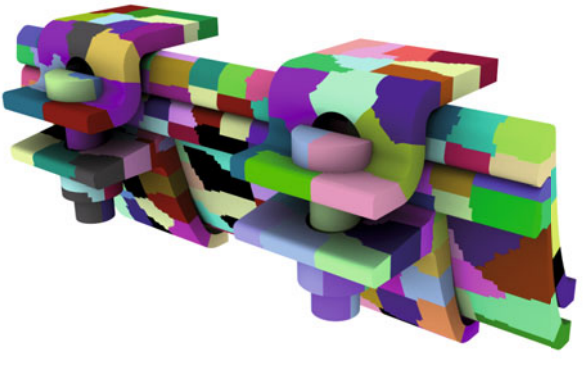

Fig. 13 Domain decomposition

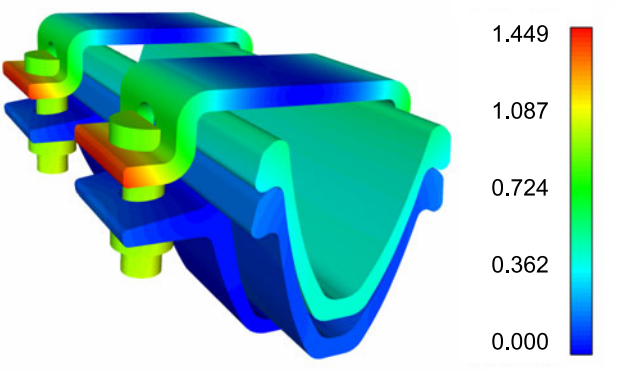

Fig. 14 Frictionless case: total displacement

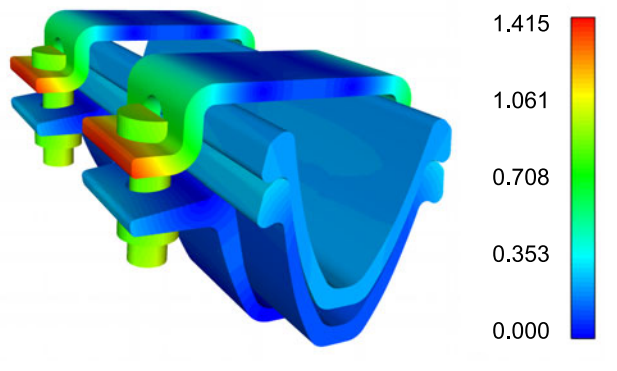

Fig. 15 Coulomb friction: total displacement

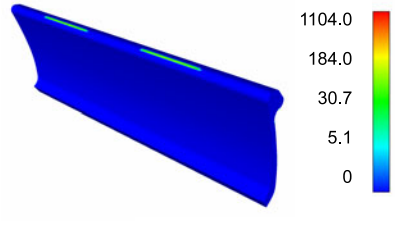

Fig. 16 Frictionless case: normal contact pressure (view 1) [MPa]

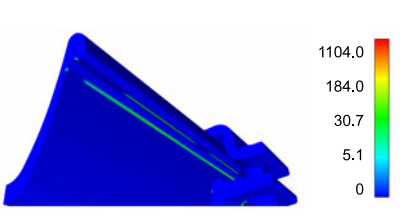

Fig. 17 Frictionless case: normal contact pressure (view 2) [MPa]

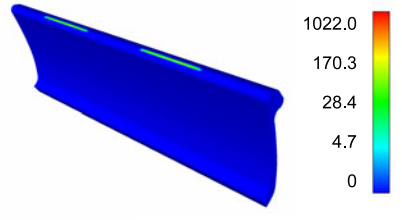

Fig. 18 Coulomb friction: normal contact pressure (view 1) [MPa]

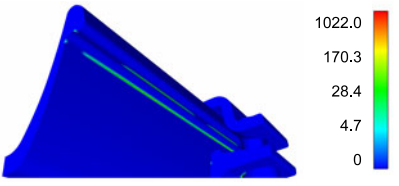

Fig. 19 Coulomb friction: normal contact pressure (view 2) [MPa]

10 Comments and Conclusions

We have presented the scalability results related to the application of the Total BETI based domain decomposition method with the natural coarse grid preconditioning and of our recently developed algorithms for the solution of convex QPQC problems to the solution of 3D multibody contact problems of elastostatics. We considered the frictionless contact, the contact with the Tresca friction and with the Coulomb friction. We have shown that an approximate solution of the discretized elliptic variational inequality which describes the equilibrium of a system of elastic bodies in mutual contact for frictionless case and for the Tresca friction may be obtained in a number of matrix–vector multiplications bounded independently of the discretization parameter provided the ratio of the decomposition and the discretization parameters is kept bounded.

Numerical experiments with the academic benchmark are in agreement with the theory. The power of our algorithms for the solution of problems with the Coulomb friction has been demonstrated also on a real world problem from mechanical engineering. We have documented also the parallel scalability inherited from the basic BETI scheme. The solution of auxiliary linear problems in the inner loop may be improved by standard preconditioners [40, 57] and may be adapted to the mortar discretization [41, 58] or to the solution of more general problems, such as the problems with anisotropic friction, quasistatics and dynamics problems.

Acknowledgements. This research has been financially supported by the grants GA CR 201/07/0294 and the Ministry of Education of the Czech Republic No. MSM6198910027.

References

[1] Avery, P., Farhat, C.: The FETI family of domain decomposition methods for inequality-constrained quadratic programming: Application to contact problems with conforming and nonconforming interfaces. Comput Methods Appl. Mech. Engrg. 198, 1673–1683 (2009)

[2] Bazaraa, M.S., Shetty, C.M., Sherali, H.D.: Nonlinear Programming, Theory and Algorithms. Wiley, New York (1993)

[3] Bebendorf, M.: Hierarchical Matrices: A Means to Efficiently Solve Elliptic Boundary Value Problems. Lecture Notes in Computational Science and Engineering, vol. 63. Springer, Berlin (1978)
[4] Bebendorf, M., Rjasanow, S.: Adaptive low–rank approximation of collocation matrices. Computing 70, 1–24 (2003)
[5] Bouchala, J., Dostál, Z., Sadowská, M.: Theoretically supported scalable BETI method for variational inequalities. Computing 82, 53–75 (2008)
[6] Bouchala, J., Dostál, Z., Sadowská, M.: Scalable Total BETI based algorithm for 3D coercive contact problems of linear elastostatics. Computing 85, 189–217 (2009)
[7] Brzobohatý, T., Dostál, Z., Kovář, P., Kozubek, T., Markopoulos, A.: Cholesky decomposition with fixing nodes to stable evaluation of a generalized inverse of the stiffness matrix of a floating structure. Internat. J. Numer. Methods Engrg. 85(5), 493–509 (2011)
[8] Burczyński, T., Adamczyk, T.: The boundary element formulation for multiparameter structural shape optimization. Appl. Math. Model. 9, 195–200 (1985)
[9] Costabel, M.: Boundary integral operators on Lipschitz domains: Elementary results. SIAM J. Math. Anal. 19, 613–626 (1988)
[10] Dostál, Z.: An optimal algorithm for bound and equality constrained quadratic programming problems with bounded spectrum. Computing 78, 311–328 (2006)
[11] Dostál, Z.: Optimal Quadratic Programming Algorithms with Applications to Variational Inequalities. Springer Optimization and its Applications, vol. 23. Springer, New York (2009)
[12] Dostál, Z., Kozubek, T.: An optimal algorithm with superrelaxation for minimization of a quadratic function subject to separable constraints with applications (submitted)
[13] Dostál, Z., Kučera, R.: An optimal algorithm for minimization of quadratic functions with bounded spectrum subject to separable convex inequality and linear equality constraints. SIAM J. Optim. 20, 2913–2938 (2010)
[14] Dostál, Z., Schöberl, J.: Minimizing Quadratic Functions Subject to Bound Constraints with the Rate of Convergence and Finite Termination. Comput. Optim. Appl. 30, 23–43 (2005)
[15] Dostál, Z., Friedlander, A., Santos, S.A., Malík, J.: Analysis of semicoercive contact problems using symmetric BEM and augmented Lagrangians. Eng. Anal. Bound. Elem. 18, 195–201 (1996)
[16] Dostál, Z., Friedlander, A., Santos, S.A.: Solution of coercive and semicoercive contact problems by FETI domain decomposition. Contemporary Mathematics 218, 82–93 (1998)
[17] Dostál, Z., Horák, D., Kučera, R.: Total FETI – an easier implementable variant of the FETI method for numerical solution of elliptic PDE. Commun. Numer. Meth. Eng. 22, 1155–1162 (2006)
[18] Dostál, Z., Kozubek, T., Horyl, P., Brzobohatý, T., Markopoulos, A.: Scalable TFETI algorithm for two dimensional multibody contact problems with friction. J. Comput. Appl. Math. 235, 403–418 (2010)
[19] Dostál, Z., Kozubek, T., Vondrák, V., Brzobohatý, T., Markopoulos, A.: Scalable TFETI algorithm for the solution of multibody contact problems of elasticity. Internat. J. Numer. Methods Engrg. 82, 1384–1405 (2010)
[20] Dostál, Z., Domorádová, M., Sadowská, M.: Superrelaxation and the rate of convergence in minimizing quadratic functions subject to bound constraints. Comput. Optim. Appl. 48, 23–44 (2011)

[21] Dostál, Z., Kozubek, T., Markopoulos, A., Brzobohatý, T., Vondrák, V., Horyl, P.: A theoretically supported scalable TFETI algorithm for the solution of multibody 3D contact problems with friction. Comput. Methods Appl. Mech. Engrg. (published online, 2011)
[22] Dostál, Z., Kozubek, T., Markopoulos, A., Menšík, M.: Cholesky decomposition of a positive semidefinite matrix with known kernel. Appl. Math. Comput. 217, 6067–6077 (2011)
[23] Dureisseix, D., Farhat, C.: A numerically scalable domain decomposition method for solution of frictionless contact problems. Internat. J. Numer. Methods Engrg. 50, 2643–2666 (2001)
[24] Duvaut, G., Lions, J.L.: Inequalities in Mechanics and Physics. Springer, Heidelberg (1976)
[25] Eck, C., Steinbach, O., Wendland, W.L.: A symmetric boundary element method for contact problems with friction. Math. Comput. Simulat. 50, 43–61 (1999)
[26] Farhat, C., Géradin, M.: On the general solution by a direct method of a large scale singular system of linear equations: application to the analysis of floating structures. Internat. J. Numer. Methods Engrg. 41, 675–696 (1998)
[27] Farhat, C., Mandel, J., Roux, F.X.: Optimal convergence properties of the FETI domain decomposition method. Comput. Methods Appl. Mech. Engrg. 115, 365–385 (1994)
[28] Glowinski, R., Le Tallec, P.: Augmented Lagrangians and Operator Splitting Methods. SIAM, Philadelphia (1989)
[29] Greengard, L.F., Rokhlin, V.: A fast algorithm for particle simulations. J. Comput. Phys. 73, 325–348 (1987)
[30] Greengard, L.F., Rokhlin, V.: A new version of the fast multipole method for the Laplace equation in three dimensions. Acta Numerica 229–269 (1997)
[31] Han, H.: The boundary integro–differential equations of three–dimensional Neumann problem in linear elasticity. Numer. Math. 68, 269–281 (1994)
[32] Hlaváček, I., Haslinger, J., Nečas, J., Lovíšek, J.: Solution of Variational Inequalities in Mechanics. Springer, Berlin (1988)
[33] Kikuchi, N., Oden, J.T.: Contact Problems in Elasticity. SIAM, Philadelphia (1988)
[34] Kornhuber, R.: Adaptive monotone multigrid methods for nonlinear variational problems. Teubner, Stuttgart (1997)
[35] Kornhuber, R., Krause, R.: Adaptive multigrid methods for Signorini's problem in linear elasticity. Comput. Visual. Sci. 4, 9–20 (2001)
[36] Kozubek, T., Markopoulos, A., Brzobohatý, T., Kučera, R., Vondrák, V., Dostál, Z.: MatSol – MATLAB effcient solvers for problems in engineering, `http://www.am.vsb.cz/matsol`
[37] Kučera, R.: Convergence rate of an optimization algorithm for minimizing quadratic functions with separable convex constraints. SIAM J. Optim. 19, 846–862 (2008)
[38] Kupradze, V.D., Gegelia, T.G., Baseleisvili, M.O., Burculadze, T.V.: Three–dimensional problems of the mathematical theory of elasticity and thermoelasticity. North–Holland Series in Applied Mathematics and Mechanics, vol. 25. North–Holland, Amsterdam (1979)
[39] Langer, U., Pechstein, C.: Coupled FETI/BETI solvers for nonlinear potential problems in (un)bounded domains. In: Ciuprina, G., Ioan, D. (eds.) Proceedings of the SCEE 2006, Mathematics in Industry, vol. 11, pp. 371–377. Springer, Heidelberg (2007)
[40] Langer, U., Steinbach, O.: Boundary element tearing and interconnecting methods. Computing 71, 205–228 (2003)
[41] Laursen, T.A.: Computational Contact and Impact Mechanics. Springer, London (2002)

[42] Liu, Y., Nishimura, N.: The fast multipole boundary element method for potential problems: A tutotial. Eng. Anal. Bound. Elem. 30, 371–381 (2006)
[43] Maischak, M., Stephan, E.P.: Adaptive hp–versions of BEM for Signorini problems. Appl. Numer. Math. 54, 425–449 (2005)
[44] McLean, W.: Strongly Elliptic Systems and Boundary Integral Equations. Cambridge University Press (2000)
[45] Of, G.: BETI–Gebietszerlegungsmethoden mit schnellen Randelementverfahren und Anwendungen. PhD Thesis, University of Stuttgart (2006)
[46] Of, G.: The all–floating BETI method: numerical results. In: Domain Decomposition Methods in Science and Engineering XVII. Lecture Notes in Computational Science and Engineering, vol. 60, pp. 295–302. Springer, Berlin (2008)
[47] Of, G., Steinbach, O.: The all–floating boundary element tearing and interconnecting method. J. Numer. Math. 17, 277–298 (2009)
[48] Of, G., Steinbach, O., Wendland, W.L.: Applications of a fast multipole Galerkin boundary element method in linear elastostatics. Comput. Visual. Sci. 8, 201–209 (2005)
[49] Pechstein, C.: Boundary element tearing and interconnecting methods in unbounded domains. Appl. Num. Math. 59, 2824–2842 (2009)
[50] Rjasanow, S., Steinbach, O.: The Fast Solution of Boundary Integral Equations. Mathematical and Analytical Techniques with Applications to Engineering. Springer, New York (2007)
[51] Sadowská, M., Dostál, Z., Kozubek, T., Markopoulos, A., Bouchala, J.: Scalable total BETI based solver for 3D multibody frictionless contact problems in mechanical engineering. Eng. Anal. Bound. Elem. 35, 330–341 (2011)
[52] Sauter, S.A., Schwab, C.: Boundary Element Methods. Springer Series in Computational Mathematics, vol. 39. Springer, Berlin (2011)
[53] Schöberl, J.: Solving the Signorini problem on the basis of domain decomposition techniques. Computing 60, 323–344 (1998)
[54] Steinbach, O.: Fast evaluation of Newton potentials in boundary element methods. East–West J. Numer. Math. 7, 211–222 (1999)
[55] Steinbach, O.: Stability Estimates for Hybrid Coupled Domain Decomposition Methods. Lecture Notes in Mathematics, vol. 1809. Springer, Heidelberg (2003)
[56] Steinbach, O.: Numerical Approximation Methods for Elliptic Boundary Value Problems. Finite and Boundary Elements. Springer, New York (2008)
[57] Toselli, A., Widlund, O.B.: Domain Decomposition Methods – Algorithms and Theory. Springer, Heidelberg (2005)
[58] Wohlmuth, B.I.: Discretization Methods and Iterative Solvers Based on Domain Decomposition. Springer, Berlin (2001)
[59] Wohlmuth, B.I., Krause, R.: Monotone methods on nonmatching grids for nonlinear contact problems. SIAM J. Sci. Comput. 25, 324–347 (2003)
[60] Wriggers, P.: Contact Mechanics. Springer, Berlin (2005)